Photobioreactors in Life Support Systems

A microalgae-based reactor concept operating under microgravity conditions

zur Erlangung des akademischen Grades eines
DOKTORS DER INGENIEURWISSENSCHAFTEN (Dr.-Ing.)

von der Fakultät für Chemieingenieurwesen und Verfahrenstechnik des
Karlsruher Instituts für Technologie (KIT)

genehmigte
DISSERTATION

von
M. Sc. Ines Wagner
aus Karlsruhe

Referent: Prof. Dr.-Ing. Clemens Posten
Korreferent: Prof. Dr. rer. nat. Christoph Syldatk

Tag der mündlichen Prüfung: 02.02.2018

„Es ist kein weicher Weg von der Erde zu den Sternen.“ (Lucius Annaeus Seneca)

„Die Natur kennt keine Probleme, nur Lösungen.“ (Carl Amery)

„Juschten, mir han Huddel.“ (Anonym)

Danksagung

Die vorliegende Arbeit entstand während meiner Tätigkeit am Institut für Bio- und Lebensmitteltechnik, Bereich III: Bioverfahrenstechnik am Karlsruher Institut für Technologie (KIT). Ich danke allen, die zum Gelingen beigetragen haben.

An erster Stelle möchte ich mich sehr herzlich bei Herrn Prof. Dr.-Ing. Clemens Posten bedanken, dass ich diese Arbeit in seiner Arbeitsgruppe durchführen konnte. Die gewonnenen Erfahrungen während dieser Zeit haben sowohl meinen fachlichen wie auch persönlichen Horizont erweitert. Die konstruktiven Diskussionen und Ihre Offenheit haben es mir ermöglicht eigene Ideen umzusetzen und weiterzuentwickeln.

Herrn Prof. Dr. rer. nat. Christoph Syldatk danke ich recht herzlich für die freundliche Übernahme des Korreferates.

Herzlicher Dank geht an die gesamte Arbeitsgruppe Bioverfahrenstechnik für die gute Zusammenarbeit und die tolle Zeit inner- und außerhalb des Institutes. Mein besonderer Dank geht an Tomasz Duczmal, Christian Steinweg und Lena von Riesen für Ihre unermüdliche technische Unterstützung. Frau Taisija Schaffell, Kristin Pluntze, Anna Rommel und Astrid Wahlig danke ich für Ihre Hilfe bei der Verwaltung der Projekte. Meinen Kollegen Linda, Ioanna, Matthias, Mirco, Inga und Kira danke ich für die erheiternden und schönen Momente während dieser Zeit.

Dem Institut für Lebensmittelverfahrenstechnik möchte ich für die Ermöglichung der Partikelgrößenanalytik danken.

Weiterhin möchte ich mich bei meinen Projektpartnern, Prof. Gerd Klöck (Hochschule Bremen), Prof. Thomas Happe (Ruhr-Universität Bochum) bedanken. Besonderer Dank gilt Euch, den „Modu-Mädels“ Siv, Anja und Franziska für die tolle Zusammenarbeit während dieses außergewöhnlichen Projektes. Ich werde unsere gemeinsame Zeit und unsere Flüge mit Schwerelos-Anteil nie vergessen. Weiterer Dank gilt dem Projektpartner OHB System AG, besonders Prof. Klaus Slenzka, Sandra Podhajsky und Benjamin Harting.

Dem Institut für Membrantechnologie, ITM CNR um Prof. Alberto Figoli und Dr. Francesco Galiano danke ich für die freundliche Bereitstellung ihrer Membranen.

Ganz herzlich möchte ich bei meinen Studenten bedanken, ohne deren tatkräftige Mitarbeit die Vielzahl an Versuchen nicht möglich gewesen wäre. Ich danke deshalb Nischa Maier-Knapp, Julieta Colosimo, Noemí Guitierrez-Carmona, Andrea Lamos, Javiera Riquelme-Warnke, Tobias Kabbeck, Felix Kasper, Chloé Smith, Marius Meier, Hannes Frey, Virág Sari, Johannes Kühn, Manuel Merkel,

Benedict Wieters und Gina Kaysan, die durch ihre Praktika, Studien-, Bachelor-, Diplom- und Masterarbeiten einen wesentlichen Beitrag zum Erfolg dieser Arbeit beigetragen haben.

Dem Deutschen Zentrum für Luft- und Raumfahrt (DLR) danke ich für die finanzielle Förderung des Projektes.

Zu guter Letzt, aber im Herzen an erster Stelle, möchte ich meiner gesamten Familie, besonders meinen Eltern und Lieselotte für Ihre unermüdliche mentale und tatkräftige Unterstützung und stete Motivation danken. Durch Euch wurde dies Alles erst möglich.

Karlsruhe im Februar 2018

Ines Wagner

Summary

Life support systems are needed to enable long-term manned spaceflights or establish extraterrestrial installations on other planets. These systems are composed of several modules housing representatives of all trophic levels (microorganisms, higher plants and vertebrates), similar to Earth ecosystems. The photosynthetic activity of eukaryotic microalgae or prokaryotic cyanobacteria always was the central process these systems were based on.

Several approaches where life support systems, also including human beings, were tested failed, as loops of mass fluxes could not be closed or an accumulation of toxic substances was detected in atmosphere, water or soil, leading to a collapse of the system. This was resulting from a lack of knowledge on the interdependencies within these highly complex systems. New approaches are based on a bottom-up philosophy were each single module is studied accurately and the in- and outputs in terms of mass and energy fluxes are defined qualitatively and quantitatively. Once each module is characterized, these individual parts can be connected gradually where a complete life support system is achieved as a final result. A new approach is introduced with the ModuLES (Modular Life Support and Energy System) concept where in a first step a phototrophic module based on the green microalga *Chlamydomonas reinhardtii* is developed and studied.

Microalgae are suitable candidates for phototrophic modules within those life support systems. Additionally to their high growth rates compared to higher plants (Chisti 2007), they show highest light energy to biomass conversion efficiency. Besides their capacity for air regeneration they can also be used to enhance the nutritional value of food and feed (Spolaore 2006, Becker 2004). From a technical perspective, microalgae can be easily grown as suspension cultures or as immobilized cells also during long-term continuous cultivations which is a prerequisite for their space application.

Challenges on the reactor and process level result from the unique nature of the space environment. The absence of gravity, resulting in the absence of buoyancy and convective forces, low pressures, cosmic radiation and extreme temperatures are factors that limit design possibilities. Gas supply to algae cultures has to be established by a diffusion-based bubble-free aeration technique. Energy limitation demands a system running with maximum energy efficiency. For the microalgae reactor itself this means that its yield has to be optimized on volume, time and weight. Light is provided artificially with the help of LEDs. A major question is in what quantity and what quality light has to be provided to microalgae cultures to achieve highest energy conversion efficiencies. Another important aspect is the aeration technique used. In this work bubble-free aeration with membranes is studied. Furthermore, pressure and the effects of lowered pressure on algal cultures are in the focus of research. Additionally, the stability of long-term microalgae cultivations and the effects of perturbations on the system were studied within this work.

For evaluation of energy-efficient LED illumination mono- and dichromatic illumination with red, blue and green LED light and color combinations was compared to full-spectrum illumination in terms of photo conversion efficiency (PCE), specific pigment concentration and effects on morphology and cell size. Semi-fed-batch cultivations were conducted in plate reactors with planar LED illumination from low to saturating intensity. For photo conversion efficiencies an increase of 200% from 5% for warm-white to 15% for a dichromatic 90/10 red/blue color combination was measured for low light intensities of 25 µE m^{-2} s^{-1}. With this red/blue color combination the so far highest PCE value was measured. The results have shown that for achieving highest conversion efficiencies a high proportion of red light at 680 nm combined with a small amount of blue photons is beneficial. Furthermore, it was shown that there are effects based on sensory pigments influencing PCE values. For green photons, it was demonstrated that a cell growth was measurable for all tested light intensities and PCE values similar to white and blue illumination were determined.

When higher light intensities up to saturation values are applied, a saturation effect was verified for the red/blue 90/10 color combination and the resulting PCE values are similar for warm-white control and the dichromatic combination around light intensities from 150 to 300 µE m^{-2} s^{-1}. These findings result from the different light attenuation profiles in dependence on light absorption for different wavelengths.

With respect to morphology and cell size, results have shown that especially red and blue photons have a remarkable effect on cell size. Blue light illumination results in bigger cell diameters based on a delayed cell division (Oldenhof 2004 a, 2004 b, Münzner and Voigt 1992); red light leads to smaller cells and a more oval cell shape. Within this work at least for red light there seems to be a transient nature of this influence which was also verified during continuous cultivations. Green light seems to provoke aggregation of cells where a possible underlying mechanism is still unknown.

Lowest specific pigment contents for all tested light intensities were found for the red/blue 90/10 color combination, which supports the results found for PCE values. Ratios of Chl a/b, Chl a/Car and Chl b/Car are dependent on the light color and the PFD applied. Saturation with an increase in PFD is reached earlier for the dichromatic red/blue 90/10 combination at 100 µE m^{-2} s^{-1} compared to full spectrum control at 150 µE m^{-2} s^{-1}. Adaptation mechanisms in form of state transitions and a change of absorption cross section of cells can be assumed to be responsible for the detected results.

Furthermore, the results have shown that the détour-effect is applicable for microalgae cultures. Supported by results for light attenuation coefficients, it was shown that low absorbing wavelengths, e.g. green photons, can penetrate deeper into algal cultures than high absorbing wavelengths. Therefore, green photons can be used to promote growth at higher cell densities. A trichromatic illumination is promising to further enhance process productivity. First a red/blue combination with a high amount of red light and a low proportion of blue light is used for illumination and green photons are added while gradually replacing red/blue photons with increasing cell density.

Results reveal that by adjusting wavelengths of irradiated light to absorption spectra of the microalga *C. reinhardtii* also taking into account sensory pigments and their action spectra, an increase of photo conversion efficiencies compared to full-spectrum illumination is possible. Red light of 680 nm shows high efficiency, whereas the addition of a small proportion of blue photons can further enhance energy conversion due to effects of physiological functions controlled by sensory pigments. These findings were also found consistent during continuous cultivations.

The testing for suitable membrane materials for aeration of a space photomodule revealed that there are measurable differences of CO_2 and O_2 mass transfer coefficients between the different membrane materials tested for the developed gas liquid testing system. The measured k_L values are in the range of 10^{-6} m s^{-1}. Whereas for porous membranes very similar $k_{L,O2}$ values were found, the values for dense solution-based membranes differ to a high extent. Highest O_2 mass transfer coefficients were found for silicone membranes. In total, the k_L values found for O_2 are slightly larger than those for CO_2, whereas among $k_{L,CO2}$ values there is a higher variation. Highest $k_{L,CO2}$ values were found for porous membranes. It was shown that the abiotic factors T, salt concentration and pH (in case of CO_2 mass transfer) are important influencing factors on $k_{L,O2}$ and $k_{L,CO2}$.

Higher O_2 towards CO_2 mass transfer is, additional to the overall k_L values, the most important membrane parameter for its suitability towards a bubble-free aeration of a photomodule. The highest O_2/CO_2 selectivity factor measured accounted for 2.2 for a dense membrane. In total, the dense membranes tested, especially silicone membranes, showed O_2/CO_2 selectivity factors above one, whereas porous membranes only showed values around one or below. For this reason porous membranes are not suitable for designing a long-term bubble-free membrane aeration of phototrophic processes. Dense solution-based membranes should be considered where selectivity factors are further increased. Water losses per membrane area and time were measured which showed a higher variation for dense membranes, depending on thickness and kind of material.

A novel membrane reactor system using flat sheet membranes was developed and tested in batch and continuous mode during this work. A configuration with two different membranes and two different gas phases was found best for a long-term bubble-free aeration, although ultimately no complete inhibition of bubble formation could be achieved. A bubble formation was identified as the main challenge for membrane-aeration. This is a consequence of the oversaturation of the liquid phase with dissolved gases and the lower solubility of oxygen compared to carbon dioxide. A reduction of bubble formation of 40% was achieved by using two different membranes and two gas phases with a high driving force for O_2 removal.

During batch cultivations, peak volumetric OPR and CUR values of 0.4 mmol L^{-1} h^{-1} for an irradiating PFD of 200 µE m^{-2} s^{-1} could be obtained, which is slightly lower than for the homogeneously mixed, bubble-aerated stirred tank reactor for the same irradiating light intensity. This could be enhanced by

optimizing mixing, once a final membrane setup and design is fixed in dependence on the specific application case and its requirements.

Experiments with lower pressures, down to 700 mbar, have demonstrated that within the range of pressures tested, no fatal threshold was found. However, an effect on growth of the alga was found in so far as specific growth rates of *C. reinhardtii* CC-1690 cells decreased whereas volumetric and specific CUR increased. As OPR seems not to be affected within the tested pressure range, results indicate that there is no influence of lowered pressure on the light reaction of photosynthesis. A possible signaling effect of lowered pressure or a deviation from atmospheric pressure resulting in distinct physiological effects is still unclear. The results revealed that for the *C. reinhardtii* wildtype strains tested, lowered pressure or sudden pressure changes in the range of 300 mbar are not causing aggregate formation of cells as presumed before.

The long-term stability of gas exchange rates was demonstrated during continuous cultivations in two different reactor systems. The effects of perturbations in form of light intensity step changes exerted on cultures in both systems were analyzed for gas exchange rates, time constants and changes in specific pigment contents. For the homogenously mixed bubble-aerated reactor with cylindrical illumination stable steady-state CUR and OPR values were installed within a cell concentration range of 0.5 to 3.5 g L^{-1}. After light intensity step changes (in the range of 20 to 2400 µE m^{-2} s^{-1}) the original volumetric gas exchange rates were reinstalled with the same time constants as the new equilibrium was established. Kinetic curves determined from these step changes can be used for a comparison of reactor systems. Time constants found, as T,63%, are in the range of 13 to 39 minutes.

For the membrane-aerated reactor with planar, one-sided illumination the same stability of gas exchange rates was found within the tested cell concentration range of 0.1 to 2 g L^{-1}. The determined PI-curves can be used to adjust the cell concentration needed to obtain a desired gas exchange rate of the photomodule within a life support system. Time constants showed a higher variation than those measured in the comparative system and were in the range of 27 to 319 minutes. Similar to the results found for continuous cultivations inside the bubble-aerated ideally mixed reactor, the least variation in time constants is measured for the highest cell densities inside this plate type reactor geometry for one-sided illumination. Time constants determined for the membrane reactor are on the average four times higher than those determined with the ideally mixed system.

Specific pigment contents of the cells showed adaptation within 24 hours after the perturbation was performed for cells in both systems. The pigment content was adjusted to the average light intensity inside the reactor. In total this reveals that cells are adapting quickly (in case of gas exchange rates within minutes, for pigment contents within 24 hours) to stepwise light intensity changes even if the perturbations were only exerted for short times (1.5 hours in case of the ideally mixed bubble-aerated reactor). The results shown within this work demonstrate that, if perturbations in form of light intensity changes are exerted on the photosynthetic cells, the culture is able to restore its initial gas

exchange rate under the conditions of an axenic culture. This is an important finding relevant for the long-term stability of a photomodule within a life support system.

Within this work a concept for the ModuLES-PBR, as a microalgae based module within a life support system, was developed and tested. During parabolic flight tests of the ModuLES-PBR it was shown that both hardware and algae were robust towards the changing gravity conditions. The results of parabolic flights indicate that the algae showed a high photosynthesis rate comparable to ground conditions. The ModuLES-PBR system has proven its suitability for longer tests under microgravity conditions during satellite missions.

It can be concluded that the green microalga *C. reinhardtii*, based on the results presented, is a suitable photosynthetic microorganism for a photomodule within a life support system working under microgravity conditions. The reactor itself with its challenges of energy-efficient illumination, bubble-free membrane aeration, long-term stability of gas in- and output as well as robustness during pressure changes seems promising for future research under space conditions.

Zusammenfassung

Um längere bemannte Weltraummissionen durchzuführen, oder Habitate auf anderen Planeten aufzubauen, werden Lebenserhaltungssysteme benötigt. Diese Systeme sind aus mehreren Modulen aufgebaut, bestehend aus Mikroorganismen, höheren Pflanzen und Wirbeltieren. Sie beinhalten Vertreter aller trophischen Stufen, ähnlich wie Ökosysteme auf der Erde. Seit jeher ist die photosynthetische Aktivität von eukaryotischen Mikroalgen und prokaryotischen Cyanobakterien der zentrale Prozess, auf dem die Entwicklung dieser Systeme aufbaut.

Mehrere Ansätze zum Test der geschaffenen Systeme, bei denen auch Menschen integriert waren, sind fehlgeschlagen, da Stoffkreisläufe nicht geschlossen werden konnten oder sich toxische Substanzen in der Luft, im Wasser oder im Boden angehäuft hatten. Dies führte zum Zusammenbruch der Systeme. Gründe hierfür waren ein Mangel an Wissen um die Wechselbeziehungen innerhalb dieser hoch komplexen Systeme. Neue Ansätze basieren auf einer *Bottom-up*-Methode, bei der zunächst jedes Modul einzeln sehr genau erforscht wird und Stoff- und Energieflüsse qualitativ und quantitativ genau bestimmt werden. Nach der genauen Charakterisierung der Einzelmodule können diese schrittweise gekoppelt werden um schließlich ein Gesamtsystem zu erhalten. Durch das ModuLES- (Modulares Lebenserhaltungs- und Energiesystem) Konzept wird ein neuer Ansatz vorgestellt, bei dem in einem ersten Schritt ein phototrophes Modul basierend auf der Grünalge *Chlamydomonas reinhardtii* entwickelt und beforscht wird.

Mikroalgen sind geeignete Kandidaten für phototrophe Module innerhalb dieser Lebenserhaltungssysteme. Zusätzlich zu ihren hohen Wachstumsraten, verglichen mit höheren Landpflanzen (Chisti 2007), zeigen sie höchste Effizienz was die Umwandlung von Lichtenergie in Biomasse betrifft. Neben ihrer Eignung zur Regeneration der Atemluft können sie auch zur Erhöhung des Nährwertes von Nahrung und Futtermitteln verwendet werden (Spolaore 2006, Becker 2004). Aus der technischen Perspektive lassen sich Mikroalgen einfach als Suspensionskulturen oder auch als immobilisierte Zellen und zudem auch in längeren kontinuierlichen Prozessen kultivieren, was Voraussetzungen für ihren Einsatz im Weltall sind.

Herausforderungen auf der technischen und der Prozess-Ebene resultieren aus den einzigartigen Bedingungen des Weltalls. Die Abwesenheit von Schwerkraft, was in der Abwesenheit von Auftrieb und konvektiven Kräften resultiert, geringe Drücke, kosmische Strahlung und extreme Temperaturen begrenzen die Möglichkeiten innerhalb des Designs. Die Gasversorgung der Algen muss auf eine diffusionsbasierte, blasenfreie Art erfolgen. Die begrenzte Energieverfügbarkeit verlangt ein System, das mit maximaler Energieeffizienz arbeitet. Der Mikroalgenreaktor selbst muss bezüglich seiner Ausbeute auf Volumen, Zeit und Masse optimiert werden. LEDs werden als künstliche Lichtquelle eingesetzt. Hauptfragestellung ist hierbei in welcher Quantität und welcher Qualität Mikroalgenkulturen beleuchtet werden müssen um maximale Energieeffizienz zu erzielen. Ein anderer

wichtiger Aspekt ist die verwendete Begasungstechnik. In dieser Arbeit wurde eine blasenfreie Begasung mit Membranen untersucht. Darüber hinaus sind Druck und ein reduzierter Druck und sein Einfluss auf Algenkulturen ein Forschungsschwerpunkt. Zusätzlich wurden innerhalb dieser Arbeit die Langzeitstabilität kontinuierlicher Kultivierungen und die Effekte von Störungen auf das System erforscht.

Zur Untersuchung energieeffizienter LED Beleuchtung wurde mono- und dichromatische Beleuchtung basierend auf rotem, blauem und grünem LED Licht mit Kombination der Farben verwendet. Die Farbbeleuchtung wurde mit weißer Beleuchtung hinsichtlich Photokonversionseffizienzen, spezifischem Pigmentgehalt, und Auswirkungen auf Morphologie und Zellgröße untersucht. Semi-Fed-Batch-Kultivierungen wurden in planar beleuchteten Plattenreaktoren unter geringer bis sättigender Lichtintensität durchgeführt. Eine Steigerung der Photokonversionseffizienz (PCE) von 200%, von 5% für warm-weiße Beleuchtung auf 15% für eine rot/blau 90/10 Farbmischung, wurde bei geringer Lichtintensität von 25 µE m^{-2} s^{-1} erreicht. Mit dieser rot/blau Farbmischung wurde der bisher höchste PCE-Wert erreicht. Die Ergebnisse haben gezeigt, dass für das Erreichen höchster Konversionseffizienzen einer hoher Rotanteil (680 nm) kombiniert mit einem geringen Blauanteil vorteilhaft ist. Darüber hinaus wurde gezeigt, dass es einen Einfluss durch sensorische Pigmente auf den PCE-Wert gibt. Für grüne Photonen wurde ein messbares Zellwachstum bei allen getesteten Lichtintensitäten gezeigt, und die ermittelten PCE-Werte sind vergleichbar mit weißer und blauer Beleuchtung.

Für höhere Lichtintensitäten bis zur Sättigung wurde ein Sättigungseffekt für die rot/blau 90/10 Farbkombination bestätigt. Die hierbei resultierenden PCE-Werte der warm-weiß beleuchteten Kontrolle und der zweifarbigen Kombination sind ähnlich für Lichtintensitäten zwischen 150 und 300 µE m^{-2} s^{-1}. Diese Resultate basieren auf unterschiedlichen Profilen der Lichtabschwächung in Abhängigkeit der Lichtabsorption für verschiedene Wellenlängen.

Hinsichtlich der Morphologie und Zellgröße haben die Ergebnisse gezeigt, dass besonders rote und blaue Photonen einen bemerkenswerten Einfluss auf die Zellgröße haben. Beleuchtung mit blauem Licht resultiert in größeren Zelldurchmessern basierend auf einer verzögerten Zellteilung (Oldenhof 2004 a, 2004 b, Münzner und Voigt 1992), rotes Licht führt zu kleineren Zellen mit einer ovaleren Form. Innerhalb dieser Arbeit wurde zumindest für rotes Licht gezeigt, dass diese Effekte nur vorübergehend auftreten. Dies wurde zudem durch kontinuierliche Kultivierungen bestätigt. Grünes Licht scheint zu einer Aggregation der Zellen zu führen, wobei ein möglicher, zugrundeliegender Mechanismus noch unbekannt ist.

Niedrigste spezifische Pigmentkonzentrationen wurden bei allen getesteten Lichtintensitäten für die rot/blau 90/10 Kombination gemessen, was die Ergebnisse der PCE Werte bekräftigt. Die Verhältnisse von Chl a/b, Chl a/Car und Chl b/Car sind abhängig von Lichtfarbe und PFD. Eine Sättigung mit Steigerung der PFD wird eher bei der dichromatischen rot/blau 90/10 Kombination bei 100 µE m^{-2} s^{-1}

erreicht, verglichen mit der weiß-beleuchteten Kontrolle, die eine Sättigung bei 150 µE m^{-2} s^{-1} zeigt. Anpassungsmechanismen in Form von *State Transitions* und eine Änderung des Absorptionsquerschnitts der Zellen können als verantwortliche Mechanismen für die gemessenen Ergebnisse vermutet werden.

Zudem haben die Ergebnisse gezeigt, dass der Détour-Effekt auf Mikroalgenkulturen bezogen werden kann. Unterstützt durch die Ergebnisse der Lichtabschwächungskoeffizienten, wurde gezeigt, dass gering absorbierende Wellenlängen, wie beispielsweise grüne Photonen, eine höhere Eindringtiefe in Algenkulturen aufweisen als hoch absorbierende Wellenlängen. Aus diesem Grund können grüne Photonen zur Verstärkung des Wachstums bei hohen Zelldichten genutzt werden. Eine trichromatische Beleuchtung könnte weiterhin die Prozessproduktivität erhöhen. Hierbei soll zunächst eine rot/blau Kombination mit hohem Rotanteil und geringem Blauanteil genutzt werden, die schrittweise bei Ansteigen der Zelldichte durch grüne Photonen ersetzt wird.

Die Ergebnisse belegen, dass durch eine Anpassung des eingestrahlten Lichtes an das Absorptionsspektrum von *C. reinhardtii*, auch unter Beachtung von sensorischen Pigmenten und deren Aktionsspektren, eine Erhöhung der Photokonversionseffizienzen im Vergleich zur Ganzspektrum Beleuchtung möglich ist. Rotes Licht von 680 nm zeigt eine hohe Effizienz, wobei die Addition von einem geringem Anteil Blaulicht noch eine weitere Steigerung der Energieausbeute zulässt. Dies beruht auf Effekten von physiologischen Funktionen unter Kontrolle von sensorischen Pigmenten. Diese Erkenntnisse wurden auch innerhalb kontinuierlicher Kultivierungen bestätigt.

Die Tests zur Auswahl geeigneter Membranmaterialien zur Begasung von Weltraum-Photomodulen ergaben, dass es messbare Unterschiede zwischen den verschiedenen Membranmaterialien bezüglich ihrer CO_2 und O_2 Stofftransportkoeffizienten innerhalb des entwickelten Gas-Flüssig-Testsystems gibt. Die gemessenen k_L-Werte liegen im Bereich von 10^{-6} m s^{-1}. Während für poröse Membranen sehr ähnliche $k_{L,O2}$ Werte gefunden wurden, variieren die Werte für dichte Löslichkeitsmembranen sehr stark. Höchste Sauerstoff-Transportkoeffizienten wurden für Silikonmembranen nachgewiesen. Allgemein lagen die Werte für Sauerstoff in geringer Weise über denen für CO_2, wobei sich für die $k_{L,CO2}$-Werte eine größere Variation zwischen den getesteten Membranen ergeben hat. Höchste CO_2 Stofftransportkoeffizienten wurden dagegen für poröse Membranen gefunden. Es wurde gezeigt, dass die abiotischen Faktoren Temperatur, Salzkonzentration und pH (im Falle des CO_2 Transports) wichtige Einflussfaktoren auf den $k_{L,O2}$ und $k_{L,CO2}$ sind.

Eine höhere O_2 Transportrate gegenüber dem CO_2 Transport ist, zusätzlich zu den k_L Werten, der wichtigste Membranparameter für die Eignung zur blasenfreien Begasung eines Photomoduls. Der höchste innerhalb dieser Arbeit gemessene O_2/CO_2 Selektivitätsfaktor liegt bei 2,2 für eine dichte Membran. Generell wurden bei den getesteten dichten Membranen, besonders den Silikonmembranen, O_2/CO_2 Selektivitäten über 1 gemessen, wobei die gemessenen Faktoren für poröse Membranen bei 1 oder geringer liegen. Aus diesem Grund eignen sich poröse Membranen nicht zum Design einer

langfristig blasenfreien Membranbegasung eines phototrophen Prozesses. Dichte Löslichkeitsmembranen sollten hierfür in Betracht gezogen werden, bei denen die Selektivitätsfaktoren weiter erhöht werden. Wasserverluste pro Membranfläche und Zeit wurden bestimmt; sie zeigten eine höhere Variation bei dichten Membranen, in Abhängigkeit von Dicke der Membran und dem Material.

Ein neuartiges Membranreaktorsystem unter Verwendung von Flachmembranen wurde entwickelt und in Batch und kontinuierlich betriebenen Versuchen während dieser Arbeit getestet. Eine Konfiguration mit zwei unterschiedlichen Membranen und zwei verschiedenen Gasphasen wurde als beste Kombination für eine Langzeit blasenfreie Begasung gefunden, wobei letzten Endes keine komplette Vermeidung von Blasenbildung erreicht werden konnte. Eine Entstehung von Blasen, als Konsequenz aus Übersättigung der Flüssigphase mit gelösten Gasen und der im Vergleich zu CO_2 geringeren Löslichkeit von O_2, wurde als größte Herausforderung der Begasung mittels Membranen identifiziert. Eine Reduktion des gebildeten Blasenvolumens von 40% wurde durch die Verwendung von zwei verschiedenen Membranen und zwei Gasphasen bei einer hohen Triebkraft für den O_2-Austrag erreicht.

Im Verlauf der Batchkultivierungen, betrugen die maximale volumetrische OPR und CUR 0,4 mmol L^{-1} h^{-1} bei einer PFD von 200 µE m^{-2} s^{-1}, was geringfügig unter den erreichbaren volumetrischen Raten für den homogen durchmischten und blasenbegasten Rührwerksreaktor bei gleicher eingestrahlter Lichtintensität liegt. Dies könnte durch eine optimierte Mischleistung verbessert werden, nachdem eine finale Membrankonfiguration und ein Design je nach Anwendungsfall und sich daraus ergebenden Anforderungen festgelegt wurde.

Experimente mit reduziertem Druck, bis zu 700 mbar Absolutdruck, haben gezeigt, dass innerhalb des getesteten Druckbereiches kein letaler Grenzwert erreicht wurde. Jedoch konnte ein Einfluss auf das Wachstum der Alge in Form von einer reduzierten spezifischen Wachstumsrate von *C. reinhardtii* CC-1690 Zellen bei einer Erhöhung der volumetrischen und spezifischen CUR gefunden werden. Da die OPR innerhalb des Druckbereiches von 1000 mbar bis 700 mbar nicht verändert ist, zeigen diese Ergebnisse, dass kein Einfluss des reduzierten Druckes auf die Lichtreaktion der Photosynthese besteht. Ein möglicher Signaleffekt von geringerem Druck oder einer Abweichung vom Atmosphärendruck und davon ausgelösten eindeutigen physiologischen Effekten ist noch unbekannt. Die Ergebnisse ergaben, dass der geringere Druck sowie die Drucksprünge im Bereich bis 300 mbar keine Bildung von Aggregaten der *C. reinhardtii* Wildtyp Stämme auslösten, was zuvor vermutet wurde.

Die Langzeitstabilität der Gasaustauschraten wurde innerhalb kontinuierlicher Kultivierungen in zwei verschiedenen Reaktorsystemen gezeigt. Die Auswirkungen von Störungen in Form von sprunghaften Änderungen der Lichtintensität auf die Kulturen wurden in beiden Systemen anhand der Gasaustauschraten, Zeitkonstanten und Änderungen der spezifischen Pigmentkonzentrationen

analysiert. Im homogen durchmischten blasenbegasten Reaktor mit zylindrischer Beleuchtung wurden stabile CUR und OPR Werte im Fließgleichgewicht für Zellkonzentrationen im Bereich von 0,5 bis 3,5 g L^{-1} eingestellt. Nachdem die Lichtsprünge (im Bereich von 20 bis 2400 µE m^{-2} s^{-1}) ausgeführt waren, wurden die ursprünglichen volumetrischen Gasaustauschraten wieder hergestellt; dies geschah mit den gleichen Zeitkonstanten wie sich auch zuvor das neue Gleichgewicht während des Sprunges eingestellt hatte. Kinetiken, die basierend auf den Lichtsprüngen erstellt wurden, können zum Vergleich der Reaktorsysteme genutzt werden.

Die ermittelten Zeitkonstanten im Membranreaktor, ermittelt als T,63 %, liegen im Bereich von 13 bis 39 Minuten. Im membranbegasten Reaktor mit planarer, einseitiger Beleuchtung wurde die gleiche Stabilität der Gasaustauschraten nachgewiesen; in diesem Fall für getestete Zellkonzentrationen im Fließgleichgewicht von 0,1 bis 2 g L^{-1}. Die ermittelten PI-Kurven können dazu genutzt werden die benötigte Zellkonzentration einzustellen, die für eine gewünschte Gasaustauschrate eines Photomoduls innerhalb eines Lebenserhaltungssystems nötig ist. Die Zeitkonstanten, die im membranbegasten System ermittelt wurden, zeigten eine höhere Variation und liegen im Bereich von 27 bis 319 Minuten. Auch in diesem Reaktorsystem wurden die geringsten Variationen der Zeitkonstanten für die höchsten Zelldichten gemessen. Zeitkonstanten, die im Membranreaktor bestimmt wurden, sind im Mittel viermal höher als die, die im ideal durchmischten System bestimmt wurden.

Spezifische Pigmentkonzentrationen der Zellen zeigten in beiden Systemen eine Anpassung innerhalb von 24 Stunden nach Ausübung der Störung. Die Pigmentgehalte passen sich hierbei an die mittlere Lichtintensität im Reaktor an. Allgemein lässt sich erkennen, dass die Zellen sich schnell (im Fall der Gasaustauschraten innerhalb von Minuten, im Falle der Pigmentkonzentrationen innerhalb von 24 Stunden) an die sprunghafte Änderung der Lichtintensität angepasst haben. Dies geschah auch für den Fall, dass diese Störungen nur für kurze Zeit (1,5 Stunden im Falle des blasenbegasten ideal durchmischten Reaktors) auftraten. Die Ergebnisse innerhalb dieser Arbeit zeigen, dass, wenn Störungen in Form von Sprüngen der Lichtintensität auf die photosynthetischen Zellen einwirken, die Kultur in der Lage ist die ursprünglichen Gasaustauschraten wiederherzustellen unter den Bedingungen einer axenischen Kultur. Dies ist eine wichtige Erkenntnis für die Langzeitstabilität eines Photomoduls innerhalb eines Lebenserhaltungssystems.

Innerhalb dieser Arbeit wurde ein Konzept für den ModuLES-PBR, als mikroalgenbasiertes Modul eines Lebenserhaltungssystems, entwickelt und getestet. Innerhalb von zwei Parabelflugkampagnen zum Test des Reaktors wurde bewiesen, dass Hardware und Algen sehr robust gegenüber den wechselnden Schwerkraftbedingungen sind. Die Ergebnisse der Parabelflüge zeigen eine hohe Photosyntheserate der Algen vergleichbar mit Bodenbedingungen. Das ModuLES-PBR System hat seine Tauglichkeit für längerfristige Tests unter Schwerelosigkeitsbedingungen innerhalb von Satellitenmissionen gezeigt.

Es kann geschlossen werden, dass die Grünalge *C. reinhardtii*, basierend auf den präsentierten Ergebnissen, ein geeigneter photosynthetischer Mikroorganismus für ein Photomodul innerhalb eines Lebenserhaltungssystems unter den Bedingungen der Schwerelosigkeit ist. Der Reaktor selbst, mit den Herausforderungen einer energieeffizienten Beleuchtung, einer blasenfreien Membranbegasung, einer Langzeitstabilität der Gas-In- und Outputs und einer Robustheit gegenüber Druckschwankungen scheint vielversprechend für die zukünftige Forschung unter Schwerelosigkeitsbedingungen zu sein.

Table of Contents

1 Introduction

Spreading life beyond Earth to other planets and into outer space was and still is a major dream for mankind. To reach those distant places, closed systems sustaining life during spaceflight and on planetary stations are of crucial importance.

Those systems that need to be developed are based on the central process of photosynthesis which enabled the evolution of life on Earth. Light energy is converted into biochemical energy and the oxygen formed during this process once accumulated in the atmosphere. This was followed by the formation of ecosystems on Earth. Photosynthesis is also needed to maintain life and human activities in hostile environments like space. In general, there are also theoretical approaches for using life support systems not only for space but also for remote regions, for example desert areas, which share the same conditions threatening life.

For several decades research is engaged in studying closed controlled life support systems for manned space missions and their dynamic behaviour and limitations. Different concepts for biological life support systems were developed and to some extent, with a limited number of trophic levels, tested during satellite missions. On ground also tests were conducted where human beings were part of these artificial ecosystems. For all times, microalgae were part of those life support systems as representatives of the first trophic level.

Major functions that those systems need to fulfil are a purification of water, a regeneration of atmosphere, food production, waste recycling as well as supply of energy. However, the practical realization of those systems, whether tested on ground or under space conditions, revealed that loops of material flows could not be closed completely. This led to an imbalance in atmosphere composition or also an accumulation of toxic substances. These problems indicate that the interdependencies of the system components were not yet fully understood as a result from the high complexity of those life support approaches.

This work focuses on the potentials of eukaryotic microalgae for life support systems. In contrast to former approaches, a novel concept as bottom up approach is established, where research is focused on a single photosynthetic module based on the green microalga *C. reinhardtii*. The in- and outputs of masses of this single system shall be clearly defined in order to build up a whole life support system by coupling other modules which in turn were studied and described in detail respectively. Furthermore, special requirements and frame conditions relating to the design of photobioreactors for space conditions are discussed within this work. A novel concept of a membrane-aerated, energy-efficient photobioreactor for application in microgravity is introduced.

1.1 Objectives and Outline

In Chapter 2 the theoretical foundation for this work is outlined, whereas Chapter 3 provides detailed information on materials and methods. Further information on techniques and media used can be found as supplementary material in Chapter 11 (Appendix). Research focuses on the development of a membrane-aerated, energy-efficient photobioreactor module based on the microalgae *C. reinhardtii* for application under space conditions. Related research topics are the energy-efficient illumination with LEDs, a diffusion-based bubble-free aeration of microalgae cultures with membranes, the effects of lowered pressure on photosynthetic efficiency as well as the long-term stability of continuous cultures and the effects of perturbations.

The research on energy-efficient artificial illumination focuses on finding optimal wavelengths to achieve highest light energy to biomass conversion for different illumination intensities. Moreover, effects of light color on physiology and morphology of the cells are investigated. Light is introduced by LEDs. Biomass yields from light energy for mono- and dichromatic illumination are determined with respect to the different energy content of red, blue, green and warm-white light. Also long-term effects of mono-and dichromatic illumination on *C. reinhardtii* cultures are studied during continuous cultivation processes. Further on, light attenuation in the reactor volume in dependence on the applied wavelength shall be studied. Results and discussion are provided in Chapter 4.

Bubble-free membrane aeration is a prerequisite for the exchange of gases in microalgae photomodules under microgravity conditions with the aspect of maximal energy efficiency. A first goal is to find suitable membrane materials for CO_2 supply and O_2 removal by quantifying mass transfer coefficients for those gases and water losses of the materials. Based on these first quantitative data it can be evaluated if those membranes meet the requirements for aeration of the microalgal module. Further on, first cultivations of the alga *C. reinhardtii* in batch mode with different membrane configurations and a defined gas composition shall be established inside a novel lab scale membrane reactor. Here, also the aspect of mono- and dichromatic illumination shall be combined by using white light as control and red/blue combinations. Results and discussion are outlined in Chapter 5.

As pressure is an important abiotic factor for microalgal processes in space as well as on ground, the effects of lowered pressure and sudden pressure changes are studied within this work. Effects on the photosynthetic activity in form of specific growth rates, gas exchange rates and pigment content shall be determined during batch cultivation in a homogeneously mixed, bubble-aerated photobioreactor. A fatal threshold value of pressure changes shall be detected by sudden pressure changes. Also effects on morphological appearance and aggregation shall be studied during these experiments. Analysis of results of these pressure experiments is outlined in Chapter 6.

Chapter 7 shows results and discussion on experiments focused on the long-term stability of continuous microalgae cultures and the effects of perturbations. Two different reactor systems with

different aeration techniques are compared for their gas exchange rates. Perturbations in form of light intensity step changes are exerted within steady-state phases in both systems. Time constants of system responses with respect to changed CO_2 uptake and O_2 production rates are determined and used to compare the two different systems. By this means, the lab scale membrane-aerated photobioreactor can be compared to the bubble-aerated well-mixed stirred tank photobioreactor with regard to stability and system response to light intensity changes. This is relevant for its application in space modules where energy shortages may impair constant lighting conditions. Also the effects on specific pigment concentrations in response to light intensity step changes are studied.

Chapter 8 deals with the developed concept of the ModuLES-PBR which is tested during parabolic flights and ground campaigns. First data on hardware stability, gas transfer and physiology of the alga under the changing gravity conditions during the parabolas is collected during batch and continuous processes and compared with experiments on ground as control. Furthermore, data of gas exchange rates can be compared to other reactor systems. The ModuLES-PBR also combines the aspects of membrane aeration and energy-efficient LED illumination with colors.

2 Fundamentals and state of the art

2.1 Life support systems and challenges of space environment for living beings

2.1.1 Characteristics of life support systems

In order to conduct long-term space missions or to spread life from Earth to other planets, closed systems, known as life support systems, are needed. The following chapters aim to introduce concepts and give definitions of life support systems. Furthermore, the concept of the ModuLES project focusing on the ModuLES-PBR is introduced.

2.1.1.1 Life support system: definition, classification and development approaches

From a thermodynamic point, human beings can be considered as open systems: there is an exchange of energy and matter with the environment. Environment, with its own structure, is regarded as closed terrestrial life support system, designated as “biosphere”. A biosphere is defined as basically closed system regarding matter, but an open system regarding energy. For longer space missions or the installation of extraterrestrial habitats the aim is to develop technical systems able to ensure the biological autonomy of a human being which is separated from its original biosphere. That means the provision of a controlled and physiological acceptable environment for human beings living either inside a spacecraft, a space station or a planetary settlement. A system ensuring the autonomy of a crew is called a life support system (LSS) (Eckart 1996, Tamponnet 1991). In a traditional view, a life support system is composed of three main components, being air, water and food. A wider classification also includes habitability aspects which make a life or an environment pleasant or desirable, thus aspects also relating to human psyche. Life support systems can principally be divided into five main areas:

- Atmosphere management
    - Control of: composition, temperature, humidity, pressure, contamination
    - Regeneration
    - Ventilation
- Water management
    - Provision of potable water
    - Recovery and processing of waste water
- Production of Food and Storage
    - Provision of food
    - Production of food
- Waste management (Human waste/trash)

    - Collection
    - Storage
    - Processing
- Crew safety
    - Fire detection, suppression
    - Radioactive radiation shielding

Until the present day a very successful way to provide these requirements for short duration missions is to carry air, food and water onboard and to store the waste, which is returned to Earth again. However, for longer space missions with an increasing number of crew members and the installation of planetary bases, regenerative, closed environmental life support systems (CELSS) (Clément 2006) are required as supply loads get heavier and a resupply is not affordable or possible (Eckart 1996).

The functions of a life support system can be grouped into the categories of non-regenerative (not subject to recycling like system monitoring) and regenerative (relating to fields which are subject to recycling: water, oxygen, food). Systems where there is no recovery of resources are designated as open loop systems, whereas systems with recovery of resources are termed closed loop systems (Eckart 1996).

For open loop systems food, water and oxygen originates from storages that must comply in terms of quantity to the needs during the mission. Advantages of those open loop systems, extensively used for space missions, are a high degree of reliability and simplicity with the huge disadvantage that they cannot be used for longer missions as resource requirements increase linearly with duration and number of crew members. Concerning oxygen, food and water it takes more than 8000 kg of load to support one person for one year without recycling according to Schwartzkopf (1992), which underlines the necessity of regenerative, closed loop systems.

For closed loop systems a starting supply of resources is brought from Earth and wastes are recycled to recover useful resources. With an increasing degree of closure, quantities of resources which have to be resupplied decrease. Disadvantages of those systems are the higher power and thermal requirement. Myers (1963) developed a method to determine breakeven points relating to the dependency of mission length and economically feasible recycling. For shorter missions water and atmosphere recycling would be profitable whereas full recycling is economically feasible for longer missions.

Life support systems can be classified into physico-chemical (sub-) systems and bioregenerative systems (Eckart 1996). Currently used spacecraft life sustaining systems are based on open-loop physico-chemical systems. Analysis proved that hybrid systems incorporating both approaches might be most promising to achieve the above-mentioned goals (Schwartzkopf 1992). In the case of physico-

chemical life support systems the human being is the only biological component. The physico-chemical subsystems are able to fulfill the following basic life support functions: atmosphere management, water management and waste management (Eckart 1996). Physico-chemical technologies comprise for example mechanical devices like fans, pumps, filters, as well as whole physical or chemical reactors (for example incinerators, distillation columns). Advantages of these technologies are that they are fast acting, but a huge power demand and their single function characteristic is a major drawback (Schwartzkopf 1992). In the past it was shown that for regenerable physico-chemical subsystems in a LSS the loops for water and oxygen can be closed (Eckart 1996). However, future systems have to be able to close also the carbon loop. Especially planetary settlements on Moon or Mars require a maximum of regeneration as a resupply would be too expensive at such distances (Eckart 1996). In order to close also the carbon loop, advanced life support systems have to be developed where there is a regeneration of metabolic waste products and a production of food.

A regenerative process, where biological systems are used, is called a biological life support system (BLSS), (Figure 2-1 A).

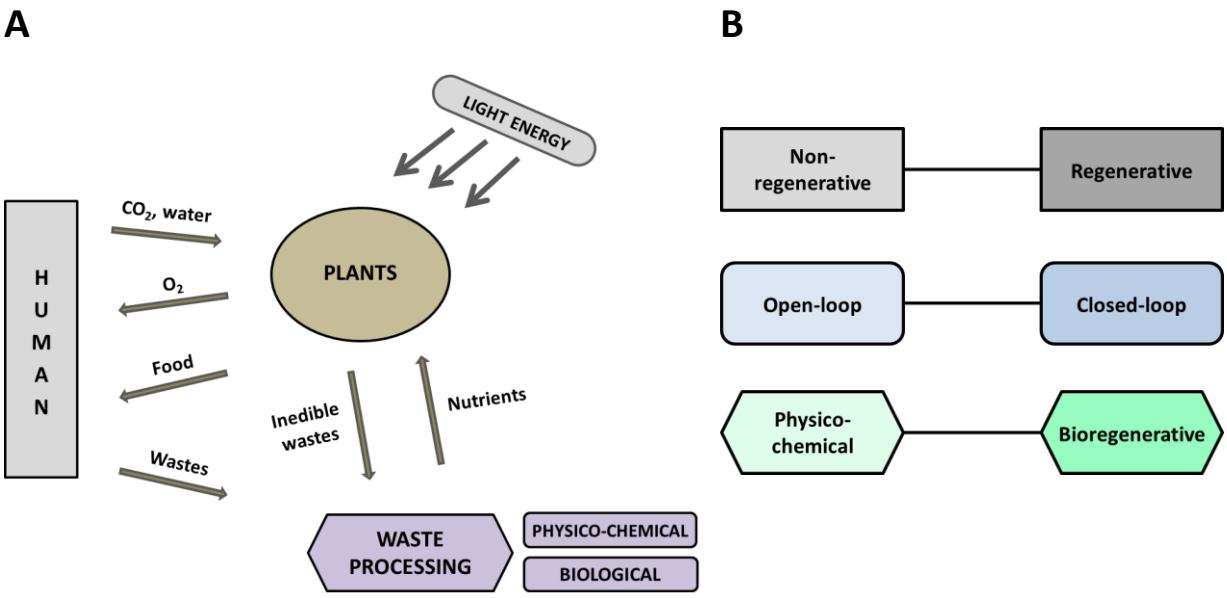

Figure 2-1. Life support systems. A) Principle of a biological life support system (BLSS). Modified after Leiseifer (1983). B) Classification of life support systems (Slenzka 2002).

One very important aspect is the degree of closure of a developed life support system. According to Rygalov (2014) the highest degree of closure so far was achieved during the BIOS-3 experiment with 93%, whereas a maximum theoretical degree of closure is expected to be around 95% (oral presentation).

Relating to the development and design of closed environmental life support systems one has to distinguish between two approaches: the holistic and the reductionist approach. The holistic approach (which was used for the development of Biosphere-2 in Arizona) (Turner 1989) is based on a natural evolutionary development of a system where organisms (including humans) are assembled in a closed environment and mutual adaptation occurs leading to a stable homeostatic ecological system being in equilibrium. The reductionist approach is based on the division into subsystems with the development of external control mechanisms which can come into action if system stability cannot be guaranteed by intrinsic mechanisms. Subsystems are then combined to form the entire system with both internal and external control mechanisms. Disadvantages and advantages of both approaches are discussed by Schwartzkopf (1992). One drawback of the holistic approach is that the outcome of the evolutionary process cannot be directed. Major advantages of the reductionist approach are the time and cost efficiency and the establishment of a system consisting of highly defined and controlled subsystems. Disadvantageous is the fact that this approach may not lead to a life support system with natural ecological control mechanisms.

2.1.1.2 History and examples of life support systems

The first practical approaches for the design of life support systems came up early in the 1960ies (Gitelson 1976) whereas the awareness of the problem emerged after the first success in the field of cosmonautics by the end of the 1950ies (Mezhevikin 1994). Until the present day several concepts for biological life support systems were designed and some small subsystems with one or two trophic levels of the food chain were even tested during satellite missions (Wang 2004 a, Wang 2008). These were either comprised of only producers like plants or also included consumers like fish or fish larvae. With ongoing research closed control systems even including men were created and tested during longer periods of several months on ground. One example which gained public attention was the experimental complex of "BIOS-3" (Gitelson 1976) in the 1970ies.

In the 1960ies, Nichoporovich and Semenenko were among the first ones having the idea of using microalgae for designing life support systems (Soeder 1986). In the following, eukaryotic microalgae and photosynthetic cyanobacteria always played a major role in the development of CELSSs mainly because of their photosynthetic capabilities as members of the first trophic level producing oxygen as essential basis of human and animal life (Gitelson 1976, Wang 2004 a, Wang 2004 b, Wang 2008). The second stage of "BIOS-3" in 1976 also included a species of green microalgae, namely *Chlorella* (Gitelson 1976). Differences between these approaches were the number of compartments, trophic levels and the degree of complexity. Highest complexity so far reported can be attributed to the Biosphere-2 experiment in the desert of Arizona in 1991 (Turner 1989). Some of the reported life support systems and concepts including microalgae (and cyanobacteria) are listed in Table 2-1.

Table 2-1. Reported life support systems or research approaches including microalgae and/or cyanobacteria.

	Species used	Experiments	Purpose/aim	References
BIOS-3	*Chlorella vulgaris*, wheat and various vegetable plants, three humans	Ground experiment: closed system, several months	Development of a closed control system with man included as part/operator of it	Gitelson 1976
CAES	*Chlorella pyrenoidosa* as producer, snail *Bulinus australianus* as consumer	Spacecraft experiment: SHENZOU-II, 7 days in 2001	Development of a closed aquatic ecosystem (CAES), study effect of microgravity on it	Wang 2004 b Wang 2008
Aquacells/ OmegaHab	*Euglena gracilis*, fish *Oreochromis mossambicus*	Satellite experiments: four biosatellite flights in 2013	Development of a closed loop gas cycle (CO_2, O_2)	Strauch 2008
MELISSA	Compartment I: Human gut bacteria Compartment II: *Rhodospirillum rubrum* Compartment III: *Nitrosomonas and Nitrobacter* Compartment IVa: *Arthrospira platensis* Compartment IVb: higher plants Compartment V: crew	Four bioreactors, one with cyanobacterium *Spirulina platensis*, one higher plant compartment	Development of a "Micro Ecological Life Support System Alternative" for life support in space	Gódia 2002 Farges 2008

The C.E.B.A.S. (Closed Equilibrated Biological Aquatic System)/AquaHab system (from 1986 to 2003) developed by German researchers from universities and industry was tested as mini-module during three shuttle flights from 1998 to 2003. The system consisted of a fish module (*Xiphophorus*) where major focus was put on effects of space environment on its morphology, physiology and development. Hornweed plants served as oxygen producer, fish and snails as consumers. Water was recycled by a biofilter (Clément 2006).

The Aquacells/OmegaHab (*Oreochromis mossambicus Euglena gracilis* Aquatic Habitat) project from German researches from 1998 to 2013 was focused on the establishment of a closed loop gas cycle regarding O_2 and CO_2 as closed ecological bioregenerative life support system. The system was comprised of a phototrophic compartment housing the microalga *Euglena gracilis*, a flagellate capable of gravitaxis, connected to a heterotrophic compartment with a fish (*Oreochromis mossambicus*) where its behavior under microgravity conditions and especially the effects on the morphology of the inner ear should be studied. Overall objectives were the investigation of ecophysiological,

gravitational-, developmental- and systems-biology aspects in space environment. The experiment was flown during four biosatellite flights (FOTON M-1, M-2, M-3 and BION M-1) in 2013. For the BION M-1 campaign more species were tested: microalgae, fish, snails as well as higher water plants.

In recent times also complex systems like MELISSA (Micro Ecological Life Support System Alternative) were developed (Gódia 2002). MELISSA started in 1988 and was supported by ESA (European Space Agency). The system is composed of a loop of interconnected continuous bioreactors which shall be used as life support system in space. Four bioreactors housing different microbial species and one higher plant compartment are interconnected. The operation at pilot scale was reported in literature (Gódia 2002). To the present day the complete system has not yet been tested during parabolic or satellite flights. Primarily bacterial compartments have been tested during parabolic flights.

With time, also the complexity of the hardware of life support system approaches increased as the duration of space travel increased and also the requirements of the experiments became more sophisticated (Slenzka 2002).

Outcomes and conclusions from the approaches so far tested until the present day

After accessing the payloads of the BION M1 flight, the microalgae *E. gracilis* was the only surviving organism of the OmegaHab module, whereas fish, snails and also the higher plants were found dead. Speculations for the reasons for failure include an unforeseen contamination and a failure of the lighting system. Concerning more complex systems there is also a gain of knowledge. Biosphere-2 was a closed ecological system which was tested from 1991 to 1994 whereas the degree of closure was stepwise increased. Overall the system had a high degree of closure with a leak rate < 10% per year and housed 3800 species of plants and animals as well as eight human beings for almost two years. A high degree of closure is important also for studying changes in the biogeochemical cycles and the atmospheric composition. Problematic during the closed running of this complex system was that the atmospheric O_2 concentration decreased from the initial 21% to about 14% after roughly 500 days of closure. CO_2 concentrations in the atmosphere increased from 350 ppm (0.035%) to a maximum of 4000 ppm (0.4%) with huge day/night oscillation of about 600 ppm (Alling 2005). In order to lower these high CO_2 concentrations in the atmosphere, a physico-chemical precipitator had to be used. A total of 81% of food was grown inside the Biosphere-2 systems for the eight human beings on an area of 2000 m² whereas the agricultural harvest amount was highly depending on ambient light levels. After artificial light was added to the ambient light the food cycle could be closed completely in the third year of closure (Marino 1999). Concerning the plant substrate, this system was the first closed system using soil as substrate for plants instead of the commonly used hydroponics (Alling 2005). As an overall conclusion it was monitored that the atmospheric composition was the most dynamic

component of the biosphere and that there was more interaction of the atmosphere, the soil life and the water body then expected before.

Concerning the MELISSA project no long-duration tests with an integrated human have yet been done due to multiple instabilities monitored in the microbial modules. However, a higher closure degree is planned (Rygalov 2014).

ModuLES-concept as bottom-up approach

A novel approach was introduced with the ModuLES- (Modular Life Support and Energy System) concept which was started in 2012 supported by the German Space Agency, DLR Space Management. Scientific partners from Ruhr-University Bochum, the University of Applied Sciences Bremen, Karlsruhe Institute of Technology and an industrial partner with expertise in aquatic life support systems (OHB System AG, Bremen) worked together in order to develop a first phototrophic module based on the green microalga *Chlamydomonas reinhardtii*.

In contrast to former approaches, a modular life support system shall be developed as a bottom-up-approach where in a first step module after module is designed and the in- and outputs of every interface are exactly defined and quantified (Figure 2-2 A). By combining a first phototrophic module and a heterotrophic module a subsystem will be created where a further integration of other modules finally leads to a closed, functional system. A combination of physico-chemical and bioregenerative modules shall sustain a long-term stable operation to be used for long-term space missions (also on the International Space Station, ISS), extraterrestrial habitats, but also for remote applications on Earth. Major criteria are to maximize efficiency, a long-term stability, the generation of energy and all the aspects a life support system has to fulfill (compare to 2.1.1.1).

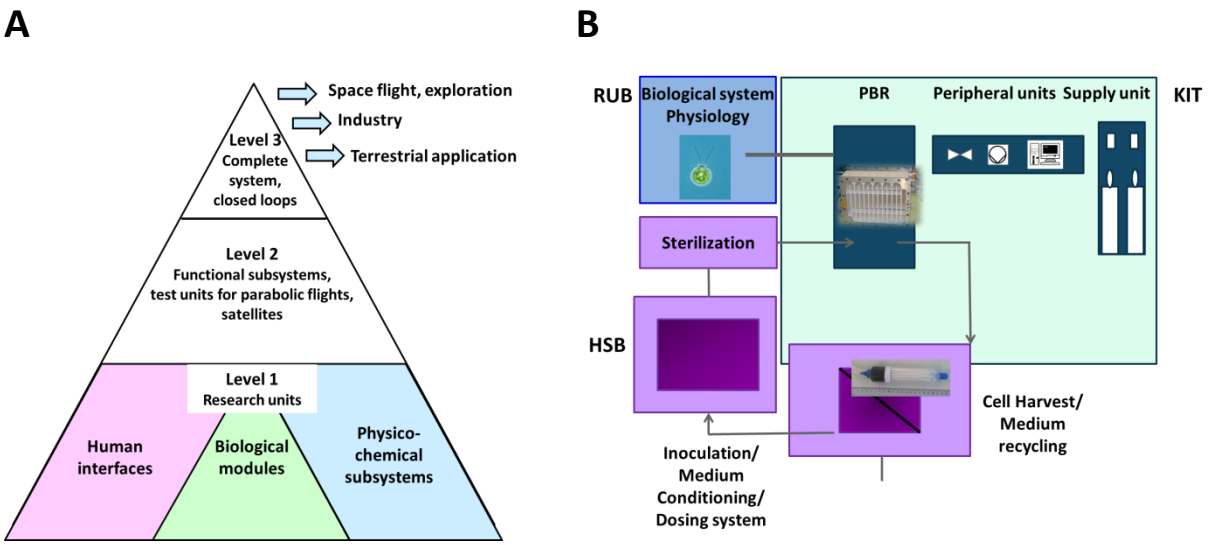

Figure 2-2. ModuLES concept. A) ModuLES as bottom-up approach. B) Project partners ModuLES-PBR and distribution of tasks.

The first module to be developed within this concept is the ModuLES-Photobioreactor (PBR). Primarily, this reactor system shall consume CO_2 and produce O_2 and biomass with maximum efficiency as a key element of a modular life support system. A parabolic flight model of this system was studied during two flight campaigns in September 2013 and February 2014 where the hardware was tested during changing gravity conditions and first physiological data were collected to elucidate possible effects on the algae.

Challenges of future life support and energy systems are factors like reliability and efficacy by redundant and complementary systems (for example bioregenerative, hybrid systems) with maximal efficient modules with defined in- and outputs. These systems shall also lead to spin-off projects with respect to terrestrial applications (energy-storage, conservation of resources, see also 2.1.1.3). Goals of the ModuLES concept are to make use of synergistic effects by combining hybrid systems and integrate a systems biology research approach.

Tasks were divided among the three research groups which are shown in Figure 2-2 B. Research of KIT was focused on the development of the reactor and its peripheral units like illumination and mixing. Researchers from HSB developed a cell harvesting system and should provide devices for medium recycling and substrate dosing. Partners from RUB focused on the physiology of the alga and the composition of the medium as well as on PAM fluorometry measurements to study the short-term effects of changed gravity on the photosynthetic efficiency of the alga.

There are several specifications concerning the ModuLES-PBR which are a result from microgravity conditions, general requirements for life support systems and experimental requirements:

- Modular design
- Bubble-free membrane aeration
    - No buoyancy
    - Energy efficiency
    - Diffusion-based aeration, measurement instrumentation
- Efficient illumination technology
    - Maximal efficient light energy to biomass conversion
    - Maximal PCE – photo conversion efficiency
- Long-term stability during continuous processes
    - Closed-loop system
    - Maximal CO_2 uptake and O_2 production rates
- Technical functionality
    - Measuring technology, control technology
    - Physiological control, stress markers

Details of the concept for the ModuLES-PBR systems are depicted in the results part of this work (Chapter 8).

2.1.1.3 Reasons for space research and potential terrestrial applications of LSS

Besides the importance for testing modules or whole life support systems under space conditions for being able to sustain human life for a longer period on the surface of other planets or during longer spaceflight missions, there are also other benefits from these research approaches.

In general, biological space research experiments will help increasing our knowledge of how organisms function under microgravity conditions which gives us new insight in fundamental biological processes (Clément 2006). Space biology research exposes organisms to conditions (primarily microgravity and cosmic radiation) which they have never experienced before during evolution. Generally the exploration of space is due to intrinsic human needs to explore, to seek and to increase scientific knowledge. Special focus lies on enhancing the understanding of life in the universe and finding possible traces of (former) life on other planets. Furthermore, it might be useful or necessary to utilize potential resources of other planets (Eckart 1996).

Besides their application in space exploration and habitation, closed bioregenerative life support systems also have potential terrestrial applications (Eckart 1996) as space and remote terrestrial environments often share the same problems such as a lack of water, clean air, food and energy supply (Polyakov 2010). Relating to this approach, the problem until the present day is, that only few of the potential applications have been clearly defined, although especially concerning bioregenerative life support in space, there is a huge potential for spin-off technologies deriving from that. Potential concrete applications of research on closed ecological systems and life support can be divided into the categories (Eckart 1996): ecological research and environmental protection, bioregeneration of atmosphere, water, and waste, highly efficient cultivation of plants and microorganisms as well as design and support of habitats and research facilities. These approaches are reinforced by an increasing awareness for the ecological challenges man is facing on Earth such as global warming, extinction of species, loss and degradation of natural ecosystems, industrial pollution and the outrunning of non-renewable fossil-fuels (Alling 2005).

2.1.2 Space environment: hostile habitat and research tool in space biology

In general, outer space is a hostile environment for living beings characterized by the absence of gravity, atmosphere and therefore atmospheric pressure, the threat of cosmic radiation, the absence of circadian rhythms, extreme temperatures as well as hypoxia (Wang 2004 a, Rea 2008, Clément 2006). Simultaneously, these unique conditions create an exciting environment for various studies on living organisms from single cells to human beings (Clément 2006). In the following chapters the most important space factors, microgravity and radiation are depicted with related experimental results on effects on living organisms. The influence of pressure and hypobaric conditions with respect to

microalgal growth is another factor discussed in 2.2.1.5. As mentioned before, there are various factors impeding the spread of life into space. Cells and higher organisms are facing totally different conditions they have never encountered during evolution on Earth. One example is that fluids behave completely different under microgravity conditions (under 0 g conditions fluids are dominated by surface tension, diffusion and Marangoni effects, see also chapter 2.3) and as the cell interior behaves in part like a fluid, this may also have decisive effects on intracellular processes in a microalgal cell (mechanical, biochemical and physiological). This is also a challenge for the homeostasis of the cell (Clément 2006).

2.1.2.1 Microgravity: perception and effects on organisms

As a major factor influencing organisms in space environment, microgravity has to be mentioned, where it is important to distinguish between direct and indirect effects of microgravity. Microgravity conditions create an environment for cells and careful analysis has to be conducted to differ between direct and indirect contribution of microgravity.

Indirect effects of Microgravity

Indirect effects of microgravity are the absence of sedimentation, the absence of gravity-driven convection, the absence of hydrodynamic shear, hydrostatic pressure, atmospheric pressure, and reduced mechanical forces which are acting on cells. Hence, it is very interesting to study how cells will respond to this altered environment where most of the forces acting on them on ground are missing. The effects of hydrodynamic shear on microalgae, for example, created by a fluid moving along a fixed object (Clément 2006), and the effects of its absence in the case of external influences, is an interesting parameter to study in the microgravity environment. Relating to that are mechanical forces acting on cells in normal gravity conditions and their absence or reduction in space environment without having artificial mechanical forces introduced by stirrers for example.

Direct effects of Microgravity

The direct effects of microgravity cells are exposed to, relate to the missing surface attachment of cells, the tendency of forming a spherical shape and the disorganization of microtubules responsible for the cellular cytoskeleton in space. In cell tissues, cells have a decreased tendency to undergo apoptosis during their stay in microgravity conditions. The increased dominance of surface tension forces and Marangoni convection is assumed to favor cell-cell interaction for cells in liquid suspension. Besides, diffusion becomes a dominant force for mixing in microgravity which is masked by buoyancy convection and sedimentation on Earth (Clément 2006). For cells in closed reactor systems in space environment, the restoration of mass transfer, shear and vibration (mechanical forces) by means of mixing systems can favor cell culture under these conditions and compensate possible altered cellular functions.

Gravity perception and effects on cell growth and development

A major question in space biology is by which mechanisms cells perceive gravitational forces and what effects on growth and development are resulting. The search for a gravity sensor at cellular level gives insight in the gravity-sensing mechanisms. Higher organisms possess special gravity-sensing organs using the direction of the gravitational vector for orientation. Examples are otolith organs in mammals which are part of the vestibular apparatus in the inner ear. Vertebrates show the same structure for this gravity sensing system in form of otoliths, tiny calcium carbonate crystals, resting on a layer of specialized nerve cells. The weight movement of the otoliths lying on these cells gives information about linear acceleration in three planes to the brain. For lower vertebrates and insects these sensing systems are also present, but simpler.

For plants, gravity has a tremendous influence on development (gravimorphism), orientation (gravitropism) and growth. Besides, plants respond to environmental factors like light, temperature, water, wind, magnetic and electric fields (Clément 2006). Gravity directs the growth of roots which show positive gravitropism and shoots (with negative gravitropism) of plants. The mechanism of perceiving gravity is still discussed in literature. All approaches are associated with a gravity-induced sedimentation of statoliths within the cytoplasm. More precisely, the sedimenting organelles, called amyloplasts, are membrane-bound and contain starch. Until the present day it is unclear if it is the movement of these organelles within the cytoplasm or the pressure that they put on the membrane in specific areas in the cell that is responsible for gravity perception. Mosses which also show gravitropism possess special zones where amyloplasts sediment in relation to the gravitational vector (Schwuchow 2002). It is also assumed, that the whole protoplasm of plant cells, and not only the amyloplasts, might play a role for gravisensing (Wayne 1992). Also for some algae, these seem to be involved in sensing gravity; here the particles are composed of barium sulphate crystals (Clément 2006) as it was reported for the statoliths of the macro alga *Chara* (Sievers 1996). Details for gravity perception in *C. reinhardtii* are outlined in chapter 2.2.1.4.

The group of ciliates and flagellates, where *C. reinhardtii* also belongs to, are important organisms for space research as they are capable of gravitaxis and gravikinesis. The latter one is defined as a regulation of swimming velocity to compensate sedimentation of the cell as a result from gravity. For the flagellate alga *Euglena gracilis* sensitivity to gravity was proven to be based on mechanosensitive Ca-channels (Häder 2005). A mechanical load, assumed to be the cytoplasm which has a higher density than the medium, is the activator of these channels triggering a signal transduction cascade.

Concerning effects of the gravitational force on the development of organisms, studies with centrifuges indicate that the lower life forms, like single-cell organisms (bacteria, protozoa) as well as invertebrates are independent of the gravitational force concerning their development (Clément 2006). For bacteria, like *E. coli* and *B. subtilis*, a higher growth rate of the flight group was monitored during

spaceflight (Mattoni 1971, Mennigmann 1986) which may be attributed to indirect effects of microgravity relating to the changes in the cellular microenvironment (Clément 2006). However, also contradictory results were published by Gasset (1994) and Bouloc and d'Ari (1991). Further experiments showed a result that might be problematic for longer space missions and crew health issues: *E. coli* and *S. aureus* possess a higher antibiotic resistance during spaceflight compared to ground control based on a thicker cell membrane developed during the flights (Planel 2004). More results for effects of space flight conditions on growth and physiology of bacteria are reviewed in Clément (2006). For these simple forms of cells it is assumed that mostly indirect effects of microgravity play a role for growth and signal transduction.

Concerning eukaryotes, an important factor for space biology research is that cellular organelles possess a higher density than one which corresponds to the density of the cytoplasm. As a result, at 1 g, the organelles exert a certain pressure on the cytoskeleton which disappears under 0 g conditions. This may lead to possible effects relating to the signal transduction chains contained in the cytoskeleton (Clément 2006). Moreover, it was proven by experiments, that the assembly of components of the cytoskeleton is dependent on gravity in that extent that the self-assembly of the microtubules does not take place in 0 g (Tabony 2002). A distinction must be drawn between direct gravitational and indirect gravitational effects on the cellular level. Indirect effects may result from a changed cellular microenvironment, for instance missing convection and sedimentation under microgravity, influencing the distribution of nutrients and wastes in the surrounding medium of a cell. Not only might the cytoskeleton be influenced by gravity, but also the physiology of cells. Whereas passive transport of small molecules is based on diffusion, the active transport by protein channels might be influenced by gravity (Clément 2006). Also for intracellular transport processes this might be true. Furthermore, the energy of motile cells for swimming to avoid sedimentation is not needed in microgravity and could be used instead for growth or other processes. A higher cell proliferation was reported for the ciliate *Paramecium* which might be caused by the fact, that under microgravity conditions, the swimming requires less energy than on Earth which could be used for cell division and metabolism (Planel 1982). This might also be attributable to other swimming organisms like the alga *C. reinhardtii*.

For plants, it was proven that the cell wall contains less amounts of cellulose and lignin under microgravity conditions (Cowles 1984, Nedukha 1996). Also on the metabolic level effects of microgravity were monitored, relating to a reduced electron chain transport in dwarf wheat (Stutte 2005). During attempts to grow higher plants in a complete life cycle problems of sterility and a delayed development were encountered (Kordyum 1997, Merkys 1990). In general, studies in space environment have shown that plants are affected by the conditions concerning changed growth (decreased cell division), biomass production and development (chromosomal abnormalities). Li and coworkers (2004) studied the effects of simulated microgravity conditions on reactive oxygen species

(ROS) on the cyanobacterium *Anabena sp*. which showed higher susceptibility under microgravity conditions compared to 1g control. Studies of Balan and coworkers (2006) with *N. salina* and *A. platensis* during parabolic flights showed fluctuation in the values of photosynthetic yields measured with PAM fluorometry. However, as gravity changes rapidly during parabolic flights it is not possible to conclude if the monitored changes were due to a reduced or an increased gravity or a combination of both.

As a summary, it can be assumed that the microgravity environment influences organisms through direct and indirect effects and that also single cells react to changes of gravity.

2.1.2.2 Radiation effects

Life on Earth is continuously exposed to space ionizing radiation, basically divided into three categories relating to its origin. Galactic cosmic radiation GCR, with energies between 1 and 10 GeV, which originates from outside the solar system from supernovae explosions, is composed of protons, α-particles and high-ionizing high energy particles HZE. Solar cosmic radiation (SCR) comprises low energy solar wind particles and the high-energy solar particle events (SPE). The latter is originating from bursts of energetic particles from the sun, which mainly consist of protons with energies up to 1 GeV. A third form of radiation on Earth is the geomagnetically trapped particle radiation with electrons (up to 7 MeV) and protons with energies of hundreds of MeV and low energy heavy ions (Rea 2008). To a large extent the Earth's magnetic field, based on its deflecting effect, and the atmosphere is a shield against radiation. Beyond Earth's atmosphere, GCR is mainly composed of protons (H nuclei) and α-particles (He particles) whereas 98% of GCR is atomic nuclei and 2% electrons. These 98% of nuclei consist of 87% protons, 12% He ions and 1% heavier ions (comprises HZE particles), (Clément 2006).

The terrestrial average annual effective dose, relating to cosmic rays, accounts for 0.3 mSv which is around 100 times lower than in outer space. In low Earth orbit another radiation source, the Van Allen belts, are important for space stations like ISS. This source is caused by interactions of GCR, SCR with the Earth's magnetic field and the atmosphere. Overall, radiation doses account for 20 mSv per month (Reitz 1995). In deep space, radiation may reach peak levels of 3 mSv per day calculated for organisms behind a shielding structure of a spacecraft (De Angelis 2004). On Mars, for example, living beings will be exposed to much higher radiation doses than on Earth (almost 100 times higher concerning cosmic ionizing radiation) as a result from a lack of an effective magnetic field or a notable atmosphere. A major health concern for living organisms in space, especially for long-term missions, is attributed to HZE particles (most important iron nuclei), which make up only 1% of GCR (Clément 2006). As adequate shielding is not yet available and damage caused by this kind of radiation is tremendous, it is the main radiation component space biologists are focused on. Besides HZE, neutrons possess the highest biological effectiveness and therefore cause most damage together

with HZE particles (Rea 2008). Their interactions with materials of space craft devices can lead to secondary radiation like γ-rays and neutrons with different energies (Miroshnichenko 2003). For radiation exposure the upper limit on Earth for the public accounts for 1 mSv per year, with an occupational limit for 20 mSv per year (lifetime limit is 400 mSv), set by the International Committee on Radiation Protection (ICRP).

Cosmic radiation or more precisely, ionizing radiation, could mainly lead to damage of DNA (primarily DNA strand breaks) and proteins if repair and defense mechanisms fail (for example production of stress proteins, activation of the immune defense system), acting through ionization and excitation of electrons in atoms and molecules. As radiation is a strong mutagen, it is considered as a major driver of evolution. A distinction must be drawn between direct damage by energy deposition or indirectly by a generation of reactive oxygen species after the breakdown of water molecules. Further details on mechanisms of direct and indirect radiation effects are mentioned in Clément (2006) and to some extent in chapter 2.2.1.4 for *C. reinhardtii*.

Conservation of genetic stability and cellular reproducibility are the two main components for the development and maintenance of life, which both are threatened by ionizing radiation. Radiation effects on living organisms are therefore a major topic in space biology research. An increased rate of chromosomal aberrations was found in crew members, a higher number of mutations in the fruit fly *Drosophila* and the nematode *C. elegans* as well as chromosomal damage and abnormalities in various plants relating to exposure to cosmic radiation (Clément 2006). In general, radiation sensitivity is related to the DNA amount per cell and the capacity of repair mechanisms. According to Korogodins thesis (Korogodin 1966) the most devastating effect is correlating with highest growth rates being the most susceptible cell condition in terms of radiation exposure. The order of most resistant organisms starts with single-stranded viruses, double-stranded viruses (if viruses can be considered as organisms), followed by bacteria, algae and yeast. For eukaryotes, haploid cells are more sensitive than diploids. The bacterium most resistant to radiation is *Deinococcus radiodurans* which can tolerate doses up to 4kGy (Clément 2006). Hence, algae in general can be considered as quite tolerant against radiation. In general, the lower life forms (bacteria, protozoa) as well as invertebrates seem to be relative insensitive to radiation (Clément 2006).

Radiation is not the only environmental factor in space. Also possible combined effects of radiation, microgravity and other factors are of major research interest. Effects resulting from a combined action of radiation and microgravity were assumed after several studies relating to cells, higher plants and several development stages of insects and mammals which were reviewed by Horneck (1999). Here, embryonic stages are especially sensitive to a synergistic interaction of microgravity and radiation.

2.2 Potential of microalgae with respect to remote applications

Remote habitats like outer space, other planets or even desert regions on Earth often share the same problems impeding the spread of life. Special environmental factors in space or extraterrestrial habitats act on biological systems. The application of bioregenerative life support systems is considered to be the key for making these hostile environments amenable for (human) life. Also for extreme regions on Earth, like deserts, these life support systems are developed in order to establish sustainable settlements fighting against soil erosion and desertification (Polyakov 2010, Nelson 2003). Interestingly, almost all concepts for these closed autonomous life support systems rely on microalgae as basic parts. In general, plants (and algae) were used in spaceflights in the early beginnings in the space program. First, plant seeds were sent to space in 1960 whereas various species were studied in space environment since then (Clément 2006).

There are various reasons why eukaryotic microalgae are of major interest for this approach. A major function, that has to be fulfilled by a sustainable life support system, is the regeneration of atmosphere in form of oxygen production and removal of carbon dioxide with carbon being fixed into complex molecules. In order to accomplish this function, an organism capable of photosynthesis is needed. Potential candidates originate from the group of higher plants, eukaryotic microalgae as well as prokaryotic cyanobacteria. These primary producers constitute the basis of the food chain on Earth and their integration in life support systems ensures closed material cycles of gases and minerals. Thereby the sun provides the driving energy which is both valid for material cycles on Earth as well as in space where life support systems for space application in some way mimic the Earth cycles.

Eukaryotic microalgae possess several unique features which favors their use for closed control life support systems in comparison with higher plants or prokaryotic cyanobacteria.

Disadvantages of several cyanobacterial species are, among other things, their filamentous form displaying basic difficulties for bioprocess engineering and an establishment of suspension cultures and their production of toxic substances whereas production rates are reported to increase under conditions with reduced gravity (Xiao 2010).

Compared to that, eukaryotic microalgae show numerous traits which are important for an organism which should build up the first module of a life support system. Their fast growth rates surmounting those of higher plants, their high photosynthesis rates (Chisti 2007) and their high light to biomass conversion yields (up to 5 fold higher compared to higher plants) (Zhu 2008) are the most promising characteristics.

In contrast to cultures of higher plants, microalgae cultures only need CO_2, light and aqueous media containing some mineral salts. Microalgae exhibit shorter growth cycles than higher plants.

Furthermore, harvesting techniques for microalgae can be implemented more easily than those for higher plants.

Concerning interfaces with other modules or specifically the “human module”, microalgae show gas exchange characteristics able to meet human requirements (Javanmardian 1992, Wharton 1988). For example, during BIOS experiments with the green alga *Chlorella* it was shown that a culture volume of 20 L with its specific production rates can supply one man concerning oxygen and water.

Also concerning the provision of food, microalgae can play a significant role: because of their unique composition (for instance polyunsaturated fatty acids, rich in protein) they are used for increasing the nutritional value of food and feed (Spolaore 2006) while indigestible compounds like cellulosic fibers or lignin can be completely avoided. Algae cells could be used as a whole after a drying step for human nutrition (Becker 2004). Concerning carotenoids, especially *C. reinhardtii* represents a good source without the necessity of additional processing (Gille 2016).

From the perspective of process engineering and the cultivation of microalgae in photobioreactors, eukaryotic microalgae also possess various positive traits. With microalgae, where most species are unicellular, in contrast to filamentous cyanobacteria like *Arthrospira platensis*, suspension cultures as well as immobilized cultures can be realized, also in continuous cultures (Tang 2012, Maeda 2006, Lamers 2010). In general, for continuous microalgae cultures, no manual maintenance is required, a complete automated cultivation can be conducted by pure process engineering.

A media recycling system is needed for fresh media supply which automatically refills consumed substrates after analysis of composition. In order to harvest algae biomass, flocculation techniques (chemical or electroflocculation), or simple centrifugation or sedimentation can be used. For space application of photobioreactor concepts (Oguchi 1989) also the use of hollow fiber membrane modules for filtration is reported. After filtration, the cell free medium is fed to the media supply unit for dosage of nutrients and filled back into the system to create a closed loop system.

However, even if numerous aspects justify the usage of microalgae as basis or a first module of a closed life support system, potential obstacles have to be carefully considered and taken into account while designing such a system or just a first part of a whole system. Major questions which need to be addressed for that approach are relating to the long-term stability of continuous microalgae cultures in respect to cosmic radiation and genetic stability of algae. Another aspect, also related to resistance and self-restoration capability to radiation is that microalgae physiology does not have to change during continuous processes (ideally steady-state conditions) in space environment.

In the following chapters the chosen green alga *C. reinhardtii* is described with respect to its suitability for a module of a life support system.

2.2.1 *Chlamydomonas reinhardtii* as model organism

The green alga *Chlamydomonas reinhardtii* is one of the best studied eukaryotic microalgae and a model organism for various aspects. Therefore it is often termed photosynthetic yeast (Rochaix 1995). It is the alga chosen for a first microalgae-based module for a life support system which is described within this work. The results of genomic sequencing were published in 2007 (Merchant 2007).

2.2.1.1 Classification and scientific significance

Chlamydomonas reinhardtii belongs, within the domain of eukaryotes, to the kingdom of plantae, the phylum of chlorophyta (green algae), the class of chlorophyceae, the order of Chlamydomonales and the family of Chlamydomonadaceae. More than 500 different species make up the genus of *Chlamydomonas* whereas most of them are distributed in fresh water but also in soil water. Some cryophilic species like *Chlamydomonas nivalis* are able to thrive in cold regions on snow (Hoek, 2002). Replication is possible via asexual and sexual replication. Reasons for its importance as model organism for algae biotechnology (Harris 2001) are divers. The ability of this alga to grow either photoautotrophically, mixotrophically as well as heterotrophically is particularly interesting for genetic or biochemical analysis. By using mutants various aspects concerning photosynthesis as well as mitochondrial functions and cellular interactions can be studied. Besides its flexibility concerning energy metabolism, all of the three genomes (nuclear, mitochondrial, chloroplast) are sequenced and annotated (Merchant 2007). Almost all strains of *C. reinhardtii* used in the laboratory originate from an isolate from G. M. Smith in 1945 which was diverging into three main lines, the Sager-line, the Cambridge-line and the Ebersold/Levine-137c-line. The latter is not able to consume nitrate as N-source as a result of a loss of the enzyme nitrate reductase. Thus, these cells need ammonia as main medium component (Harris 2009). Within this work, primarily the wildtype CC-1690 mt^+ (Sager 21 gr) was used.

2.2.1.2 Morphology

Chlamydomonas reinhardtii is a unicellular round to ellipsoid biflagellate with an average size of 10 µm length and about 3 µm width. *C. reinhardtii* cells show a polar structure with two flagella at the front side and one single hoof- or cup-shaped chloroplast which partly surrounds the nucleus. The two flagella have the same size (between 1.5-2 times longer than the cell body) and are located at the front (apical) side of the cell. The chloroplast can make up 40% of the total cell volume for photoautotrophically grown cells. The nucleus is about 2-4 µm in diameter and contains a nucleolus. Its surrounding double-membrane merges into the endoplasmic reticulum. About one to four Golgi apparatuses can be found in proximity to the nucleus (Rochaix 1995). The structure of one cell is shown in Figure 2-3 A.

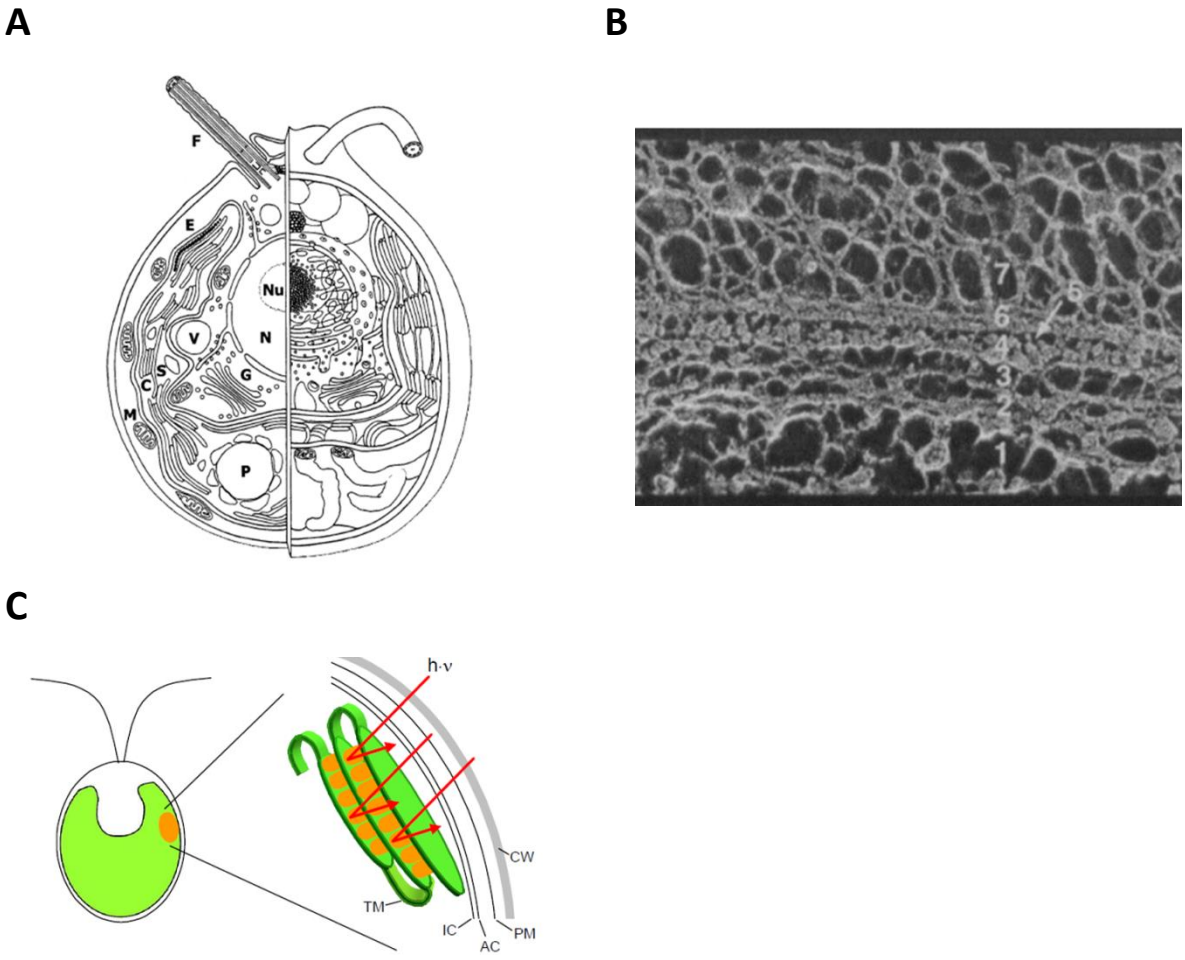

Figure 2-3. The model organism *Chlamydomonas reinhardtii*. A) Structure of a *C. reinhardtii* cell: Nucleus (N) with nucleolus (Nu), two isoform flagellae (F), cup-shaped chloroplast (C) with the eye spot (E), starch-containing pyrenoid (P), mitochondria (M), golgi vesicle (G), starch grains (S) and vacuoles (V) (Nickelsen 2000). B) Cross section of the cell wall of *C. reinhardtii*. Numbers indicate the wall layers; 130,000 fold magnification (Goodenough 1985). C) Eye spot of *C. reinhardtii*: PM: plasma membrane, AC: outer chloroplast membrane, IC: inner chloroplast membrane, TM: thylakoid membrane, CW: cell wall (Berthold 2007).

The cell wall consists of glycoproteins rich in hydroxyproline where sugar components (mainly composed of galactose, arabinose, mannose and glucose) are bound to. In contrast to earlier assumptions, the wall of *C. reinhardtii* cells does not contain cellulose. Seven layers are building the cell wall whereas three of them (layer 2, 4 and 6) are termed "central triplett". Whereas layer 3 and 5 are void spaces, layer 2 consists of a network of densely woven filaments. Layer 4 shows a granular structure and the outer layer 6 a crystalline structure. Layer 1 and 2 are insoluble, whereas the outer layers 4 and 6 are soluble to chaotropic salts and can be separated from the cell. The outer layers are only bound via electrostatic or hydrophobic forces whereas layer 2 is more tightly bound to the cell membrane. *C. reinhardtii* is able to reproduce its cell wall after a loss within two to three hours (Robinson 1978).

A double-membrane encloses the chloroplast where also pyrenoids can be contained. Inside the chloroplast, several (two to twenty) thylakoids are arranged in stacks of different sizes. Also the circular chloroplast DNA is contained, in form of small aggregates, termed nucleoides with 1-2 µm diameter. Pyrenoids, which are mainly containing the enzyme RuBisCO, possess a round shape without a clear spatial definition and are important sites for starch production within the cell. At this location within the cell, CO_2 is fixed by the enzyme RuBisCO after local accumulation of carbon concentrating mechanisms (CCM). Grains of starch crossed by thylakoids are accumulating around the pyrenoid. These starch granules are particularly prominent in cells suffering from nutrient limitation (for example N- and P-limitation) (Ball 1990).

One important part of the cell is the eyespot (or stigma) which is visible as red-orange spot, next to the plasma membrane (Figure 2-3 C). It consists of several layers of carotenoid-containing lipid vesicles which are localized in the stroma of the chloroplast in close vicinity to the plasma membrane, thereby separated by the thylakoid membranes (Melkonian 1984). The eyespot plays a role for light perception for phototaxis, a directed movement toward a light source (or away from it). Details of phototaxis are depicted in Chapter 2.2.1.4. Resulting from a higher refractive index of those vesicles, compared to the layers of thylakoid membranes, and a distance of 125 nm between them (Melkonian 1984) light beams hitting them at right angels are partly reflected. Only with light beams of wavelengths around 500 nm (four times the distance between the layers) there is a constructive interference (Kreimer 1990, Schaller 1997).

Chlamydomonas reinhardtii is also able to determine the direction of incoming light. There are photoreceptors in the plasma membrane next to the eye spot which are shielded from the eye spot from light beams hitting the spot from backside. Light beams hitting at right angle are amplified by constructive interference whereas this is maximal at wavelengths of 500 nm. When the angle of the incoming light beam is smaller, constructive interference amplifies light with smaller wavelengths (Hegemann 1998).

A *C. reinhardtii* cell also contains two contractile vacuoles in the apical part of the cell and further organelles of eukaryotic cells like membrane-bound organelles (lysosome, peroxisome, glyoxysome). The two vacuoles pump water penetrating the cell in a hypotonic environment out of the cell. Between the vacuoles there is the point of attachment of the flagella with the cell body. The contraction of the two vacuoles is not synchronous but chronologically shifted. The endoplasmic reticulum is arranged next to the nucleus, surrounded by a Golgi-apparatus. Mitochondria are located between chloroplast and plasmalemma as well as within the cytoplasma and make up only 1-3% of the total cell volume of phototrophically grown cells. Also lipid droplets, ribosomes, as well as membrane-bound bodies like lysosomes, peroxysomes and glyoxysomes can be found in a *C. reinhardtii* cell. Further details on cell organelles for this alga can be found in (Harris 2009, Hoek 2002, and Witman 2009).

Concerning liquid cultures of *C. reinhardtii*, colonies or cell clusters of adherent, non-motile cells termed as palmelloids, can be found under specific conditions, for instance Ca^{2+} limitation, high phosphate concentration, when chelating agents are present or organic acids which cannot be used as substrates. However, exact details and conditions leading to the formation of these palmelloids are not known yet. Often an extracellular gelatinous matrix, consisting of acidic polysaccharides is produced where these aggregated cells are embedded in. Mostly four to eight cells are contained by a cell wall and sometimes aggregates of those cell groups are built. Cells contained in these palmelloid structures show a normal morphology. It is assumed that palmelloids result from an erroneous cell division (Harris 2009). Several methods have been tested and discussed in order to dissolve those aggregates, for example lowering the pH or changing lighting from continuous to day/night cycles. Especially the 21gr-line of *C. reinhardtii*, which was the origin of the strain CC-1690, tends to form those palmelloid structures very often. In contrast to that, strains from the Ebersold-Levine-line hardly show these clusters. Independently from those palmelloids, CC-1690 cells also build secondary aggregates which do not originate from an erroneous cell division but are a result of various biotic and abiotic factors. This may be related to reports of auto-flocculation of algal species induced either by CO_2-limitation or other abiotic stimuli such as O_2 deprivation (Pittman 2011).

2.2.1.3 Protective mechanisms against osmotic effects

In order to assess effects of pressure changes or the hypobaric environment of space on microalgae, the effects of osmotic pressure might be relevant. In general, cell volume, hydrostatic pressure and osmolality are controlled by several signaling cascades which are responsible for important cellular functions like exocytosis and apoptosis (Zonia 2007). As the cells are continuously exposed to changes of osmotic conditions in their environment, either in soil or in water, cells need to develop adaptation mechanisms to avoid excessive swelling or shrinking. In relation to the cellular environment, it can be distinguished between isotonic, hypertonic and hypotonic conditions. As osmotic effects either lead to an increasing pressure or a decreasing pressure inside the cell, it can be assumed that the perception of pressure by algal cells acts via similar mechanisms like the perception of osmotic effects. For this reason, protective mechanisms against osmotic effects are considered as hints concerning stability of cells against pressures different from atmospheric conditions. In general, it is assumed that aquaporins, channels allowing the flow of H_2O and small neutral solutes across membranes, have a function as osmosensors and act as cell volume regulators in all kind of cells (Hill 2004). In the genome of *C. reinhardtii* there are hints for two putative aquaporins (Komsic-Buchmann 2014).

A first protective device is the cell wall of *C. reinhardtii* described in chapter 2.2.1.2. Inside cells the so called turgor pressure exists. The turgor pressure describes the difference of osmotic pressure between the intracellular and the extracellular environment. Osmotic pressure is defined as force exerted against a selectively permeable membrane by a solution with different solute concentrations

on either side of a membrane (Zonia 2007). It is a consequence of diffusion of water along an ion concentration gradient across a semi-permeable membrane which is the cellular wall or membrane in this case. In case of different osmotic pressures between environment and intracellular volume, a balance of water potentials is installed. The water potential ψ or osmotic potential is defined as potential for water to move across a selectively permeable membrane and is calculated as the difference between hydrostatic pressure p and osmotic pressure π:

Equation 2-1. Water potential.

$$\psi = p - \pi$$

Under the assumption that the hydrostatic pressure inside the cell (p_i) is equivalent to the pressure in the environment (p_0), an inflow of water in the cell is resulting for a decreasing osmotic pressure in the environment (π_0). For cell-wall containing organisms the cell wall keeps the cell volume constant whereas the pressure inside the cell increases. It increases as long as the water potentials inside and outside the cell are balanced:

Equation 2-2. Balance of intracellular and extracellular water potentials.

$$\psi_i = \psi_0$$

Equation 2-3. Definition of turgor pressure.

$$Turgor = p_i - p_0 = \pi_i + \pi_0$$

According to Bisson and Kirst (1995), cells without a cell wall cannot maintain a turgor pressure. As a logical consequence, flagellate algae like *Chlamydomonas* do not have a turgor pressure as the site where the flagellae emerges is a weak point of the cell wall. This might be the gap between the flagella and the so called flagella rings which is covered by material similar to the inner layer of the cell wall (Ringo 1967, O'Toole 2003). Hence, algae without a cell wall and algae with flagella need other methods for adaption to osmotic differences. One method is the accumulation of inorganic (monovalent ions like Na^+, K^+, Cl^-) or organic osmolytes (sugars, polyols and heterosides) inside the cytoplasm in case of a hypertonic environment. Ions are easily available but in higher concentrations could impede cellular metabolism. Organic osmolytes not only regulate osmotic pressure but protect, as solutes, also proteins and stabilize the cell membrane. Moreover, they possess a high solubility and are not charged at neutral pH. However, their provision is slower and energy dependent. For *C. reinhardtii* it is assumed that osmotic regulation is related to the function of two contractile vacuoles (Komsic-Buchmann 2014). These are able to pump water out of the cell in case of a hypotonic medium (Luykx 1997). As a result the authors assume that *Chlamydomonas* is able to sense cell size and osmolarity of the medium independently and adapts the function of the contractile vacuoles to these changing conditions (Komsic-Buchmann 2014).

2.2.1.4 Suitability for life support systems with respect to microgravity and radiation

Concerning the choice of species for life support systems and in general space studies, factors like size, weight and maintenance issues for that organism as well as available support hardware and techniques are essential (Clément 2006). A microorganism selected for use in a life support system module for space application should show a sufficient metabolic activity under the conditions present in a pressurized module in space environment. This environment is mainly characterized by the absence of effective gravity, the part of the cosmic radiation spectrum that penetrates the surrounding material of the module which can interact with both the material and the contained organisms as well as the lack of circadian rhythms (24 hour day rhythm with dark periods) (Clément 2006).

Chlamydomonas reinhardtii, as representative of eukaryotic microalgae, is a photosynthetic organism which is of interest for selection as part of a first phototrophic module within a life support system. As this green alga is among the species showing the highest efficiency of photosynthesis during spaceflight experiments (Rea 2008), the alga might be a suitable organism for a first microalgae-based module within a life supporting system in space flight. Moreover, it is one of the best investigated species with respect to physiology and genetics and therefore an ideal model organism. However, other microalgae species would be better suited concerning food applications. Yet, the combination of more than one microalgae species within closed life support systems would be beneficial, each with specific main functions. Concerning susceptibility to cosmic radiation, the alga seems to be relatively tolerant. Studies from Rea and coworkers (2008) have shown that *C. reinhardtii* does not seem to be negatively influenced by increased radiation concerning O_2 production and yield of photosystem II. One hypothesis is that PSII has a role for capturing and utilizing ionizing radiation. Oxygen evolution of the cells even seems to be stimulated. However, it seems that also the light intensity, the algae were exposed to, simultaneously to radiation in space flight, has an influence on the degree of vulnerability against radiation. This could be based on a negative synergistic effect of light and cosmic radiation, as high light causes photoinhibition also producing free radicals. Studies with *C. vulgaris* in continuous cultures by Gitelson and coworkers (2003) showed that after a first decrease of growth rate following exposure to UV radiation, a growth rate resulted which was higher than the initial one being a good example for the self-restoration capacity of the described system.

General reasons for using *Chlamydomonas reinhardtii* as organism for a first module are numerous: resulting from its importance as model organism for algae biotechnology, a vast amount of knowledge of studies, also –omics studies, is accessible with a complete sequencing of the three genomes. Another aspect is that *C. reinhardtii* as a microalgae species, is able to produce hydrogen (Frenkel 1952) under certain conditions (anaerobic, S-limitation) (Melis 2000, Lehr 2012) which is of importance for a possible energy supply approach within a CELSS. H_2 formation is catalyzed by the enzyme hydrogenase. This might also be realized by a second module. The alga also shows strong growth on municipal wastewater (Kong 2010) and therefore can be used for waste water recycling in a

life support system. Furthermore, *C. reinhardtii* is an algae species, with highly studied environmental perception mechanisms, regarding movements in relation to light (phototaxis), gravitational field (gravitaxis) and gravitational and viscous torques in a flow (gyrotaxis).

Phototaxis is defined as directed movement of a motile organism in relation to a light source or stimulus. This may either be a movement toward this light source, termed positive phototaxis, or a movement away from this light source (negative phototaxis). For this motile behavior, the eyespot of *C. reinhardtii* plays a central role. Details of composition, sensitivity relating to intensity and wavelength are further depicted in 2.2.1.2. Besides, there is the photophobic response in *C. reinhardtii* and other green algae, which is defined as a reorientation of swimming direction resulting from a sudden increase in light intensity.

Gravitaxis is the orientation of the swimming motion of an organism relative to the gravitational field. In general, it is an energy-depending behavior demanding a coordinated movement of flagella. Most microalgae show negative gravitaxis, swimming upwards in the gravitational field. It is a slow process with mean velocities of about 4-8 µm s^{-1}, whereas the normal swimming velocity of *Chlamydomonas* is about ten times higher (Bean 1977). Furthermore, it is independent from the phototactic movement of *Chlamydomonas* (Bean 1977, Yoshimura 2003, Kam 1999). Reasons for this behavior are assumed to be originating from an inhomogeneous mass distribution or a geometric fore and rear asymmetry. According to Roberts (2006) the gravitactic movement in *Chlamydomonas* is explicable in only physical terms without any biosensor involved. Kam and coworkers (1999) showed that mechanosensitive Ca^{2+}-channels, which were assumed to attribute to the gravitactic behavior, were not involved. Furthermore, they tested by complete inactivation of flagella, if biochemical processes are at all involved in this movement. Their result was, according to Roberts (2006), that there is no involvement of mechanosensitive channels for gravitaxis in *Chlamydomonas reinhardtii*. Kam and coworkers (1999) assumed that gravitaxis is caused by an inhomogeneous mass distribution in the cell. Roberts (2006) showed that primarily shape orientation, and only to a minor extent a longitudinal density gradient, is responsible for the upward orientation of this alga. Therefore, it is questionable if the abiotic factor pressure acts, when it is affecting cells at all, via the mechanisms of gravitropism.

In general, there is the assumption, that the smaller the organism, the less affected it is by gravity, meaning that microorganisms are principally affected by viscosity and Brownian movement (Clément 2006). For high acceleration, there is a higher tolerance of smaller organisms, compared to bigger ones (Smith 1975). However, there is a clear agreement of the existence of gravitropism of the green alga *C. reinhardtii*.

Gyrotaxis is defined as directed motion by orientation of the cellular axis in relation to gravitational and viscous torques and velocity gradients in a flowing fluid (Kessler 1985). Hence, it seems that both

gravitaxis and gyrotaxis are based on physical mechanisms related to cellular geometry and weight distribution for *C. reinhardtii*.

The wildtype of *C. reinhardtii*, which is chosen for this work, is CC-1690 wildtype mt^+ (Sager 21 gr), Sager's basic wildtype strain which was used as source for the majority of cDNA libraries within the Chlamydomonas Genome Project. This wildtype is able to metabolize nitrate as N-source possessing the enzyme nitrate reductase and could, analogously to the cyanobacterial compartment in the Melissa concept (see chapter 2.1.1.2), be integrated after nitrifying bacteria have converted NH_4^+ to nitrate (Farges 2008).

2.2.1.5 Pressure: perception and effects relating to *C. reinhardtii* and other microalgae

Within this work, a special attention is put on one of the indirect effects of microgravity: pressure and the absence of pressure. For the design of algae-based life support modules and also for optimization of photobioreactor geometries and hydrodynamics in general, major questions that should be taken into account are the perception of pressure and pressure changes by microalgae and the effects of this abiotic factor on photosynthetic efficiency, kinetics, physiology and morphology of the cells. Whereas a lot of fundamental knowledge is existing on the effects of other abiotic factors like pH and temperature on the aforementioned parameters, literature on pressure perception and its effect on microalgae and their photosynthetic performance is rare and there is no consistent conclusion.

On Earth with its gravitational field, there is also a considerable gradient of hydrostatic pressure along the body axis on which various cells are dependent on for normal function (Clément 2006). The absence of this gradient in microgravity conditions is one possible reason for the loss of bones in mammals during space residence. Concerning a direct perception of pressure by microalgae, possible receptors related to this abiotic factor have to be regarded. Most likely receptor candidates for that are mechanoreceptors. Mechanosensitive ion channels developed early in evolution and exist in species from all three domains of life. It is assumed that the first signal transduction cascade evolving through evolution was the pressure-induced activation of the mechanosensitive channels (Kung 2005). Several hints for the existence of mechanoreceptors in *Chlamydomonas reinhardtii*, located within the cell membrane and on flagella, can be found in literature (Yoshimura 1996, Yoshimura 1998, Fujiu 2011) possibly playing a role for pressure perception maybe also in an indirect way. Those receptors are assumed to be involved in the regulation of cell volume and morphogenesis. Besides, other mechano-sensitive receptors are reported to be located within the cytoplasm and the chloroplast membrane important for chloroplast organization (Nakayama 2007).

For elucidation of pressure effects on microalgae, Min and coworkers (2014) developed a microfluidic experimental system for distortion of the cell membrane by compression and tested it on *C. reinhardtii* cells. Outcomes of these experiments were a deflagellation of the cells, a higher number of daughter cells and also smaller cells after cell division. Cells under compression in that apparatus also showed

higher lipid productivities than under control conditions. Other green algae species showed various effects to higher pressure and pressure changes: the disassembly and uptake of flagella inside the cell (reported for *Polytomella agilis* (Brown 1978)), an inhibition of photosynthesis (lower CO_2 uptake, lower O_2 production and reduced growth) reported for different algae and diatom species (Pope 1973) as well as *Scenedesmus obliquus* (Schreiber 1973) as reaction to high hydrostatic pressures. The latter reported the reversibility of those effects on photosynthesis. While these studies were conducted for effects of higher pressures, only few studies for influences of lowered pressure have yet been published. Richards and coworkers (2006) studied the effects of a hypobaric environment (down to 100 mbar absolute pressure) on the higher plant *A. thaliana* with the results that the net photosynthetic rates increased for decreasing pressure when the pCO_2 was at limiting concentrations. In contrast to that, photosynthetic rates were insensitive to a pressure decrease for saturating pCO_2 concentrations. An interesting study of Qin and coworkers (2014) with cyanobacterial species and hypobaric environments of 500 mbar absolute showed several important results. The authors report reduced growth rates for all species tested, an increased Car/Chl a-ratio, a reduced phycocyanin content and more extracellular polymeric substance.

Beside the presence of mechanoreceptors, characteristics of *C. reinhardtii* like the presence of flagella, the ability for gravitaxis as well as gyrotaxis should also be taken into account, as mentioned in the previous chapter. The presence and the composition of the cells flagella is important in so far as there are experimental hints suggesting that they are weak spots for cell wall integrity resulting in the inability of the cell to maintain a turgor pressure (Bisson 1995). So far, no clear conclusion can be found in literature concerning this aspect. Until the present day it cannot be excluded to 100% that mechanoreceptors are not involved for perception of gravity and gravitaxis (Yoshimura 2003). This could also be important for revealing possible effects of lowered pressure.

For the development of life support systems based on microalgae modules it is important to know which critical pressure thresholds do exist and if slight deviations from Earths atmospheric pressure are beneficial for photosynthetic activity.

It is also important to reveal if pressure changes are responsible for cellular aggregation effects, in the case of *Chlamydomonas reinhardtii* relating to palmelloids and secondary aggregates. Further technical aspects are depicted in chapter 2.3.3.

2.2.2 Metabolism of *Chlamydomonas reinhardtii*

C. reinhardtii is able to grow photoautotrophically with CO_2, heterotrophically with acetate, as well as mixotrophically while using both carbon sources (Heifetz 2000). However, the alga is not capable to metabolize glucose or similar saccharides (Harris 2009). This capability allows the proliferation of the cells under a variety of nutritional conditions with various differences in active metabolism for these types of nutrition. In case of the photoautotrophic way, light energy is used to reduce CO_2 via the

Calvin-cycle to glycerinaldehyde-3-phosphate whereas under heterotrophic conditions acetate is degraded to glyceraldehyde which is subsequently channeled to the glyoxylate-cycle (Heifetz 2000). According to several studies, acetate influences metabolism in various ways, for example through a transient inhibition of photosynthesis (Endo 1996), a reduced expression of special proteins of light harvesting antenna (Kindle 1987) and CO_2 fixation (Goldschmidt-Clermont 1986). For cultures grown under light with acetate, a stimulation of respiration is reported (Endo 1996, Fett 1994) which might be explained by an increased activity of the alternative oxidase (Weger 1990). For increasing acetate concentrations Heifetz and coworkers (2000) report a decreased CO_2 fixation and O_2 production rate. Furthermore, it was shown that the part of carbon in biomass originating from photosynthetic fixation is reduced by 50% when acetate is contained in the medium.

2.2.2.1 Photosynthesis

The term photosynthesis means „built by light" and is defined as process with which photoautotrophic organisms like plants and algae convert light energy into chemical energy. Low-energy substances like CO_2, water and salts are converted into energy-rich organic components like sugar or other organic molecules and oxygen. The reaction takes place inside the chloroplast, specialized organelles and is described by the overall formula:

Equation 2-4. Photosynthesis

$$nCO_2 + nH_2O \xrightarrow{h\cdot\nu} (CH_2O)_n + nO_2$$

The process of photosynthesis can be divided into two main reactions: the light reaction and the Calvin-cycle, which is also called dark reaction. The process of light reaction is characterized by a conversion of light energy into chemical energy in from of ATP and reduction equivalents (NADPH) during photolysis of water and a resulting release of oxygen. During the dark reaction this energy stored is consumed for CO_2-fixation in form of sugar molecules (Campbell 2009).

Light harvesting complexes (LHC)

One step prior to the storage of light energy in form of chemical energy, photons have to be absorbed by several cellular pigments. *C. reinhardtii* cells contain three different types of accessory pigments (see also chapter 2.3.2.3): chlorophyll a (Chl a), chlorophyll b (Chl b) and carotenoids (Car). Their absorption spectrum lies within the so called PAR (photosynthetic active radiation) range, the wavelength range between 400 and 700 nm. Besides these accessory pigments, *C. reinhardtii*, like other photosynthetic organisms, contains sensory pigments. Details of this topic are depicted in chapter 2.3.2. During absorption of a photon by a pigment molecule one electron of this molecule is shifted to a higher energy level, what is termed excited state. Only those photons are absorbed which possess exactly the energy corresponding to the difference between ground state S_0 and excited state S_1 of the pigment molecule. Hence, the frequency (quotient of light velocity and wavelength) of

absorbed radiation has to be in resonance to the difference in energy of the two states of the molecule (resonance condition). This is the reason for the characteristic absorption maxima of the different pigment types (Häder 1999).

Pigments are part of the photosystems which are integrated inside the thylakoid membrane of the chloroplast. Together with special proteins those pigments build the light harvesting complexes (LHC). These constitute the light harvesting antenna of the photosystems' reaction centers. The antenna complexes contain all three of the accessory pigments (Chl a, Chl b, Car) of around 250 to 400 molecules, which collect light energy and transfer it to the reaction centers. A pair of Chl a molecules acts as central molecules in these reaction centers which are able to use the photons absorbed by the antenna in a photochemical reaction.

Two different photosystems are linked by an electron transport chain and interact during light absorption. They are termed, relating to their discovery, photosystem I (PSI) and photosystem II (PSII). They both possess a characteristic reaction center which is comprised of a special primary electron acceptor and a pair of Chl a molecules. These are identical for both photosystems but are associated with different proteins in the thylakoid membrane, which is the reason for their different absorption maxima. PSI is characterized by a central pair of Chl a molecules with peak absorption at 700 nm (therefore termed P700); PSII contains a Chl a pair with a maximum absorption at 680 nm (P680). The reaction center of PSII contains, beside the Chl a pair, two different chlorophyll binding proteins as well as a heterodimer of the D1 and D2 proteins. The D1 protein has an important role in repair mechanisms during high light conditions (Ohad 1984). The direction of energy flow is from PSII to PSI (Stern 2009) as PSII is on a higher energy level than PSI while absorbing photons with higher quantum energy at a lower wavelength than PSI. When light energy is absorbed, a delocalized outer electron is lifted from the singlet basic state S_0 to a higher excited state, as pigment molecules possess vast π electron systems. Only red and violet light photons can excite Chl a molecules. The S_2 state for violet light is unstable with the result that energy is dissipated as heat for S_2 to S_1 state transition. Transition of S_1 to S_0 is slower so that different energy transforming processes occur.

Of importance for photosynthesis are the production of an electrical polarized state and the energy transfer. This Förster resonance energy transfer (FRET), or resonance energy transfer, is important for pigment molecules in close proximity to each other whereby S_1 excitation energy is transferred from antenna to reaction center. With the help of the oscillation electrical field of an excited electron an electron in the receiving molecule in S_0 state is transferred to higher S_1 state by resonance. A little amount of energy is hereby lost in form of heat. Within the reaction center charge separation occurs with the transfer of energy rich electrons and the initiation of a redox reaction. One electron of the Chl a dimer is transferred to a higher energy level and afterwards transferred to an electron acceptor to

start the electron flow. The Chl a molecule is oxidized with that step and is now positively charged (Raven 2005, Häder 1999).

Light reaction

The excited S_1 state is the initial state for the following photochemical processes within the light reaction of photosynthesis. This state is only stable for about a nanosecond. For isolated pigments this energy difference is dissipated in form of heat and photons resulting in characteristic fluorescence emissions. For *in vivo* conditions the excited electrons are transferred to specific transport molecules and thus the installation of ground state is prevented for the purpose of energy storage. The following electron transport can occur in two different ways (Raven 2005, Barsanti 2006, Campbell 2009) designated as non-cyclic and cyclic electron transport.

a) Non-cyclic electron transport

In the case of non-cyclic electron transport, the excited electrons do not return to their original site but are transferred finally to a carrier molecule which is $NADP^+$. This means that continuously new electrons have to be supplied which is accomplished by oxidation of water molecules resulting in oxygen and protons. The non-cyclic or linear version of the electron transport involves both photosystems and two electron transport chains for the production of NADPH. It is also called the Z-scheme of electron flow (Figure 2-4 A).

For the reduction of $NADP^+$ to NADPH electrons have to be transferred to a higher energy level and therefore, they have to be excited twice, first in PSII and then in PSI. First PSII (P680) is excited by light energy and electrons in the reaction center which are in S_1 state are transferred to a primary electron acceptor, called pheopytin and subsequently to the electron transport chain. One electron per P680-chlorophyll is transferred which makes the chlorophyll a strong oxidant which is positively charged and the missing electrons are replaced by electrons resulting from the splitting of water (photolysis). This oxidation of water molecules produces one molecule oxygen and four protons from two molecules water. The two missing electrons are balanced by the water splitting enzyme complex and transferred to the P680 molecules. The excited electrons of PSII are transferred from the primary acceptor via an electron transport chain to PSI. The electron transport chain involves quinone, cytochromes and further metal binding proteins. This exergonic electron flow is used to build up a proton gradient across the thylakoid membrane which is used by the enzyme ATP-synthase to build ATP from ADP through non-cyclic photophosphorylation. When the electrons reach the lower energy level of the transport chain they balance the missing electrons of the P700 chlorophyll molecules in the reaction center of PSI. This imbalance in electrons is caused by light absorption, analogous to PSII, and a subsequent excitation and transfer of electrons to the primary electron acceptor of PSI, A_0. From here, electrons are transferred to the protein ferredoxin (Fd). The enzyme $NADP^+$-reductase finally

transfers the electrons to $NADP^+$ yielding NADPH. Besides ferredoxin, the electron transport chain involves phylloquinone A_1 and flavoprotein. NADPH is used as reducing agent in the Calvin cycle during sugar synthesis.

Per oxygen molecule built, four electrons are transferred and eight protons are transported across the membrane ($2H^+$ per e^-). About eight photons are absorbed for building two molecules ATP and two molecules NADPH. Besides NADPH, also ATP is used in the following dark reaction for the synthesis of glucose and other sugars.

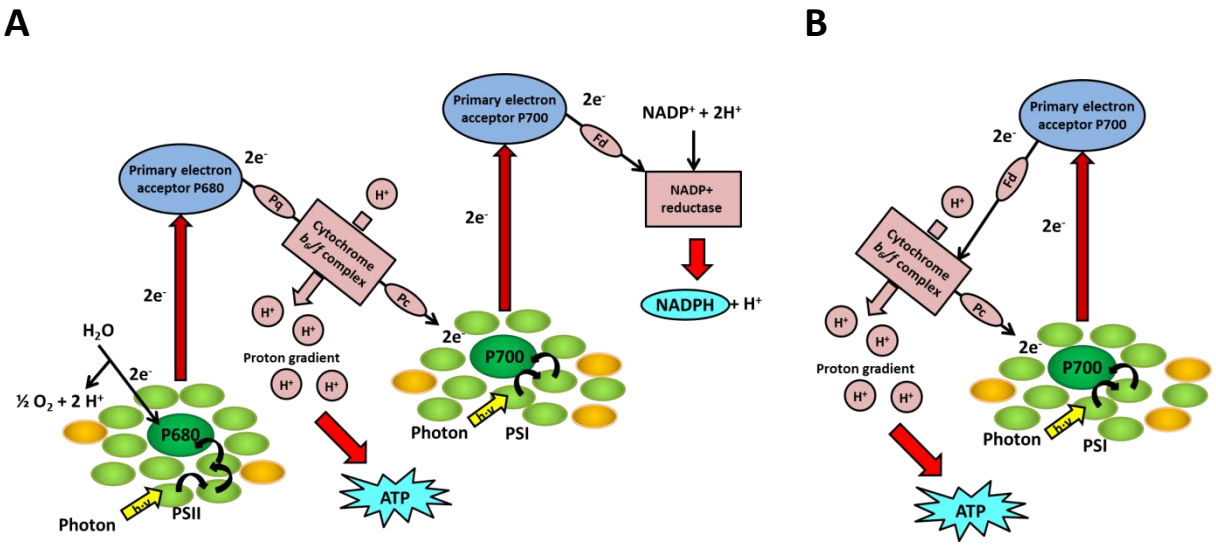

Figure 2-4. Types of electron transport during photosynthesis. A) Non-cyclic or linear electron transport, known as Z-scheme of photosynthesis. Pq: plastoquinone, Pc: plastocyanin, Fd: ferredoxin. B) Cyclic electron transport.

b) Cyclic electron transport

The cyclic electron transport only involves PSI (Figure 2-4 B). The electrons are not transferred to $NADP^+$ but return to the P700 chlorophyll pair using the same transport chain which is also involved in the non-cyclic transport. After excitation the electrons are initially transferred to the primary acceptor A_0 then to the electron transport chain linking PSII and PSI hereby returning to the reaction center of PSI. The cyclic transport represents a kind of short circuit where the excited electrons are continuously returned to P700 along the electron transport chain. This means that there is no net electron transport and no water is split and neither oxygen nor NADPH is produced. This is in contrast to the non-cyclic version. Analogously to the non-cyclic version, the production of ATP is achieved by cyclic photophosphorylation.

It is assumed that the cyclic transport is used for regulation of the ATP-NADPH ratio in the chloroplasts. This is necessary as for the non-cyclic electron transport ATP and NADPH are produced in almost equimolar amount, but the Calvin cycle consumes more ATP than NADPH (ratio of 3:2 is

needed) (Shikanai 2007). The need for ATP and NADPH for anabolic processes is also different for different cellular components like starch or lipids. This additional demand in ATP can be met by a temporarily increased cyclic electron transport. For the cyclic transport one photon has to be absorbed per electron transferred. One proton is transported across the membrane against the gradient and four protons and four photons are needed in total for the building of one molecule ATP. Hence, for both non-cyclic and cyclic transport four photons are needed for one ATP molecule, with the difference that during the non-cyclic transport additionally one molecule of NADPH is produced.

Different assumptions for the regulation and control between cyclic and non-cyclic electron transport exist. As the photosynthetic protein complexes are spatially separated on the thylakoid membrane there seems to be only little influence of each process to the other. The cyclic transport is of constitutive type for CO_2 limitation conditions and increases for high light intensities for photo protection. Otherwise, it is assumed that linear and cyclic transports compete for reducing equivalents where for constant illumination the non-cyclic transport version is favored by the cell because of its higher efficiency. In *Chlamydomonas*, the regulation of cyclic and non-cyclic transport is highly influenced by state transitions in state 2 (see following chapter "optimization of light absorption"). This can be seen as a method to balance different excitation of the two photosystems by a different spectral distribution of the exciting light (Eberhard 2008, Finazzi 2005).

Dark reaction (Calvin cycle)

During the Calvin cycle the stored energy in form of ATP and reducing equivalents produced in the light reaction is used for fixation of carbon from CO_2. The reactions of the Calvin cycle occur inside the stroma of the chloroplast. Basically, the cycle can be divided into three steps (Figure 2-5):

Step 1: Carbon fixation

The enzyme ribulose-1,5-bisphosphate carboxylase/oxygenase (RuBisCO) catalyzes the addition of a CO_2 molecule by covalent bonding to the C5 body ribulose-1,5-bisphosphate (RuBP) resulting in a C6 molecule. This is unstable and disintegrates by hydrolyzing into two molecules of the C3 molecule 3-phosphoglycerate.

Step 2: Reduction

The two molecules 3-phospholgycerate are phosphorylated under consumption of ATP yielding 1,3-bisphosphoglycerate. The pair of electrons transferred to NADPH during light reaction is used for reduction of 1,3-bisphosphoglycerate to glycerinaldehyde-3-phosphate (G3P), hence converting a carboxyl group to an energy richer carbonyl-group. For three molecules of CO_2 six molecules of glyceraldehyde-3-phosphate (G3P) are produced whereas one of these C3 bodies is transferred out of the cycle so that an equal amount of carbon atoms enters and leaves the cycle.

Step 3: Regeneration of RuBP as CO_2 acceptor

In different steps and under ATP consumption the carbon backbones of the remaining five C3-molecules are rearranged that again three molecules of the C5-body RuBP are produced. These are used for addition of three molecules CO_2 in the next round of the cycle.

For the production of one molecule glyceraldehyde-3-phosphate nine ATP and six NADPH molecules are consumed or per CO_2 molecule fixed two NADPH and three ATP. These are provided by the light reaction. Three cycles are needed for the formation of one molecule glyceraldehyde-3-phosphate which is transported into the cytosol of the cell. Glyceraldehyde-3-phosphate leaving the cycle is used as precursor for the synthesis of macromolecules like glucose and starch. In the cytosol glucose is formed by reversal of the first four steps of glycolysis. Glucose can be used for a further formation of sucrose suitable for transport. The remaining glyceraldehyde-3-phosphate inside the chloroplast is converted to starch being a carbon storage form. Starch is stored temporarily during the light period in the form of starch granules in the stroma and inside the plasmatic interior of the chloroplast and can be broken down again during the dark night period.

The enzyme RuBisCO catalyzes the reductive carboxylation reaction, the oxygenation reaction occurs during photorespiration (2.2.2.2). Both reactions hereby compete for the same active center of the enzyme. A so called selectivity factor describes the ratio of both relative enzymatic reaction rates, here carboxylase to oxygenase. For chlorophyta with a type 1B RuBisCO this selectivity factor accounts for 54 to 83% (Giordano 2005). As this is a relatively low affinity for CO_2, local partial pressures of CO_2 and O_2 are decisive. By evolution most microalgae species developed the so called carbon concentrating mechanisms (CCM) which increase the concentration of carbon dioxide in local proximity to RuBisCO in the pyrenoid. Besides the low affinity for CO_2 the enzyme also shows a low conversion rate with about three molecules per second. These are the reasons why big amounts of the enzyme are contained in the chloroplast (RuBisCO accounts for 20 to 50% of the overall cell protein). Low conversion rates hereby result from the fact that the partial pressure of CO_2 is lower than the $K_{m,CO2}$ value (half saturation constant relating to Michaelis-Menten-kinetics). $K_{m,CO2}$ for algae is in the range of 15 to 200 µM (Moroney 2001). For *C. reinhardtii* the ratio of $K_{m,\,CO2}$ photosynthesis to $K_{m,CO2}$ RuBisCO accounts for 1:30 indicating that CCM mechanisms are necessary to improve enzyme kinetics. Relative RuBisCO selectivity accounts for 61 and $K_{m,CO2}$ for 29 µM for this green alga (Badger 1998). Also important is the influence of the ratio of partial pressures of CO_2 and O_2 on the growth and rate of photosynthesis as solubility of gases changes for different pressures which may arise in modules of life support systems in microgravity. Vance and Spalding (2005) came to the conclusion that the ratio of CO_2 to O_2 had no influence on photosynthetic rate and algal growth. They attribute their results to the fact that CCMs in *C. reinhardtii* balanced the increased intracellular O_2 content. Kliphuis and coworkers (2011) came to a contrary result. They measured a decreased growth

rate and biomass yield for a decreased ratio of CO_2/O_2 which they attributed to an increased oxygenase activity of RuBisCO.

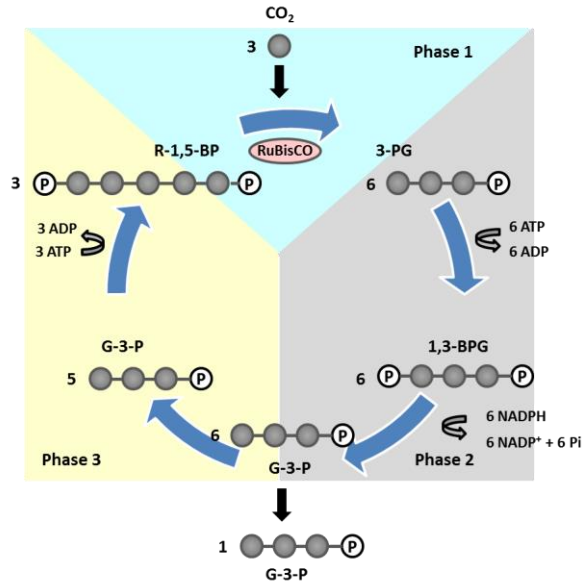

Figure 2-5. Calvin-cycle or dark reaction. R-1,5-BP: ribulose-1,5-bisphosphate; 3-PG: 3-phosphoglycerate; 1,3-BPG: 1,3-bisphosphoglycerate; G-3-P: glyceraldehyde-3-phosphate.

Optimization of light absorption and efficiency on the cellular level

As light energy is not always provided to an optimal extent, photosynthetic organisms have developed several mechanisms on the cellular level to adapt to different lighting conditions. By a dynamic regulation of the light harvesting complexes on the one hand, the efficiency of light absorption is maximized; on the other hand, damages of the photosynthetic apparatus by too much light and resulting reactive oxygen species are minimized. This process is known as photo acclimation and can act in different ways (Stern 2009, Falkowski 1997, Eberhard 2008, Finazzi 2006). There are three types of photo acclimation mechanisms which are distinguished by their time constants: qE-quenching, state transitions (qT), and the regulation of the antenna size. The first two mechanisms, qE-quenching and state transitions are measurable components of the non-photochemical quenching (NPQ) of the fluorescence of the chlorophyll molecule.

qE-quenching is an energy depending, fast quenching process in the range of seconds by means of heat dissipation of an excited chlorophyll molecule. Specific xanthophylls, which belong to the group of carotenoids, like violaxanthin and zeaxanthin as well as the protein PsbS are involved in this regulatory process by responding to a low pH inside the thylakoid lumen (Müller 2001, Dreuw 2005, Demmig-Adams 2006).

A short-term (in the range of minutes), reversible redistribution of the light-harvesting antenna between PS I and PD II is designated as state transition (qT). State transition also belongs to non-

photochemical quenching. It is a mechanism for adaptation of the relative absorption cross sections of PSI and PSII (Finazzi 2002) to changes in the spectral quality of light characterized by a reorganization of the photosynthetic membranes in response to a regulatory kinase sensing the physiological state of a photosynthetic cell (Wollman 2001). This leads to a reorganization of the photosynthetic membranes. The light harvesting antenna of the two photosystems have a different pigment composition whereas PSI contains a bigger part of Chl a and PSII more Chl b molecules resulting in different absorption maxima. As both photosystems are acting in series during photosynthetic electron transport an imbalance in excitation energy would result in relation to the spectral composition of irradiating light and thus in a decrease of the overall yield of light absorption. Hence, state transitions are not only important for avoiding damage through excess excitation energy but also for optimization of absorption efficiency (Wollman 2001). By means of phosphorylation a redistribution of mobile LHCII proteins to PSI and therefore also excitation energy occurs. Two states are existing: linear state 1 and cyclic state 2 whereas for state 1 electron flow is linear, for state 2 cyclic electron flow around PSI is present. The ratio between linear state (1) and cyclic state (2) electron transport is variable. For plants state transitions only play a minor role where about 20% of LHC of PSII is transferred to PSI, but for *C. reinhardtii* state transitions are a very important adaptation mechanism (Müller 2001), where in dependency on growth conditions about 80% of the PSII antenna is transferred to PSI in state 2 (Delosme 1996).

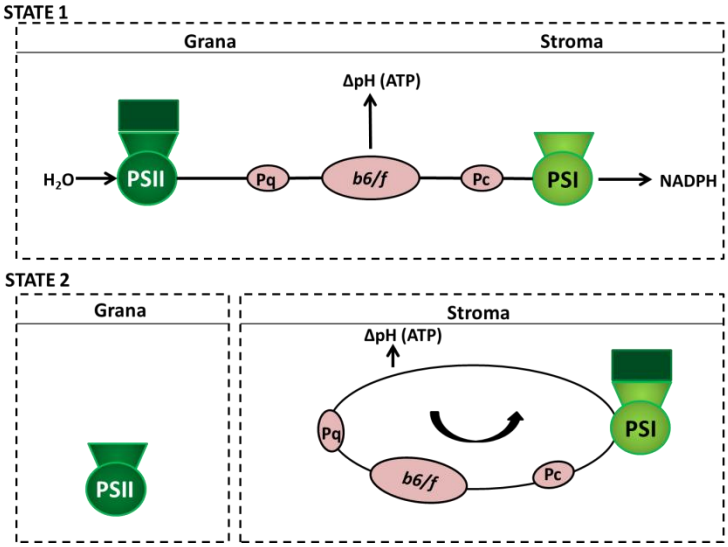

Figure 2-6. State transition as adaptation mechanism to light conditions in *C. reinhardtii*. State 1 and 2 are characterized by two different modes of electron transfer. ΔpH (ATP) indicates ATP generation via a pH gradient across the membrane. Pq, plastoquinone, Pc, plastocyanin, grana: thylakoid grana with PSII membrane domains, stroma: thylakoid stroma lamellae with PSI membrane domains; modified after Finazzi (2002).

For *C. reinhardtii* it was shown that the transition from state 1 to state 2 induces a switch from non-cyclic to cyclic electron flow with a clear cause-effect relationship concerning redistribution of antenna and the switch to cyclic electron flow (Finazzi 2002) (see Figure 2-6). In state 1, PSII and PSI

are functionally connected in the non-cyclic electron transfer mode with NADPH generation and ATP. During transition from state 1 to state 2 there is a redistribution of LHCII (drawn in dark green) from PSII to PSI and the partly migration of b6/f complex from grana to the stroma induces cyclic electron flow around PSI. This mode of electron flow only generates ATP. In *C. reinhardtii* state transitions have the main function to switch the photosynthetic apparatus from the oxygenic type with the two photosystems functionally connected in series with O_2 production and CO_2 fixation to the bacterial type acting as an ATP generator with cyclic electron flow around PSI (Wollman 2001). Hence, the process of state transitions provides high flexibility for the photosynthetic cell.

A third mechanism is the regulation of the antenna size at very high light intensities which is a slower adaptation than the aforementioned ones. Time constants are in the range of hours to days and involve a regulation of transcription and translation during gene expression in cell nucleus as well as chloroplast. Genes coding for proteins involved in the synthesis of light harvesting complexes are involved. This primarily involves the LHCB family, which codes for different chlorophyll binding LHC proteins in the nucleus. The lower the temperature and the CO_2 concentrations a *C. reinhardtii* cell is exposed to, the lower the light intensity triggering a regulation of antenna size. Therefore, it is assumed that excitation energy, CO_2 fixation and the expression of LHC genes are regulated by a negative feedback mechanism (Teramoto 2002). Cells adapted to high light conditions possess a reduced amount of chlorophyll per cell and show an increased Chl a/Chl b ratio compared to cells adapted to low and below saturating light intensities. Both parameters, the specific chlorophyll content per cell and the Chl a to Chl b ratio are indicators for changes on the antenna and the reaction centers of the photosynthetic cells. Relating to a chromatic adaptation of *C. reinhardtii* cells it was shown that this is primarily accomplished by an adjustment of PSI/PSII ratio (Melis 1996).

2.2.2.2 Photorespiration

The enzyme RuBisCO, as mentioned before, also possesses an oxygenase activity which is important for low CO_2 and high O_2 partial pressures. Hence, photorespiration involves the binding of oxygen instead of CO_2 to the enzyme RuBisCO. In contrast to plants, the process only occurs in two organelles, the chloroplast and the mitochondria in *C. reinhardtii*. More than 20% accounts for photorespirative activity of the enzyme in relation to the CO_2 assimilation (Eberhard 2008). In this case ribulose-1,5-bisphosphate is oxidized yielding two molecules glycolate which are transferred out of the Calvin cycle (Figure 2-7 A).

Inside the mitochondria glycolate is oxidized to glyoxylate which is converted to the amino acid glycine (Nakamura 2005). Two molecules of glycine are converted to one molecule serine which is subsequently processed into hydroxypyruvate and through another step into glycerate under consumption of reducing equivalents. Glycerate is transported into the chloroplast where it is phosphorylated yielding 3-phosphoglycerate under ATP consumption. This enters the Calvin-cycle

again (Wingler 2000). Whereas for CO_2 fixation in the Calvin-cycle three ATP and two NADPH molecules are needed, additionally two ATP and one NADPH are necessary to balance the outcomes of the oxygenase activity of RuBisCO. Hence, no additional CO_2 is fixed during the glycolate pathway but only the results of the oxygenase activity are undone under energy consumption.

In contrast to mitochondrial respiration, neither ATP nor NADH is formed during photorespiration (Raven 2005, Stabenau 2005). From an energetic perspective, photorespiration diminishes the efficiency of photosynthesis. However, there is a physiological benefit of photorespiration. It is assumed that the process of photorespiration is a kind of safety valve to get rid of excess energy to avoid damage to the photosystems by photo oxidation processes (Wingler 2000, Kozaki 1996). This can be important for growth under limited conditions, for instance by CO_2 limitation, which could result in an inhibition of the Calvin-cycle resulting in a decreased cellular demand of ATP. But the ATP production rate is dependent on the amount of photons absorbed and hence dependent on light intensity. This situation would result in too much energy built as more ATP is produced than consumed. The flow of energy has to be maintained to prevent photo oxidation damage to the photosystems. To realize this, the continuous provision of ADP and $NADP^+$ is needed. Also from the perspective of evolution, photorespiration can be explained. The enzyme RuBisCO with the specific CO_2 affinity developed through evolution about 2.5 billions of years ago, where CO_2 concentration in the atmosphere was sufficiently high (up to 10% (v/v) assumed) while the O_2 concentration was zero in the first atmosphere where later cyanobacteria developed as first photosynthetic organisms. Slowly, atmospheric oxygen concentration increased with the progressive photosynthetic activity of the first photosynthetic organisms. At this point the catalytic mechanism of RuBisCO was already fixed. By photorespiration it is possible to regain at least a part of the carbon (75%) which would have been lost. As mentioned before, photorespiration can be seen as protective mechanism against reactive oxygen species when the cell is exposed to high light intensities and low intracellular CO_2 concentration (Barsanti 2006).

To ensure a sufficient photosynthetic efficiency even at low CO_2 concentrations, microalgae species have developed different CCMs, as already mentioned before. In order to avoid a carbon limitation in the Calvin-cycle, *C. reinhardtii* possesses an inducible CO_2 concentrating mechanism (CCM). Through an active transport, bicarbonate from the environment is taken up and dehydrated enzymatically to increase the intracellular CO_2 concentration (Spalding 2008). Studies indicate that the expression of CCM-genes is only induced at conditions of CO_2 lower than 0.5% in the gas phase. Additionally, the half saturation constant for CO_2 is reduced under such conditions. At very low CO_2 concentrations, below 0.01%, an additional decrease of maximal photosynthesis velocity was reported (Spalding 2008, Vance 2005). As also the active uptake of bicarbonate consumes energy, this results in a reduction of photosynthetic yield. In photobioreactor cultivations this can be circumvented by a

sufficient supply of CO_2 (Lehr 2009) shifting the activity of RuBisCO to the side of carboxylation which minimizes the amount of photorespiration.

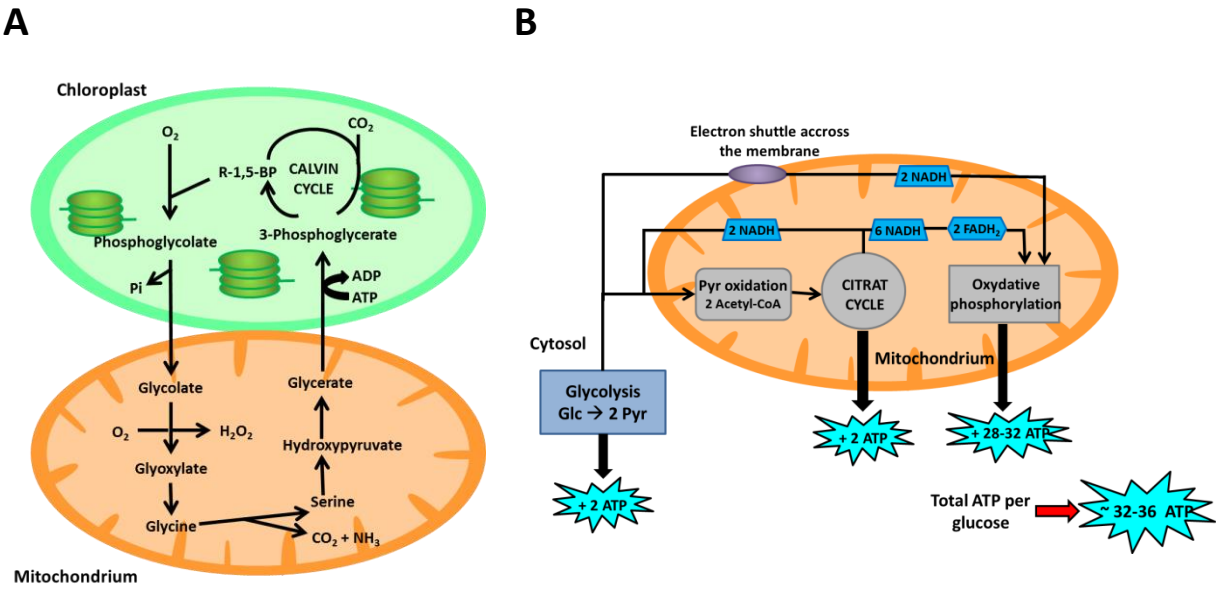

Figure 2-7. Metabolism of *C. reinhardtii*. A) Photorespiration. R-1,5-BP: ribulose-1,5-bisphosphate. B) Respiration. Glc: glucose, Pyr: Pyruvate.

2.2.2.3 Respiration

Only parts of the energy-rich macromolecules built during photosynthesis are used for cellular growth. A big amount of assimilated carbons is used as energy storage. This enables phototrophic organisms for a certain time to proliferate independently from light energy. In such phases, for example during night periods, the metabolism is rearranged in such a way that it resembles the one of heterotrophic organisms. The energy-rich assimilates are dissimilated in catabolic processes under release of energy. Hence, respiration is the counterpart of photosynthesis concerning products and educts. Respiration is based on the overall equation starting from glucose:

Equation 2-5. Dissimilation

$$C_6H_{12}O_6 + 6O_2 + 6H_2O + 32ADP + 32P_i \rightarrow 6CO_2 + 12H_2O + 32ATP$$

Several processes are occurring successively during respiration where sugars and other organic molecules are converted into CO_2 and water. By hydrolysis of storage molecules like starch and sucrose the monosaccharides fructose and glucose are formed. A main process for the breakdown of glucose and all carbohydrates that can be broken down into glucose is the process of glycolysis which is located in the cytosol resulting in the important precursor molecule pyruvate. Alternatively, glucose phosphate can also be degraded via the pentose phosphate pathway yielding pentoses and CO_2. Respiration starts with glucose as C6-body which is split during glycolysis inside the cytosol into two molecules pyruvate (C3-body). Pyruvate is subsequently split inside the mitochondria, via acetyl-CoA

during the citrate-cycle and the respiratory chain finally into CO_2 and H_2O. The respiratory chain consists of a sequence of redox reactions, where electrons of the substrates are transferred finally to oxygen. Analogous to the photosynthetic electron transport, the energy released in those exergonic processes is used to build up a proton gradient across the membrane which is used for ATP synthesis. This is called oxidative phosphorylation (Figure 2-7 B).

As mentioned above, an alternative way is the pentose phosphate pathway, which is preferred during the absence of light and or the growth on acetate as organic carbon source. Glucose-phosphate is split into pentoses (C5 sugars) and CO_2 inside the cytoplasm and the chloroplasts. Important is the provision of NADPH and specific sugar phosphates with three, four, five, six or seven carbon atoms as supply for other biosynthetic pathways (Perez-Garcia 2011).

2.2.2.4 Starch metabolism

Starch is composed of the two polysaccharides amylopectin and amylose. Amylopectin can be built up of up to 10^5 linked glucose molecules with no exact upper threshold for its size. It is the main framework of the starch granule which exhibits a semi-crystalline structure causing its water insolubility. Amylose only makes up 10-30% of starch and has no influence on the structure of the starch granule. Starch granules can be found inside the chloroplast matrix in *C. reinhardtii* cells. At low light intensities and low CO_2 concentration they form a kind of shell around the pyrenoids (Ball 1990). In various steps during starch synthesis, molecules of ADP-glucose are bound by starch synthases to the non-reducing ending of a α-1,4 chain to extend amylopectin and amylose chains. Side chains are formed by hydrolytic cleavage (Harris 2009).

An intensive starch production in *C. reinhardtii* cells occurs under nutrient limitation and therefore in phases of decreasing growth rate (Ball 1990). Remarkable is that under nitrogen limitation a first reduction in photosynthetic activity is initiated, which is measurable as a decreased oxygen production and a decreasing specific chlorophyll content. Starch production and synthesis of lipids is enhanced by the cell. One theory assumes that under nutrient limitation the cells try to avoid an excess energy production by photosynthesis which could lead to cell damage (Juergens 2015). According to Kuchitsu (1988) the starch content of the cells decreases for decreasing CO_2 amounts in the supplied air during cultivations of *C. reinhardtii* where starch in the cytoplasm is degraded. In contrast to that, a shell of starch located around the pyrenoid is accumulated. Studies conducted by Gardner and coworkers (2013) showed that a maximum starch content was measured for cells grown under aeration with 5% CO_2 (v/v) and nitrogen limitation conditions. However, starch was degraded rapidly afterwards within one day. They assumed that after a peak in starch content was reached, cells degrade it again and start the synthesis of lipids, as maximum lipid contents were measured shortly after.

2.2.2.5 Lipid metabolism

Lipids play a major role as constituents of the cellular membrane. In contrast to other organisms, lipids of the plastid membranes in *C. reinhardtii* cells are produced inside the chloroplasts instead of the endoplasmic reticulum (Harris 2009). Triacylglycerides (TAG) are lipids which are not part of the cellular membrane. They are used as storage components for fatty acids and build free fat droplets and oleosomes in the cytoplasm of the cell.

There is only little knowledge on influences on the production of TAG. It is assumed that triacylglycerides are mainly produced when *C. reinhardtii* cells are exposed to various kinds of abiotic stress factors. Phosphate and nitrogen limitation conditions lead to a strong change in lipid composition of the cells. Instead of polar lipids, neutral lipids and TAG are built under limitation conditions whereas under saturated nutrient conditions there is only a low intracellular TAG content (Weers 1997). Another assumption is that there is a relation between TAG production and the autophagic degradation of the chloroplast membrane and the chlorophyll molecules under nitrogen limitation (Davey 2014, Siaut 2011). It is likely that cells exposed to abiotic stress conditions remove polar lipids from the membranes and convert it to neutral storage lipids. A further result was that starch was produced more rapidly than TAG and that an increase of salt concentration in the medium had a positive influence on lipid production (Siaut 2011). Also high light intensities have an influence on lipid production (Harris 2009).

2.3 Requirements and challenges of photobioreactor design for space conditions

The space environment with its specific characteristics requires photobioreactors for microalgae fulfilling certain additional requirements which they do not necessarily have to fulfill on ground. Obstacles or challenges concerning the aspect of designing such a reactor system are the unique environmental factors in outer space like extreme temperatures and temperature changes and low atmospheric pressure. Especially microgravity conditions and consequences like the absence of buoyancy and virtually all convective forces limit design possibilities. Besides, energy supply is limited for a remote system which means in effect that the system has to work in a highly energy-efficient way whereas the microalgae reactor itself should have a yield optimized on volume, time and weight (Klanjscek 2001).

Primarily, microgravity conditions constitute a special challenge for engineering of photobioreactor systems. This relates to the fact that fluids behave differently in space environment which is especially important in case of suspension cultures. Whereas pressure (as hydrostatic pressure) and buoyancy are dominating fluid behavior on Earth, under microgravity physical properties like diffusion, surface tension and Marangoni effects (flow based on differences in surface tension) become dominant (Clément 2006). This also may influence intracellular processes (compare to chapter 2.1.2). Indirect

effects of microgravity are the absence of sedimentation and the gravity-driven convection resulting in the fact that without an external influence on that, slow diffusion processes are the only way for exchange of heat and nutrients, and hence, for mass transport.

Important factors for a stable and safe reactor operation under microgravity conditions are a bubble-free performance, as with the lack of buoyancy, bubbles would remain in suspension and lead to several problems. Details are depicted in chapter 2.3.1. As mentioned before, the lighting technique, the quantity and quality of light are major factors determining the overall energy efficiency of the system. For this work efficient illumination is a major topic and is the focus of chapter 2.3.2.

Besides the absence of gravitational force, a lower pressure or also the absence of pressure is another important environmental factor acting, depending on the housing, on the reactor and its peripheral devices. For instance, during parabolic flights, the ambient pressure may drop down to values around 700 mbar or even lower. This becomes also pivotal thinking of potential production sites for microalgae-based processes in high-altitude regions, which offer a high solar radiation at lower ambient temperature and lowered pressure. Here, pressure lowers per meter altitude whereas for regions at 4000 m altitude ambient pressure accounts for only 600 mbar. But also for photobioreactors at ground level sudden pressure changes resulting from hydrostatical pressure and mixing conditions or peripheral devices like pumps can have effects on algal cells. Details relating to this topic are listed in chapter 2.3.3.

The weight of the bioreactor and the whole system is another decisive issue not that important on ground. This not only concerns the construction as such but the weight of the enclosed water body. Process intensification has to lead to high biomass concentrations and minimization of dark zones which can be further optimized to some extent.

Algae physiology does not have to change during long-term cultivation; that means that for continuous processes a steady-state condition with specific rates has to be maintained for long durations in the range of months. This also implies that possible techniques for re-inoculation are established which allow a new start of cultivation in case of a system failure as a result from severe contamination or technical failure. Concerning long-term stability and contamination, a major question to address in research is the co-cultivation of several algal species or even of the alga with specific contaminants enabling a stable culture with a net oxygen production, avoiding the infection of pathogenic contaminants. Relating to technical failures, being a breakdown of the lighting system or an intermittent shortage in energy, the systems response to these perturbations has to be tested with regard to time constants and a quantitative analysis of system performance after normal conditions have been re-installed and if the system gets back to its original steady-state conditions.

Within this work a special focus is on the topics of bubble-free aeration via membranes, illumination of microalgae in life support systems, pressure reduction and pressure changes as well as long-term stability of cultivations.

2.3.1 Aeration of microalgae for remote applications with membranes

2.3.1.1 Motivation for using membranes for PBR aeration

In the following, characteristics of bubble-free aeration of photobioreactors with the help of membranes are depicted.

One main factor having influence on the overall costs and productivity of microalgal cultivations is the supply with CO_2 (Carvalho 2006, Ferreira 1998, Drexler 2014). There are various types of aeration techniques and devices where the simplest method for aeration of especially large open outdoor systems or shaking flasks on the lab scale consists of the bubble-free surface aeration. Here, carbon dioxide enters the liquid culture via the culture surface being the interface between the gas and liquid phase. A limited mass transport as a result from a limited liquid surface is one big disadvantage of this simple method (Carvalho 2006). For aeration of airlift reactors or bubble columns conventional methods of supplying CO_2 by means of bubble-based aeration techniques are used (Barbosa 2003). In this case, bubbles of air (mostly enriched in CO_2) are also used for mixing of the culture. Aeration rings or spargers are used for bubble-aeration of stirred-tank photobioreactors, where bubbles are dispersed by rotation stirrers of various types. Also porous membranes may be used for bubble-aeration while a certain pressure is applied leading to bubbles entering the culture broth.

Concerning a microalgae photobioreactor for space application where no gravity dependent processes and hence buoyancy are present, it is not feasible to apply a bubble-aeration technique. In this case bubbles would remain in the liquid phase and would coalesce (Colin 2008) and may interfere with measuring devices and also pumps in the periphery. They could even negatively affect cell growth. Furthermore, bubble-aeration techniques, which are conventionally used, contain disadvantages like the loss of CO_2 via the exhaust gas phase, caused by a small residence time of gas bubbles inside the liquid and a high resistance of mass transfer from gas to liquid phase (Heussler 1978). Losses of CO_2 constitute a major cost factor in microalgae cultivations and have to be avoided or at least reduced (Ferreira 1998, Talbot 1991). Cells may also be impaired by the shear stress resulting from bursting gas bubbles at the liquid-gas interface in algal photobioreactors with bubble aeration (Frahm 2007). Also energetic expenses for a gas liquid separation, in case of a bubble-aerated photobioreactor applied in microgravity conditions, would impede the overall efficiency of such a system where maximal energy efficiency is one of the essential characteristics of a life support system module (compare to 2.1.1). As a consequence, it is inevitable to switch to a completely bubble-free aeration technique.

One possible way to accomplish this goal is the aeration via membranes in a purely diffusion-based manner. In this case, no pressure difference is applied and the mass transport of CO_2 is only driven by a concentration gradient. This gradient of different partial pressures of CO_2 exits between the two phases separated by the membrane (see chapter 2.3.1.3). Transport of CO_2 across the membrane is accomplished by pure diffusion. This can avoid the losses of unused CO_2 to the atmosphere and enable an accurate control of the CO_2 transfer rate obtaining the gas directly dissolved in water being available for the cells without the resistance of gas-liquid mass transport (Ferreira 1998). As the liquid and gas phases in the case of diffusion-based membrane aeration are not dispersed into each other, the respective flow rates of both fluids can be set independently of each other without underlying limited operating conditions. The total surface area of the membrane is available even though flow rates of gas and/or liquid might be set to a minimum (Ferreira 1998). The reason why a bubble-free membrane-aeration has been used in mammalian cell cultures for almost 30 years is that sensitive cells, like usually mammalian cells are, profit from a bubble-free aeration technique due to reduced shear forces (Frahm 2009).

2.3.1.2 Classification and selection of suitable materials for aeration of PBRs

Membranes can be classified according to their nature, geometry and separation type (Khulbe 2007). In general, membranes can be classified into homogenous or heterogeneous, symmetric or asymmetric concerning their structure, solid or liquid. Membranes can possess a positive or negative charge; they can be neutral or bipolar. For all membrane types a driving force as a gradient of pressure, or concentration is applied to induce mass transfer across the membrane. Apart from biological membranes which possess many disadvantages like limited operating parameters relating to T, pH, and susceptibility to microbial attacks (Xia 2003), synthetic membranes can be classified into organic (polymeric), inorganic (ceramic, metals) membranes and hybrid forms (Galluci 2011). Silicones possess an intermediate position between inorganic and organic materials because of their inorganic backbone and their organic groups. Inorganic membranes possess a high tolerance to a wide range of pH as well as to chemicals. However, the majority of industrial membranes are polymeric membranes, either natural (e.g. rubber, cellulose) or synthetic polymers (e.g. polyamide, polystyrene, PTFE). Within this work a special focus is on polymeric membranes (especially synthetic polymers) and silicones. An overview of available commercial polymer membrane materials as well as other potential promising polymers for membrane application is published by Ozdemir and coworkers (2006).

By their inner structure, membrane materials can be divided into porous and dense materials where differences for mass transport result (Galluci 2011) (compare to chapter 2.3.1.3). Intermediate forms are composite membranes combining both porous and dense characteristics. These composite membranes are composed of a thin either dense, or very fine microporous, selective layer on a thick porous supporting structure (Mohanty 2011), (Figure 2-8 A).

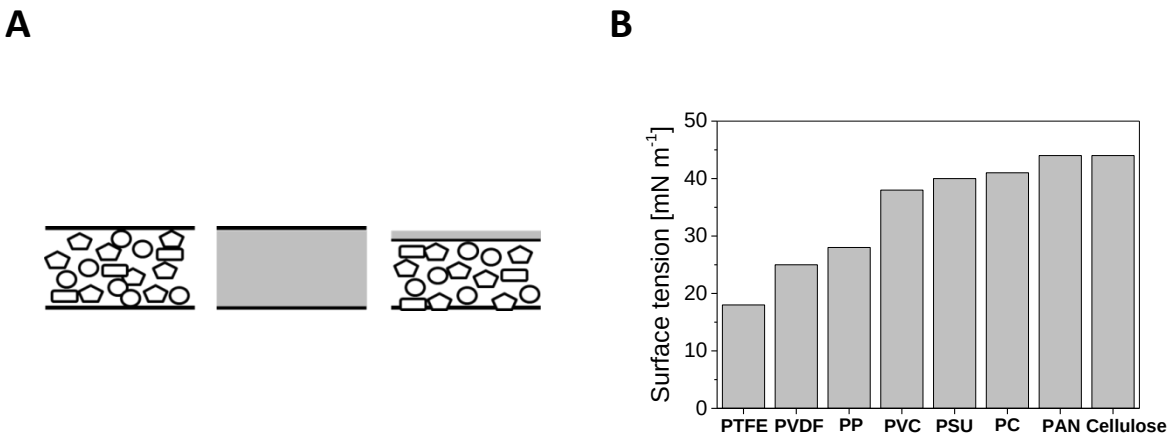

Figure 2-8. Classification and characteristics of membranes. A) Membrane structures; from left to right: isotropic microporous membrane, non-porous dense membrane, thin-film composite anisotropic membrane; modified after Baker (2000). B) Surface tension of certain membrane materials as indicator for hydrophobicity. The higher the value of surface tension, the more hydrophilic the material is. PTFE: polytetrafluoroethylene, PVDF: polyvinylidenefluoride, PP: polypropylene, PVC: polyvinylchloride, PSU: polysulfone, PC: polycarbonate, PAN: polyacrylonitrile; modified after Galluci (2011).

Materials for membrane fabrication can be also classified into either hydrophobic or hydrophilic, according to their tendency to adsorb water, where hydrophobic surfaces repel water and hydrophilic surfaces do readily adsorb water. This is based on the surface tension of the material. Galluci and coworkers (2011) list some surface tension values of certain polymer materials. The higher the value the more hydrophilic the material is. Starting with low surface tension in mN m^{-1} for PTFE, it increases for: polyvinylidenefluoride, polypropylene, polyvinylchloride, polysulfone, polycarbonate, polyacrylonitrile, and cellulose (Figure 2-8 B). Concerning membrane application, surface tension is important for wetting of materials, pressure requirements and in the case of a gas-liquid system and porous membranes the water loss across the system. It is also important for the fouling behavior of a membrane as in general hydrophilic membranes are less prone to fouling.

Relating to the geometry of the membrane, flat sheets, spiral wound, tubular and hollow fiber geometries can be distinguished. Hollow-fiber geometries have the advantage of allowing highest ratios of membrane area to reactor volume (Galluci 2011). Mostly several hollow fibers are arranged into bundles whereas both directions of mass transport are possible and also pressure or vacuum could be applied. For the outside-in configuration there is the general advantage of a higher surface-to-volume ratio then for the inside-out version.

There are various materials from which membranes can be manufactured. These differ in their performance characteristics like mechanical strength, resistance to fouling, hydrophobicity and tolerance towards chemicals and process parameters like pH and T. Common membrane materials used for application in bioreactor aeration are polymers like polytetrafluoroethylene PTFE,

polypropylene PP, polyethylene PE and silicone-elastomers. In general, silicone rubber materials show high permeability to gases (Robb 1968).

Even liquid membranes or micro-encapsulated membranes have been introduced as new concepts (Figoli 2001), particularly as gas separation membranes for the oxygen enrichment in air. For the same purpose, also silicone rubber membranes can be applied as oxygen shows higher permeability than nitrogen in these materials (Robb 1968). Membrane materials can also be functionalized by different functional groups, metal ions or carrier molecules. Examples are liquid membranes with mobile carrier molecules. Traditional oxygen carrier systems are hemoglobin, or metal ion complexes based on nickel, for example (Figoli 2001). Also membranes made of modified polyetheretherketones (for example PEEKWC) are promising for gas separation purposes. Their final morphology, porous or dense, symmetric or asymmetric, depending on their specific application purpose, can be highly controlled during the production process (Buonomenna 2004).

Common parameters influencing the choice of membrane type for reactors are membrane separation selectivity, life time of the membrane, mechanical and chemical stability as well as the costs for the material (Galluci 2011). Membrane materials that are suitable for the application in space photobioreactors should have several important characteristics which are closely related to the design of such a reactor (compare to Figure 2-9). Most important factors are the transparency of the materials, their mechanical stability, and also fouling behavior. Compatibility with sterilizing procedures is also of great importance for such membrane materials.

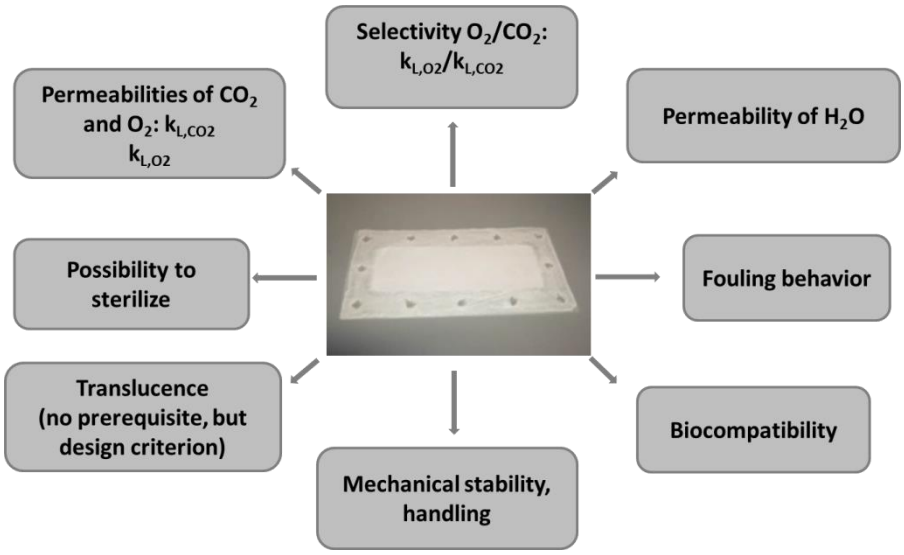

Figure 2-9. Membrane characteristics important for their usage in photobioreactors.

Fouling is one of the biggest problems concerning membrane application in various fields hampering a faster commercialization of membrane technology (Galluci 2011). Membrane fouling is defined as the deposition and accumulation of colloids, solutes, microorganisms and cell debris on the surface of a membrane and/or inside its pores (Meng 2009). Factors influencing the fouling behavior are surface

charge and hydrophobicity of the membrane material, the cell density of the suspension in contact with the membrane as well as the amount and the composition of extracellular polymeric substances (EPS) (Germain 2005) and soluble microbial products (SMP). Interestingly, the degree of fouling may also be influenced by the growth stage of the algae, where exponentially growing cells cause less fouling. Relating to surface charge, membrane materials which are negatively charged may repel negatively charged cells. Only minor fouling is reported for negatively charged hydrophilic membranes (Sun 2013). Drexler and Yeh (2014) conclude in their review that membrane fouling in microalgae reactors is mainly due to cake formation and only to a minor degree by blockage or hydrophobic adhesion of cells. A reduction of membrane fouling during long-term cultivations was achieved by a higher fluid velocity and an additional coating with functional materials like polyvinylalcohol (PVA) (Drexler 2014, Hwang 2013).

Application fields where membranes are used in microalgae technology, besides aeration, are solid/liquid separation (biomass concentration, dewatering, cell retention) and also solute/liquid separation for product recovery and effluent recycling where other techniques cannot be used (Drexler 2014). Also membrane biofilm reactors are used (Galluci 2011). Other application fields of membranes possibly interesting for life support systems are desalination of water (for instance with PVDF hollow-fibers) (Simone 2014), for removal of water from gas streams with ECTFE (ethylene-chlorotrifluoroethylene copolymer) membranes (Drioli 2014) which could be used for dehumidification of PBR exhaust gas streams.

Concerning membrane material selection the first research within this work was focused on the use of membranes in artificial lungs, as the gases concerned, O_2 and CO_2, are also of primary interest for PBR aeration (only reverse direction of mass transport) and more publications are available. Common materials used for artificial lungs (blood oxygenators) are usually in the form of hollow fibers and mostly composed of hydrophobic polymers like PP but also silicones (Federspiel 2014, Bartlett 2005). Polypropylene (PP), PVDF and silicon-based polymeric membranes (e.g. polyvinyltrimethylsilane PVTMS) are examples for common membrane materials used for gas exchange in microalgae technology (Drexler 2014). However, concerning these approaches one should clearly distinguish between approaches using pressure differences creating small bubbles (Fan 2008, Cheng 2006) and concentration difference driven processes where the operation is bubble-free. For microalgae modules applied in space life support systems, approaches with bubble-free diffusion-based membrane aeration should be favored relating to energy efficiency and the absence of buoyancy.

2.3.1.3 Theory of mass transfer with membranes

For assessment of membrane aeration for photobioreactors and the design of membrane area and geometry, principles of mass transfer with membranes have to be collected. Mass transfer is defined as movement of mass from one location to another. The two main types of mass transfer are convection

and diffusion. In this work the diffusion-based aeration of photobioreactors is in focus of research. In the case of a membrane-aerated PBR the membrane acts as interface between gas and liquid phase which both have different concentrations of (dissolved) gases. These concentration gradients act as driving force for the movement of the substance from one phase to the other (Burghardt 2010).

Diffusion and convection

Diffusion is defined as movement of a chemical compound in a fluid mixture based on a random molecular mixing process as consequence of a thermal agitation of molecules which finally leads to homogenization of the mixture. Velocity of diffusion is fastest in gases (with around 5 cm min^{-1}), followed by diffusion in liquids (0.05 cm min^{-1}) and slowest in solids (10^{-5} cm min^{-1}) (Cussler 2009, Burghardt 2010). Diffusion is slowed down by molecular collisions whereas the distance between two collisions for a diffusing molecule in a gas phase is called *mean free path* (see also "Differences of mass transfer in porous and dense membranes") which accounts for 10^{-5} cm (Burghardt 2010). These are reasons for the positive effect of an increased temperature (increased mean molecular velocities, Brownian motion) and the negative effect of high pressures (higher concentration of molecules and more collisions) on the rate of diffusion.

Convection is usually a more rapid process; here, a compound is not only transported by Brownian motion, but by a macroscopic movement, for instance agitation or by currents of fluid resulting of temperature differences.

At the interphase between two phases the velocity of flow is zero (no-slip condition) as a result there is no convection within the boundary layer. Hence, mass transfer is only based on diffusion within that zone and can be mathematically explained by Ficks law and the two film model.

Ficks law

Ficks law relates the diffusive flux J to a concentration gradient while assuming steady-state conditions. It defines that the flux goes from regions of high concentration to regions of low concentration, whereas the magnitude of flux is proportional to the concentration gradient. The following equation describes the one-dimensional flux:

Equation 2-6. Ficks first law for one-dimensional diffusional flux J.

$$J_a = -D_{ab} \cdot \frac{dc_a}{dz}$$

with:

J_a – diffusional flux of substance A [mol m^{-2} s^{-1}]

D_{ab} – diffusion coefficient of A through B [m^2 s^{-1}]

dc_a/dz – concentration gradient along the axis of diffusion [mol m^{-3} m^{-1}]

The negative sign emphasizes that diffusion occurs in the direction of a drop in concentration.

Two film theory

The two film theory is a theoretical model describing mass transfer across an interphase. Several assumptions are underlying this theory. It is assumed that there are two laminar layers, (in this case a liquid film and a gas film), which are formed on both sides of the fluidic interface. The flux of molecules that occurs across the liquid and gas films is driven by the concentration gradient (ΔC) across each layer or film between bulk phase and interface.

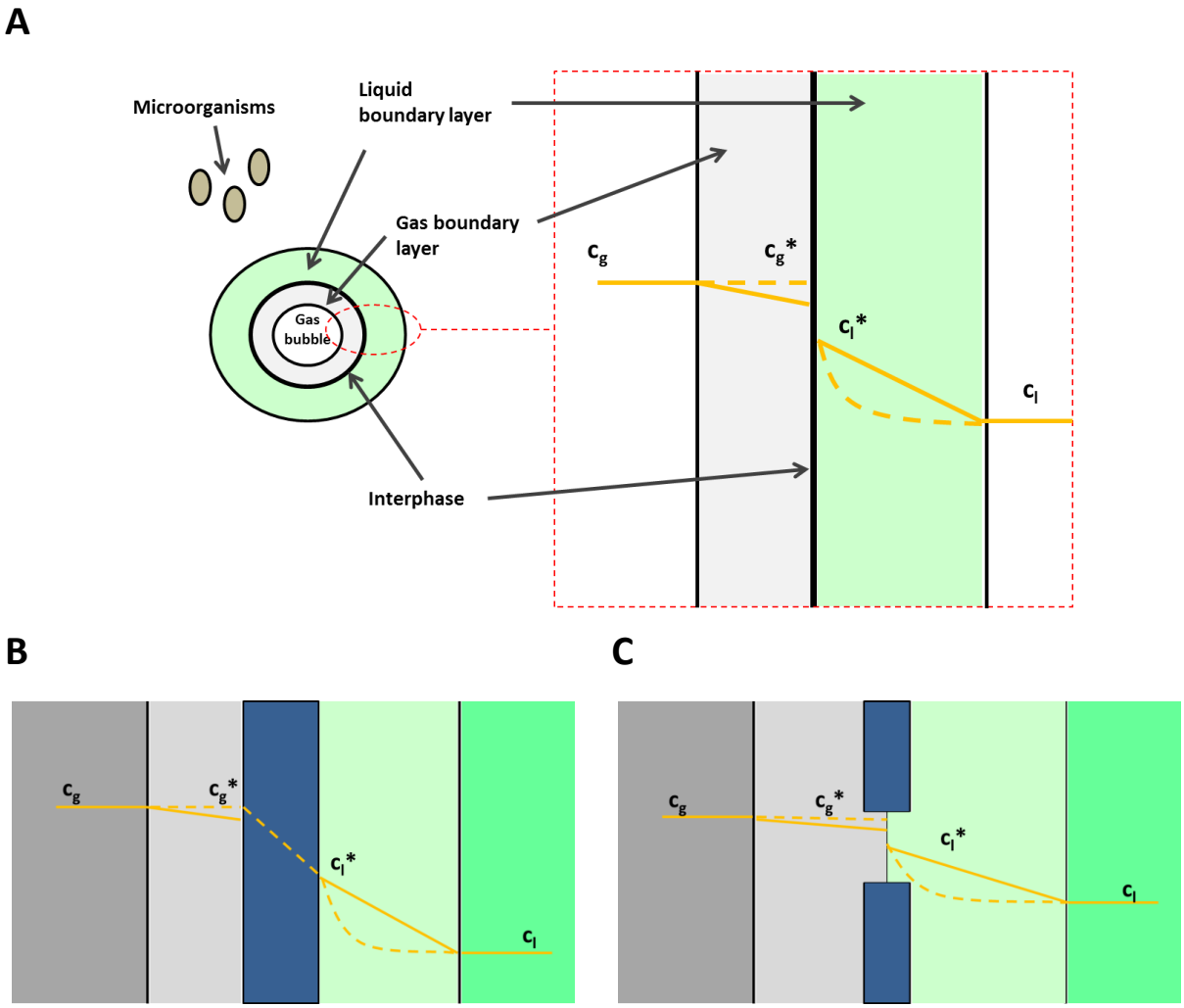

Figure 2-10. Mass transfer at interphases described by the two-film theory. A) Mass transfer of a gas component from a gas bubble to the liquid bulk phase in case of bubble aeration of a bioreactor. Direction of mass transfer along the concentration gradient is from gas to liquid phase. Dashed lines indicate the realistic concentration course; modified after Chmiel (2011). B) Mass transfer of a gas component from the gas phase across a dense membrane to the liquid bulk phase. The gas component is dissolved in the membrane material. C) Mass transfer of a gas component from the gas bulk phase to the liquid bulk phase in case of a porous membrane.

It is assumed that the resistance to transfer through the interface occurs in the thin stagnant films, also called laminar boundary layers, where transport of molecules is only driven by diffusion, and no convective motion is present. The two film theory is based on assuming that the concentration of the gas in the liquid at the interface and the concentration of the gas in the gaseous phase are in equilibrium (i.e. saturation). The equilibrium relationship is described by Henry´s law. In the bulk stream of both gas and liquid the concentrations are assumed to be constant by mixing. In the case of bubble aeration, the two-film theory can be applied for description of mass transfer for a gas component from a gas bubble to the liquid phase (Figure 2-10 A). Also for bubble-free aeration with membranes this theory can be used (Figure 2-10 B and C).

As diffusion in gases is much faster than in the liquid, the boundary layer on the gas side can be neglected and $c_g = c_g^*$. At the interphase therefore the following equations for the fluxes can be applied:

Equation 2-7. Flux on the gas side of the interface.

$$J = -K_g \cdot \left(c_g - c_g^*\right)$$

Equation 2-8. Flux on the liquid side of the interface.

$$J = -K_l \cdot \left(c_l^* - c_l\right)$$

with:

J – Mass flux [mol m^{-2} s^{-1}]

K_g – overall mass transfer coefficient on the gas side [m s^{-1}]

K_l – overall mass transfer coefficient on the liquid side [m s^{-1}]

c_g^*, c_l^* – equilibrium concentrations at interphase for gas and liquid [mol m^{-3}]

c_g, c_l – bulk concentrations in gas and liquid phase [mol m^{-3}]

The driving force of mass transfer is the concentration gradient. The overall resistance coefficient for mass transfer 1/K is defined as:

Equation 2-9. Overall mass transfer resistance as sum of single resistances.

$$\frac{1}{K} = \frac{1}{K_g} + \frac{1}{K_l}$$

1/K incorporates all resistances for mass transfer across an interphase. By using Henry's law equilibrium concentrations can be calculated from bulk concentration with a known Henry coefficient for a certain temperature and at pressures close to atmospheric pressure:

Equation 2-10. Equilibrium conditions at interface.

$$H \cdot c_g = c_l^*$$

Henry's law

At the interphase between a gas and a liquid there is an exchange of gas molecules by diffusion between gas and liquid phase. The entry of gas molecules into the solution is proportional to the partial pressure of the gas and the exit is proportional to the concentration of the gas in the solution. This is defined by Henry's law:

Equation 2-11. Henry's law.

$$H_x = \frac{c_x}{p_x}$$

with:

H_x – Henry coefficient for component x [mol m^{-3} Pa^{-1}].

The overall liquid mass transfer resistance is composed of:

Equation 2-12. Liquid mass transfer resistance

$$\frac{1}{K_L} = \frac{1}{k_l} + \frac{1}{H \cdot k_g}$$

For the overall gas mass transfer coefficient it can be written:

Equation 2-13. Gas mass transfer resistance

$$\frac{1}{K_G} = \frac{1}{k_g} + \frac{H}{k_l}$$

For soluble gases, such as CO_2 and O_2, Henry coefficients are much larger than one. Moreover, values of k_g are larger than k_l as gas diffusion is much faster than diffusion in the liquid and gas boundary layer is smaller than the liquid analogue. Because of that it can be written (Ferreira 1998):

Equation 2-14. Simplified mass transfer resistance

$$\frac{1}{K_L} = \frac{1}{k_L}$$

This suggests that mainly all the resistance to interfacial mass transfer of soluble gases lies in the liquid-film at the interface (Chisti 1989).

For the case of membranes, an additional mass transfer resistance for the membrane material is introduced (Côté 1988):

Equation 2-15. Overall resistance for mass transfer across membranes

$$\frac{1}{K_L} = \frac{1}{k_L} + \frac{1}{k_M}$$

Mass transfer coefficients that were measured during this work are the coefficients summarizing resistances of liquid boundary layer and membrane material, as it is more difficult to isolate the resistance of the membrane itself by the testing procedure.

Differences of mass transfer in porous and dense membranes

For dense and porous membranes there are differences in mass transport mechanisms. For porous membranes, mass transport is dependent on membrane properties and different transport mechanisms can be distinguished (Galluci 2011):

- Poiseuille mechanism: average d_{pore} > average free path of fluid
- Knudsen mechanism: average d_{pore} ~ average free path of fluid
- Surface diffusion: permeating molecule is adsorbed on pore wall
- Capillary condensation: permeating molecule condenses inside a pore due to capillary forces
- Multi-layer diffusion: for strong molecule-surface interactions
- Molecular sieving: for very small pore diameters, only very small molecules permeate

For porous membranes, there are also differences for hydrophobic and hydrophilic materials relating to a gas liquid separation and the gas liquid interface. In case of porous membranes, gas and liquid are in direct contact. For hydrophobic materials the interface between gas and liquid interface will be built more towards the liquid side inside a pore whereas for hydrophilic materials the interface is shifted towards the gas side. This implies that the pores are either primarily filled with gas or liquid respectively (compare to Figure 2-11).

Hence, for porous membranes, gas and liquid interphase are in contact to each other, where Henry's law can be applied in equilibrium (Figure 2-10 C). It is important for the application of porous

membranes for a bubble-free aeration that the *bubble-point* of the membrane is not reached. The *bubble-point* defines the Δp above which gas bubbles are formed and detach from the pores of the membrane. For example, in case of a PP membrane (thickness of 400 µm) with a pore size of 0.3 µm a bubble-point of 13 mbar Δp is reported (Aunins 1993).

In case of dense membranes, mass transport is based on a solution-diffusion mechanism. This process consists of several sub stages, involving the adsorption of the gas molecule to the membrane surface, the dissolution of the molecule into the material matrix, diffusion inside the membrane material along a gradient toward the other side, desorption of the molecule on the liquid side and dissolution in the liquid phase.

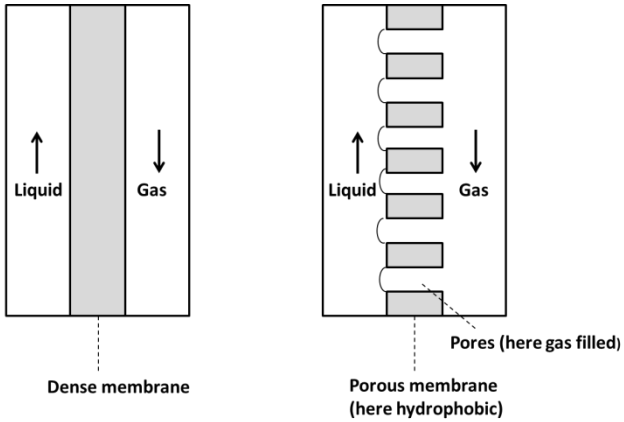

Figure 2-11. Dense and porous membranes in mass transfer from gas to liquid. Difference between dense and porous membranes relating to mass transfer across gas liquid interphases.

Mass transfer through membranes applied for gas exchange in photobioreactors

For a photobioreactor aerated via membranes the gas phase with a specific composition is separated from the liquid phase by the membrane. The two gases of interest for gas exchange in a microalgae reactor are CO_2 and O_2. As for CO_2 and water there is a chemical reaction influencing dissolved gas concentration, this has to be considered for assessment of CO_2 supply via membranes for photobioreactors.

CO_2 system

The mass transfer of CO_2 across the gas/liquid interface can be described by a dynamic equilibrium reaction. Two opposing gas transfer processes, CO_2 absorption and stripping occur continuously and simultaneously (Shanableh 2007) (Figure 2-12 B). A dynamic equilibrium is reached when both rates are equal. CO_2 dissolves into water establishing equilibrium between the dissolved CO_2 and H_2CO_3, carbonic acid, followed by the dissociation of carbonic acid as weak acid in two steps:

Equation 2-16. Dissociation of carbonic acid as equilibrium reaction.

$$CO_2 + H_2O \leftrightarrow H_2CO_3$$

$$H_2CO_3 + H_2O \leftrightarrow H_3O^+ + HCO_3^-$$

$$HCO_3^- + H_2O \leftrightarrow H_3O^+ + CO_3^{2-}$$

In equilibrium the amount of each of the CO_2 species is dependent on the actual pH. This dependency, called Bjerrum plot, is shown in Figure 2-12 A.

According to Shanableh (2007) the general model for CO_2 transfer (Equation 2-17) from gas phase to liquid phase is only valid when the initial pH does not change. They also calculated the contribution of each of the carbon species to the total flux of CO_2 across the gas-liquid interphase.

Besides the work of Shanableh (2007) also Ferreira and coworkers (1998) have developed mathematical models for simulating a dynamic equilibrium for CO_2 transfer from the gas to the liquid phase. Concerning CO_2 uptake, *C. reinhardtii* is able to consume both CO_2 and HCO_3^- (Moroney 2001) whereas especially the latter one is actively transported across the plasmalemma. However, CO_2 is the preferred species of dissolved inorganic carbon.

Modeling of mass transfer for membrane aeration of photobioreactors

Mass transfer equations based on their respective mass transfer coefficients and based on Fick's law of diffusion and the two-film theory with Henry's law can be set up. In case of CO_2 the transfer rate (CTR, carbon dioxide transfer rate) across the membrane is given by:

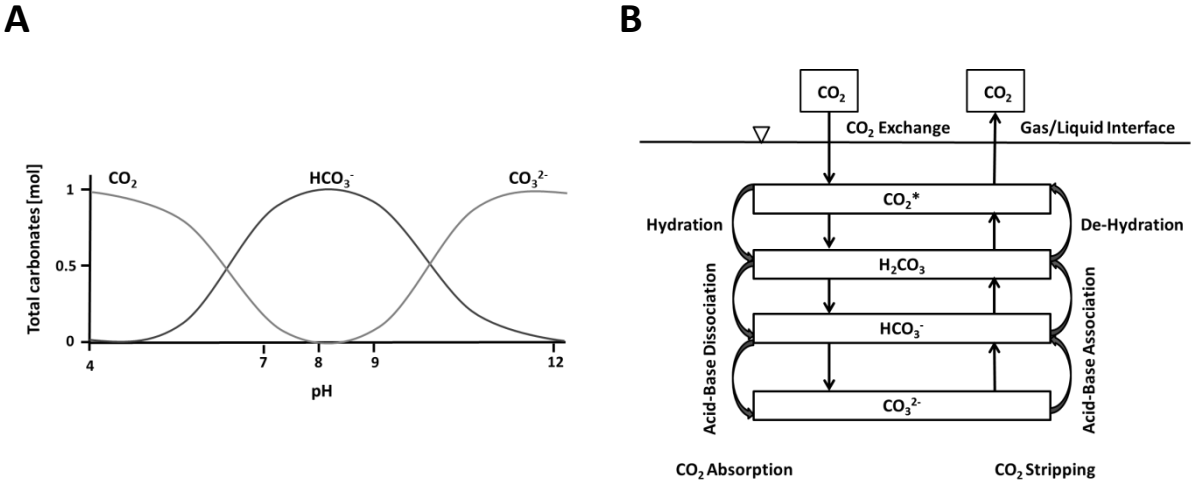

Figure 2-12. Carbonate system and CO_2 transfer across a gas-liquid interphase. A) Bjerrum plot showing pH dependent concentrations of carbonate species; modified after Lindsay (1979). B) CO_2 transfer across a gas-liquid interphase; modified after Shanableh (2007).

Equation 2-17. Carbon dioxide transfer rate across a membrane for diffusion-based aeration.

$$CTR = J_{CO2} = k_{L,CO2} \cdot a \cdot \left(c^*_{CO2} - c_{L,CO2}\right)$$

With:

CTR – carbon dioxide transfer rate [mol CO_2 m^{-3} s^{-1}]

J_{CO2} – flux of CO_2 across the membrane, analogously to Fick's law [mol CO_2 m^{-3} s^{-1}]

$k_{L,CO2}$ – CO_2 mass transfer coefficient [m s^{-1}]

a – specific transfer area [m^{-1}]

c^*_{CO2} – CO_2 concentration at interphase in equilibrium [mol m^{-3}]

$c_{L,CO2}$ – CO_2 concentration in bulk liquid phase [mol m^{-3}]

($c^*_{CO2} - c_{L,CO2}$) – concentration gradient acting as driving force [mol m^{-3}]

$k_{L,CO2}$, as a constant, in this case represents the mass transfer coefficient for CO_2 related to resistance for mass transport of the membrane and the boundary layer on the liquid side (resistance by the boundary layer on the gas side can be neglected), (Ferreira 1998). OTR, the oxygen transport rate is calculated in an analogous manner.

In almost all publications the mass transfer of gases across membranes is calculated as permeability P, often expressed in Barrers [cm^3 s^{-1} cm^{-1} $cmHg^{-1}$], being defined as quotient of diffusion coefficient D [cm^2 s^{-1}] and Henry-coefficient or the product from diffusion coefficient and solubility S (cm^3 cm^{-3} $cmHg^{-1}$) (Robb 1968):

Equation 2-18. Permeability in relation to diffusivity and Henry coefficient.

$$P = \frac{D}{H}$$

Equation 2-19. Permeability in relation to diffusivity and solubility.

$$P = D \cdot S$$

Permeability is a function of temperature and pressure.

During this work mass transfer with membranes is compared and quantified in terms of mass transfer coefficients k_L.

The value of $c_{L,CO2}$ (Equation 2-17) can be measured constantly with a sensor inside the liquid phase of the PBR. The value of c^*_{CO2} represents the concentration at the interface. The value for the

concentration of the gas in the gas phase will change along with the length of the reactor in the case of a horizontal setup due to the mass transfer between liquid and gas phase as shown in Figure 2-13 A analogously for bubble aeration, where also the overall pressure changes when a gas bubble rises from the bottom of a reactor to the gas-liquid interphase.

A

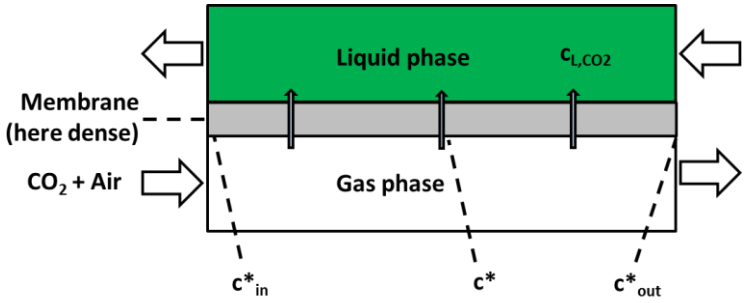

B

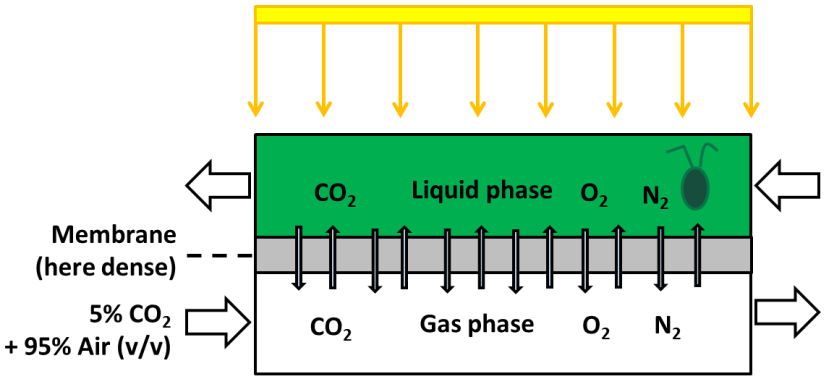

Figure 2-13. Application of membranes for aeration of photobioreactors. A) Logarithmic mean concentration difference of a gas component, here CO_2, for calculation of gas transfer in a membrane-aerated photobioreactor. Membrane and reactor are in horizontal orientation. B) Mass transfer of gases across the membrane, CO_2 and O_2, in an illuminated photobioreactor with a certain inlet gas concentration and a horizontally mounted membrane.

For this reason, the driving force (c^*_{CO2} - $c_{L,CO2}$) is calculated as logarithmic mean concentration gradient as shown in Equation 2-20 (Storhas 1994):

Equation 2-20. Mean logarithmic concentration difference for calculation of gas transfer.

$$(c^*_{CO2} - c_{L,CO2}) = \Delta(c_{CO2})_M = \frac{\left(c^*_{CO2}\right)_{in} - \left(c^*_{CO2}\right)_{out}}{\ln\left(\frac{\left(c^*_{CO2}\right)_{in} - c_{L,CO2}}{\left(c^*_{CO2}\right)_{out} - c_{L,CO2}}\right)}$$

Accordingly, CTR can be calculated as follows:

Equation 2-21. CTR calculation with mean logarithmic concentration difference.

$$CTR = k_{L,CO2} \cdot a \cdot \Delta\left(c_{CO2}\right)_M$$

This logarithmic mean concentration difference is especially important for calculation of transfer rates in case of hollow fiber membranes, where there is a long distance concerning membrane surface important for the gas transfer.

Selectivity of a membrane

An essential parameter for a long-term bubble-free phototrophic cultivation is the selectivity α (-) of a membrane towards gases. In this case it can be expressed via the mass transfer coefficients for gas A and gas B (determined under exactly the same testing parameters) by the following equation:

Equation 2-22. Selectivity of a membrane for gases A and B.

$$\alpha_{A/B} = \frac{k_{L,gasA}}{k_{L,gasB}}$$

An important principle relating to the topic of selectivity of a membrane is the so called "upper-bound" relationship (Figoli 2001, Robeson 2008). This principle was formulated for the membrane separation of gases, published in 1991 and was shown for various gas pairs (O_2/CO_2, however, is not mentioned). It describes the fact, that the separation factor in general decreases with increasing permeability of the faster permeating gas for a pair of gases to be separated. This relationship is related to an upper bound relationship where the log of the separation factor plotted against the log of the permeability of the gas faster permeating yields a limit for polymeric membranes while it was revealed that the diffusion coefficient decided the upper bound limits.

In general, dense membranes, where mass transport is governed by dissolution of the gas component in the material matrix, are considered to be advantageous concerning the selective transport of O_2 against CO_2. For silicone rubber, solubilities and diffusion rates were investigated by Robb in 1968. Here, diffusion rates for O_2 account for $1.6 \cdot 10^{-5}$ cm^2 s^{-1} and $1.1 \cdot 10^{-5}$ cm^2 s^{-1} for CO_2. The molecular diameter is also affecting diffusion in dense membranes, where CO_2 with almost 3.2 Å has a higher molecular diameter than O_2 with 2.9 Å (Robb 1968). The Lennard-Jones constant of the gases seems to be important for solubilities of gases in materials. Permeability is reported to be the product of diffusion rate and solubility whereas a 5-fold higher permeability of CO_2 than for O_2 is reported in dimethyl silicone rubber (Robb 1968).

Some properties of silicone towards CO_2, O_2 and N_2 are listed in the following table:

Table 2-2. Characteristics of silicone relating to mass transport of gases, according to Aunins (1993) and Robb (1968).

Parameter	O_2	N_2	CO_2
Permeability coefficient P [kg m/(s m² N/m²)]	$6.4 \cdot 10^{-15}$	$2.6 \cdot 10^{-15}$	$4.8 \cdot 10^{-14}$
Diffusion coefficient D [m²/s]	$1.6 \cdot 10^{-9}$	$1.5 \cdot 10^{-9}$	$1.1 \cdot 10^{-9}$
Henry-coefficient H [N/m²/(kg/m³)]	$2.5 \cdot 10^{5}$	$5.77 \cdot 10^{5}$	$2.29 \cdot 10^{4}$

There is also literature on solubilities of oxygen in water and organic liquids, where high solubility of oxygen is reported for diethylether (Fischer 1922). Important to note is that a transmembrane pressure was applied for the tests and mass transport was not purely based on concentration gradients acting as driving force. Also Lund and coworkers (2002) used a pressure gradient for permeability measurements for hollow fiber membranes. According to Robb (1968) in these times no direct diffusion measurements of gases in silicone rubber have been published which makes it difficult to compare own values quantitatively.

CO_2 uptake and oxygen production rate

From the biological side, the carbon dioxide uptake rate (CUR) by the cells has to be described and quantified. From the stoichiometry of photosynthesis, it is known that 1 mol of CO_2 is converted to 1 mol of O_2, resulting in CUR = OPR in molar terms. CUR is a physiological characteristic of the culture which is limited by the metabolic activity of the microalgae. This, in turn is limited by photosynthesis and therefore light intensity. With the elementary biomass composition and the carbon content of the biomass, the CO_2 uptake rate is directly coupled to the biomass production rate.

Equation 2-23. Carbon dioxide uptake rate in relation to specific CO_2 uptake and biomass concentration.

$$CUR = q_{CO2} \cdot c_X$$

With:

q_{CO2} – specific CO_2 uptake rate [mol CO_2 g^{-1} CDW h^{-1}]

c_X – cell concentration [g L^{-1}]

μ – specific growth rate [h^{-1}]

$Y_{X/CO2}$ – yield coefficient biomass from CO_2 [g CDW mol^{-1} CO_2]

Equation 2-24. Specific CO_2 uptake rate in relation to specific growth rate and Yield coefficient.

$$q_{CO2} = \frac{\mu}{Y_{X/CO2}}$$

For algae species, rich in carbohydrates (> 40% of dry weight), like *Chlorella vulgaris* and *Chlamydomonas reinhardtii* (John 2011), the CO_2 requirement is about 1.7 up to 2.5 g CO_2 per g biomass produced.

For *C. reinhardtii*, q_{CO2} has a value of 0.117 mol CO_2 kg^{-1} CDW s^{-1} with a stoichiometric CO_2 requirement of 1.85 g CO_2 per g biomass and a biomass production rate of 1 g L^{-1} d^{-1} during exponential growth (data not published).

The amount of CO_2 that has to be transported via the membrane finally depends on the illumination intensity to the culture. Typical values of CTR for artificially illuminated reactors are in the range of 2 g L^{-1} d^{-1} (data not published).

Determination of CUR is accomplished for the case when the CTR is known, in case of bubble-free membrane aeration with the following formula and based on the accumulation term dc_{CO2}/dt according to Garcia-Ochoa (2010):

Equation 2-25. Calculation of CUR when CTR is known

$$CUR = k_{L,CO2} \cdot a \cdot \left(c^*_{CO2} - c_{L,CO2}\right) - \left(\frac{dc_{CO2}}{dt}\right)$$

In case of a quasi-stationary operation, the membrane area-to-volume ratio a can be calculated from CTR − CUR = 0 and depends, in turn, on the mass transfer coefficient $k_{L,M}$ of the membrane.

Equation 2-26. Specific membrane transfer area as area-to-volume ratio.

$$a = \frac{A}{V} = \frac{CTR}{k_{L,M} \cdot \left(c^* - c_L\right)}$$

As for porous membranes the main resistance for mass transfer is on the liquid side, for calculation of specific transfer area the total membrane surface A is considered, rather than just the area covered by the pores (membrane porosity multiplied by membrane area), (Fereirra 1998).

By using hollow-fiber modules highest values of specific membrane transfer areas can be achieved. For hollow fiber modules applied for gas exchange in photobioreactors specific areas of 0.83 cm^{-1} (Farges 2012) up to 2.53 cm^{-1} (Ferreira 1998) are reported. For their space PBR concept, Cogne and

coworkers (2005) used a flat sheet membrane and a specific area of 0.15 cm^{-1}. Concerning blood oxygenators and artificial lungs specific areas of 28 cm^{-1} are applied, whereas lung alveoli area accounts for 290 cm^{-1} (Federspiel 2014).

The CTR and OTR are also influenced by factors relating to reactor design, most important, membrane material, porosity, selectivity of the material for O_2/CO_2, specific transfer area a, and also to culture conditions such as bulk liquid velocity (thickness of boundary layer), salinity, and viscosity of the medium as well as culture temperature.

2.3.1.4 Solubility of gases in liquids and bubble formation

As phototrophic growth of the algae involves the production of oxygen, the removal of the produced oxygen is another very important aspect (Ferreira 1998). The accumulation of dissolved oxygen and an increase in dO_2 concentrations may lead to inhibition of photosynthesis (Rubio 1999, Fan 2008) and may provoke bubble formation by oversaturation. Relating to the latter aspect, a critical factor is the relatively low solubility of oxygen in water, around 8 mg L^{-1} at 25°C with air atmosphere.

Table 2-3. Solubility of gases in water at 1.013 bar (1 atm) in mg kg^{-1} water.
According to Storhas (1994).

Gas \ T [°C]	25	30	35
O_2	39.31	35.86	33.15
N_2	17.34	16.14	14.93
CO_2	1453	1263	1104
Air-O_2	8.23	7.51	6.94

For the saturation concentration with relation to Henry's law there is a dynamic equilibrium between both directions of diffusion, where the saturation concentration is proportional to the partial pressure in the gas phase. The constant of proportionality is termed solubility, or solubility coefficient. Solubility of gases in liquids decreases with increasing temperature, higher salt concentration and in general a high amount of dissolved solids. Only for very high pressures there is no proportional relation between gas pressure and equilibrium concentration any more. Hence, major environmental factors influencing solubility are pressure and temperature. According to Henry´s law, the mass of a gas dissolved in a liquid at a constant temperature is proportional to the total pressure exerted on the solvent. Therefore, when the pressure on a given volume of water increases, the capacity of that volume of water to hold the dissolved gas also increases (Weitkamp and Katz 1980). Pressure is increased in water by hydrostatic head according to equation:

Equation 2-27. Hydrostatic pressure.

$$p_{hydrostat} = \rho \cdot g \cdot h$$

Where $p_{hydrostat}$ is the hydrostatic pressure [kg m^{-1} s^{-2}], ρ is the density of the liquid [kg m^{-3}], g is the gravitational constant [9.81 m s^{-2}] and h is the depth in the fluid at which the pressure is measured [m] (Giancoli and Boyle 2005). Hydrostatic pressure increases rapidly with depth, greatly increasing the capacity of deeper water to hold dissolved gas as compared to shallow water. The capacity of water to hold dissolved gas is inversely related to temperature (Weitkamp and Katz 1980) (Table 2-3).

Bubbles can be formed whenever there is a supersaturation with respect to total dissolved gas. Gas supersaturation occurs when the total dissolved gas pressure (TDG) exceeds the local solution pressure. The total dissolved gas pressure is determined by the summation of the aqueous gas partial pressures including the partial pressure of water vapor:

Equation 2-28. Definition of supersaturation as prerequisite for bubble formation.

$$(TDG = pN_2 + pO_2 + pCO_2 + pAr + pH_2O) > p_{local}$$

In such circumstances the water is termed “supersaturated” with respect to total dissolved gas (Scardina 2004). In other words, the total oversaturation is defined as a condition where the sum of the partial pressures of all dissolved gases including the water vapor pressure (TDG = total dissolved gas pressure) is greater than the mechanical pressure (atmospheric pressure plus hydrostatic pressure) at the site of bubble formation. Dissolved gas supersaturation can be a result from chemical, mechanical, or microbial processes (Scardina 2002). Following the supersaturation of a dissolved gas, similar to the growth of crystals, a nucleation step follows prior to bubble formation. Bubble formation is regarded as a diffusion-controlled process (Hey 1994) and two types of nucleation have to be distinguished (Scardina 2001, Scardina 2004):

- Homogeneous nucleation (*de novo* nucleation)
- Heterogeneous nucleation

In the case of homogenous nucleation, also called *de novo* nucleation, bubble formation is spontaneous and random, but only occurs under very harsh conditions, when the difference between dissolved gas pressure and ambient pressure is higher than 100 atm (Harvey 1975). Hence, this type of bubble nucleation is very rare. The second type, heterogeneous nucleation, starts at nucleation sites, being surface imperfections or particles (also algae cells) and also from pre-existing gas pockets in cavities. The gas diffuses into those already existing gas pockets, which leads to bubble growth and detachment from the solid surface. For this type of nucleation only less dissolved gas supersaturation is required and therefore it can occur whenever a water based liquid is supersaturated (Hey 1994).

Factors influencing the size and the number of bubbles are the degree of supersaturation, the viscosity of the solution (Hey 1994), and the number of nucleation sites which is positively influenced by surface active agents (Jackson 1994), the hydrophobicity and smoothness of surfaces, whereas rough hydrophobic surfaces lead to an increased number of bubbles even for low supersaturations (Ryan 1998, Hey 1994). Increasing gas supersaturation positively affects bubble formation by generating more bubbles from previously dormant nucleation sites as well as an increased mixing intensity or in general a higher energy input into the system (Jackson 1994, Scardina 2001). An increased temperature also leads to more bubble formation (as Henry's coefficients are reduced) and faster diffusion kinetics (Hikita 1984).

After the nucleation of bubbles a new equilibrium is installed by diffusion of other dissolved gases to that newly formed gas volume. At this new interphase there is diffusion in both directions of all dissolved gases. Hence, oxygen in the case of a phototrophic cultivations is the driver for supersaturation, but the volume of gases also includes N_2 and CO_2 besides O_2 (Scardina 2001). There are no gas bubbles which only contain one gas species for atmospheric conditions. This is in contrast to the building of crystals from a mixture of salts in solution. Moreover, a gas bubble, once formed can only grow bigger, when there is a positive balance of diffusion into the gas bubble.

By using mass balancing for gas volumes and surrounding liquid supersaturated with a dissolved gas, the formation of bubble volumes can be modeled. Important is that also the partial pressure of water vapor is considered. In a detailed model, also dissociation of dCO_2 in relation to pH is considered. The ideal gas law can be used for this model as deviations from using the real gas law only account for 0.4% (Scardina 2001). Another influencing factor is the aforementioned ambient pressure of the site of bubble formation. For detachment of bubbles from a surface the angle of contact is important (Lubetkin 1989).

Scardina (2001, 2004) developed an apparatus to validate model predictions and to physically measure the total volume of gas developed after acidification of a water body and supersaturation with CO_2. Crucial for model prediction of experimental results was an accurate measurement of atmospheric pressure, as this factor has a big influence on the resulting bubble volume. However, model prediction of bubble formation provided accurate results.

According to Stumm (1981) the equilibrium for the system of a liquid where bubbles have been formed can be calculated by using conventional equations for all equilibriums, partial pressures, and mass balance equations for nitrogen, oxygen and carbon dioxide (nitrogen and argon are normally lumped together because both are biologically inert gases):

Equation 2-29. Bubble atmosphere and solution equilibrium.

$$[O_2]_{aq} = k_{O2} \cdot pO_2$$

$$[N_2]_{aq} = k_{N2} \cdot pN_2$$

$$[CO_2]_{aq} = k_{CO2} \cdot pCO_2$$

where $[O_2]_{aq}$, $[N_2]_{aq}$ and $[CO_2]_{aq}$ are the concentrations of the respective dissolved gases [M]; pO_2, pN_2 and pCO_2 are the partial pressures in gaseous state [atm] and k is Henry´s law constant [M atm^{-1}].

Once bubbles are formed, the sum of bubble partial pressures will be:

Equation 2-30. Calculation of bubble partial pressures:

$$pO_2 = (p_b - p_{wv}) \cdot \frac{O_{2(g)}}{O_{2(g)} + N_{2(g)} + CO_{2(g)}}$$

$$pN_2 = (p_b - p_{wv}) \cdot \frac{N_{2(g)}}{O_{2(g)} + N_{2(g)} + CO_{2(g)}}$$

$$pCO_2 = (p_b - p_{wv}) \cdot \frac{CO_{2(g)}}{O_{2(g)} + N_{2(g)} + CO_{2(g)}}$$

where $O_{2(g)}$, $N_{2(g)}$ and $CO_{2(g)}$ are the amounts of respective gas in gaseous state [mol]; p_b is the total pressure of gases within the bubble (assumed atmospheric pressure) [atm] and p_{wv} is the water vapor total pressure [atm].

Dissolved gases from the liquid diffuse into the bubble in gaseous form, therefore, the gaseous mass balance will be:

Equation 2-31. Mass balances for gases after bubble formation.

$$p_{atm}(\%O_2) \cdot k_{O2} \cdot V = [O_2]_{aq} \cdot V + O_2$$

$$p_{atm}(\%N_2) \cdot k_{N2} \cdot V = [N_2]_{aq} \cdot V + N_2$$

$$p_{atm}(\%CO_2) \cdot k_{CO2} + Alk - \frac{K_{HCO3^-} \cdot [CO_2]_{aq}}{[H^+]} = [CO_2]_{aq} + \frac{CO_2}{V}$$

where p_{atm} is the atmospheric pressure [atm]; $\%O_2$, $\%CO_2$ and $\%N_2$ are the normal percentages occurring in atmospheric air; V is the solution volume (assume 1 L) [L]; Alk is the bicarbonate

alkalinity [M]; K_{HCO3-} is the first acid dissociation constant for bicarbonate; and $[H^+]$ is the hydrogen ion concentration [M]. After solving the system of equations listed above, the ideal gas law can then be used to calculate the total volume of bubbles formed at equilibrium. The ideal gas law was used, since calculations indicated that use of the real gas law only alters predictions by less than 0.4% under water conditions:

Equation 2-32. Calculation of total bubble volume with ideal gas law.

$$p \cdot V_g = n \cdot R \cdot T$$

$$p = p_b - p_{wv}$$

$$n = O_{2(g)} + N_{2(g)} + CO_{2(g)}$$

$$\frac{p_{wv}}{p_b} = \frac{V_{wv}}{V_b}$$

$$V_b = V_{wv} + V_g$$

where V_g is the bubble volume from aqueous dissolved gases; R is the ideal gas law constant; V_{wv} is the bubble volume from water vapor; and V_b is the total bubble volume (Scardina 2001).

For modeling bubble formation various simplifications can be made on the basis of physics (Kostoglou 2007):

- Thermal and mass diffusivity are two orders of magnitude larger in the gas phase of the bubble than in the surrounding liquid. For this reason transient and convection effects can be ignored inside the bubble compared to the liquid.
- The density and thermal conductivity of the bubble gas are negligibly smaller in comparison with those of the liquid.
- Thermodynamic equilibrium is assumed at the interface with the assumption of an ideal mixture.

Bubble formation is mainly divided into two stages, the expansion/growth of the bubble (when the surface forces dominate) and the detachment (when buoyancy forces dominate). In cases of multiple bubbles generation, a coalescence step usually precedes the detachment. The buoyancy forces in the detachment process are very low in the case of small bubbles, and the larger the bubbles are, the higher the buoyancy force gets (Kulkarni 2005). Under microgravity conditions the buoyancy force is reduced and therefore bubbles will grow larger and will stay longer on the nucleation surface (Qiu 2002).

In order to establish a bubble-free gas exchange for cultivation of phototrophic cells, a suitable reactor design, with a certain specific geometry of the membrane and a high selectivity for O_2 related to CO_2 is needed. A possible solution is the application of different membranes for the supply of CO_2 and the removal of oxygen with different mass transport coefficients for the two gases. Besides, an exact monitoring of total dissolved gas (TDG) pressure inside the liquid phase with the help of a saturometer is advisable.

2.3.1.5 New membrane materials and concepts to solve selectivity problems and avoid bubble formation during PBR cultivations

In order to achieve higher selectivities for oxygen toward CO_2 new membrane materials or approaches relating to functionalized membranes are in the focus. Promising examples are chitosan-based membranes where metal ions can be added to increase O_2/CO_2 selectivity. Chitosan membranes can also be produced in hollow-fiber form (Mirmohseni 2012) and various others (Elwakeel 2010) with good mechanical strength. Concerning its O_2/CO_2 selectivity a promising study was published by Bai and coworkers (1988). Chitosan-acetic acid polymer membranes where functionalized with metal ions and values of $\alpha_{O2/CO2}$ of around 30 were achieved with Ni ions.

Another example are liquid membranes with mobile carrier molecules (Figoli 2001) where a dual-mode transport mechanism makes it possible to uncouple flux from driving force, resulting in appreciable oxygen fluxes at very low driving forces (Petropoulos 1970, Paul 1976). This could be beneficial for avoiding oversaturation by enabling O_2 removal at very early stages of cultivation and thus low driving forces where DO concentrations are still close to starting concentrations and therefore very small partial pressure gradients between liquid and gas phase adjacent to the membrane.

Sawdon and Peng (2015) used perfluorocarbon (PFC) emulsions for oxygen entrapment in tubular photobioreactors, as during cultivations high oxygen concentrations are monitored in the liquid phase which inhibit photosynthesis of microalgae. These PFC emulsions were used as gas-carrier vehicles and thereby decreased DO concentration from 47% to 4% during cultivation.

Further enhancement of solubility and selectivity of silicone elastomers regarding oxygen should also be in the focus of research for membranes applicable for bubble-free aeration of photobioreactors.

2.3.1.6 Application examples of membranes for aeration of bioreactors

This subchapter summarizes the application of membranes for bubble-free aeration of bioreactors and particularly photobioreactors. Furthermore, some concepts for membrane-based photobioreactors for space application are displayed. More details of the mentioned concepts are collected and reviewed in Wagner (2015).

Membranes have been used for aeration in bioreactors for cultivation of shear-sensitive mammalian cells since the end of the 1980s. Membranes for aeration of animal cell cultures are mainly applied in

the form of hollow-fiber modules as well as tubular membranes (Frahm 2009, Côté 1988 and 1989, Ahmed 1992 a, b, Lehmann 1987) either directly placed inside the bioreactor (Vorlop and Lehmann 1988, Frahm 2007) or outside, in the periphery (Schneider 1995). Materials often used were polypropylene, silicone, and PTFE. In some approaches (Vorlop and Lehmann 1988, Frahm 2007) the membrane fibers were also moved with the help of a motor in order to increase turbulence on the membrane surface for an enhanced mass transfer. In general, the specific membrane area was used as a scale-up factor.

However, transfer of the elaborated membrane technology from heterotrophic cultures to phototrophic cultures is challenging. Although mass transfer rates are similar between animal cell and microalgal culture, the directions of oxygen and carbon dioxide transfer are reversed. As oxygen is less soluble in water than CO_2 (see 2.3.1.4) this may lead to problems concerning oversaturation and consequent bubble formation.

Membrane-aerated photobioreactors

Also for cultivation of phototrophic microorganisms membranes have been used for a bubble-free aeration, although more approaches based on using pressure differences across the membranes creating small bubbles have been reported so far (Fan 2008, Cheng 2006). In the following work, these approaches will not be further discussed as they do not seem to be suitable for space application.

Detailed experiments by Lee and Hing (1989) focused on the use of silicone tubing to supply *Chlorella pyrenoidosa* cultures with CO_2 inside an airtight stirred-tank reactor. Different surface areas and partial pressures of CO_2 (in air) were tested, whereas the membrane tubing was coiled inside the reactor. They measured maximal CO_2 accumulation in the liquid under cell-free conditions when a maximal specific surface area of the membrane was used. They also used pure CO_2 during cultivation which reached a peak concentration at small biomass concentrations of 100 mbar (10 % v/v) dissolved CO_2 in the liquid. This did not result in an inhibition of cell growth. For maximal cell densities of around 2.6 g L^{-1} during the end of the cultivation the dissolved CO_2 concentration in the culture medium was almost constant around 1 % pCO_2.They emphasize the advantage of bubble-free aeration with membrane tubing compared to conventional bubble-aeration that the CTR can be actively controlled (at a chosen membrane geometry) by adjusting partial pressure on the gas side. The maximum and minimum CTR can be chosen by selecting specific membrane tubing geometries. By selecting appropriate geometries and partial pressures it is even possible to use pure CO_2. This makes it possible to avoid high investment costs for gas mixing in larger scales without being concerned with inhibition at elevated dissolved carbon dioxide concentrations.

A review about the use of hydrophobic microporous membranes for aeration of photobioreactors is provided by Ferreira and coworkers (1998). One of their potential applications is the CO_2 supply in

photobioreactors for microalgae cultivation. The pores of hydrophobic porous membranes are filled with gas and the resistance of the membrane to the mass transfer can be neglected in comparison to the resistance of the liquid phase. Problems that can arise are pressure drops, laminar flows, and obstruction by solid particles in the liquid by using long fibers with small diameter to meet the needs of mass transfer related to reactor working volume. They also attribute the major resistance for the mass transfer for gases such as O_2 and CO_2 to the liquid phase. However, in their study both systems tested were open to the atmosphere which makes it difficult to monitor the dissolved gas concentrations in this case and therefore compare the different setups.

A comparison of plain bubbling against aeration by hollow-fiber modules (hydrophobic polypropylene fibers, as well as hydrophilic polysulfone fibers) was also conducted by Carvalho and Malcata (2001) for transfer of CO_2 into microalgal cultures. For aeration with membrane hollow fibers, higher k_La values were determined than for plain bubbling. Besides, they also mentioned further advantages of using membrane modules for aeration like the possibility of circulating the gases and using lower gas pressures and thereby reducing the overall process costs.

Membrane-aerated photobioreactors for space

Also in the field of space application and research on life support systems concepts for bubble-free membrane-aerated photobioreactors have already been described by various authors (Cogne 2005, Ai 2008, Farges 2012). A more detailed description of these approaches is reviewed in Wagner (2015).

Cogne and coworkers (2005) designed a closed membrane-aerated photobioreactor and implemented it for batch cultivation of the cyanobacterium *Arthrospira platensis*. By designing and using a model they are able to predict biomass and pressure during space cultivations within that novel photobioreactor. Until now, this reactor has not yet been used in parabolic flight tests or satellite missions under long-term microgravity conditions. The reactor is composed of a cylindrical chamber with a flat sheet membrane separating the gas and liquid compartments. A porous 0.2 µm PTFE membrane (thickness of 60 µm) with a surface area of 20 cm² is used for gas exchange. One possible drawback of using porous membranes is the increased permeability to water vapor, compared to dense membranes, which may lead to volume variations as well as bubble formation on the liquid culture side. Sensors for OD, pH, T as well as pressure are integrated in the system. A magnetic stirrer, situated on top of the membrane surface, is used for mixing. For process control O_2 production was measured indirectly as pressure increased within the gas chamber. After a certain threshold pressure (1.5 bar absolute pressure) was reached, the gas chamber was flushed with N_2 after releasing the overpressure. Gas bubbles were observed on the liquid side of the reactors since the first hours of process time. They were able to correlate pressure in the gas phase with biomass concentration in the linear phase of the cultivation and detected a faster pressure increase after each N_2 flushing as a higher driving force generated a temporarily higher mass transfer. This membrane-aerated PBR concept for

space application represents a preliminary system that can be used for the development of a final system applicable for cultivations under microgravity conditions.

Ai and coworkers (2008) developed and tested another ground-based photobioreactor for CELSSs with the cyanobacterium *Arthrospira platensis*. Here, in contrast to the approach by Cogne (2005), the exchange of gases was accomplished with separate hollow fiber modules for CO_2 (porous polyethylene fibers) and O_2 (PTFE fibers) respectively, that are integrated in the bypass system where a diaphragm pump is used for circulation. In dependence on the actual pH of the medium, the CO_2 module is either flushed with pure CO_2 (if pH > 9.5) or the flushing is stopped completely (if pH < 8.0). In this approach O_2 removal is accomplished by using a lowered pressure to increase mass transport of the oxygen produced through the membrane. Above DO concentrations of 10 mg L^{-1} the vacuum pump is switched on and below 6.0 mg L^{-1} it is switched off again. During cultivation, the temperature of the medium was kept between 28 and 32°C; at this temperature the saturation concentration for O_2 is 7.5 mg L^{-1} for 30°C and air oxygen concentration (having the atmospheric concentration of gases dissolved in the medium). As the upper threshold for control was 10 mg L^{-1} there is a risk of oversaturation with oxygen and a potential formation of bubbles. However, the authors do not mention if bubble formation was monitored during testing. As a pressure difference (lowered pressure) was applied for O_2 removal, this approach by Ai and coworkers was not purely based on a concentration difference acting as the driving force for mass transfer.

A third concept based on a hollow-fiber PTFE module was proposed by Farges and coworkers (2012). A hollow-fiber membrane contactor consisting of microporous hydrophobic membranes is used for gas exchange. This module was used in preliminary tests for mass transfer coefficients for CO_2 without cells.

A similar concept was introduced by Brechignac and Schiller (1992). An external gas exchange module consisting of hydrophobic membrane fibers (polypropylene) is a central part of their approach. Interestingly, they also proposed a very different, second option for liquid-gas separation under microgravity conditions based on a cylindrical bioreactor with an axially rotating paddle. This generates a fluid layer of cell suspension on the inside of the bioreactor and would allow a conventional bubble aeration of the culture.

Another photobioreactor primarily designed and implemented for CELSSs is described by Javanmardian and Palsson (1992). Experiments, both in batch and continuous mode, were run with *C. vulgaris*. The separate gas exchange for O_2 and CO_2 is realized by external hollow-fiber cartridges operating under reduced (in case of O_2 removal) and increased (for supply of CO_2) pressure. So, this approach is not purely diffusion-based. During steady-state conditions of continuous *Chlorella* cultures ($c_X = 4 \cdot 10^8$ cells ml^{-1}, D = 0.15 d^{-1}) volumetric OPRs accounted for 5 mmol O_2 L^{-1} h^{-1}. Based

on these production rates a volume of 200 L is needed to support the O_2 requirement of one human being.

A similar concept is also proposed by Oguchi and coworkers (1989) based on a membrane module for *Spirulina* cultures with an integrated biomass harvesting system operating in semi-continuous mode. Two fiber modules (porous, hydrophobic PP, pores 0.04 µm) are integrated in the bypass system: one for CO_2 supply, the second for O_2 removal with connection to a continuously running vacuum pump.

The concept of Mori (1989) is relying on one hollow-fiber membrane module (porous PP membranes) for gas exchange of CO_2 and O_2. The gas phase used was a mixture of CO_2, O_2 and N_2 with varying composition in relation to dissolved CO_2 and O_2 concentrations on the liquid side. An optimal growth and gas exchange of the system was achieved with volumetric CO_2 and O_2 concentrations of 10% respectively.

So far, no results from parabolic flight campaigns or satellite tests with these membrane-aerated photobioreactor concepts have yet been published.

2.3.1.7 Consequences for potential bubble-free membrane aeration of microalgae-photobioreactors for remote/spaceflight application

As a summary, there are only a few approaches reported that rely on a mass transfer that is purely diffusion-based; the vast majority of concepts with membranes for aeration of photobioreactors for space application relies on pressure difference. The concept proposed by Cogne and coworkers (2005) is relying on diffusion; however, bubbles have been formed in an early stage of the cultivation. This indicates that some additional important factors have to be reflected for the realization of a long-term bubble-free cultivation based on membranes for aeration.

A crucial factor is the selectivity of the membrane for the two gases of interest CO_2 and O_2, whereas selectivity factors should be higher for O_2 in relation to CO_2. This is in accordance to the stoichiometry of photosynthesis and the different solubilities of these gases in the liquid. Additional factors are a suitable specific transfer area and partial pressures on the gas side that contribute to a bubble-free membrane aeration of microalgae reactors also for long-term cultivations.

2.3.2 Illumination of microalgae for remote applications

As mentioned earlier in chapter 2.1, maximal efficiency in regards to energy is a major criterion of a successful implementation of a module within a life support system. This implies that algae are grown in a very energy-efficient way. Both on a technical and on a biological level, the transfer of energy has to be at its optimum. In this work special focus is put on the optimization of light to biomass conversion. Relating to this, there are several ways to approach this goal by process design or genetic engineering. To achieve this optimal energy conversion, widespread problematic effects playing a role for outdoor ground cultivations (like light reflection or adsorption of cells to reactor walls and

technical devices) have to be completely avoided. Lighting is a major aspect relating to energy efficiency of such a system. The question how and in what quantity and quality light is provided for a photosynthetic organism to achieve maximum energy efficiency and stability is essential. Concerning a suitable light intensity range, dependencies of intensity and growth rate have to be regarded for the chosen alga.

2.3.2.1 Light kinetics and photo conversion efficiency

Figure 2-14 A represents a typical curve for light kinetics of microalgae with three characteristic ranges:

I) The phase of photolimitation is characterized by a linear increase of photosynthesis rate as specific growth rate with increasing irradiance. Above the compensation point I_c a first photosynthetic activity can be measured, where cell maintenance equals photosynthesis. The optimal point is defined by I_k where only little further increase of photosynthesis rate can be achieved with increasing light intensity.

II) A constant maximum photosynthesis rate characterizes the phase of photosaturation, where the efficiency of photons decreases because not every absorbed photon is used for CO_2-fixation as a consequence of limited RuBisCO fixation and capacity of electron transport chain. An excess of energy is dissipated as heat during non-photochemical quenching NPQ.

III) The phase of photoinhibition is characterized by a decreasing photosynthesis rate with increasing irradiance (beyond I_h). In this phase the production of photo-protective pigments like carotenoids is induced. The degree of photoinhibition is depending on intensity and duration of light exposure. However, microalgae are capable of adaption to low and high-light conditions by photoacclimation.

In dependence on photobioreactor geometry and lighting system, light intensity is different in different zones of the reactor and average growth rates are obtained by integration along the light path.

An important factor determining the efficiency of a microalgae-based module in a life supporting system is the efficiency with which light energy can be converted into biomass. This yield parameter is termed photo conversion efficiency, PCE. This comparative parameter also takes into account anabolic reactions, following the process of photosynthesis, which is in contrast to the regularly used photosynthesis efficiency, PE. The photo conversion efficiency PCE [J/J] is the yield describing the efficiency with which absorbed light is converted into biomass (Equation 2-33):

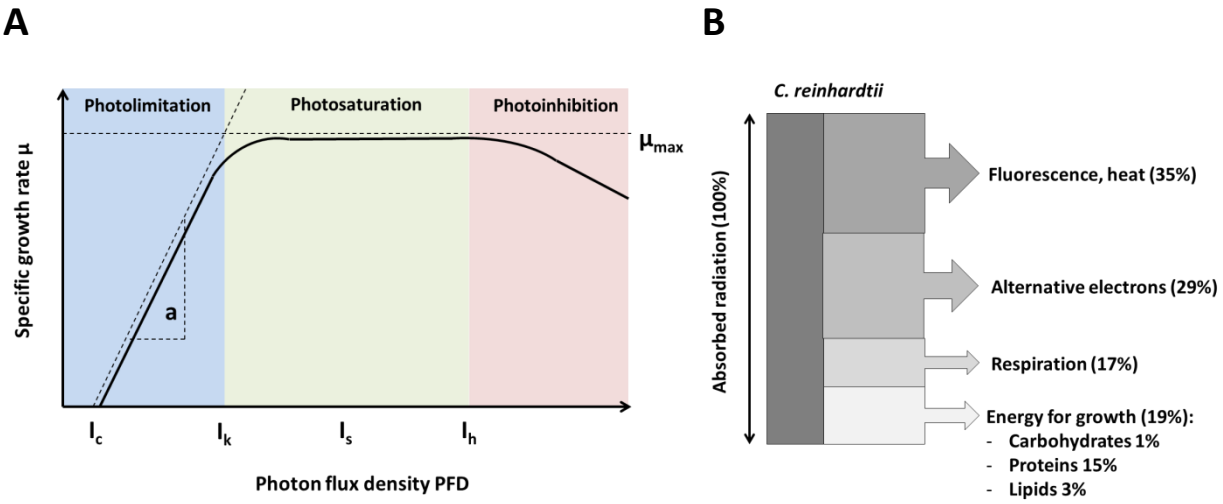

Figure 2-14. Light kinetics and conversion efficiency of photosynthesis. A) Typical light kinetics for microalgae. a: slope of curve in light limited range, I_c: compensation irradiance, I_k: transition point between light limited and light saturated growth as optimal intensity, I_s: saturating irradiance, I_h: inhibiting irradiance. B) Energy balance from photon to biomass for *C. reinhardtii* under chemostat conditions with light irradiance at I_k; according to Posten (2012).

Equation 2-33. Photo conversion efficiency

$$PCE = \frac{H_B}{I}$$

With:

H_B - Biomass heat of combustion [J]; with h_B as specific algae biomass heat of combustion [J kg^{-1}] being around 20 MJ/kg (Lehr 2009, Schaub 2007)

I - absorbed light energy [J]

Maximum theoretical PCE values are reported to be around 9% for microalgae under white illumination, whereas higher plants only achieve efficiencies around 4-6% (Zhu 2008).

For pure red illumination at 680 nm an energetic yield of 24% from photon to glucose conversion is achieved, based on the assumption that 10 photons per mol glucose are needed. As glucose is metabolized by the cells, another 30-40% reduction of this yield has to be included leading to a gross yield of around 15 to 17%.

Figure 2-14 B illustrates a balance for light energy to biomass conversion in the case of a continuous culture (chemostat, enabling optimal cultivation conditions) of the green alga *C. reinhardtii* illuminated with an optimal light intensity I_k. Here a value of 19% is given for the highest possible bound energy in the cells being the upper biological limit.

2.3.2.2 Quantum energy of wavelengths and theoretical maximum of conversion yields

For 100% absorption of radiation, 35% of energy is lost by dissipation in form of heat and fluorescence (Figure 2-14 B). This loss could be reduced by using mutant strains with reduced antenna sizes. Further losses relate to the quantum energy of photons in dependence on their energy content U (Figure 2-15 A): highly energetic photons, for example from the blue range, lead to NPQ to get rid of excess energy avoiding damage to the photosynthetic apparatus. Another 29% is lost by alternative electrons which are losses within the photosynthetic process itself, for instance during CO_2-fixation. Losses caused by respiration account for 17% and can be minimized by avoiding dark zones in the reactor. The production of biomass and oxygen is coupled and fixed by stoichiometry with 1 mol CO_2 being converted to 1 mol O_2 which results in 19% as the highest possible bound energy in the cells which constitutes the upper biological limit. For 680 nm illumination 24% is assumed to be the upper limit.

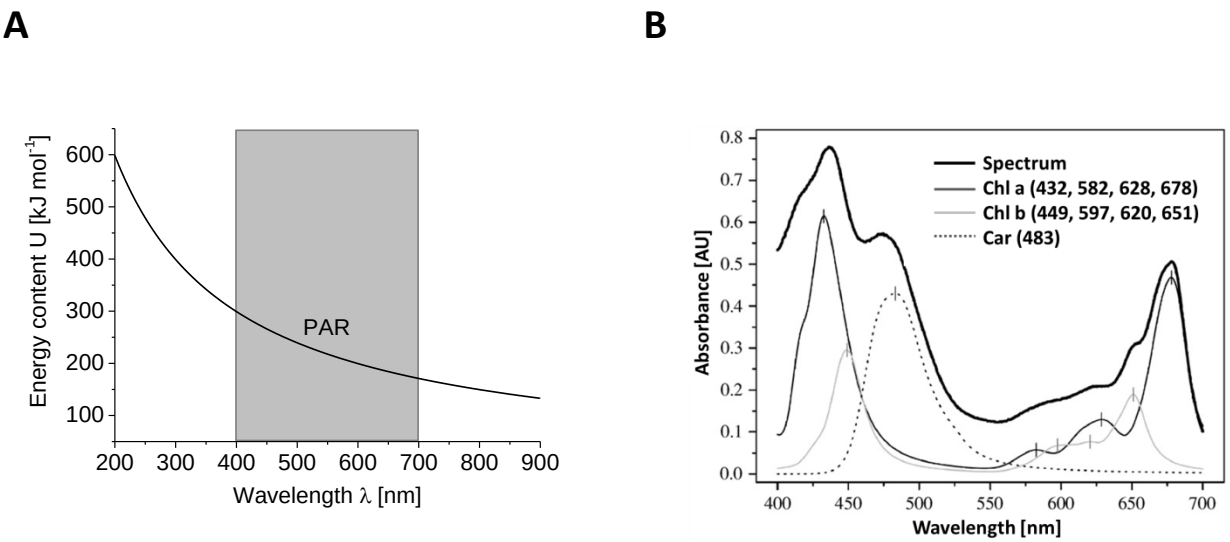

Figure 2-15. Quantum energy and absorption spectrum. A) Energy content U of photons in dependence on their wavelength λ. B) *In vivo* absorption spectrum of *C. reinhardtii* cells. The modified spectrum was measured on the chloroplast thylakoid membrane system by Rodríguez and coworkers (2007). Spectrum range 400-700 nm, step size 0.5 nm, scan rate 100 nm s^{-1}, 10,000 values per wavelength.

For the efficiency of light to biomass conversion, the wavelengths of irradiated light are also important, as depending on the light color used, different photo conversion efficiencies (PCE) are resulting.

Different colors of LED illumination were used for example for experiments concerning the growth of the moss *Physcomitrella patens* as representative of plants (Cerff 2012). Besides, there are several studies concerned with the influence of light colors on the growth of microalgae which are reviewed in the following chapter.

For the calculation of efficiencies, the quantum efficiency based on the energy content of photons depending on their wavelengths has to be taken into account for mono- and dichromatic illumination (Equation 2-34).

Equation 2-34. Energy content U of photons depending on their wavelength λ.

$$U = N \cdot h \cdot \frac{c}{\lambda}$$

U – energy content of photons [J E^{-1}], [J mol^{-1}]

N – Avogadro's number [mol^{-1}], (N = 6.022×10^{23} mol^{-1})

h – Planck's constant [J s], (h = 6.626×10^{-34} J·s)

c – speed of light [m s^{-1}], (c = 2.998×10^{8} m s^{-1})

λ – wavelength [nm]

Another important factor for the overall efficiency of a phototrophic life support module is the kind of artificial illumination that is used. Artificial sources have to be used if no sunlight is present or if conducting sunlight with the help of fiber-optic structures is too laborious or not suitable because of design aspects. Besides conventional halogen lamps, illumination with LEDs is more and more used for photobioreactor illumination (Carvalho 2011, Nedbal 2008, Gordon 2007, Bitog 2011). Using LED technology for lighting gives several degrees of freedom relating to reactor geometry, chosen light color and optional light cycles.

A detailed evaluation of light spectra is essential where artificial illumination is used and predetermined (for example concerning the production of high-value substances, or the use of algae-based modules within life support systems for space application), especially regarding energy optimization. With the knowledge on light absorption and action spectra of green microalgae, the question has to be posed if an illumination with white LED light or halogen lamps is optimal for achieving highest light to biomass conversion efficiencies or if a mono- or dichromatic illumination with specific wavelengths should be favored. To find optimal wavelengths for illumination of microalgae modules, profound knowledge on pigment composition, accessory as well as sensory pigments, and their physiological role has to be collected and carefully reflected. Within this work, special focus is put on the green alga *C. reinhardtii* (wildtype CC-1690).

2.3.2.3 Accessory pigments, absorption, and action spectra of *Chlamydomonas reinhardtii*

The green alga *C. reinhardtii*, chosen for the project mentioned, possesses accessory pigments including chlorophyll a and b as major components of photosystems, as well as carotenoids being essential for cell survival because of their photo protective and antioxidant properties (they may act as

quenchers of ROS). Another function of carotenoids is to broaden the absorption spectrum and thus help the organism to make use of a bigger part of the emitted sunlight spectrum (Kreimer 1990). Carotenoids present in the green alga comprise β-carotene, neoxanthin, violaxanthin, and lutein as well as loroxanthin being all associated with photosynthetic reaction centers in the chloroplast of the cell (Schaller 1997). During high light stress, a part of violaxanthin is converted to zeaxanthin (Hegemann 1998). Besides their function as photosynthetic pigments localized in the chloroplast, carotenoids (β-carotene) are also part of the eyespot lens and act as precursor molecules for retinal, the chromophore covalently linked to the rhodopsin photoreceptors of the eyespot which is responsible for phototaxis (Nagel 2002, Nagel 2005).

Relating to the goal to maximize efficiency, suitable wavelengths for monochromatic illumination have to be found which implies that absorption and action spectra of the alga have to be regarded. An *in vivo* absorption spectrum for living cells of *C. reinhardtii* was measured with a special apparatus (Gualtieri 1989) und published by Rodríguez and coworkers (2007). The spectrum was measured on chloroplast thylakoid membrane systems of *C. reinhardtii* wildtype cells (Figure 2-15 B).

Major peaks of absorption can be seen in the blue as well as in the red region of the spectrum, whereas the maximum in the red region is at 680 nm. In the blue spectral range the maximal peak is around 435 nm whereas a smaller peak is around 470 nm. For this reason, wavelengths in the blue and red regions of the spectrum seem to be promising light colors for an efficient illumination system of microalgae photobioreactors. An important issue concerning pigment composition of the cells is the question if a direct excitation of auxiliary pigments such as chlorophyll b is necessary or if it is sufficient to excite chlorophyll a only.

Chlorophyll b and carotenoids (also called auxiliary pigments) absorb light according to their specific absorption spectra and transfer the resulting energy to chlorophyll a (Förster resonance energy transfer) which drives light reaction of photosynthesis. Questionable is the fact if the role of these auxiliary pigments only consists of transferring their absorbed energy to chlorophyll a, or if they have other physiological functions. Emerson and Rabinowitsch (1960) put their research focus on that question and published the theory of the Emerson effect. They described the red drop during illumination of a *Chlorella* culture (among others) with wavelengths higher than 685 nm, where chlorophyll a is the only molecule absorbing the light with that particular wavelength. The quantum efficiency ϕ_{max} in terms of oxygen production was determined, meaning the ratio of produced O_2 mols to mols absorbed light quants. The red drop describes the strong decrease of ϕ_{max} in this long-wave radiation range compared to the efficiency achieved with light at around 600 nm. Additionally, around 650 nm, a drop can be measured. They concluded that for photosynthesis, working with maximum efficiency, it is a prerequisite that light is absorbed by at least two pigments: chlorophyll a and one of the auxiliary pigments.

Furthermore, it was assumed that there are two *in vivo* forms of chlorophyll a wherein one form absorbs far-red light and the other form is either directly excited by near-red light or indirectly via energy transfer from auxiliary pigments. The enhancement effect was also described within the same work, describing that when light at 650 nm and light at 720 nm are used simultaneously for illumination of algae, the quantum yield is as high as with light at 600 nm. This could be explained by the fact that long-wave light around 720 nm can only be used efficiently for oxygen production via PSI if simultaneously light with lower wavelength around 650 (PSII maximum) is present. It also appears when these wavelengths are illuminated one after another if the dark time period in between is short; this is called the Hill effect.

With the help of these experiments the conclusion was drawn that oxygen production is at PSII which has its absorption maximum in a lower wavelength range of red. The general conclusion from this is that it seems to be necessary that both Chl a and one of the auxiliary pigments are excited to keep photosynthesis running with maximum efficiency.

In general, the determined quantum yields based on absorbed photons for *Chlorella* suspensions published by Emerson and Lewis (1943) as well as for a variety of higher plants published by McCree (1972) (Figure 2-16) show that there are slight differences for PAR wavelengths. Also in recent literature the quantum yield for a green alga, in this case *Nannochloropsis oculata* shows a similar relation to the wavelength absorbed (Tamburic, 2014). In terms of stoichiometry, every absorbed photon has the same biological effect on the mechanistic level. However, losses during “processing” of photons with different wavelengths within the photosynthetic apparatus result in those quantum yields measured. This has relevance for finding optimal wavelength combinations for high efficiency illumination of microalgae.

Plants and microalgae use light not only for energy supply during photosynthesis but also as an environmental stimuli with a certain intensity, wavelength and direction. This environmental signal is perceived by several photoreceptors and a certain response is generated (Takemiya 2005). The green alga *Chlamydomonas reinhardtii* also possesses sensory pigments responsible for phototaxis as well as other physiological functions in addition to those accessory pigments. For choosing optimal wavelengths for highly efficient illumination these also should be taken into account.

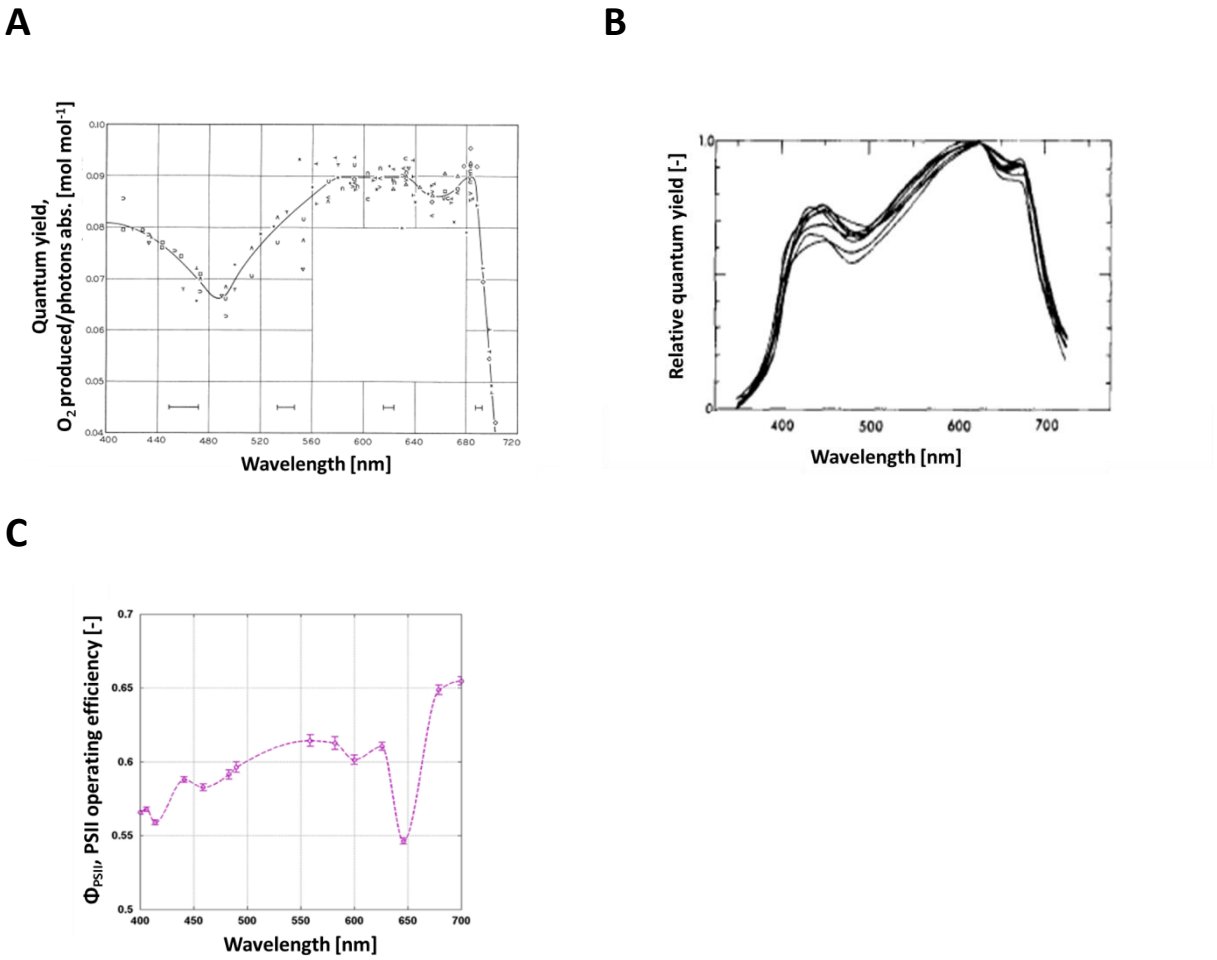

Figure 2-16. Quantum yields in dependence on wavelength. A) Quantum yield measured for *Chlorella* samples based on absorbed photons by Emerson and Lewis (1943); modified. B) Average relative quantum yield for higher plants; modified after McCree (1972). C) Quantum yield measured as PSII operating efficiency for *Nannochloropsis oculata* cells published by Tamburic (2014); modified.

2.3.2.4 Sensory pigments of *Chlamydomonas reinhardtii* and physiological role

Several sensory pigments of *C. reinhardtii* have been identified until the present day: seven rhodopsins (whereas the role of two of them is clear, being ChR1 and ChR2, the role of the remaining five is still not known), one phototropin (UV, blue), and two cryptochromes (blue). The existence of a phytochrome being sensitive to red light is still not proven but strongly assumed. Quite unusual receptors found in this alga are the aforementioned channelrhodopsins (ChR1, a proton channel and ChR2, a cation channel) which act as light-gated ion channels during photoreception for phototaxis and photophobic response.

Phototaxis of *C. reinhardtii*

Farmintzin was the first one to describe phototactic behavior for *C. reinhardtii* in 1867 (Haupt 1959, Farmintzin 1878). This phototactic behavior (for definition see chapter 2.2.1.4) is strongest in the exponential growth phase and also independent of photosynthesis, indicating that also

heterotrophically grown cultures show that behavior (Stavis 1973). The action spectrum of phototaxis has the highest peak in the blue range of wavelengths (at 503 nm), whereas only light from near UV up to wavelengths of 550 nm induces a phototactic response (Nultsch 1971). Both responses, positive and negative phototaxis, are influenced by light intensity (low light mostly positive, high light mostly negative) (Häder 1981) as well as factors like calcium and magnesium ion concentration in the medium (Haldall 1957), adaptation to actual light conditions of the cells (Mayer 1968), and the rate of photosynthesis (Takahashi 1993). However, only during later studies photoreceptor pigments were identified and rhodopsin was discovered to have a function for phototropism interacting with the orange-colored "eye spot" (see chapter 2.2.1.2), providing information about the direction of the incoming light. As early as in the 1850s, scientists attributed a function for light perception to the orange-colored spot of *C. reinhardtii* cells which is visible under the light microscope (Farmintzin 1878, Ehrenberg 1883).

It was shown that the eye spot consists of several layers of carotenoid containing lipid globules which are localized within the stroma of the chloroplast next to the plasma membrane while being separated from each other by thylakoid membranes (Melkonian 1984). As these vesicles possess a higher refractive index than the layers of thylakoid membranes and resulting from a distance of 125 nm between them, light beams hitting them at right angles are partly reflected (Melkonian 1984). Only when light at wavelengths around 500 nm (four times the distance between the layers) hits these structures constructive interference results (Kreimer 1990, Schaller 1997). The cells are further able to determine the angle of incoming light. There are photoreceptors in the plasma membrane next to the eye spot. These are shielded by the eye spot from light beams hitting the spot from the back side. Light beams hitting at right angles are amplified by constructive interference and this is maximal for photons of 500 nm. For smaller angles of incoming light beams constructive interference amplifies light with wavelengths smaller than 500 nm (Hegemann 1998). In 1984 it was proven by Foster and coworkers (Foster 1984) that a rhodopsin is the responsible photoreceptor for phototaxis. A rhodopsin with an action spectrum peak around 495 nm is also involved in controlling the photophobic stop response. This peak is similar to the one of phototaxis action spectrum at 503 nm. Studies have proven that two proteins are acting as ion channels, termed channelrhodopsin 1 (ChR1) and channelrhodopsin 2 (ChR2) with action spectrum peaks of 500 nm and 460 nm respectively (Nagel 2002, Nagel 2005). Consequently, it seems reasonable that ChR1 is responsible for phototaxis and the photophobic stop response with an action spectrum peak around 500 nm, whereas the exact function of ChR2 is not known. There are other works (Sineshchekov 2002) reporting slightly shifted maxima for rhodopsin A and B (correlating to ChR1 and 2, respectively) being 510 nm and 470 nm. Rhodopsin A is responding quickly to high light intensities and B slowly to low light.

As a summary, light in the UV and blue region (action spectrum peak at 503 nm) is attributed to phototactic movement of the alga which has to be considered for illumination of *C. reinhardtii* cells.

Role of the circadian clock for phototaxis

The phototactic movement of *C. reinhardtii* is also controlled by the cell's circadian clock which provides a rhythm to that behavior (Mittag 2005). This was in focus of several studies, in particular the reset of the circadian rhythm of phototactic behavior in response to different wavelengths. For cells of *C. reinhardtii* CC-124 this reset was shown for blue light at 440 nm, and for green (at 540 nm) and red light (640-660 nm) during experiments conducted by Forbes-Stovall and coworkers (2014). Kondo and coworkers (1991) had the same results for the cell-wall-deficient strain CW15 of *C. reinhardtii* for blue and red light but with another peak in the action spectrum for blue at 520 nm. The authors also assume that the action spectrum peaks are different from that responsible for phototaxis and that there are photoreceptors responsible for setting the clock differing from the one leading to phototaxis. If phytochrome is responsible for the action spectrum peak at 660 nm for resetting the circadian clock of phototaxis still remains unclear. It is assumed by the authors that photoreceptors, different from the one responsible for phototaxis, act together in resetting the clock for photomotile behavior, and therefore also for the circadian rhythm of phototaxis, wavelengths in the blue region, but also in the green and red range, play a role.

Further physiological roles of blue light

Besides inducing phototaxis and photophobic response in *C. reinhardtii*, blue light also plays a role for cell division. *C. reinhardtii* cells can divide into two, four, eight (Harris 2009) or even 16 daughter cells during cell division (Vítová 2011). Cell division is initiated at several critical cell sizes (Oldenhof 2004 a) and there are several hints in literature that point to a role of blue light for influencing cell division. Studies conducted by Münzner and Voigt (1992) resulted in a delay in cell division in *C. reinhardtii* wildtype cultures (137C mt^+) induced by blue light compared to cultures grown with red and far-red light. White light also caused that effect in cells grown heterotrophically before. The related action spectrum of cell division delay contains peaks at 400 and 500 nm, whereas the one at 500 nm is attributed to rhodopsin which is reported to play a role in phototaxis (Foster 1984, Beckmann 1991, Foster 1988, Hegemann 1988). The same effect of blue light on cell division was found by Oldenhof and coworkers (2004 b) compared to red light ($\lambda > 590$ nm) for *C. reinhardtii* wildtype (cc125 mt^+) cells. Blue illuminated cells also showed an increased size before they undergo cell division compared to the red light control. They conclude that light from the blue wavelength range has a role for controlling the time when cell division starts and leads to an inhibition of cell division at the minimal critical cell size. However, the blue light filter that they used during their experiments also transmitted light with a wavelength higher than 680 nm which makes it difficult to come to a final conclusion. Further research of these authors (Oldenhof 2004 a) also showed effects of red and blue light on the time of cell division, the synthesis of DNA, and the presence of cyclin-dependent kinases (CDKs) of *C. reinhardtii* wildtype cultures (cc125 mt^+). CDKs (serine/threonine

protein kinases) have a function for controlling the progression of the eukaryotic cell cycle. Under activation they initiate DNA synthesis and mitosis. Besides delaying cell division, blue light and white light also delays DNA synthesis compared to red light. Also CDK activity occurred later in blue illuminated cultures. However, there is no detailed knowledge on the exact mechanisms of how blue light affects these processes.

Additional to the aforementioned functions, blue light also plays a key role in the sexual life cycle of *C. reinhardtii* controlled by a phototropin photoreceptor (Huang and Beck 2003). In general, the sexual life cycle of *C. reinhardtii* has three phases that can be influenced by light: gamete formation, the maintenance of mating competence in gametes, and the germination of zygotes. This blue light-sensitive phototropin is assumed to primarily control developmental processes.

Not only the cell division of the green alga *C. reinhardtii* seems to be strongly controlled by wavelengths: Kim and coworkers (2014) report that blue light also has an influence on cell size and cell division of another green alga, *Chlorella vulgaris*. Blue light (450 nm) led to an increased cell size, and red light (660 nm) to smaller cells with high cell division activity. They also applied the wavelengths at different growth stages: when first illuminated with blue light and shifted to red light illumination, higher biomass as well as lipid productivities could be achieved. This was resulting from that fact that blue light first creates big cells and the shift to red light leads the cells to divide actively.

A receptor sensitive for blue light also has a function for controlling several important enzymes, for example, RuBisCO and carbonic anhydrase (Dionisio 1989 a, b). Moreover, it controls reproductive stages (Huang and Beck 2003) and gamete formation (Weissig 1991). The cryptochrome encoded by the gene CPH1 is one further blue light receptor that has been identified in *C. reinhardtii* whereas its particular function still is unclear. It is very light-labile and only present during heterotrophic cultivation in the darkness (Huang and Beck 2003).

Red Light

Concerning the range of red wavelengths until now, no red light receptor has yet been identified; however, there are certain hints within the genome indicating its existence (Grossmann 2004). It is known that red photons have influence on gene regulation and development of *C. reinhardtii*.

Green light: green gap and détour-effect for low absorbing wavelengths

Another important question arising, concerning absorption spectra of microalgae and emission spectra of the sun and a warm-white LED light, is for example the issue with the “green gap” of photosynthesis (see Figure 2-17 A).

There are different opinions in literature concerning the green gap in absorption spectra of microalgae (Tredici 2010, Kruse 2005). The term “green gap” of photosynthesis roughly describes the range of

the spectrum between 500 and 600 nm where chlorophyll a and b do not absorb light. However, absorption and action spectra of green microalgae also show absorption and photosynthetic activity within this gap region (Grossmann 2004, Rodríguez 2007, Schaller 1997, Gualtieri 1989), but there is a need for experimental prove including achievable yields for biomass and oxygen production under green light illumination.

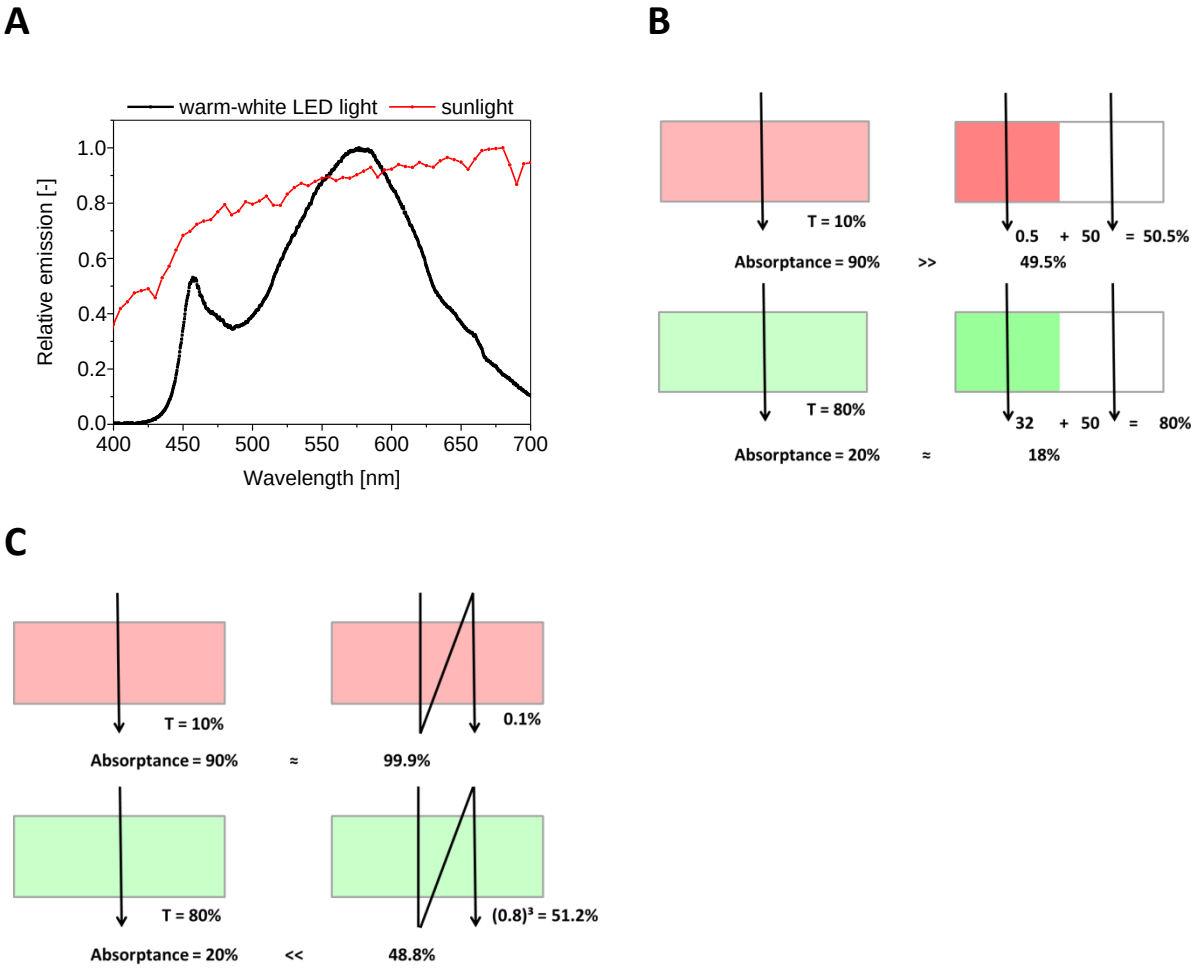

Figure 2-17. Green light, sieve- and détour-effect for high and low absorbing wavelengths. A) Normalized emission spectra of the sun and a warm-white LED within PAR range. B). Sieve-effect with pigments uniformly distributed (left side) and two-fold concentrated (right side) for high absorbing (red) monochromatic wavelength and weak absorbing (green) monochromatic wavelengths. C) Détour-effect; on the left side: no détour-effect, on the right side: elongation of the light path by a factor of 3 by the détour-effect. For highly absorbed red light the increase in absorptance is small, for weak absorbing wavelengths the increase is large; modified after Terashima (2009).

Concerning light penetration in plant leaves, it is reported that 80% of green light, which is the prevailing wavelength in the deeper leave, is absorbed, as a result of light scattering within the leaf inner structures. Once green photons are absorbed they are efficient drivers for photosynthesis (Terashima 2009, Terashima 2011). Relating to the photosynthetic quantum yield, green photons are said to be even more efficient than blue photons based on absorbed quanta. There are two interesting effects that were shown for light absorption by plant leaves and which play a role for absorption of

green light (Figure 2-17 B, C): the sieve- ("flattening"-) as well as the détour-effect (Terashima 2009); the latter is originating from the diffusive nature of the plant leaf tissue leading to an increased light path length (Vogelmann 1993). The sieve-effect is characterized by a large decrease in absorptance in case of high absorbing monochromatic light (red) whereas for weak absorbing wavelengths the decrease in absorptance is small. The détour-effect is characterized by an increase in absorptance due to light diffusion. This can be seen when the light path is lengthened whereas there is a big difference for wavelengths with weak absorption (like green photons) and wavelengths with strong absorption. Hence, for light strongly absorbed, like red and blue, the sieve-effect leads to a tremendous reduction of absorptance whereas the détour-effect leads to a slightly increased absorptance. For wavelengths weakly absorbed, the influence of the sieve-effect for absorptance is small whereas the détour-effect has a large positive effect on it.

If microalgae suspensions at certain high cell densities can also be seen as tissue-resembling structures showing a measurable absorbance of green light fueling photosynthesis is investigated during this work. Theoretically this détour-effect should be relevant for all ranges of rather low absorbing wavelengths. There are also some studies that included photons from the green gap for illumination of microalgae and higher plants. Johkan and coworkers (2012) proved that for higher plants like *Lactuca sativa* pure green light illumination (PFD of 300 µE m^{-2} s^{-1}) was effective to promote growth of the plants and that particularly green photons at 510 nm were available for active plant growth and more efficient than higher wavelengths within the green range. Green photons with wavelengths near the blue range of the spectrum are absorbed by blue light receptor phototropin promoting substantial plant growth (Takemiya 2005). These results indicate that green light at higher light intensities is available for morphogenesis and photosynthesis in *Lactuca sativa*. However, there is also discussion about green light that antagonizes functions relying on red and blue photons in plant growth and development (Folta 2007). Besides phototropin, phytochromes and cryptochromes are assumed to be sensors for green light in higher plants (Folta 2007). Those photoreceptors (also contained in the alga *C. reinhardtii*, with strong assumptions on the existence of a phytochrome) are sensitive for green light but with a low processing efficiency compared to red and blue wavelengths (Folta 2007). Kim and coworkers (2004) described positive effects of additional green photons to red and blue in cultivation of *Lactuca sativa* with a white illuminated control. They assume a repeated reflection of green photons within the leaf structure from chloroplast to chloroplast and therefore described the functional principle of the aforementioned détour-effect. Further studies (Brodersen 2010, Sun 1998) on higher plant leaves showed that red and blue photons are almost completely absorbed by the initial cell layers. Green photons can penetrate deeper and drive CO_2 fixation more efficiently in deeper located cells or in multiple cell layers.

Even for microalgae cultivations studies with green photons are available. Studies with the freshwater green alga *Scenedesmus bijuga* with focus on biomass production in high-density cultures were

conducted by Mattos and coworkers (2015). They compared red and blue wavelengths with green light and a white illuminated control. They also studied light distribution with increasing path length and cell density for red, blue and green photons compared to white. For different measured path lengths the trends for transmission were consistent where green, followed by white, red and blue light was the order from high to low transmission. This is resulting from high scattering coefficients and a low absorbance coefficient of Chl a and b for low absorbing wavelengths like green photons (e.g. 530 nm). These low absorbing wavelengths are able to penetrate deeper into high density cultures. They suggest an additional use of low absorbing green photons to high absorbing red and blue light in later cultivation phases at high cell densities to improve overall productivity.

2.3.2.5 Light attenuation profiles

In order to assess and compare illumination with different wavelengths to full spectrum illumination in respect to growth and overall productivity as well as yield values (PCE), knowledge on light intensity distribution with the path length and at different cell densities has to be gained. Important are light absorption and attenuation characteristics for differently absorbed wavelengths to model growth rate for different volume elements of a whole photobioreactor volume.

One approach is proposed by Yun and coworkers (2001). They determined light attenuation coefficients in case of *C. vulgaris* cultures theoretically using light absorption spectra and emission spectra of different light sources. The determined coefficients were used to evaluate light attenuation models like Lambert-Beer's law, Cornet and hyperbolic models for the quantitative description of light penetration into microalgal cultures. Blue, green, yellow, red and full spectrum light was provided by halogen lamps and specific filters. The spectral PFD of transmitted light through an algal suspension can be calculated based on the spectral irradiances of the light sources (emission spectra) and absorption spectra of the algae. As defined by Geider and Osborne (1992) the transmittance spectra $T(\lambda, c_X)$ can be obtained from absorbance spectra $D(\lambda, c_X)$ using the equation:

Equation 2-35. Calculation of transmittance spectra based on absorption.

$$T(\lambda, c_X) = 10^{-D(\lambda, c_X)}$$

The spectral PFD of transmitted light $P(\lambda, c_X)$ can thus be calculated using spectral irradiances of light sources $E_0(\lambda)$:

Equation 2-36. Calculation of spectral PFD of transmitted light.

$$P(\lambda, c_X) = \frac{T(\lambda, c_X) \cdot E_0(\lambda)}{N \cdot h \cdot c / \lambda \cdot 10^9}$$

For describing the attenuation of monochromatic light, the attenuation coefficient a(λ, c_X) can be calculated based on light path length l, the spectral PFD of transmitted monochromatic light P(λ, c_X) and the spectral PFD of incident light P_0(λ):

Equation 2-37. Coefficient of light attenuation for monochromatic light.

$$a(\lambda, c_X) = -\frac{1}{l} \cdot \ln\left(\frac{P(\lambda, c_X)}{P_0(\lambda)}\right)$$

The calculated coefficients can be plotted versus c_X for different monochromatic lights. As expected, highest values of a(λ, c_X) were determined for blue and red photons, lower values for green light whereas differences were bigger for higher cell densities (Yun 2001) meaning that green photons can penetrate deeper into algal cultures. Up to cell dry weight concentrations of 0.5 g L^{-1}, and therefore rather low cell densities, the relation was linear. They also used this approach to calculate attenuation for polychromatic light A(λ, c_X) using PFD of incident light P_{T0} and the PFD of transmitted light $P_T(c_X)$:

Equation 2-38. Coefficient of light attenuation of polychromatic light.

$$A(c_X) = -\frac{1}{l} \cdot \ln\left(\frac{P_T(c_X)}{P_{T0}}\right)$$

The PFDs of transmitted and incident lights can be calculated from the respective spectral irradiances (emission spectra) E_0(λ) and E(λ,c_X), as well as the transmission spectrum of the algal suspension T(λ, c_X):

Equation 2-39. PFD of transmitted light.

$$P_{T0} = \int_{400}^{700} P_0(\lambda) d\lambda = \int_{400}^{700} \frac{E_0(\lambda)}{N \cdot h \cdot c \cdot 10^9 / \lambda} d\lambda$$

$$P_T(c_X) = \int_{400}^{700} P(\lambda, c_X) d\lambda = \int_{400}^{700} \frac{T(\lambda, c_X) \cdot E_0(\lambda)}{N \cdot h \cdot c \cdot 10^9 / \lambda} d\lambda$$

Using the determined attenuation coefficients, the PFD can be calculated using Lambert-Beer's law which is primarily used for simplicity reasons. However, the authors also used the Cornet model (Cornet 1992) and a hyperbolic model, whereas the latter was the one best fitting to the attenuation coefficients determined for different cell densities and for all light colors used. This hyperbolic model was used before by several authors (Radmer 1987, Fernandez 1997) for estimation of light attenuation and is described by following equation with A_{max} as maximum attenuation coefficient and a and b as constants:

Equation 2-40. Hyperbolic model for estimation of light attenuation in microalgal cultures.

$$A(c_X) = \frac{A_{max} \cdot c_X}{b + c_X}$$

However, as this model was empirically determined from the attenuation curves it does not further enhance the understanding of light attenuation in culture suspensions. The authors also mentioned that none of the models was able to describe the relation of light source and light attenuation and hence more work needs to be done to acquire a universal model for exact quantification of light attenuation in algal cultures and different light colors.

2.3.2.6 Design aspects of space photobioreactors relating to lighting and overall efficiency

An essential point relating to the design of a photobioreactor for a module of a life support system is the question of how the illumination device is implemented in the design. One of the simplest forms of a photobioreactor is a plate type PBR, where either lighting from one side or from both sides is possible. Jacobi and coworkers (2012 a) examined light distribution (Figure 2-18) for different reactor types.

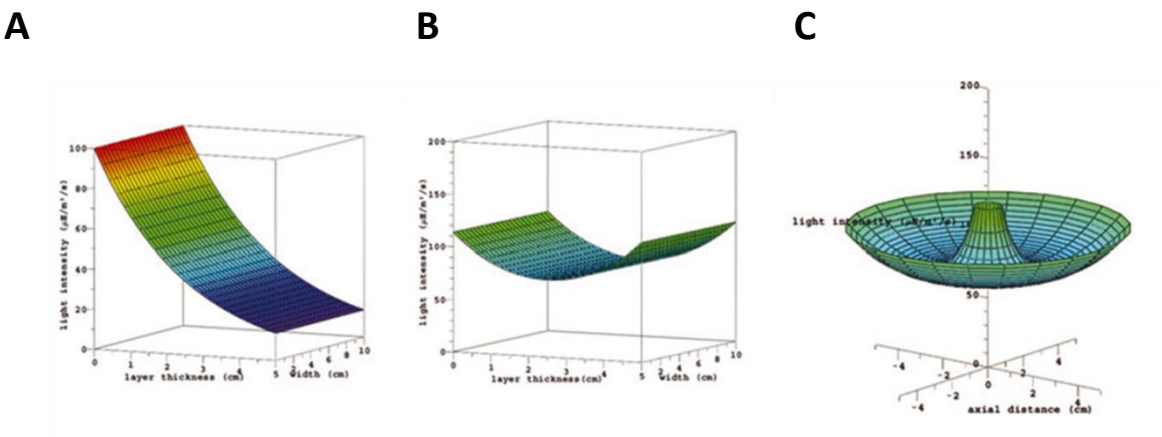

Figure 2-18. Typical light intensity distribution in different reactor types for a light intensity of 100 µE m^{-2} s^{-1} and the same extinction coefficients ε and layer thickness D. A) One-sided illumination of a plate-type reactor. B) Double-sided illumination of a plate-type reactor. C) Cylindrical reactor with external illumination (Jacobi 2012 a).

For one-sided illumination an exponentially decreasing light intensity profile is resulting. When this type of illumination approach is used, good mixing and a more turbulent flow regime are necessary to minimize the time a single cell is exposed to dark volume elements with insufficient illumination. When double-sided illumination is applied no turbulent flow regime is necessary as there is a homogeneous light distribution within the reactor depth. Along the trajectory of one cell moving from one point in the reactor to another almost the same incident light intensity is irradiating the whole reactor volume. Concerning overall energy efficiency the ability of using laminar flow regimes is also advantageous.

Another important factor highly influencing internal energy efficiency (electrical energy to light energy conversion) is the kind of light source chosen. In order to minimize energetic losses in the form of heat, LEDs are chosen for illumination for a microalgae module (Carvalho 2011, Lee 1994). For internal efficiency of LEDs the color chosen is also important inasmuch as red LEDs, for instance, consume 30% less energy than blue or white LEDs (Cerff 2012).

Besides their energetic benefits, LEDs possess further advantages like their small size and low weight enabling a good adjustment for various reactor structures and sizes. Especially for an illumination with an absorption specific emission spectrum in long-term cultivations, it is advantageous that LEDs possess a narrow spectral output (half-power bandwidths of about 20-30 nm) and a long durability (Carvalho 2011, Lee 1994). The long lifetime of LEDs (about one year in continuous PBR operation) (Kommareddy 2003) especially makes them the optimal choice among several possible light sources.

Aiming at a maximum energy efficiency of a PBR module for life support also implies that volume and mass is minimized whereas the efficiency of the volume "working" inside such a module is maximized. In terms of a microalgae reactor this means that biomass concentration has to be maximized and, on the other hand, volumetric productivity relating to oxygen production and CO_2 consumption (Javanmardian 1991). For a one-sided illumination of a plate reactor the cell density concentration should be at a certain value where there is just no transmission of light on the unlighted side, as transmission of light would mean loss of energy. Relating to that Pruvost (2012) and Takache (2012) described the *Luminostat* regime which means that light is fully absorbed with no dark zones in the culture bulk. At this point maximal biomass productivity at a given incident PFD is achieved for full light attenuation with no dark zones (Souliès 2016).

2.3.2.7 Illumination concepts and designs for biological life support systems in spaceflight

During the development of biological life support systems one special focus is the reduction of electrical power demand and therefore lighting techniques are of special interest. Several studies were and are conducted by NASA related to hybrid solar and artificial illumination systems for bioregenerative life support systems (Cuello 2002). Besides LEDs (Massa 2006) microwave lamps are also in the spotlight of research resulting from their excellent power conversion efficiencies (Cuello 2002). Several experiments concerned with the cultivation of higher plants for bioregenerative space applications and optimal illumination have shown that a power ratio of red to blue with 90/10 achieves the highest yields in plant biomass (Cuello 2002). However, there is still need of proving that blue and red photons alone can be used for optimal growth of specific plants (Pinho 2012).

2.3.2.8 Consequences for potential mono- and dichromatic illumination

Based on the current knowledge about accessory and sensory pigments of the green alga *C. reinhardtii* and their role in microalgae growth and physiological functions, it seems promising to use mono-and dichromatic illumination for the chosen microalga for the development of a life support

photobioreactor module. Particular wavelengths according to the action spectrum *in vivo* should be chosen for experimental studies. One option for additional experiments is to test the influence on growth and PCE while exciting the phototaxis photoreceptor at the corresponding wavelength or also together with blue wavelengths for photoreceptors of the circadian clock of phototactic behavior.

Despite experiences from experiments with mono- and dichromatic illumination for higher plant cultivation for almost two decades (Kuwahara 2011) this knowledge gained has not been widespread within microalgae illumination techniques aside from physiological studies on photoreceptors and their function and a few studies on cultivation lighting based on colors. One example is the work of Kuwahara (2011) who tested red (655 and 680 nm) and blue (474 nm) laser light as well as combinations of each of the red ones with blue for cultivation of *C. reinhardtii* compared to a control culture illuminated with white fluorescent light. For dichromatic mixtures they used a power ratio of 90 % red to 10 % blue according to common plant lighting techniques (Cuello 2002). Both dichromatic combinations resulted in an increased cell number compared to monochromatic red illumination and white control. It was proven that with pure red laser light at both wavelengths tested the same cell count was achieved compared to the white control. Reasons for the successful usage of dichromatic illumination with red and fewer blue photons could be, as aforementioned, the stimulation of high expression or control of important enzymes such as RuBisCO (Dionisio 1989 a) and carbonic anhydrase, the latter playing a major role in CCMs in that alga. RuBisCO is reported to be under blue light control (Dionisio 1989 a) and the induction of carbonic anhydrase is regulated by two light-mediated steps (Dionisio 1989 b) whereas one of them requires blue light. It was also proven that the first photosynthesis-dependent step in regulation of induction of that enzyme also required red light. However, Lee and coworkers (1994) used only red LED lights (at 680 nm peak) in a photoautotrophic cultivation of *Chlorella vulgaris* to achieve high cell densities. Only in recent times studies focusing on photobioreactor productivity as function of light quality in continuous microalgae cultures have been published (De Mooij 2016, Baer 2016). Also the addition of green light to red and blue for high density algal suspensions is discussed (Mattos 2015).

2.3.3 Technical aspects of hypobaric conditions on PBRs

As mentioned before, microalgae are interesting species for application in basic modules within CELSSs (controlled ecological life support systems) (Gitelson 1976). For this reason they have to withstand the environmental conditions present. Besides the aforementioned factors like microgravity, radiation, hypoxia and extreme temperature gradients there are low atmospheric pressures prevailing on other planets or even vacuum in space (Wang 2004 a, Rea 2008) that have an influence on reactor design, for example with respect to wall thickness. Even during parabolic flights, in which those systems have to be tested in, pressure reduction plays a role as values decrease to almost half the atmospheric pressure on Earth which is acting on the hardware, software and biological components.

Also on the ground under atmospheric conditions microalgae contained as suspension cultures in various types of photobioreactor systems are exposed to pressure changes, local pressure peaks and reductions. These pressure patterns can either be caused by peripheral devices like pumps or by expansions or reduction of flow cross-sections or simply by hydrostatic pressure differences when a single cell moves along flow paths inside a reactor. The pressure aspect is also an important factor for possible locations of microalgae processes in high-altitude near-tropical regions with high solar radiation where pressure or more precise a lower pressure is a critical factor possibly having an influence on productivity; for instance, ambient pressure in regions at 4000 m altitude decreases down to almost 600 mbar.

On the reactor level, an overall pressure drop also influences partial gas pressure and solubilities and may also lead to bubble formation. For this reason pressure has to be monitored carefully during cultivations under microgravity conditions as well as studied for its influence on dissolved gas concentrations and on microalgae physiology during microalgae cultivations on ground.

Also concerning effects like agglomeration and subsequent sedimentation of microalgae during cultivation within various ground photobioreactors, reasons for this behavior are highly discussed. Those phenomena, leading to reduced productivity of microalgae based processes might be resulting from fast pressure changes alone or in combination with other factors.

Within this work experiments with moderate pressure reductions and sudden pressure changes were conducted. Also parabolic flight data where pressure decreased to about 700 mbar might show possible effects of this abiotic factor on growth, CO_2 uptake and the oxygen production of the green microalga *C. reinhardtii*, wildtype CC-1690. Also effects on morphology are studied via light microscopy. Studies should show if fatal threshold values of pressure reduction can be identified and if and within which time frame adaptation mechanisms permit cell survival.

2.3.4 Long-term stability of continuous cultivations: time constants and process control

For long-term operation the only feasible process type is a continuous culture where optimal conditions can be maintained for a longer time. Achievable cell densities in a continuous photoautotrophic cultivation of a *Chlorella sorokiniana* strain in a photobioreactor are reported to account to 20 g L^{-1} (Pirt 1980). For high cell densities inside a PBR module, an optimization of medium composition has to be realized upstream, together with the development of feeding strategies. A well-balanced medium composition has to be developed, while avoiding the accumulation of inhibiting metabolites or other compounds during a long-term process (Lee 1994). A further optimization parameter is the maximum volumetric oxygen productivity OPR (oxygen production rate) based on the reactor volume (Javanmardian 1991). For batch cultivations these rates in general reach peak values at the end of the exponential growth phase when growth merges from exponential to

linear phase. According to Lee and coworkers (1994) a theoretical maximum O_2 production rate of 25-400 fmol O_2 per cell and h can be expected, based on the assumption that one mole of chlorophyll can produce 50-400 mol O_2 per h and the chl-content per cell is in the range of 0.5-1 fmol for *Chlorella*.

With regards to an oxygen producing and CO_2 consuming life support module it is also important to consider gas exchange rates of the heterotrophic modules to be supplied with the photosynthetic product. For a human being of 70 kg body weight in a non-stressed condition at rest the breathing rate accounts for 7.5 L min^{-1} with an exhaust gas composition of 17% (v/v) O_2 and 3.2% (v/v) CO_2 (Brake 1999). Breathing rates may rise up to 65 L min^{-1} for maximal physical effort. For normal resting conditions oxygen uptake rates account for 0.3 L O_2 min^{-1} and CO_2 production for 0.24 L CO_2 min^{-1}. This is about 800 mmol O_2 h^{-1} and 650 mmol CO_2 h^{-1} for a 70 kg standard human being at resting conditions. Fatal thresholds for gas composition to be inhaled account for values above 10% (v/v) CO_2 and values below 10% (v/v) O_2. These are important basic data that have to be in accordance with modules for air regeneration in a life support system.

In summary, essential factors and parameters to realize high-density phototrophic microalgal cultures are a high surface-to-volume ratio, the use of an efficient light source, an efficient light delivery, and an efficient gas transfer as well as a medium dosing and recycling system.

2.3.4.1 System perturbation and time constants

For the assessment of stability of a continuous microalgae culture inside a life support system the systems reaction to perturbations and resulting time constants are essential. In general, biological time constants range from very fast reactions in the range of picoseconds for the primary process of vision, over enzyme catalyzed reactions in the range of some milliseconds to the doubling time of eukaryotic cells which may account up to several hours or even days. The synthesis of larger proteins can last up to several seconds which also should be taken into account for the setting of time constants and parameters for process control involving molecular changes or adaptations (Klempnauer 2008).

For microalgae, time constants of about 15 mins for metabolic profile changes in response to light shift experiments for red and blue lights were reported by Jungandreas and coworkers (2014) for *P. tricornutum* in semi-continuous airlift-cultures. These were attributed to a direct control of enzyme activity by blue and red light. Later transcriptional changes are reported to occur about 30 minutes to one hour after shift changes.

In general the so called Deborah number defines the ratio of the biological relaxation time to the time interval of environmental changes (Storhas 1994). When the changes resulting from circulation or mixing times are in the same range as the internal cellular regulation mechanisms, the system is affected and changes (for example pigment content for microalgae) can be detected. This can be

applied for changes of light intensity and the adaptation of microalgae by means of specific pigment content and composition.

2.3.4.2 Process control in continuous processes and analysis of time constants

In order to assess the systems behavior to perturbations occurring during steady-state conditions of a continuous process, it is necessary to consider process control concepts and the definition of system behavior from the perspective of the time response of the control system composed of the algae and the technical system (reactor, measuring devices with their respective time constants). Such perturbations can be regarded as disturbance variables in process control acting on the control system. In case of an algae module within a life support system these perturbations could occur in the form of power limitations or inconsistencies leading to a failure of illumination or a sudden decrease or even increase in light intensity. Also a sudden drop of pressure, changes of gas composition adjacent to the membrane for aeration, or other factors might occur. These perturbations act immediately and can be experimentally mimicked by step changes of certain parameters during the steady-state run of a continuous algae cultivation process.

A typical control circuit is basically composed of the controller, the system and the feedback loop. Types of time response of controlled systems can be generally divided into systems with and without compensation. In the case of compensation the steady-state is constant for $t \rightarrow \infty$ after a step function was applied to the system. A further characteristic is the kind of transient response (dynamic behavior) which divides the controlled system into systems without delay and with delay of first, second and higher order. Systems with dead-times react to every change of correcting variable not until the dead-time has expired.

Systems with compensation often only have proportional relation of control variable x and correcting variable y; they are proportional control systems with Kp as proportional constant of the system with dimensions [Kp] = [x]/[y].

Control systems with compensation are further divided into systems without delay, with first order delay and delay of higher order. In this work further focus is put on first and higher order delay as they are mostly applicable to a photobioreactor system.

These systems are characterized by a delayed response of the controlled variable x to the correcting variable y. For first order delay the term PT1 is used for second or higher order delay PT2 or PTn respectively. Details for systems without compensation are outlined in Mann (2009).

A typical control circuit, composed of the controlled system and the controller, can follow the same types of time responses and can be described by mathematical models, either built theoretically or experimentally (Mann 2009). For the experimental method to set up mathematical models a test signal (step function, impulse function, ramping function or sine function) is used to measure the time

response of the control system and a mathematical model is adapted with a help of a catalogue of models. This test signal can be used in form of a step change, impulse change or ramp and the systems response (for example termed step response in case of a step change of the test signal) is recorded. Within this work, only step functions were applied.

One major task of this work is the investigation of the light step influence on *Chlamydomonas reinhardtii* cultures and the determination of time constants for the system response following the light steps. Environmental changes cause a complex response in biological systems, depending on the organism and source of change. To describe the response of a system, the control theory develops mathematical models to describe the static and dynamic behavior of systems. In this special case with light steps in a continuous *Chlamydomonas reinhardtii* culture, it is possible to describe the step response with the first order lag model (PT1), (Figure 2-19).

Here, a proportional delay system with a certain number of reservoirs (PT response) describes the systems' reaction after a step change with a time delay in response either first order (PT1) or second order (PT2). The two characteristic parameters for both are the time constant T and the static reinforcement k_s (Figure 2-19 A). For determination of these parameters, several steps are necessary.

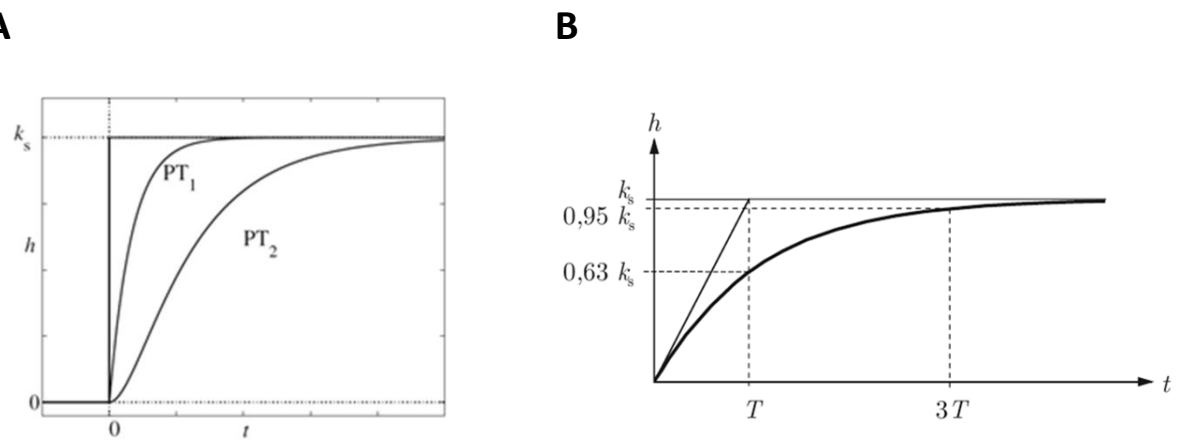

Figure 2-19. Characteristics of PT1 and PT2 elements. A) Difference between step response h(t) of a first order lag model (PT1) and a second order lag model (PT2) and static reinforcement k_s. B) Step response h(t) of a PT1 element (thick line) with the graphical solution using the point of intersection between k_s and a tangent at t = 0 (lines) and the alternative method "63% rule" and "95% rule" (dotted line), Lunze (2008).

An alternative option to determine k_s and T is with the "63% rule" or similarly the "95% rule" (Figure 2-19 B). This is possible as at the time t = T the step response has the value:

Equation 2-41. 63% rule for time constant determination.

$$h(T) = k_s \cdot \left(1 - e^{-1}\right) \approx 0.63 \cdot k_s$$

Or respectively, for t = 3T:

Equation 2-42. 95% rule for time constant determination.

$$h(3T) = k_s \cdot \left(1 - e^{-3}\right) \approx 0.95 \cdot k_s$$

During this work the system responses were analyzed as PT1 system responses. Time constants were calculated based on the "63% rule". After k_s values were determined, proportional constants Kp were calculated. Time constants T,63% and Kp values were used as comparative parameters for assessing system performance of a membrane-aerated reactor system and a bubble-aerated ideally mixed reactor.

3 Materials and methods

3.1 Microalgae strains

In this work wildtype strains of the green alga *Chlamydomonas reinhardtii* were used, which are described in the following.

3.1.1 *Chlamydomonas reinhardtii* CC-1690

Chlamydomonas reinhardtii CC-1690 wildtype mt^+ (Sager 21 gr) (Sager 1955, Pröschold 2005) was used as a model organism in this work for the majority of experiments. It was the chosen wildtype strain for the ModuLES-project as a nitrate consumer and being a C. *reinhardtii* wildtype strain highly characterized in literature in various " –omics" studies.

3.1.2 *Chlamydomonas reinhardtii* WT13

C. reinhardtii wildtype WT13 (Schönfeld 2004) originating from the original Ebersold/Levine line 137c (CC-125mt^+) (Harris 2001, Pröschold 2005) was used in order to study agglomeration effects of pressure reduction and pressure changes in comparison to CC-1690 cells which tend to form palmelloids and secondary aggregates (Harris 2009) very easily in liquid cultures.

3.2 Media, strain maintenance and pre-cultures

3.2.1 Media

For pre-cultures and cultivations of the alga *C. reinhardtii* CC-1690 TP-NO_3 (TRIS phosphate nitrate) medium was used as standard medium (see Appendix 11.1 for detailed composition) without acetate to enable pure photoautotrophic growth. Trace elements were used according to Kropat et al. (2011) without ammonium. In case of cultivations inside a stirred tank 1.8L model reactor (3.3.4, Appendix 11.2, Figure 11-3) as well as some of the cultivations inside the lab scale membrane-aerated photobioreactor, the medium was used without Tris as buffer to lower the risk for contamination. In order to install the same osmolarity of 2 g L^{-1}, KCl was used in these cases. The pH was installed to 7.2 for all cultivations if not stated otherwise. For pre-culturing and cultivations inside the stirred photobioreactor cells of *C. reinhardtii* WT13 were grown photoautotrophically on TP medium (Harris 2009) with Hutner's trace elements (see Appendix 11.1.2). The pH was installed to 7.0 in this case. Media were steam sterilized in pressure-resistant glass bottles, except for cultivations in the stirred tank 1.8L model reactor, where the medium was *in situ* autoclaved (except for ammonia, which was autoclaved separately in closed bottles and added afterwards). For feeding the cultures to extent the linear growth phase for PCE determination concentrated 10x TP-NO_3 medium was used (Appendix 11.1.2).

3.2.2 Strain maintenance and pre-cultures

Strain maintenance was realized by plating these different *C. reinhardtii* strains on solid agar plates with the respective medium (see 3.2.1). Plates were illuminated with warm-white LED light (PFD = 20 µE m^{-2} s^{-1}) in an incubator at 25°C. Every two to three months plate-cultures were renewed. Pre-cultures, as liquid cultures for all cultivations, were grown pure photoautotrophically in 500 mL Erlenmeyer-flasks (with 200 mL culture volume) on a LED rotary shaker (see 3.3.3) illuminated with warm-white light at light intensities of around 50 µE m^{-2} s^{-1} at 25°C and 100 rpm. In order to ensure axenic conditions of the cultures, a specific testing procedure was performed. Liquid samples were used by plating aliquots of 1 mL on agar plates favoring the growth of bacteria and fungi (Appendix 11.1.3) that were incubated for 48 h at 30°C and checked for colony growth.

3.3 Experimental setups

In the following, the different experimental setups for all of the experimental work are depicted. First, the experimental approaches concerning the topic of membrane-aeration are listed, followed by efficient lighting of space photobioreactors and experiments studying the effects of lowered pressure and pressure changes on the cells. Additionally, the setup of the photobioreactor concept of the ModuLES-PBR, which was tested during two parabolic flight campaigns and during ground cultivations and the related pre-culture system, is shown.

3.3.1 Experimental setup for membrane tests

A closed gas tight testing chamber (inner dimensions 4 x 12.5 x 3.2 cm) was used to determine mass transfer coefficients for CO_2 and O_2 as well as water permeability for several membrane materials (see 3.4.1) in a gas-liquid environment. Figure 3-1 shows the overall experimental setup. Further details are shown in Appendix 11.2.1. Dimensions and technical data of the testing system are listed in the following table.

Table 3-1. Dimensions of the membrane testing chamber and overall characteristics of the testing system.

Part, characteristic	Dimensions
Inner liquid compartment	4 x 12.5 x 2 cm
Volume of liquid compartment V_L	100 ml
Inner gas compartment	4 x 12.5 x 1.2 cm
Volume of gas compartment V_G	60 ml
Active membrane surface A_M	50 cm²
Specific transfer area membrane $a_M = A_M/V_{L,total}$	7.4 m^{-1}
Total liquid volume of system $V_{L,total}$	677 ml

The flat sheet membrane was fixed with the help of 12 screws between the liquid and the gas part of the testing chamber made of polyvinylchloride. Polyurethane foam (10 ppi, pores per inch) was integrated inside the gas chamber to provide mechanical stability of the membranes. A flat gasket made of Viton® (fluoroelastomer) was installed between the two compartments (see Appendix, Figure 11-1). Liquid and gas flows were circulated in a countercurrent manner. Liquid flow (100 ml min^{-1}) was realized via a peristaltic pump (Ecoline ISM1-B, pumphead 280, Ismatec) along the peripheral loop consisting of gastight fluoroelastomer tubing (Viton®, d_I = 4.8 mm, wall thickness 1.6 mm, Masterflex). Within the liquid loop a glass bottle of 500 ml volume (filled with dH_2O and mixed by a magnetic stirrer) was integrated to decrease specific membrane area (a = A/V = 7.4 m^{-1}, with a membrane surface of 50 cm^2) as the pCO_2 probe (InPro5000, Mettler Toledo), used to monitor the increase of dissolved CO_2 in the liquid, has a long response time. The total liquid volume accounted for 677 ml. Probes for pCO_2, pH (Polylite Plus ARC, Hamilton Company) and pO_2 (VisiFerm DO Arc Hx 120, Hamilton Company) were integrated inside the liquid peripheral loop with the help of stainless steel adapters. Mixtures of nitrogen and CO_2, or O_2 respectively, were supplied via pressurized gas bottles; gas flows were adjusted with the help of mass flow controllers (MKS Instruments) and gas streams were mixed. Gas flows were optionally saturated with water vapor by bubbling through a water filled bottle integrated in the gas loop before gases entered the chamber. In order to measure relative humidity and consequently water loss across the membrane, a hygrometer (BB sensor, FF-GLT-20MA-INT-TE1) was installed in the exhaust gas stream. The experimental setup was placed inside an electrically heated and water cooled cabinet (Certomat® HK, B. Braun, Melsungen AG, Germany).

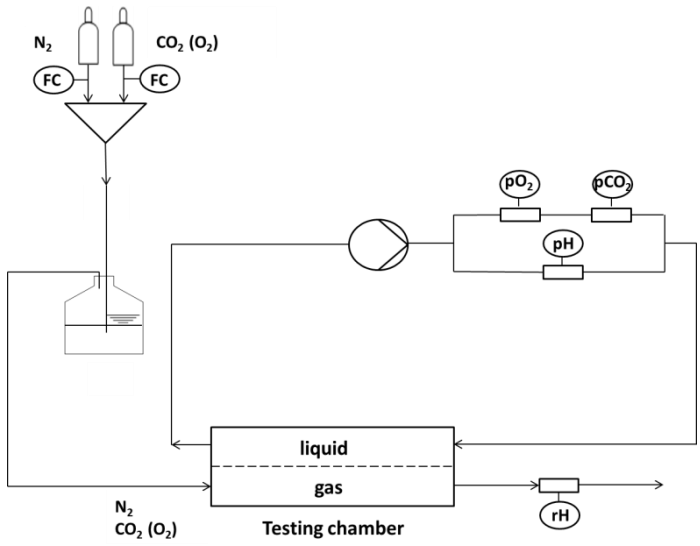

Figure 3-1. Experimental setup for membrane tests. The membrane is indicated by the dashed line; FC = flow control; rH = relative humidity.

3.3.2 Membrane-aerated lab scale photobioreactor

Cultivations of the alga *C. reinhardtii* CC-1690 with diffusion-based membrane aeration were conducted with the help of a modular 200 mL lab scale photobioreactor (Figure 3-2 A-D, technical drawings in Appendix, Figure 11-2) where flat sheet membranes were integrated between gas and liquid compartments. Cultivations were conducted in order to find optimal combinations of membrane materials with their respective transfer coefficients, and gas mixtures to enable a long-term bubble-free aeration inside photobioreactors for microgravity conditions. Furthermore, gas exchange rates should be determined as these are crucial parameters defining the interfaces for the coupling to a heterotrophic compartment. This membrane-aerated photobioreactor was developed as horizontal plate type reactor, representing one volume element of the ModuLES-PBR which is realized as mini-raceway reactor (compare to chapter 3.3.6). Flat sheet membranes were used exclusively throughout this work; however the usage of membrane tubing, coiled inside the liquid chamber, is also possible. The reactor consists of up to three compartments, separated by membranes.

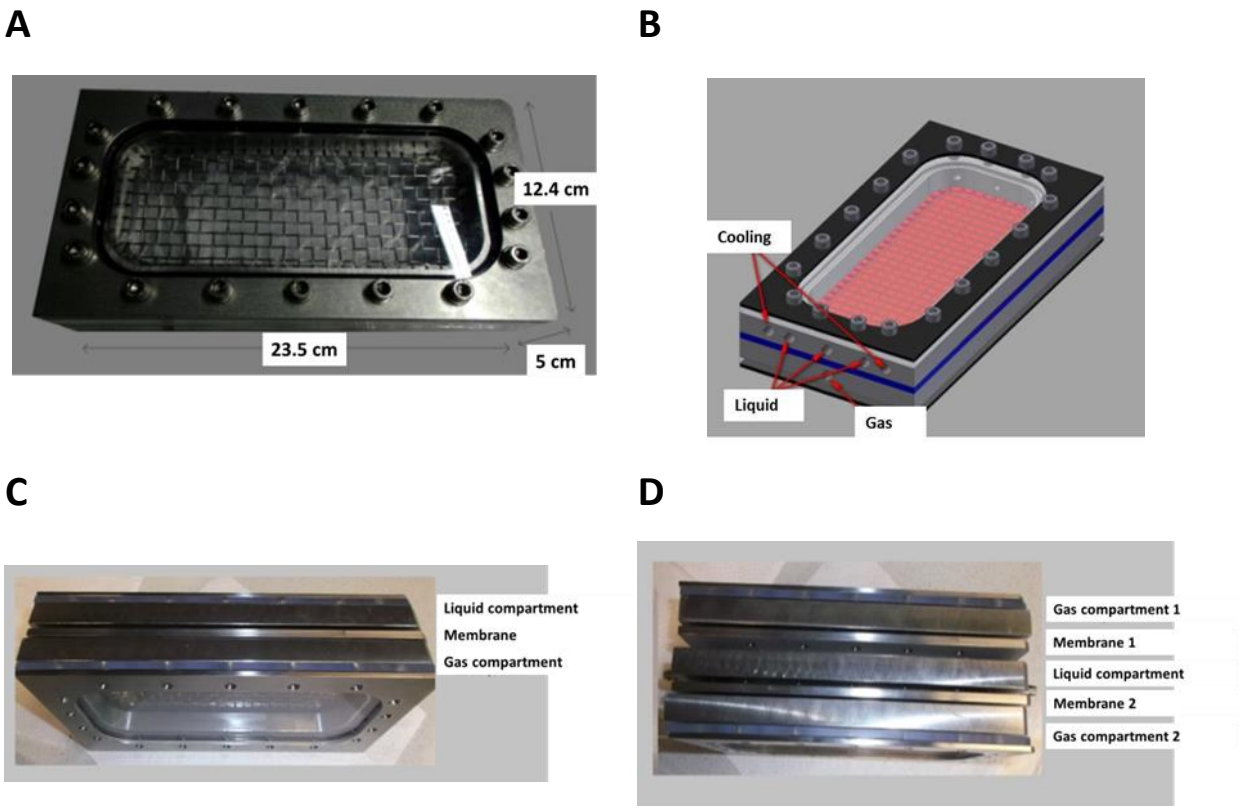

Figure 3-2. Membrane-aerated lab scale photobioreactor. A) Top view of the 200 mL membrane reactor with dimensions. B) Top view of the reactor with liquid and gas inlets as well as cooling. C) Side view of the one-gas-compartment-version of the reactor. D) Side view of the two-gas-compartment-version of the reactor.

The reactor was made of stainless steel (V4A) with front and back sides of translucent polycarbonate (Makrolon GP clear 099 5mm, Glasschmid, Karlsruhe, Germany). All gaskets were made out of gas tight fluoroelastomer. Modularity was realized in that way as the reactor can be run with either one gas

compartment (one membrane), or two gas compartments and two membranes. It would also be possible to couple a heterotrophic compartment to either side of the membrane adjacent to the algae suspension. This modular design allows a high flexibility for various set parameters being inlet CO_2, or O_2 concentration. For the one-gas-compartment-configuration the liquid compartment was mounted on top; for the two gas compartment configuration, the algae suspension was circulated in between the lower und the top gas compartment (Figure 3-2 C, D).

The following table shows the most important dimensions and design parameters. Three inlet holes connected to the tubing with polyethylene flow distributors ensured a homogenous flow over the membrane surface where rounded corners should minimize dead zones within the liquid compartment. Mixing of the algae suspension was accomplished with the help of a peristaltic pump (Ecoline ISM1-B, pumphead 380, Ismatec) integrated in the periphery whereby the liquid was circulated in countercurrent to the gases.

Table 3-2. Technical data, and design parameters of the modular membrane photobioreactor.

Part, characteristic	Dimensions
Outer compartment dimensions	12.4 x 23.5 cm
Inner dimension of liquid compartment	7.4 x 18.5 x 1.7 cm
Volume of liquid compartment V_L	232.73 ml
Inner dimension of gas compartment(s)	7.4 x 18.5 x 1.5 cm
Volume of gas compartment(s) V_G	205.35 ml
Active membrane surface A_{M1} for one membrane configuration	136.9 cm²
Active membrane surface A_{M2} for the two membrane configuration	273.8 cm²
Specific transfer area $a_M = A_{M1}/V_{L,total}$	52 m^{-1} - 37 m^{-1}
Total liquid volume of system $V_{L,total}$	263 ml - 370 ml
Distance of LED panel to reactor surface	10 cm

As some adjustments of the periphery were accomplished in between the single cultivations, the total liquid volume changed and therefore the specific transfer area a_M of the membrane was calculated for every experimental approach. The periphery was built of a gas tight fluoroelastomer tubing (Fluran-5500A, d_I = 4.8mm, wall thickness 1.6 mm, Idex Health & Science, Wertheim, Germany) where small stainless steel cubes (equipped with O-rings made of fluoroelastomer) allowed the integration of probes for pressure (Type PR-35 XHT, Keller AG, Druckmesstechnik, Winterthur, Schweiz), pH (ARC Sensor, Hamilton Germany GmbH, Höchst), pO_2 (amperometric, In-Pro 6800, Mettler-Toledo

GmbH, Gießen, Germany) and pCO_2 (InPro 5000, Gießen, Mettler- Toledo GmbH, Germany). The amperometric oxygen sensor was hereby connected to the controller ADI 1010 (Applikon Biotechnology, Delft, Netherlands). Temperature was measured by a sensor with an integrated Pt100 resistor at the inlet of the reactor compartment. Holes in the frame of the liquid compartment enabled the circulation of cooling water for temperature control. Sampling could be accomplished with the help of several SafeFlow valves (B. Braun, Melsungen, Germany) connected to LuerLock adapters integrated in the peripheral loop. These were also used for optional addition of antifoam, for balancing liquid volume by addition of medium or for the removal and quantification of produced gas volume originating from oversaturation with oxygen.

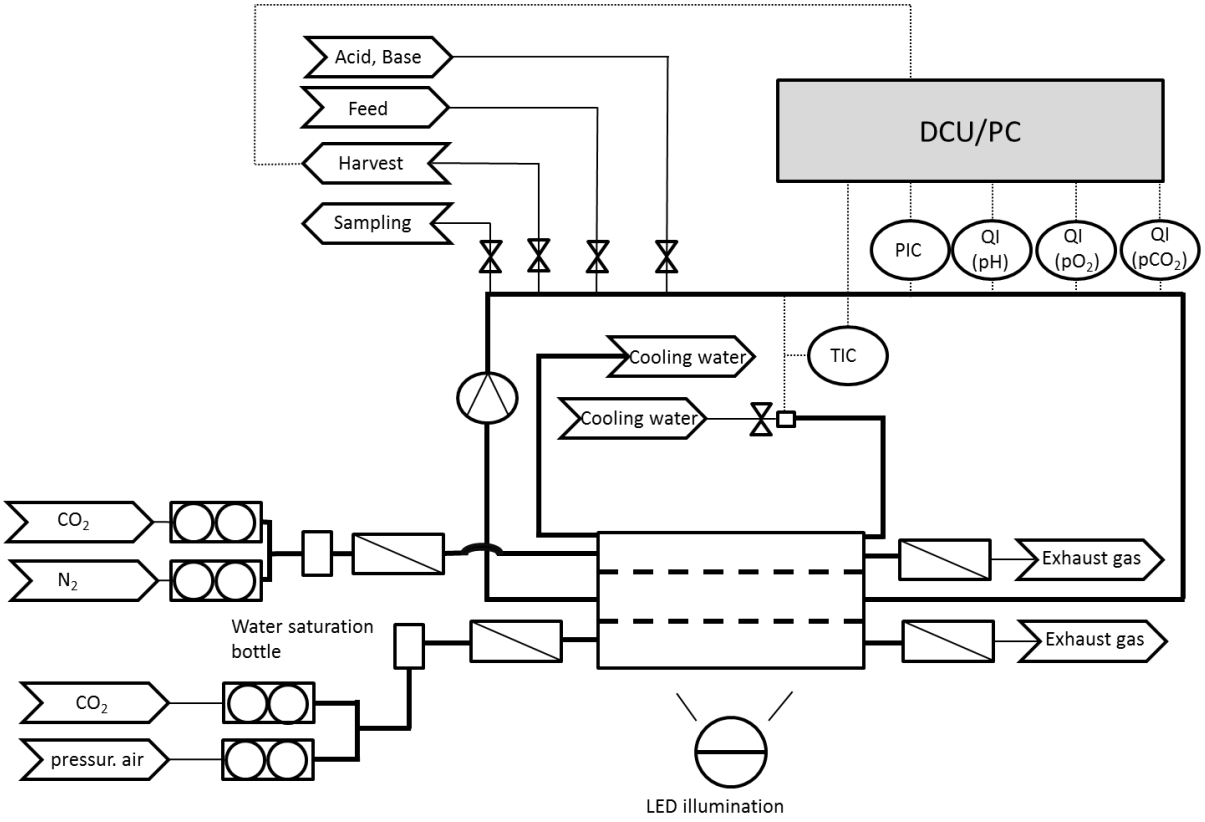

Figure 3-3. Piping and instrumentation diagram (P&ID) for the membrane reactor. Diagram shows the reactor system in continuous process mode. TIC: temperature indicate control; PIC: pressure indicate control (via harvest flow rate); QI: quality indicate for pH, pCO_2, pCO_2; DCU: digital control unit; dashed lines within the reactor chamber represent membranes.

Adjacent to the liquid compartment, membranes were integrated with the help of 18 stainless steel screws and ring gaskets, or flat gaskets for certain membrane materials made of fluoroelastomer. A metal grid on the gas side ensured mechanical stability of the membranes even for the case of slight pressure differences. The gas compartments were continuously flushed with a defined gas mixture (or mixtures in case of two-compartment-configuration) at a controlled flow rate (MassFlow, MKS Instruments). To minimize a loss of culture volume originating from evaporation, the inlet gas was bubbled through a water bottle to saturate it with water vapor. Exhaust gas from the reactor could be

analyzed for its composition via GC analysis (3000A MicroGC, Agilent Technologies, Waldbronn, Germany) after passing through condensate trapping bottles. Mass flow meters were calibrated using a Gilibrator II (Sensidyne, St. Petersburg, USA) and the process control system BioProCon based on LabView. Sensor data was monitored via the BioProCon software, based on LabView (National Instruments, USA) which was also used to control temperature and gas flows. Illumination was accomplished using either warm-white LED light (330 LEDs on a SMD, NS6L083BT, Nichia, Japan) or dichromatic red/blue illumination at a molar ratio of 90 red to 10 blue photons (supplied with 120 red LEDs, peak = 680 nm, Marubeni, Tokio, Japan, SMBB680-1100-02 and 120 blue LEDs, LUXEON® Rebel LXML-PR01-0500, Royal Blue 447.5 nm, Lumileds, Aachen, Germany, per SMD) in accordance to the results summarized in Chapter 4. Light intensity used throughout all cultivations was 200 µE m^{-2} s^{-1} on the illuminated surface of the reactor. Only during the steady-state phase of continuous cultivations the light intensity was changed stepwise in the range of 20-1600 µE m^{-2} s^{-1} for white and 0-300 µE m^{-2} s^{-1} for dichromatic illumination (see chapter 3.4.6).

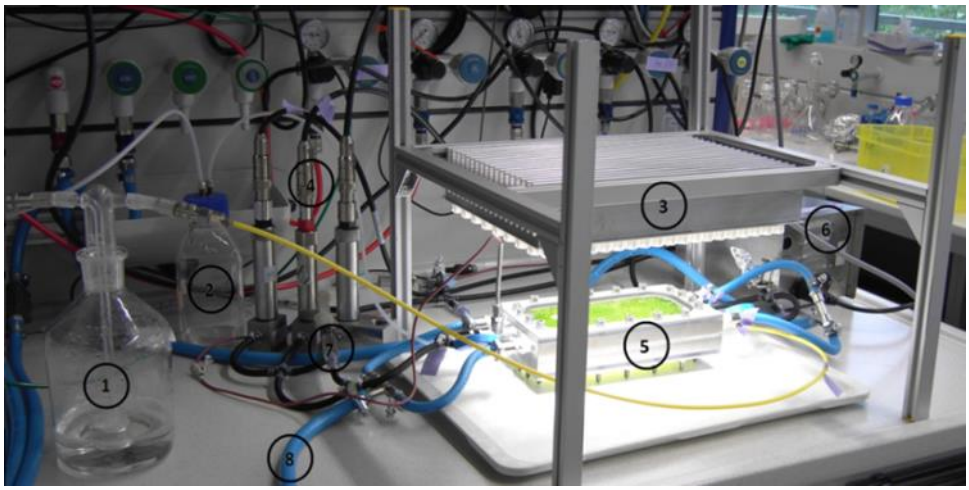

Figure 3-4. Setup of membrane-aerated photobioreactor with periphery in batch mode. (1) Inlet air water vapor saturation bottle, (2) capture bottle for condensate, (3) warm-white LED panel, (4) probes for DO, dCO_2, pH, p, T, (5) photobioreactor with membrane(s), (6) pump, (7) sampling via safelock, (8) cooling water circuit. Optionally exhaust gas is connected to GC for analysis of CO_2, O_2 and N_2.

For continuous cultivations, flexible media bags (5 L volume, Flexboy® Sartorius Stedim) were used for feed and harvest. The feed bag was filled with 5 L sterile, CO_2-saturated medium (1% CO_2 (v/v) in N_2) where gas bubbles were removed under the cleanbench prior to assembling the peripheral loop. Feed and harvest bags were coupled via fluoroelastomer tubing (Fluran-5500A, d_I = 1.6 mm, wall thickness 1.6 mm, Idex Health & Science, Wertheim, Germany) to the sampling connectors in the peripheral loop. Pumps (Miniplus 3, Gilson) for both feed and harvest ensured controlled dilution rates for the continuous procedure.

3.3.3 LED shaker system

With the help of an LED shaker system (Cerff 2012), developed at the Institute of Bioprocess Engineering (KIT), cells were horizontally illuminated and cultivated as pre-cultures for further experiments in other reactor types. Furthermore, this setup was used to determine a correlation factor for cell dry weight (bio dry mass) and optical density of the wildtype CC-1690 of *C. reinhardtii*, either without active aeration or with active aeration. Moreover, smaller experimental approaches studying agglomeration and dissolution of palmelloid structures were also conducted in rotating Erlenmeyer flasks illuminated from below with LEDs. The illumination device allows a simultaneous cultivation of 12 flasks which are illuminated independently via SMD-LEDs (Nichia, type NS6L083AT) and collimating lenses (6° radiation angle, IMM Photonics GmbH). The illumination system was mounted on an orbital shaker (KS 501 digital, IKA Werke, Germany) placed inside an incubator (MKK1200, Flohr Instruments). For some experiments, cultures were actively aerated with air enriched in CO_2 via custom made aeration devices made of glass tubes equipped with sterile filters, for surface aeration as well as submerge aeration with bubbles. In the latter case perforated rubber covers were mounted on the glass tubes to create bubbles. For control of gas flow rate and mixture of air and CO_2 mass flow meters (MassFlow, MKS Instruments) with a controller (Multi Gas Controller 647B, MKS Instruments) were used connected to a flow distributor for equal aeration of 12 flasks. For surface aeration glass tubes were shorter, only reaching just above the liquid surface.

3.3.4 Stirred tank photobioreactor

A stirred tank 2-L photobioreactor (STPBR, KLF 2000, Bioengineering AG, Switzerland, Appendix 11.2.3) with a glass vessel was chosen for µ-I-kinetic studies (see also Figure 11-15), for continuous cultivations as well as for batch cultivations under hypobaric conditions and pressure changes. It was equipped with a customized cylindrical white LED illumination device based on SMD-LEDs (surface-mounted device), (Jacobi 2012 a). For the illumination warm-white LEDs (type NS6L083AT, Nichia, Japan) and collimating lenses (6° radiation angle, IMM Photonics GmbH) with intensities from 0 to 1600 µE m^{-2} s^{-1} were used. For some of the batch cultivations under lowered pressure a new LED panel with cold-white light (type NFSW036BT, Nichia, Japan) was used due to technical failure of the older one. Control of LEDs was realized via the process control system BioProCon based on LabView, National Instruments. Mixing was realized by a two-stage disk agitator where baffles ensure homogenous mixing conditions with dispersion of nutrients and suspension of cells. Air enriched in CO_2 was introduced as bubbles via a gassing ring below the stirrer. Flow rate and composition were controlled via two mass flow meters (M&W Instruments MSR D5111 for air and Massflow MKS 1179B for CO_2). Calibration of air flow rate was accomplished with the help of the Gilibrator (Sensidyne, St. Petersburg, USA). Temperature was measured via a Pt100 resistor element and controlled via an electrical heating rod and a cooling rod flushed with cooling water. The pH was measured online (Polylite Plus 225, Hamilton) with a measurement amplifier (Thornton M300-Modul,

Mettler Toledo) and controlled via addition of base or acid by peristaltic pumps (Alitea XV, Bioengineering). With the help of an online probe (AvaSpec-3648) the optical density of the culture suspension was determined. Stirrer speed and temperature were controlled via the Bioengineering controller (Bioengineering AG, type IFM); other parameters like pH and flow rate were controlled via the software BioProCon based on LabView (National Instruments, USA). Off-gas was analyzed for its O_2 and CO_2 concentration based on paramagnetic behavior of O_2 and infrared absorption of CO_2 with the exhaust gas analyzer (Sick-Maihak, Germany).

Table 3-3. Dimensions of the 2-L stirred tank photobioreactor with bubble aeration.

Parameter	Abbreviation	Dimension
Height glass tank	H	300 mm
Inner diameter glass tank	d_I	100 mm
Stirrer diameter	d_S	60 mm
Volume, total	V_{total}	2356 cm³
Working volume	V_R	1800 cm³
Illuminated surface	A	827 cm²
Illuminated surface/volume ratio (SVR)	A/V_{total}	0.35 cm^{-1}
Slenderness ratio	H/d_I	3.0
Stirrer-/inner diameter ratio	d_S/d_I	0.6

Further design details of this reactor are depicted in Appendix 11.2.3. A light intensity profile for different cell densities and incident light intensities is shown in Appendix 11.6.3.1.

For continuous cultivations, an in- and outflow of medium and culture suspension was installed with tubing and attached piercing pins and septa connected to the reactor cover. In this case flow rate for in- and outlet was adjusted manually concerning pump speed (Miniplus 3, Gilson) to achieve a constant cell density and steady-state conditions. Calibration curves of pumps are shown in Appendix, 11.3.

For cultivations under lowered pressure and pressure changes some modifications had to be integrated in order to enable pressure control and aeration during the batch processes. Additionally, more sensors were integrated in the reactor lid: a probe for dissolved CO_2 as pCO_2-sensor (InPro5000, Mettler Toledo) with measurement amplifier M400 (Mettler-Toledo) as well as an optical pO_2-sensor (VisiFerm DO Arc Hx 120, Hamilton Company). Furthermore, a pressure sensor was integrated in the exhaust gas line above the sterile filter. For pressure reduction and control, a vacuum pump acting as membrane pump (KnF LAB SC920) was installed inside the exhaust gas loop. Vacuum resistant silicone tubing was used to connect reactor and pump. As bioreactors are usually designed for

withstanding slightly higher than atmospheric pressure, for instance, during steam autoclaving at around 1 bar overpressure, changes concerning sealing and connections had to be accomplished. Swagelock-valves were added to the reactor periphery tubing in order to avoid pressure compensation through sterile filters of peripheral bottles for inoculum, for example. An exit gas cooler and a pressure gauge with a shutoff valve were integrated inside the exhaust gas line together with a pressure sensor. For online sensors, placed at the reactor lid, two sealing rings, instead of only one, were built in, one between sensor and adapter and the second between adapter and reactor lid.

3.3.5 Plate reactors

Experiments to determine effects of mono- and dichromatic illumination, in semi-fed-batch and continuous mode, were conducted in plate type reactors in two different scales. Continuous cultivations however, where only conducted in the bigger scale version. Mini- and midiplate reactors were used for these experiments with working volumes of 0.2 and 1 L respectively (internal measurements of 140 x 100 x 20 mm for mini- and 350 x 200 x 20 mm for midiplates) consisting of stainless steel frameworks with two glass panes as front and back side. More details of miniplate composition were already mentioned in Jacobi (2012 b). A porous PTFE membrane (1 µm THOMAPOR-Poröse Platte, RTC Reichelt Chemietechnik, Heidelberg, Germany) fixed in the bottom plate was used for aeration. The resulting bubbles were used for mixing in both reactor types after applying pressurized air enriched in CO_2. Inlet and exhaust gas loops were equipped with sterile filters (0.2 µm). Sampling was achieved by using sterile syringes and SafeFlow valves with Luer-lock adapters (B. Braun, Melsungen, Germany) and a needle inside the plates reaching into the liquid phase. Two mass flow meters (MassFlo, MKS Instruments, München, Germany) were used to control flow rate and composition of inlet air. For miniplates temperature was kept constant using an incubator (Flohr Instruments, The Netherlands); for midiplate cultivation T was kept constant using cooling water circuits in the stainless steel frame and the process control system BioProCon written in LabView (National Instruments). The pH was uncontrolled in both reactor types. Dimensions and parameters of mini- and midiplate reactors are shown in the following table. More details are mentioned in Jacobi (2012 b). With the same thickness of 2 cm, midiplate reactors have a five times higher volume than the smaller version.

Concerning measurement instrumentation for semi-fed-batch cultures in midiplates, a temperature (Pt100 resistor) and a pH sensor (pH ARC Sensor, Hamilton Bonaduz AG, Switzerland) were integrated via the reactor lids.

Table 3-4. Dimensions and parameters of mini- and midiplate reactors

Parameter	Abbreviation	Dimensions mini- /midiplates
Height	H	140 mm / 350 mm
Filling level	h	100 mm / 250 mm
Width	W	100 mm / 200 mm
Thickness	d	20 mm / 20 mm
Working volume	V_R	200 cm³ / 1000 cm³
Illuminated surface (one side)	A	100 cm² / 500 cm²
Illuminated surface/volume ratio (SVR)	A/V_R	0.5 cm^{-1} / 0.5 cm^{-1}

For continuous cultivations in midiplate reactors additionally an optical pO_2 sensor (Hamilton, Visiferm Arc 120, Hamilton Bonaduz AG, Switzerland) was integrated. A four-channel peristaltic pump (Ismatec Reglo ICC, Cole-Parmer, Wertheim, Germany) connected to the process control system BioProCon was used to deliver feed medium and harvest cell suspension for both plates at a controlled pump rate. To control cell density inside the reactors, the transmitted light of an infrared LED was measured with a UV-Vis-detector (Avantes, AvaSpec) which was installed at the front side of the plate reactors. Via the integration of a PI-controller the transmission was kept constant as a control variable. The pump rate for feed and harvest was used as correcting variable. Further details are mentioned in chapter 3.4.6.

3.3.5.1 Illumination of miniplate reactors

In case of miniplate reactors, on the one hand, LED panels with warm-white LED light were used as control, on the other hand, panels with red and blue LEDs, and panels with red and green LEDs were used to test different monochromatic illuminations as well as combinations of red and blue and red and green light. Warm-white LED light was supplied using 60 LEDs (NS6L083BT, Nichia, Japan) with 6° collimating lenses (IMM Photonics GmbH, Unterschleißheim, Germany) at a distance of 10 cm from the illuminated surface of the plate reactor. Color LED illumination for miniplates was realized as mixture of red and green (18 red LEDs, Epitex L680-02AU, Kyoto, Japan, 18 green LEDs, Winger® WEPGN1-S1 Power LED Star green (520 nm) 1W, Dessau-Roßlau, Germany), and red and blue (30 red LEDs, Epitex L680-02AU, Kyoto, Japan, 30 blue LEDs, LUXEON® Rebel LXML-PR01-0500, Royal Blue 447.5 nm, Lumileds, Aachen, Germany). The differently colored LEDs were homogeneously distributed and each color was individually controlled and also monochromatic red, blue as well as green illumination was applied. Light for miniplates was controlled via BioProCon written as a routine in LabView (National Instruments).

3.3.5.2 Illumination of midiplates

In case of midiplate reactors, again warm-white LED illumination was used as control and red and blue LEDs for mixtures of colored illumination. Warm-white LED light for control was supplied using 330 LEDs (NS6L083BT, Nichia, Japan) at a distance of 15 cm from the illuminated reactor surface. Red/blue LED light was supplied by 120 red LEDs (peak = 680 nm, Marubeni, SMBB680-1100-02) and 120 blue LEDs (LUXEON® Rebel LXML-PR01-0500, Royal Blue 447.5 nm, Lumileds, Aachen, Germany). Emission spectra of color LEDs compared to full-spectrum warm-white LEDs are shown in Chapter 4, Figure 4-1 A.

3.3.6 ModuLES-PBR: pre-culture and photobioreactor tested in parabolic flights

A novel membrane-aerated photobioreactor concept was developed for space application and was tested in two parabolic flight campaigns and on the ground. This should reveal how hardware and software of the system withstand changing gravity conditions and give first hints for effects of changed force of gravity on algal physiology and overall photobioreactor performance. For that cells of *C. reinhardtii* CC-1690 were first pre-cultured during one week at the laboratories of Novespace, France.

3.3.6.1 Pre-culture system for parabolic flights

Penicillin-flasks with a volume of 4 L made of borosilicate glass were used to culture cells on orbital shakers (KS 501 digital, IKA Werke, Germany) equipped with horizontally mounted SMD-LED panels with warm-white (NS6L083BT, Nichia, Japan) and red/blue LED illumination (red LEDs, peak = 680 nm, Marubeni, Tokio, Japan, SMBB680-1100-02 and blue LEDs, LUXEON® Rebel LXML-PR01-0500, Royal Blue 447.5 nm, Lumileds, Aachen, Germany). The flasks were inoculated with liquid cultures transported by car in 2 L borosilicate bottles aerated with air by air pumps (air pump 100, Eheim, Deizisau, Germany) and illuminated with warm-white LED light-strips from construction market in order to achieve a starting cell concentration for the main reactor cultivation of about 2 g L^{-1} after one week. Surface aeration was accomplished via a pressurized gas bottle with a prefilled gas mixture of 5% CO_2 (v/v) in air. In the gas line several pressure reducers (double-stage pressure regulator and relief valve HBS 200-3-2.5, Air Liquide, France) were installed and with the help of rotameters (PKB Process Instruments) the flow rates were installed. Gas flows were equally distributed to six flasks via flow splitters and sterile filters at the inlet and outlet of the lids enabled axenic conditions.

3.3.6.2 ModuLES-PBR: concept and design

For the ModuLES-PBR a concept based on a plate-type reactor was used, and realized as a mini-raceway reactor that can be illuminated either from one side or from both sides. In the first approach one-sided illumination with either warm-white LEDs or dichromatic red/blue LED lighting was used. Warm-white LEDs from Ledxon (SMD3528 warm white 3000K, Ledxon Company, Landshut,

Germany) were used for the first parabolic flight campaign and red and blue LEDs from Epitex (Kyoto, Japan, red: SMT680, blue: SMT450) for the second parabolic flight campaign. Datasheets of LEDs used are shown in Appendix 11.4.1.

For the diffusion-based bubble-free aeration flat sheet membranes fixed on both sides of the mini-raceway reactor (either horizontally or vertically mounted) were used to supply CO_2 to the cells as well as for removal of O_2 produced. The system was composed of two gas compartments (gas exchange and gas collection) flushed with different gas mixtures and one liquid compartment (2 L volume) housing the algae. Gas- and liquid-containing compartments had a meandering shape with the gas flow circulating in countercurrent to the liquid flow. Mixing was realized by a peristaltic pump (Ecoline ISM1-B, pumphead 380, Ismatec) installed in the periphery. Concerning membranes it was possible either to use the same membrane on both sides of the algae compartment or use different membranes adjacent to the two gas compartments.

The PBR stack consisted of two connected stacks of fluid chambers. Each stack was comprised of two photobioreactor chambers, two gas exchange compartments, one gas collection compartment, and two panels of LED for illumination (Figure 3-5). The MSH (ModuLES Scientific Hardware) had dimensions of 34.5 cm x 25.6 cm x 22.5 cm; the mass was about 15 kg, including the 2 L of algae culture. The liquid and gas chambers were made of autoclavable Tecapro MT (Ensinger, Wales). The liquid compartments had a thickness of 1.5 cm (light path) in which the algae culture circulated along the meander-shape. Each photobioreactor chamber had a volume of about 500 ml. The two photobioreactor chambers were connected in series, obtaining the final culture volume of 1 L for each stack, or 2 L total of liquid volume with both stacks. One PBR chamber in each stack included an optical window through which optical density of the algae suspension could be measured. The PBR liquid chambers were separated by the membrane from the gas collection chamber, which was also made from autoclavable Tecapro MT (polypropylene, Ensinger, Mid Glamorgan, Wales), with a thickness of 2 cm. The gas chamber also had a meander-shape and a volume of 650 ml. The gas collection chamber included temperature and pressure sensors, as well as an optical window for O_2 measurements. The gas exchange chamber was identical to the gas collection chamber. Membranes were placed between the chambers (Figure 3-5 C), and sealed via a round seal. With a specific membrane surface area of 47 m^{-1} this value of the ModuLES-PBR was similar to the smaller membrane reactor used for lab experiments (compare to Table 3-5 and Table 3-2).

Transparent Lexan (Lexan* 9030 FA Sheet, Sabic Innovative Plastics, Pittsfield, USA) plates were attached to outer sides of gas exchange chambers, through which algae were illuminated by the adjacent LED panels. The LEDs were supported by an aluminium frame. Each LED PCB (printed circuit board) was equipped with a thermal sensor Pt100.

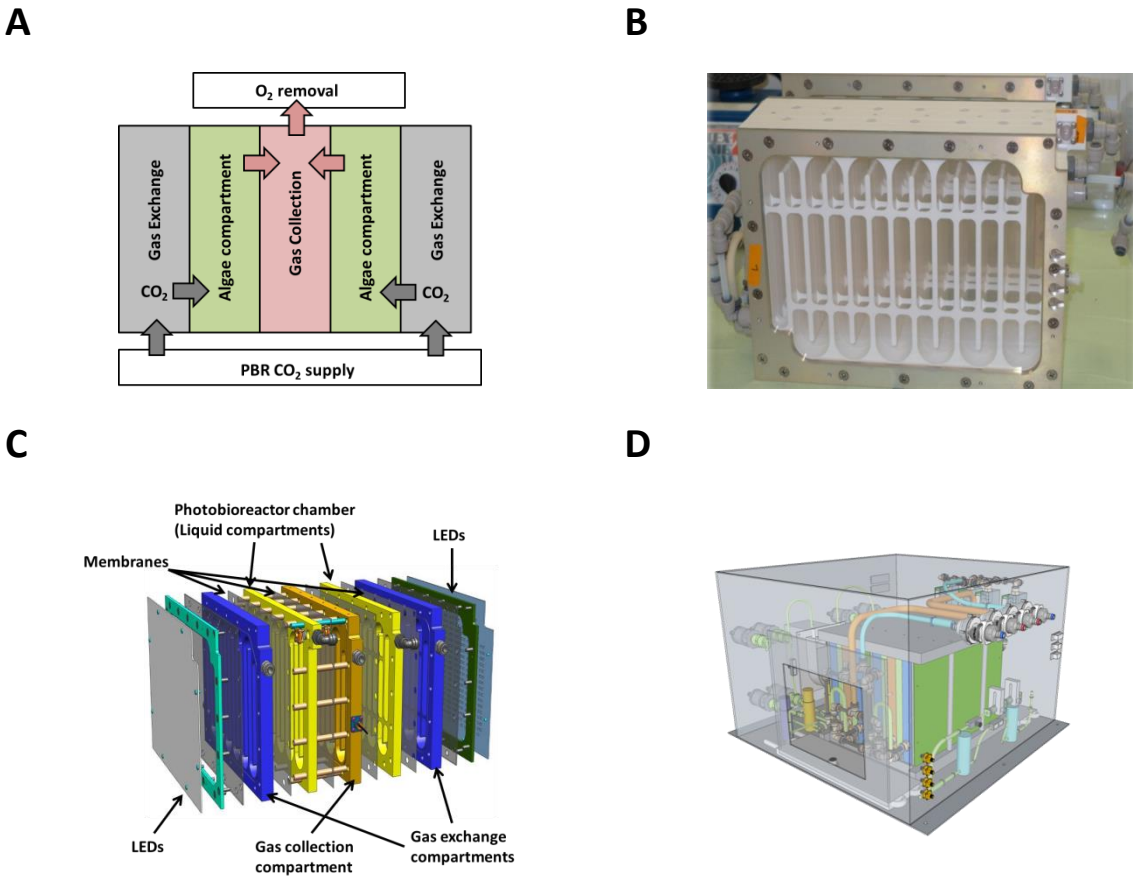

Figure 3-5. ModuLES-PBR. A) Gas exchange in the ModuLES-PBR with two gas compartments. B) Front view of one of the ModuLES-PBR stacks. C) Stack compartments with LEDs and membranes. D) ModuLES-PBR (ModuLES scientific hardware, MSH) inside the MSC (ModuLES standard container), Podhajsky (2014).

The liquid loop was made of rigid PTFE tubing (AdTech, d_o = 6.4 mm) and Viton (Saint Gobain, d_o = 4.8 mm) with Push Fit Fittings (John Guest). This loop connected the stacks of each 500 ml so that an overall reactor stack liquid volume of 2 L with an overall system volume of 2.7 L was resulting. The algae suspension was pumped with the help of a peristaltic pump (Ismatec VC380) through the whole system. The housing (MSC - modules standard container) was made of aluminium panels with a small Lexan window for optical inspection. The MSC contained the double-stack reactor including the peripheral pump for mixing. Quick Disconnect adapters for fluids (Walther Präzision) and gases (Colder Products Company) were used for liquid and gas loop connections to the system like feed medium supply and for flushing of gas loops.

The gas loops were connected via gas tight PTFE tubing (AdTech) and PTFE gas chambers to increase the volume, resulting in 6.5 L in case of the gas exchange loop, 2 L in case of gas collection loop. Air pumps (rotary vane air pump, model G12/02-4EB, Thomas) in both gas exchange and collection loop were used to circulate the gases along the loop. The gas exchange loop was used for CO_2 supply and the gas collection loop was used for O_2 removal. A gas collection bag (Tedlar gas sampling bag, 3.8 L, PVDF, Kleinfeld Labortechnik), connected with a three-way-valve to the loop, served to collect the

gas volume from the collection loop after the parabolic flight in order to analyze the gas volume for its CO_2, N_2 and O_2 composition via GC analysis. The gas loops were flushed with a pre-defined mixture of gas prior to the flights and then closed. The oxygen partial pressure inside the gas collection loop was monitored. The sample bag was integrated directly into the continuous flow path and removed after landing for the analysis.

Table 3-5. Dimensions and characteristics of the ModuLES-PBR.

Part, characteristic	Dimensions
Outer compartment dimensions	34.5 cm x 25.6 cm x 22.5 cm
Volume of 4 liquid compartments	2000 ml
Volume of one liquid compartment V_C	500 ml
Total liquid volume of reactor system V_{total}	2700 ml
Volume of single gas compartment, gas exchange	650 ml
Volume of single gas compartment, gas collection	650 ml
Total volume gas exchange	6.5 L
Total volume gas collection	2 L
Active membrane surface A_{M1} of the 4 liquid compartments, one membrane side is considered	1279 cm²
Total membrane surface $A_{M,total} = 2 \cdot A_{M1}$= (A(Gas exchange membranes) + A(Gas collection membrane)) · 4	2558.4 cm²
Specific transfer area relating to one membrane side, a = A_{M1}/V_{total}	47.4 m^{-1}
Specific transfer area relating to total membrane surface (two sides) of gas exchange and collection side and total liquid volume, a = $A_{M,total}/V_{total}$	94.8 m^{-1}
Distance of LED panel to reactor surface	1.5 cm

There were various sensors installed in the liquid loops as well as in the gas loops. The gas exchange loop (GE-loop) was equipped with an air flow meter (Honeywell), a relative humidity and temperature sensor (Honeywell) as well as optical CO_2 and O_2 partial pressure sensors (Carbonoxy, Pewatron, Munich, Germany). The gas collection loop was equipped with a pressure sensor (Kulite) and an O_2 sensor (Firesting O_2 meters 4 channels, Pyroscience sensor technology, Copenhagen, Denmark).

Integrated in the liquid loop there were in total three optical density sensors (OD at 750 nm), four sensors for absolute pressure, three sensors for temperature, one optical sensor for dissolved CO_2 (PDS-005, DSP 4000mc, 2 channel, Polestar Technologies Inc., USA), dissolved O_2 (OEM Firesting

O_2 meter, Pyroscience sensor technology, Copenhagen, Denmark) and for pH (optical sensor, PDS-004, DSP 4000mc, 2 channel, Polestar Technologies Inc., USA). A fluorescence measurement was realized with the help of a PAM sensor (Junior PAM, Walz Mess- und Regeltechnik, Effeltrich, Germany) using actinic white light integrated in a small bypass loop which was flushed in normal mode and closed in PAM acquisition mode. PAM analysis was used to detect possible changes in photosynthetic activity upon changed gravity conditions.

A sampling unit was integrated in the periphery of the reactor consisting of 12 standard luer tip syringes (20 mL syringe, Braun, Melsungen) which were modified and pre-filled with each 5 mL RNA fixative (supplier). With the help of a movable piston, which was automatically shifted, the sample was taken at the desired time with the help of a push button. The liquid volume of the system was kept constant, meaning that the sample volume taken (5 mL each) was directly balanced with fresh medium from the storage tank.

For continuous cultivation, fresh medium was fed from a storage bag (500 mL, single usage Bioprocess Containers™) with the help of another peristaltic pump (peristaltic pump, Instech 625/275) into the reactor. For fresh media supply there were two media bags (each 500 mL, CX5-14 film, HyClone Labtainer BioProcess Container™ Thermo Scientific) filled with different liquid media. One feed medium (volume of 380 mL) was saturated with 1% CO_2 in air (v/v) (relating to 100% CO_2 saturation) which was used for the continuous chemostat feed. The other medium was not saturated with CO_2 (volume contained was 350 mL) and only used to increase the pH when needed.

In the normal operating mode the algae suspension was pumped (peristaltic pump, Instech 625/275) at the same rate to a biomass harvesting container (500 mL, CX5-14 film, HyClone Labotainer BioProcess Container™ Thermo Scientific). This harvesting container could be coupled to a filtration unit for solid/liquid separation. Additionally, a volume compensator bag was coupled to the loop. Its activation was triggered by pressure monitoring of the liquid loop. Above overpressures of 300 mbar the three-way-valve changed its status and the volume compensation bag acted as relief valve.

Control loops were established for several parameters in order to enable a long-term stable cultivation. The pH was kept constant by dosing either 1% CO_2 saturated (v/v) or unsaturated feed media into the liquid loop as soon as pH was out of range (7.0 ± 0.5). Temperature was controlled and kept constant at 23 ± 2°C by a feedback-controlled Peltier element circuit with a heat sink with an axial fan also in proximity to LED panels. Data was monitored and stored at 5 s intervals. For the safe operation mode a temperature drop to 16°C or rise to 28°C was defined as threshold for a short-term period (for instance 0.5-1 h, when the flight was delayed). As the process was run in a continuous mode, the dilution rate was installed and kept constant during parabolic flight. During long-term ground testing it was regulated manually. Pressure was controlled by feeding rate from the medium compensation bag. A drop of pressure down to about 700 mbar absolute pressure was tolerated during flight duration. In

total the system was comprised of two racks, one with the biological components/the biological module and one which incorporated the electronics.

For mass transfer of gases to supply algal cells with CO_2 and remove O_2, one of the gas compartments contained 5% CO_2 (v/v) in air (in relation to 100% CO_2 saturation; termed gas exchange loop) for the CO_2 supply to keep dissolved CO_2 in the liquid at a level of 1%. The second gas compartment (termed gas collection) was used for O_2 removal and was flushed with a mixture of 1% CO_2 in N_2 (v/v) to create a high driving force for the O_2 transfer across the membrane. During two parabolic flight campaigns and ground experiments a dense flat sheet membrane made of polymethylpentene with 50-µm thickness (TPX compare to Table 3-6) was used. For a first hardware test during the first parabolic flight campaign, illumination of cells was achieved by warm-white LED illumination with a PFD of 200 µE m^{-2} s^{-1} (corresponding to about 42 W m^{-2}) whereas in the second flight campaign red (emission peak at 680 nm) and blue LEDs (peak at 450 nm) were used for dichromatic illumination at a ratio of 90/10 red/blue photons.

Technical realization, measurement, and control of this reactor system were accomplished by OHB System AG, Germany, (Podhajsky 2014).

3.4 Cultivation conditions and procedures

3.4.1 Membrane materials tested

For assessment of mass transfer coefficients for CO_2 and O_2, selectivity factors as well as water vapor permeability of membrane materials, in total 17 material samples in form of flat sheets were tested inside a gas-liquid-system. A gas-liquid system was chosen as it mostly resembled the later application system in form of a membrane photobioreactor. However, advantageous of a gas-gas testing systems is that the resistance of the membrane itself to mass transport can be measured directly, without having the influence of liquid boundary layers (Lund 2002). There were porous and dense membranes among the tested membranes, partly with supporting layers for increasing stability and ease of handling purpose. Membrane properties like thickness, porosity (in case of porous membranes), and degree of transparency are listed in Table 3-6.

In case of membranes with supporting layers, the supported side was facing the gas phase when the membrane was installed inside the chamber.

For cultivations inside the modular membrane photobioreactor, a suitable selection of several membranes was tested, either in the one-gas-compartment-configuration or in combination in the two-gas-compartment-configuration. These membranes were the dense polymethylpentene membrane (TPX, Goodfellow, 50 µm), various dense silicone elastomer membranes (Wacker old, Wacker 80, 100, 200) as well as porous ACP (PALL) and PE (Accurel Membrana) membranes.

Table 3-6. Overview of all membrane materials tested.

Manufacturer/membrane/ material/type	Abbreviation used in this work	Pore size [µm]	Thickness [µm]	Transparency
Membrana/ Accurel® / Polypropylene/ PP 1E (R/P)	Accurel PP	0.1	100	no
PALL/ Emflon®/ PTFE/ PTF020LH0A-SAMP	PTFE 0.2	0.2	250	no
PALL/ Emflon®/ PTFE/ PTF002LH0A-SAMP	PTFE 0.02	0.02	200	no
Goodfellow/ Silicone elastomer-Film/ Silicone elastomer/ SI301050	Goodfellow	dense	50	yes
PALL/ FluoroTrans® Membrane/ PVDF/ P/N PVM020C3R	PVDF 0.2	0.2	120	no
PALL/ Supor®-200R/ PES/ P/N S80526	PES 0.2	0.2	200	no
Goodfellow/ TPX®/ Polymethylpentene/ ME311050/1	TPX	dense	50	yes
PALL/ Versapor®-200R/ Acrylic Copolymer/ P/N S80273	ACP	0.2	300	no
Wacker/ ELASTOSIL® LR 3003/30 A/B /Silicone elastomer	Wacker, old	dense	200	yes
Wacker/ ELASTOSIL® Film 2030 250/40/ Silicone elastomer	Wacker 40	dense	40	yes
Wacker/ ELASTOSIL® Film 2030 250/80/ Silicone elastomer	Wacker 80	dense	80	yes
Wacker/ ELASTOSIL® Film 2030 250/100/ Silicone elastomer	Wacker 100	dense	100	yes
Wacker/ ELASTOSIL® Film 2030 250/200/ Silicone elastomer	Wacker 200	dense	200	yes
SBS symmetric Membrane	SBS sym	dense	30	yes
SBS asymmetric Membrane	SBS asym	dense	30	no
PDMS + silicalite Membrane	PDMS	dense	30	no
PVA Membrane	PVA	dense	30	no

3.4.2 Procedures for determination of k_L values, selectivity and water loss

In order to determine $k_{L,CO2}$ and $k_{L,O2}$ values of the membrane materials, step changes inside the testing chamber for a gas liquid system were applied. The respective gas was stripped out of the liquid with nitrogen und then a step change to a volumetric gas concentration of 50% CO_2 or O_2 in N_2 was applied. The accumulation of the respective gas in the liquid was recorded and used for the calculation of the transfer coefficient. By measuring the relative humidity in the off-gas leaving the chamber the water loss per membrane area and time could be determined.

To begin an experiment for assessment of mass transfer coefficients and water loss of a membrane material, sensors for dissolved gases, pH and relative humidity were calibrated. The pH sensor was calibrated with two standard solutions at pH 4 and pH 7. The optical dissolved oxygen sensor was calibrated after saturating distilled water with pure O_2 as 100% value and with N_2 as 0%. The pCO_2 sensor was calibrated using distilled water saturated with specific gas mixtures with different defined volumetric CO_2 concentrations in air (v/v): 5, 10, 15, 30, 50, and 60%. The relative humidity sensor was calibrated with the help of saturated salt solutions. The sensor was placed in the gas phase above a saturated water magnesium chloride solution and the value in equilibrium was set at 33% relative humidity (for temperature range 5-45°C). The second point was calibrated with a saturated NaCl-H_2O solution giving a relative humidity of 75% in the range of 10-45°C.

After assembly of the testing chamber, the respective membrane and the periphery with the sensors, the system was filled with distilled water. For fitting of silicone-elastomer membranes these were previously soaked in EtOH (76% v/v) in order to optimize handling. The liquid flow was adjusted to 100 ml min^{-1} (pump rate 7 rpm, v = $1.98 \cdot 10^{-3}$ m s^{-1}), and a gas flow of 40 ml min^{-1} with pure N_2 was started to strip out the remaining dissolved gases. For some experiments the gas flows were saturated with water vapor by bubbling through a water filled bottle integrated in the gas loop before gases entered the chamber. For the rest of experiments the gases were not saturated with water vapor to measure water loss with dry inlet air. Temperature was kept constant at 25°C (± 0.5°C), unless stated otherwise, with the help of an electrically heated and water cooled cabinet (Certomat® HK, B. Braun, Melsungen AG, Germany).

In the case of the standard CO_2 step changes, the starting pH of the distilled water was adjusted to a constant value of 6.7 for all the experiments. Step changes to 50% CO_2 (v/v) ended at an approximate pH of 4.5. The adjustment of the initial pH was done in order to have the same concentrations of the different carbon species in equilibrium at the beginning of the step change for the different experiments for all of the tested materials. After a constant minimal dissolved gas concentration of the respective gas was measured, the step change was started by applying 50% (v/v) CO_2, or O_2 respectively, in N_2 (gas flows were both adjusted to 20 ml min^{-1}). The step change experiment was ended when equilibrium, and hence a constant dissolved gas concentration in the liquid, was reached.

Online data was monitored and saved via the control system BioProCon written in LabView (National Instruments, USA). Analysis of online data for determination of mass transfer coefficients is described in section 3.6.1.1 and for water loss in section 3.6.1.3.

3.4.2.1 Influence of thickness of dense membrane materials on k_L values

By testing membranes of the same material with different thicknesses, the influence of this factor on transfer coefficients can be tested. Suitable for these experiments were dense silicone elastomer membranes with 40, 80, 100 and 200 µm thickness (Wacker 40, 80, 100 and 200). They were tested for both CO_2 and O_2 transfer and $k_{L,O2}$ and $k_{L,CO2}$ values were calculated. For porous membranes this was not possible as there were no membranes available made from the same material in several thicknesses.

3.4.2.2 Influence of temperature on mass transfer coefficients

As temperature is a very important factor influencing the process of diffusion it was also tested during mass transfer experiments in the case of O_2 and for three temperatures: 20, 25 and 30°C and two porous membranes, PP membrane (Membrana, Accurel) and the PTFE membrane (PALL, PTFE, pore size 0.02 µm).

3.4.2.3 Influence of liquid velocity on mass transfer coefficients

In order to study the influence of the liquid flow velocity on the value of k_L, step changes at different pump speeds were carried out. The flow rates tested were 50, 100 and 200 mL min^{-1} (corresponding to pump speeds of 4, 8 and 15 rpm) and the membrane used for such step changes was PTFE 0.02. In theory the flow rate has a direct influence on the thickness of the laminar phase adjacent to the membrane, which in turn influences mass transfer. At higher flow rates, the laminar phase will become smaller according to theory and therefore the influence should be seen in the results by a classical saturation curve approaching the value of k_L for pure membrane resistance.

Flow velocity (Equation 3-2) was calculated from the pump calibration curve (see Appendix, Figure 11-4 B) and the cross sectional area of the testing chamber based on continuity Equation 3-1:

Equation 3-1. Continuity equation

$$\dot{V} = v_1 \cdot A_1 = v_2 \cdot A_2$$

Equation 3-2. Liquid flow velocity inside the testing chamber

$$v_{Chamber} = \frac{\dot{V}}{A}$$

with A: cross-sectional area of testing chamber (liquid compartment) = 0.0008 m^2

3.4.2.4 Influence of salt concentration and pH on $k_{L,CO2}$

As also salt concentration is an important influencing factor on mass transfer of gases, first of all experiments with culture medium (TP-NO_3) compared to dH_2O were conducted. For these tests the porous PTFE membrane (PALL, pore size 0.02 µm) was used.

As CO_2 dissociates in water and there are pH-dependent reaction rates, influencing the driving force for mass transfer of CO_2, all of the tests before where conducted exactly in the same pH range with the same starting pH for every material tested. In order to determine the influence of pH and salt concentration on the $k_{L,CO2}$ value, another series of tests was conducted. This is especially important for the quantitative accuracy and the applicability of the determined $k_{L,CO2}$ values for the design of a membrane-aerated photobioreactor. Another fact being decisive is that the used pCO_2 sensor only detects dissolved CO_2 (dCO_2) as species but no carbonate species. For these tests the porous PP membrane (Membrana, Accurel) was assembled in the testing chamber. Distilled water at different pH values, buffered algae medium (TP-NO_3) at different pH values and medium without a buffer were used for these experiments.

3.4.3 Cultivation conditions and procedure for the membrane-aerated PBR

In order to study diffusion-based membrane aeration for microalgae cultures, cells of *C. reinhardtii* CC-1690 were cultivated photoautotrophically inside a modular lab scale membrane photobioreactor (see chapter 3.3.2). In first approaches batch cultivations with either one or two gas compartments were conducted to characterize growth and gas exchange of the alga inside this membrane-aerated photobioreactor. Moreover, the formation of bubbles resulting from oversaturation with oxygen had to be quantified and compared for different membrane configurations at fixed gas compositions.

A further series of experiments was focusing on long-term continuous cultivations inside this reactor. Initially, a suitable control approach to enable a continuous cultivation with constant cell densities in steady-state conditions had to be found, without having an online optical density sensor. Once steady state was set, stepwise changes of light intensity were used to determine the system behavior to these perturbations and time constants for oxygen production could be determined. These light step changes were conducted for different steady-state cell concentrations and resulting light conditions and growth rates.

Calibration of sensors was performed analogously to chapter 3.4.2. Throughout the majority of experiments the liquid flow rate was constant at 100 ml min^{-1}, the gas flow rate for the first experiments was 200 ml min^{-1}, later on it was reduced to 100 ml min^{-1}.

The two gas compartments were termed gas exchange loop which was used to supply CO_2 for the cells and therefore flushed with a 5% CO_2 (v/v) in air mixture. The second gas compartment was termed gas collection loop and used for removal of oxygen from the algae compartment. For this reason it was

flushed with 1% CO_2 (v/v) in N_2 in order to have a high driving force for the diffusive transport of oxygen out of the algae suspension, while containing a low volumetric CO_2 concentration which was defined as setpoint for concentration of dissolved CO_2 in the liquid in steady-state conditions. This designation and gas mixtures were analogous to the gas loops of the ModuLES-PBR.

The reactor parts were autoclaved independently, including the membranes which were capable of being vapor sterilized, and the system was assembled inside a clean bench. Standard TP-NO_3 medium (Appendix 11.1.1) was used to fill the liquid loop of the reactor. The pH was adjusted to 8 instead of 7.2. Before the reactor was inoculated, the gas loops were flushed at set flow rates and with the desired mixtures to allow the gases, according to their respective concentration gradients and according to the respective k_L values of the membrane material used, to dissolve inside the liquid loop until equilibrium is reached. This also resulted in a decrease of pH from 8 to about 7.2-7.4.

Table 3-7. Cultivation conditions in the membrane-aerated photobioreactor.

Cultivation number	Illumination Color, PFD [µE m^{-2} s^{-1}]	Number of gas compartments	Membranes	Process mode
C1	ww, 200	1	TPX	Batch
C2	ww, 200	2	TPX, Wacker 80	Batch
C3	r/b, 200	2	TPX, TPX	Batch
C4	ww, 200	2	TPX, Wacker 200	Continuous
C5	ww, 200	2	TPX, TPX	Continuous
C6	90/10 r/b, 200	2	TPX, TPX	Continuous
C7	90/10 r/b, 200	2	TPX, Wacker 200	Continuous

Inoculation was accomplished by adding 20 mL volume of an exponentially growing pre-culture (see section 3.2.2) via a syringe into the liquid loop while simultaneously withdrawing the same volume of medium at another sampling port to keep the same volume on the liquid side. Also sample volumes taken during cultivation were balanced with sterile fresh medium immediately.

Several cultivations in batch mode (thereof two in one-gas-compartment-configuration and six in two-gas-compartment-configuration), and four cultivations in continuous mode were performed with the membrane reactor, whereas seven cultivations are discussed in detail within this work (as shown in Table 3-7).

The cultivations were carried out at a constant temperature of 25 ± 0.5°C and a constant light intensity of 200 µE m^{-2} s^{-1} at the surface of the algae compartment. For cultivations C1, C2 and C4, C5, warm-white LED light was used (NS6L083BT, Nichia, Japan) for the resting cultivations C3, C6 and C7

dichromatic red/blue illumination (red: peak = 680 nm, Marubeni, SMBB680-1100-02; blue: LUXEON® Rebel LXML-PR01-0500, Royal Blue 447.5 nm, Lumileds, Aachen, Germany) at a 90 to 10% molar ratio was used in relation to the experiments focusing on optimized illumination. The pH was recorded online but not controlled, just occasionally when it was out of tolerance range ($6 < pH < 8$) highly diluted NaOH or HCl (0.5 M) was added. Antifoam (Antifoam A, Sigma-Aldrich) was added in a 1:100 dilution as required.

Information on procedures during continuous cultivations inside the membrane photobioreactor is given in chapter 3.4.6.

3.4.4 Cultivation conditions for determination of effects of light quality

Cultivations for assessment of mono- and dichromatic illumination were conducted as semi-fed-batch cultivations, where cells where fed manually with concentrated medium to extend the duration of the linear growth phase. The PFD was kept constant during the cultivations and intensities tested ranged between 25-300 µE m^{-2} s^{-1}. Reactors were filled with TP-NO_3 medium (pH = 7.2) and the liquid was aerated with 5% CO_2 (v/v) in air (0.35 and 0.25 vvm for midi- and miniplates, respectively) prior to inoculation with one week old pre-culture at an approximate biomass concentration of 0.02 g L^{-1}. The pH was uncontrolled in both reactor versions and varied in the range of 6.5 and 7.5.

For shift experiments, where illumination color changed during the cultivation, cells were illuminated with pure blue light till the end of the exponential growth phase and then the illumination was switched to pure red light. For experiments with color shifts to study the détour-effect, the cells were first grown under 90/10 red blue illumination until light transmission (light measurements see section 3.4.4.1) approached zero and were then grown under pure green illumination. In order to determine efficiency of mono-and dichromatic illumination and compare this to full-spectrum illumination the photo conversion efficiency (PCE) was used as yield for biomass production from absorbed light. For this reason conditions with only light limitation but no nutrient limitation had to be provided. Cultures were therefore fed manually with 10x TP-NO_3 medium to extend the linear growth phase where almost all light is absorbed. This was done analogously for every illumination condition. Hence, conditions were therefore only light-limited and not nutrient-limited. In this linear phase also samples for analysis of cell size distribution, cell dry weight, microscopic analysis (unless otherwise stated), specific pigment as well as starch content were taken. Experiments to study long-term effects of color illumination were conducted in midiplate reactors and continuous cultivation. Details are mentioned in section 3.4.6.

3.4.4.1 Light measurements for plate reactor cultivations

Light measurements of irradiation intensity on the surface of the reactor (I_0), transmission (T) and reflected light (R) were performed using the planar quantum sensor from Walz (MQS-C, Walz connected to a LI-250 Light Meter, Licor, Walz Mess- und Regelungstechnik, Effeltrich, Germany).

The averaged function of the sensor was used where the values of 15 s measurement were averaged and taken as measured values. A spectral response curve of the planar quantum sensor can be found in Appendix 11.6.1.1.

3.4.5 Cultivation conditions for studies with lowered pressure and pressure changes

For assessment of effects of lowered pressure and pressure changes on the cells' photosynthetical activity and morphology, algae were cultivated photoautotrophically at photon flux densities of 200 µE m^{-2} s^{-1} (compare to calibration procedure for cylindrical LED panel in Appendix 11.6.2.2). The cultivations were started by inoculation from pre-cultures at approximate cell dry weight concentration of 0.2 g L^{-1}.

The algae suspension was aerated by sparging 4.8% CO_2 (v/v, 0.035 vvm) at a total aeration rate of 63 ml min^{-1} into the reactor with the intention to ensure CO_2 saturated conditions above 0.5-1% dCO_2 in the liquid, also for lower pressures down to 700 mbar absolute with the corresponding solubilities according to Henry's law (Equation 2-11). For small pressure differences, the influence of the overall pressure on the Henry coefficient can be neglected and for this reason the calculation of gas solubilities for pressures down to 700 mbar was performed with Henry coefficients for atmospheric pressure of 1013 mbar. Above dCO_2 concentrations of 0.5-1% optimal growth rates are enabled according to CO_2 kinetics (Dillschneider 2014). For this reason, inlet CO_2 gas concentrations were chosen high enough to ensure dCO_2 concentrations above this critical range, even at the lowest pressure tested and during phases of maximum CO_2 uptake rates. Hence, CO_2 limitation conditions were avoided for the conducted experiments with lowered pressure even though gas solubilities were reduced accordingly.

The two mass flow controllers (MKS Instruments) were calibrated for each absolute pressure applied. The calibration procedure for mass flow meters for lowered pressure is described in Appendix 11.6.2.1.Temperature was kept constant at 25°C; pH was controlled at 7.2 by dosing 2M HCl and 2M NaOH into the medium. The stirring rate was also kept constant throughout the cultivations at 250 rpm. Inoculation was performed under atmospheric pressure. Only around 12 h after start of cultivation, before cells started to grow exponentially, the pressure was reduced stepwise to the respective absolute pressure desired. Pressure during batch cultivations, once lowered, was kept constant for the rest of the process time. Cells were grown at 1 atm, 900, 800 and 700 mbar. In total 7 batches were performed with CC-1690 cells, four of them under warm-white illumination (at 1000, 900, 800 and 700 mbar respectively) and three under cold-white illumination (1000, 800 and 700 mbar) whereas the total PFD was the same. Another batch cultivation was performed with the WT13 strain to compare possible aggregation events with cells of the CC-1690 strain. One additional experiment was performed with CC-1690 cells where pressure was changed stepwise during the

exponential phase to determine a fatal threshold value and below that value, a possible adaptation of cells.

3.4.6 Cultivation conditions for long-term cultivations and effects of perturbations.

In order to study long-term stability of a phototrophic cultivation, determine time constants of the systems behavior in response to perturbations and quantify gas exchange rates, several experiments in different reactor types with bubble aeration and diffusion-based membrane aeration were performed.

Table 3-8. Turbidostat cultivations inside the stirred tank photobioreactor. The cultivation 4 with two runs of step changes and two different steady-states is numbered as two cultivations (K4 and K5).

Cultivation number	Average c_X [g L^{-1}]	Basic illumination [µE m^{-2} s^{-1}]	Step change 1	Step change 2	Step change 3	Step change 4	Step change 5
K1	3.5	200	400	800	1600	100	20
K2	1.0	200	400	800	1600	100	20
K3	0.5	200	400	800	1600	100	20
K4	1.3	200	400	800	1600	100	-
(K5)	0.9	200	400	800	1600	100	20
K6	0.5	800	1600	2400	400	80	20
K7	0.5	400	800	1600	200	40	20

First experiments were performed in the bubble-aerated stirred tank photobioreactor (compare to 3.3.4), as the technical realization was easier than in the other approaches. During this series of tests step changes in form of light intensity were performed during the steady-state phase. In total, a number of six continuous cultivations were run in the system, whereby in each cultivation five step changes at different steady-state cell densities were performed. During cultivation K4/K5 (Table 3-8) two steady-state phases with different cell concentrations and nine light step changes were established. The basic illumination intensity was 200 µE m^{-2} s^{-1} for K1 to K5, from which intensity was changed stepwise up- and downwards and kept constant at that new value for 1.5 h. The time span between the light steps was 24 h each. The analysis of specific pigment content should reveal how fast algae adapt to their new illumination conditions by changing pigment composition and the overall amount per cell. Continuous cultures were run as manually controlled turbidostat cultures where pump rates were adjusted to the actual growth rate. Temperature and pH were controlled at 25°C and 7.2 respectively. Stirrer speed was constant at 250 rpm.

Light steps were conducted within steady-state phases where constant offline OD_{750} values and amounts of O_2 and CO_2 in exhaust gas were taken into account. Light intensity steps were performed

with a duration of 1.5 h each, whereas this duration was sufficient to establish a new quasi steady-state, monitored as constant pH values (pH control was off during the step duration) and constant offgas analysis values. Samples for offline analysis were taken every 24 h before the next step change was performed.

Continuous cultivations were also established inside the membrane-aerated photobioreactor testing long-term stability, process control and gas exchange rates during steady-state conditions. Also for this reactor type, step changes in light intensity with warm-white LED as well as with dichromatic red/blue 90/10 illumination were performed. These were aimed to determine time constants for comparison with the larger scale ModuLES-PBR data acquired during parabolic flight campaigns. In contrast to the STPBR step changes, the duration of steps inside the membrane reactor varied, as time to establish a new equilibrium varied and was higher than for the ideally mixed reactor.

Table 3-9. Continuous cultivations with light intensity step changes within the membrane-aerated reactor.

Cultivation number	Average c_X [g L^{-1}]	Color, basic PFD [µE m^{-2} s^{-1}]	Step changes, step intensity [µE m^{-2} s^{-1}]					
			1	2	3	4	5	6
C4	2.2	ww, 200	400	800	1600	100	20	-
C5	0.25	ww, 200	400	800	1600	1200	100	20
C6	0.13	90/10 r/b, 200	300	100	20	-	-	-
C7	0.5	90/10 r/b, 200	300	20	-	-	-	-

Continuous cultivations in plate type reactors were conducted in form of turbidostat cultures where transmission of an infrared LED was measured by a spectrophotometer. The transmission, as controlled value, was kept constant with a PI controller with the pumping rate of feed and harvest pump as correcting variable. Here, the illumination intensity was kept constant, while the part of red and blue light was changed stepwise after a new steady-state was established. For the second cultivation P2 (see Table 3-10), a warm-white illuminated continuous control culture was running in parallel. For red/blue illumination cells were first grown under a 90/10 red/blue illumination during batch phase and the beginning of the continuous phase until a first steady-state was established. During continuous cultivation P1, in total 11 color step changes were performed; during continuous cultivation P2 four color step changes were exerted.

Table 3-10. Continuous cultivations in midiplates under dichromatic red/blue illumination with light color changes.

Cultivation number	$c_{X,avg}$ [g L^{-1}]	PFD [µE m^{-2} s^{-1}]	Step change 1/7	Step change 2/8	Step change 3/9	Step change 4/10	Step change 5/11	Step change 6
P1	1.0	200	100 r	50/50 r/b	75/25 r/b	90/10 r/b	100 b	10/90 r/b
			20/80 r/b	30/70 r/b	40/60 r/b	90/10 r/b	100 r	
P2	0.5	25	90/10 r/b	100 r	100 b	50/50 r/b		

3.4.7 Procedures and conditions for cultivations inside the ModuLES-PBR

The ModuLES-PBR was tested during two parabolic flight campaigns in September 2013 and February 2014 as well as during one experimental run on ground.

To establish a diffusion-based, bubble-free aeration for microgravity conditions, flat sheet membranes were used in this first approach for CO_2 supply and O_2 removal. Membrane sheets were fixed on both sides of the mini-raceway reactor which was mounted vertically for parabolic flight campaigns. For aeration, two gas compartments were flushed with different gas mixtures separated by the flat sheet membranes from the liquid compartment with a total volume of 2 L. Gas- and liquid-containing compartments possess a meandering shape with the gas flow circulating in countercurrent to the liquid flow. Liquid mixing was realized by a peristaltic pump installed in the periphery; for air mixing after filling the loops, air pumps were used.

For establishing the continuous process, fresh medium was fed from storage with the help of another pump into the reactor and algae suspension was pumped at the same rate to a biomass harvesting container that could be coupled to a filtration unit for solid/liquid separation.

For membrane aeration the sandwich type structure enabled the use of different flat sheet membranes, which could be changed in between cultivations. Moreover, it was possible to use different membranes on both sides of the algae compartment to enable high flexibility for membrane configurations. One of the gas compartments contained 5% CO_2 (v/v) in air for the CO_2 supply to keep dissolved CO_2 in the liquid at a level of 1%. The other compartment was used for O_2 removal and was flushed with a mixture of 1% CO_2 in N_2 to create a high driving force for the O_2 transfer across the membrane. During two parabolic flight campaigns and the ground experiment, a dense flat sheet membrane made of polymethylpentene with 50-µm thickness (Goodfellow TPX, see also 3.4.1) was used on both sides.

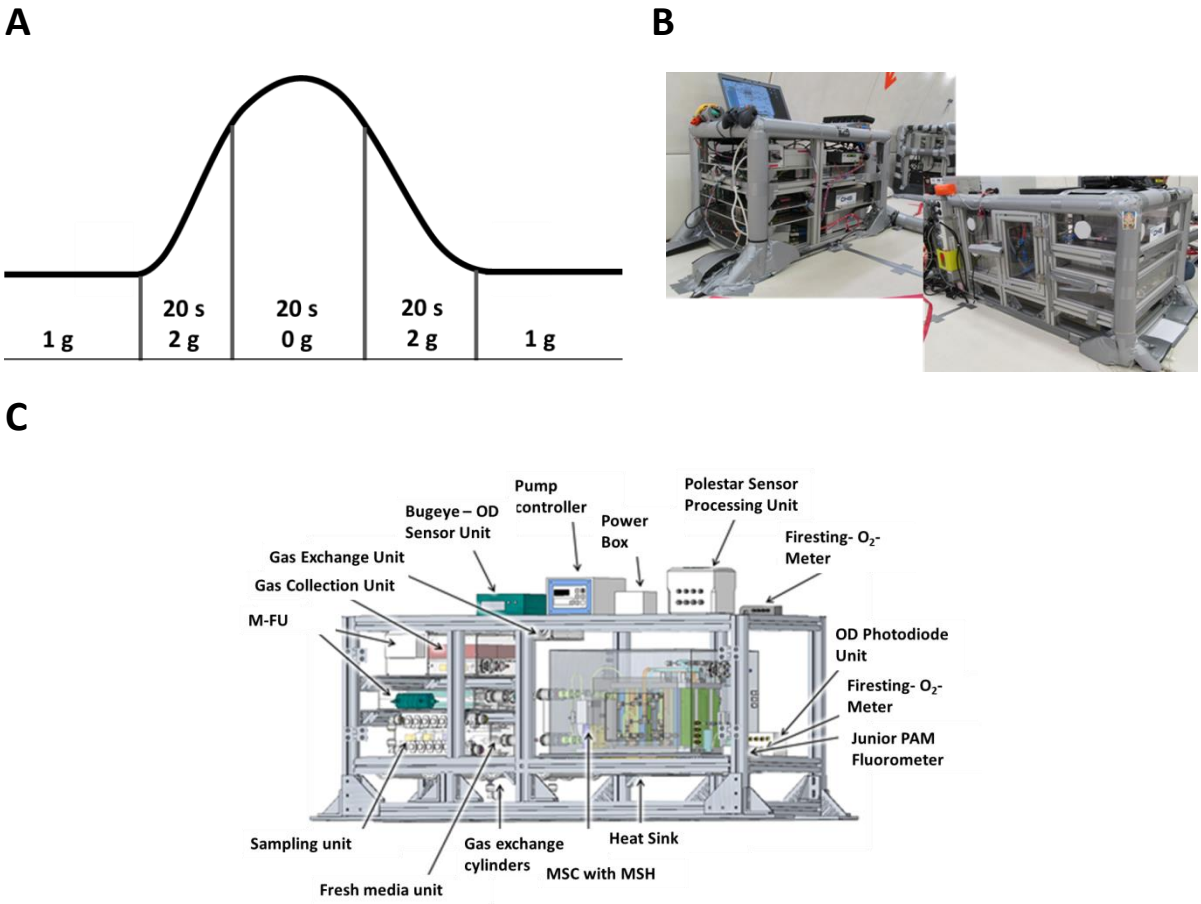

Figure 3-6. Parabolic flight campaign with the ModuLES-PBR. A) Parabolic flight trajectory with duration of different g phases. B) Mounted stacks of the ModuLES-PBR inside the airplane. The stack in the background contained the electronics; the one in the front contained the reactor with the peripheral system. C) Experiment rack of the ModuLES-PBR system with peripheral parts, OHB System AG (Podhajsky 2014).

In order to detect physiological effects of the gravity changes during parabolic flights, the reactor was equipped with measurement instrumentation. This reactor system included optical sensors for CO_2 and O_2 partial pressures within the gas loops, as well as optical sensors for dissolved CO_2 and O_2 on the liquid side. Cell concentration measured as optical density at 750 nm (OD_{750}), temperature, pH and pressure were measured to monitor the cultivation process. Using fluorescence measurement with the help of a PAM sensor it was possible to detect putative changes in the photosynthetic activity during parabolic flights. Liquid samples of algae suspension were taken using a sampling unit integrated in the periphery of the reactor consisting of 12 syringes pre-filled with RNA fixative. By an automated suction mechanism representative samples were taken from the continuously flushed sampling line at the desired time. As the liquid loop was a closed, completely filled compartment without a gas phase, the volume on the liquid side had to be kept constant, meaning that the sample volume taken (5 mL each) was directly balanced with fresh medium from the storage tank.

The pH was controlled by dosing either CO_2 saturated or unsaturated media. Temperature was controlled by a feedback-controlled Peltier circuit. Dilution rate D of the continuous process was set

constant for parabolic flights and was manually regulated during long-term ground testing. Technical realization, measurement, and control of this reactor system were accomplished by OHB System AG, Germany (Podhajsky 2014).

The system could be run in different modes during an experiment (nominal operative mode, sampling mode, PAM acquisition mode and the system safe mode). During the nominal operative mode the reactor was run as continuous process where the main peristaltic pump was used for mixing. For continuous operation the fresh/harvested media were injected and collected at the same rate adjusted to a previously calculated growth rate. During the sampling mode a sample was taken from the liquid loop. In this case, all pumps were switched off and the bypass loop was opened. The syringe in the sampling unit was released to take a sample. The PAM acquisition mode was performed at 5 second intervals during the parabolic flight. The liquid flow was stopped inside the PAM cuvette in order to ensure a reliable data acquisition. The "Safe Mode" represented the minimum condition to keep the algae alive in case of emergency or during a period without the control software. During the system safe mode the light intensity was set to a minimum value of 20 µE m^{-2} s^{-1} which represents I_c in PI-curve. The peristaltic pump for mixing kept the algae in suspension to avoid sedimentation and the air pumps of the gas loops were running to move the gases along the membrane surface. An UPS system (uninterruptable power supply) was used to provide the power to the system for 20 minutes. This mode could be manually activated.

The reactor setup for the first parabolic flight campaign included the earlier described PBR system without the filtration unit. Cells were illuminated with warm-white LEDs (data sheet in Appendix 11.4.1.1) at a photon flux density of 200 µE m^{-2} s^{-1} (see Table 3-11).

Table 3-11. Overview of the parabolic flights with the ModuLES-PBR. C = Continuous, B = Batch

	Parabolic flight campaign 23				**Parabolic flight campaign 24**		
Flight number	1	2	3	4	1	2	3
Number of parabolas flown	31	31	31	31	25	36	31
Process mode	C	B	C	C	B	C	C
Harvest mode executed	no	no	no	no	no	yes	yes
Illumination color	ww	ww	ww	ww	90/10 r/b	90/10 r/b	90/10 r/b
PFD [µE m^{-2} s^{-1}]	20-200	20-200	20-200	20-200	20-300	20-300	20-300

For the second campaign, red-blue light with a peak at 450 nm and 680 nm (data sheet in Appendix 11.4.1.2) was applied. The illumination was controlled manually and was set to a fixed ratio of 90%

red to 10% blue photons, analogously to ground experimental results. The PFD during the second campaign was varied between 20-300 µE m^{-2} s^{-1}. For flight two and three of the second campaign, the filtration unit was included, which concentrates algae biomass as retentate on one side and filtered media as permeate on the other side, collecting those in separate bags as a first step toward a future media-recycling for long duration space missions. During the second campaign, it was possible to adjust the illumination intensity manually as well as the saturation pulse frequency for the PAM measurements. For continuous mode of the system the setpoint cell density accounts for 2 g L^{-1} bio dry mass, corresponding to $4 \cdot 10^7$ cells mL^{-1}. Optical sensors were calibrated accordingly.

As the algae could not be cultured in the airplane overnight (no power, no temperature control), they were cultured in the lab and got filled into the PBR under sterile conditions early in the morning of the parabolic flights. The PBR was transferred to the airplane and was integrated into the remaining ModuLES-infrastructure that was already mounted inside the airplane. The PBR was connected with all sensors, and the algae-loop between PBR, sampling unit, fresh media and harvesting/filtration unit was closed. The gas loops were flushed prior to the flights for CO_2 supply and oxygen removal to avoid pressurized gas bottles in the airplane. The gas loops were flushed with a mixture of 5% CO_2 in air (v/v) and 1% CO_2 in N_2 (v/v), respectively. The gas flow rates in both loops were adjusted to 100 mL min^{-1}, the liquid flow rate to 200 mL min^{-1}. The continuous flow rate was set to 2.6 mL min^{-1} corresponding to the maximum specific growth rate μ_{max} = 0.08 h^{-1} at a PFD of 200 µE m^{-2} s^{-1} of CC-1690 cells. The duration of the gas loop flushing period was depending on the time of PBR integration and door closure of the airplane for starting the flight. Prior to starting the flight, the power-up of the airplane engines required a power shut down of all experiments. To ensure the illumination of the algae and prevent sedimentation in that time span, battery power was required for at least 20 minutes. In that time the illumination was reduced to 20 µE m^{-2} s^{-1} PFD, with only the main peristaltic pump working during that safety mode.

Sampling during the flights was accomplished according to protocols at different times during the flight in relation to parabolas and g forces. Light step changes were performed during the second campaign in order to limit the dissolved oxygen concentration, to avoid bubble formation and inhibition of photosynthesis.

Additionally, one ground experiment in continuous mode was run with the ModuLES-PBR in order to collect data for assessment of reactor performance as 1g control. Furthermore, one flight day was simulated to get ground control data to study effects of parabolic flight conditions on the algal cells. The following table summarizes the ground test conducted.

Table 3-12. Overview of ground experiments with the ModuLES-PBR.

Characteristics	Continuous cultivation with flight day simulation	
	Simulation of PFC24 flight day	**Subsequent chemostat cultivation**
Duration	5 hours	3 days
Specials	Gas loops flushed before start, closure of loops analogous to flight conditions	Continuously flushing of gas loops, flow rates reduced to 100 ml min^{-1}
Aims	Collect ground control data for flight comparison	Overall performance in continuous mode, comparison with membrane reactor
Sensors	Failure of dCO_2 sensor: no signal available	Failure of dCO_2 sensor: no signal available

3.5 Analytical methods

Further details of the analytical methods, which were used during this work, are depicted in Appendix 11.5.

3.5.1 Optical density

Optical density of liquid culture samples was measured in triplicate measurements using a UV-Vis-spectrophotometer (Lambda 35, Perkin Elmer, USA) at a wavelength of 750 nm against distilled water as blank. The measurement of optical density is based on the scattering of light beams hitting particles in suspension. This is applicable as at a wavelength of 750 nm no absorption by algal pigments occurs. Samples with OD_{750} values > 0.3 [AU] were diluted with distilled water in order to have a linear correlation of CDW and optical density.

3.5.2 Cell dry weight

A gravimetric determination of cell dry weight concentration CDW [g L^{-1}] was accomplished with triplicate measurements using 20-30 mL culture volume. The algae suspension was centrifuged (Hettich, Rotina 420R) using dried and weighed stainless steel tubes for 30 min at 4500 rpm and 4°C. The supernatant was discarded and the resting pellet washed twice with the same volume of distilled water (resuspended and centrifuged again). After drying the pellet at 80°C for 48 h it was cooled down to room temperature in a desiccator and the difference in weight was determined on a high-resolution balance.

Furthermore, cell dry weight concentration was determined with the help of a correlation factor from the optical density at 750 nm OD_{750}, compare to section 3.5.1. Details for determination of this correlation factor are depicted in Appendix 11.5.1.

3.5.3 Photon flux density (PFD)

Photon flux density was measured for different reactor geometries with two quantum sensors. A spherical quantum sensor (QSL-2101, Biospherical Instruments) was used for calibration of current of the LED control unit and the resulting light intensity inside the cylindrical illuminated reactor. For this measurement the reactor was filled with algae suspension of wildtype CC-1690 at a cell dry weight concentration of about 0.4-0.5 g L^{-1}. At this cell density light is distributed homogenously inside the cylindrically illuminated reactor, which was determined during a former experiment with CC-1690 cells inside this reactor (compare to Appendix 11.6.3.1, Figure 11-14). The sensor was placed centered inside the reactor volume. The calibration curve showing linear correlation between current and light intensity for both warm-white and cold-white LEDs is shown in Appendix, Figure 11-12. For planar illumination systems (plate reactors, membrane reactor and shaking flasks) a planar quantum sensor (MQS-C, Walz connected to a LI-250 Light Meter, Licor, Walz Mess- und Regelungstechnik, Effeltrich, Germany, see spectral response curve in Appendix 11.6.1.1) was used to measure illumination intensity (see also 3.4.4.1). Calibration of mini- and midiplate reactor LED panels is shown in Appendix 11.6.1.2.

3.5.4 Pigment analysis

The pigment content (Chl a, Chl b, Car) was determined in form of triplicate measurements based on a cell disruption and a simultaneous extraction with acetone (Lichtenthaler and Buschmann, 2001 and Porra, 2002). Solid-liquid separation of cells and medium was accomplished by centrifugation (Mikro 220R, Hettich, Germany) at 4°C, for 10 min at 11000 rpm. The cell pellets were resuspended in 1 mL 80% (v/v) acetone saturated with Na_2CO_3. Five stainless steel beads were added per micro test tube and cell disruption was performed using a swing mill for 5 min at 30 Hz. After removal of the beads the tubes were centrifuged again (11000 rpm, 10 min, 4°C) to separate cell debris and sodium carbonate. The supernatant, containing the pigments in solution, was measured for absorption at the wavelengths 470, 646.6, 663.6 and 720 nm inside a UV-Vis-spectrophotometer against 80% (v/v) acetone as blank. Samples were diluted with 80% (v/v) acetone as soon as one of the four values approached A = 0.5. Using the following equations (modified after Lichtenthaler and Buschmann, 2001) pigment concentrations in µg mL^{-1} were calculated. The absorption value at 720 nm corresponds to the background noise resulting from remaining solid matters or undissolved salts.

Equation 3-3. Chl a concentration

$$Chla = 12.25 \cdot \left(A_{6636} - A_{720}\right) - 2.55 \cdot \left(A_{6466} - A_{720}\right)$$

Equation 3-4. Chl b concentration

$$Chlb = 20.31 \cdot \left(A_{6466} - A_{720}\right) - 4.91 \cdot \left(A_{6636} - A_{720}\right)$$

Equation 3-5. Carotenoid concentration

$$Car = \frac{\left[1000 \cdot \left(A_{470} - A_{720}\right) - 1.82 \cdot Chla - 85.02 \cdot Chlb\right]}{198}$$

3.5.5 Exhaust gas analysis

The exhaust gas of the stirred tank photobioreactor was analyzed for its O_2 and CO_2 concentration with the help of a gas analyzer (Sick-Maihak, Germany). A minimum flow rate of 250 ml min^{-1} was required. For this reason the model reactor was equipped with a gas collection bag in the exhaust gas stream. The required control via a two series-connected three-way solenoid valve was performed using the process control system BioProCon. Following this measurement, volumetric uptake and production rates for CO_2 and O_2 could be calculated according to section 3.6.3.

3.5.6 Cell size distribution

As cell size was one of the comparison parameters for studying effects of mono-and dichromatic illumination on microalgae cultures, this factor was analyzed based on laser diffraction (Beckman Coulter LS 32 and LS 13320, Beckman Coulter, USA) at the Institute of Process Engineering in Life Sciences I: Food Process Engineering, Karlsruhe Institute of Technology. In laser diffraction analysis a laser beam hits a particle collective and each particle generates a certain scattered light distribution which depends on the particle size. For smaller particles, bigger angles of scattering are measured.

Until otherwise mentioned, samples for cell size distribution analysis were taken during the linear growth phase of the cultivation. Prior to the analysis, the refractive index of the TP-NO_3 medium was determined (refractive index medium, n_{medium} = 1.334) and from literature (Aas, 1996) a suitable refractive index for green algae was taken (refractive index green algae, n_{algae} = 1.146).

For analysis, a theoretical sphere is used which is compared to the irregular formed particle (in this case the cell which is the disperse element). The equivalent diameter is the diameter of a sphere having the same properties like the irregular formed cell under the same conditions. In this case the property is the particle volume. Hence, the volume based particle size equals the diameter of the sphere that has the same volume as a given particle, which is described by:

Equation 3-6. Equivalent diameter

$$d_3 = 2\sqrt[3]{\frac{3V_p}{4\Pi}}$$

With:

d_3: diameter of the representative sphere [µm]

V_p: particle volume [L]

The particle size distribution is described by the cumulative distribution curve Qr (x_i) and the density distribution curve q_r (x_i). The cumulative distribution Qr (x_i) represents the proportion of the particle collective whose characteristic x is smaller than a given value x_i (Schwister 2005):

Equation 3-7. Cumulative distribution

$$Q_r(x_i) = \frac{amountparticle x < x_i}{totalitypa\,rticles}$$

The density distribution qr describes the proportion of the particle collective whose property is between two limits x_{1i} and x_{2i} in relation to the interval width Δx_i:

Equation 3-8. Density distribution

$$q_r(x_i) = \frac{dQ_r(x_i)}{dx_i} = \frac{amountparticle x_{1i} < x < x_{2i}}{\text{int}\,ervalwidth \Delta x_i}$$

3.5.7 Light microscopy

Cell size and also morphology of the cells were examined regularly with the AxioScope A1 light microscope (Zeiss, Germany). Also the possible occurrence of bacterial or fungal contaminants was monitored via lightmicroscopic images. Sample examination was performed with and without differential phase contrast. Digital images were taken with an Infinity2-camera (Klughammer, Germany) and were further modified by the corresponding software.

3.6 Calculated/derived parameters

In the following, parameters are depicted that were calculated from the analyzed parameters and online process data.

3.6.1 Calculated parameters related to membrane aeration

From sensor data concerning dissolved gas concentration and relative humidity of the membrane testing unit, several parameters important for the design of a membrane-aerated photobioreactor were calculated.

3.6.1.1 Mass transfer coefficients

From online data of increasing dissolved gas concentrations with time k_L values were determined. For this the following equation, analogous to the CTR equation (theoretical chapter, Equation 2-17), was used:

Equation 3-9. Mass transfer equation used for k_L-Fit in Origin

$$\frac{dc}{dt} = k_L \cdot a \cdot \left(c^* - c\right)$$

$$\frac{dc}{\left(c^* - c\right)} = k_L \cdot a \cdot dt$$

$$\int \frac{1}{\left(c^* - c\right)} dc = \int k_L \cdot a \cdot dt$$

The constant k_L in this case represents the mass transfer coefficient for the respective gas representing the resistance for mass transfer of the membrane and the boundary layer on the liquid side (resistance of the boundary layer on gas side can be neglected). In order to determine the k_L-value of each membrane for both O_2 and CO_2, Equation 3-9 for mass transfer is integrated, obtaining the equation:

Equation 3-10. Fitting equation for step changes

$$c = c^* + C_1 \cdot e^{-k_L \cdot a \cdot t}$$

with C_1 as integration constant. Online data was fitted to this equation using the software Origin (version OriginPro 9.0.0). The function "ExpDec1" was used for the exponential fitting corresponding to the equation:

Equation 3-11. Function for k_L-fitting in Origin

$$y = y_0 + A_1 \cdot \exp\left(-\frac{1}{t_1} \cdot x\right)$$

Where k_L corresponds to:

Equation 3-12. k_L-determination from fit function

$$k_L = \frac{1}{t_1 \cdot a}$$

k_L-values [m s^{-1}] were calculated and plotted for all of the tested membrane materials tested at T = 25°C and the mentioned flow rate settings.

3.6.1.2 Selectivity

Selectivity of the membrane materials for O_2 versus CO_2 was determined as:

Equation 3-13. Selectivity factor α of a membrane material for O_2 versus CO_2

$$\alpha_{O2/CO2} = \frac{k_{L,O2}}{k_{L,CO2}}$$

3.6.1.3 Water loss

The permeation of water vapor per membrane area and time was calculated based on the data recorded by the hygrometer in the off-gas leaving the testing chamber. Based on the following thermodynamic data the mass flow of water in the exhaust gas of the experimental setup was calculated from the difference of relative humidity between inlet and outlet.

- T = 298.15 K, 25°C
- p = $1.01325 \cdot 10^5$ Pa
- gas flow rate = 0.0024 $m^3\ h^{-1}$
- saturation pressure water vapor (25°C) $p_{S,25°C} = 0.031697 \cdot 10^5$ Pa
- specific gas constant, water R_{H2O} = 461.5 J $kg^{-1}\ K^{-1}$
- relative humidity gas φ [%]: from online data of hygrometer

Knowing the difference ΔrH in humidity of gas entering (rH_{in}) and leaving the chamber (rH_{out}) the partial pressure of water vapor $p^*_{w,25°C}$ at 25°C can be calculated, according to Equation 3-14.

Equation 3-14. Calculation of partial pressure of water vapor based on difference in relative humidity of gas

$$p^*_{w,25°C} = \varphi \cdot p_{S,25°C} = \left(\frac{rH_{out} - rH_{in}}{100} \right) \cdot p_{S,25°C}$$

The mass flux of water $\dot{m}_{w,25°C}$ transported in the gas stream is calculated by Equation 3-15.

Equation 3-15. Mass flux of water transported in gas stream

$$\dot{m}_{w,25°C} = \frac{p^*_{w,25°C}}{R_{H2O} \cdot T} \cdot \dot{V}$$

Tests were carried out using both dry inlet air and humid inlet air to compare the differences in water loss for both approaches.

3.6.2 Photo conversion efficiency

An important parameter used for comparison of efficiency of different illumination systems is the photo conversion efficiency PCE [$J\ J^{-1}$]. It is defined as yield with which absorbed light is converted into biomass. For lipid-poor green algae (Lehr 2009, Schaub 2007) a biomass calorific value H_B of 20 MJ kg^{-1} is assumed and taken for PCE calculation. PCE values were determined within the linear growth phase under light-limited conditions (see section 3.4.4).

Only the absorbed light energy in Joule, calculated from irradiated, reflected and transmitted light, was taken into account for the calculation of the light to biomass conversion yields.

As photons of the applied wavelengths transport different energy levels, light energy conversion factors had to be determined for calculation of the yield value. Light energy conversion factors F, depending on the wavelength and molar fractions (in case of dichromatic illumination), were calculated from emission spectra of LEDs, for PAR photosynthetic active radiation of 400-700 nm and quantum energy of photons according to Equation 3-16 - Equation 3-18.

Equation 3-16. Quantum energy of photons.

$$U = N \cdot h \cdot \frac{c}{\lambda}$$

U – energy content of photons [J mol^{-1} photon = J E^{-1}]

N – Avogadro's number (N = $6.022 \cdot 10^{23}$) [mol^{-1}]

h – Planck's constant (h = $6.626 \cdot 10^{-34}$) [J s]

c – speed of light (c = $2.998 \cdot 10^{8}$) [m s^{-1}]

λ – wavelength [nm]

Factors F were calculated along with U within PAR range from LED emission spectra (see Figure 4-1 A) according to:

Equation 3-17. Quantum energy from LED emission spectra

$$U = \frac{1}{I} \cdot \int_{400nm}^{700nm} \phi(\lambda) d\lambda$$

I – irradiated light [µE m^{-2} s^{-1}]

Φ(λ) – radiant flux at different wavelengths λ [J m^{-2} s^{-1}]

Equation 3-18. Calculation of conversion factors from quantum energy of photons

$$F = \frac{1}{U}$$

Table 3-13 shows light energy conversion factors F [mol J^{-1}] or [µE J^{-1}] for color mono- and dichromatic illumination as well as warm-white illumination.

Table 3-13. Light energy conversion factors

Light color/Mixture	Conversion factor F [µE J^{-1}]
Warm-white	4.67
Red (680 nm)	5.65
Blue (447 nm)	3.71
Green (520 nm)	4.49
90 % red 10 % blue	5.46
80 % red 20 % blue	5.26
70 % red 30 % blue	5.07
50 % red 50 % blue	4.68
25 % red 75 % blue	4.19
10 % red 90 % blue	3.91
90 % red 10 % green	5.54

In order to calculate the PCE, the energy fixed as biomass has to be calculated:

Equation 3-19. Energy fixed in form of biomass.

$$E_B(t) = CDW(t) \cdot H_B \cdot V(t)$$

With:

$E_B(t)$ – as biomass fixed energy [J]

CDW (t) – cell dry weight built [g L^{-1}]

H_B – biomass calorific value [J g^{-1}], here assumed to be 20 MJ kg^{-1}

V(t) – working volume of reactor [L], time dependent

t – process time [s]

Absorbed light energy was calculated according to:

Equation 3-20. Calculation of absorbed light energy from incident, reflected and transmitted light energy.

$$E_L(t) = \frac{(I(t) - T(t) - R(t)) \cdot A(t) \cdot t}{F}$$

$E_L(t)$ – absorbed light energy [J]

I(t) – irradiated light [µE m^{-2} s^{-1}]

T(t) – transmitted light [µE m^{-2} s^{-1}]

R(t) – reflected light [µE m^{-2} s^{-1}]

A(t) – illuminated surface [m^2]

F – light energy conversion factor [µE J^{-1}] (Table 3-13), depending on the wavelength and molar fractions

PAR-based PCE values were determined during the light-limited linear growth phase at high cell densities > 1 g L^{-1} for every lighting condition described by linear fitting E_B and E_L versus process time. PCE is calculated as ratio of those slopes according to:

Equation 3-21. Calculation of PCE.

$$PCE = \frac{m_B}{m_L} \cdot 100\%$$

PCE – Photo conversion efficiency [%]

m_B – slope of linear fitting for build biomass versus process time [J s^{-1}]

m_L – slope of linear fitting for absorbed light energy versus process time [J s^{-1}]

Values were averaged over at least three independent experiments.

3.6.3 Carbon dioxide uptake and oxygen production rate (CUR, OPR)

Volumetric carbon dioxide uptake and oxygen production rates (CUR, OPR) [mmol L^{-1} h^{-1}] were the most important parameters defining interfaces of a phototrophic microalgae module to other heterotrophic modules of a life support system. The rates were calculated, depending on the reactor system conditions, based on two different methods. In case were exhaust gas analysis was established, the calculation method based on the gas balancing method (Garcia-Ochoa 2010). This method was used for calculation of volumetric CUR and OPR taking into account CO_2 and O_2 concentration of the gas streams entering and leaving the reactor. For calculation (according to Equation 3-22, Equation 3-23), all gases were considered ideal with the assumption of constant molar fractions of nitrogen and inert gases in the in- and outlet gas.

Equation 3-22. Calculation of volumetric CUR based on gas balancing method.

$$CUR = \frac{\dot{V}_{air,in}}{V_M \cdot V_L} \cdot 60 \frac{\text{min}}{h} \cdot \left[x_{CO2,in} - x_{CO2,out} \right]$$

Equation 3-23. Calculation of volumetric OPR based on gas balancing method.

$$OPR = \frac{\dot{V}_{air,in}}{V_M \cdot V_L} \cdot 60 \frac{\min}{h} \cdot \left[x_{O2,out} - x_{O2,in} \right]$$

A different method (compare to Equation 3-24, Equation 3-25) was used in case where the gas transfer rate was known. This was the case for the membrane-aerated cultivations; gas uptake and production rates were calculated from the gas concentration profile data, knowing the respective transfer rate (Garcia-Ochoa 2010).

Equation 3-24. Calculation of volumetric CUR knowing the CTR

$$CUR = k_{L,CO2} \cdot a \cdot \left(c^*_{CO2} - c_{CO2} \right) - \left(\frac{dc_{CO2}}{dt} \right) = CTR - \left(\frac{dc_{CO2}}{dt} \right)$$

Equation 3-25. Calculation of volumetric OPR knowing the OTR

$$OPR = k_{L,O2} \cdot a \cdot \left(c^*_{O2} - c_{O2} \right) + \left(\frac{dc_{O2}}{dt} \right) = OTR + \left(\frac{dc_{O2}}{dt} \right)$$

In case of the two-compartment-version of the membrane reactor, the balance boundary was set around each membrane separately (Figure 3-7) and the equations were extended:

Equation 3-26. Calculation of volumetric CUR for two membranes, two gas compartments

$$CUR = CTR_1 + CTR_2 - \left(\frac{dc_{CO2}}{dt} \right)$$

Equation 3-27. Calculation of volumetric OPR for two membranes, two gas compartments

$$OPR = OTR_1 + OTR_2 + \left(\frac{dc_{O2}}{dt} \right)$$

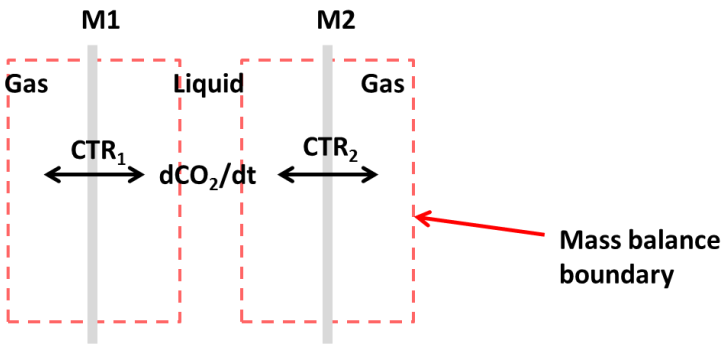

Figure 3-7. Mass balance boundaries for calculation of gas transfer rates for the two compartment version of the membrane reactor. Gas transfer is shown for CO_2, with M1,2 = membrane 1,2.

3.6.4 Photosynthesis quotient PQ

The photosynthesis quotient PQ was calculated from volumetric maxima of gas exchange rates during batch cultivations, or mean values for steady-state conditions during continuous cultivations, of CUR and OPR according to Equation 3-28:

Equation 3-28. Photosynthesis quotient

$$PQ = \frac{OPR}{CUR}$$

3.6.5 Time constants

Time constants of system response curves, following step changes of light intensity, during continuous cultivations were determined as T,63% time constants by using online sensor data. In case of the stirred tank photobioreactor the pH signal was used; in case of the membrane reactor online data of the pO_2 sensor was used. The response curves were fitted according to a PT1 element with the help of the software Origin. After determination of the terminal value of the response, the time constant T,63% was calculated (compare to Chapter 2, 2.3.4.2).

4 Efficient illumination of microalgae for life support systems

In this chapter results and discussion concerning the effects of mono- and dichromatic LED illumination on photo conversion efficiencies (PCE), cell morphology, as well as pigment content are provided. The optimization of light utilization regarding energy efficiency under the consideration of accessory and sensory pigments and their physiological functions is of crucial importance for the feasibility of microalgae-based modules integrated in life support systems.

Investigations started with the selection of suitable wavelengths for mono- and dichromatic illumination, followed by first experiments under low light intensities to test for most efficient color combinations during manual fed-batch cultures. Experiments under higher and saturating light intensities should reveal the differences in light absorption characteristics for different wavelengths and the resulting light to biomass conversion yields. Further studies were concerned with long-term effects of mono- and dichromatic illumination during continuous cultures. For every serial experiment, warm-white LED illumination was used as control. Morphology of cells, in form of cell size and aggregation conditions, as well as specific pigment concentrations were further parameters for comparison.

4.1 Selection of wavelengths

Figure 4-1 A shows the emission spectra of the chosen color LEDs together with the spectrum of warm-white control LEDs for the assessment of efficient illumination of *C. reinhardtii* cultures. LED colors were selected with the background of the existing accessory and sensory pigments of *C. reinhardtii* (compare to chapter 2.3.2.3 and 2.3.2.4) and according to the *in vivo* absorption spectrum of *C. reinhardtii* (Rodríguez 2007, panel B, full spectrum thick black line) as peak absorption wavelengths are most promising for an energy-efficient illumination. This spectrum was measured by means of *in vivo* absorption microspectroscopy on the thylakoid membrane of the chloroplast of living cells. The full spectrum was measured, whereas the relative contribution of Chl a, Chl b and carotenoids was computed based on templates for the specific pigment absorption spectra for this alga. Details of this method are given by Evangelista et al. (2006). The apparatus for *in vivo* absorption spectroscopy is described by Gualtieri et al. (1989).

Red LEDs with a peak emission at 680 nm were chosen in accordance with the absorption peak within the red range and related to the optimal energy content of 680 nm photons; a peak emission of 447.5 nm was chosen for blue LEDs as compromise between the peaks of Chl a, Chl b, and Car absorption within the blue range. Green LEDs with peak emission at 520 nm were chosen according to the minimum (range of 515 to 570 nm) in the absorption spectrum. In general, care should also be taken if there are additional local peaks in the *in vivo* absorption spectrum of a photosynthetic organism which are beyond the range of PAR definition from 400-700 nm. Their relevance should be

assessed and taken into account for wavelength selection. For the total energy efficiency of the lighting system also the internal efficiency of LEDs (power to output conversion) is important whereas the color chosen makes a difference inasmuch as red LEDs need 30% less energy than blue or white LEDs (Cerff 2012).

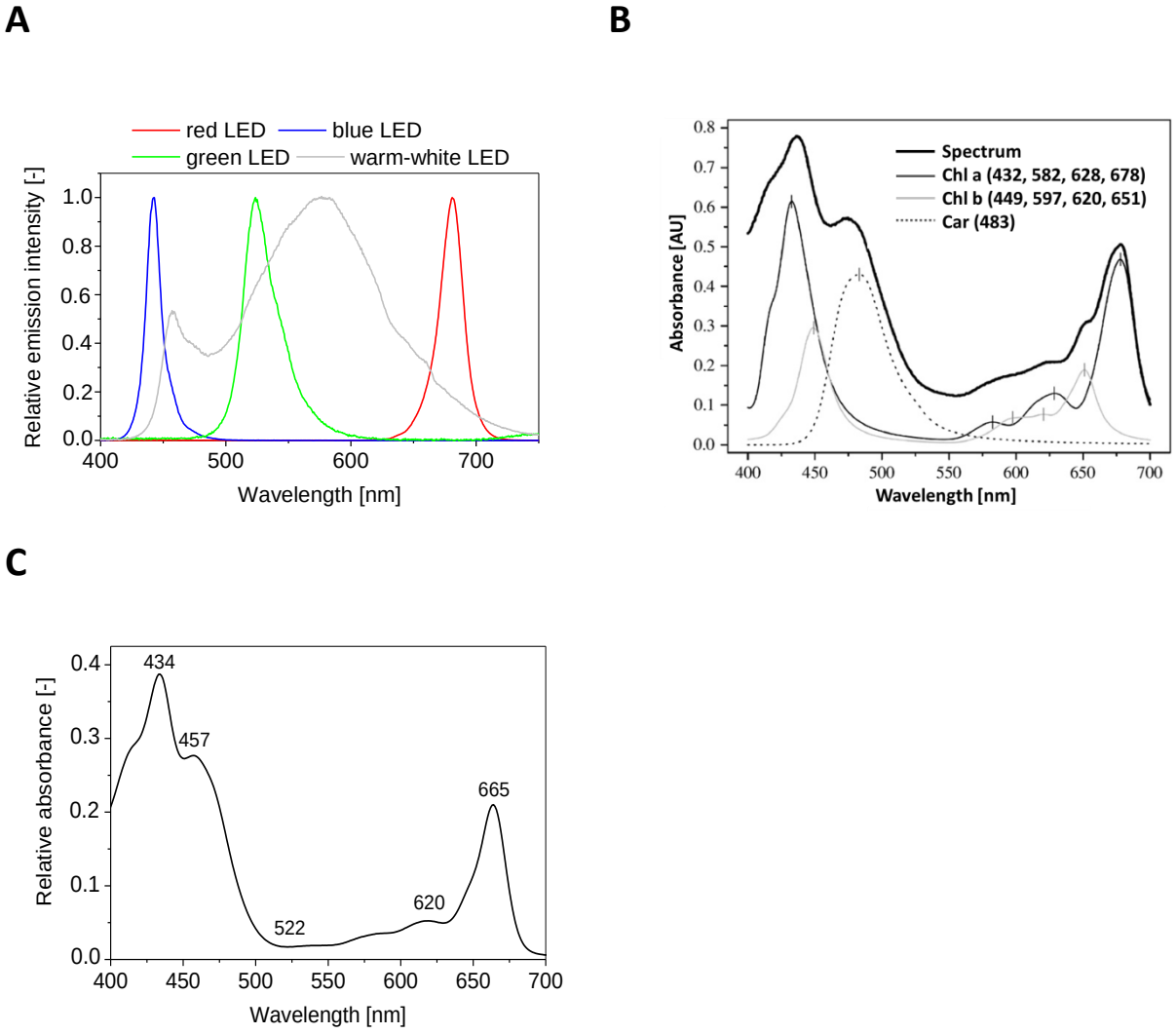

Figure 4-1. Selection of LEDs for studies of efficient illumination of microalgae for life support systems. A) Emission spectra of LEDs chosen. B) *In vivo* absorption spectrum measured on the thylakoid membrane system of a *C. reinhardtii* cell, modified from Rodríguez (2007). C) Absorption spectrum of extracted pigments dissolved in 80% (v/v) acetone solution; method according to chapter 3.5.4.

The absorption spectrum of extracted pigments dissolved in 80% acetone/water (v/v) (panel C, Figure 4-1) shows a peak shifted to the left at 665 nm compared to the *in vivo* spectrum. Therefore attention should be paid by comparing absorption spectra of *in vivo* measurements, being the ones that have to be considered for choosing illumination wavelengths, and spectra measured on pure pigments dissolved in various solvents.

4.2 PCE values for different wavelengths and color combinations

As a major factor for efficiency comparison of different light colors compared to full-spectrum illumination, photo conversion efficiencies (PCE) based on quantum energy of absorbed irradiation are used.

Related to the topic of light attenuation, biomass productivity and light to biomass conversion efficiency, one has to distinguish between kinetic, stoichiometric and thermodynamic effects (Souliès 2016). In terms of stoichiometry, there is the hypothesis that all absorbed photons have the same contribution to photosynthetic rates. Hence, on the basis of the absorbed quantum efficiency, all absorbed photons from the PAR range should have the same physiological effect in form of mols oxygen produced.

This was and still is a highly discussed topic in photosynthetic research. For a variety of plants the quantum yield of PAR photons was measured by McCree (1972); for *Chlorella* suspensions the yield of oxygen from absorbed photons was measured by Emerson and Lewis (1943) and for the green alga *N. oculata* by Tamburic and coworkers in 2014 (see theoretical section 2.3.2.3, Figure 2-16). As it was shown in the theoretical section, there are differences in quantum yield in relation to wavelength measured for higher plants and microalgae cultures, whereas highest yield values were found for red wavelengths.

However, in thermodynamic terms, the accessory pigments use the photons with different efficiencies in relation to their wavelength. As the photosystems operate at specific energy levels corresponding to red wavelengths of 680 and 700 nm, red light is used more efficiently than blue light (Souliès 2016). In this work also light color combinations were examined, also bearing in mind that *C. reinhardtii* is equipped with several sensory pigments with their respective action spectra, which can have an influence on the overall PCE.

Another important factor is the light distribution in the reactor volume. The illuminated fraction γ is defined as ratio of the reactor depth at which a complete light attenuation occurs to the overall reactor depth (Souliès 2016). For high absorbing light conditions it follows that $\gamma < 1$; for low absorbing conditions it is $\gamma > 1$. The condition where $\gamma = 1$ is termed “luminostat regime” with maximal biomass productivities, full light attenuation and no dark volumes (Souliès 2016). Additional to this concept of the illuminated fraction, it is important how the ratio of reactor volume within photosaturation and the volume within photolimitation is; meaning the ratio of the reactor depth at which the resulting PFD per cell is within the light saturated range in terms of PI-curve to the overall reactor depth.

The following subchapters summarize the experimental results of light color studies in terms of PCE values for low light and higher light intensity conditions.

4.2.1 Low light intensity conditions

For the first studies with mono- and dichromatic illumination, low light intensities, with a total PFD of 25 µE m^{-2} s^{-1} on the irradiated surface, were applied. Experiments were conducted in miniplate reactors with one-sided illumination. Two colors were combined in molar ratios given on the basis of µE photons.

Table 4-1 and Figure 4-2 A show photo conversion efficiencies as mean values with standard deviation based on absorbed photons with their respective quantum energies for different mono- and dichromatic illuminations, full-spectrum warm-white illumination as well as shift experiments from blue to red monochromatic illumination at the end of the exponential growth phase (Wagner, 2016). All of these experiments were conducted under conditions with only light limitation but no nutrient limitation, ensured by feeding the cultures during the linear light limited growth phase. Additionally, ratios of biomass built per photons absorbed are shown (Figure 4-2 B). These values originate from the same data sets and were also determined during the linear growth phase analogous to PCE calculation.

Table 4-1. Results for PCE_{PAR} values as well as ratios of biomass built in mg per photons absorbed in mol and kJ determined under low PFDs. Results for determination of PCE_{PAR} values (Wagner 2016) for different mono- and dichromatic illuminations compared to warm-white control for low light intensities with an overall PFD of 25 µE m^{-2} s^{-1} in miniplate reactors at 25°C. Ratios of biomass built from photons absorbed in mg mol^{-1} and mg kJ^{-1}.

Light color/combination	PCE_{PAR} [%]	$Biomass_{built}$/ $Photons_{abs}$ [mg mol^{-1}]	$Biomass_{built}$/ $Photons_{abs}$ [mg kJ^{-1}]
Warm-white	5.02 ± 1.01	0.65 ± 0.27	2.84 ± 1.24
Red (680 nm)	12.24 ± 1.45	1.52 ± 0.40	8.50 ± 1.36
Blue (447 nm)	6.25 ± 0.66	0.89 ± 0.22	3.34 ± 0.81
Green (520 nm)	3.85 ± 0.79	0.36 ± 0.12	1.63 ± 0.53
Shift (blue to red)	11.42 ± 1.50	1.17 ± 0.33	7.89 ± 1.53
90 % red 10 % blue	14.78 ± 1.11	1.71 ± 0.07	9.35 ± 0.39
80 % red 20 % blue	10.97 ± 1.90	1.15 ± 0.08	6.06 ± 0.41
70 % red 30 % blue	11.79 ± 1.36	1.30 ± 0.31	6.60 ± 1.58
50 % red 50 % blue	9.54 ± 2.71	1.02 ± 0.33	4.77 ± 1.55
25 % red 75 % blue	7.25 ± 1.53	0.93 ± 0.38	3.83 ± 1.50
10 % red 90 % blue	4.8 ± 1.09	0.79 ± 0.22	3.08 ± 0.86
90 % red 10 % green	11.53 ± 1.84	1.29 ± 0.31	7.57 ± 1.73

A PCE of 5.02 ± 1.01% was achieved with full-spectrum warm-white illumination used as control. Concerning monochromatic illumination, highest conversion yields were determined for pure red illumination accounting for 12.24% (± 1.45%); pure blue illumination with a PCE of 6.25% is close to warm-white. With pure green illumination a PCE value of 3.85% was calculated. Shift experiments, where blue illumination was switched to red illumination at the end of the exponential growth phase, lead to a value of 11.42%.

Interestingly, under low light conditions, highest PCE_{PAR} values were achieved with dichromatic red blue illumination at a molar ratio of 90 to 10% with 14.78 ± 1.11%. With increasing blue proportion, yield values decrease where a 10% red, 90% blue mixture corresponds to a PCE value of 4.8 ± 1.09%. A dichromatic mixture of red and green photons at a molar ratio of 90 to 10% leads to a PCE value of 11.53 ± 1.84%, thereby not surmounting the red/blue combination at the same molar ratio.

On the basis of these results (Table 4-1 and Figure 4-2), a clear influence of mono- and dichromatic illumination can be seen compared to warm-white control for *C. reinhardtii* CC-1690 cells for low light intensities.

As far as monochromatic illumination is concerned, the highest light to biomass conversion efficiency (12.24 ± 1.45%) is achieved with pure red (680 nm) light illumination. Red light of 680 nm is optimal from an energetic perspective correlating to Chl a absorption maximum, as well as to the cumulated total *in vivo* absorption spectrum (Figure 4-1 B). However, absolute values for all red lighting combinations may be slightly overestimated since the used light sensor only shows around 70-80% sensitivity for wavelengths around 680 nm (compare to Appendix 11.6.1.1, Figure 11-8).

Warm-white and blue light achieve similar PCE values around 5-6%, respectively. This is slightly lower than could be expected from the assumption that all photons have the same quantum yield. This is also displayed by ratios of biomass built per photons absorbed (Figure 4-2 B) where especially the PCE values for blue illumination show that, although blue wavelengths carry highest energy within PAR range, energy to biomass conversion is drastically lower than for red photons which transport less energy. This contradicts the hypothesis that every absorbed photon, independent from its energy, has the same effect on photosynthesis.

For pure green illumination at 520 nm at low light intensities, a PCE of 3.85% was determined which is not much lower than for full-spectrum illumination. This proves that green photons can promote growth of the alga.

As highest PCE values measured were achieved with dichromatic red/blue illumination at a molar ratio of 90 to 10%, it can be concluded that there is a clear influence of sensory pigments on growth as red should yield the highest values seen from an energetic perspective. PCE values decrease when the

amount of blue light is increased. This physiological growth behavior is accompanied by a changing morphological appearance (see chapter 4.3).

The maximum value of around 15% PCE achieved with red/blue 90/10 illumination is close to the theoretical maximum PCE value as for red photons of 680 nm the theoretical photosynthesis efficiency PE for the photosynthetic light to glucose conversion is 24% (see chapter 2.3.2.1). Therefore, as biomass formation is one step further, this value of 24% is reduced by 30-40% and should be close to 15-17%.

When blue photons are replaced by green photons in the same molar ratio, a PCE similar to pure red illumination is achieved (11.53 ± 1.84%), which is lower than the value determined for the red/blue combination. This result underlines the fact that for growth of the alga in closed photobioreactors photons within the blue wavelength range are beneficial combined with a high proportion of red light at 680 nm. Furthermore, it shows that there are effects based on sensory pigments having also influence on the overall yield coefficient of light to biomass conversion.

Shift experiments, where blue light was switched to red lighting via the end of the exponential growth phase, could not achieve highest light to biomass conversion as it was reported for *Chlorella vulgaris* by Kim and coworkers (2014). They reported effects of an increased cell size and activation of cellular metabolism by blue-light-photoreceptors during the early exponential phase combined with a high division rate promoted by red light during the linear growth phase. These effects finally resulted in a higher *C. vulgaris* biomass concentration in comparison to cultivation with red, blue or warm-white light. This could not be shown for *C. reinhardtii* CC-1690 during this work. Only the effect of blue and red photons on cell size was clearly visible by microscopic images (see 4.3).

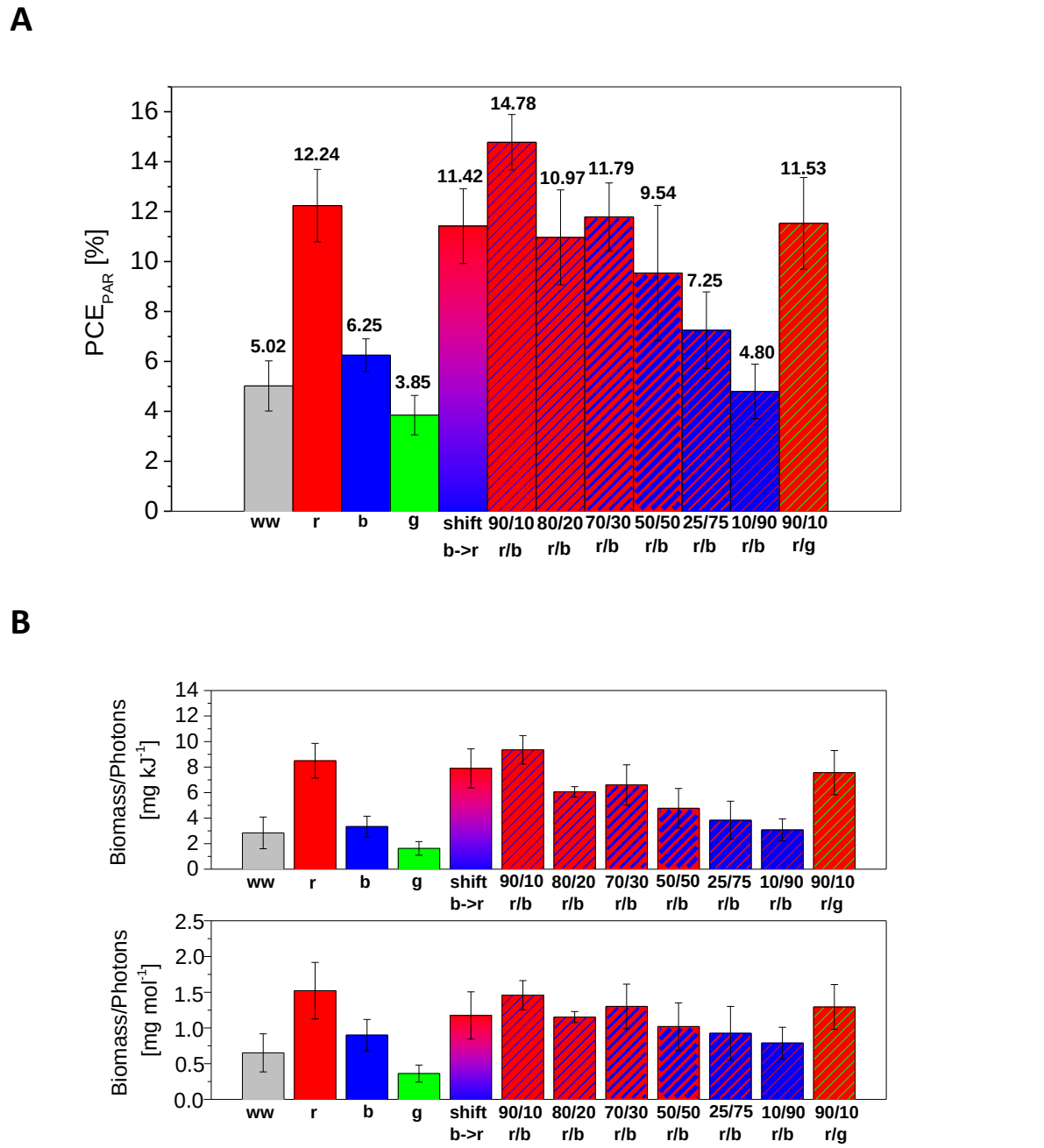

Figure 4-2. Light to biomass conversion in dependence on light colors compared to full-spectrum illumination. A) PCE_{PAR} values for mono- and dichromatic illumination and shift experiment compared to warm-white control at low overall PFDs of 25 µE m^{-2} s^{-1} in miniplate reactors at 25°C. Abbreviations indicate: ww = warm-white control; r = 100% red; b = 100% blue; g = 100% green; shift = shift from 100% blue to 100% red illumination at the end of exponential growth; r/b 90/10 = red/blue 90/10%; r/b 80/20 = red/blue 80/20%; r/b 70/30 = red/blue 70/30%; r/b 50/50 = red/blue 50/50%; r/b 25/75 = red/blue 25/75%; r/b 10/90 = red/blue 10/90%; r/g 90/10 = red/green 90/10%. Numbers indicate the mean values out of at least three replicates. Error bars indicate standard deviations, Wagner (2016). B) Ratios of biomass built per photons absorbed in mg mol^{-1} and mg kJ^{-1} derived from the same data set.

4.2.2 Higher and saturating light intensity conditions

As experiments were conducted at low light intensities, further studies were necessary to determine PCE values at higher light intensities, also approaching saturating light intensities. This is important to see where maximal yield coefficients can be achieved to select optimal PFDs for a most energy-efficient operation of a microalgae-based module under microgravity conditions.

A

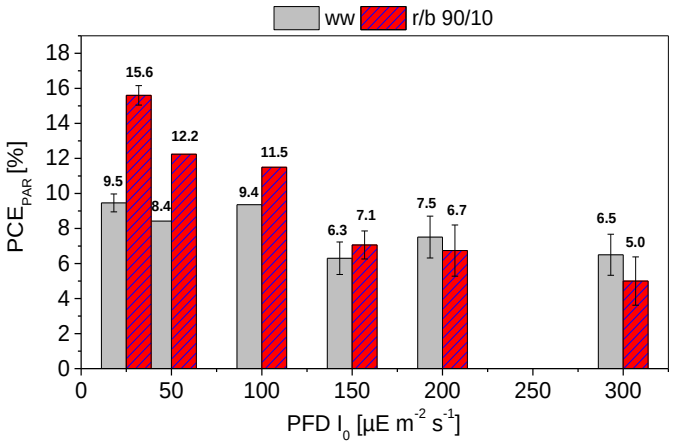

B

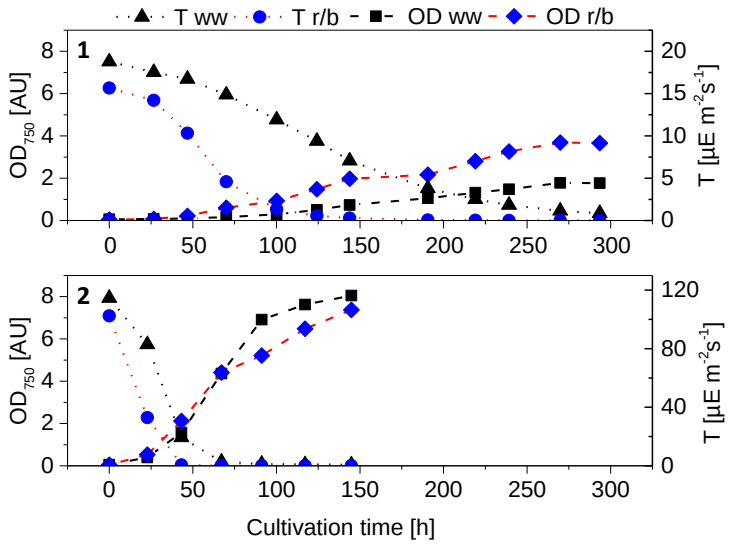

Figure 4-3. PCE values and transmission for higher and saturating light intensities. A) PCE_{PAR} values for red/blue 90/10 illumination compared to warm-white control for different I_0 PFDs: 25, 50, 100, 150, 200 and 300 µE m^{-2} s^{-1} determined for cultivations of *C. reinhardtii* CC-1690 in midiplate reactors at 25°C. (ww = warm-white; r/b 90/10 = red/blue 90/10%). Numbers indicate mean values and error bars represent standard deviation. For PFDs of 50 and 100 µE m^{-2} s^{-1} there are no duplicate cultivations. B) Values of transmission T (µE m^{-2} s^{-1}) and optical density OD_{750} (AU) during cultivation at a PFD of 25 µE m^{-2} s^{-1} (1) and 150 µE m^{-2} s^{-1} (2) for warm-white control and red/blue 90/10 illuminated culture in midiplate reactors at 25°C. Linear growth phase was extended by feeding with concentrated medium as soon as light transmission values approached zero, Wagner (2016).

Experiments were conducted in larger scale midiplate reactors as well as miniplate reactors (not every PFD tested) with PFDs of 25, 50, 100, 150, 200 and 300 µE m^{-2} s^{-1}. Results (except for 300 µE m^{-2} s^{-1} value) were also published to some extent (Wagner 2016).

Figure 4-3 A shows results for PCE values determined for dichromatic red/blue 90/10 illumination compared to warm-white illumination. Panel B shows growth curves (as OD_{750} values) and light transmission for cultivations with a PFD of 25 µE m^{-2} s^{-1} and 150 µE m^{-2} s^{-1} in midiplate reactors at 25°C for white and dichromatic red/blue illumination (Wagner 2016).

Concerning dichromatic illumination with red and blue photons at a 90 to 10% ratio, highest PCE values were measured at low light intensities of 25 µE m^{-2} s^{-1}. The maximum PCE with 15.60 ± 0.55% is slightly higher than the value measured in the smaller scale reactor, which can be explained by better mixing conditions.

With increasing PFD, PCE values for red/blue illumination decrease within the tested range, where lowest PCE values for red/blue 90/10 illumination were measured for 300 µE m^{-2} s^{-1} with 5.0 ± 1.4%. In contrast to that, PCE values do not differ very much within the range of tested light intensities for full-spectrum warm-white illumination. PCE_{PAR} values vary between 6-9%, whereas from integration of µ along with light path there should be a slight decrease of PCE with higher PFD as light saturation occurs. The slightly higher PCE for a PFD of 200 and 300 compared to 150 µE m^{-2} s^{-1} could be explained by measurement errors and is reflected as standard deviation.

No clear difference in PCE values between dichromatic and full-spectrum illumination can be detected anymore for light intensities between 150 and 300 µE m^{-2} s^{-1}. A possible explanation for similar PCE values at these higher light intensities when full-spectrum and dichromatic illumination are compared is that a saturation effect occurs. Around light intensities of about 200 µE m^{-2} s^{-1} no net difference in PCE values between full spectrum and dichromatic red/blue 90/10 illumination can be determined any more. This effect is likely to be resulting from the different absorption characteristics of light wavelengths where wavelengths in the red and blue range are better absorbed than full-spectrum illumination leading to a sharper decrease of light intensity along the light path inside the plate reactor. This becomes pivotal at higher light intensities. This fact is noticeable by an earlier decrease of transmitted light on the dark side of the reactor for cultures illuminated with the red/blue light mixture (see Figure 4-3 B) for both low (1) and high light intensities (2), where at high light intensities the slope of light decline is larger.

Resulting from that, cells in cultures illuminated by red and blue photons from one side suffer earlier from light limitation with increasing reactor depth than control cultures illuminated with less absorbing warm-white light at the same incident PFD. In other words, in this case light saturation for

red/blue illumination only exists in some parts of the reactor volume and to a lesser extent than for full-spectrum illumination.

With increasing irradiated light intensities there is a decrease of PCE values for both illuminations as more cells come to saturation range of the PI-curve and there is not net increase in mean µ integrated along the light path for one-sided illumination. A possible advancement could be the application of double-sided illumination with reduced PFDs and a dichromatic 90/10 red/blue illumination. To further elaborate this approach, the µ distribution along the depth of the culture for different light mixtures and intensities should be determined with the help of light penetration modeling based on experimental results.

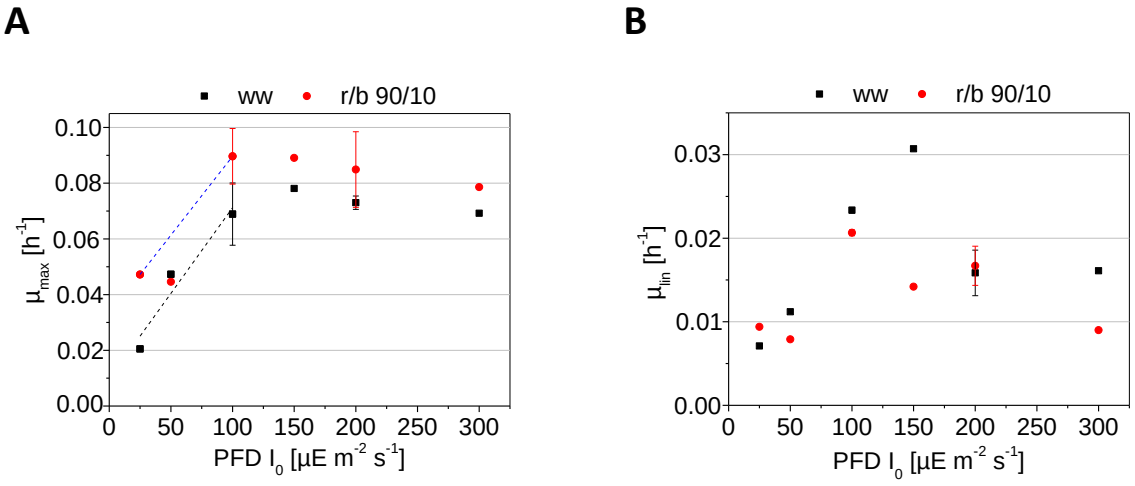

Figure 4-4. µ-I_0-kinetics for red/blue and full-spectrum illumination.
A) μ_{max}-I_0 curve for cultivations in midiplate reactors at 25°C for warm-white control and 90/10 red/blue illumination. B) μ_{lin}-I_0 curve for midiplate reactor cultivations for warm-white and 90/10 red/blue illumination.

Figure 4-4 A shows μ_{max} in dependence on the applied PFD I_0 in midiplates for both warm-white and dichromatic 90/10 red/blue illumination. This kinetic shows that maximum specific growth rates are higher for dichromatic illumination at every PFD tested (the value for 50 µE m^{-2} s^{-1} is considered as statistical outlier) and that saturation point is around 100 µE m^{-2} s^{-1}, whereas saturation point for warm-white is later around 150 µE m^{-2} s^{-1} for one-sided illumination in midiplate reactors. Hence, the aforementioned assumption of an earlier saturation for high absorbing wavelengths is proven. The slope of both curves in the light limited range is very similar for both illumination approaches. However, more experiments in the light limited range should have been performed to achieve a higher certainty for the course in that specific range.

Panel B shows the μ_{lin}-I_0 curve for both lighting approaches. Maxima correspond to saturation intensities reflecting the μ_{max}-I_0 curve. A better light penetration at higher intensities in the linear phase of the cultures is shown for warm-white light as values of μ_{lin} are higher.

4.3 Influence of light color on cell size and morphology

All samples taken during the experiments with light colors were analyzed regularly by light microscopy and the corresponding software for cell size and morphological characteristics. Cell size distribution was measured by laser diffraction within the linear growth phase.

A **B**

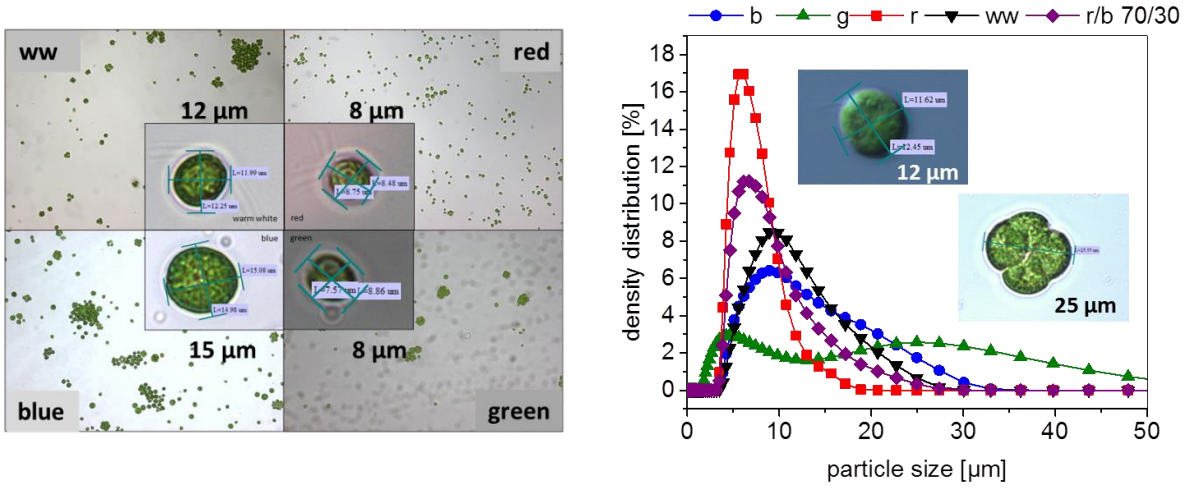

C

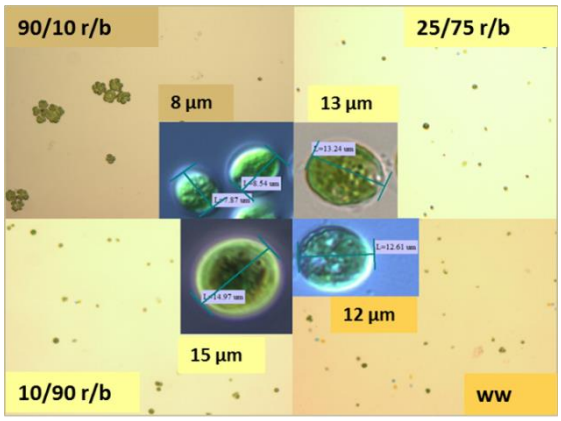

Figure 4-5. Influence of light color on cell size. A) Microscopic images analyzing cell size under different monochromatic illumination versus warm-white control at low PFDs of 25 µE m^{-2} s^{-1} in miniplates at 25°C. From upper left: warm-white, red, blue, green. B) Cell size distribution as density distribution of cultures grown under monochromatic (blue, green, red) as well as dichromatic red/blue 70/30 illumination compared to warm-white control at PFDs in miniplate reactors (Wagner 2016). C) Effects on cell size and shape of higher percentages of blue light compared to white control. Bright field, 100x magnification, phase contrast at 400x magnification.

Figure 4-5 shows microscopic pictures (A) and particle size distribution curves (B) for cultures illuminated mono- and dichromatically compared to warm-white control (Wagner 2016). The largest cell diameters can be determined for blue light illumination (up to 15-20 µm), where the smallest diameters can be detected for cells grown under pure red illumination (around 8 µm).

Panel B of this figure shows particle density distribution in % versus equivalent diameter in µm representing the size of the cells. A peak of the curve around 9 µm is detected for control samples with warm-white illumination; red illuminated cultures show most commonly cell diameters around 6 µm. The blue peak is similar to the warm-white control at 9 µm; however, this curve is broader indicating a broader distribution of cell sizes and that bigger cell sizes are more frequent than in control. A peak around 7 µm is determined for dichromatic 70/30 illumination between that of pure red and white control. Cell size distribution curve for green illumination shows a bimodal distribution indicating that not only single cells were present, but also cell aggregates as indicated by the microscopic picture (see also Figure 4-7 C). For pure red illumination cells mostly dominate as single cells or dividing cells showing a narrow distribution curve. Sauter diameters account for 10.95 µm (warm-white), 11.73 µm (blue) and 7.19 µm (red).

The results shown in panel A and B of Figure 4-5 suggest that light color has a remarkable effect on cell size and also aggregate formation for the tested light intensities. Blue light leads to bigger cell sizes and red photons to smaller cells compared to warm-white control. Increased cell diameters for blue and also for white light (compared to red; white light also contains blue photons) can be explained by the already known fact that blue light leads to an increase of the critical cell size at which cells undergo cell division (Münzner and Voigt 1992). This relation is assumed to be based on the influence of blue photons on cyclin-dependent kinases associated with DNA replication and mitosis (Oldenhof 2004 a). Besides *C. reinhardtii*, this effect of light color on cell size was also reported for *Chlorella vulgaris* (Kim 2014).

Cell size and morphology of CC-1690 cells were studied during all further cultivations with different illumination colors and combinations and with different light intensities (between 25-200 µE m^{-2} s^{-1}) with the help of lightmicroscopic images and the corresponding software to determine cell diameters. For warm-white illumination there were no differences of average cell sizes between the single approaches and the inoculum sample and no dependencies on the PFD applied were monitored. For monochromatic red illumination at 680 nm differences of cell sizes in the course of cultivation time were detected. Similar to the earlier described effect (compare to Figure 4-5 A, B) the average cell size decreased to 6-7 µm (see Figure 4-6 A, left, on day ten of cultivation during linear growth, compare also to an average of 8 µm in part A of Figure 4-5) whereas after about 16 days of cultivation cell sizes increase again to the normal “control” size of the inoculum (right side panel A, still in linear growth phase as cultures were fed regularly). Together with the cell diameter also the cell shape changed from almost round to oval simultaneously with decreasing cell diameter (Figure 4-6 A).

For blue light the effects of increased cell diameters were also found for higher PFDs of 150 and 200 µE m^{-2} s^{-1} (in this case 12-13 µm, see Figure 4-6 B), in accordance to the first results (part A, B of Figure 4-5) whereas this effect was detected after about four days of cultivation (during linear growth

phase). During the cultivation under blue light no decrease back to the initial cell diameter was monitored which might have been detected during longer cultivations at later times.

For green illumination similar results like for warm-white illumination were detected, neither cell size nor shape was influenced tremendously. This is in part contrary to the results in part A and B of Figure 4-5, where cell size was decreased. Further experiments with daily cell size measurements by laser diffraction would have been necessary to assess this in more detail.

For red illumination, after the decrease in average cell size monitored at about four days after inoculation (cell already showed linear growth at this point) which was seen earlier, there is a reverse development monitored with re-installation of initial cell diameters. This can be interpreted as transient effect of light color on cell size (in the case of red light also cell shape) which was only persisting in the first days of cultivation under red light.

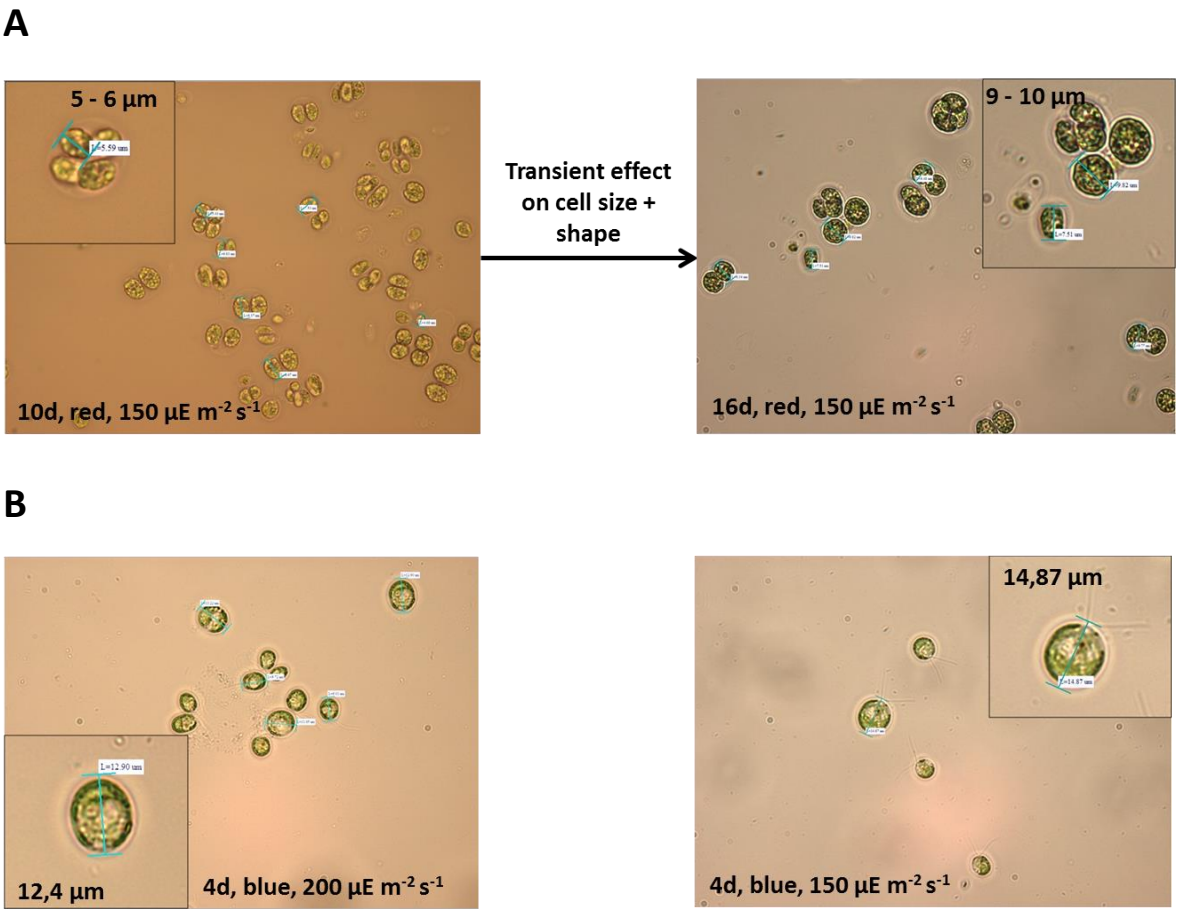

Figure 4-6. Effects of light color on cell size and morphology in dependence on PFD and cultivation time. A) Cells illuminated with pure red at 150 µE m^{-2} s^{-1}, left: culture after ten days of cultivation: average cell diameter decreases to about 5 µm, cells show an oval shape. Right: transient effects with reverse development, cells show an initial cell diameter of about 10 µm, and a more round shape, 400x magnification, bright field. B) Cells under pure blue light after four days of cultivation, left side at a PFD of 200, right side at 150 µE m^{-2} s^{-1}, 400x magnification, bright field.

For blue light the effect on cell size was detected later and possibly a reverse development could have been detected in later stages of cultivation. If these transient effects are monitored also during continuous cultivations the following chapter 4.6 summarizes.

For red light a high amount of dividing cells was monitored throughout the cultivations, reflecting the aforementioned effect on cell division, where red light promotes a higher doubling rate at smaller critical cell sizes.

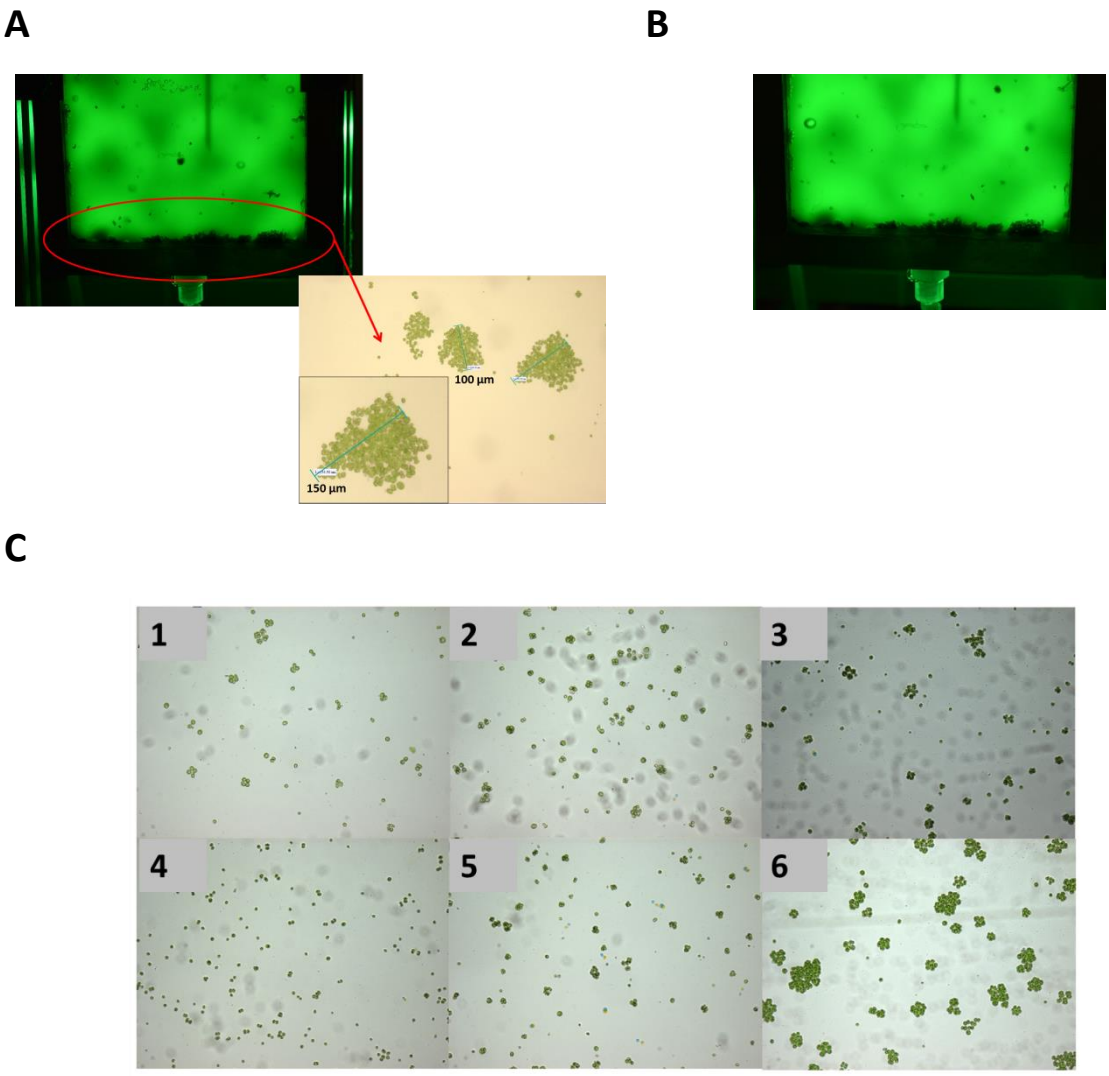

Figure 4-7. Effects of monochromatic green light on morphology at both low and high light intensities. A) Cells grown under low green light conditions (PFD = 25 µE $m^{-2}s^{-1}$) in miniplates at 25°C. Upper part showing a picture of algae suspension in miniplate with green illumination and aggregate forming cells. Lower part represents lightmicroscopic image from a sample of this cultivation with aggregates with diameters ranging up to 150 µm. B) Picture of algae suspension in miniplate with green illumination and aggregate forming cells during cultivation under green light at 200 µE m^{-2} s^{-1}. C) CC-1690 cells during linear growth phase illuminated with different light colors at low light intensities of 25 µE $m^{-2}s^{-1}$ in miniplate reactors at 25°C, light microscope, 100x magnification, bright field: 1: warm-white, 2: blue, 3: green_a, 4: red, 5: 70/30 red/blue, 6. green_b.

Concerning pure green illumination and the effects on morphology, the results show that *C. reinhardtii* CC-1690 cells tend to form aggregates more easily when illuminated with green photons (520 nm) than with red or blue photons. Further studies with green light, also at higher light intensities, up to saturation, confirm this first assumption.

Figure 4-7 shows effects of monochromatic green illumination both at low (part A and C) and high light intensities (B) on macroscopic cell morphology of *C. reinhardtii* CC-1690. Further experiments at a PFD of 200 µE m^{-2} s^{-1} were conducted to assess if the effect of green light favoring cellular aggregation also prevails at higher intensities which was confirmed. However, this phenomenon is a first observation; a biological based explanation cannot yet be given at this point. Also for warm-white illumination a higher tendency to form large aggregates (> 100 µm) was monitored which can be explained by the high amount of green photons emitted (compare to Figure 4-1 A). However, as discussed before, the wildtype strain CC-1690 highly tends to form primary and secondary aggregates were reasons are not yet discovered. Pre-culture cells illuminated with warm-white light also kept growing in aggregated form even when illuminated with red and blue light to some extent. However, a clear tendency of green photons to promote this behavior was detected throughout all cultivations.

Possible reasons for this behavior can be divided into two aspects. One explanation might be that by building aggregates cells in suspension try to increase absorption by increasing light path length by a higher reflection of incoming photons similar to plant leaf structures. This would require a kind of quorum sensing. Technically, light refraction and reflection change for a suspension primarily containing aggregates compared to a cell suspension with single cells; additionally, the inner-filter effect appears for aggregates. However, it is not clear if there is a net increase of light path length for aggregated cells.

A second explanation, which is possibly most reasonable, would be that green photons excite, via sensory pigments, a coordinated aggregation event of single cells in suspension where an evolutionary benefit seems to underlie. A related reason might be based on a stress condition cells are exposed to during illumination with green low absorbing wavelengths originating from a lack of energy. However, also under higher light intensities this aggregation reaction was observed. Furthermore, this effect might also be related to a formation of microbubbles following O_2 production inside those aggregates. As a consequence the density is reduced leading to a flotation effect which allows a change of location probably faster than for motile single cells. This would allow a movement to an environment with more favorable light conditions.

In terms of bioprocess techniques there are both disadvantages, like diffusion limitation and decreased productivities, as well as advantages of aggregation as cell liquid separation is easier resulting from an increased cell aggregation under monochromatic green illumination of *C. reinhardtii* cells.

The monitored transient effects of pure red light on cell diameter and shape were independent of the applied PFD (25 to 200 µE m^{-2} s^{-1}). However, so far these transient effects of red light are not described in literature. It might be explained by a habituation or adaptation effect in relation to the enzyme CDK being involved in cell division and cell size in *C. reinhardtii*. This transient nature might also be explained by the existence of an optimal cell size from an energetic perspective relating to intracellular pressure or transport mechanisms. For long-term cultivations this optimal cell size is reinstalled.

More detailed experiments with regular cell size distribution analysis and a variation in PFD should confirm these results. If these effects on cell size and morphology resulting from light color experiments monitored for *C. reinhardtii* CC-1690 are transposable to other species (other than cell division and cell size for *C. vulgaris*) is beyond the scope of this work and would be speculative. However, it seems likely that at least for other species within the phylum of chlorophyta some effects should be transposable relying on the same mechanistic models.

4.4 Pigment content in dependence on applied wavelengths and intensity

For every experiment in large and small scale plate reactors, specific pigment concentration as well as starch contents of the cells were measured during the linear phase of the cultivations under different light colors. First of all, the differences in specific pigment concentrations depending on lighting conditions were studied. The results of specific pigment concentrations are shown for different illumination colors under low light intensities in miniplate reactors (Figure 4-8, see also Appendix 11.6.1.3, Table 11-12), (Wagner 2016).

Results for red/blue 90/10 versus warm-white illumination also at higher light intensities (up to 200 µE m^{-2} s^{-1}) in miniplate reactors are shown in Figure 4-9 A and Appendix 11.6.1.3, Table 11-13. Results for larger scale midiplate reactors are shown in Figure 4-9 B and Appendix 11.6.1.3, Table 11-14.

Under low light conditions (Figure 4-8) cells contain a specific chlorophyll a concentration in control of 45.6 ± 6.5 mg g^{-1} CDW. The experiments with red light, light shift from blue to red, the combination with 90% red/10% blue light and the mixture of 90% red/10% green all yield a lower specific Chl a concentration, especially red light with 33.5 ± 0.3 mg g^{-1} and the red/green mixture with 32.2 ± 3.7 mg g^{-1}. All other illumination approaches yield higher concentrations with a maximum of 58.0 ± 2.4 mg g^{-1} Chl a for 80% red/ 20% blue.

The distribution for specific Chl b concentrations is similar, but at lower levels: 16.9 ± 1.0 mg g^{-1} for the warm-white control illumination, a maximum was measured for 80% red/ 20% blue light illumination with 20.8 ± 1.0 mg g^{-1} and a minimum of 10.2 ± 0.3 mg g^{-1} for red light.

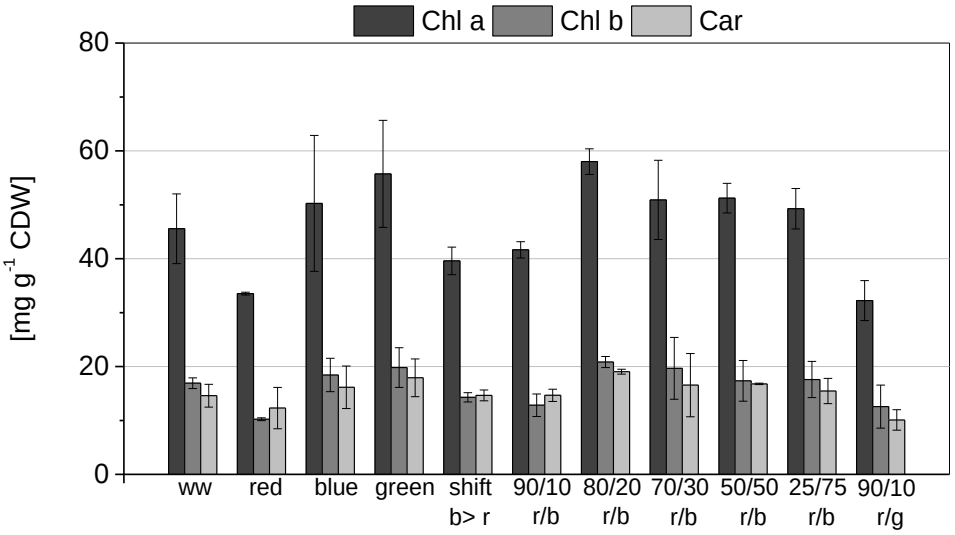

Figure 4-8. Specific pigment concentration for cells of *C. reinhardtii* CC-1690 grown under different mono- and dichromatic illumination compared to warm-white control at low light intensities. Results for low light intensities (25 µE m^{-2} s^{-1}) including shift experiments and warm-white illuminated control in miniplates at 25°C (Wagner 2016).

Carotenoids concentration is similar for control, shift and 90% red/10% blue light with 14 mg g^{-1}. For red light illumination a Car content of 12.3 ± 3.8 mg g^{-1} is measured. Here, 90/10 red/green illumination yields the lowest concentration with 10.1 ± 1.9 mg g^{-1} whereas all other mono- and dichromatic combinations show a higher amount of carotenoids per cell dry weight. Again, a maximum value is measured for cells illuminated with 80/20 red/blue light.

Cells illuminated with higher light intensities above 25 µE m^{-2} s^{-1} show decreasing specific pigment concentrations for both control and dichromatic red/blue 90/10 illumination with increasing PFD in both scales of plate reactors (Figure 4-9 A and B).

Around the saturation point, of about 150 µE m^{-2} s^{-1}, the amounts of Chl a, Chl b and Car are on the same level for white and dichromatic illumination; around 13 to 14 mg g^{-1}, 6 mg g^{-1} and 6 to 7 mg g^{-1}, respectively, for midiplates and on a slightly higher level for cells grown in smaller scale reactor with 15, 12 to 14 and 12 mg g^{-1}, respectively. With further increasing PFDs (here, only 200 µE m^{-2} s^{-1} tested) specific concentrations for all pigments analyzed seem to increase again for higher scale reactor cultivations (Figure 4-9 B, Appendix Table 11-14) whereas concentrations are clearly higher for red/blue illumination (Chl a at 25.9 ± 2.4 mg g^{-1}, Chl b 17.7 ± 3.2 mg g^{-1}, Car 8.0 ± 1.0 mg g^{-1}) than for white control (Chl a at 16.0 ± 1.3 mg g^{-1}, Chl b 12.1 ± 1.5 mg g^{-1} and Car 5.8 ± 0.4 mg g^{-1}). Data of specific pigment concentration in smaller scale reactors at this light intensity for red/blue is not available due to contamination problems.

The measured low specific chlorophyll concentrations of cells cultivated under monochromatic red and dichromatic 90% red/ 10% blue and 90/10 % red/green illumination at low light intensities (Figure

4-8) are due to the high efficiency of the photosynthesis apparatus irradiated with these wavelengths. As there is a strong photolimitation condition under low light intensity and high cell density during the linear growth phase, cells are forced to increase the chlorophyll concentration in order to absorb enough light energy to survive and produce new biomass. The higher the photosynthesis' efficiency the less chlorophyll per cell is necessary. As red photons provide the ideal wavelength and quantum energy for photosynthesis, it is obvious that cultivation under red light should have the lowest chlorophyll concentration. A dichromatic illumination with 90% red and 10% blue photons still provides enough red light to perform photosynthesis on a high level efficiency as chlorophyll concentration is relatively low as shown by the results.

Furthermore, a lower percentage of red light seems to influence the efficiency of photosynthesis crucially as there is a big difference between chlorophyll concentration of 90% red/ 10% blue and 80% red/ 20% blue light illumination. This is also maybe due to the low light intensity of approximately 25 µE m^{-2} s^{-1} and could be different with stronger illumination. Cells cultivated under green light show a specific chlorophyll concentration similar to cells grown under blue light which is surprising as a much higher concentration would have been expected due to the fact that the wavelengths of green light are the less favorable for photosynthesis. However, cells grown under pure green illumination never reached such a strong level of photolimitation at the dark side of the reactor (determined by light transmission measurement) like in cultivations illuminated with other colors.

As seen before, the dichromatic mixture of 90% red to 10% green photons leads to the same specific pigment concentrations like pure monochromatic red illumination. Compared to the two color mixture of 90/10 red and blue, the results show that the effect of a small addition of blue photons to red is different from the effect of a small addition of green photons. This can be explained by the higher influence of blue light via the action of sensory pigments in this alga. As a result, the 90/10 red/blue combination leads to different PCE values and specific pigment contents compared to red photon and 90/10 red/green illumination.

Specific pigment concentrations of cells grown under higher light intensities are lower for both conditions (dichromatic red/blue 90/10 and control warm-white) as seen in panel A and B of Figure 4-9. For saturating light intensities, around 150 µE m^{-2} s^{-1}, there is no difference between high absorbing red/blue light and warm-white control.

When the PFD is further increased to 200 µE m^{-2} s^{-1}, specific pigment concentrations of the cells, measured during the linear, light limited growth phase, increase for red/blue illumination. Also for pigment concentrations of cells illuminated with full-spectrum illumination a slight increase for all pigments analyzed is measured at least for higher scale cultivations which show better mixing conditions. A possible explanation for this increase in specific pigment concentrations is the aforementioned fact that more cells come to saturation range of the PI-curve and there is no net

increase in mean µ integrated along the light path for one-sided illumination. This is more pronounced for highly absorbing wavelengths in the red and blue range with an optimal mixture of red and blue at a 90 to 10% ratio, as decrease of light intensity along the light path is sharper than for full-spectrum illumination. These results reflect the results for PCE values at higher PFDs for both tested illumination conditions. For highly absorbing wavelengths saturation conditions with respect to light intensity are reached earlier than for full-spectrum illumination.

A

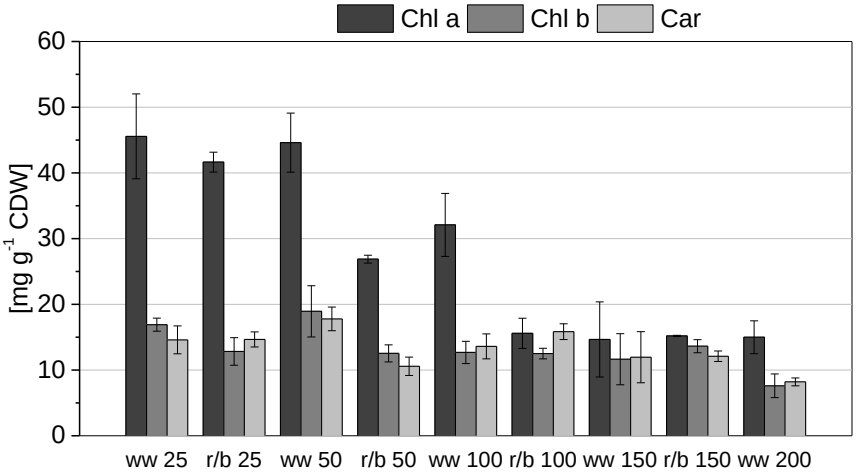

B

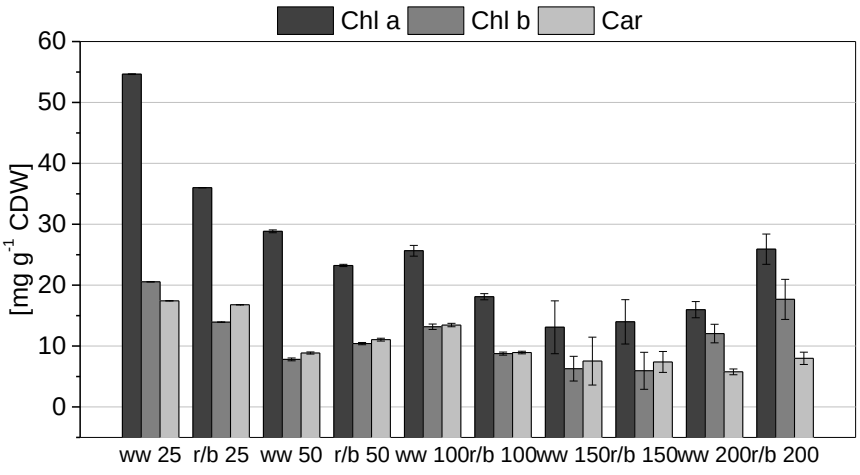

Figure 4-9. Specific pigment concentration for cells of *C. reinhardtii* CC-1690 grown under different mono- and dichromatic illumination compared to warm-white control. A) Specific pigment concentration results for low to saturating light intensities as I_0 for warm-white control and dichromatic 90/10 red/blue illumination in miniplates at 25°C. For 200 µE m^{-2} s^{-1} only values for control are available. B) Specific pigment concentration results for low to saturating light intensities for warm-white control and dichromatic 90/10 red/blue illumination in higher scale midiplates at 25°C. Analyzed pigments were chlorophyll a, b as well as carotenoids.

Further interesting are the different relations of the pigments to each other (see Figure 4-10, Figure 4-11) and their specific share at the overall pigment content (Figure 4-12).

A very important parameter is the ratio of Chl a to Chl b (Figure 4-10 A). As depicted in chapter 2.2.2.1, this ratio, together with the specific chlorophyll content per cell, is an important indicator for changes in the antenna and the reaction centers of the algal cells and may give insight on adaptation mechanisms like state transitions. Algae adapted to high light conditions show a reduced amount of Chl per cell and an increased Chl a/Chl b ratio. A putative stoichiometric relation of Chl a and Chl b is mentioned by Grossman and coworkers (2004).

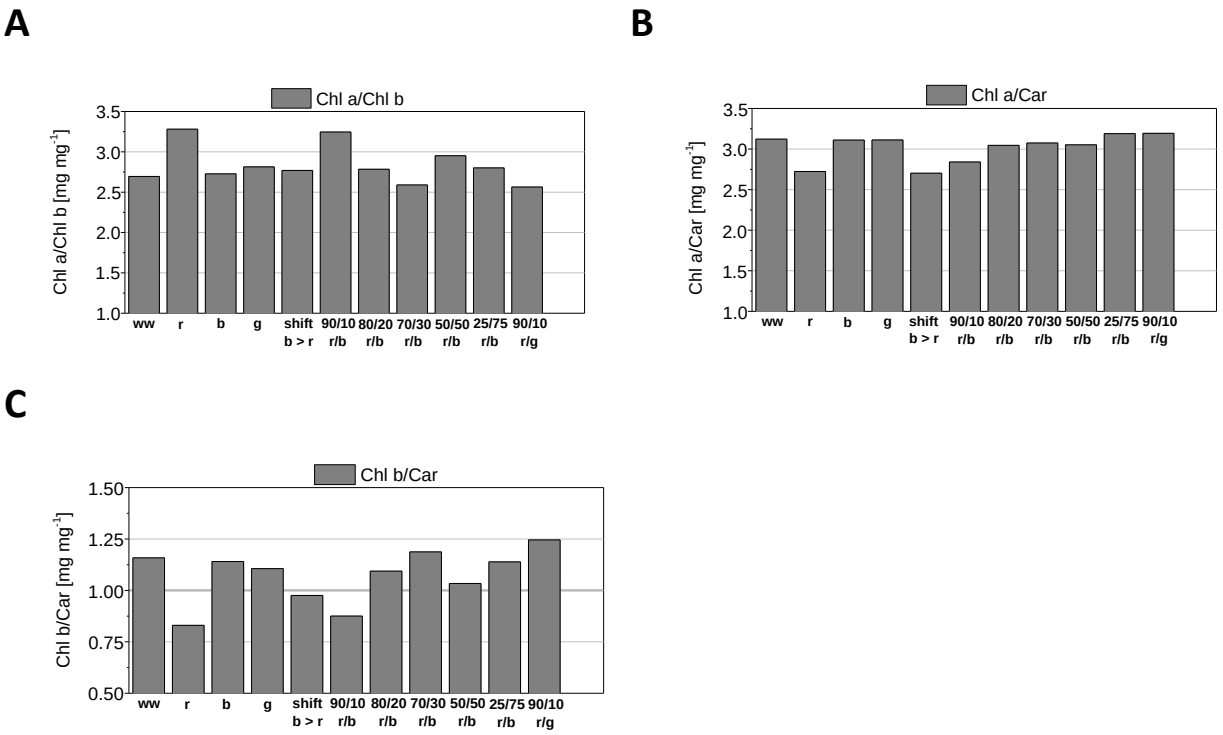

Figure 4-10. Effect of light color and intensity on pigment composition as ratios of pigments. A) Chl a/ Chl b ratio for all tested light colors at low PFDs of 25 µE m^{-2} s^{-1} in miniplate reactors at 25°C. B) Chl a/ Car ratio, PFD of 25 µE m^{-2} s^{-1}, miniplate reactors, 25°C. C) Chl b/ Car ratio, low PFDs of 25 µE m^{-2} s^{-1}, miniplate reactors, 25°C.

Figure 4-10 A shows the Chl a to Chl b ratio for all of the tested lighting approaches at low PFDs of 25 µE m^{-2} s^{-1} in miniplate reactors at 25°C. Concerning one color and full-spectrum illumination cells illuminated with pure red at 680 nm show the highest ratio with 3.3 mg mg^{-1} where the other results account for 2.7 and 2.8 mg mg^{-1}. Concerning dichromatic and shift illumination, the highest Chl a/b ratio was measured for 90/10 red/blue with 3.3 mg mg^{-1}. All other approaches yield values between 2.6-2.9 mg mg^{-1}.

In general, a high Chl a/b ratio is associated with small antenna sizes as the central pair of Chl a molecules is kept while Chl b molecules are reduced for decreasing antenna size (Melis 1996). This

would indicate that the approaches with red and 90/10 red/blue illumination lead to cells with smaller antennas than the other approaches. Moreover, it could also indicate that light energy is primarily processed by PSI as this photosystem contains more Chl a molecules. This could be related to state 2 conditions (Wollman 2001) and it could be a result of performed state transitions (compare to chapter 2.2.2.1). State 2 is described by cyclic electron transport around PSI and only ATP generation.

Concerning green light and red/green illumination, Figure 4-10 B and C show that the ratio of Car to Chl a and Chl b (here shown as Chl a/Car and Chl b/Car) is not increased compared to the other approaches, despite the assumption that carotenoids help to broaden the absorption spectrum within the green gap. For this reason a high Car content and relation to the other pigments (and therefore low Chl a/Car and Chl b/Car ratios) could have been expected. Also the share of carotenoids at the overall pigment content is not increased for green and red/green illumination (Figure 4-12 D). However, as Figure 4-10 A shows, the ratio of Chl b to Chl a is increased for these two approaches compared to red and red/blue. Therefore, it seems likely that green light at 520 nm is primarily absorbed by Chl b.

Figure 4-10 C shows the ratio of Chl b to carotenoids, where most prominent are the approaches red, shift and 90/10 red/blue leading to ratios below 1. The dichromatic illumination with 90/10 red/green yields the highest value with 1.25. Concerning the ratio of Chl b to Car (Figure 4-10 C) only for the approaches with pure red, 90/10 red/blue and the shift from blue to red illumination the specific Car concentration of the cells is higher than the Chl b concentration (Chl b/Car ratio: 0.8-0.9), whereas for all of the other light mixtures and white control Chl b/Car ratio is around 1.0-1.2. Another interesting fact is that the ratio of Chl b to Car is lowest for highest efficiency illumination conditions being red, 90/10 red/blue and shift from blue to red, with the only exception of 90/10 red/green.

Figure 4-11 shows the respective ratios of the pigments in relation to the irradiated light intensity as PFD I_0. Chl a/Chl b ratios of 90/10 red/blue compared to full-spectrum illumination are shown in panel A averaged for small and larger scale plate reactors. For both illumination approaches the ratio decreases from 2.5 to 3 down to 1.5 with increasing PFD, whereas there is an earlier decrease for high absorbing wavelengths.

Further panels B and C show ratios of Chl a/Car and Chl b/Car for the same averaged results. In total, these ratios show that light saturation is reached earlier for high absorbing wavelengths (around 100 µE m^{-2} s^{-1}) than for white control, where saturation is reached at 150 µE m^{-2} s^{-1}. This is in perfect accordance to the μ_{max}-I_0 curve in Figure 4-4 A. Hence, light saturation points are different for high and low absorbing wavelengths. One method besides the calculation of attenuation coefficients and modeling light distribution is to analyze ratios of Chl a, b and Carotenoids in dependency on applied light intensity for different colors.

These results point to adaptation mechanisms in response to light intensity and wavelength conditions which are exerted by state transitions and probably an adjustment of packing density of thylakoids in the chloroplast which is termed absorption cross section. From an evolutionary perspective, photosynthetic cells could anticipate light conditions by sensing the changing composition of sunlight with the daytime period and adjust the photosynthetic apparatus with state transitions and the amount of pigments per cell to optimize light utilization.

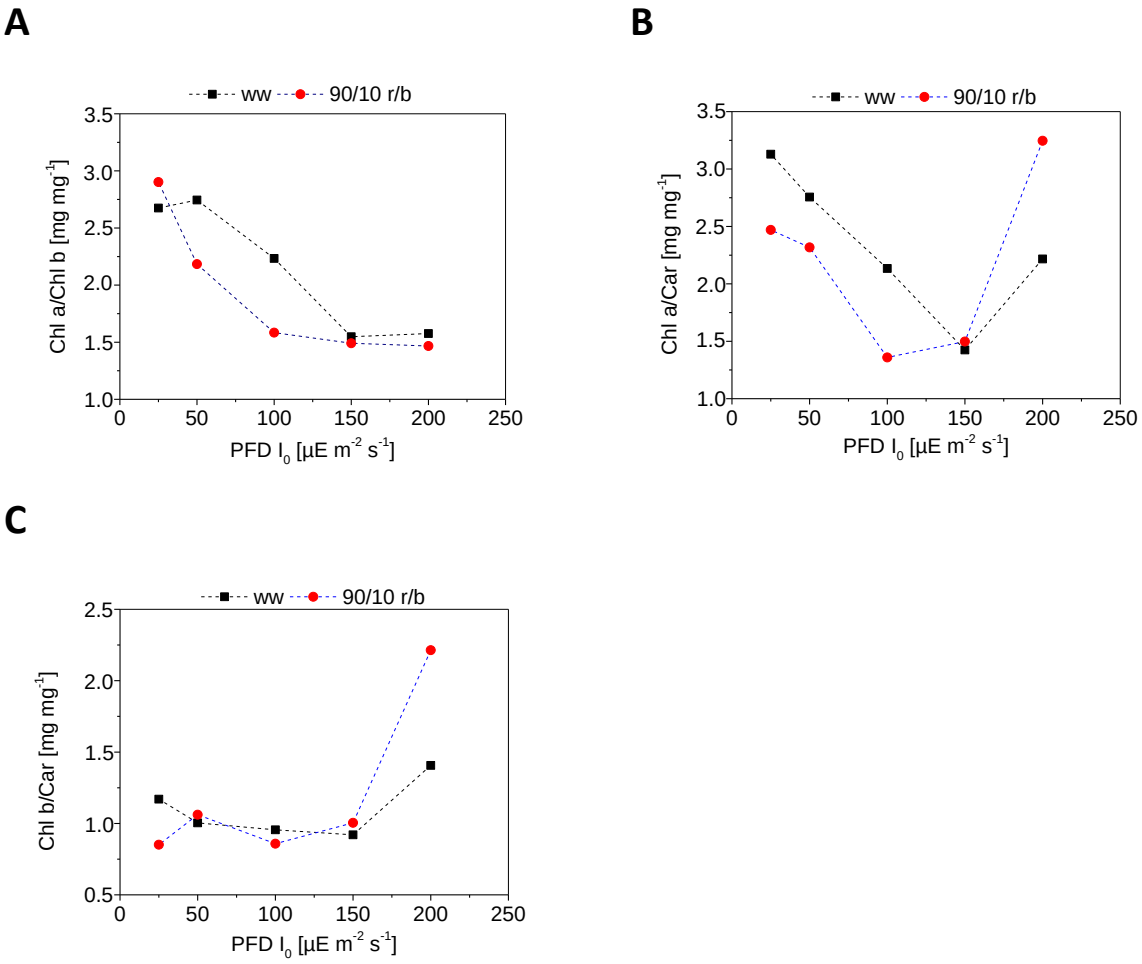

Figure 4-11. Specific pigment composition for different color illumination approaches compared to full-spectrum control. A) Ratio of Chl a to Chl b for 90/10 red/blue compared to warm-white control as mean values for small and higher scale plate reactors in dependence on light intensity. B) Ratio of Chl a to Car for 90/10 red/blue compared to warm-white control as mean values for small and higher scale plate reactors in dependence on light intensity. C) Ratio of Chl b to Car for 90/10 red/blue compared to warm-white control as mean values for small and higher scale plate reactors in dependence on light intensity.

Figure 4-12 gives another view with the total amount of specific pigments (part A) and ratios of Chl a (part B), Chl b (panel C) and Car (panel D) in relation to the total amount of pigments. The approaches with the highest PCE values show the lowest total pigment concentrations per cell (A). The share of carotenoids of total pigments (D) is the highest for the most efficient approaches except for the

red/green mixture which also points to the fact that cells under pure green or red/green illumination do not increase their carotenoid content to better absorb green wavelengths.

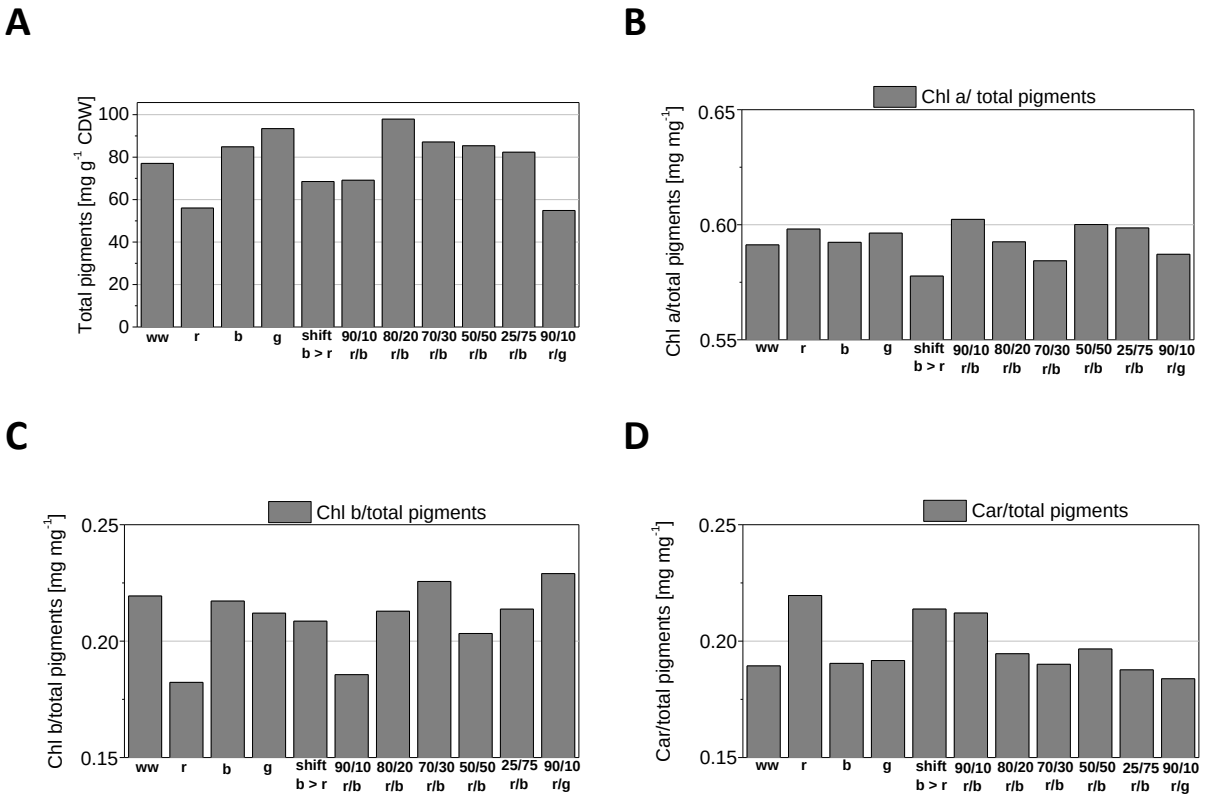

Figure 4-12. Specific pigment composition for all tested light color approaches in miniplates at 25°C. A) Specific total pigments for all light colors in miniplates at 25°C. B) Ratio of Chl a to total pigments. C) Ratio of Chl b to total pigments. D) Ratio of Car to total pigments.

In further studies also longer experiments in continuous cultures were conducted (see chapter 4.6). Experiments for PCE determination were conducted as semi-fed-batch cultivations so that linear growth phases were extended resulting in only light-limited, but no nutrient-limited conditions. During this phase PCE values were calculated. Still, long-term adaptation concerning pigment concentration has to be studied in continuous cultivations.

For higher light intensities (as mentioned for one-sided plate reactor illumination within this work) there are no relevant differences in pigment concentrations between red/blue and warm-white any more as mean the PFD per cell is in saturation range (Figure 4-9 A and B for 150 µE m^{-2} s^{-1}). Intracellular limitations are prevailing in this range of the PI-curve, which are mainly caused by the RuBisCO turnover rate, so that different wavelength compositions of irradiated light have not that much of an effect compared to low light intensities. As pre-cultures were illuminated with moderate light intensities, around 50 µE m^{-2} s^{-1}, acclimation to either low or high light conditions, before cultivations were started, can be excluded.

4.5 Absorption characteristics and détour-effect for microalgae cultures

As light attenuation is dependent on wavelength and absorption characteristics of the photosynthetic organism (absorption spectrum, pigment content and composition and therefore extinction coefficient ε) as well as morphological characteristics of the cells determining reflection and scattering, it is an important parameter which changes during batch cultivations.

One major question was concerned with the usage of low absorbing wavelengths, for example green photons (here 520 nm); if absorption can be increased by an increased light path length in case of microalgae cultures similar to the détour-effect described for plant leaf structures (compare to chapters 2.3.2.4 and 2.3.2.5).

First experiments with monochromatic green illumination gave first hints for a better absorption above a certain threshold cell density (compare to panel A, Figure 4-13). Here, in contrast to other illumination colors (as comparison dichromatically 70/30 red/blue illuminated cultures are shown), growth was only linear until a process time of about 12 days, where cell dry weight was around 0.18 and 0.22 g L^{-1}, respectively. After this point an exponential increase was monitored. This could be a result from an exponential rise of diffuse reflection or scattering effects with the result that a green photon diffuses several times through a chloroplast and the total likelihood for absorption increases.

Further experiments were therefore conducted with higher inoculum concentrations (see Figure 4-13 B) as well as with a longer duration to reach this critical cell density (compare to Figure 4-13 C). As the diagram in panel B shows, a direct exponential growth is monitored for starting cell densities around 0.2 g L^{-1}. A higher inoculum concentration around this critical value leads to a higher growth rate. These results reinforce the assumption of the possible transfer of the détour-effect for plant leaf structures to algae suspensions.

Long-term cultivations in fed-batches for 30 days have shown that the critical cell density for the détour-effect of green light (520 nm) for this alga is between 0.2 and 0.4 g L^{-1} CDW (panel C). In contrast to the white illuminated culture, which was even inoculated at a slightly lower CDW, the cell density in green illuminated cultures only shows an exponential growth after this critical cell concentration has been reached. This is also valid for transmission values for green cultures which show a more pronounced plateau phase than for the white control.

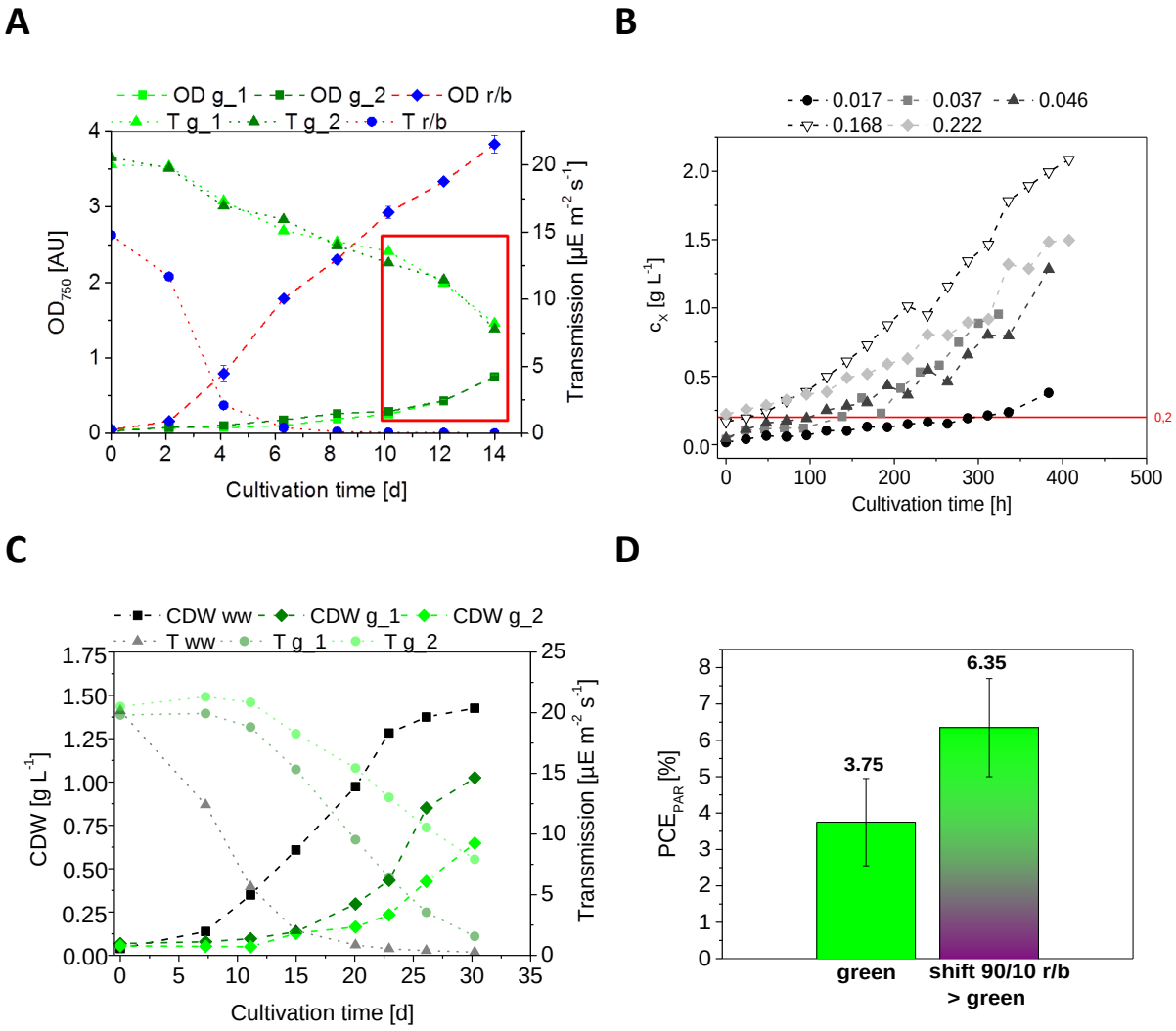

Figure 4-13. Green light and détour-effect for low absorbing wavelengths. A) First cultivation with green light with 25 µE m^{-2} s^{-1} in parallel to 70/30 red/blue illumination at the same inoculum concentration of 0.015 g L^{-1} in miniplate reactors at 25°C. OD_{750} and transmission values are depicted. On day 12 CDW accounts for 0.18 and 0.22 g L^{-1}, respectively. B) Variation of inoculum concentration with pure green illumination. c_X was varied with 0.017, 0.037, 0.046, 0.168 and 0.222 g L^{-1} cell dry weight concentration. Cells were illuminated with green light at a low PFD of 25 µE m^{-2} s^{-1}. C) Long-term cultivation under green light in comparison with warm-white for 30 days: depicted are OD_{750} values and transmission. D) Comparison of PCE values determined for a miniplate reactor culture illuminated with a PFD of 25 µE m^{-2} s^{-1} where growth is only linear, with cultures first illuminated with 90/10 red/blue at the same PFD and after transmission fell below 0.8, shifted to pure green illumination where in the linear phase the PCE was determined.

Final experiments were conducted to compare PCE values determined for pure green illumination from the beginning and cultures which have been grown first on dichromatic red/blue to reach a higher cell density and where red/blue light is then replaced with green illumination at the same PFD. Here, the algae suspension was first illuminated dichromatically with 90/10 red/blue illumination (PFD = 25 µE m^{-2} s^{-1}) until transmission intensity decreased below 0.8 µE m^{-2} s^{-1}; at this point cultures were illuminated with pure green light at the same intensity. During the linear growth phase, where both approaches were illuminated with pure green light, the PCE was determined and compared with the previous approaches under green illumination at lower starting cell densities. As it can be seen

from Figure 4-13 D, the PCE was almost doubled from 3.8 ± 1.2% to 6.4 ± 1.4% with the increase in cell concentration under green illumination. Therefore the applicability of the détour-effect for low absorbing wavelengths from plant leaf structures to microalgae suspensions was proven.

This effect can be used for enhancing microalgal growth and productivity for higher cell densities. Cultures first grown under 90/10 red/blue light at a certain PFD can be switched to trichromatic illumination by adding green photons at a certain cell density and therefore mean light intensity in the culture volume while maintaining the same initial PFD. Thereby the red to blue ratio of 90/10 should be kept constant, but intensity of both colors is reduced where the difference to the initial PFD is replaced by green photons penetrating deeper into the culture. This was already proposed by Mattos and coworkers (2015).

Another important aspect is light attenuation and resulting light gradients in dependence on the applied wavelengths, cell dry weight concentration, extinction coefficients and specific pigment composition and concentration. First data were collected where transmission spectra were measured for miniplate reactor cultivations in linear growth phase of the cells for different light colors.

Figure 4-14 and panel A of Figure 4-15 show transmission spectra for miniplate reactor cultures under red, blue and warm-white illumination at different days of cultivation and with increasing cell densities.

For pure red illumination (Figure 4-14 A) a peak shift to the right (from 681 to 696 nm) is visible for higher cell densities and increasing light limitation conditions. Furthermore, there are three local maxima visible at 661, 679 and 696 nm. Panel B shows just the same spectra, only normalized to relative transmission PFD. For pure blue illumination (part C and D) there is almost no difference in peak wavelength of transmitted light. For warm-white illumination (Figure 4-15 A) the green range peak is shifted to the left (from 577 nm to 569 nm) whereas the peak in the blue region 457 stays constant for higher cell density conditions. Additionally around 685 nm there is a local minimum for the transmitted light at later cultivation stages. Interestingly, there is a higher reduction (around 70%) of transmittance of blue photons (around the peak of 457 nm), whereas the transmittance of green photons around 570 nm is only reduced by 40% with increasing cell densities.

In case of red transmission peaks the shift of transmission curves to the right could be explained by a Stokes shift, which is even more pronounced in polar solvents like water. It is based on the fluorescence of chlorophylls, mostly Chl a molecules of PSII after light absorption; emitted wavelengths possess less energy and therefore a higher wavelength.

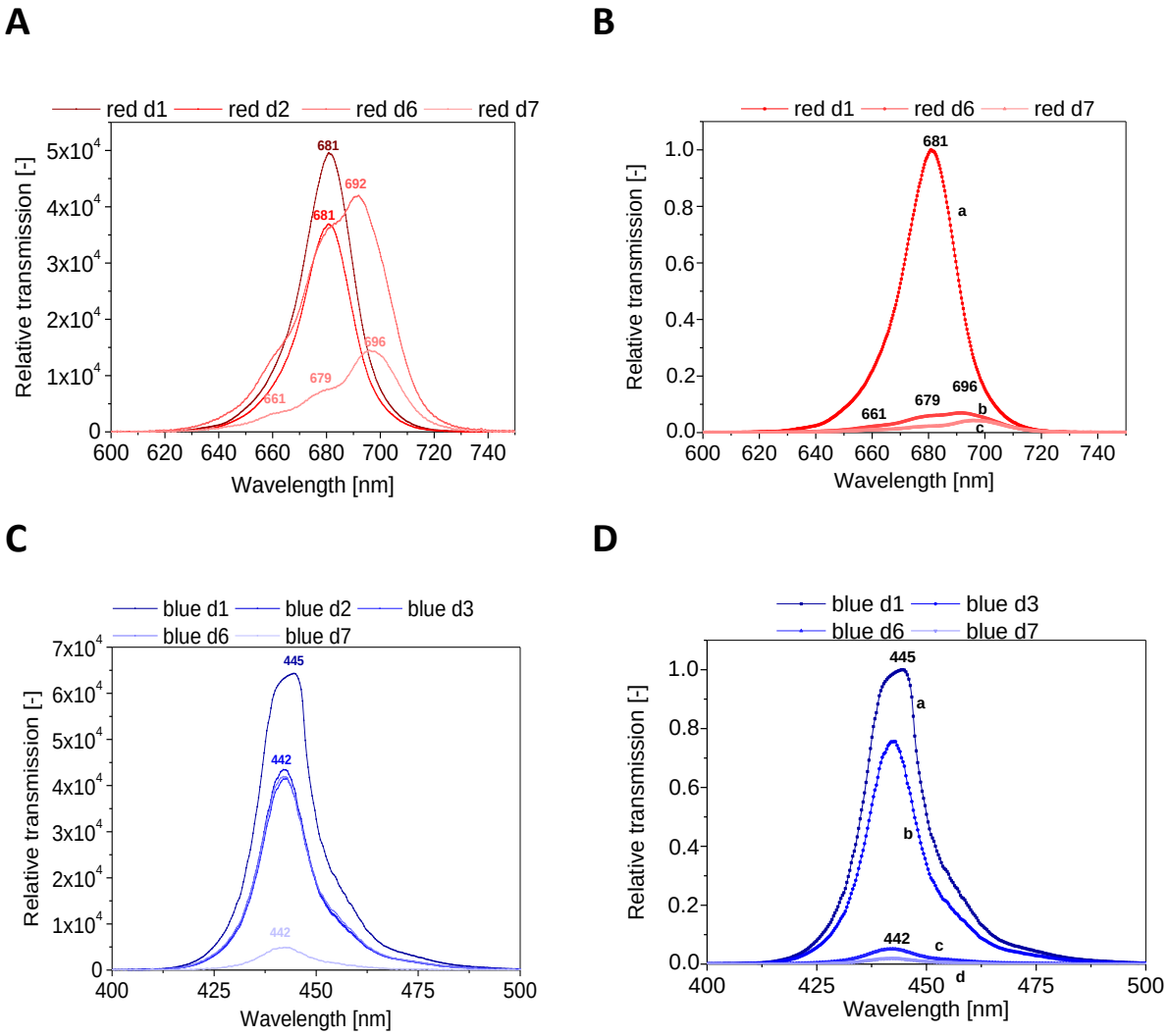

Figure 4-14. Transmission spectra for red and blue light during miniplate reactor cultivations in linear growth phase. A) Transmission spectra for pure red illumination at different days of cultivation from c_X = 0.03 to 0.89 g L^{-1} in miniplates at a low PFD of 25 µE m^{-2} s^{-1}. B) Same transmission spectra for red illumination normalized to transmission PFD with c_X of a) 0.03, b) 0.67 and c) 0.89 g L^{-1}. C) Transmission spectra for pure blue illumination at different days of cultivation from c_X = 0.03 to 0.48 g L^{-1} D) Same transmission spectra for blue illumination normalized to transmission PFD with c_X of a) 0.03 b) 0.13 c) 0.35 and d) 0.48 g L^{-1}.

Panel B of Figure 4-15 shows transmission spectra measured for cells under pure green and warm-white illumination at a low PFD, also in linear phase. For comparison, the normalized emission spectra (E) of green and warm-white LEDs are shown. Transmission intensity accounted for 17 µE m^{-2} s^{-1} (green_1), 13 µE m^{-2} s^{-1} (green _2) and T = 9 µE m^{-2} s^{-1} (ww) at the time of measurement. For both green illuminated cultures there is a right shift in transmission peak which is now at 532, 533 nm respectively, around 10 nm shifted to the right compared to emission peak at 524 nm.

Figure 4-15 C shows absorption spectra of extracted pigments for cells illuminated with white and green light; in comparison to Figure 4-1 C, the same local maxima and minima can be measured in the absorption spectrum of extracted pigments of CC-1690 cells grown under pure green light and warm-

white light as control for low PFDs. Both cultures were in linear growth phase. Transmission intensities accounted for T = 13 µE m^{-2} s^{-1} (green) and T = 9 µE m^{-2} s^{-1} (ww) at that time of measurement.

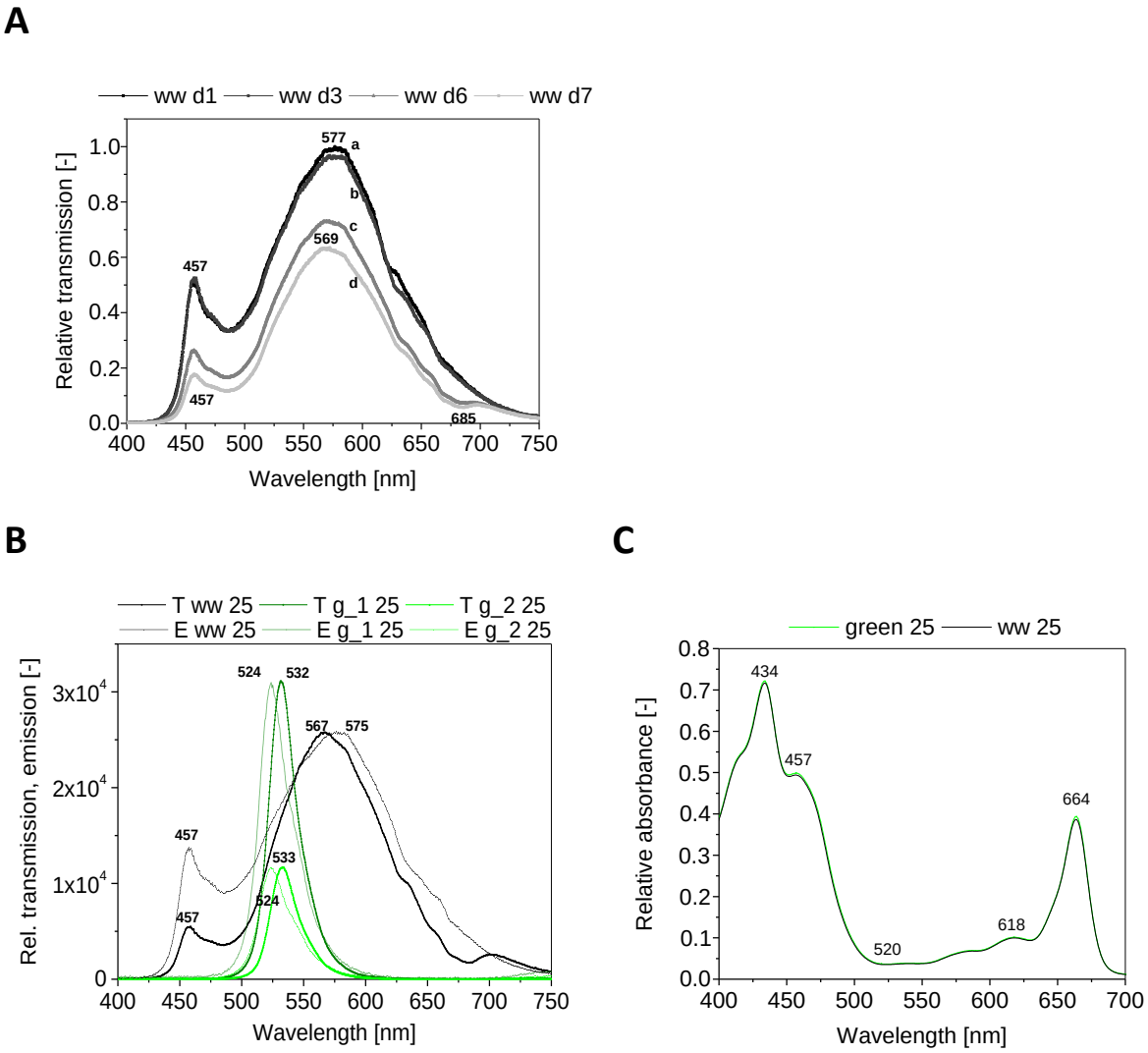

Figure 4-15. Transmission spectra for warm-white and green light during miniplate reactor cultivations in linear growth phase as well as absorption spectrum of extracted pigments of cells cultivated under pure green light. A) Transmission spectra for warm-white illumination at different days of cultivation from a) c_X = 0.03, b) 0.05, c) 0.06 to d) 0.15 g L^{-1}. B) Transmission spectrum for pure green and warm-white illumination at 25 µE m^{-2} s^{-1} and a cell dry weight concentration of 0.13 g L^{-1} (green_1), 0.4 g L^{-1} (green_2) and 0.3 g L^{-1} (ww) in miniplate reactors in linear phase; the cultivation was started at a CDW of 0.017 g L^{-1}. For comparison normalized emission spectra of LEDs are shown. C) Absorption spectra of extracted pigments for cells cultured under pure green light and warm-white in miniplate reactors at 25 µE m^{-2} s^{-1} both in linear phase. CDW green: 0.4 g L^{-1}, CDW ww: 0.3 g L^{-1}.

In order to establish kinetic models of microalgal growth depending on light distribution in photobioreactors, it is essential to describe light attenuation quantitatively. Yun and coworkers (2001) theoretically calculated light attenuation coefficients in *C. vulgaris* suspensions based on light absorption spectra and emission spectra of different light colors (see 2.3.2.5). This method was used

for calculation of monochromatic attenuation coefficients for red (680 nm) and blue (445 nm). Polychromatic attenuation coefficients were additionally calculated for green and warm-white.

Figure 4-16 A and B show the transmitted spectral PFDs of warm-white, blue and red light for increasing cell densities. For red and blue the spectral transmitted PFDs decrease down to almost zero at cell densities around 0.5 g L^{-1}. For warm-white there is also a decrease visible, but the highest CDW (0.15 g L^{-1}) applied is much lower than for the other approaches.

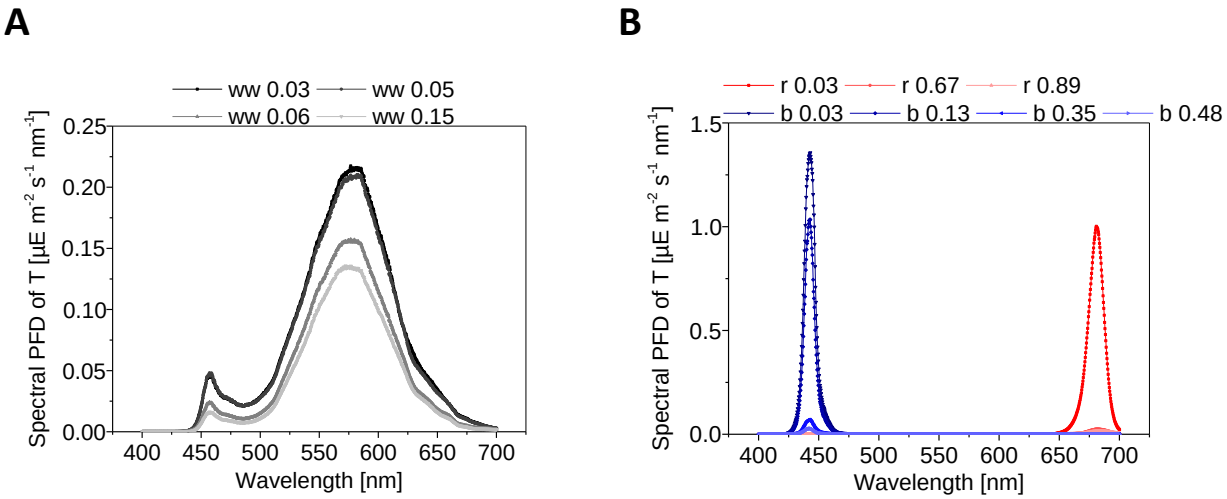

Figure 4-16. Transmitted spectral PFD of warm-white, blue and red light. A) Spectral photon flux densities of transmitted light for warm-white LED at I_0 = 25 µE m^{-2} s^{-1} for different cell densities: 0.03, 0.05, 0.06 and 0.15 g L^{-1}. B) Spectral PFDs of transmitted light for blue and red LEDs at 25 µE m^{-2} s^{-1} for increasing cell densities; red: 0.03, 0.67 and 0.89 g L^{-1}; blue: 0.03, 0.13, 0.35 and 0.48 g L^{-1}.

Panel A and B of Figure 4-17 show poly- and monochromatic light attenuation coefficients calculated according to Yun et al. (2001). Both coefficients are highly affected by the spectral irradiance of the incoming light. The coefficients for blue and red light are larger than those of white and green, whereas for all of them there is no linear correlation with cell density of *C. reinhardtii*.

White light and green light penetrates deeper into the algal culture which becomes pivotal at higher cell concentrations. Highest attenuation is shown for blue light. This is in accordance with monochromatic light attenuation coefficients for the two tested wavelengths 445 nm and 680 nm. Yun and coworkers (2001) found similar correlations although they tested red light at 650 nm.

These attenuation coefficients can be used to model PFD as a function of cell density and light path for different spectral irradiances. Further experiments should verify these coefficients for higher incident light intensities and higher cell densities as in this calculation only incident PFDs of 25 µE m^{-2} $s^{-1}$and cell densities up to 1.5 g L^{-1} were considered as there was only limited data on spectral transmitted light available.

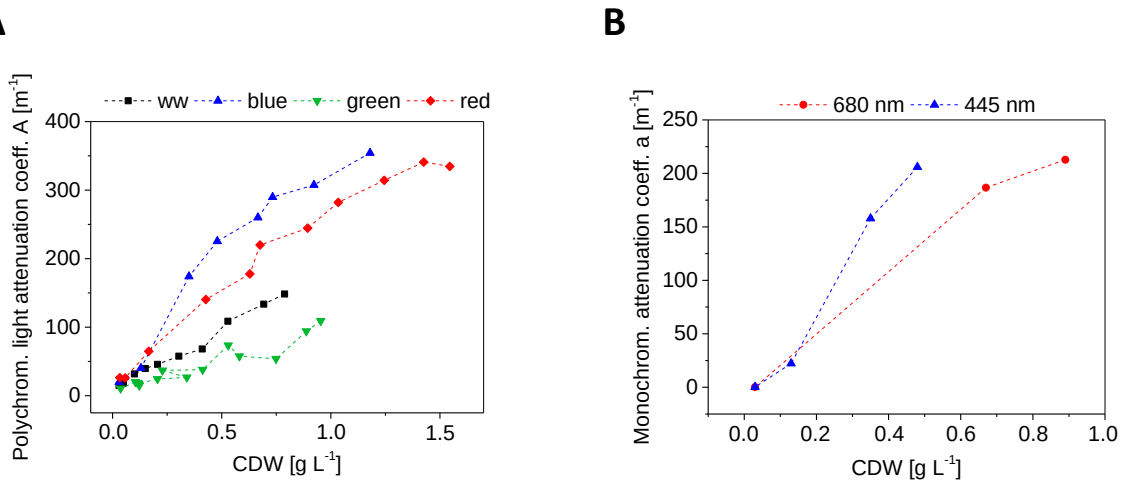

Figure 4-17. Light attenuation for mono- and polychromatic light. C) Polychromatic light attenuation coefficients A for warm-white, blue, green and red. D). Monochromatic light attenuation coefficient a for red at 680 nm and blue at 445 nm.

4.6 Long-term effects of light colors

Continuous cultivations were conducted in midiplate reactors with red/blue illumination in order to assess long-term effects of color illumination and study the effects of color changes.

For the first approach, illuminated with a saturating light intensity of 200 µE m^{-2} s^{-1}, there was no control; for the second a warm-white illuminated control was established. For the second approach the PFD applied for both reactors was 25 µE m^{-2} s^{-1}. A turbidostat was established based on the measurement of the transmitted light which was kept constant by a PI-controller. Cultures were, at a given irradiated intensity of 200 and 25 µE m^{-2} s^{-1}, respectively, kept constant at cell densities between 0.5 g L^{-1} and 1.2 g L^{-1}. For this cell density range a linear growth would result in the corresponding batch cultivation with the given PFD. During steady-state phases, changes of light colors were performed stepwise and the light color was kept constant until a new quasi steady-state was established. As a criterion of a new (quasi) steady-state balance, a constant dilution rate in form of the controlled pump speeds in response to transmission measurement was used.

4.6.1 Effects of light changes on growth rate

During these continuous cultivations no PCE values were determined; however, an assessment of light color efficiency for photosynthesis on the basis of influence on the growth rate is possible by monitoring the controlled dilution rates necessary to keep the cell density at a constant value.

Process data of the continuous cultivation at an overall PFD of 200 µE m^{-2} s^{-1} with dichromatic red/blue illumination and light color changes is shown in Figure 4-18 A, together with microscopic pictures showing algae suspension samples taken at different times during the continuous cultivation. Panel B shows calculated averaged specific growth rates for the specific phases with color combinations of red and blue photons.

A

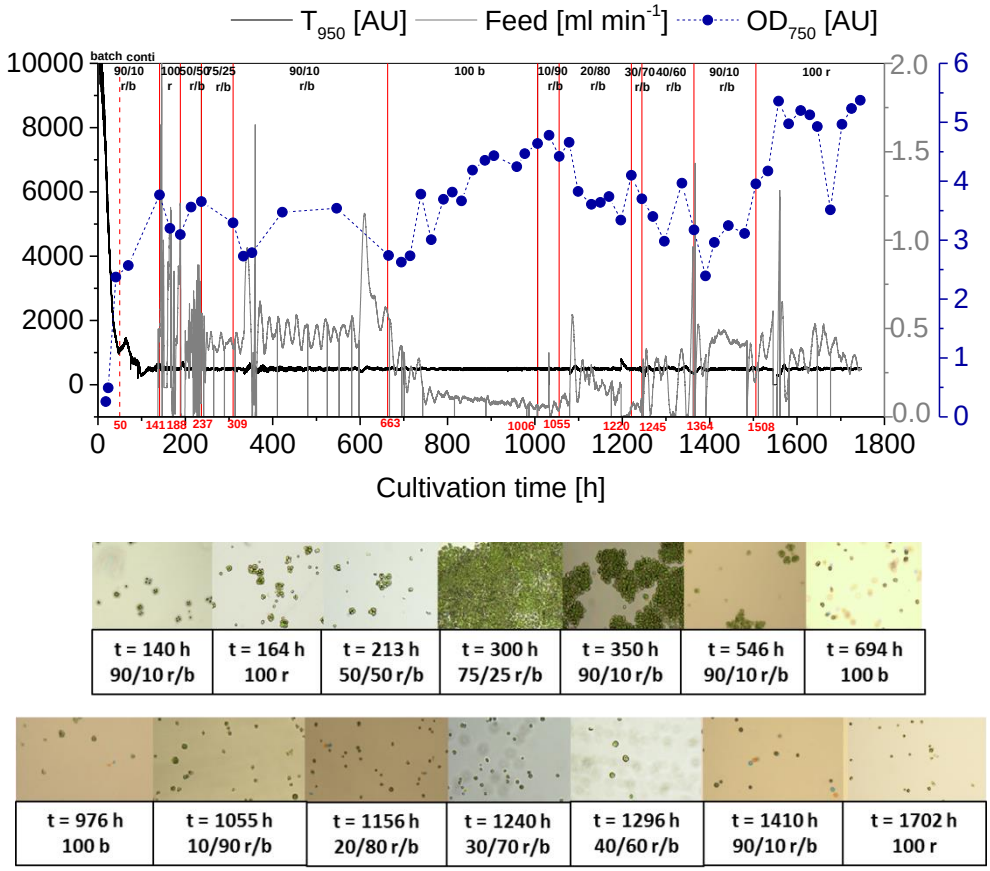

B

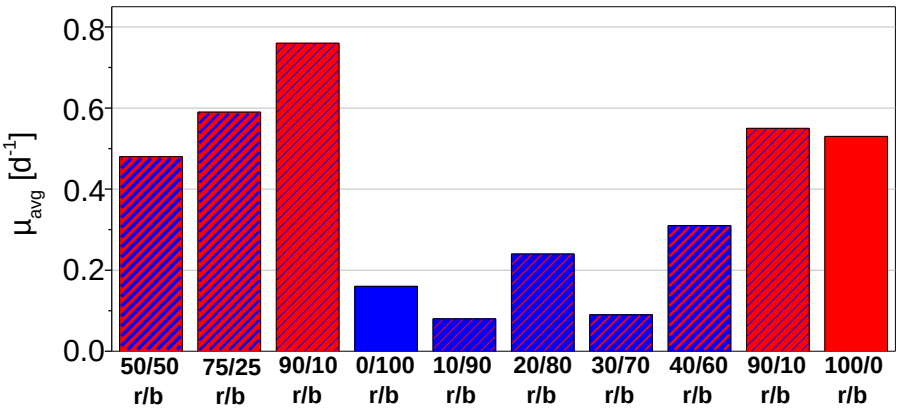

Figure 4-18. Long-term effects of mono- and dichromatic illumination on specific growth rates during a continuous cultivation for a saturating PFD of 200 µE m^{-2} s^{-1}. A) Online and offline data of a continuous cultivation under mono- and dichromatic illumination at a saturating PFD of 200 µE m^{-2} s^{-1}: Transmission of infrared light 950 nm (mV), offline OD_{750} (AU), feed rate (ml min^{-1}). Times for light color changes are marked with a red vertical line. Microscopic pictures showing strong agglomeration of cells (bright field, 100x magnification). B) Averaged specific growth rate µ (in d^{-1}) determined in steady-state phases of continuous culture at 200 µE m^{-2} s^{-1} with red and blue illumination with color changes.

Panel A shows online and offline data of this cultivation where red vertical lines mark color changes. Panel B depicts the averaged specific growth rate μ_{avg} which was calculated for average feed rates for the specific color phases. Remarkable was a strong agglomeration of cells in the first phase of the continuous process from about t = 250 h to t = 600 h which was probably induced by a dosage of antifoam (see lower part of panel A with microscopic images). These agglomerates with maximum sizes of up to 500 µm lead to an interference with OD and transmission measurements hindering a stable steady-state establishment of the process. Therefore, the average growth rates determined can be only analyzed qualitatively, not quantitatively. However, the determined averaged specific growth rates shown in panel B, compared within times of agglomeration and the ones compared for times without agglomeration, reflect the results of overall PCE determination of previous chapter.

Highest growth rate, within each phase respectively, was measured for 90/10 red/blue illumination (at a steady-state CDW of 1.0 g L^{-1}).

Figure 4-19 A and B show online and offline data of the continuous cultivations at a low PFD of 25 µE m^{-2} s^{-1} under red and blue light as well as the warm-white control. Several software outtakes and also a failure of the pump-controller connection at t = 360 h led to noise signals of online data and in case of the control reactor to a partial cell washout which delayed the establishment of the respective steady-state conditions. Nevertheless, online data of feed rates was averaged and used for calculation of specific growth rates. Both reactors were run at cell dry weight concentrations of 0.5 g L^{-1} during the continuous phase.

Figure 4-19 C shows the calculated specific averaged growth rates (in d^{-1}, right y-axis) determined from an averaged feed signal during the continuous cultivation under mono- and dichromatic illumination at an overall PFD of 25 µE m^{-2} s^{-1} compared to the continuous cultivation under warm-white light as control. Values account for: μ_{ww} = 0.4 d^{-1}, $\mu_{90/10r/b}$ = 0.95 d^{-1}, μ_r = 0.88 d^{-1}, μ_b = 0.41 d^{-1}, $\mu_{50/50r/b}$ = 0.63 d^{-1}. For comparison, the PCE values determined during semi-fed-batch cultivations (as previously described) are plotted on the left y-axis. The specific growth rates determined during the continuous cultivation are in perfect accordance to the PCE values; both determined under light-limited conditions.

Hence, during long-term continuous cultivations there are no other effects on growth and photosynthesis detected than stated for short-term cultivation with mono- and dichromatic illumination. A quantitative comparison with data shown in panel B of Figure 4-18, for a PFD of 200 µE m^{-2} s^{-1}, shows that the values for 25 µE m^{-2} s^{-1} seem to be a little high. This could be resulting from agglomeration problems leading to an overall perturbation of steady-state conditions and hence lower µ values for the higher PFD.

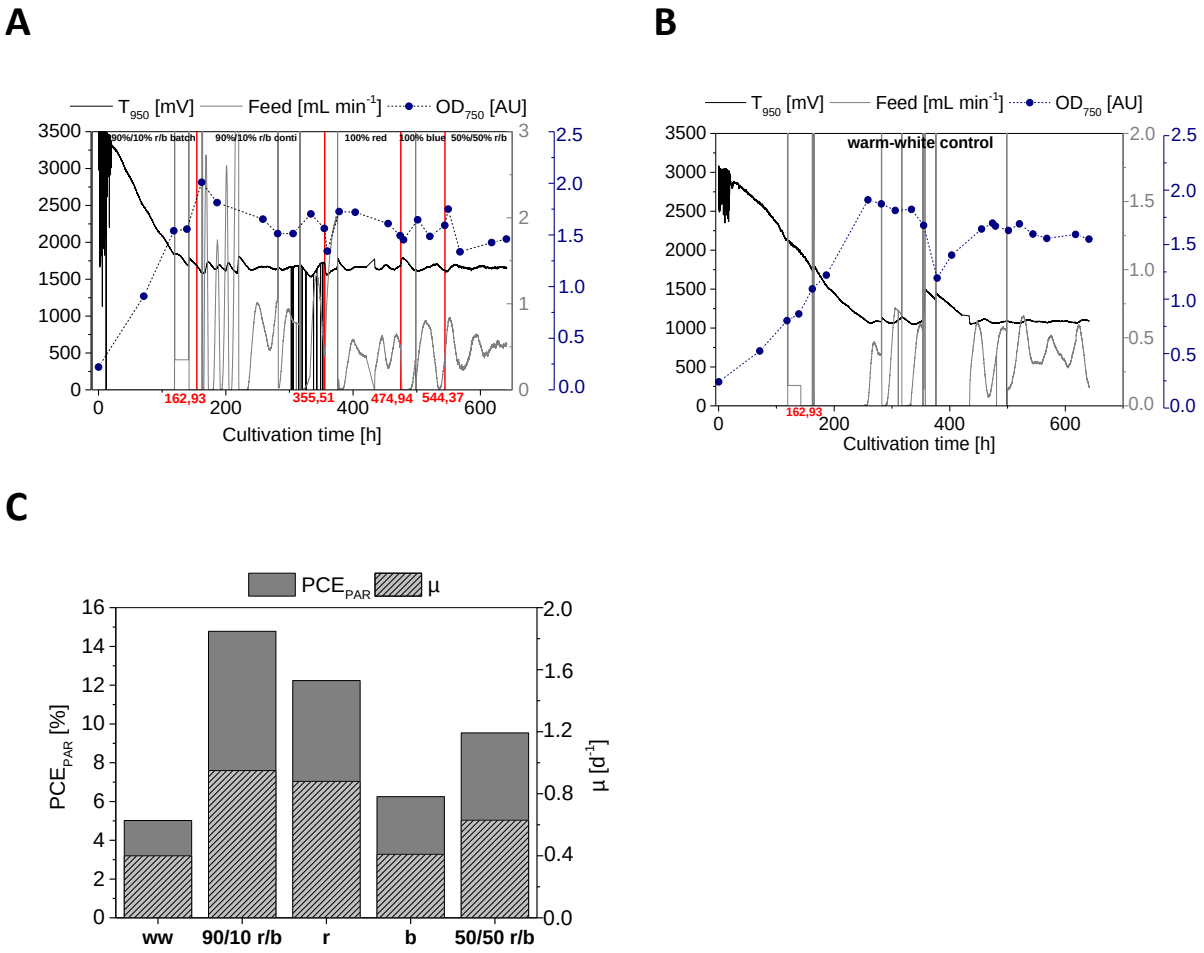

Figure 4-19. Long-term effects of mono- and dichromatic illumination on specific growth rates during a continuous cultivation at a low PFD in comparison to PCE values determined in semi-fed-batch cultivations. A) Online and offline data of a continuous cultivation under mono- and dichromatic illumination at an overall PFD of 25 µE m^{-2} s^{-1}: Transmission of infrared light 950 nm (mV), offline OD_{750} (AU) and feed rate (mL min^{-1}). Times for light color changes are marked with a red vertical line. B) Online and offline data of a continuous cultivation under warm-white illumination at an overall PFD of 25 µE m^{-2} s^{-1}: Transmission of infrared light 950 nm (mV), offline OD_{750} (AU) and feed rate (mL min^{-1}). Continuous process was started after 162.93 h which is marked by a red vertical line. C) Averaged specific growth rate µ (in d^{-1}) determined in steady-state phases of the continuous culture at 25 µE m^{-2} s^{-1} with red and blue illumination with color changes compared to warm-white continuous control. As comparison PCE_{PAR} values determined in semi-fed-batch cultivations (see previous results) are depicted.

4.6.2 Long-term effects of red and blue illumination on cell size and morphology

For semi-fed-batch cultivations effects of light color on the cell size, shape and morphology were monitored, where red light illumination resulted in smaller, oval shaped cells and blue light in larger cell diameters. These effects seem to be independent on the applied PFD (between 25-200 µE m^{-2} s^{-1} tested). At least for red light, it was shown that the decline in cell diameter is a reverse, transient effect which was monitored for cultivation times of about 16 days.

Continuous cultures with mono- and dichromatic red/blue illumination also served to assess the long-term effects on cell size and morphology.

During the continuous process at an overall higher PFD with red/blue illumination and color changes (compare to Figure 4-18) no tremendous effect of light color and cell size could be monitored compared to the results discussed before. However, a slight increase of cell diameter was monitored for pure blue illumination and a decrease with increasing red content (compare to Figure 4-20 A).

A

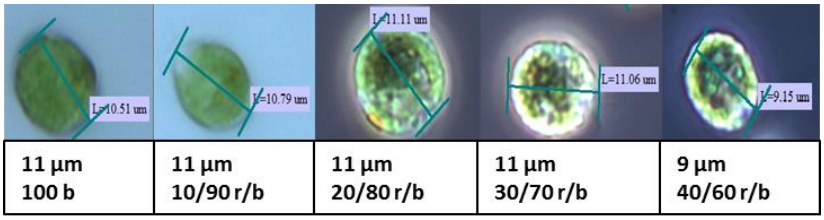

B

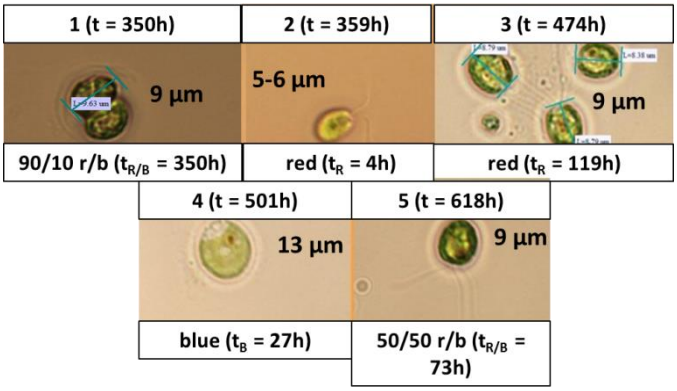

Figure 4-20. Long-term effects of mono-and dichromatic illumination on cell size, shape and morphology. A) Lightmicroscopic images depicting cell diameter for different blue light and blue/red light phases during the continuous cultivation at higher light intensities of 200 µE m^{-2} s^{-1}. B) Development of cell size, shape and morphology during a continuous culture with red and blue light changes at a PFD of 25 µE m^{-2} s^{-1}. Process time is depicted in the left upper corner, the time after the last color change is given at the bottom of the picture sections; magnification 400x.

During the continuous culture with warm-white illumination at a lower PFD of 25 µE m^{-2} s^{-1} no effect on the cell size and shape was monitored for about 500 h of the continuous process. Only smaller aggregates of six or eight daughter cells were visible, which can be defined as palmelloids. For the red/blue illuminated continuous process with light color changes (compare to 3.4.6) at a low PFD there were effects on cell size and shape visible (Figure 4-20 B). Under 90/10 red/blue dichromatic illumination the cells kept their initial cell size of about 10 µm like in the control reactor. After the color change to 100% red light the cell diameter decreased to 5-7 µm, already monitored four hours after the change. After almost 100 h of pure red illumination the cell diameter increased again to the control value. At a process time of 480 h light was changed to 100% blue and almost 27 h later the cell

diameter increased to 12-14 µm. 70 h after the change to blue light maximal cell diameters of 23 µm occurred. This corresponds to an increase in cell diameter of 250% from the initial value. On the average, a diameter of about 13-14 µm was prevailing during pure blue illumination. The light change to 50/50 red/blue illumination induced a decrease of cell diameter to initial values after 100 h. Throughout the continuous process with mono- and dichromatic illumination no aggregates, neither bigger nor smaller ones, were detected for all of the light color phases.

As far as these results indicate, there is, similar to the results of cultivations in semi-fed-batch cultivations, an effect of red and blue light on the cell size and shape also during continuous processes. These effects occur at different times after the light color has changed. They seem not to be dependent on the PFD used, in the ranges of 25-200 µE m^{-2} s^{-1} tested.

However, for the continuous cultivation at saturating light intensities of 200 µE m^{-2} s^{-1} the effects seem to be less pronounced.

At least for pure red illumination (680 nm) these effects on cell diameter and shape are of transient nature, where cells restore their initial size after about 16 days of cultivation time. This points to an adaptation or a habituation of the processes involved (cell division, CDK enzyme) and should be further studied by regular particle size analysis by laser diffraction or other means.

4.6.3 Long-term effects of red and blue illumination on pigment content

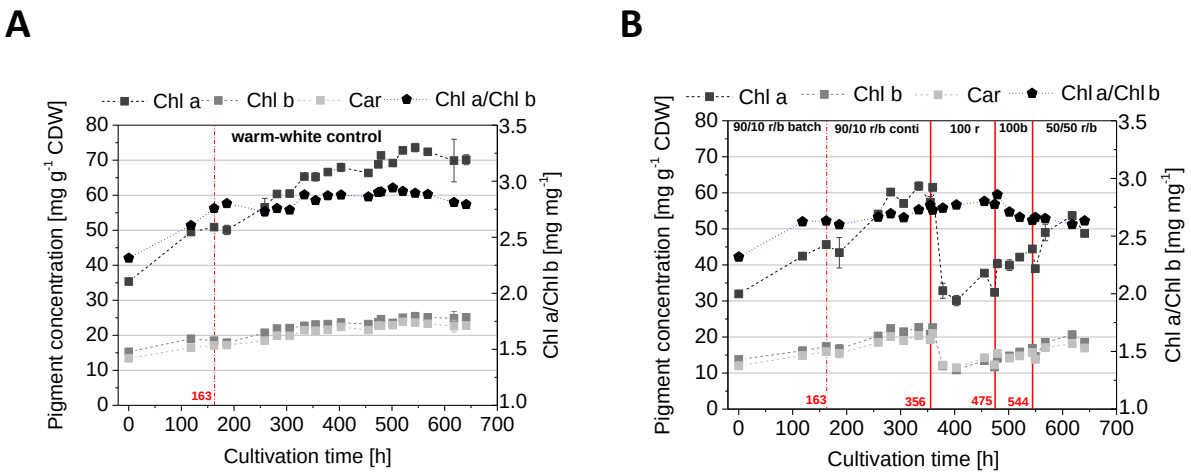

Figure 4-21. Long-term effects of mono- and dichromatic red/blue illumination at a low PFD on pigment content. A) Long-term effects of warm-white illumination at a low PFD (25 µE m^{-2} s^{-1}) during continuous cultivation. Vertical red line marks batch to continuous process shift. B) Long-term effects of red and blue illumination at a low PFD (25 µE m^{-2} s^{-1}) during continuous cultivation. Vertical red line marks batch to continuous process shift as well as light color changes from 90/10 r/b to pure red, to pure blue and to 50/50 r/b.

Figure 4-21 A and B shows specific pigment contents of cells continuously cultivated under red/blue illumination and the white control at a low PFD of 25 µE m^{-2} s^{-1}. Panel A shows the results of the warm-white control culture and panel B for dichromatic red/blue cultivation with light color changes.

For the warm-white control the specific steady-state pigment contents are on the average slightly higher than for the red/blue continuous cultivation, in accordance to the results in 4.4. The Car content is lower than the Chl b content throughout the continuous cultivation under warm-white illumination.

During the red/blue continuous cultivation (panel B) there are clear changes in specific pigment composition visible which occur in relation to light color changes. Lowest contents were measured for pure red illumination, whereas the following light color phases obviously were too short to establish new steady-states in terms of pigment composition, under the assumption that pure blue illumination and 50/50 red/blue illumination should provoke highest specific pigment contents among the light combinations tested (compare to Figure 4-12 A) although first changes in specific pigment concentrations were detected early after the color changes of 4 to 5 h after the change. However, more samples in smaller time intervals should have been taken to assess this in detail and determine time constants for adaptation in specific pigment composition. Also phases with a specific illumination should have been tested for a longer time to be sure that an equilibrium has been established.

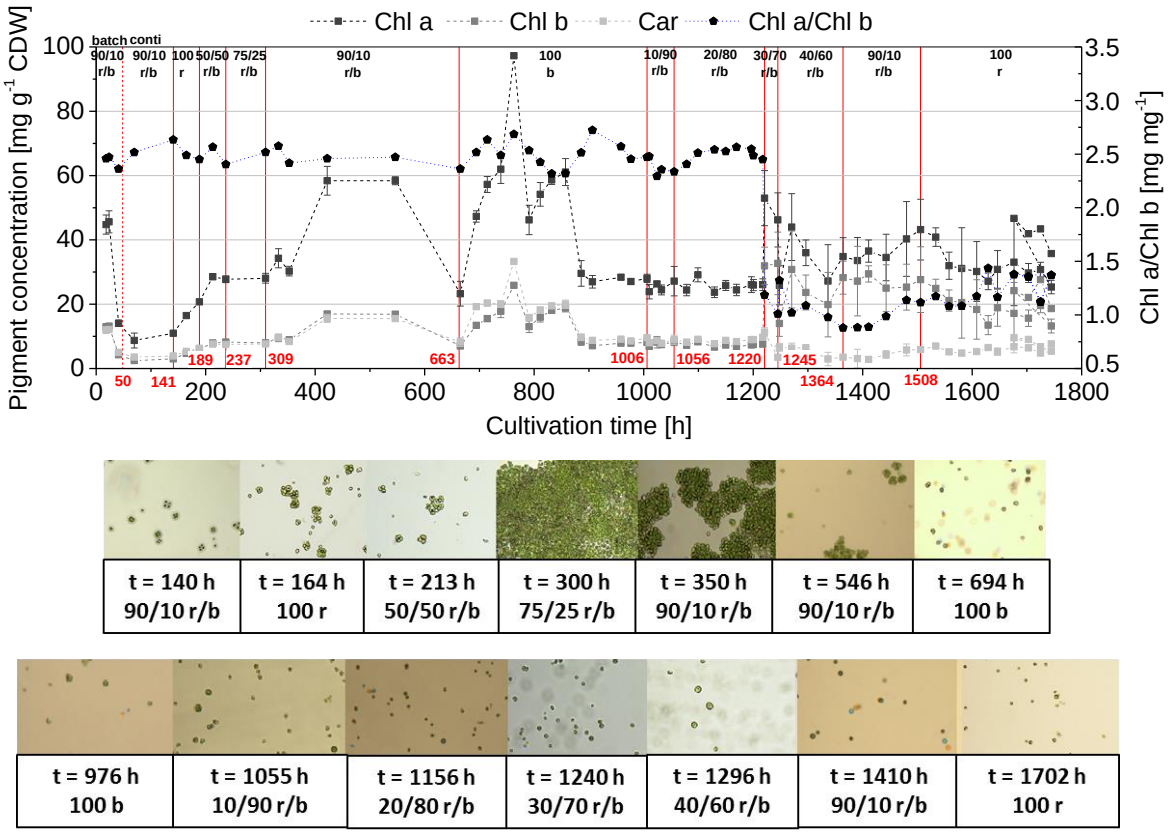

Figure 4-22. Long-term effects of mono- and dichromatic red/blue illumination at a saturating PFD on pigment content. Long-term effects of red and blue illumination on specific pigment concentration at a saturating PFD (200 µE m^{-2} s^{-1}) during continuous cultivation. Vertical red line marks batch to continuous process shift as well as light color changes. For comparison, again microscopic images show cellular aggregation during the continuous process.

For the continuous culture at a saturating PFD of 200 µE m^{-2} s^{-1} fluctuations are visible for specific pigment content, not only provoked by color changes (Figure 4-22) but also by changing aggregation conditions and therefore changes in steady-state optical density and cell dry weight concentrations. However, it is visible that specific pigment concentrations at high light are lower than for low light continuous cultures in accordance to previous results. As aggregations prevail from t = 250 h to t = 600 h and larger optical density fluctuations and large error bars for specific pigments from t = 1200 h to the end of cultivations no clear discussion is possible for these results.

4.7 Summary of results for efficient illumination

Results of the experiments concerned with an efficient illumination of *C. reinhardtii* cultures show that an increase in efficiency of light to biomass conversion is achievable with pure red (680) and dichromatic red/blue 90/10 illumination. The highest PCE_{PAR} values of about 15% were achieved with dichromatic illumination at a molar ratio of 90% red to 10% blue at low PFDs of 25 µE m^{-2} s^{-1} which are close to the theoretical limit (Wagner 2015). With a light to biomass conversion efficiency of 5% for full-spectrum warm-white illumination this is an increase of 200% for low light intensities.

This study has shown that for growth of *C. reinhardtii* in closed photobioreactors photons within the blue wavelength range are beneficial combined with a high proportion of red light at 680 nm. Besides, it was shown that there are effects based on sensory pigments also having influence on PCE values. With respect to the green wavelength range, regarded as non-usable for photosynthetic growth, even at low light intensities, a cell growth was measurable, with PCE values similar to white or blue illumination.

For higher PFDs and one-sided illumination of plate reactors a saturation effect was verified for red/blue illumination with similar PCE values for white control and 90% red/10% blue illumination at around 150-300 µE m^{-2} s^{-1} PFD. Reasons for similar light to biomass conversion yields at this point are the good absorption and resulting bad light penetration within the plate reactor resulting in earlier zero light transmission for dichromatic illumination and therefore strong light limitation conditions for the cells. Hence, overall PCE values decrease with increasing PFD for dichromatic illumination as saturation is reached and there is no net increase in mean µ integrated along the light path.

From the energetic perspective, a total energetic efficiency of 7.5% results, in case of a dichromatically at low PFDs illuminated photobioreactor system. Here, an electrical LED efficiency of 50% and a PCE of 15% (for 90/10 red/blue at 25 µE m^{-2} s^{-1}) are assumed.

With respect to cell size and morphological features like aggregation, results of this work have shown that light color, especially blue light, as further studies have proven, has an remarkable effect. Blue light leads to bigger cell sizes, by delaying cell division (Oldenhof 2004 b, Münzner and Voigt 1992). Red light leads to smaller cell diameters and an oval shape. At least for red light these effects seem to

be transient pointing to an adaptation effect which was also shown for continuous cultures. These effects seem to be mostly independent of the applied PFD within the tested range. However, the effects were more pronounced at lower PFDs. Green light tends to provoke cell aggregation whereas the mechanism behind is still unclear.

Lowest specific pigment concentrations were found for cells cultivated under pure red as well as dichromatic illumination of 90% red and 10% blue indicating a high efficiency of photosynthetic apparatus from low light intensities until saturation point. Above this point specific concentrations are higher and as light penetration is better for low absorbing white light at higher PFDs, specific pigment concentrations of dichromatic illuminated cultures surmount those of white control. Ratios of Chl a/b, Chl a/Car and Chl b/Car are dependent on light color and PFD applied and show the saturation intensities for warm-white and red/blue. Saturation is reached earlier for 90/10 red/blue (around 100 µE m^{-2} s^{-1}) compared to warm-white (around 150 µE m^{-2} s^{-1}). The results shown point to adaptation mechanisms in form of state transitions and an adjustment of absorption cross section of cells.

The results conducted have proven that the so called détour-effect is also applicable for microalgae cultures and together with the results for light attenuation coefficients it was shown that low absorbing wavelengths, for example green photons, can penetrate deeper into algal cultures and promote growth at higher cell densities. Therefore, it is advisable to use trichromatic illumination where first red/blue illumination is used and green photons are added with increasing cell density.

Experiments during this work have shown that by adjusting wavelengths of irradiated light to absorption spectra of *C. reinhardtii* an increase of photo conversion efficiencies compared to full-spectrum illumination is possible. Red light at 680 nm shows high efficiency, but the addition of small amounts of blue photons can achieve highest efficiencies due to effects of physiological functions controlled by sensory pigments. The results from semi-fed-batch cultivations were also found consistent during continuous cultures.

Future studies should continue the search for an optimal wavelength combination and should reveal if a trichromatic illumination with red, blue and green LEDs can further enhance PCE values or if additional wavelengths within the blue region are optimal. The three light colors could also be applied independently in varying amounts depending on the actual cell concentration during batch cultivations with respect to light penetration. Also red light at 680 nm could be applied together with the total blue range spectrum to cover most of the action spectra peaks of sensory pigments using filters on white light which allow the transmission of blue photons.

Future studies should reveal if activation of rhodopsins, responsible for phototaxis, by irradiating light corresponding to their action spectrum, is beneficial for overall efficiency within mixed

photobioreactors or if excess energy for phototactic behavior is wasted thereby reducing light to biomass conversion.

For future experiments it could also be interesting to choose illumination wavelengths which are a little aside from the actual peak in absorption spectrum, in case of red light, for instance at 660 nm. There are methods to optimize light penetration in photobioreactors based on biological approaches where the microalgal antenna complex is reduced in size leading to a reduced absorption and optical density. As a technical approach, the irradiation with wavelengths just aside from the actual absorption peaks (e.g. 660 nm instead of 680 nm for red photons) should be used. Theoretically this should mimic antenna reduced mutants where light penetration is optimized as wavelengths next to the absorption peaks are used which can penetrate deeper into the cultures.

In further experiments μ_{max}-I_0 curves should also be produced for pure red and pure blue illumination conditions to underline the results found for red/blue illumination at higher PFDs and to use this data for simulation of light attenuation profiles.

For the design of an artificially illuminated photomodule operating with maximal energy efficiency the application of a double-sided illumination for plate type reactors with a reduced PFD seems to be promising for a 90/10 red/blue illumination.

Future experimental approaches should further focus on long-term cultivation in continuous mode to deepen the knowledge about pigment acclimation concerning spectral composition at different intensities. The analysis of the results should also be completed by modeling growth rate distribution along the light path for different colors and intensities, based on the acquired experimental data. This is important to determine possible limits for the conclusions drawn. A deeper knowledge about interdependencies of light and cellular functions triggered by sensory pigments is essential for the development of optimal illumination systems not only for space application of microalgae-based life support systems.

5 Bubble-free membrane aeration of photobioreactors

5.1 Selection of suitable membrane materials

Investigations were done systematically to study the applicability of certain membrane materials for their usage in photobioreactors for aeration in a bubble-free manner. Parameters which are most important to judge whether a membrane material can be used for aeration of photobioreactors, are the transfer coefficients for CO_2 and O_2, the selectivity factor for these two gases, the water loss of the membrane material per area and time as well as its fouling-behavior. Thus, these parameters were investigated with the help of a gas-liquid testing system.

5.1.1 Mass transfer coefficients for O_2 and CO_2

Figure 5-1 shows mass transfer coefficients for O_2 (panel A) and CO_2 (panel B) for testing conditions outlined in section 3.3.1 and 3.4.2 for a gas-dH_2O system for 17 membrane materials tested. Table 5-1 displays mean values with standard deviations together with selectivity and water loss values which are discussed in the following chapters. The mass transfer coefficients displayed are mean values of at least three separate measurements under the same testing conditions.

Concerning O_2 mass transfer, values measured under these conditions are in the range from $1.2 \cdot 10^{-6}$ to $7.4 \cdot 10^{-6}$ m s^{-1} and are therefore slightly higher than those measured for CO_2 which are in the range of $5.4 \cdot 10^{-7}$ to $6.7 \cdot 10^{-6}$ m s^{-1}. For oxygen mass transfer, highest values were achieved with silicone membranes where a maximum value was recorded for the new Wacker Silicone membrane with a thickness of 40 µm ($k_{L,O2} = 7.4 \cdot 10^{-6}$ m s^{-1}). Also for the dense SBS asymmetric membrane a high $k_{L,O2}$ of $6.7 \cdot 10^{-6}$ m s^{-1} was measured. Lowest oxygen transfer coefficients were detected for the PVA membrane with $1.2 \cdot 10^{-6}$ m s^{-1} followed by $2.5 \cdot 10^{-6}$ m s^{-1} for the dense TPX (polymethylpentene) membrane. It is remarkable that for porous membranes (columns with patterns) $k_{L,O2}$ values are similar, around $5 \cdot 10^{-6}$ m s^{-1}, even though membrane materials are differing. For dense, solubility membranes the measured values are very different, depending on membrane material and thickness (when made from the same material, compare to Figure 5-2 A).

For CO_2 transfer, the results show a different finding: first of all, in total the values are lower than those for O_2; second, highest CO_2 transfer coefficients are detected for porous membranes, where a maximum value of $k_{L,CO2} = 6.7 \cdot 10^{-6}$ m s^{-1} is measured for the PVDF membrane (pore size 0.2 µm), followed by a $k_{L,CO2}$ of $6.2 \cdot 10^{-6}$ m s^{-1} for the PTFE membrane with a pore size of 0.2 µm. As for oxygen, also for CO_2 transfer lowest values were recorded for the PVA membrane ($k_{L,CO2} = 5.4 \cdot 10^{-7}$ m s^{-1}) followed by the value for the TPX membrane ($k_{L,CO2} = 1.5 \cdot 10^{-6}$ m s^{-1}). Furthermore, concerning porous membranes, there is a higher difference in $k_{L,CO2}$ values than for oxygen.

Table 5-1. Membrane parameters measured by a gas-liquid testing system. Mass transfer coefficients for O_2 and CO_2, selectivity factors for O_2/CO_2 as well as water loss in ml per membrane surface area and day.

	Manufacturer/ membrane name/ material	Abbreviation used in this work	$k_{L,O2}$ [m s^{-1}]	$k_{L,CO2}$ [m s^{-1}]	$\alpha_{O2/CO2}$ [-]	Water loss [ml $m^{-2}d^{-1}$]
a	Goodfellow/ Silicone elastomer-Film/ Silicone elastomer	Goodfellow	$5.87 \cdot 10^{-6} \pm 3.41 \cdot 10^{-7}$	$4.97 \cdot 10^{-6} \pm 6.21 \cdot 10^{-7}$	1.18	190
b	Wacker/ ELASTOSIL® LR 3003/30 A/B /Silicone elastomer	Wacker, old	$4.58 \cdot 10^{-6} \pm 6.08 \cdot 10^{-7}$	$2.95 \cdot 10^{-6} \pm 6.71 \cdot 10^{-8}$	1.55	85
c	Goodfellow/ TPX®/ Polymethylpentene	TPX	$2.50 \cdot 10^{-6} \pm 3.82 \cdot 10^{-8}$	$1.45 \cdot 10^{-6} \pm 1.40 \cdot 10^{-7}$	1.73	25
d	Membrana/ Accurel/ Polypropylene	Accurel PP	$5.35 \cdot 10^{-6} \pm 1.28 \cdot 10^{-6}$	$5.53 \cdot 10^{-6} \pm 2.50 \cdot 10^{-7}$	0.97	188
e	PALL/ Versapor®/Acrylic Copolymer	ACP	$5.12 \cdot 10^{-6} \pm 1.86 \cdot 10^{-7}$	$5.49 \cdot 10^{-6} \pm 3.03 \cdot 10^{-7}$	0.93	190
f	PALL/ Emflon/ PTFE	PTFE 0.02	$4.49 \cdot 10^{-6} \pm 3.45 \cdot 10^{-7}$	$4.34 \cdot 10^{-6} \pm 1.20 \cdot 10^{-7}$	1.04	194
g	PALL/ Emflon/ PTFE	PTFE 0.2	$4.71 \cdot 10^{-6} \pm 9.76 \cdot 10^{-7}$	$6.18 \cdot 10^{-6} \pm 1.66 \cdot 10^{-6}$	0.76	197
h	PALL/Supor®/ PES	PES 0.2	$4.78 \cdot 10^{-6} \pm 3.93 \cdot 10^{-8}$	$5.22 \cdot 10^{-6} \pm 8.38 \cdot 10^{-7}$	0.92	201
i	PALL/FluoroTrans® PVDF Membrane/ PVDF	PVDF 0.2	$4.79 \cdot 10^{-6} \pm 1.48 \cdot 10^{-7}$	$6.68 \cdot 10^{-6} \pm 6.64 \cdot 10^{-7}$	0.72	197
j	Wacker/ ELASTOSIL®Film 2030 250/40/ Silicone elastomer	Wacker 40	$7.43 \cdot 10^{-6} \pm 1.80 \cdot 10^{-7}$	$4.91 \cdot 10^{-6} \pm 9.26 \cdot 10^{-8}$	1.51	168
k	Wacker/	Wacker 80	$6.47 \cdot 10^{-6} \pm 1.56 \cdot 10^{-6}$	$4.66 \cdot 10^{-6} \pm 5.65 \cdot 10^{-7}$	1.39	163

	ELASTOSIL®Film 2030 250/80/ Silicone elastomer					
l	Wacker/ ELASTOSIL®Film 2030 250/100/ Silicone elastomer	Wacker 100	$6.15 \cdot 10^{-6} \pm 4.0 \cdot 10^{-8}$	$4.41 \cdot 10^{-6} \pm 4.05 \cdot 10^{-7}$	1.39	155
m	Wacker/ ELASTOSIL®Film 2030 250/200/ Silicone elastomer	Wacker 200	$5.89 \cdot 10^{-6} \pm 1.1 \cdot 10^{-7}$	$4.15 \cdot 10^{-6} \pm 3.74 \cdot 10^{-8}$	1.42	124
n	SBS asymmetric Membrane	SBS asym	$6.70 \cdot 10^{-6} \pm 1.83 \cdot 10^{-7}$	$5.36 \cdot 10^{-6} \pm 1.95 \cdot 10^{-7}$	1.25	236
o	SBS symmetric Membrane	SBS sym	$5.97 \cdot 10^{-6} \pm 1.20 \cdot 10^{-6}$	$3.04 \cdot 10^{-6} \pm 3.01 \cdot 10^{-7}$	1.97	140
p	PDMS + silicalite Membrane	PDMS	$5.35 \cdot 10^{-6} \pm 5.37 \cdot 10^{-8}$	$4.16 \cdot 10^{-6} \pm 1.15 \cdot 10^{-7}$	1.29	236
q	PVA Membrane	PVA	$1.18 \cdot 10^{-6} \pm 7.07 \cdot 10^{-8}$	$5.39 \cdot 10^{-7} \pm 4.14 \cdot 10^{-8}$	2.19	240

Comparative values from literature are rare, due to the fact that most values are measured for gas-gas systems. Farges and coworkers (2012) determined mass transfer coefficients in a gas-liquid system where a $k_{L,CO2}$ value of $8.6 \cdot 10^{-6}$ m s^{-1} was measured for a porous hollow fiber PTFE membrane module (pore size 0.2 µm; pH 8) which is only slightly higher than the value determined during this work of $6.2 \cdot 10^{-6}$ m s^{-1}. This slight deviation can be explained with different testing conditions. In general, the reported gas transfer values for surface aeration are in the range of 10^{-5} m s^{-1}, whereas bubble-aeration k_L values are in the range of 10^{-4} m s^{-1} (Storhas, 1994). In case of bubble-aeration mass transfer is facilitated as the motion of ascending gas bubbles leads to a decrease of the liquid boundary layer thickness adjacent to the gas bubble. All k_L values determined within this work are one magnitude smaller than surface aeration, whereas highest mass transfer values for membrane aeration are around $7 \cdot 10^{-6}$ m s^{-1} and therefore close to 10^{-5} m s^{-1} for surface aeration.

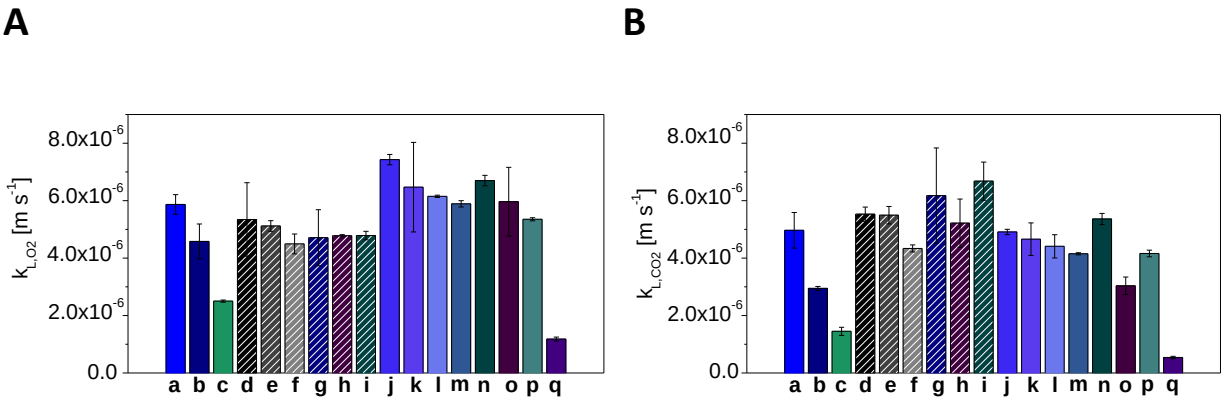

Figure 5-1. Mass transfer coefficients for O_2 and CO_2 of all membranes tested. Values were measured with a gas-liquid system and step changes of inlet gas composition from 0 to 50% (v/v). All tests were performed at 25°C and the same liquid and gas velocities with dry inlet air. Mean values and standard deviations represent at least three individual measurements.
A) Oxygen mass transfer coefficients for all membranes tested. B) Carbon dioxide mass transfer coefficients for all membranes tested.

Differences in k_L values for oxygen and CO_2 are resulting from different diffusion coefficients D ($m^2\ s^{-1}$) of both gases in gases, liquids and solids in case of dense solution membranes. In case of porous membranes, also other diffusion mechanisms like for example Poiseuille and Knudsen diffusion (chapter 2.3.1.3) and the Henry-coefficients at the gas liquid interface inside the pores play a role. For these diffusion mechanisms inside porous materials the relation of the average free path length to the average pore size as well as the density of the gas plays a role. Diffusion coefficients of O_2 and CO_2 in gases are in the range of 10^{-5} $m^2\ s^{-1}$, whereas D_{O2} in air ($1.76 \cdot 10^{-5}$ $m^2\ s^{-1}$ at 0°C) is higher than D_{CO2} in air ($1.48 \cdot 10^{-5}$ $m^2\ s^{-1}$ at 8.9°C). Also in water, the diffusion coefficient of O_2 (D_{O2} = $2.1 \cdot 10^{-9}$ $m^2\ s^{-1}$ at 25°C) is higher than for CO_2 ($1.92 \cdot 10^{-9}$ $m^2\ s^{-1}$). These higher diffusion rates of oxygen compared to CO_2 in air and water can explain the overall slightly higher mass transfer values for oxygen. Additional to that, solubility in the membrane material and diffusion coefficients of the gases in the material are of crucial importance in case of dense membranes. Most of the dense membranes were made of silicone. Diffusion coefficient of oxygen in silicone is higher than that of CO_2 in silicone (compare to Table 2-2).

Hence, for air, water and silicone, oxygen diffusion is slightly faster than diffusion of CO_2 which could explain the overall higher mass transfer coefficients.

In case of a gas-gas testing system it is possible to directly measure only the resistance for the gas transfer of the membrane, in contrast to a gas-liquid system, where the liquid boundary layer has an influence (Lund, 2002). However, a gas-liquid system in this case was better to simulate the case of application inside a membrane-aerated photobioreactor.

5.1.2 Influencing factors on mass transfer coefficients

Different series of tests were conducted to study the influence of several factors on mass transfer coefficients, being the thickness of the dense membrane material, temperature, liquid velocity, salt concentration as well as pH in case of CO_2 transfer.

5.1.2.1 Thickness of dense solution-based membrane materials

A first influencing factor studied was the thickness of membrane material in case of dense solution-based materials. The dense material chosen was Wacker Elastosil Film (see Table 5-1, j, k, l, m), a silicone elastomer with thicknesses of 40, 80, 100 and 200 µm.

As can be seen from Figure 5-2 A, with increasing thickness of the membrane, mass transfer coefficients decrease for both gases tested. This can be explained with a longer diffusion path which gas molecules have to travel along. A linear correlation can be found for the thicknesses tested. Theoretically, it can be assumed that with decreasing thickness of the membrane material down to zero, the k_L values increase to a value in the range of 10^{-5} m s^{-1} (surface aeration) where only the liquid boundary layer creates the resistance for mass transfer.

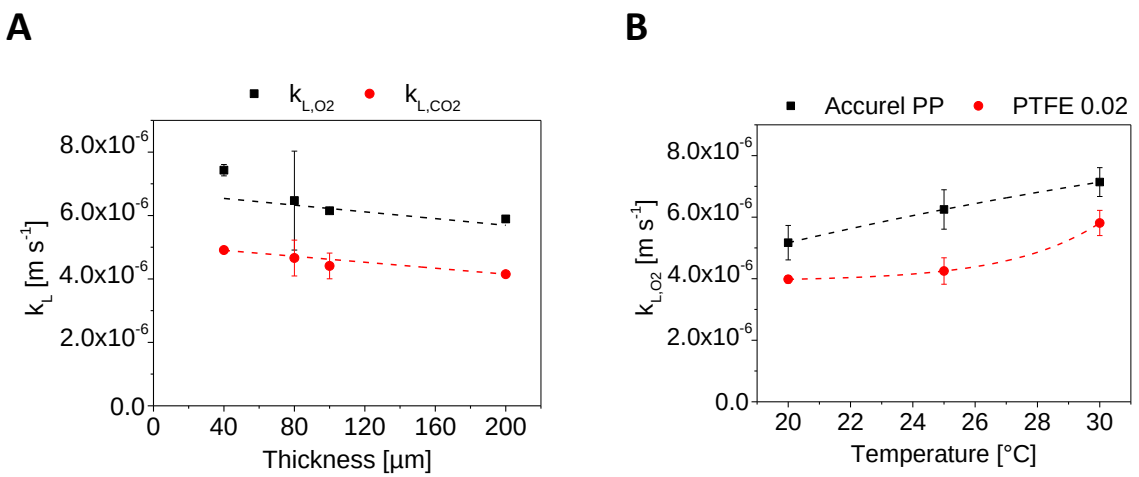

Figure 5-2. Influence of membrane thickness and temperature on mass transfer.
A) Dependence of mass transfer coefficients for O_2 and CO_2 on the thickness of a solution-based dense silicone elastomer membrane. B) Influence of temperature on mass transfer coefficients of O_2 measured on porous membranes Accurel PP and PTFE 0.02 for 20, 25 and 30°C.

5.1.2.2 Temperature

As another important factor on mass transfer of gases, temperature was tested. Only temperatures within the range of possible applied temperatures for microalgae cultivations (20-30°C) were tested because of a higher relevance for application. Two porous membranes made from polypropylene (Accurel PP) and PTFE 0.02 were applied for this testing series where only $k_{L,O2}$ values were determined.

Temperature has an influence on diffusional mass transfer as with a higher temperature molecule mobility increases. Furthermore it has an influence on the viscosity of liquids in case of diffusion in the liquid phase. For diffusion of a molecule in a liquid there is a nonlinear correlation of diffusion coefficient D with temperature, where viscosity of the liquid is a function of temperature. As in this case water, showing a Newtonian behaviour, was used as liquid phase, viscosity of the liquid decreases exponentially with increasing temperature. A net exponential increase in k_L values with increasing temperature is expected for mass transfer across membranes.

As Figure 5-2 B shows, even though the temperature difference between the tested temperatures is only 10 degrees, an influence on mass transfer coefficients is measurable. There is an increase in oxygen mass transfer coefficients with increasing temperature. Theoretically, there should be an exponential increase in k_L values with temperature. In general, for chemical processes the factor with which the rates increase with an increase in temperature are higher than for physical processes like diffusion rates.

The increase in mass transfer coefficients can be explained by an increased diffusion for higher temperature based on faster molecular movements of gas molecules with higher temperature and therefore a higher diffusion rate. The experiments show, that an increase of temperature of 10 K, mass transfer coefficients increase by a factor of 1.4. Theoretically, there should be an increase of 20% for a temperature difference of 10 K for physical processes (hence a factor of 1.2). In this case, $k_{L,O2}$ values are increased by a factor of 1.4, which is close to the theoretically expected factor.

5.1.2.3 Liquid velocity on the membrane/ mean velocity in chamber cross section

According to theoretical considerations concerning laminar boundary layers on the liquid side which display a major part of the overall resistance to mass transfer, it should be possible to decrease the size of this boundary layer by increasing the bulk velocity of the liquid. A stepwise increase of velocity, at a constant given gas flow rate, should result in a saturation type curve for mass transfer coefficients. Then, this saturation value of k_L should display the resistance of the membrane for mass transfer.

For this reason a series of tests was performed where bulk liquid velocity as mean liquid velocity in the chamber cross section was increased and k_L values for oxygen were determined. Two porous membranes were applied. Here, liquid velocities applied can be compared to velocities of ascending bubbles in case of bubble aeration. However, these are in the range of 0.02-0.3 m s^{-1} depending on the bubble diameter, and therefore are still at least one dimension higher than the mean bulk velocities in the experiments presented.

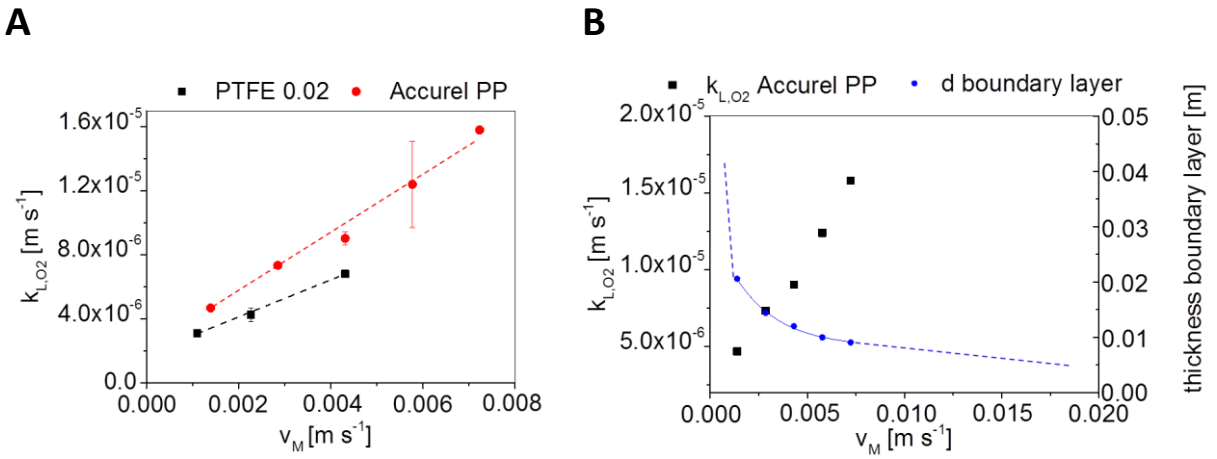

Figure 5-3. Influence of mean bulk liquid velocity on mass transfer. A) Dependence of oxygen mass transfer coefficient on mean bulk liquid velocity measured with two porous membranes. B) $k_{L,O2}$ value measured with the Accurel PP membrane for different mean bulk liquid velocities and the calculated theoretical boundary layer thickness d.

As Figure 5-3 A shows, there is an increase in k_L values with increasing liquid velocity. Also Ferreira and coworkers (1998) showed that k_L values increase with increasing liquid flow rate. They found a rather saturation curve correlation which they attributed to the influence of the decreasing thickness of the laminar boundary layer. Panel A of this figure shows that for the experiments performed within this work no saturation value was reached and a rather linear correlation was found. This might be explained by the fact that the testing system geometry did not allow to use this assumption for laminar boundary layers. The effect of an increased mass transfer is assumed to result in this case from a higher mixing condition. Hence, a convective mass transport is dominating the diffusive transport in this case.

Part B of the figure shows the thickness of the laminar boundary layer in dependence on liquid velocity. As this is dependent on plate length (here length of the chamber) a mean value was calculated. A hyperbolic curve is resulting where the influence of the boundary layer decreases with increasing bulk liquid velocity. As the theoretical layer thickness at these low liquid velocities is higher than the actual height of the liquid chamber, the assumption cannot be applied for the used geometry and flow regimes. The theory is based on a stationary plug flow which is not present in the experimental set up caused by the point inlets of the liquid where a more turbulent flow regime is resulting. Thus for calculation of mass transfer coefficients the linear correlation shown in panel A of the figure should be used for determination of mass transfer for the geometrical similar membrane-aerated photobioreactor. Also Schneider and coworkers (1995) described experiments where liquid flow velocities were varied during mass transfer coefficient determination. Here, mass transfer coefficients also increased with increasing flow rate.

In general, this series of experiments underlines the necessity for geometrical similarity of the testing chamber for determination of k_L values and the actual membrane reactor which should have the same flow patterns in order to achieve valuable results for gas transfer design.

5.1.2.4 Salt concentration and pH

Other factors possibly having an important influence on mass transfer in a gas liquid system with membranes are salt concentration and pH in case of CO_2 transfer.

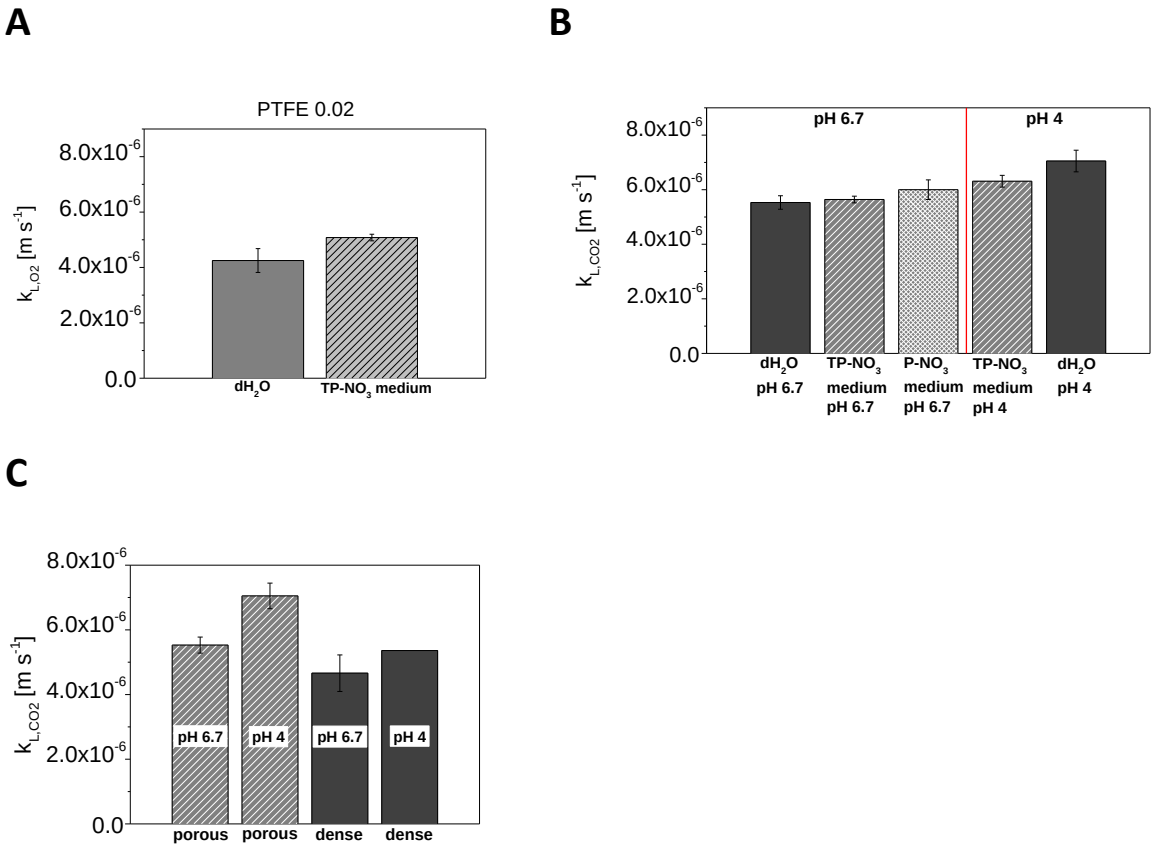

Figure 5-4. Influence of salt concentration and pH on mass transfer coefficients. A) Oxygen mass transfer coefficients measured for distilled water and for TP-NO_3 medium for the same porous PTFE 0.02 membrane. B) CO_2 mass transfer coefficients at two different pH values of 6.7 and 4 for different liquids: distilled water, TP-NO_3 medium and unbuffered P-NO_3 medium. For all approaches the porous Accurel PP membrane was used. C) CO_2 mass transfer coefficients measured with distilled water at two different pH values of 4 and 6.7 for a porous (Accurel PP) and a dense (Wacker 80) membrane.

Figure 5-4 A shows that $k_{L,O2}$ values are similar for distilled water and TP-NO_3 medium measured with the porous PTFE 0.02 membrane. The value measured with medium is only slightly higher. This was assumed as the medium used only contains a low salt concentration, with an ionic strength of 0.014 mol L^{-1} for the unbuffered P-NO_3 medium.

Figure 5-4 B and C show the influence of pH on the CO_2 transfer coefficient. As outlined in the theoretical part of this work, in case of CO_2 it is important to consider its chemical reactions in water

where equilibrium constants are dependent on pH. Panel B shows $k_{L,CO2}$ values for different liquids at pH 6.7 and pH 4 in case of a porous PP membrane (Accurel, Membrana). As for all tests of this series the same membrane was used, the differences of $k_{L,CO2}$ values can be directly attributed to the influence of the liquid medium.

A first result is that distilled water and TP-NO_3 medium at the same pH of 6.7 yield similar values for $k_{L,CO2}$. This is important, because all $k_{L,CO2}$ determinations were performed at a pH of 6.7 with distilled water. The fact that there is no difference in $k_{L,CO2}$ for distilled water and TP-NO_3 medium at that pH means that all values determined with water at pH 6.7 can be used for a quantitative design of CO_2 transfer for cultivations with TP-NO_3 medium inside the membrane-aerated photobioreactor at pH values around 6.7.

In contrast to that, there is a higher difference between $k_{L,CO2}$ values at the lower pH 4 for different liquids. Reasons for this are based on the pH dependent carbonate system and the salting-out effect. This effect describes that the solubility of gases in liquids decreases with increasing salt concentration. As at a pH of 4 dissolved CO_2 is the predominating carbonate species, the salting-out effect has a higher influence at lower pH than at pH 6.7. At a pH of 6.7 the prevailing carbonate species is hydrogen carbonate (see Bjerrum plot Figure 2-12 A). As the medium has a slightly higher salt concentration than distilled water, the solubility of CO_2 is lower in the medium. Hence, the lower solubility of CO_2 in TP-NO_3 medium at pH 4 is the reason for the lower $k_{L,CO2}$ value compared to distilled water at pH 4. The overall increasing $k_{L,CO2}$ values with lowered pH are also based on the pH dependency of the carbonate system. The lower the pH, the higher the amount of dissolved CO_2 species, the faster the pCO_2 sensor detects an input of CO_2 into the system. Therefore, a lower pH leads to a higher $k_{L,CO2}$ value. For the unbuffered medium at pH 6.7 there is a lower resulting pH (final pH of 4.8) during the ongoing CO_2 step change compared to the buffered medium (final pH of 5.1) at the same pH. $k_{L,CO2}$ values increase with decreasing pH values based on the pH dependency of the carbonate system. Furthermore, there is an influence of the salt concentration below pH values of 6.7. For pH values < 6.7 the salting-out effect has an influence based on the high amount of CO_2 species of the carbonate system.

As the highly mobile H^+ ions might diffuse faster in pores, which are mainly filled with gas, than through dense materials, leading to a different charge distribution in the case when the counter ions diffuse slower, there should be an electrochemical potential and hence a different influence on mass transfer for porous in contrast to dense membranes. Therefore, this experiment was repeated with a dense solution-based membrane and distilled water, where the difference in $k_{L,CO2}$ values for different pH values is expected to be smaller for dense than for porous membranes.

Panel C shows CO_2 transfer coefficients for distilled water at pH 6.7 and pH 4 for a porous (Accurel PP) and a dense membrane (Wacker 80) in comparison. As the results show, the influence of pH value

with distilled water is smaller for dense membranes in contrast to the porous membrane. These results underline the assumptions outlined above.

5.1.3 Selectivity factor for O_2/CO_2

Figure 5-5 A shows selectivity factors $\alpha_{O2/CO2}$ which are based on mass transfer coefficient measurements in a gas-dH_2O system at T = 25°C. As discussed in the theoretical section (2.3.1.3) the selectivity factor of the membrane of O_2 versus CO_2 (Equation 2-22) is of critical importance for a stable bubble-free aeration of a microalgae culture. The selectivity factor $\alpha_{O2/CO2}$, determined as ratio of k_L values, should be > 26, as solubility of CO_2 in water is 26 times higher than for O_2, expressed by Henry-coefficients, in order to avoid bubble formation.

Figure 5-5 A shows that there is a great difference of selectivity factors between the membranes tested. Whereas selectivity factors of porous membranes are similar and in the range of 0.7-1.0, there is a higher variation among the dense solution-based membranes. Here, $\alpha_{O2/CO2}$ values vary between 1.2-2.2. The highest O_2/CO_2 selectivity factor of 2.2 was measured for the dense PVA membrane, followed by 1.97 for the dense SBS symmetric membrane. The lowest O_2/CO_2 selectivity factor was detected for the porous PVDF membrane (pore size 0.2 µm) with $\alpha_{O2/CO2} = 0.72$.

The reason for the bigger difference in selectivity among dense membranes can be explained by the solution-based manner of mass transfer. The gas molecules have to dissolve into the dense membrane material, where the different diffusion coefficients of O_2 and CO_2 as well as the molecular structure of the membrane material and distribution of free spaces inside the molecular scaffold, siloxane units in case of silicone elastomer membranes, play a role. This leads to a more heterogeneous result for selectivity ratios. Interestingly, the ratio of diffusion coefficients for O_2/CO_2 in silicone is about 1.45 (see Table 2-2), which is displayed by selectivity factors of all the silicone based membranes (b, j-m, Table 5-1) with 1.4-1.6. The only exception is the value determined for the Goodfellow Silicone membrane (line a, $\alpha_{O2/CO2} = 1.2$).

For porous membranes, where gas and liquid are in direct contact inside the pores, there are less differences in mass transfer for the two gases leading to selectivity factors around 1. Here, Henry coefficients and diffusion coefficients of CO_2 and O_2 in gas and water play a major role for selectivity. As discussed before, diffusion coefficients are higher for O_2 in water and air and the ratio of D_{O2}/D_{CO2} is about 1.09 and 1.19, respectively. Henry coefficients display a ratio of 26 at 25°C where the coefficient for CO_2 is higher than that for O_2 (higher solubility of CO_2 in water). It seems that for selectivity in porous membranes, diffusion coefficients of both gases in air and water have a major influence and selectivity factor $\alpha_{O2/CO2}$ is around 1.

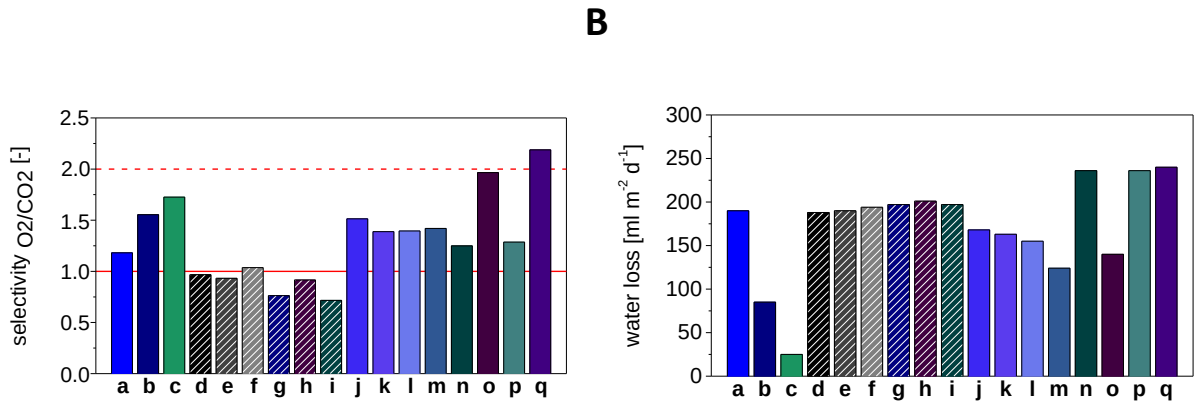

Figure 5-5. Selectivity factor $\alpha_{O2/CO2}$ and water losses of all membranes tested. A) Selectivity factor $\alpha_{O2/CO2}$ for all membranes tested based on k_L values at 25°C. B) Water losses in ml m^{-2} d^{-1} measured as water vapor transported in exhaust gas stream at 25°C with dry inlet air for all membranes tested.

As outlined in the theoretical section, a higher selectivity for O_2 towards CO_2 is necessary to circumvent the problem of bubble formation as a result of photosynthetic activity and lower solubility of oxygen in water. Therefore, based on the results obtained within this work and theoretical considerations, porous membranes are not suitable in order to design a long-term bubble-free membrane aeration of phototrophic processes. Dense solution-based membranes which show a higher mass transfer of oxygen than for CO_2 should be considered. If bubble formation shall only be avoided by the factor selectivity, at least a value of 26 for $\alpha_{O2/CO2}$ is necessary, relating to the ratio of Henry coefficients of the two gases.

5.1.4 Water loss

The water loss per time and membrane surface area of the tested membranes for dry inlet air is shown in Figure 5-5 B. Where water loss values for porous membranes do not show a great variation, there are differences in water vapor diffusion among dense membranes. Water loss values for porous membranes are in the range of 188-201 ml m^{-2} d^{-1}, whereas for dense membranes the values vary between 25-240 ml m^{-2} d^{-1}. A minimal water loss was measured for the dense TPX membrane, which was used during parabolic flight campaigns with the ModuLES-PBR (results see chapter 8.2). The highest loss in water vapor was detected for the dense PVA membrane. These values should be taken into consideration only with the thickness of the applied membranes especially in the case of dense membranes.

The factor of water vapor transfer is important for the design of a photobioreactor for space application whereas the other factors like mass transfer coefficients for O_2 and CO_2, selectivity and specific gas transfer area are higher prioritized. However, water losses are necessary to determine in order to balance liquid volume loss. This could be achieved by increasing feed flow rate for a continuous culture by a certain factor or adding sterile water like a substrate component. Also

regarding the exhaust gas stream it is necessary to determine the relative humidity to adjust this value to the desired value for human breathing air in a space module.

5.1.5 Mass transfer values required for aeration of a microalgae culture

In order to design a membrane-aerated bioreactor for cultivation of microalgae under space conditions, it is necessary to evaluate CO_2 requirements in form of CO_2 uptake rates at given illumination intensities and compare them in a quantitative way to the CO_2 transfer rates based on k_L values measured and the specific surface areas a of both the lab scale photobioreactor and the ModuLES-PBR.

The following assumptions were taken into account for calculation of CO_2 requirement and CO_2 transfer:

- Photon flux density chosen: **PFD = 200 µE m^{-2} s^{-1}**
- Photo conversion efficiency **PCE_{PAR}** for warm-white illumination is **8%** (compare to a PCE of 7.5% measured for 200 µE m^{-2} s^{-1} in midiplates for warm-white illumination, chapter 4.2.2)
- Light energy conversion factor F for warm-white light within PAR: **F = 4.67 µE J^{-1} (or µmol J^{-1})**, hence 1 J m^{-2} s^{-1} = 4.67 µE m^{-2} s^{-1}.
- Specific mass transfer area a:
  - Lab scale MBR: a = **51 m^{-1}**
  - ModuLES-PBR: a = **47.4 m^{-1}**
- Total liquid volumes of two reactor geometries:
  - Lab scale MBR: **V_{total} = 0.263 – 0.370 L (0.263 L for calculation)**
  - ModuLES-PBR: **V_{total} = 2.7 L**
- Total illuminated surface A (one-sided illumination) for two different geometries
  - Lab scale MBR: **A_{MBR} = 0.01369 m^2**
  - ModuLES-PBR: **$A_{ModuLES}$ = 0.1279 m^2**
- Biomass calorific value: **H_B = 20 kJ g^{-1} CDW**
- Stoichiometric CO_2 demand of **1.85 g CO_2 g^{-1} CDW**

For a PFD of warm-white light applied to the surface of 200 µE m^{-2} s^{-1} the energy per surface is:

Equation 5-1. Calculation of illuminated energy per surface

$$200\frac{\mu E}{(m^2 s)}\cdot\frac{1}{4.67}\frac{\mu E}{J}=42.83\frac{J}{(m^2 s)}$$

About 8% of that light energy is converted into biomass: 3.43 J m^{-2} s^{-1}. With a biomass calorific value of 20 kJ g^{-1} CDW this will give:

Equation 5-2. Calculation of biomass built per illuminated surface and time

$$3.43\frac{J}{(m^2 s)}\cdot\frac{1}{20000}\frac{gCDW}{J}=1.715\cdot10^{-4}\frac{gCDW}{(m^2 s)}$$

With a stoichiometric CO_2 demand of 1.85 g CO_2 per g CDW this leads to a CO_2 requirement per illuminated surface of $3.173\cdot10^{-4}$ g CO_2 m^{-2} s^{-1}. For the **lab scale MBR** with an illuminated surface of 0.01369 m² this will give a CO_2 requirement of **$4.34\cdot10^{-6}$ g CO_2 s^{-1}**; for the **ModuLES-PBR** with a total illuminated surface of 0.1279 m² the CO_2 requirement accounts for **$4.06\cdot10^{-5}$ g CO_2 s^{-1}**.

Relating to the total reactor liquid volumes, **volumetric CO_2 requirements of $1.65\cdot10^{-5}$ g CO_2 L^{-1} s^{-1}** (equals to **$3.75\cdot10^{-7}$ mol CO_2 L^{-1} s^{-1}**) and **$1.50\cdot10^{-5}$ gCO_2 L^{-1} s^{-1}** (equal to **$3.42\cdot10^{-7}$ mol CO_2 L^{-1} s^{-1}**) are calculated for the lab scale MBR and the ModuLES-PBR respectively. These values represent the required CTR values.

On the reactor side, it is important which specific mass transfer area is resulting from the design of the membrane reactor and which gas composition (ratio of CO_2) is chosen. In case of the lab scale MBR the specific surface a accounts for **52 m^{-1}**, whereas a = **47.4 m^{-1}** for the ModuLES-PBR. When a gas composition of **5% CO_2 (v/v)** (1.7 mol m^{-3} as dissolved CO_2 concentration) is chosen for a one-gas-compartment-version and a dissolved CO_2 concentration of **0.34 mol m^{-3}** (corresponding to a **1% pCO_2**) and neglecting the gas side boundary layer resistance, the membrane should have a $k_{L,CO2}$ value of:

Equation 5-3. Calculation of the required mass transfer coefficient for CO_2

$$k_{L,CO2}=\frac{CTR}{a\cdot\left(c^{*}_{CO2}-c_{CO2}\right)}=\frac{CTR}{a\cdot\left(\frac{p^{*}_{CO2}}{H_{CO2}}-c_{CO2}\right)}$$

In case of the lab scale MBR, the membrane $k_{L,CO2}$ has to account for:

Equation 5-4. Required $k_{L,CO2}$ value in case of the lab scale MBR

$$k_{L,CO2}=\frac{CTR}{a\cdot\left(c^{*}_{CO2}-c_{CO2}\right)}=\frac{3.75\cdot10^{-4}\frac{molCO_2}{m^3 s}}{52\frac{1}{m}\cdot\left(1.7\frac{mol}{m^3}-0.34\frac{mol}{m^3}\right)}=5.30\cdot10^{-6}\frac{m}{s}$$

For the ModuLES-PBR the $k_{L,CO2}$ has to be at least:

Equation 5-5. Required $k_{L,CO2}$ value in case of the ModuLES-PBR

$$k_{L,CO2} = \frac{CTR}{a \cdot \left(c^*_{CO2} - c_{CO2}\right)} = \frac{3.42 \cdot 10^{-4} \frac{molCO_2}{m^3 s}}{47.4 \frac{1}{m} \cdot \left(1.7 \frac{mol}{m^3} - 0.34 \frac{mol}{m^3}\right)} = 5.31 \cdot 10^{-6} \frac{m}{s}$$

These values are very similar. Compared to the results for CO_2 mass transfer coefficients of the membranes tested within this work, the calculations show that the measured k_L values are in the same range of 10^{-6} m s^{-1}. Nine out of the 17 membranes tested showed $k_{L,CO2}$ values of around $5 \cdot 10^{-6}$ m s^{-1} or higher. Additionally, these coefficients could even be lower in case of a two-gas-compartment-configuration with a second gas mixture and a second membrane where CTR is higher.

If a gas atmosphere of 10% CO_2 (v/v) and the one-gas-compartment-/one-membrane-configuration is chosen, $k_{L,CO2}$ values should only account to $2.4 \cdot 10^{-6}$ m s^{-1} for both reactor geometries. 15 out of 17 membranes tested showed $k_{L,CO2}$ coefficients above this value.

For a two gas compartment version with two membranes (M1 and M2), the CTR can be expressed as:

Equation 5-6. Calculation of the required CTR for two membranes and two gas compartments

$$CTR_{required} = CTR_{M1} + CTR_{M2}$$

For this configuration, several combinations of membranes with their specific $k_{L,CO2}$ values are possible.

In total, these calculations have shown that even for flat sheet membranes a sufficient CO_2 supply can be guaranteed. Even membranes with lower $k_{L,CO2}$ can be applied when either CO_2 concentration in the gas phase is increased and, or, specific mass transfer surface is increased by using hollow fiber membranes.

5.2 Application of membranes for a bubble-free aeration of photobioreactors

Within this work, a first photobioreactor concept based on bubble-free membrane aeration for space application was developed and tested where several parameters were varied. As a first approach, flat sheet membranes were used within this work where the gas transfer was located inside the reactor. As outlined in the material and methods part, there were two configurations of the membrane reactor: one membrane and one gas compartment and the version with two membranes and two gas compartments. Here, two exemplary batch cultivations for both configurations are compared and discussed for several growth parameters as well as pressure and bubble volume development. Continuous cultivations and results of light intensity step changes within the lab scale membrane reactor are displayed in chapter 7.

5.2.1 Dissolved gas concentrations, bubble formation and gas transfer rates

Figure 5-6 A, B shows equilibrium gas concentrations and pH before the reactor was inoculated, for both configurations as comparison. As it can be seen, different gas equilibrium concentrations and pH values result for those two approaches, resulting from the given driving forces and the k_L values of the membrane(s) used. For the two-gas-compartment-approach, a reduced dissolved O_2 concentration of about 7.5%, compared to 24% dO_2, is resulting, which is an advantage for the phototrophic cultivation concerning O_2 accumulation. Concerning the dO_2 concentration for the one compartment version, the reason that the actual concentration is higher than would be resulting from a 5% CO_2 in air mixture (dO_2 of 19%) is due to the higher $k_{L,O2}$ of the TPX membrane compared to CO_2 ($\alpha_{O2/CO2}$ = 1.73). However, a perfect equilibrium has not been reached yet where with ongoing time dissolved CO_2 and O_2 concentrations should display gas concentrations.

In the following, batch cultivations with the two different configurations are compared regarding pressure and the bubble volume formed. Resulting from O_2 accumulation and the lower solubility of O_2 towards CO_2, gas bubbles formed during all cultivations which were removed manually. Hence, a quantification of the volume built was possible. As panel A and B of Figure 5-7 show, a clear reduction of gas volume built and hence bubble formation, as well as overpressure, was achieved for the configuration with two membranes and two gas compartments with two different gas compositions by optimizing gas transfer. By using the two-gas-compartment-configuration the gas volume built was reduced by 40% (a total of 144 ml compared to 85 ml) and maximum pressure peaks reduced by 85% (0.35 bar to 0.05 bar). However, there still was bubble formation and therefore an overpressure built up inside the closed liquid compartment. This can be solved by a higher selectivity factor $\alpha_{O2/CO2}$ of the membrane for O_2 removal.

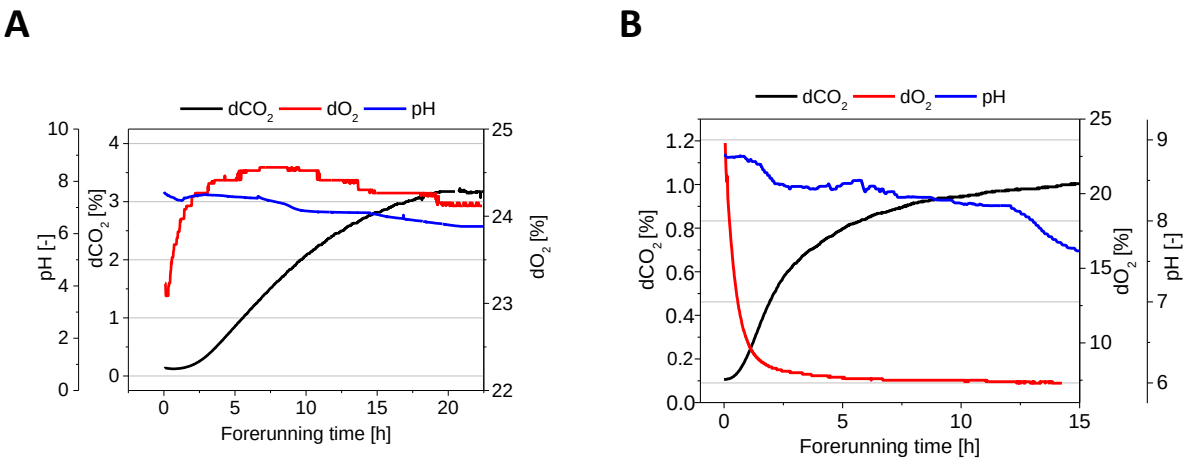

Figure 5-6. Dependence of equilibrium gas concentrations on membrane and reactor configuration inside the membrane-aerated photobioreactor. A) Forerunning process data before inoculation showing equilibrium gas concentrations and pH with one gas compartment (5% CO_2 in air) and TPX membrane. B) Forerunning process data before inoculation showing equilibrium gas concentration and pH with two gas compartments (5% CO_2 in air; 1% CO_2 in N_2 (v/v)) and TPX and Wacker 80 membranes.

For all following cultivations in batch and continuous mode, the two-gas-compartment-configuration was chosen. Part C of Figure 5-7 shows online process data of one batch cultivation with the two-compartment-configuration. During exponential growth of the cells, dCO_2 decreases down to 1% indicating that for batch cultivations CO_2 gas concentrations on the O_2 removal side (gas collection) should be slightly increased above 1% to keep dCO_2 levels above 1%, even during phases with maximal CO_2 uptake rates and therefore avoid CO_2 limitation conditions. Dissolved O_2 concentrations reached maximum values of 23% by the end of the exponential growth phase which are below the reported photosynthesis inhibiting O_2 levels of 40% (Rubio 1999, Fan 2008). In contrast to that, during cultivations with only one gas compartment, dO_2 levels surmounted 60% leading to massive bubble formation and possibly an inhibition of photosynthetic activity.

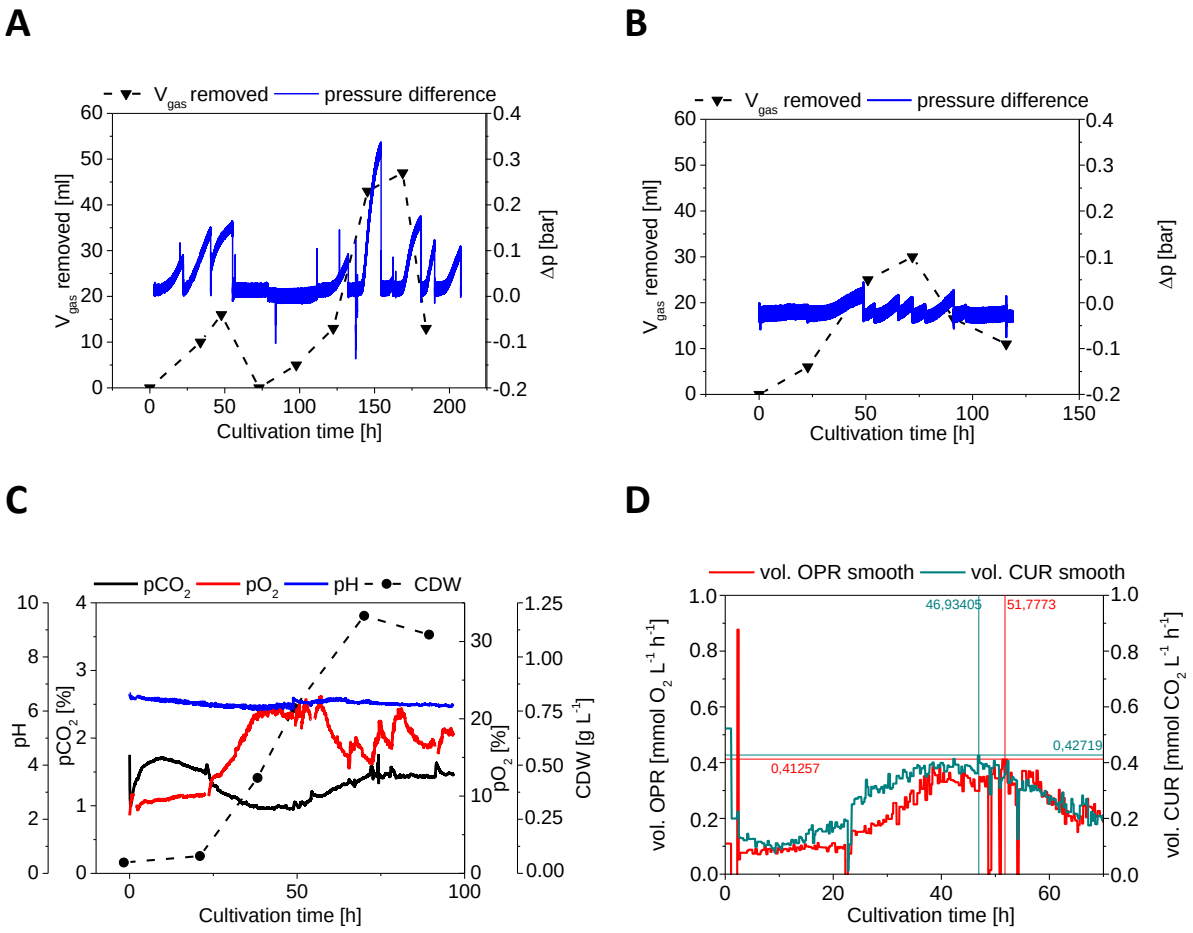

Figure 5-7. Online and offline data of batch cultivations inside the membrane-aerated photobioreactor at 200 µE m^{-2} s^{-1} warm-white illumination. A) Gas volume built and pressure inside the liquid compartment for the one compartment configuration with the TPX membrane for CO_2 supply and O_2 removal and a gas phase composition of 5% CO_2 (v/v) in air. B) Pressure difference and gas volume inside the liquid compartment for the two compartment configuration: TPX membrane for CO_2 supply and Wacker 80 membrane for O_2 removal; gas phases of 5% CO_2 (v/v) in air and 1% CO_2 (v/v) in N_2 respectively. C) Online process data for the two-compartment-configuration with TPX and Wacker 80 membrane displaying dissolved gas concentrations, pH as well as correlated cell dry weight during the batch cultivation. D) Calculated volumetric CO_2 uptake and O_2 production rates related to CDW during the batch cultivation.

Based on Equation 3-24 and Equation 3-25, volumetric CO_2 uptake and O_2 production rates were calculated (Figure 5-7 D). Maximal volumetric CUR in this case accounts for 0.43 mmol L^{-1} h^{-1} whereas the peak OPR accounts for 0.42 mmol L^{-1} h^{-1}. These peak gas transfer rates correlate with the late exponential to linear growth phase. A photosynthetic quotient PQ of 0.98 is resulting. Volumetric gas exchange rates, PQ values as well as growth rates were used to compare this membrane reactor in batch and continuous mode with the ideally mixed bubble-aerated reactor.

5.2.2 Comparison of gas exchange rates for bubble and membrane aeration

In order to connect the algal photomodule to a heterotrophic compartment for the long term, it is important to quantify volumetric CO_2 uptake and O_2 production rates under certain growth conditions. Moreover, these values can be used to compare the novel diffusion-based membrane-aerated reactor concept to conventional bubble-aerated reactors under similar conditions, like the same light intensities. The following data are mean values of at least three cultivations with the same lighting conditions and media. In case of the MBR the two-gas-compartment-configuration was chosen equipped with a TPX and a Wacker 80 membrane.

Table 5-2. Comparison of cultivation parameters from batch cultivations under warm-white LED illumination of 200 µE m^{-2} s^{-1} inside the membrane-aerated reactor and the bubble-aerated stirred tank photobioreactor (STPBR).

Reactor system	μ_{max} [h^{-1}]	vol. CUR_{max} [mmol L^{-1} h^{-1}]	vol. OPR_{max} [mmol L^{-1} h^{-1}]	PQ [-]
MBR (TPX, Wacker 80)	0.060 ± 0.014	0.42 ± 0.01	0.41 ± 0.02	0.97 ± 0.02
Bubble-aerated STPBR	0.051 ± 0.012	1.00 ± 0.08	1.07 ± 0.32	1.08 ± 0.37

As data in Table 5-2 shows, there are differences between the two completely different reactor and aeration approaches for the same irradiant light intensity: whereas maximum specific growth rates are similar with 0.06 and 0.05 h^{-1}, volumetric gas exchange rates differ. For volumetric gas exchange rates, there is a clear tendency that rates are higher (factor of 2.4 for CUR, respectively 2.6 for OPR) in the conventional ideally mixed bubble-aerated PBR.

In total, it can be summarized that volumetric gas exchange rates are higher in the ideally mixed bubble-aerated reactor. Higher volumetric rates are a result of better mixing conditions and a faster gas transfer as k_L values of bubble-aeration are one magnitude higher than for membrane-aeration. Interestingly, PQ values are similar, about 1, for both reactor systems.

Results of continuous cultivations inside the membrane PBR, also in comparison to the results of cultivations inside the STPBR are displayed in Chapter 7.

Furthermore, also dichromatic illumination was used for comparison with full-spectrum warm-white illumination at 200 µE m^{-2} s^{-1} according to Chapter 4. This is necessary in order to combine bubble-free membrane-aeration with energy-efficient illumination. However, in contrast to experiments conducted in mini- and midiplate reactors, as described in Chapter 4, it was not possible to determine PCE values for this reactor configuration. For this reason, gas exchange rates are used as comparison parameters between warm-white and 90/10 red/blue illumination.

Table 5-3 shows results for batch cultivations illuminated with warm-white and with red/blue light at the same PFD. As most of the batch cultivations listed in this table were switched to continuous mode, only few samples, if any, were taken during batch phase to reduce the contamination risk. For this reason, cell densities at gas peak rates during batch phase were not determined. Hence, specific gas exchange rates are not available.

Table 5-3. Comparison of maximum volumetric gas exchange rates from batch cultivations and batch phase of continuous cultivations under warm-white and red/blue 90/10 LED illumination of 200 µE m^{-2} s^{-1} inside the membrane-aerated reactor.

Illumination color, cultivation number	vol. CUR_{max} [mmol L^{-1} h^{-1}]	vol. OPR_{max} [mmol L^{-1} h^{-1}]	PQ [-]
ww, C2	0.43	0.42	0.98
ww, C4	0.41	0.39	0.95
Mean values ww	**0.42**	**0.41**	**0.97**
90/10 r/b, C3	0.40	0.32	0.8
90/10 r/b, C6	0.37	0.39	1.05
90/10 r/b, C7	0.30	0.29	0.97
Mean values 90/10 r/b	**0.36**	**0.33**	**0.94**

As it can be seen from these gas exchanges rates, for CO_2 uptake and O_2 production, both illumination colors lead to similar results, whereas slightly higher values are achieved with full-spectrum illumination. This is consistent with PCE values determined in Chapter 4.2.2 for higher PFDs and one-sided illumination of plate type reactors.

Concerning membrane fouling, no specific tests were performed. For the dense membranes TPX and silicone membranes with different thicknesses, which were used throughout the cultivations presented within this work, almost no membrane fouling occurred. Membranes were easily cleaned with rinsing water after the cultivation and no adverse effect on gas transfer was measured.

The acquired maximal volumetric CUR measured during the experiments can now be related to the required $k_{L,CO2}$ value of a membrane. A maximal vol. CUR of 0.4 mmol CO_2 L^{-1} h^{-1} would require a membrane $k_{L,CO2}$ value of $1.6 \cdot 10^{-6}$ m s^{-1}. Except for two membranes, all of the membrane samples tested showed $k_{L,CO2}$ values higher than this required value.

In relation to the oxygen requirement of a resting human (800 mmol O_2 h^{-1}, compare to Chapter 2.3.4), a reactor volume of 2000L would be necessary, based on a maximal vol. OPR of 0.4 mmol L^{-1} h^{-1} measured for this reactor system in batch mode.

5.3 Summary of results for bubble-free membrane aeration

The results of the series of experiments for selection of suitable membrane materials have shown that there are measurable differences of CO_2 and O_2 mass transfer values between the membranes tested during this work for the gas-liquid testing system built. In total, k_L values for both gases are in the range of 10^{-6} m s^{-1} which is one magnitude lower than for surface aeration (10^{-5} m s^{-1}) and two magnitudes lower than for bubble aeration (10^{-4} m s^{-1}).

Concerning $k_{L,O2}$ values, porous membranes show similar mass transfer behavior, whereas $k_{L,O2}$ values for dense membranes differ to a higher extent. Highest $k_{L,O2}$ values were achieved with silicone membranes. O_2 mass transfer values measured, in total, were slightly higher than those for CO_2. For CO_2 mass transfer values show a higher variation than for O_2. In contrast to O_2, highest $k_{L,CO2}$ values were measured for porous membranes.

For dense solution membranes, differences in k_L values for O_2 and CO_2 are resulting from different diffusion coefficients of both gases in gases, liquids and solids. For porous membranes also other diffusion mechanisms like Poiseuille and Knudsen diffusion and the Henry-coefficients at the gas liquid interface inside the pores play a role. For these diffusion mechanisms inside porous materials the relation of the average free path length to the average pore size as well as the density of the gas are important factors. The higher diffusion rates of O_2 compared to CO_2 in air and water can explain the overall slightly higher mass transfer values for oxygen. Additional to that, solubility in the membrane material and diffusion coefficients of the gases in the material are of crucial importance in case of dense membranes. Diffusion coefficient of oxygen in silicone, where most of the dense membranes tested were made of, is higher than that of CO_2 in silicone. Hence, for air, water and silicone, oxygen diffusion is faster than CO_2 which can explain the overall higher mass transfer coefficients.

The testing series for influencing factors on k_L values shows that abiotic factors like T, salt concentration and pH (in case of CO_2 mass transfer) are influencing mass transfer coefficients for O_2 and CO_2. Furthermore, the thickness of the membrane material, in case of dense membranes, as well as the bulk liquid velocity have an influence on k_L values. These factors have to be taken into account, first of all, for designing a membrane-aerated phototrophic cultivation process and second, also during analysis of gas transfer rates under the specific cultivation conditions.

For selectivity factors $\alpha_{O2/CO2}$ there is a higher difference in values measured for dense membranes, as a result of the solution-based manner of mass transfer. The highest factor is measured for a dense membrane where $\alpha_{O2/CO2}$ accounts to 2.2. For the porous membranes tested, the values are around 1 or slightly below. As outlined before, a higher selectivity for O_2 towards CO_2 is necessary to circumvent the problem of bubble formation as a result of photosynthetic activity and lower solubility of oxygen in water. Therefore, based on the results obtained within this work and theoretical considerations, porous membranes are not suitable in order to design a long-term bubble-free membrane-aeration of phototrophic processes. Dense solution-based membranes, which show a higher mass transfer of oxygen than for CO_2, should be considered.

For water loss values a maximum of 240 ml m^{-2} d^{-1} was measured for a dense membrane. In general, dense membranes show, dependent on their thickness, a high variation in water vapor loss. For porous membranes the values measured are similar. During this work, hydrophilic membranes showed immediate water loss during testing and for this reason they are not suitable for application inside an algal photobioreactor for space application.

During calculation of CTR values achievable with the membranes tested, it was shown that even for flat sheet membranes a sufficient CO_2 supply can be guaranteed under the assumptions made.

For studying the application of membranes for a bubble-free aeration of a photobioreactor, a novel membrane reactor system using flat sheet membranes was developed during this work. The system is flexible for its membrane configuration and can be run either using one membrane and one gas compartment or two membranes and two compartments. A series of tests in batch mode was run to determine the ideal setup for long-term cultivations where the configuration with two separate membranes showed optimal starting dissolved gas concentrations in equilibrium before the cultivation was started. Therefore, a configuration with two membranes, one for CO_2 supply and the second for O_2 removal with two different gas compositions on each side is chosen.

First cultivations inside the membrane reactor were run in batch mode where bubble formation was observed resulting from O_2 accumulation and oversaturation of the liquid with gases. By using the two-membrane/two-gas-compartments-configuration, the bubble volume built during cultivation was reduced. However, with the setup used it was not possible to avoid bubble formation completely. This

fact was taken into account for establishing a control system for continuous cultures which have been performed in later stages of this work.

Relating to maximal gas exchange rates during batch cultivations, peak volumetric CUR and OPR account for 0.4 mmol L^{-1} h^{-1}, with a PQ of 0.97. These volumetric rates are only half the rates which are obtained for the same irradiating intensity inside the ideally mixed STPBR with cylindrical illumination. However, this is a result from better mixing conditions and the different light intensity gradients. Also for the membrane reactor the full spectrum illumination was compared to red/blue 90/10 illumination at the same PFD of 200 µE m^{-2} s^{-1} leading to the conclusion that volumetric gas exchange rates are similar. This is a result from light saturation conditions at this PFD of 200 m^{-2} s^{-1} for a plate type reactor geometry with one-sided illumination as discussed in Chapter 4.2.2.

Future work on membrane application for photobioreactor aeration should primarily focus on selectivity factors $\alpha_{O2/CO2}$ of dense membrane materials. In order to further increase this factor, it seems promising to test chitosan-acetic acid membranes functionalized with Ni-ions, as selectivity factors $\alpha_{O2/CO2}$ of about 30 were published by Bai and coworkers (1988). Also liquid membranes with carriers or dense SBS membranes with increased selectivity as outlined in the theoretical Chapter 2.3.1.5 are promising.

By using the determined k_L values, simulations with variation of specific surface area a, and gas composition can be used to find optimal solutions for each application case respectively.

6 Effects of lowered pressure on microalgae cultures

For the assessment of effects of lowered pressure and pressure changes on microalgal growth, gas exchange rates, pigment concentration and morphology, experiments with *C. reinhardtii* CC-1690 and WT13 were conducted in batch mode inside a stirred tank photobioreactor with bubble-aeration with warm-white and cold-white light. Cultivations were started under atmospheric pressure and stepwise the pressure was lowered during the lag phase of the growth to the desired pressure value. This pressure was kept constant for the rest of the cultivation. For one experiment it was tested how sudden pressure changes, applied during exponential growth phase, affect cell survival, and morphology aiming to find a possible fatal threshold value. The applied pressure limits (1000-700 mbar) were chosen as a compromise between technical feasibility and relevant pressures for high-altitude microalgae cultivations on Earth (600 mbar for 4 km altitude) and the proposed 540 mbar for lunar or other extraterrestrial bases as a compromise between engineering and human demands, specified by NASA (2004). With the photobioreactor used, no lower pressures than 700 mbar could be tested. The results shown were published in Wagner (2017) to some extent.

6.1 Influence of pressure reduction on growth, gas exchange and pigment formation

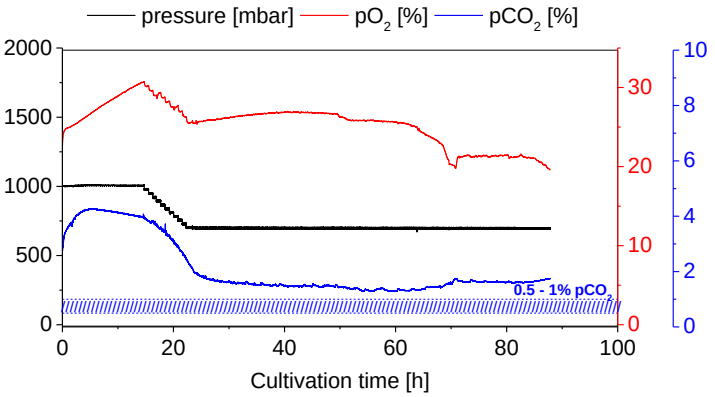

Figure 6-1. Typical plot of pressure and dissolved gas concentrations of CO_2 and O_2 for a batch cultivation at 700 mbar. Lines show the critical CO_2 concentration range of 0.5 to 1% dCO_2; modified after Wagner (2017).

Figure 6-1 exemplarily shows the development of pressure, dCO_2 and dO_2 during a batch cultivation at 700 mbar pressure. In general, it is important to note that the sensors used for dCO_2 and dO_2 measure concentrations (whereas partial pressures are displayed) and calibration was performed under atmospheric pressure conditions. As concentrations of dissolved gases during pressure reduction decrease, as a result from decreased solubility with lower pressure, the online signals for pO_2 and pCO_2 also decrease. The pressure signal shows how pressure was reduced stepwise after inoculation

and how concentrations of dCO_2 and dO_2 develop. As the medium was not saturated yet with the gas mixtures, there is an increase in pCO_2 in the beginning. Concerning CO_2 limitation, it is shown that even during phases where CUR was maximal, pCO_2 values are higher than the critical pCO_2 of 0.5-1% in the liquid medium for atmospheric pressure and related to a pure CO_2 atmosphere as 100% pCO_2. Optimum growth rates are considered to correlate with CO_2 partial pressures above 0.5%. This critical concentration can be extracted from CO_2 kinetics (Dillschneider 2014). Therefore, throughout all the experiments of this study, CO_2 limitation conditions can be excluded, even though gas solubility decreased with lowered pressure.

Figure 6-2 shows the results of cultivations with CC-1690 cells in batch mode under different constant lowered pressures at the same PFD of 200 µE m^{-2} s^{-1} with warm-white and cold-white light regarding maximum specific growth rate μ_{max}, maximum volumetric and specific oxygen production rate OPR and maximum volumetric and specific carbon dioxide uptake rate CUR (for calculation see section 3.6.3, Equation 3-22, Equation 3-23), (Wagner 2017).

Figure 6-2 A shows that maximum specific growth rate in control was at 0.060 h^{-1} for warm-white and 0.050 h^{-1} for cold-white light, and decreases for lowered absolute pressure with a minimum at 700 mbar at 0.035 h^{-1} for warm-white and 0.033 h^{-1} for cold-white light.

Panel B of Figure 6-2 shows the relation of maximum specific growth rate of *C. reinhardtii* CC-1690 as a function of pressure in the range of atmospheric pressure down to 700 mbar for both lighting colors. As there is no knowledge about the kinetic model for the abiotic factor pressure yet, it is questionable how such a curve would look like. It can be assumed that growth rate is maximal for atmospheric pressure and lowers for both increased and lowered pressure so that one distinct peak maximum exists. *Chlamydomonas nivalis*, for example, as one representative of the genus *Chlamydomonas*, is commonly spread in alpine high-altitude regions (3-3.6 km altitude) where atmospheric pressure accounts for only 70 to 60% of pressure at sea level. So far, only adaptation mechanisms to the extreme temperatures in these regions have been studied for *C. nivalis*. However, Qin and coworkers (2014) also showed a reduction of growth rate for several cyanobacterial species at 500 mbar absolute pressure. Beside the factor lowered pressure, also CO_2 limitation conditions could have provoked this outcome as cultures (both under lowered pressure and control) were not aerated and gas compositions was only at atmospheric air CO_2 levels (for 500 mbar only half of the gas contents for CO_2 and O_2, respectively). Thus, no clear comparison can be drawn with the reported results. In case of extraterrestrial life support installations, for instance on the moon, a possible reduction of pressure would reduce the necessary technological complexity and the costs for resupply (Qin 2014). Therefore a photosynthetic organism, capable to grow at a sufficient growth rate under these low pressure conditions, could become an essential part of such a system.

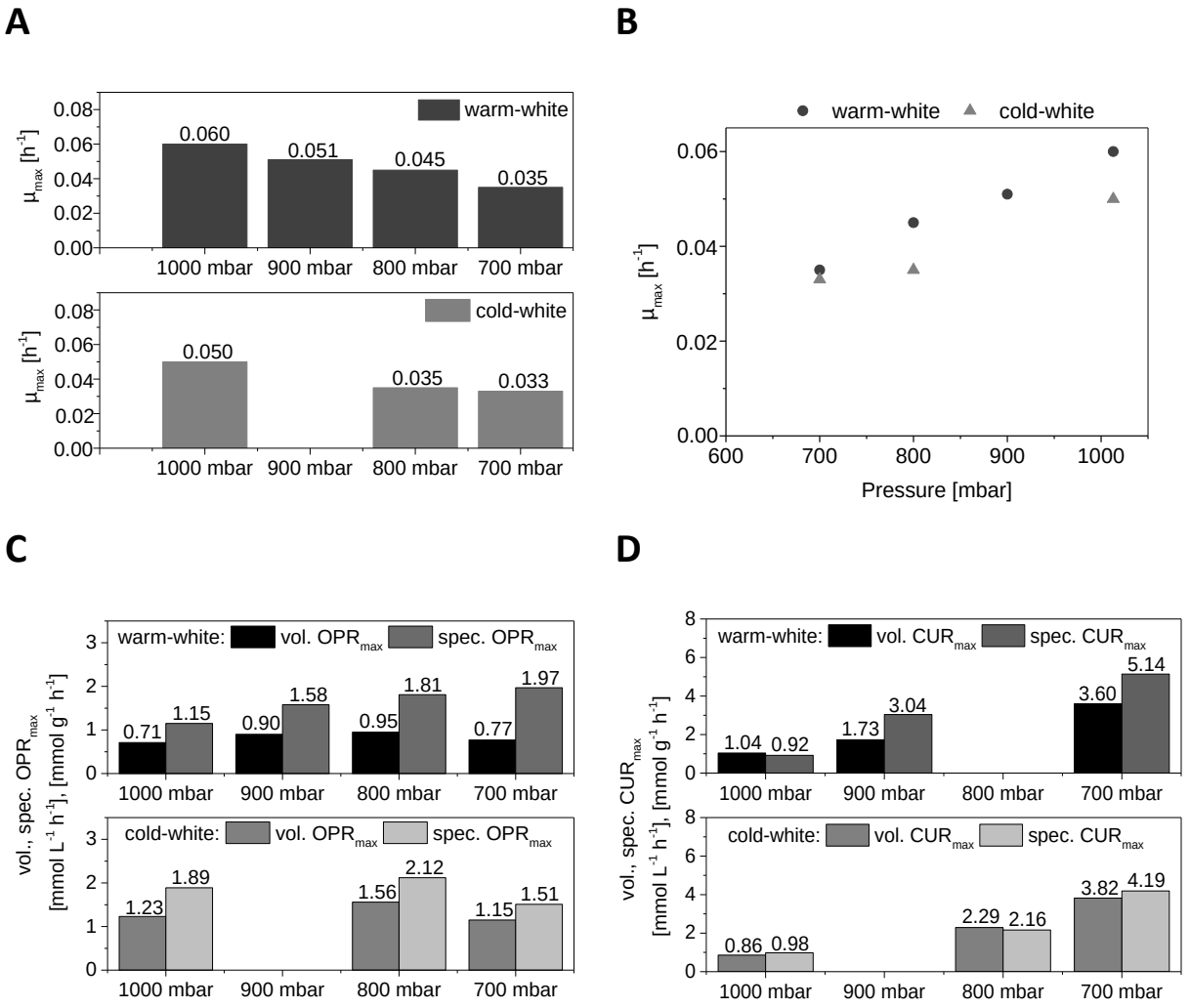

Figure 6-2. Influence of lowered pressure on growth and gas exchange rates of *C. reinhardtii* CC-1690 cells during batch cultures for warm-white and cold-white light. A) Dependency of maximum specific growth rate μ_{max} on pressure. B) Growth kinetic as function of pressure for the tested pressure range. C) Influence of pressure reduction on maximal volumetric and specific OPR and D) on maximal volumetric and specific CUR. Experiments were conducted in batch mode at a PFD of 200 µE m^{-2} s^{-1}, 4.8% (v/v) CO_2, at T = 25°C, using TP-NO_3-medium, Wagner (2017).

For volumetric oxygen production rates, maximum values (compare to panel C, Figure 6-2) for both lighting conditions show no differences for varying absolute pressures down to 700 mbar within the limits of accuracy. All volumetric OPR_{max} values are within the range between 0.71-0.95 for warm-white and between 1.15-1.56 mmol O_2 L^{-1} h^{-1} for cold-white light. Volumetric rates of oxygen production show no influence of pressure within the tested limits. For specific OPR, values seem to increase for warm-white light from 1.15 to 1.97 mmol O_2 g^{-1} h^{-1}, which is in contrast to the values obtained for cold-white light showing no influence of pressure reduction. The increase in specific OPR values for warm-white illumination could also be only apparent and caused by erroneous CDW-OD correlation factors for aggregated cells which were prevailing for the 700 mbar cultivation (see 6.3). For this reason, the assumption, that lower pressures lead to a change in specific and volumetric OPRs,

cannot be verified by the experiments within the limits of measurement accuracy for absolute pressures down to 700 mbar for both light colors. Further experiments should verify these results.

For maximum volumetric CUR values (panel D) a high dependency on absolute pressure was detected for both lighting colors: values increase from atmospheric pressure to 700 mbar with a volumetric CUR_{max} of 1.04 to 3.60 mmol CO_2 L^{-1} h^{-1} for warm-white; for cold-white they increase from 0.86 to 3.82 mmol CO_2 L^{-1} h^{-1}. The same tendency is shown by the specific CUR values: they increase from 0.92 to 5.14 mmol CO_2 g^{-1} h^{-1} for warm-white, for cold-white light from 0.98 to 4.19 mmol CO_2 g^{-1} h^{-1}.

Results indicate that at least for CO_2, there seems to be an influence of pressure on gas exchange rates. Further research should verify these results and should reveal reasons why oxygen production rates seem to be unaffected, also in regard to the application of microalgae based modules in life support systems for space application. As CUR and OPR values were calculated based on exhaust gas analysis at atmospheric pressure and not on CO_2 and O_2 sensor data, there is no influence of reduced gas solubility for lower pressures on these calculated values. However, this apparent decrease of PQ from 1.1 to 0.26 (mean values for both lighting conditions) could not be separately verified.

Concerning dissolved CO_2 concentrations in the liquid there is a reduction of CO_2 concentration at lower pressure as a result of reduced solubility (compare to Figure 6-1). However, the inlet CO_2 gas concentration of 4.8% (v/v) was chosen high enough to ensure a sufficient CO_2 concentration in the liquid (above the critical 0.5 to 1% dCO_2) even at lowest tested pressures of 700 mbar. Above this concentration, according to CO_2 kinetics, as discussed before, optimal growth rates are enabled.

Results of starch analysis for reduced pressure are displayed in Appendix 11.6.2.3. Starch was measured during the linear growth phase shortly before stationary phase began, as for *C. reinhardtii* starch production is maximal under nutrient limitation conditions (in particular nitrogen, Juergens 2015, see chapter 2.2.2.4). As the results show, no effects of reduced pressure on specific starch concentrations can be detected with these experiments, within the range of measurement accuracy (Wagner 2017). Values account for an average of 0.4 g g^{-1} starch per cell.

Future analysis should also focus on possible enhanced lipid production of this alga under different pressures, as it was reported by Min et al. (2014) for *C. reinhardtii* cells after membrane distortion. Lipid accumulation could lead to a change of photosynthesis quotient. According to references (Kuchitsu 1988) the unchanged starch contents point to an unchanged CCM activity as an increase in its activity often is accompanied by a degradation of starch granules inside the chloroplast. This could be detected under conditions of C- limitation with simultaneous light saturation conditions.

Also specific pigment concentration (Figure 6-3) and a possible influence of pressure on their formation were of interest within this study. As pigment content and composition highly depend on the resulting average light intensity per cell, which is a function of time for a batch culture, only samples

taken from cultures with different pressure but with almost the same cell dry weight concentration, and therefore same light intensity distribution conditions, were compared for analysis.

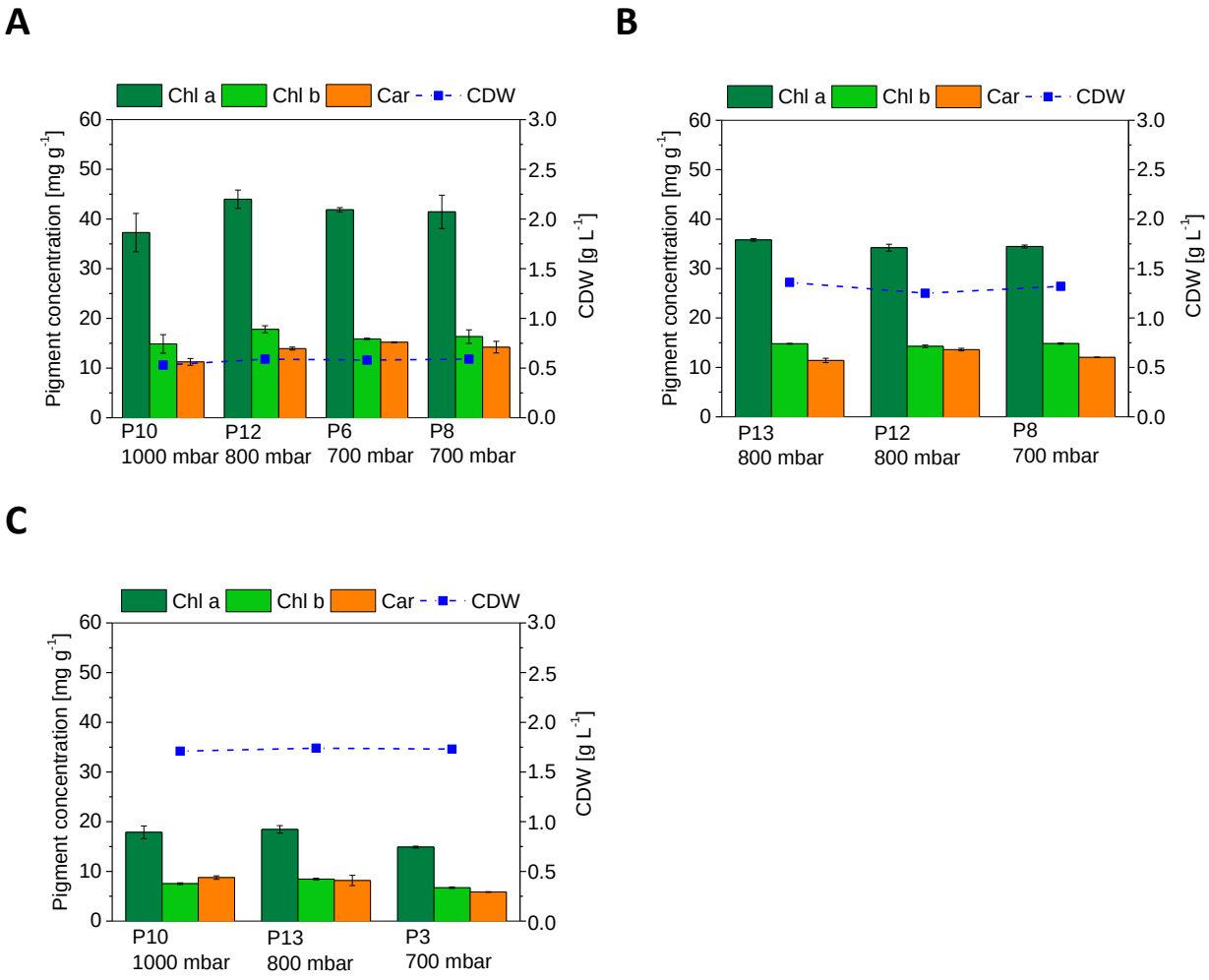

Figure 6-3. Specific pigment concentration for batch cultivations with *C. reinhardtii* CC-1690 under different pressures. A) Specific pigment concentrations (Chl a, Chl b, Car) of cells during different batch cultures (P10, P12, P6, P8) for 1000, 800 and 700 mbar at similar cell dry weight concentrations around 0.6 g L^{-1}. B) Specific pigment concentrations of cells for batch cultures at 800 and 700 mbar (P13, P12, P8) for process times with cell dry weight concentrations of around 1.4 g L^{-1}. C) Results for specific pigment concentrations for CDW of around 1.8 g L^{-1} for cultivations at 1000, 800 and 700 mbar (P10, P13, P3). Cultivation P3 was performed under warm-white illumination. All other cultivations shown were conducted with cold-white illumination.

As Figure 6-3 A-C shows, the specific pigment concentration is the same for similar cell dry weight concentrations (CDW of 0.6, 1.4 and 1.8 g L^{-1}), regardless of the pressure applied during cultivation of the algae cells.

The results presented so far tend to show that light reactions of photosynthesis are hardly influenced by the reduced pressure and the relating lower gas solubility with unchanged specific pigment contents and no tremendous influence on volumetric and specific OPR values. This would point to an increased activity of CCM to balance the reduced CO_2 concentration in the cell under lowered pressure. As a

consequence, no changes in light reactions with pigment content and OPR would be visible. This increased activity of CCM is reported to correlate with a reduction of starch content of cells for CO_2 gas concentrations from 0.3% to 1% CO_2 (v/v). As CO_2 was kept at 4.8 % (v/v) in the inlet gas within this study and also with taking into account the lowered gas solubility at 700 mbar, the CO_2 concentrations were still above 1% pCO_2 in the liquid phase (in the range of 1-2% pCO_2 for maximal CUR, see Figure 6-1). For this reason, the influence of the CCM on the starch content could be less pronounced in this study compared to references. In contrast to that, there seems to be an influence of lowered pressure on dark reactions of photosynthesis in *C. reinhardtii*, as both volumetric and specific CUR values are increased.

6.2 Effects of sudden pressure changes on cell survival

As a microalgae module for space life support systems may be exposed not only to lower pressure, but also sudden pressure changes, in total nine sudden pressure steps at one hour intervals were performed during the exponential phase of a batch culture. This is also of relevance for ground photobioreactors where cells can also be exposed to pressure changes in millisecond dimensions.

Figure 6-4 panel A shows the overview of this batch cultivation with CC-190 cells where sudden pressure changes were performed (Wagner 2017). Online OD signals, pressure and dissolved gas concentrations (both in partial pressure %) for CO_2 and O_2 as well as the natural logarithm of these online OD values (as ln(OD)) are plotted versus process time.

For dissolved gases, the stepwise reduced pressure and therefore reduced solubilities are clearly seen from the signals, whereas the steps are more easily detected for dissolved O_2, as the optic sensor has a shorter response time than the pCO_2 sensor. By regarding ln(OD) values no influence of pressure changes on maximum specific growth rate, as slope of the ln(OD) value, can be detected, implying that there was no impairment of growth measurable for these sizes of pressure changes tested.

Panel B shows an enlarged section of part A where the phases of sudden pressure changes are more easily visible and numbers correlate with the microscopic pictures in part A of Figure 6-5 (bright field, 400x magnification) taken immediately after these stepwise changes of pressure starting with a microscopic picture at atmospheric pressure (1), each picture equipped with scales indicating randomly chosen cell diameters (measured from top with apical flagella to the basis of the cell). Green boxes on the right upper corner depict the applied Δp for each step respectively.

These results imply that the pressure changes exerted on the cells had no measurable influence on algal growth (μ_{max}). During these tests no fatal threshold was reached, indicating that cells can tolerate pressure changes within the tested magnitudes (highest step with 300 mbar).

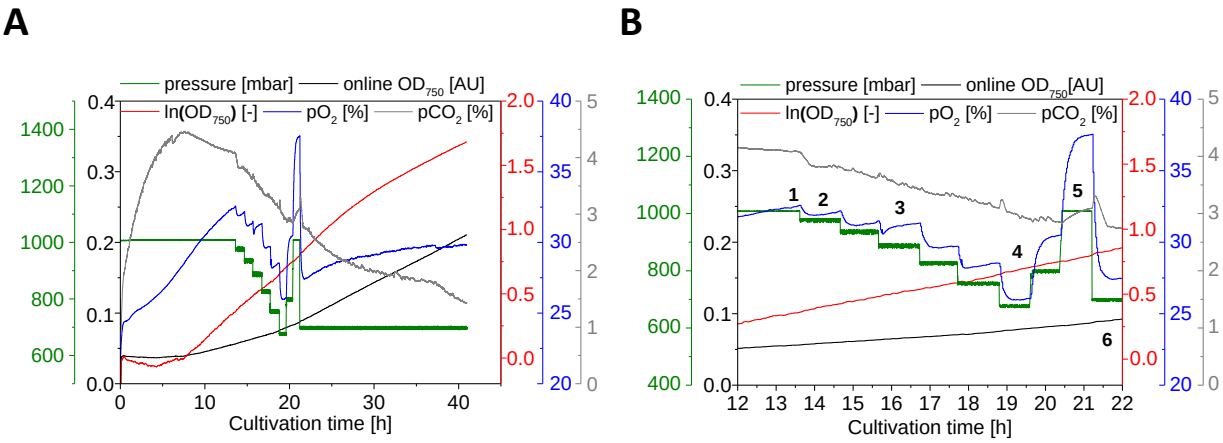

Figure 6-4. Effects of sudden pressure changes on cell growth. A) Overview of process data from the batch cultivation showing pressure changes within exponential growth phase, online OD_{750} as well as $ln(OD_{750})$. B) Section of diagram in panel A showing numbered pressure steps correlating with microscopic images in part A, Figure 6-5 (1), (Δp = 0mbar) from 30 mbar step size down to 970 mbar (2), (Δp = 30mbar), increasing negative step size each time by 10 mbar (3), (Δp = 50mbar), down to 670 mbar absolute pressure (4), (Δp = 80mbar) followed by positive step sizes of 100 and 200 mbar (5), (Δp = 200mbar), ending with a negative step size of 300 mbar from 1000 mbar down to 700 mbar (6), (Δp = 300mbar), Wagner (2017).

6.3 Effects on morphology and aggregation

As Figure 6-5 A shows, swelling and also an increase in diameter of the cells is monitored as a result of these pressure steps, starting with a step size of 50 mbar and further increasing pressure step changes (Wagner 2017). For atmospheric pressure (1) cell diameters mostly account for 10 µm, whereas the diameters account for up to 18 µm for the highest pressure difference exerted on the cells of 300 mbar (6). Another striking feature is that with increasing pressure steps, also the number of daughter cells seems to be increased: while under atmospheric pressure two or four daughter cells per cell division result, mostly eight daughter cells prevail for step sizes higher than 80 mbar (4). However, results might imply that lower and earlier pressure steps were able to trigger this reaction. Furthermore, there is the question if such short pressure steps were long enough to enable this increase in number of dividing cells; for example from two daughter cells to eight daughter cells within one membrane capsule. This has to be also related to an average doubling time of about 11 hours for a μ_{max} of 0.06 h^{-1} at this PFD. Another open point is relating to cell cycle and if pressure changes influence the cellular life cycle with its concrete phases. The detected swelling of cells might either be resulting exclusively from pressure reduction and a mechanical elongation of the cell membrane and wall and an influx of water, or also be caused by cell division.

A

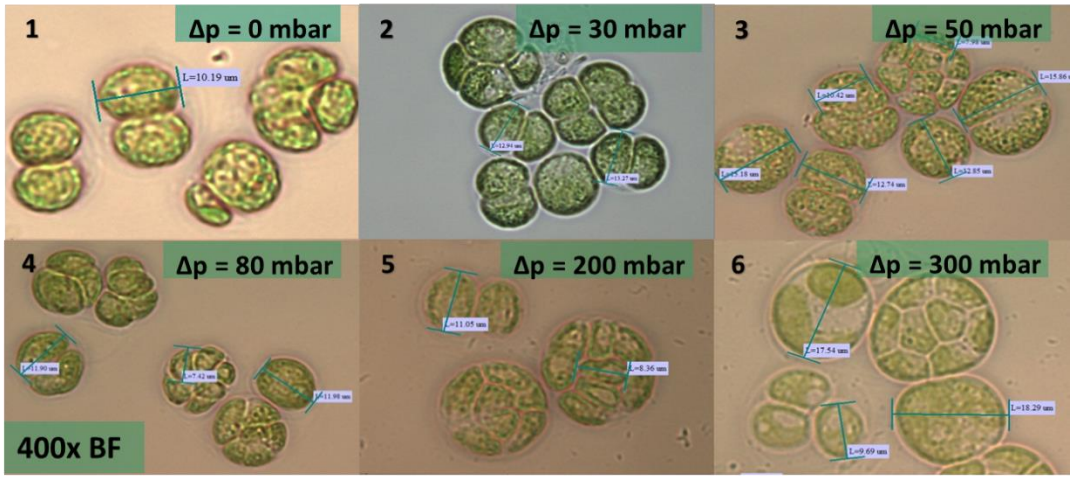

B

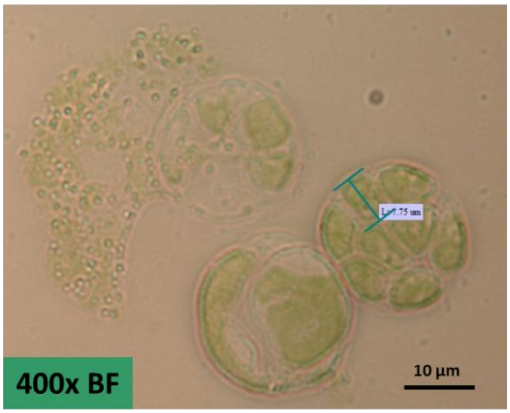

Figure 6-5. Influence of sudden pressure changes on cell morphology and survival of *C. reinhardtii* CC-1690 cells during batch cultures. A) Lightmicroscopic images, bright field BF, 400x magnification, green boxes indicate pressure step size. B) Lightmicroscopic image (BF, 400x magnification) showing cell debris after pressure changes were finished (Wagner 2017).

According to Min et al. (2014) distortion of the cellular membrane also leads to a higher number of daughter cells after division for *C. reinhardtii*. For *C. reinhardtii* cells it is known that cells divide into either two, four or eight daughter cells (Harris 2009) per division, where for optimal conditions also 16 daughter cells are reported (Vítová 2011). This kind of cell division is known as multiple fission (Bišová 2014), where the key components characterizing the environment of a photosynthetic organism, being light intensity and temperature, have a strong influence on the division number (number of daughter cells produced). Here, higher light intensities and optimal temperatures are assumed to lead to a higher division number. Light conditions seem to be the most important factor influencing multiple fission, which in turn, is seen as an adaptation mechanism to light cycles occurring in nature. Studies also indicated that signals relating cell-cycle progression and photosynthesis exist. The division number is also depending on the cell size (Bišová 2014). As Min et al. (2014) described a higher number of daughter cells after cell membrane and wall distortion, and

relating to the results of this study with lower pressures and sudden pressure changes, it is remarkable that both conditions were resulting in a higher division number, as a higher number of resulting cells generally is originating from environmental conditions enabling higher growth rates where multiple fission is an evolutionary advantage over binary fission (Bišová 2014). In other words, more optimal conditions favor increasing daughter cell numbers. So, mild stress conditions acting on cells, as exerted by Min and coworkers (2014) and those pressure patterns studied within this work seem to provoke the same mechanisms relating to cell division as optimal environmental conditions do for this green alga.

After finishing pressure changes, p was kept constant at 700 mbar. Further samples were taken several hours after these pressure changes. Here, cells showed a higher sensitivity during handling compared to cells cultivated from the beginning under such lowered absolute pressures, resulting in breaking of the cell wall and cell death where cell debris was seen with the help of lightmicroscopic analysis (compare to panel B of Figure 6-5). This was a rather qualitative observation and should be further studied in future experiments by quantitative means, for example shear stress tests. Concerning aggregate formation as response to sudden pressure changes as was assumed before, there are no aggregates detected for any of the Δp tested on CC-1690 cells. However, as microscopic analysis only involved a small number of cells, future studies should verify these findings by particle size analysis together with microscopic image analysis software.

Further experiments were conducted to reveal, if at all, lower than atmospheric pressures within the tested range, are able to provoke formation of aggregates for *C. reinhardtii* cells. Therefore, batch cultivations of two wildtype strains of this alga, CC-1690 and WT13, were conducted under a constant pressure of 700 mbar. WT13 was chosen, as for CC-1690 cells it is known that cells of the wildtype strain tend to build palmelloids (Harris 2009) as well as secondary aggregates (see chapter 2.2.1.2), triggered by various abiotic (T, pH) and biotic (bacterial contamination) factors where dependencies and causes are not yet fully revealed and understood. In contrast to that, WT13 cells neither show a tendency for palmelloids formation nor strong aggregate formation.

Figure 6-6 shows lightmicroscopic images of *C. reinhardtii* cells (Wagner 2017): panel A shows wildtype CC-1690: (1) in pre-culture at atmospheric pressure before start of cultivation; (2) immediately after inoculation, inside the photobioreactor at atmospheric pressure; (3) after the pressure reduction from 1000 mbar to 700 mbar; (4) at the end of the batch cultivation at 700 mbar. Figure 6-6 B shows lightmicroscopic images for WT13 cultivation under 700 mbar denoted with numbers five to eight. For wildtype CC-1690 it can be seen that already in pre-culture larger aggregates were prevailing, which seem to increase in diameter after inoculation, still under normal pressure. With stepwise pressure reduction these seem to suspend whereas at the end of the cultivation at 700 mbar smaller aggregates of dividing cells prevail, smaller than those present in the beginning.

On the contrary, WT13 cells neither show palmelloids nor secondary aggregates for any of the phases monitored. This shows that at least for both of the strains of *C. reinhardtii* tested in this study, constant lower pressure does not trigger aggregate formation.

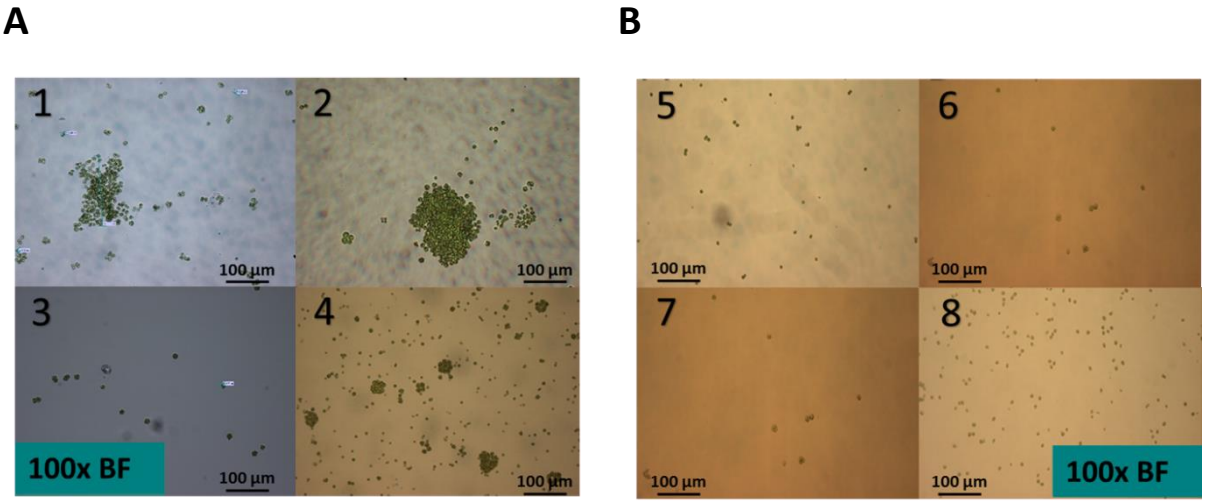

Figure 6-6. Influence of lowered pressure on formation of palmelloids and aggregates of *C. reinhardtii* CC-1690 and *C. reinhardtii* WT13 cells during batch cultures at 700 mbar pressure. A) Microscopic images (100x bright field) of *C. reinhardtii* CC-1690 cells in pre-culture at atmospheric pressure (1), in reactor at atmospheric pressure before stepwise pressure drop (2), directly after stepwise pressure reduction from 1000 mbar to 700 mbar (3), cells at the end of the batch cultivation at 700 mbar (4). B) Microscopic images (100x bright field) of *C. reinhardtii* WT13 cells in pre-culture at atmospheric pressure (5), in reactor at atmospheric pressure before stepwise pressure reduction (6), directly after stepwise pressure drop from 1000 mbar to 700 mbar (7), cells at the end of the batch cultivation at 700 mbar (8) (Wagner 2017).

6.4 Summary of results for effects of lower pressures and pressure changes

The results of this series of experiments imply that a lowered pressure, down to 700 mbar, has an influence on growth of the alga and decreases maximum specific growth rate of *C. reinhardtii* CC-1690 cells, whereas volumetric and specific carbon dioxide uptake rate increase; volumetric and specific OPR stays at the same level indicating no influence of lowered pressure on light reaction of photosynthesis, and to a small degree the impairment of growth. During these experiments neither an increase of oxygen production rate nor a reduction of it was caused by these sub lethal stresses of lowered pressure. However, a possible signaling effect of pressure or a deviation from atmospheric pressure resulting in distinct physiological effects is still unclear. Also the definition of cellular stress is related to this topic.

Similar to references, reporting negative effects of cell membrane elongation on growth of the algae (Pope 1973, Schreiber 1973), the results from these experiments under lowered pressures show decreased maximum specific growth rates. In contrast to that, as already discussed above, for the division number of *C. reinhardtii*, which is an alga carrying out multiple fission, these mild stress conditions seem to trigger a higher number of daughter cells during division, as normally more

optimal light or temperature do. Furthermore, it can be concluded from this study, that for these wildtype strains of *C. reinhardtii*, lowered pressure, or sudden pressure changes in the range of 300 mbar are not causing aggregate formation of cells which was presumed before. No lethal threshold of sudden pressure changes was reached with the conducted experiments, although cells are more susceptible to shear and mechanical stresses after exposure to a sudden pressure change of 300 mbar.

Further work should focus on starch and lipid production in *C. reinhardtii* cells under lower pressures: in this study no change of specific starch content could be detected for cells grown at lower pressures compared to control. Future experiments should also focus on a possible changed production of lipids as reported for cells after distortion of their membrane (Min 2014) and also discover long-term effects of lowered pressure during continuous cultivations. Lipids seem also be more time-stable then starch as turnover rates for starch are higher.

Pressure step changes should be kept constant for longer times in future experiments (at least in the range of doubling times) to verify these preliminary results for morphological influences of sudden pressure changes. Additionally, a bypass system with an integrated image analysis device should be developed for continuous cultivations with constant lighting conditions under lowered pressure to optimize the experimental setup.

Moreover, the existence of turgor pressure of the flagellate *C. reinhardtii* and the role of the contractile vacuoles is still unclear (see theoretical chapter 2.2.1.3 and 2.2.1.5). This could be relevant for understanding effects of the abiotic factor pressure on algal growth and photosynthetic activity.

In general, with respect to inhibition of photosynthesis by elevated O_2 concentrations (oxygenase activity of RuBisCO, see chapters 2.2.2.1 and 2.2.2.2), a lowered pressure should facilitate the mass transfer of O_2 out of the algal cell.

For a possible application of microalgae within life support systems, it is important to note that photosynthetic oxygen production rates seem not to be affected down to pressures of 700 mbar; moreover, no cell death was provoked by sudden pressure changes in the range of 300 mbar. However, deeper knowledge on how pressure and pressure changes are perceived by microalgae and which effects on photosynthetic activity, physiology, cell division and morphology are resulting is necessary to employ them for space application and also further optimize photobioreactors on ground. That includes the question if microalgae, in this work the green alga *C. reinhardtii*, are capable of pressure perception or if the responses reported in this and other works are rather responses to unspecific stimuli.

7 Long-term stability of continuous cultures

In order to study the long-term stability of the photosynthetic activity of *C. reinhardtii* cells and the effects of perturbations, continuous cultivations were performed in various reactor types from plate reactors (see Chapter 4.6), a bubble-aerated stirred tank reactor to the membrane-aerated photobioreactor. Perturbations were exerted in form of light intensity step changes and in form of step changes in spectral composition of incident light for red/blue illumination (spectral changes are displayed in Chapter 4.6). Oxygen production and CO_2 uptake rates were in focus of analysis as well as specific pigment content. Relating to a photosynthetic, microalgae-based life support module, the PFD step changes mimic an energy shortage or a failure of the lighting system. Important for these conditions is the question how fast oxygen production rates decrease, and, after the initial PFD is reinstalled, if and how fast the initial uptake and production rate is reinstalled or in general, if and after which time the system is able to install a new steady-state balance.

7.1 Influence of light step changes on gas exchange rates

7.1.1 Bubble-aerated ideally mixed reactor

First experiments in continuous cultivation mode with the alga *C. reinhardtii* CC-1690 and light step changes were conducted in the bubble-aerated stirred tank photobioreactor (STPBR) with cylindrical warm-white LED illumination. Light steps were performed in steady-state phases and each experiment was conducted at different cell densities within these phases.

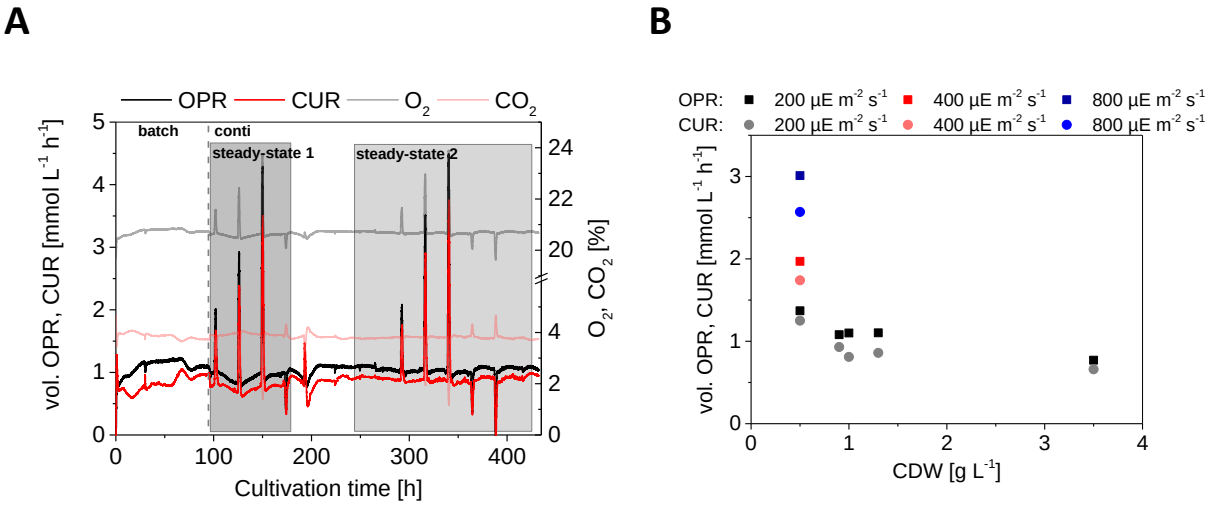

Figure 7-1. Influence of light intensity step changes during continuous cultivations on gas exchange rates in a bubble-aerated 1.8 L stirred tank photobioreactor. A) Dissolved gas concentrations and calculated volumetric OPR and CUR values during light step changes of a continuous cultivation with two steady-states at cell densities of 0.9 and 1.3 g L^{-1} respectively. B) Dependence of volumetric OPR and CUR on steady-state cell concentration for three different basic illumination intensities of 200, 400 and 800 µE m^{-2} s^{-1}.

For determination of time constants the online pH signal was used as indirect dissolved CO_2 measurement for CO_2 uptake (no pCO_2 sensor available). During the step change the pH control was stopped. Gas exchange rates were calculated based on Equation 3-22 and Equation 3-23 from O_2 and CO_2 content in exhaust air measured by Maihak gas analyzer. After a time period of 1.5 h the PFD was switched back to the initial basic illumination (see Table 3-8). Within that time both pH and exhaust gas measurements were showing constant values indicating quasi steady-state conditions. The tested light intensities were based on the afore-measured μ_{max}-I-curve of CC-1690 cells in the cylindrically illuminated photobioreactor (see Appendix 11.6.3.2, Figure 11-15) which is comparable to the light kinetic of *C. reinhardtii* WT8b+ which was determined in a previous work. In that reactor with the specific light intensity distribution, µ-I kinetics show that with a PFD of 200 µE m^{-2} s^{-1} the culture is in the photolimited range, whereas 400 µE m^{-2} s^{-1} is at the beginning of the photosaturation range (I_k) and 800 µE m^{-2} s^{-1} is within the saturated range (I_s).

Figure 7-1 A exemplarily shows CO_2 and O_2 exhaust gas contents and volumetric CUR and OPR values for the continuous cultivation 4/5 (see Table 3-8) with two steady-states at CDW concentrations of 1.3 and 0.9 g L^{-1}. For all of the different steady-states the respective average volumetric OPR and CUR values at the specific basic illumination intensity were compared and are displayed in part B.

Table 7-1. Average volumetric oxygen production rates for steady-states at different cell densities during continuous cultures in the bubble-aerated stirred tank photobioreactor.

Cultivation number (basic PFD [µE m^{-2} s^{-1}])	CDW_{avg} [g L^{-1}]	vol. OPR_{avg} [mmol L^{-1} h^{-1}]	vol. CUR_{avg} [mmol L^{-1} h^{-1}]	PQ [-]
K1 (200)	3.5	0.77	0.65	1.17
K2 (200)	1.0	1.10	0.81	1.36
K3 (200)	0.5	1.37	1.25	1.10
K4 (200)	1.3	1.02	0.86	1.19
K5 (200)	0.9	1.08	0.93	1.16
K6 (800)	0.5	3.01	2.57	1.17
K7 (400)	0.5	1.97	1.74	1.13

First of all, part A of the figure shows that the stepwise PFD changes have an effect on OPR and CUR values determined from exhaust gas analysis. Moreover, it shows that after the light was switched back to the former value the cells also restored their initial OPR and CUR values or similar rates. Part B and Table 7-1 show that there is no linear correlation between average volumetric gas exchange rates and the cell density concentration at a specific basic PFD for this cylindrical LED illumination with its particular light intensity distribution (see Appendix 3D model, Figure 11-14).

For every tested steady-state, the determined CUR values are smaller than OPR values, whereas PQ is mostly around 1.1-1.2 (Table 7-1).

Highest gas exchanges rates were measured for the lowest tested cell densities for this reactor design and illumination geometries. For other types of reactor geometries like plate reactors with one-sided illumination a different OPR und CUR profile can be expected.

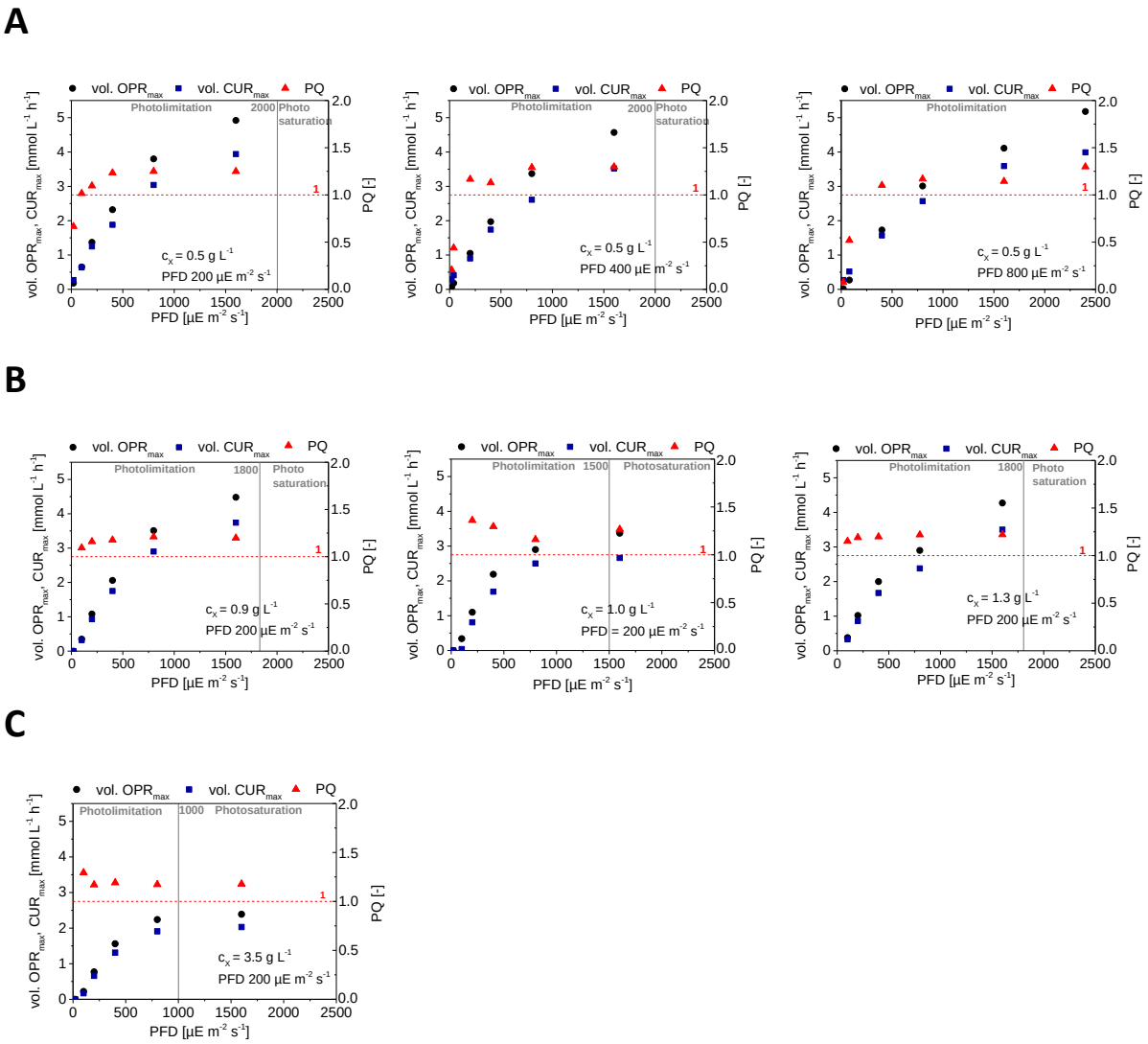

Figure 7-2. OPR, CUR and PQ values in dependence on light intensity of steps and cell density during continuous cultivations. A) Continuous cultivations at 0.5 g L^{-1} CDW for different basic illumination intensities. B) Continuous cultivations with CDW concentrations around 1 g L^{-1} at the same basic intensity of 200 µE m^{-2} s^{-1}. C). Cultivation at a CDW concentration of 3.5 g L^{-1} for a basic PFD of 200 µE m^{-2} s^{-1}.

Figure 7-2 shows maximum volumetric OPR und CUR values as well as PQ ratios in dependence on the PFD of the light intensity step change in both positive and negative direction during the continuous cultivations with cylindrical illumination.

For panel A, it can be seen that there is no linear correlation between applied light step size and gas exchange rates. Curves show the characteristic form of PI-curves for absolute PFDs for all of the three basic illumination intensities of 200, 400 and 800 µE m^{-2} s^{-1} tested for a CDW of 0.5 g L^{-1}. PQ values fall below 1 for PFDs < 200 µE m^{-2} s^{-1} indicating light limitation conditions for cylindrical illumination at a CDW of 0.5 g L^{-1} below this intensity.

For panel B and CDW values of 0.9 and 1.3 g L^{-1} identical curves are obtained. For a cell density of 1.0 g L^{-1} there seems to be an earlier saturation where PQ values increase for PFD < 200 µE m^{-2} s^{-1}. For higher cell densities of 3.5 g L^{-1} saturation is reached at lower PFDs (panel C). PQ values increase for PFDs < 200 µE m^{-2} s^{-1}.

Time constants and proportional constants Kp for light intensity changes inside the STPBR were determined based on online pH signals. By fitting the pH signal curves with Origin Software, T,63% values as time constants and Kp values (in this case corresponding to ΔpH/ΔPFD) were determined. First the cultivations with a basic PFD of 200 µE m^{-2} s^{-1} were investigated for their time constants and Kp values where also ΔpH values are plotted against cell dry weight concentrations (Figure 7-3 A-C).

Panel A shows that there is a higher variation in T,63% time constants for lower cell concentrations (in the range of 13 to 39 min for c_X < 1.5 g L^{-1}) and similar time constants (in the range of 25 to 31 min) for a higher cell concentration of 3.5 g L^{-1} in relation to the step intensity. This is based on cell shading effects for high cell densities where a change of incoming light intensity does not change the average resulting PFD within the algae suspension markedly. The only exception is for c_X = 0.9 g L^{-1} where time constants show less variation. Panel B shows pH changes in dependence on cell concentrations for the different intensity changes. A similar relation as for time constants is found for pH changes: for higher CDW the changes in pH (and therefore CO_2 uptake) are smaller than for lower cell concentrations during intensity changes. For Kp values there is a rather linear decrease with increasing cell density for light intensity steps (panel C).

In panel D, T, 63% time constants are plotted versus proportional constants Kp for light intensity steps at the same cell concentration but different basic illuminations. It can be seen, that for a basic PFD of 400 µE m^{-2} s^{-1} there is a constant relation of time constant and Kp whereas for lower and higher basic illumination intensity, time constants are dependent on Kp value.

In part E of the figure time constants are plotted versus step PFD for different cell concentrations. Curves are similar to PI-curves whereas with increasing cell concentration the influence of step intensities on time constants is less. Therefore, curves are flattened with higher CDW. This is consistent with panel A with higher cell densities based on shading effects and the resulting average PFD for light intensity steps.

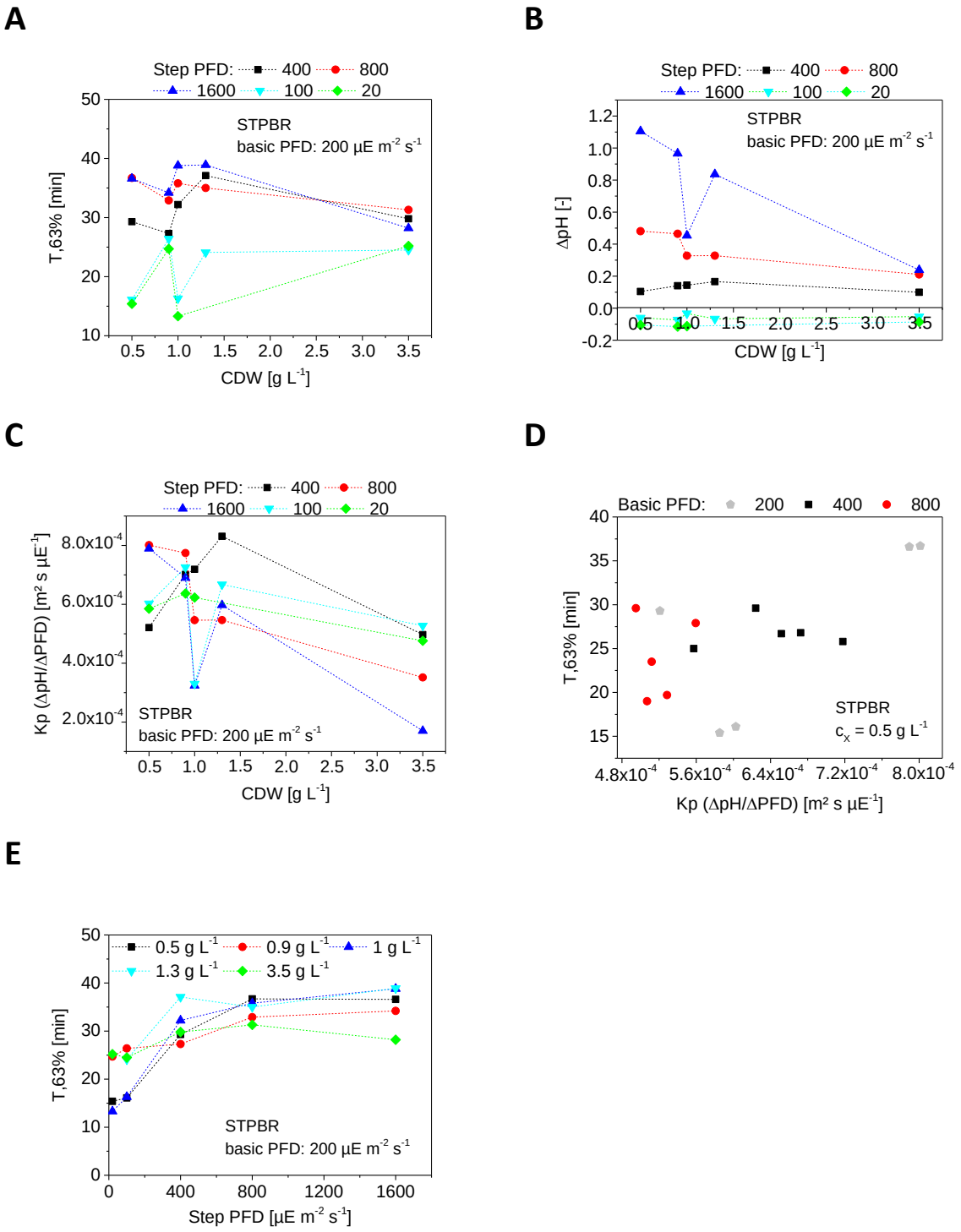

Figure 7-3. Time constants and proportional constants of light step changes during continuous cultivations with cylindrical illumination at different CDW concentrations. A) Dependence of T,63% on CDW concentration for different step changes at the same basic PFD of 200 µE m^{-2} s^{-1}. B) Relation of ΔpH and CDW for PFD step changes at a basic intensity of 200 µE m^{-2} s^{-1}. C) Relation of Kp value and CDW for different intensity step changes. D) Dependence of T,63% on Kp value for the same cell concentration of 0.5 g L^{-1} and different basic PFDs of 200, 400 and 800 µE m^{-2} s^{-1} during light intensity step changes. E) Time constants for different step PFDs and different cell concentrations and the same basic illumination intensity.

7.1.2 Bubble-free aerated membrane reactor

Further experiments with light intensity step changes were conducted in the bubble-free membrane-aerated photobioreactor to compare time constants inside this novel reactor with the ideally mixed PBR relating to its time delay. With the help of steady-state volumetric gas exchange rates CUR and OPR it is possible to scale the phototrophic compartment relating to the needs of a potential heterotrophic compartment and vice versa during the design of a life support system.

Continuous cultivations inside the membrane-aerated PBR with a gas-free liquid loop were achieved by establishing control circuits for feed and harvest flow rates. After first experiments where feed flow rate was adjusted based on online pO_2 signals which failed, the feed flow rate was set constant. The harvest flow rate was controlled, based on the online smoothed pressure signal (PI controller, P = 0.5, I = 50 min) in that form that a constant pressure inside the liquid loop was resulting. This is enabling a safe process control to avoid membrane rupture following a possible build-up of pressure from bubble formation.

After optimization of controller parameters, it was possible to achieve quasi steady-state conditions (about 100 to 200 h after start of continuous culture) where cell dry weight remained constant (in case of cultivation 1 at 2 g L^{-1}; only offline analysis possible) as Figure 7-4 A, B shows.

As in general a stable equilibrium establishes at ten times the residence time in a continuous process (here $\mu = D = 0.02\ h^{-1}$, $\tau = D^{-1} = 50$ h, time to equilibrium = 500 h), light steps were not started until a process time of 640 h and therefore 500 h after start of the continuous culture. However not for every continuous cultivation it was possible to wait for steady-state hydrodynamic conditions because of contamination risks, so that light steps were started as soon as offline cell concentration and online dissolved gas concentrations remained constant for the last 100 hours of process time. During these turbidostat cultures cells grow at a constant specific growth rate μ (for the cultivations shown between 0.009 and 0.02 h^{-1}).

Table 7-2. Gas exchange rates for steady-state phases during continuous cultivations inside the membrane reactor with different membranes for the same overall PFD and full-spectrum compared to 90/10 red/blue illumination.

Cultivation /membranes/illumination color	CDW_{avg} [g L^{-1}]	Vol. CUR_{avg} [mmol L^{-1} h^{-1}]	Vol. OPR_{avg} [mmol L^{-1} h^{-1}]	PQ [-]
C4/ TPX, Wacker 200/ ww	2.2	0.28	0.20	0.71
C5/ TPX, TPX/ ww	0.25	0.15	0.08	0.55
C6/TPX, TPX/ 90/10 r/b	0.13	0.34	0.20	0.59
C7/TPX, Wacker 200/ 90/10 r/b	0.5	0.19	0.24	1.29

Table 7-2 summarizes continuous cultivations inside the membrane-aerated reactor equipped with different membranes and for different steady-state cell densities and illumination colors for volumetric and specific gas exchange rates.

For the continuous cultivations performed during this work, there is a difference in volumetric gas exchange rates and PQ resulting from different membrane setups. Independent from illumination color, the configuration with two TPX membranes yields the lowest volumetric rates and PQ values by taking into account the different average cell densities and resulting PFD per cell. For warm-white illumination the mean volumetric CUR of the continuous cultures performed accounts to 0.22 mmol CO_2 L^{-1} h^{-1}, mean volumetric OPR to 0.14 mmol O_2 L^{-1} h^{-1}. For dichromatic illumination the vol. CUR measured was 0.27 and the vol. OPR 0.22 mmol L^{-1} h^{-1}. The mean PQ value is 0.94 and therefore higher than for full-spectrum illumination. However, as average cell densities for dichromatically illuminated cultures are lower than for warm-white illumination cultures the values are not comparable as the resulting mean PFD per cell is different.

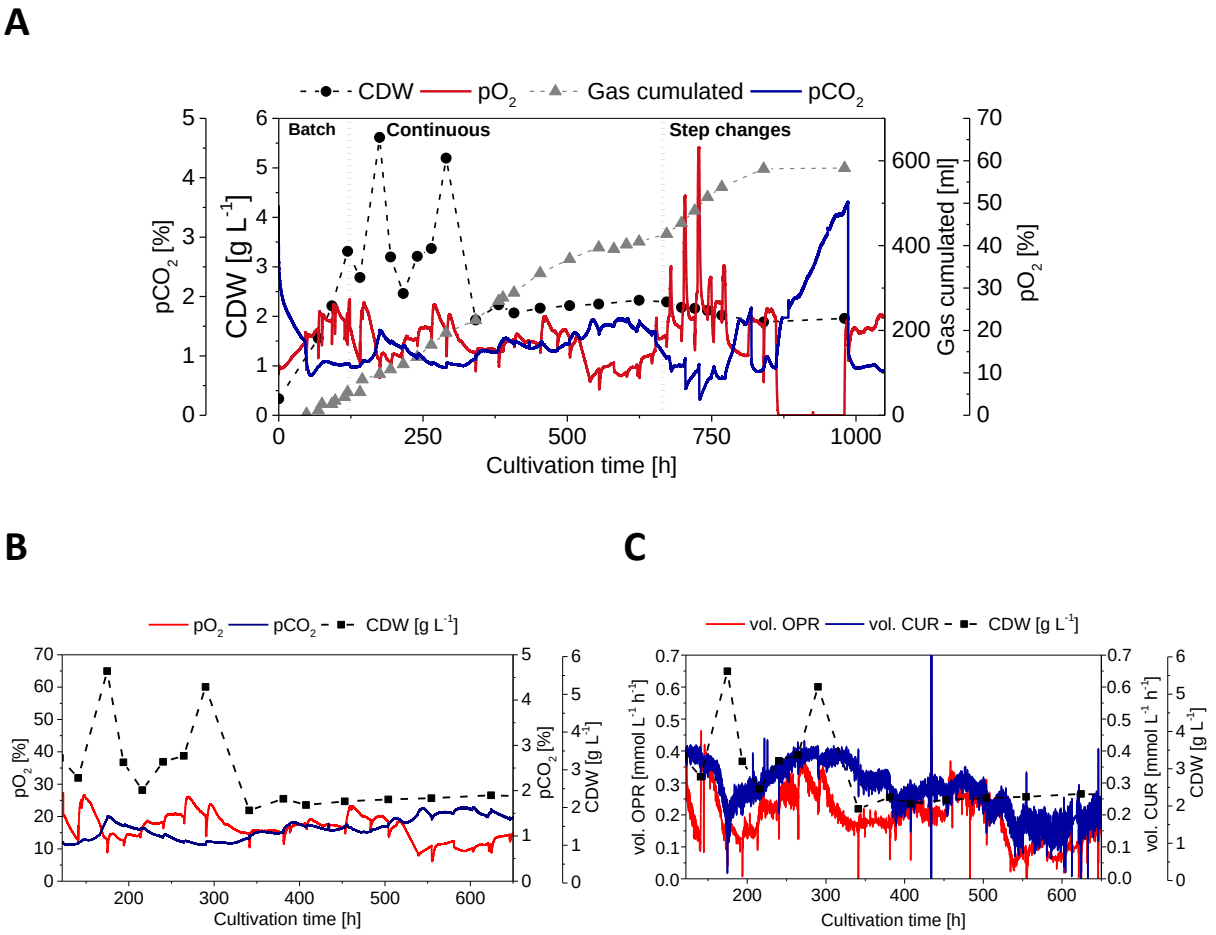

Figure 7-4. Continuous cultivation within the novel membrane photobioreactor. A) Overview of the cultivation in the MBR including batch and continuous phase with light step changes showing cell dry weight, dO_2 and cumulated gas volume produced. B) Dissolved gas concentrations, C) volumetric gas exchange rates and CDW during continuous phase of cultivation.

Light steps were started within steady-state phase of the continuous cultures according to a specific scheme (see Chapter 3.4.6, Table 3-9).

Figure 7-5 exemplarily shows dissolved O_2 concentration and calculated volumetric OPR during light intensity step changes for a continuous culture (cultivation 2 see Table 7-2) with a cell concentration of 0.25 g L^{-1}. Volumetric oxygen production rates were determined from dissolved O_2 concentration and by knowing oxygen transfer rates.

As the figure shows, during the different light intensity step changes in both positive and negative direction, the same basic volumetric O_2 production rate (here, vol. OPR_{avg} = 0.14 mmol O_2 L^{-1} h^{-1}) was reinstalled within the same duration as the new step equilibrium was reached. This was consistent for all continuous cultivations and light intensity step changes at different cell concentrations performed within the MBR.

This shows that for perturbations in form of changing lighting conditions, initial gas exchange rates can be achieved when basic illumination intensity is reinstalled. Future work shall focus on how long these perturbations can be exerted on algal cultures before the system can not be brought to initial gas exchange rates any more and how system balance is affected in case of contaminants.

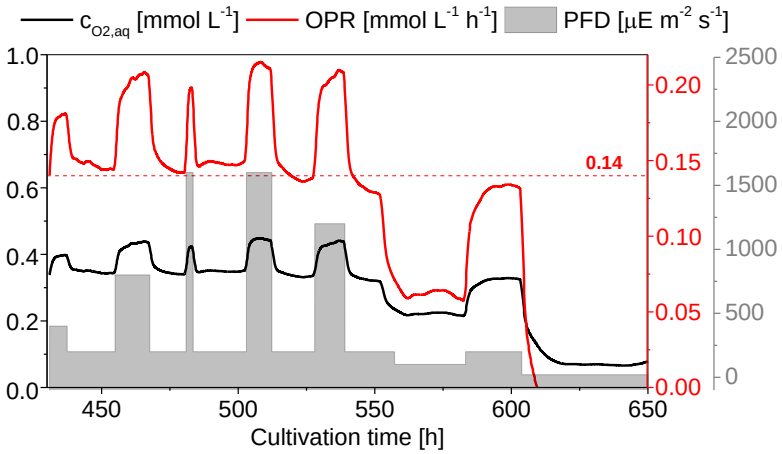

Figure 7-5. Light intensity step changes during steady-state phases of continuous cultivations inside the membrane reactor. Dissolved O_2 concentration and volumetric OPR during light step changes for a steady-state cell concentration of 0.25 g L^{-1}.

For every light step exerted a new equilibrium OPR value can be determined. By plotting these values in relation to step light intensity kinetic curves are obtained.

Table 7-3 summarizes volumetric OPR and CUR values for continuous cultures at different cell densities in steady-state phase.

Table 7-3. Volumetric CO_2 uptake and O_2 production rates for light intensity step changes in the membrane reactor. Cultivation C4: c_X = 2.2 g L^{-1}, cultivation C5: c_X = 0.25 g L^{-1}, cultivation C6: c_X = 0.13 g L^{-1}, cultivation C7: c_X = 0.5 g L^{-1}. Cultivation C4, C5: warm-white, cultivation C6, C7: 90/10 red/blue illumination.

Step to intensity [µE m^{-2} s^{-1}]	vol. OPR_{max} [mmol L^{-1} h^{-1}]				vol. CUR_{max} [mmol L^{-1} h^{-1}]			
	C4	C5	C6	C7	C4	C5	C6	C7
20	0	0	0	0	0	0	0	0
100	0.17	0.06	0.15	-	0.13	0.1	0.29	-
200	0.20	0.08	0.20	0.24	0.28	0.15	0.34	0.186
300	-	-	0.30	0.45	-	-	0.37	0.38
400	0.61	0.24			0.45	0.33		
800	1.29	0.27			1.14	0.29		
1200	-	0.28			-	0.31		
1600	1.47	0.31			1.48	0.33		

Figure 7-6 shows kinetics for volumetric O_2 production and CO_2 uptake rates for different cell densities in steady-state phases for light intensity steps and warm-white as well as dichromatic illumination.

These data can be used to design a phototrophic process inside this membrane reactor with respect to desired gas exchange rates at a specific energy input in form of illumination intensity and light color. Concerning volumetric OPR values in relation to light intensity steps, there is a saturation at a light intensity of 1600 µE m^{-2} s^{-1}. With this specific kinetic curve it is possible for this MBR system to determine the necessary light intensity for irradiance via a desired volumetric OPR at a given cell density and known k_L values of the membranes to achieve a maximal O_2 production.

In literature there are reported values for gas exchange rates within a membrane-aerated photobioreactor which can be compared to the presented membrane reactor system. Another photobioreactor primarily designed and implemented for CELSSs is described by Javanmardian and Palsson (1992). Experiments, both in batch and continuous mode were run with *C. vulgaris*. The gas exchange for O_2 and CO_2 is realized by separate external hollow-fiber cartridges operating under reduced (in case of O_2 removal) and increased (for supply of CO_2) pressure. So, this approach is not purely diffusion-based, in contrast to the system presented within this work. During steady-state conditions of continuous *C. vulgaris* cultures ($c_X = 4 \cdot 10^8$ cells ml^{-1}, D = 0.15 d^{-1}) volumetric OPRs

achieved accounted for 5 mmol O_2 L^{-1} h^{-1}. Highest volumetric OPR during continuous cultures inside the MBR was about 1.5 mmol O_2 L^{-1} h^{-1}. However, during cultivations presented within this work inside the MBR, the maximal cell density was only about 2 g L^{-1}.

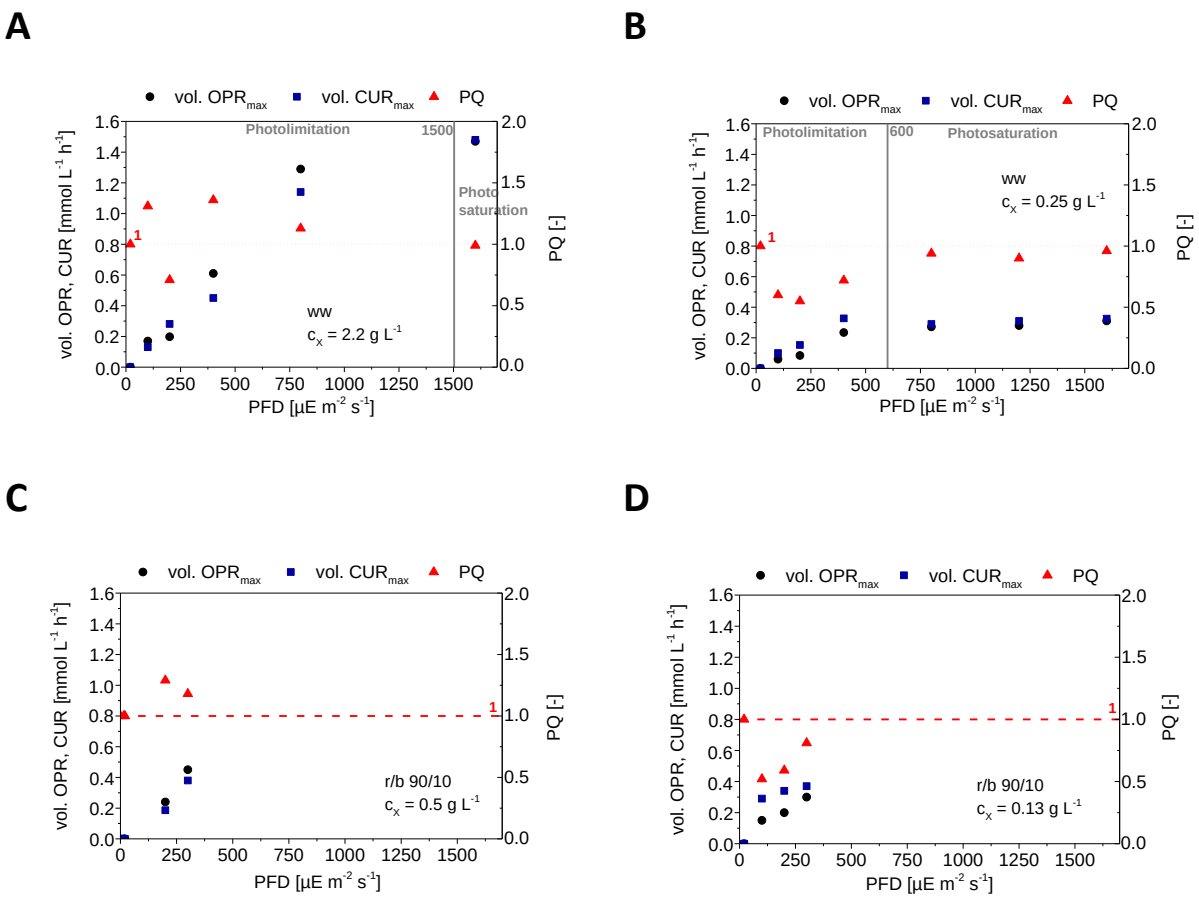

Figure 7-6. Gas exchange rate kinetics for light intensity step changes inside the membrane reactor for different steady-state cell concentrations. A) Volumetric gas exchange rates as well as PQ for continuous cultivation 1 inside the MBR at c_X = 2.2 g L^{-1} for light intensity step changes for warm-white light. B) Gas exchange rates and PQ for continuous cultivation 2 at c_X = 0.25 g L^{-1} inside the MBR during intensity steps for warm-white light. C) Gas exchange rates for continuous cultivation 4 at c_X = 0.5 g L^{-1} and 90/10 red/blue illumination. D) Gas exchange rates for continuous cultivation 3 at c_X = 0.13 g L^{-1} and 90/10 red/blue illumination.

Also time constants were determined for each of the light steps conducted in the membrane reactor (Table 7-4). In contrast to step changes in the STPBR, where time constants were determined from pH signal (indirectly measuring CO_2 uptake), in this case time constants were determined based on the pO_2 signal. Time constants determined by this means can be used to adjust controller parameters, where the dissolved O_2 concentration is the control variable and light intensity the correcting variable. Furthermore, these time constants are used to compare the different reactor systems.

Table 7-4. Time constants (T, 63%) determined for light intensity step changes in the membrane-aerated photobioreactor during steady-state phases for different cell densities under warm-white and red/blue 90/10 illumination with a basic PFD of 200 µE m^{-2} s^{-1}. C4: ww, 2.2 g L^{-1}; C5: ww, 0.25 g L^{-1}; C6: r/b 90/10, 0.13 g L^{-1}; C7: r/b 90/10, 0.5 g L^{-1}.

Light step to intensity [µE m^{-2} s^{-1}]	Time constant T, 63% [min]			
	C4	C5	C6	C7
300	-	-	73±7	-
400	88	74	-	-
800	45	82	-	-
1600	101	37±6	-	-
1200	-	84	-	-
100	121	153	89	-
20	100	190	319	27

Figure 7-7 shows results of light intensity step changes with respect to time constants and proportional constants of the system in dependence on step PFD and steady-state cell concentration. For continuous cultivations inside the membrane reactor two lighting colors, warm-white and 90/10 red/blue illumination was applied. As the possible power input for red LEDs was limited, it was only possible to increase the overall PFD of the red/blue combination to 300 µE m^{-2} s^{-1}.

Panel A shows time constants T,63% for step PFDs applied for different cell concentrations for warm-white and dichromatic illumination. As this graph shows, in contrast to the STPBR, there is no PI-curve resulting, but a rather exponential decay. In quantitative terms, time constants measured for the membrane reactor are in the range of 27 to 319 mins, showing a huge variation, whereas an average time constant determined for these experiments accounts to 105 min, which is a factor 3.9 higher than for the ideally mixed reactor.

Panel B displays time constants in relation to cell concentration for different step PFDs. Compared to the results determined for the ideally mixed reactor, a similar relation is shown: the least variation in time constants is measured for the highest cell density inside this plate type reactor geometry for one-sided illumination.

In panel C, the change in pO_2 in relation to cell concentration for the different intensity steps is shown. Here, the highest variation is shown for the highest cell concentration. This is resulting from specific OPR values and actual number of cell producing O_2.

Panel D shows Kp values as $\Delta pO_2/\Delta PFD$ in relation to cell concentration for the different step PFDs. Values show a higher variation as for the homogenously mixed reactor, where a local minimum is detected for a cell concentration of 0.25 g L^{-1}.

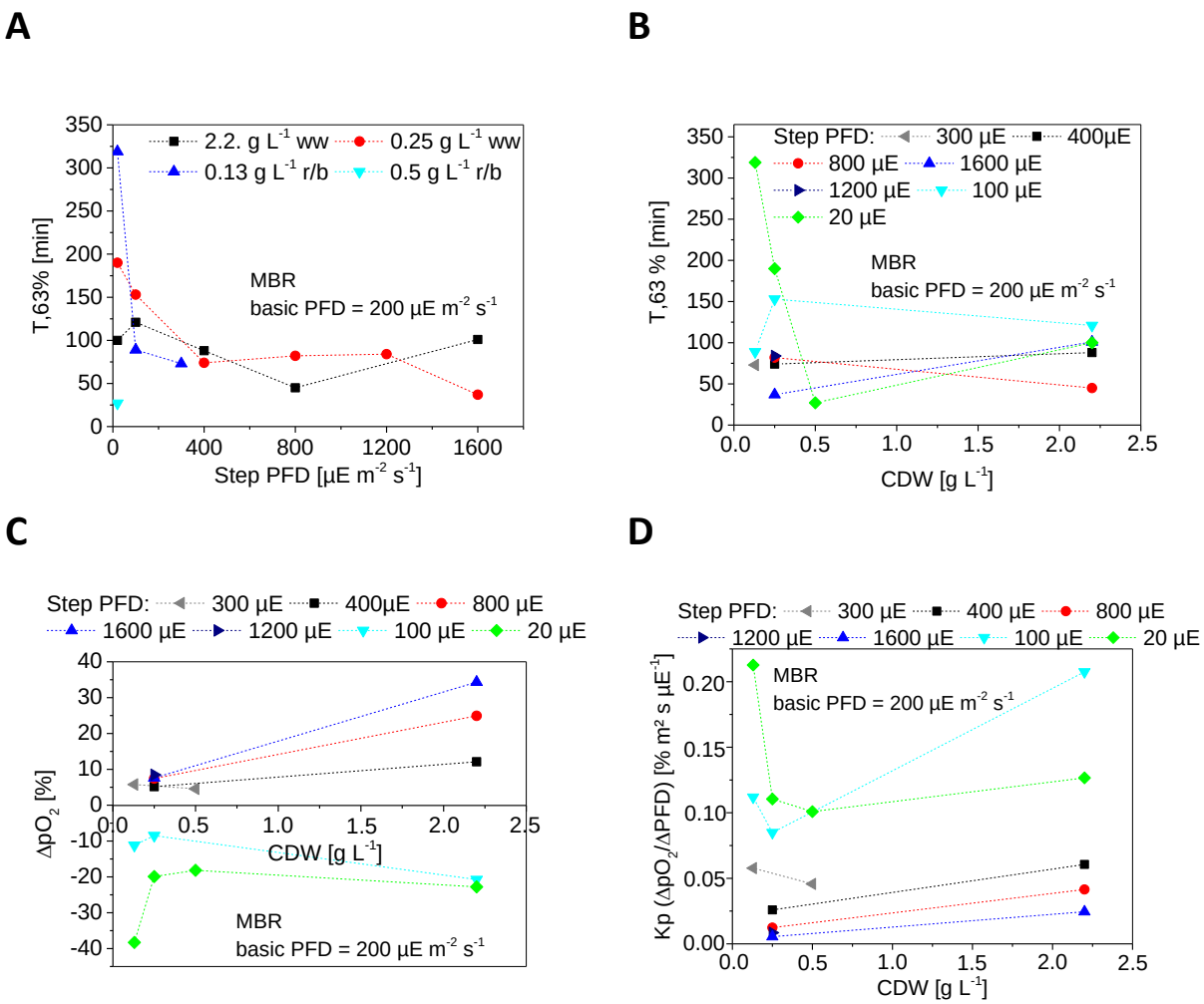

Figure 7-7. Time constants and proportional constants for light intensity step changes during continuous cultivations inside the membrane reactor. A) Time constants T,63% in relation to step PFD for different cell concentrations and for ww and for 90/10 red/blue illumination. B) Time constants in relation to cell concentration for the different step PFDs. C) Change of pO_2 in relation to cell concentration for the different step PFDs. D) Kp values in dependence on steady-state cell concentration for the different step PFDs.

A comparison with time constants of identical light intensity steps in the ideally mixed bubble-aerated STPBR (Figure 7-3) shows that time constants measured with the MBR system are on the average 4 times higher than those determined with the ideally mixed system (see Figure 7-8). This is a result from a better mixing and a higher gas transfer for bubble aeration. However, the differences of both systems relating to time delay are smaller than expected. Highest time delay measured during this work was 3.6 h relating to gas exchange.

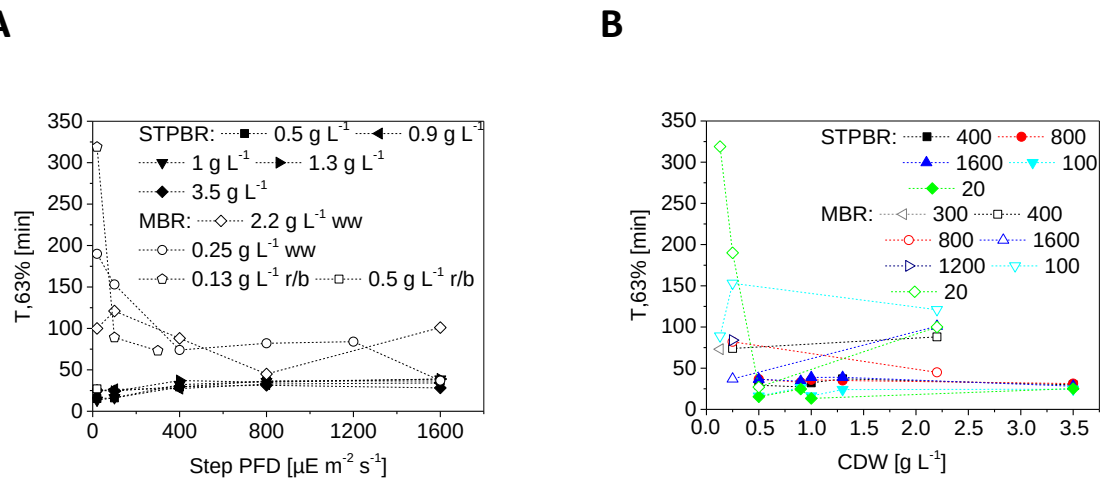

Figure 7-8. Comparison of time constants determined inside the homogenously mixed reactor with cylindrical illumination and the membrane reactor with one-sided illumination. A) Time constants T,63% in relation to step PFD for both reactor systems. B) Time constants T,63% in relation to cell concentration for both reactor systems.

7.2 Influence of light step changes on pigment concentration

During light intensity steps also the specific pigment content of the CC-1690 cells was analyzed. For continuous cultivations inside the bubble-aerated 1.8 L photobioreactor light step changes were exerted every 24 hours and samples for pigment analysis were taken just before the next step change was performed. In case of the membrane-aerated PBR, where gas transfer rates are smaller, light intensity step changes were hold longer as a new equilibrium was reached later, before intensity was switched to basic.

Figure 7-9 A, B shows effects of light intensity steps on specific pigment concentration in the bubble-aerated photobioreactor with cylindrical illumination. Part A exemplarily shows specific pigment contents for the continuous cultivation 4/5 with two steady-states at CDW concentrations of 1.3 and 0.9 g L^{-1} in the bubble-aerated photobioreactor with cylindrical illumination. For positive light intensity changes, there is a tendency for decreasing specific pigment contents and for negative light intensity changes for increasing values. These adaptations of photosynthetic apparatus can be monitored 24 h after the intensity change.

Part B sums up the results for the specific pigment contents for the different CDW concentrations inside the mentioned photobioreactor. As this graph shows, specific pigment concentrations do not change more than 10% during light intensity step changes for low (here c_X = 0.5 g L^{-1}) and high (here c_X = 3.5 g L^{-1}) CDW concentrations. For steady-state cell densities of 0.9 to 1.3 g L^{-1} inside this reactor type, intensity step changes have an influence on specific pigment concentrations where steps to higher PFDs lead to decreased pigment contents and steps towards lower intensities are followed by an increased specific pigment concentration.

As a result, it is shown that *C. reinhardtii* CC-1690 cells react, under steady-state conditions inside the ideally mixed reactor, within 24 hours to light intensity step changes by adaptation of their specific pigment content to the respective average light intensity conditions. Even relatively short changes in light intensity (here 1.5 hours) influence the cellular pigment contents. However, these effects are less pronounced for high or low CDW concentrations for this cylindrical illuminated photobioreactor which is based on the specific light distribution curve resulting from the cylindrical illumination geometry for different cell densities. For low cell densities the effect of overlapping light beams and a resulting increase of average PFD in suspension is prominent, whereas for very high cell densities with shading effects a change of incoming PFD leads to a smaller change of average light intensity per cell.

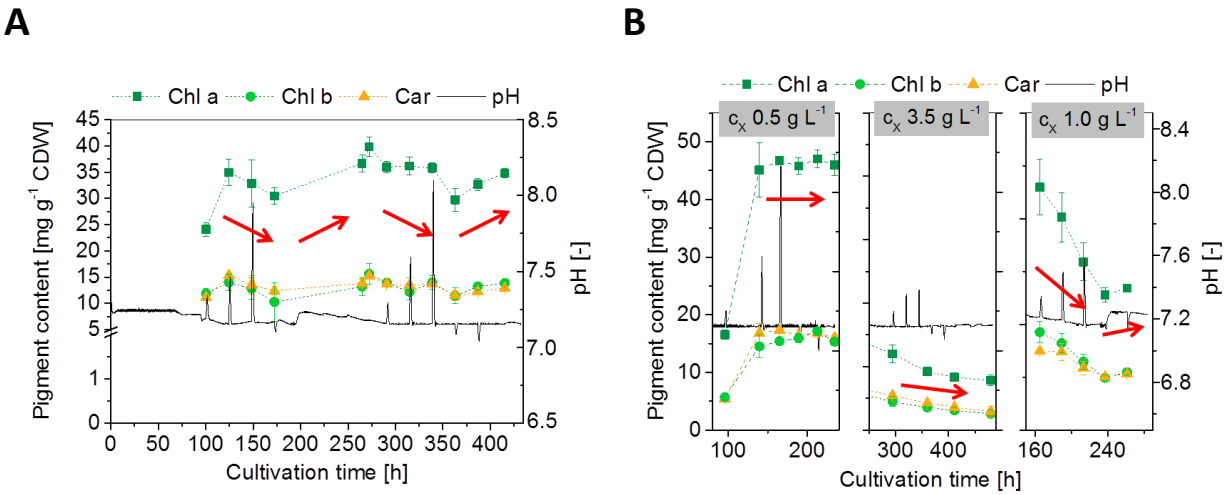

Figure 7-9. Effects of light intensity steps on specific pigment concentration for cells cultivated inside the bubble-aerated reactor with cylindrical illumination. A) Specific pigment concentrations for a continuous cultivation inside the bubble-aerated photobioreactor with cylindrical illumination and cell densities of 1.3 g L^{-1} (first four step changes) and 0.9 g L^{-1} (last five step changes). B) Comparison of effects of light step changes on specific pigment contents in the bubble-aerated photobioreactor for different steady-state CDW concentrations at the same basic PFD of 200 µE $m^{-2}s^{-1}$.

Figure 7-10 shows pigment composition in response to light intensity step changes for the membrane-aerated photobioreactor with one-sided illumination. Different cell densities during steady-states and two different light colors, warm white and 90/10 r/b were tested. Also for the single-side illuminated membrane PBR there is an influence of light intensity step changes on specific pigment concentrations. These influences are highest for the lower CDW values (here CDW of 0.13 and 0.24 g L^{-1}) tested (part A and B). In contrast, for the higher cell density of 0.5 g L^{-1} tested (panel C), the influence of light intensity steps on the cellular pigment content is less pronounced. In contrast to a cylindrical illumination, where there is hardly an effect on pigment content for low cell densities, the highest influence of light steps on pigment concentration is found for the lowest cell concentrations in case of the one-sided illumination and a plate reactor geometry. However, for higher cell concentrations inside the MBR no pigment analysis was performed but it can be expected that there is

only less influence of light steps on specific pigment content which is based on increased shading effects than for lower cell concentrations.

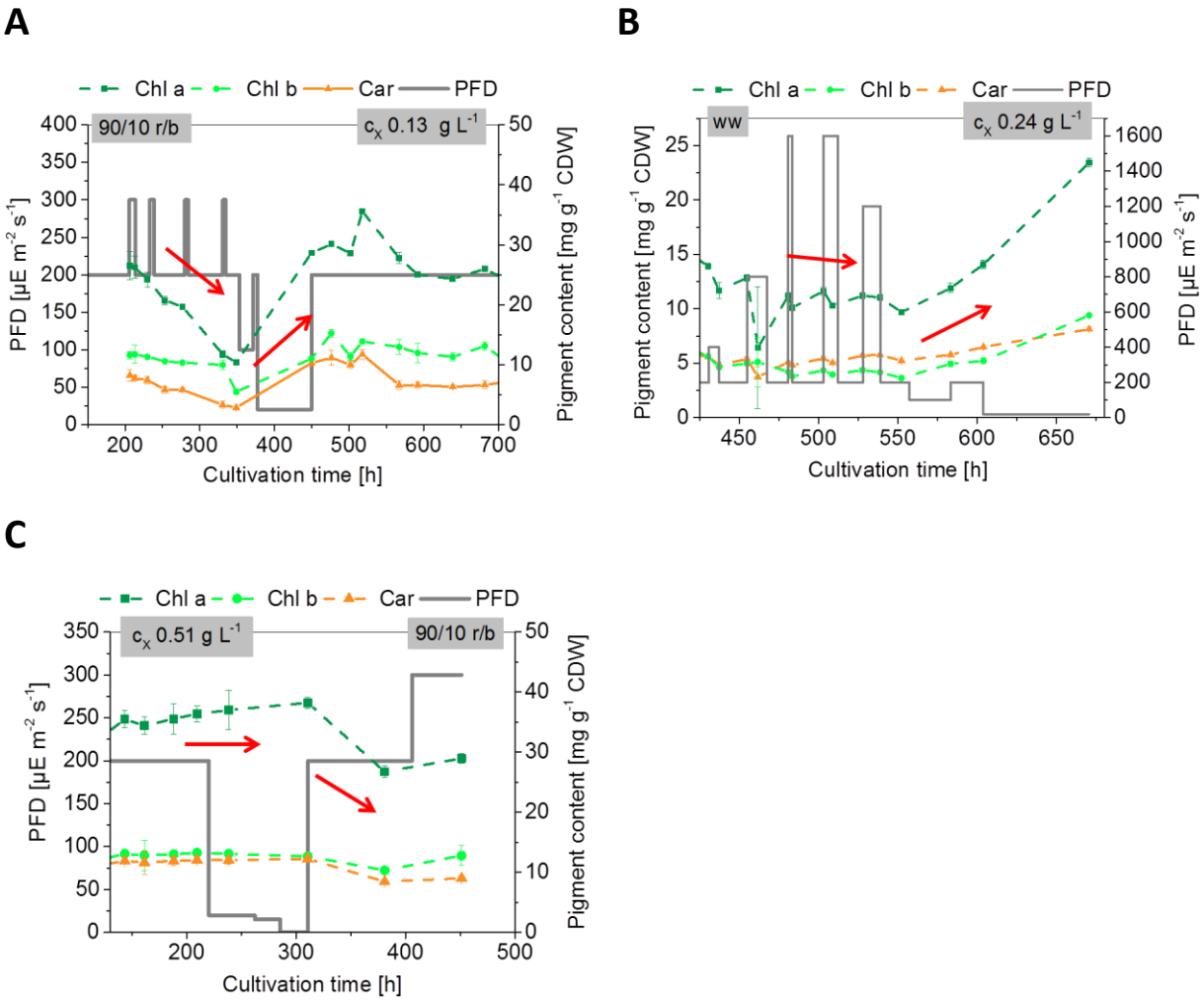

Figure 7-10. Effects of light intensity steps on specific pigment content for cells cultivated inside the membrane reactor. Effects of light step changes on specific pigment contents in the membrane-aerated PBR for different steady-state CDW concentrations at 200 µE m^{-2} s^{-1} basic illumination for 90/10 r/b and ww light color. A) Steady-state with a cell density of 0.13 g L^{-1} and 90/10 red/blue illumination. B) Steady-state with a cell density of 0.24 g L^{-1} and warm-white illumination. C) Steady-state with a cell density of 0.51 g L^{-1} and 90/10 red/blue illumination.

In general, as gas transfer rates inside the membrane-aerated PBR are smaller than for the bubble-aerated reactor, the establishment of a new equilibrium concerning dissolved gas concentrations and pH took longer than in the reactor with bubble-aeration and ideal mixing conditions. In more detail, it can be seen that especially for negative step changes, the duration for a new equilibrium for specific pigment content is longer than for positive step changes. However, adaptation time ranges of pigment contents are similar for these two reactor and illumination geometries.

All these results for the different reactor geometries with their respective light distribution curves indicate that *C. reinhardtii* CC-1690 cells are adapting quickly (for gas exchange rates within

minutes, for pigment contents and substrate uptake rates within 24 h) to stepwise light intensity changes even if these perturbations were only exerted for short times (1.5 hours for the bubble-aerated photobioreactor). Specific pigment contents adapt to the average light intensity inside the reactor for both systems tested.

7.3 Summary of results for long-term stability of continuous cultures

Experiments with continuous operation mode were run in three different reactor geometries and systems: plate type reactors with bubble-aeration and only pneumatic energy input, an ideally mixed stirred tank photobioreactor with bubble-aeration and the membrane-aerated plate type photobioreactor with external mixing with means of a bypass-integrated pump. Continuous cultivations inside the homogenously mixed STPBR as well as continuous cultivations inside the membrane reactor were specifically analyzed for their gas exchange rates and the effect of perturbations in form of light intensity step changes in both positive and negative direction during steady-state phases with constant cell and dissolved gas concentrations. Furthermore, adaptation of pigment content and time constants were of interest.

In case of the ideally mixed and cylindrically illuminated reactor, stable steady-state CO_2 uptake and O_2 production rates with only minor fluctuations were installed within a cell concentration range of 0.5 to 3.5 g L^{-1}, respectively. After light intensity step changes (with a maximal ΔPFD of 1600 µE m^{-2} s^{-1}, an absolute PFD of 2400 µE m^{-2} s^{-1} and a minimal PFD of 20 µE m^{-2} s^{-1}) the original volumetric gas exchange rates were reinstalled with the same time constants as the new equilibrium was established. Kinetic curves (PI-curves) were recorded which can be used for comparison with other systems. Time constants (in form of T,63%) calculated for the system responses to those light intensity step changes are in the range of 13 to 39 min.

In the case of the membrane reactor with plate geometry and one-sided illumination also constant gas exchange rates were reinstalled after the PFD was switched back to the initial value. The determined PI-curves can be used to adjust the cell concentration needed to obtain a desired gas exchange rate of the photomodule within a life support system. Time constants measured (also in form of T,63%) showed a higher variation as in the well mixed bubble aerated reactor and were in the range of 27 to 319 mins. Similar to the STPBR, the least variation in time constants is measured for the highest cell densities inside this plate type reactor geometry for single-sided illumination. In total, time constants measured with the MBR system are on the average 4 times higher than those determined with the ideally mixed system.

Concerning adaptation of pigment contents during light intensity steps, for both systems it was shown that there are changes in the cellular pigment content in response to the light intensity steps, detectable within 24 h after this perturbation was performed. That implies that cells are adapting quickly (for gas exchange rates within minutes, for pigment contents and substrate uptake rates within 24 h) to

stepwise light intensity changes even if these perturbations were only exerted for short times (1.5 hours in case of experiments within the bubble-aerated photobioreactor). Cells adapt their pigment concentration to the average light intensity present in the reactor at a specific time.

For a photomodule within a life support system these results indicate that, if perturbations in form of light intensity changes are acting on the photosynthetic cells, the culture is able to restore its initial gas exchange rate under the conditions of an axenic culture and with no other fatal disturbances.

Future work should focus on testing the restoration capacity of photosynthetic activity for longer dark periods ($0 \leq I_0 < I_c$) and for the presence of contaminants. However, there still is a need to design phototropic modules with devices enabling a re-inoculation of the system in case of failure and a certain amount of photomodules running in parallel for redundancy.

Future experiments should also reveal the exact relation of time constants for pigment adaptation and times of abiotic changes, for example light intensity described by Deborah numbers (Storhas 1994). This is also relevant for outdoor microalgal processes with changing light conditions as cellular pigment content and composition directly changes extinction coefficients which in turn changes light penetration at a given wavelength composition of incoming light.

8 ModuLES-PBR: results from flight and ground experiments

8.1 ModuLES-PBR concept

In this subchapter the basic concept of the ModuLES-PBR system with respect to the special requirements of space application of this photomodule is outlined. A first idea of this concept is described earlier in the theoretical section (2.1.1.2).

Based on the goal to develop a photobioreactor working with maximal energy efficiency and minimal mass with long-term stability under microgravity conditions, there are several specifications and requirements which are resulting from this primary goal:

- A high biomass concentration
- No (or as little as possible) dark reactor zones and gradients
- A continuous process with a closed medium loop and a biomass harvesting module
- Bubble-free aeration
- Energy-efficient artificial illumination

From these requirements a first concept for the ModuLES-PBR system was developed.

Concerning the reactor geometry a plate-type reactor was used for designing the ModuLES-PBR which was realized in form of a mini-raceway reactor with meander-shape that can be illuminated either from one side or from both sides (design shown under 3.3.6.2). To reach a maximal energy efficiency, a double-sided illumination with a highly-efficient red/blue 90/10 illumination shall be chosen. For this meander-shape reactor form, a gradient free aeration is guaranteed by a double-sided membrane aeration in form a flat sheets for CO_2 supply and O_2 removal. Calculations at an early stage confirmed the assumption that the use of flat sheet membranes ensures CO_2 transfer rates at given gas compositions and specific transfer area to meet the CO_2 requirements of the algae at a given irradiation intensity. A continuous process technique is chosen where a biomass harvesting module can be connected to the reactor periphery.

As a constant average light intensity per cell, a constant cell density and constant nutrient levels are essential for a long-term stable phototrophic module fulfilling life support tasks, a continuous culture technique was chosen as a batch or fed-batch process mode is not applicable. Concerning energy efficiency the photomodule has to work at the peak performance which is possible implying that irradiation and aeration work with maximal energy efficiency.

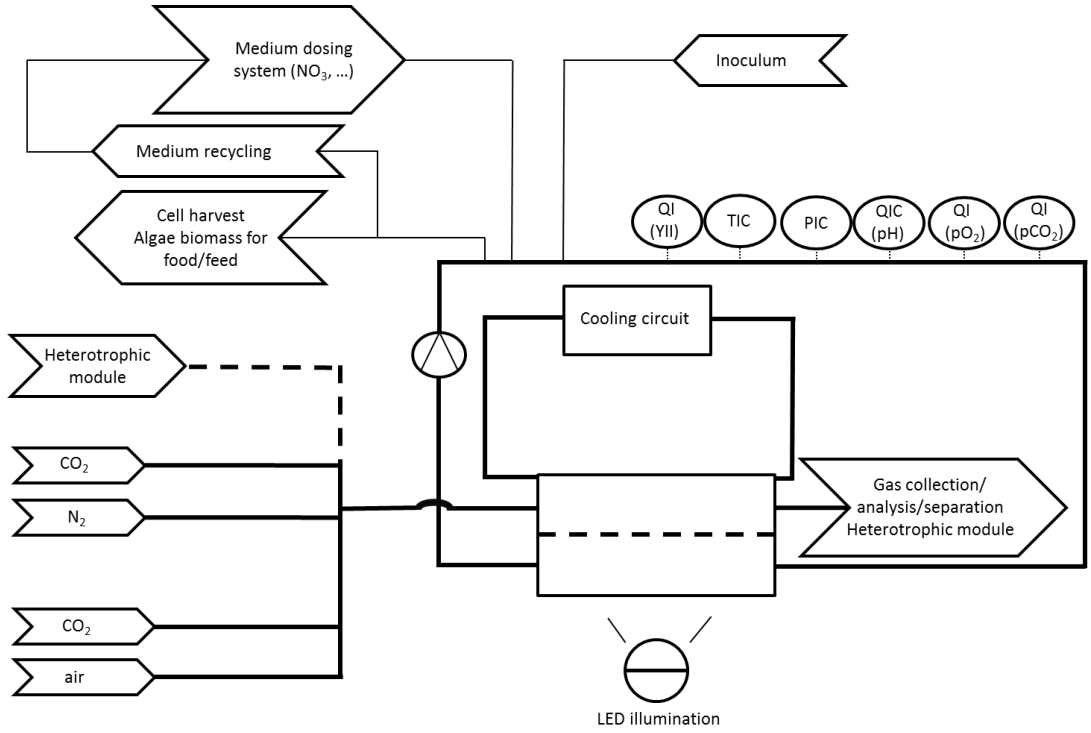

Figure 8-1. Scheme of the first ModuLES-PBR concept. TIC: Temperature indicate control; PIC: pressure indicate control; QI: Quality indicate for pO_2, pCO_2, YII; QIC: Quality indicate control for pH.

In this early stage of development of the ModuLES-PBR (see also chapter 2.1.1.2 and Figure 2-2) one-sided artificial illumination with either warm-white LEDs or dichromatic red/blue LED lighting was used.

For the first parabolic flight campaign, illumination was achieved by warm-white LED illumination whereas in a second flight campaign, red (emission peak at 680 nm) and blue LEDs (peak at 450 nm) were used for dichromatic illumination at a ratio of 90/10 red/blue photons (compare to LED specification in 11.4.1).

The two parabolic flight campaigns aimed at verifying the functionality of the reactor and all the hardware including the optical sensors under the conditions of a changing gravity field and a reduced pressure and therefore reduced gas solubilities. Furthermore, first results related to algae physiology should be collected to be able to choose if a long-term experiment under microgravity conditions, in form of a satellite flight, is promising.

Details of this concept and results from two parabolic flight campaigns were presented at the 65th International Astronautical Congress, Toronto, Canada (Podhajsky 2014).

8.2 Results from parabolic flight campaigns and ground tests

In this chapter, results and discussion are provided on experiments with the ModuLES-PBR during two parabolic flight campaigns and a ground test in form of a continuous cultivation with simulation of one flight day (Podhajsky 2014). As a first step in the ModuLES concept, after construction of the ModuLES-photobioreactor, the reactor was tested and characterized during cultivations in parabolic flights and on ground. Major criteria that have to be fulfilled are energy efficiency of the whole system with clearly defined in- and outputs. Maximum gas exchange rates at low energy requirements of the system as well as the optimization of the closure-level of the nutrient loop are in the focus for the design of the system.

The experiments during the parabolic flight campaigns were conducted in order to verify the structural and functional design of the PBR as well as to analyze and control physiological parameters of the algae. During the first parabolic flight campaign the system was not yet equipped with a biomass harvesting unit, which was integrated for the second campaign.

The main scientific objectives of the flight campaigns and the ground tests were the analysis of the applicability and effectiveness of the developed PBR under conditions of altered gravitational forces as well as ground conditions. Experiment analysis involves the determination of oxygen production rates with respect to the different gravity as well as flight conditions. Cultivation data acquired during flight campaigns is compared to a ground control cultivation to elucidate possible effects on photosynthetic activity of the algae by means of chlorophyll fluorescence measurements as well as O_2 production rates.

Analysis at the transcriptome level for certain marker genes indicating stress conditions was accomplished by project partners from the Ruhr-University-Bochum, Institute of Photobiotechnology. A harvesting unit, used for biomass filtration and media recycling constitutes the interface between the PBR and the biomass user. Parameters of this filtration unit were tested and adapted to the varying gravity conditions by project partners from University of Applied Sciences Bremen, Institute of Bioprocess Engineering.

8.2.1 Results from parabolic flight campaigns

In total two parabolic flight campaigns with four and three flight days for campaign one and two, respectively, with each a minimum of 30 parabolas were conducted to test the developed PBR and collect first experimental data. Differences between those two flight campaigns were the setup of the ModuLES-PBR: for the first campaign in September 2013 the PBR and the periphery was used without the filtration unit. Illumination was realized with warm-white LEDs at a photon flux density of 200 µE m^{-2} s^{-1}. For the second flight campaign the reactor was equipped with dichromatic red/blue illumination (peaks at 680 and 450 nm respectively). By manual control the intensities were set to a molar ratio of 90 red to 10% blue photons where the overall PFD could vary between 0-300 µE m^{-2} s^{-1}.

The setup included the filtration system which enabled a concentration of algae biomass in one bag and the collection of cell-free medium in another bag. This can be seen as first step towards a future closed-loop media recycling which is needed for long duration space missions. The software was updated for the second campaign enabling more variability of illumination intensity (by manual control) and saturation pulse frequency within PAM fluorescence measurements.

In the following sections selected results from these two parabolic flight campaigns testing the novel photobioreactor concept for microalgae cultivation under space flight conditions are depicted.

8.2.2 First parabolic flight campaign

In total four flight days with each 31 parabolas were performed whereas on three flight days the system was operated under chemostatic conditions, in this case characterized by a constant flow rate corresponding to the maximum specific growth rate μ_{max} for the applied PFD of 200 µE m^{-2} s^{-1} which corresponds to a dilution rate D of 0.08 h^{-1}. Hence, for continuous cultivations with the ModuLES-PBR for parabolic flights the flow rate was set constant and was not adjusted based on a limiting substrate. In the following the term chemostat is defined as outlined for the cultivations mentioned. Chlorophyll fluorescence via PAM measurements was recorded every 5 s.

This first flight campaign aimed at testing the complex PBR-approach. During the flights the system fulfilled its purpose as well as the scientific requirements with need for improvement relating to the sampling unit and post-flight detected leakages in the gas loop (gas exchange loop for CO_2 supply). A high signal-to-noise ratio was resulting from the fact that the standardized commercial sensors in the airflow were operating in their lower range. However, the collected data enabled first scientific results which, as a first evaluation, led to the system improvement for the second parabolic flight campaign.

Data of the last flight day of this campaign is exemplarily shown, where the reactor system was running in a chemostat mode. An overview of the flight days of this campaign is given in the methods part in 3.4.7.

Figure 8-2 shows most important sensor data from the liquid and gas loop of the ModuLES-PBR during the fourth flight of the first parabolic flight campaign, where the system was run in chemostat mode. Panel A depicts correlated cell dry weight concentrations, based on data from OD_{750} sensors located at different positions in the liquid flow. The sensor at the entry of the PBR recorded different signals from the other two throughout the whole flight. Reasonable values are shown by the other sensors at the exit of the PBR and at the entry of the bypass pump, verified by pre- and after flight analysis of cell dry weight concentration (gravimetric method) of the algae suspension, which accounts for almost 0.7 g L^{-1}. Slight oscillations of the sensor data result from a dilution effect of fresh media (caused by chemostat action and pH control) which was reinforced by the characteristic plug flow inside the reactor geometry. The deviation from the sensor at the entry of the PBR to the others

may either be due to cell adherence at some points inside the liquid loop or calibration. Data proves that cells were not washed out during the chemostat of approximately 3 hours duration. Cell dry weight concentration remained constant towards the end of the flight at around 0.65 g L^{-1}. However, a time period of three hours of chemostat conditions could not change cell density at this concentration present in a way that changes would have been expected during this short time dilution.

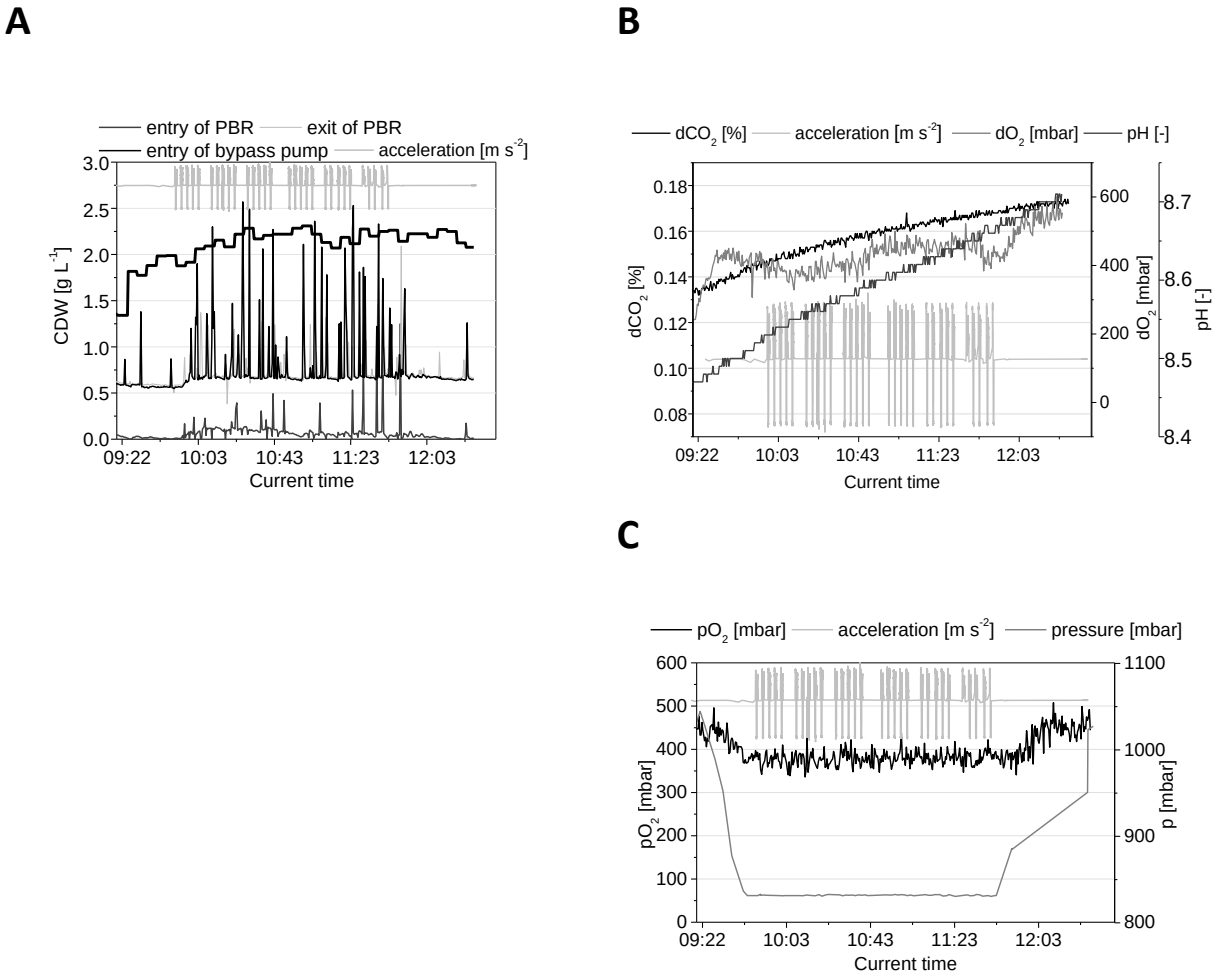

Figure 8-2. Sensor data of flight day four of the first campaign of gas and liquid loop of the ModuLES-PBR run in chemostat mode. A) Course of correlated cell density as cell dry weight CDW concentration during flight four. Three optical density probes were installed at different positions within the system: OD sensor 1 at the PBR entry, sensor 3 at the exit of the PBR, and sensor 2 at the entry to the bypass peristaltic pump. CDW values were derived from OD signals via a calibration factor. Parabolas are indicated as acceleration shown in light grey. B) Profile of dissolved CO_2 (dCO_2) in %, dissolved O_2 (dO_2) in mbar as well as pH within the algae compartment. C) Profile of oxygen partial pressure (pO_2) and pressure inside the gas collection loop for O_2 removal; Podhajsky (2014).

Panel B shows the profile of gas concentrations in the liquid loop as well as the pH within the algae compartment during the flight. The sensor measured an increase of dissolved CO_2 concentration from 0.12 to 0.18% at the end of the flight which shows the transfer of CO_2 from both gas compartments into the liquid compartment across the membranes driven by the concentration gradients. However, the desired dissolved CO_2 concentration of 1% inside the liquid loop was not reached which can be

explained by the insufficient flushing time for the gas loops before the flight started. The reason that a carbon dioxide uptake by the cells (decrease of dCO_2 concentration) cannot be seen from the recorded sensor data during the three hour flight is that the CO_2 transfer rate (CTR) across the membrane exceeds the CUR. Concerning the dissolved oxygen concentration in the algae loop an increase from atmospheric concentration up to 600 mbar towards the end of the flight was recorded. The sharp increase at 09:20 correlates with the switch from battery power to airplane power (nominal mode with full illumination intensity). Here, no net decrease of dO_2 caused by transfer of oxygen across the membrane into the gas collection loop can be seen from data as it is surmounted by the OPR of the cells. The pH inside the liquid compartment is higher than the setpoint (7.2) and increases during the whole flight up to 8.7 which is not in accordance with the increase in dCO_2 as the accumulation of CO_2 and the resulting acid should lower it. This inconsistency had to be analyzed in a follow-up experiment to verify the sensors functionality as well as their location in the system. The observed reaction might be explained by a reduced flow at the sensor position which led to a higher oxygen demand of the algae not suspended in the system.

Panel C of the figure shows that the partial pressure of oxygen inside the gas collection loop increases towards the end of the flight up to 500 mbar in accordance to the dissolved O_2 concentration of 600 mbar in the algae loop. During the parabolas the cabin pressure was lowered to 830 mbar (sometimes to minima of around 750 mbar), leading to a lower partial pressure inside the loop. The gas collection loop was flushed with a gas mixture of 1% CO_2 (v/v) in N_2 prior to the flight to create a high driving force for oxygen diffusing from the liquid compartment to the gas collection compartment. The absolute pressure inside the gas loops was equal to the absolute cabin pressure during the flight. Hence, in total a net increase from around 50 mbar pO_2 was measured in this gas loop originating from the removal of O_2 produced inside the liquid loop across the membranes. With longer experiment duration this would have increased even to a higher value, as transfer of oxygen into the gas collection loop via the membrane follows the production by the cells with time.

By establishing mass balances for gases for all three compartments (two gas compartments and one liquid compartment) uptake and production rates for the cells during the flight days were calculated (according to 3.6.3). For this flight, only OPR was calculated, as a net increase in dO_2 was measured in the algae loop, whereas for dCO_2 there was no net decrease, and therefore CO_2 uptake, monitored in online data. Furthermore, the inconsistency of dCO_2 and pH data indicate an erroneous measurement during the flight. A first order derivation of the dO_2 profile in the liquid together with OTR values for both sides across the membranes yields the following OPR values, shown in Figure 8-3 A. However, these values have to be seen as rough estimates, as at least in the gas exchange loop there was a gas leakage during the flight.

Figure 8-3 A shows that the estimated volumetric OPR fluctuated during the parabolas whereas a first local maximum of about 0.5 mmol L^{-1} h^{-1} is measured during the fourth set of parabolas. A second peak production of oxygen can be identified after the end of parabolas by towards the end of the flight with 0.8 mmol O_2 L^{-1} h^{-1}. Due to the leakages in the gas loop, oxygen transfer rates across the membranes cannot be calculated accurately and the presented production rates are therefore only a rough estimation. Nevertheless, peak OPR values of 0.5 during parabolas and 0.8 mmol O_2 L^{-1} h^{-1} after the parabolas are very similar to values measured in continuous cultures at 200 µE m^{-2} s^{-1} and a cell dry weight concentration of 3.5 g L^{-1} inside the cylindrically illuminated STPBR (here vol. OPR = 0.7 mmol L^{-1} h^{-1}). The maximum vol. OPR values measured during this campaign are slightly higher than values in continuous cultures in the membrane reactor. Here, a PFD of 400 µE m^{-2} s^{-1} at a c_X of 2.2 g L^{-1} was necessary to achieve a vol. OPR of 0.6 mmol L^{-1} h^{-1} (see chapter 7.1). Inside the ModuLES-PBR mixing conditions are slightly better than in the membrane reactor, as the meandered shape leads to turbulences, similar the formation of a Kármán vortex street, in each of the turns. This enhances mass transport and reduces mixing time. An exact calculation of OPR values should even result in higher absolute production rates. The evaluation of roughly estimated OPR values from this parabolic flight has shown that the photosynthetic production rates of O_2 yielded comparable rates like those acquired during continuous cultivations in other photobioreactor types running on ground (1 g control).

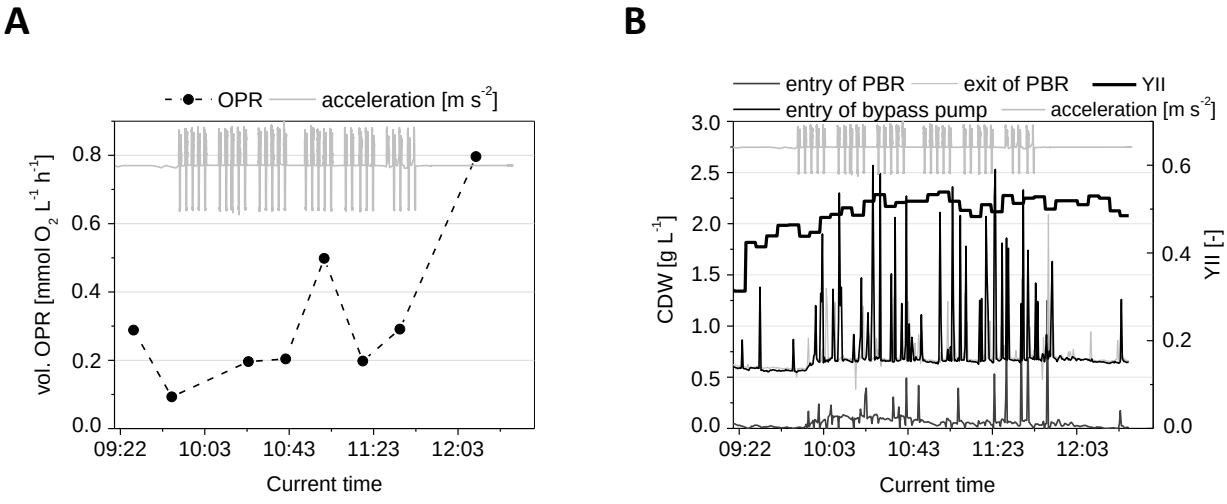

Figure 8-3. Photosynthetic activity of the cells during flight four of the first campaign with the ModuLES-PBR. A) Volumetric oxygen production rate OPR in mmol O_2 L^{-1} h^{-1} from the start of nominal mode until the end of the flight. Values represent rough estimates and originate only from accumulation term inside the liquid compartment because of leakage in the gas loop. Acceleration indicates parabolas. B) Yield of photosystem II (YII represented on right y-axis) during the flight. For comparison CDW concentration is depicted on the left y-axis; Podhajsky (2014).

Panel B in Figure 8-3 shows data of PS II yields (YII) together with CDW values as well as acceleration during the flight for comparison. In total, an increase of YII from 0.3 to 0.5 can be seen during the duration of the flight. For assessment of these values, cells of this wildtype in medium to

light saturated conditions in pre-culture flasks which are homogenously mixed, show YII values about 0.6 which proves that cells cultured in the ModuLES-PBR during the parabolic flight had a comparable photosynthetic activity as cells cultured under ground conditions.

To sum up all of the four flight days of the first campaign, the functionality of the system was proven, except the minor difficulties mentioned before. Several parts of the system with a need for improvement were identified which were addressed for preparation of the second flight campaign. These include a change of the lighting color and a manual control of the illumination intensity, an adjustable PAM saturation pulse and the integration of a filtration unit.

Although exact mass balancing was not possible, a rough estimation of OPR was achieved. However, during all flights no net decrease of dCO_2 in the algae loop could be observed which was expected, as transfer rates across the membrane inside the liquid overlaid and therefore masked the CO_2 consumption by the cells. For all of the four flight days an increase in dissolved oxygen was recorded inside the liquid compartment which also correlates to YII values measured with the help of the PAM fluorometer. Maximum YII values accounted for 0.5 which corresponds to a high photosynthetic activity. No influence of parabolas in form of changes of gravitational force on Ft and YII could be detected during this campaign which is also reflected by transcript analysis of certain stress genes (evaluation is accomplished by project partners, data is therefore not shown within this work).

8.2.3 Second parabolic flight campaign

For a second parabolic flight the illumination color was changed: instead of warm-white LED light, dichromatic illumination with red and blue in a molar ratio of 90 to 10 photons (PFD = 200 µE m^{-2} s^{-1}, manually adjustable between 0-300 µE m^{-2} s^{-1}) was used in accordance to the results acquired in ground experiments. A total of three flight days with 25 to 36 parabolas (variations of the number of parabolas were due to difficult weather conditions) were performed. With the newly integrated filtration unit biomass was collected during the last two flight days when the system was run in a chemostat mode. The light intensity was changed stepwise during all flight days, starting from a basic intensity of 200 µE m^{-2} s^{-1} down to various intensities (compare to Table 11-17). The reason for this stepwise change of PFD was to keep the dissolved O_2 concentration in the liquid below a critical threshold of 6.5 mg L^{-1} in order to prevent bubble formation following oversaturation of the liquid. The preflight flushing time of the gas loops varied in duration due to preparation of experiment and overall circumstances before the flights and therefore also the starting gas concentrations in the loops. Speed of the gas pumps and therefore the gas flow rates were the same like during the first campaign. Also liquid flow rate, dilution rate D as well as the membranes used were equal to the first campaign. In comparison to the first flight campaign, the frequency of the PAM saturation pulse was manually adjustable; in normal mode it was set to one pulse per minute and with the help of the software it was possible to set it to a higher frequency of one pulse every ten seconds for specific parabolas.

For two of the three flight days the system was run in chemostat mode (one day in batch mode). For one of the flight days where the system was run in chemostat mode it was possible to successfully collect biomass and separate cell-free medium with the help of the filtration unit. During two of the three flight days software glitches hampered the planned experimental procedure concerning light step changes and PAM frequency changes. Furthermore, the data recorded by the dissolved CO_2 sensor in the algae compartment showed an exceptional high noise-to-signal ratio.

In the following, data recorded during the first flight day in batch mode, as well as during the second flight day in chemostat with a performed cell/media separation are shown.

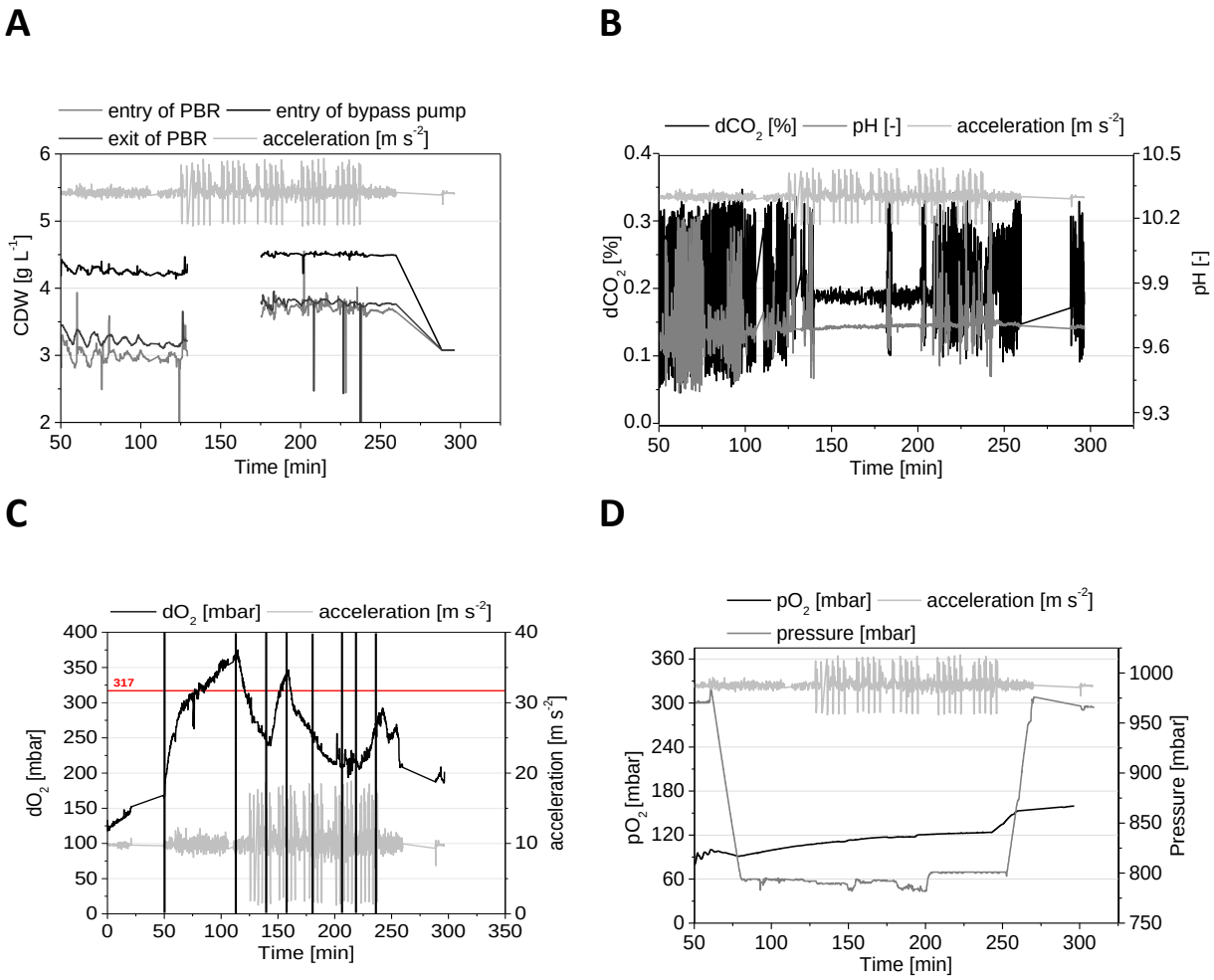

Figure 8-4. Sensor data of flight day one of the second campaign of gas and liquid loop of the ModuLES-PBR run in batch mode. A) Correlated cell dry weight concentration for batch mode during the flight. Values were derived from OD signal by a calibration factor. Acceleration indicating parabolas is shown on the right y-axis. B) Profile of dissolved carbon dioxide concentration and pH during the first flight day. Signals show high noise. C) Data of dissolved oxygen concentration as response to light step changes during the first flight day of the second campaign in batch mode. A threshold concentration of 317 mbar pO_2 corresponding to 6.5 mg L^{-1} at atmospheric pressure is shown by the red horizontal line. Black lines indicate light step changes where the first line shows the switch from safety to nominal mode after 50 min. D) Profile of partial pressure of oxygen inside the gas collection loop during first flight day in batch mode for the second campaign. On the right y-axis acceleration measured by an integrated sensor is illustrated; Podhajsky (2014).

In Figure 8-4 A the correlated cell dry weight concentration is shown for the batch cultivation during the first flight day under dichromatic illumination. As the figure shows, again, oscillation of the OD signals can be detected indicating plug flow regimes inside the reactor geometry. Towards the end of the flight, after a software failure in the middle of the flight, OD and therefore correlated CDW concentrations are even a little higher, around 3.5 to 4 g L^{-1}. This was most probably due to an offset of OD signal resulting from the software failure.

In part B of the figure signals of dCO_2 and pH sensors are plotted versus flight time. Data show a very high noise. For this reason, CO_2 uptake rates could not be determined during this flight campaign.

During all of the three flight days light step changes were conducted to avoid saturation of liquid phase with dissolved oxygen and a subsequent bubble formation by limiting dO_2 concentration. The corresponding times of step changes starting at a basic overall PFD of 200 µE m^{-2} s^{-1} are listed in Table 11-17, Appendix 11.6.4.

Algae showed adaptation to these light steps during all flights of this second campaign (a first change of the dO_2 signal is detected 5 seconds after the light intensity changed stepwise). However, as light intensity could not be kept constant until a new equilibrium was reached, it is not possible to determine time constants for comparison with ground PBR systems. As Figure 8-4 panel C shows, it was possible to keep the dissolved oxygen concentration below the critical threshold of 400 mbar by limiting the irradiance at specific times. With this, not only bubble formation has to be prevented, but also inhibition of photosynthesis, which could be relevant for oxygen concentration above this point (Sawdon and Peng 2015).

As panel D of Figure 8-4 shows, pO_2 in the gas collection loop oscillates in the beginning of the recording caused by the flushing of the gas loop with 1% CO_2 (v/v) in N_2 before the flight started. During the flight oxygen accumulated in the gas collection loop and partial pressure of oxygen increases from 80 to 150 mbar. This value was also confirmed by a subsequent analysis of the composition of the gas volume inside the gas collection bag after the flight with the help of gas chromatographic measurements (data not shown). Data also reveal that the cabin pressure decreased to 760 mbar during the flight, which is also visible for partial pressure of oxygen inside the gas loops, also marked by a sharp increase at the end of flight after 250 min when the descent of the airplane started.

By using mass balancing for all of the three compartments oxygen production rates OPR were calculated for the flight. As data recorded by the dCO_2-sensor inside the liquid loop showed high noise-to-signal ratios (see panel B Figure 8-4), it was only possible to calculate transfer and production rates for oxygen. Volumetric OPR values fluctuate during the flight, also in response to the light intensity step changes where two maxima of 0.6 and 0.5 mmol O_2 L^{-1} h^{-1} are recorded during set two

and five of parabolas. The peak OPR values measured during the parabolas are therefore comparable to the peak volumetric O_2 production rates during the first flight campaign with warm-white light. However, these peak OPR values should be tested during longer duration tests with the reactor under changing g conditions which can reveal differences in long-term O_2 production rates.

Comparing these results with a ground experiment in this novel PBR shows possible influences of changing gravity conditions present during the flights on OPR values.

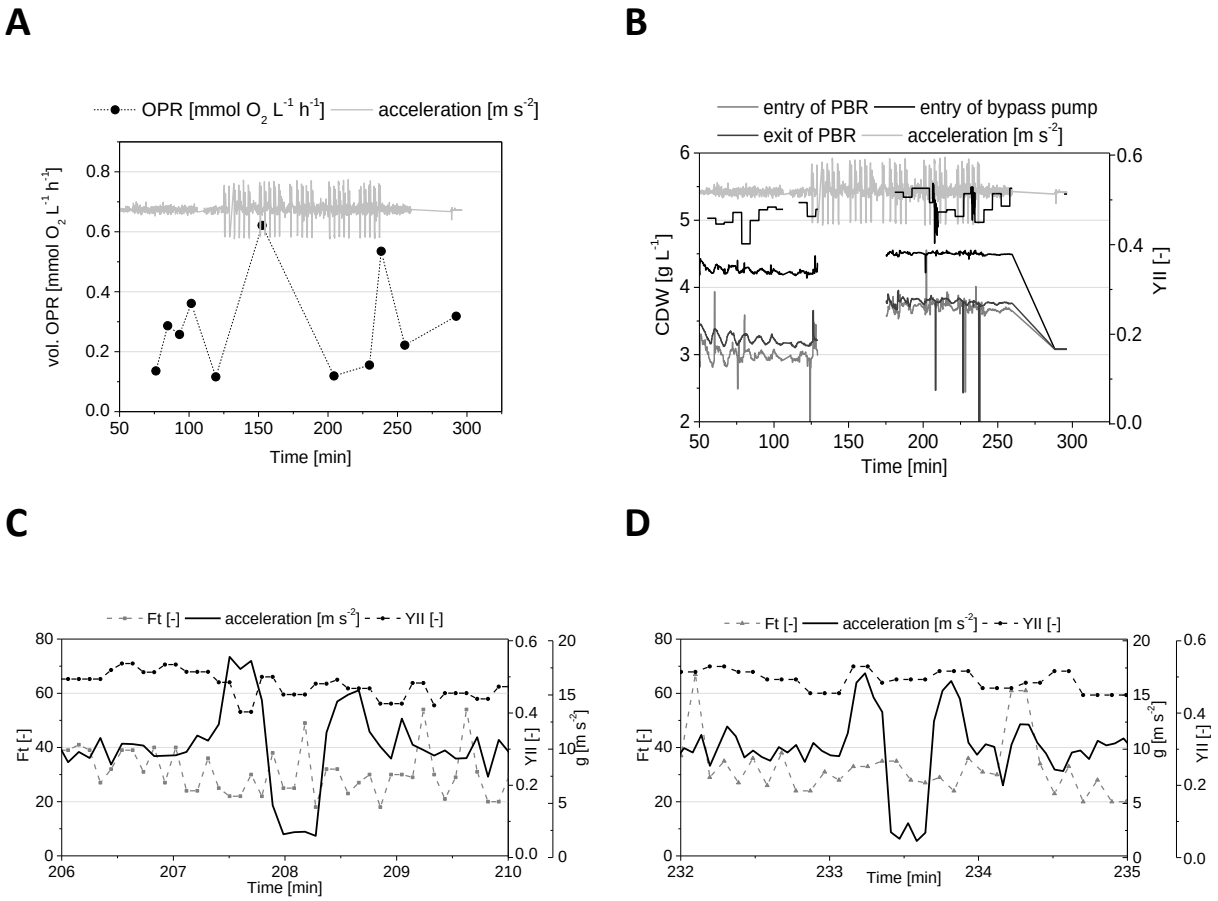

Figure 8-5. Photosynthetic activity of the cells during flight one of the second campaign with the ModuLES-PBR. A) Volumetric oxygen production rate OPR in mmol O_2 L^{-1} h^{-1}. B) Yield of photosystem II (YII) during the flight with dichromatic illumination. C) Ground fluorescence Ft and YII for parabola 18 (t = 206 – 210 min) during flight. Acceleration is depicted as black line. D) Ground fluorescence Ft and YII for parabola 24 (t = 231 – 236 min) during the first flight day of the second campaign; Podhajsky (2014).

During the duration of this flight within the second campaign *C. reinhardtii* CC-1690 cells produced 1.5 mmol O_2 L^{-1} under dichromatic illumination within 4 hours. Thus, the algae showed a high photosynthetic efficiency, which can also be seen in Figure 8-5 B showing yield of photosystem II. Values of YII increase slightly during the duration of the flight up to a value of 0.5. This is the same maximum value recorded during the fourth flight of the first campaign under warm-white illumination and chemostat mode.

Figure 8-5 C and D show basic fluorescence Ft and yield of photosystem II for the algae cells during the flight. From these data recorded, no influence of changing gravity conditions during the parabolic flight on Ft and YII for this *C. reinhardtii* wildtype cultivated inside the ModuLES-PBR can be seen. This was also shown for all flight days of both campaigns testing this novel photobioreactor with the chosen microalga.

During the second flight day of the second campaign, the system was run in chemostat mode which enabled the testing of the integrated filtration unit. After filtration towards the end of the flight a total volume of about 280 ml cell-free medium and 190 ml concentrated biomass suspension could be obtained (Figure 8-6).

Figure 8-6. Concentrated algae suspension (left side) and cell-free medium (on the right) after passage through the integrated harvesting unit during the second flight operating as chemostat. (Podhajsky 2014)

During this second campaign with three flight days the PBR system was tested with highly efficient dichromatic illumination. Besides difficulties relating to the automated sampling unit and a high noise-to-signal-ratio of the dCO_2 probe inside the liquid, the hardware functionality was verified. Furthermore, light step changes were applied in order to prevent bubble formation and avoid inhibiting dO_2 levels. During two of those three flight days the system was run in chemostat mode and it was possible to successfully use the integrated filtration unit for cell / media separation as first step towards a closed loop system with media recycling.

Comparing the first campaign with warm-white LED illumination with the second under dichromatic illumination, peak volumetric oxygen production rates are rather similar from 0.4 to 0.7 mmol L^{-1} h^{-1}.

With this system it was possible to keep the algae in a photosynthetic growth condition with high efficiency during the flights with changing gravity conditions which was proven by several probes including fluorescence signals. Based on the sensor data of gas concentrations on both gas and liquid side it was possible to calculate oxygen production rates as well as absolute amounts of oxygen produced by the cells. It was also possible to control dissolved O_2 concentration in the liquid while illuminating the cells by highly energy-efficient dichromatic illumination during the second campaign.

Optimization aspects identified during the parabolic flight campaigns include:

- Using double-sided illumination instead of one-sided illumination in order to be able to use even higher biomass concentrations inside the reactor without light limitation.
- Optimization of the overall gas transfer (especially if a higher biomass concentration is aspired) whereas a new module will need to be integrated in the system as a next step to maximize efficiency at high biomass concentrations without having the need to limit irradiance. By using other membrane materials with higher selectivity for oxygen than for CO_2 bubble formation shall be avoided completely while having high oxygen production and CO_2 uptake rates.
- Integration of a media recycling unit by analyzing the collected media from the filtration unit, which is essential for closing the algae loop for longer duration tests or spaceflight applications.

8.3 Results from ground test as continuous cultivation with flight day simulation

The ModuLES-PBR system was furthermore tested on ground. In the following section the most important data obtained during a continuous cultivation with the ModuLES-PBR on ground is outlined and discussed. This cultivation was also used to simulate one flight day of the second campaign relating to light intensity step changes and PAM data as well as samples analyzed for mRNA amounts.

8.3.1 Ground test: continuous cultivation as chemostat with flight day simulation

The third ground test was performed with chemostat conditions. First, a simulation of one flight day of the second campaign (flight day one of PFC 24) was performed as identical as possible to compare that data to flight data to study possible effects of change of gravitational field on the system and the cells. After this simulation the system was run further on in chemostat mode, just with the difference that gas loops were now flushed continuously with the specific gas mixtures.

As Figure 8-7 A and B show, dissolved O_2 concentration measured on ground is only slightly higher than during the parabolic flights. During both tests, the light intensity was changed stepwise to limit O_2 concentration and limit bubble formation. As part C and D show, volumetric OPR is also a little higher during the ground test compared to flight cultivation, although during the flight the local maxima for OPR are higher than for ground control. The same is displayed by YII values which are with 0.5 slightly lower during the flight than on ground (YII almost constant at 0.6).

However, this first indication that photosynthetic activity seems to be slightly reduced during a short-term (3 hours duration) change of gravitational field compared to ground control has to be verified during longer experiments under microgravity conditions. The slight reduction during flight conditions

might also be resulting from the lowered pressure and the lower gas solubility as cabin pressure decreased to 760 mbar.

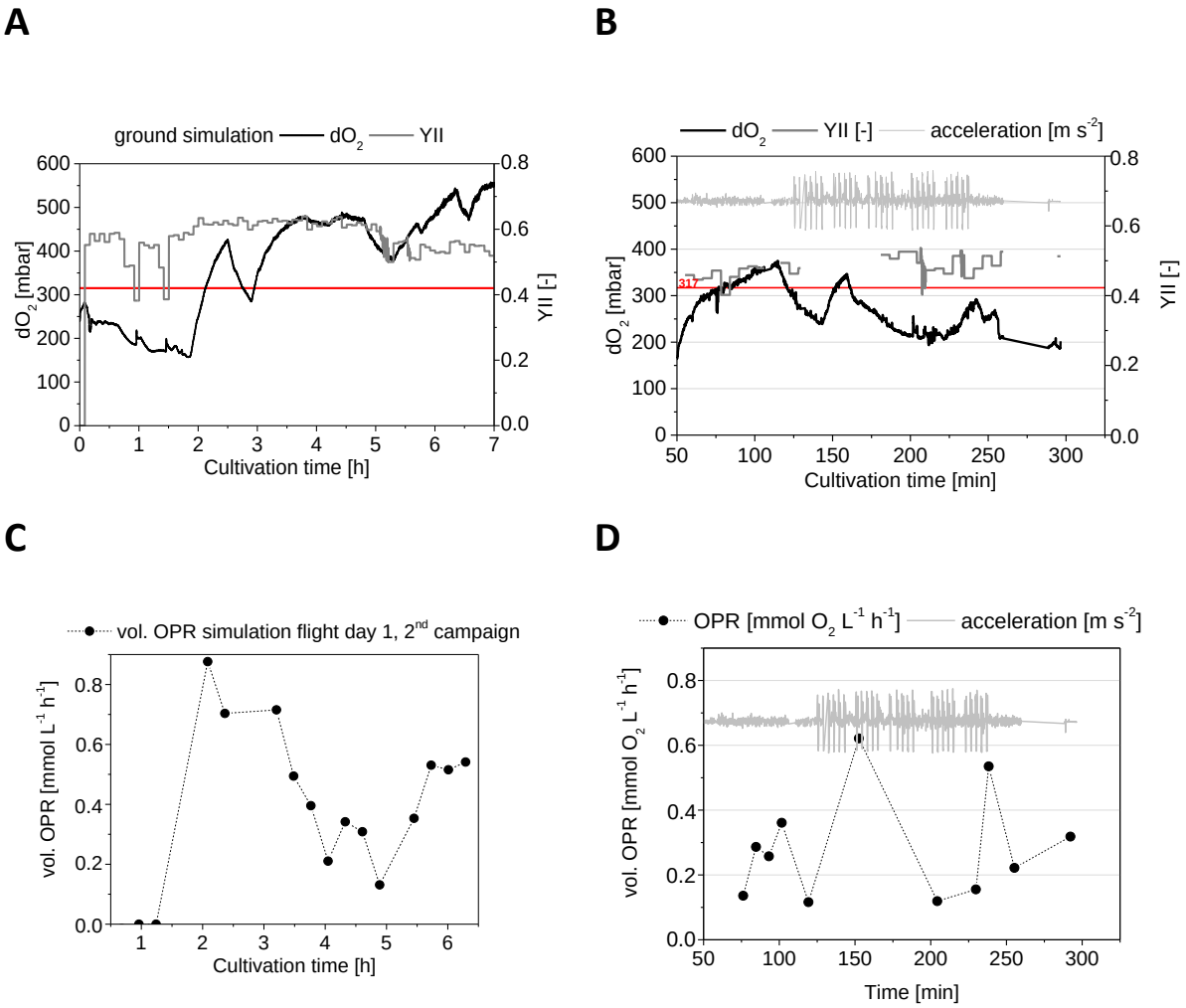

Figure 8-7. Comparison of ground simulation and flight day one of the second campaign. A) Dissolved O_2 concentration and YII during flight day simulation on ground. B) Dissolved oxygen concentration and YII measured during the first parabolic flight of the second campaign. C) Volumetric OPR during ground simulation. D) Volumetric OPR during flight day with acceleration profile.

After this flight simulation, the reactor was run in a continuous mode while the gas loops were flushed with the specific gas mixtures. Figure 8-8 A shows that dO_2 concentration fluctuated during continuous cultivation on ground and indicates that no steady-state was achieved during 50 hours of continuous cultivation. This is also displayed by YII values which decrease slightly from 0.6 after the flight simulation to 0.4. As the dCO_2 probe showed no signals during this ground test, no calculation of CUR values was possible. Part B of the figure shows volumetric OPR during continuous cultivation. Values fluctuate between 0.4-0.6 mmol L^{-1} h^{-1} and are slightly higher than steady-state vol. OPR values achieved with the membrane reactor with dichromatic red/blue illumination.

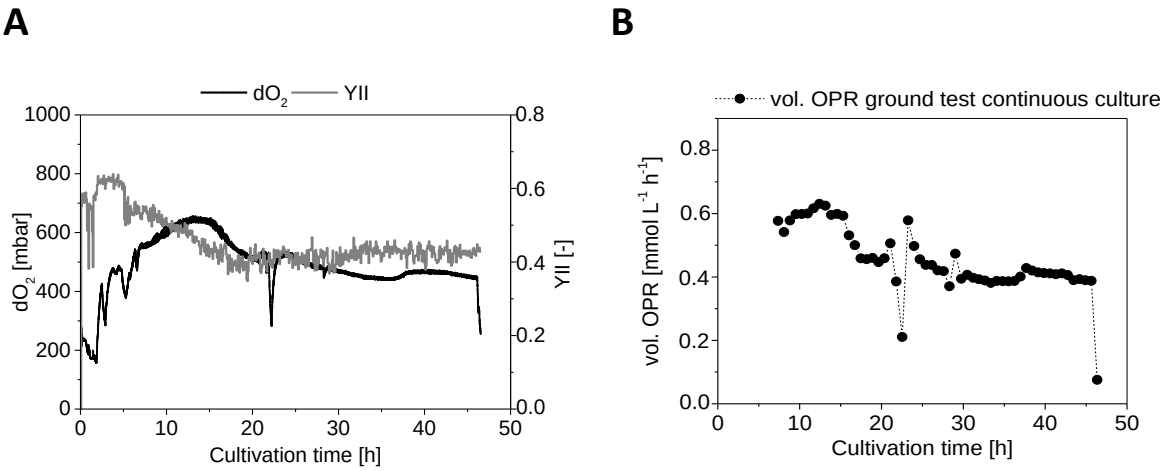

Figure 8-8. Continuous cultivation in the ModuLES-PBR on ground. A) Dissolved O_2 concentration and YII during continuous cultivation in the ModuLES-PBR. B) Calculated volumetric OPR during continuous cultivation in the ModuLES-PBR on ground.

8.4 Summary of results and conclusions from parabolic flight and ground tests

To conclude, the reactor system has proven its functionality even under the conditions of a changing gravitational field.

Concerning parabolic flight tests of the ModuLES- PBR, the results presented indicate that the algae showed a high photosynthesis rate comparable to ground conditions. After comparison with the ground experiment only a slight reduction of volumetric OPR and yield of photosystem II could be measured which could also be resulting from a lowered pressure and a lowered gas solubility during the flight. Relating to the results for effects of perturbations on continuous cultures and the quick adaptation of gas exchange rates and pigment composition presented in Chapter 7 it can be assumed that if those changing gravity conditions would have had an effect to the cells within a running closed PBR, it would have been measurable also within the 3 hour duration of a parabolic flight.

However, these tests should be verified under long-term microgravity conditions during satellite missions with ground control.

After optimization of selected membrane materials and the establishment of media recycling techniques this novel system can be applied for long-term continuous cultivations of microalgae in space environment. For future longer duration missions under microgravity conditions gas transfer has to be optimized to guarantee a stable and bubble-free membrane aeration with a pressure balancing system.

As the reactor system is suitable for enabling a maximal efficient photosynthetic activity of the algae and the algae only showed little effects in response to changing gravity conditions, it is very promising to test the system during long-term microgravity conditions in space.

9 Conclusions and Outlook

9.1 Conclusions

In the current work, the development of a photobioreactor system designed for microgravity conditions was in the focus. Here, an energy-efficient illumination of the microalga *C. reinhardtii* CC-1690, a bubble-free aeration with the help of membranes, as well as the stability of continuous microalgae cultures with respect to light intensity and color changes were major research topics. Beyond, effects of lowered pressure and pressure changes on photosynthetic growth and gas exchange were studied. First results from parabolic flight campaigns and ground control experiments that were run in the designed ModuLES-PBR were presented with close relation to ground results from the former mentioned research aspects.

Illumination colors were selected with respect to accessory and sensory pigments whereas current knowledge on physiological effects of wavelengths via sensory pigments was considered. Experiments with mono- and dichromatic illumination as well as full-spectrum illumination were studied for low and higher to saturating light intensities. A planar reactor geometry in form of plate reactors was considered with one-sided illumination. Results at lower light intensities have proven that an increase in efficiency of light to biomass conversion, measured as PCE value, is possible with red wavelengths at 680 nm as well as dichromatic red/blue 90/10 illumination. The highest PCE value measured so far of 15%, close to the theoretical limit, was achieved with a 90/10 combination of red and blue photons at low light intensities. Hence, an increase in efficiency of 200% was possible with a high portion of red combined with blue photons compared to full-spectrum illumination. Green light, regarded as useless for photosynthesis, showed efficiencies comparable to warm-white control. Results have furthermore shown that PCE values seem also be affected by effects triggered by sensory pigments. For higher to saturating light intensities, saturation effects were verified and similar PCE values were found for the red/blue combination and the white control. These results from semi-fed-batch cultivations were also found consistent during continuous cultures.

Remarkable effects of light colors on cell size and overall morphological features like aggregation were shown. Red and blue photons have a measurable effect on cell size, whereas green photons seem to provoke cellular aggregation. Concerning effects on cell size by red and blue photons, results of continuous culture experiments point to a transient nature where adaptation mechanisms lead to a restoration of an optimal cell size. Pigment content is also influenced by light colors, whereas lowest specific values were found for light combinations yielding high PCE values under low light intensities. Results of experiments under higher and saturating intensities, where full-spectrum illumination is compared to 90/10 red/blue light, point to adaptation mechanisms in form of state transitions and an adjustment of absorption cross section of cells. Within this work it was shown that the détour-effect is

applicable for microalgae suspensions where low absorbing wavelengths penetrate deeper into algal cultures and promote growth at higher cell densities.

Relating to a bubble-free aeration of microalgae cultures, the experiments conducted within this work have shown that membranes can be used where aeration is purely diffusion-based. With respect to the selection of suitable membranes, dense solution-based membranes with a high O_2 to CO_2 selectivity seem most promising. Mass transfer coefficients for different membranes for O_2 and CO_2 were determined and can be used as basis for simulation of optimal combinations of specific mass transfer surface areas, gas compositions and k_L values for each application case. k_L values for O_2 and CO_2 in the range of 10^{-6} m s^{-1} were measured which are high enough to enable a sufficient CO_2 supply to microalgae cultures. With the designed membrane testing unit it was also possible to quantify water losses of the different membrane materials as well as elucidate the effects of several influencing factors on mass transfer. First cultivations in batch and continuous mode have been run successfully in a lab scale photobioreactor with bubble-free membrane aeration. Here, a configuration with two membranes and two different gas phases was chosen to limit bubble formation. As bubble formation could not be avoided completely this was taken into account for establishing control of continuous cultures.

The experiments with lowered pressure presented within this work have demonstrated that a lowered pressure down to 700 mbar influences microalgal growth by decreasing specific growth rate, increasing carbon dioxide uptake rates whereas OPR seems to be unaffected. This indicates that light reaction of photosynthesis keeps being unaffected. Still, possible signaling effects of pressure and changes of this abiotic factor on microalgae are unclear. First experiments conducted within this work point to a relation of pressure, mechanical stress on the cell membrane and the number of daughter cells during cell division, which was already discussed in references. During experiments with sudden pressure step changes of maximal 300 mbar, no lethal threshold was found for *C. reinhardtii* CC-1690 cells.

Within the work presented, continuous cultures of the green microalga *C. reinhardtii* CC-1690 were run in a bubble-aerated, homogenously mixed photobioreactor (STPBR) with cylindrical illumination and a planar illuminated bubble-free aerated membrane photobioreactor. Comparative parameters were volumetric gas exchange rates OPR and CUR and specific pigment contents. The effects of perturbations in form of light intensity step changes were analyzed during steady-state phases at constant cell densities and time constants were measured for the overall system responses. For both reactor geometries with their different aeration concepts it was found that the original volumetric gas exchange rates were reinstalled as the former light intensity was reset. However, time constants (as T,63%) are different for the two systems compared: those found for system responses inside the membrane-aerated PBR were on the average four times higher than those determined inside the

homogenously mixed and bubble-aerated system. Pigment contents adapted during light intensity step changes in both systems in dependence on the actual average light intensity present (function of actual cell density with specific extinction coefficients, and depending on the light gradient resulting from cylindrical or planar illumination). Changes in specific pigment composition could be detected within 24 hours after the performed light intensity change, indicating a quick adaptation of cells even though these perturbations were only exerted for short times (1.5 h in case of STPBR with bubble-aeration). This indicates that a photomodule within a life support system can restore its initial gas exchange rates under axenic conditions and without any other fatal disturbances.

Within this work, the microalgae-based photobioreactor system for microgravity conditions (ModuLES-PBR) was presented and tested during parabolic flight and ground campaigns. During parabolic flights with changes of the gravitational force from 0-2g during each parabola flown, the algae showed a high photosynthesis rate comparable to ground conditions under the same lighting conditions. A comparison with the ground campaign only showed a minor reduction of volumetric OPR and PSII yield.

9.2 Outlook

Relating to the topic of an energy-efficient artificial illumination, future research should continue to focus on finding optimal wavelengths and combinations with respect to absorption and action spectra for different microalgae. A trichromatic illumination with red, blue and green photons seems promising, whereas cultures should first be illuminated with a red/blue combination where green photons are added with increasing cell densities to optimize light penetration at high cell densities. Light penetration might also be optimized by using wavelengths aside from the actual peaks in absorption spectrum mimicking mutants with reduced antenna size.

With respect to a life support photomodule operating with maximal energy efficiency, it seems promising to use a combination of 90/10 red/blue photons and a double-sided illumination with a reduced PFD for a planar geometry.

Further knowledge on long-term effects and pigment acclimation concerning spectral composition at different intensities should be gained during continuous cultivations. Starting with experimental data presented within this study modeling growth rate distribution along the light path and light attenuation profiles for different light colors at different intensities should complete the knowledge collected so far. Also more insight of interdependencies of light color and cellular functions based on the action of sensory pigments is necessary to design optimal artificial illumination systems not only for life support microalgae modules in space.

As bubble formation during a diffusion-based membrane aeration of microalgae could not be completely avoided with the chosen configuration and membranes, future work should primarily focus

on selectivity factors of O_2 towards CO_2 of dense membrane materials. Here, chitosan-acetic acid membranes functionalized with Ni-ions, SBS membranes with a further enhanced selectivity factor or even liquid membranes with carriers are promising materials.

Simulations based on the determined mass transfer values should be conducted to find the optimal combination of membranes, specific surface areas and gas compositions for every application case individually.

Furthermore, controlling of such a membrane-aerated photobioreactor should be optimized based on time constants. These controlling approaches should take into account the various potential disturbance variables acting on a microalgae module within a life support system in space.

Future work on pressure effects should focus on starch and lipid production and effects of lowered pressure and pressure changes on their synthesis and metabolism in *C. reinhardtii*. This should help to deepen the understanding of pressure effects on photosynthesis and overall on microalgal physiology. Relating to a general understanding, also the role of mechano-receptors and the existence of turgor pressure for the flagellate *C. reinhardtii* should be further focused on. For future experiments with pressure step changes, the duration of steps should be increased and exerted ideally during steady-state phases of continuous cultivations.

For the application of microalgae-based photomodules in space life support systems the long-term effects of a reduced pressure on photosynthetic activity of cells are of crucial importance. This knowledge also has relevance for further optimizing microalgal processes on ground, e.g. high-altitude regions.

Deeper knowledge on the restoration capacity of the photosynthetic activity after longer periods under limiting light conditions and for the presence of contaminants is needed to advance the development of reliable life support modules based on microalgae cultures. However, the need to foresee possibilities for re-inoculation and a certain redundancy of photomodules running in parallel is indispensable. Future experimental approaches to long-term continuous microalgae cultures should further deepen the knowledge on the relation of time constants for pigment adaptation and times of abiotic changes, as for example light intensity. This is also crucial for outdoor microalgal processes with changing lighting conditions.

To elucidate effects of long-term microgravity on photosynthetic rates, primarily pronounced as gas exchange rates, on a microalgae-based photomodule, satellite missions with longer duration of µg-phases are necessary. In order to guarantee a stable long-term bubble-free membrane aeration of the culture, simulations to find an optimal combination of membrane materials with their respective k_L values and selectivities, specific surfaces and gas compositions are crucial. Also hollow fiber membranes integrated in gas exchange modules are possible. After establishment of media recycling

systems this novel system can be applied for long-term continuous cultivations of microalgae within space environment.

In total, the presented work shows that the application of microalgae for space-photomodules is possible and there are several points were energy efficiency can be positively influenced. Challenges on the reactor as well as the biological level which arise through the unique space environment have been outlined and discussed in this work. This enables the definition of further optimization aspects to come closer to the establishment of self-reliable life support systems to spread human life beyond Earth.

10 Bibliography

Aas, E. (1996) "Refractive index of phytoplankton derived from its metabolite composition." Journal of Plankton Research **18**(12): 2223-2249.

Ahmed, T. and Semmens, M. J. (1992 a) "The use of independently sealed microporous hollow fiber membranes for oxygenation of water: model development." Journal of Membrane Science **69**: 11-20.

Ahmed, T. and Semmens, M. J. (1992 b) "The use of independently sealed microporous hollow fiber membranes for oxygenation of water: experimental studies." Journal of Membrane Science **69**: 1-10.

Ai, W., Guo, S., Qin, L. and Tang, Y. (2008) "Development of a ground-based space microalgae photo-bioreactor." Advances in Space Research **41**: 742-747.

Alling, A., Van Thillo, M., Dempster, W., Nelson, M., Silverstone, S., et al. (2005) "Lessons learned from Biosphere 2 and Laboratory Biosphere Closed Systems Experiments for the Mars on Earth Project." Biological Sciences in Space **19**(4): 250-260.

Aunins, J. G. and Henzler, H. J. (1993) "Aeration in Cell Culture Bioreactors." In.: Rehm, H.-J.; Reed, G. (Eds.) : Biotechnology, Vol. 3, 2nd ed. VCH Verlagsgesellschaft, Weinheim.

Badger, M. R., Andrews, J., Whitney, S. M., Ludwig, M., Yellowlees, D. C., et al. (1998) "The diversity and coevolution of Rubisco, plastids, pyrenoids, and chloroplast-based CO_2-concentrating mechanisms in algae." Canadian Journal of Botany **76**: 1052-1071.

Baer, S., Heining, M., Schwerna, P., Buchholz, R. and Hübner, H. (2016) "Optimization of spectral light quality for growth and product formation in different microalgae using a continuous photobioreactor." Algal Research **14**: 109-115.

Bai, R. K., Huang, M. Y. and Jiang, Y. Y. (1988) "Selective permeabilities of chitosan-acetic acid complex membrane and chitosan-polymer complex membranes for oxygen and carbon dioxide." Polymer Bulletin **20**: 83-88.

Baker, R. W. (2000). "Membrane technology", Wiley Online Library.

Balan, S. A., Kausch, M. F., Stüeken E. E. and von Appen, W. J. (2006) "The effects of microgravity

on the photosynthetic yield of *Nannochloropsis salina* and *Spirulina platensis*.“ 1st Hellenic-European student space science and technology symposium, Patras, Greece.

Ball, S. G., Dirick, L., Decq, A., Martiat, J. C. and Matagne, R. (1990) “Physiology of starch storage in the monocellular alga *Chlamydomonas reinhardtii*.” Plant Science, **66**: 1-9.

Barbosa, M. J., Janssen, M., Ham, N., Tramper, J. and Wijffels, R. H. (2003) “Microalgae cultivation in air-lift reactors: modeling biomass yield and growth rate as a function of mixing frequency.” Biotechnology and Bioengineering **82**(2): 170-179.

Barlett, R. H. (2005) “Extracorporeal Life Support. History and new directions.” Seminars in perinatology **29**(1): 2-7.

Barsanti, L. and Gualtieri, P. (2006) “Algae - Anatomy, Biochemistry and Biotechnology” CRC Press Taylor & Francis Group, Boca Raton.

Bean, B. (1977) “Geotactic Behavior of *Chlamydomonas*.” The Journal of Protozoology **24**: 394-401.

Becker,W. (2004) “Microalgae in human and animal nutrition.” In Richmond, A. (ed.), Handbook of microalgal culture. p. 312-351.

Beckmann, M. and Hegemann, P. (1991) “*In vitro* identification of rhodopsin in the green alga *Chlamydomonas*.” Biochemistry **30**(15): 3692-3697.

Berthold, P. (2007) “Analyse der Funktion des Photorezeptors Channelrhodopsin 1 der Grünalge *Chlamydomonas reinhardtii*.” Dissertation, Universität Regensburg. Urn:nbn:de:bvb:355-opus-6488.

Bišová, K. and Zachleder, V. (2014) “Cell-cycle regulation in green algae dividing by multiple fission.” Journal of Experimental Botany **65**(10): 2585-2602.

Bisson, M. A. and Kirst, G. O. (1995) “Osmotic acclimation and turgor pressure regulation in algae.” Naturwissenschaften **82**: 461-471.

Bitog, J. P., Lee, I. B., Lee, C. G., Kim, K. S., Hwang, H. S., et al. (2011) “Application of computational fluid dynamics for modeling and designing photobioreactors for microalgae production: a review.” Computers and Electronics in Agriculture **76**: 131-147.

Bonente, G., Formighieri, C., Mantelli, M., Catalanotti, C., Giuliano, G., et al. (2011) “Mutagenesis

and phenotypic selection as a strategy toward domestication of *Chlamydomonas reinhardtii* strains for improved performance in photobioreactors." Photosynthesis Research **108**: 107-120.

Bouloc, P. and D'Ari, R. (1991) "*Escherichia coli* metabolism in space." Journal of General Microbiology **137**: 2839-2843.

Brake, R. and Bates, G. (1999) "Criteria for the design of emergency refuge stations for an underground metal mine." The AusIMM Proceeding **2**: 1-7.

Brechignac, F. and Schiller, P. (1992) "Pilot CELSS based on a maltose-excreting *Chlorella*: concept and overview on the technological developments." Advances in Space Research **12**(5): 533-536.

Brodersen, C. R. and Vogelmann, T. C. (2010) "Do changes in light direction affect absorption profiles in leaves?" Functional Plant Biology **37**(5): 403.

Brown, D. L. and Rogers, K. A. (1978) "Hydrostatic pressure-induced internalization of flagellar axonemes, disassembly, and reutilization during flagellar regeneration in Polytomella." Experimental Cell Research **117**: 313-324.

Burghardt, A. (2010) "Mass transfer by diffusion." In: Chemical engineering and chemical process technology, Vol. I, Encyclopedia of life support systems.

Buonomenna, M. G., Figoli, A., Jansen, J. C. and Drioli, E. (2004) "Preparation of asymmetric PEEKWC flat membranes with different microstructures by wet phase inversion." Journal of applied polymer science **92**: 576-591.

Campbell, N. A. and Reece, J. B. (2009) "Biologie", Pearson Studium, München.

Carvalho, A. P. and Malcata, F. X. (2001) "Transfer of carbon dioxide within cultures of microalgae: plain bubbling versus hollow-fiber modules." Biotechnology Progress **17**: 265-272.

Carvalho, A. P., Meireles, L. A. and Malcata, F. X. (2006) "Microalgal reactors: a review of enclosed system designs and performances." Biotechnology Progress **22**: 1490-1506.

Carvalho, A. P., Silva, S. O., Baptista, J. M. and Malcata, F. X. (2011) "Light requirements in microalgal photobioreactors: an overview of biophotonic aspects." Applied Microbiology and Biotechnology **89**: 1275-1288.

Cerff, M. and Posten, C. (2012) "Enhancing the growth of *Physcomitrella patens* by combination of monochromatic red and blue light - a kinetic study." Biotechnology Journal **7**: 527-536.

Cheng, L., Zhang, L., Chen, H. and Gao, C. (2006) "Carbon dioxide removal from air by microalgae cultured in a membrane-photobioreactor." Separation and Purification Technology **50**: 324-329.

Chisti, M. Y. (1989) "Airlift bioreactors" Elsevier Applied Science London.

Chisti, Y. (2007) "Biodiesel from microalgae." Biotechnology Advances **25**: 294-306.

Chmiel, H. (2011) Bioprozesstechnik. Spektrum, 3. Edition.

Clément, G. and Slenzka, K. (2006) "Fundamentals of Space Biology: Research on Cells, Animals, and Plants in Space." Microcosm Press, El Segundo, California and Springer.

Cogne, G., Cornet. J. F. and Gros, J. B. (2005) "Design, operation, and modeling of a membrane photobioreactor to study the growth of the cyanobacterium *Arthrospira platensis* in space conditions." Biotechnology Progress **21**: 741-750.

Colin, C., Riou, X. and Fabre, J. (2008) "Bubble coalescence in gas-liquid flow at microgravity conditions." Microgravity Science Technology **20**: 243-246.

Cornet, J. F., Dussap, C. G. and Dubertret, G. (1992) "A structured model for simulation of culture of the cyanobacterium *Spirulina plantensis* in photobioreactors. I. Coupling between light transfer and growth kinetics." Biotechnology and Bioengineering **40**: 817-825.

Côté, P., Bersillon, J. L., Huyard, A. and Faup, G. (1988) "Bubble-free aeration using membranes: process analysis." Journal of the Water Pollution Control Federation **60**: 1986-1992.

Côté, P., Bersillon, J. L. and Huyard, A. (1989) "Bubble-free aeration using membranes: mass transfer analysis." Journal of Membrane Science **47**: 91-108.

Cowles, J. R., Scheld, H. W., Lemay, R. and Peterson, C. (1984) "Growth and lignification in seedlings exposed to eight days of microgravity." Annals of Botany **54** (Suppl 3): 33-48.

Cuello, J. L. (2002) "Latest developments in artificial lighting technologies in Dutch horticulture for bioregenerative space life support." Acta Horticulture **580**: 49-56.

Cussler, E. L. (2009) “Diffusion: mass transfer in fluid systems.” Cambridge University Press.

Davey, M. P., Horst, I., Duong, G. H., Tomsett, E. V., Litvinenko, A. C. P., et al. (2014) “Triacylglyceride production and autophagous responses in *Chlamydomonas reinhardtii* depend on resource allocation and carbon source.” Eukaryotic cell **13**: 392-400.

De Angelis, G., Clowdsley, M. S., Nealy, J. E., Tripathi, R. K and Wilson, J. W. (2004) “Radiation analysis for manned missions to the Jupiter system.” Advances in Space Research **34**: 1395-1403.

Delosme, R., Olive, J. and Wollman, F. A. (1996) “Changes in light energy distribution upon state transitions: an *in vivo* photoacoustic study of the wild type and photosynthesis mutants from *Chlamydomonas reinhardtii*. Biochimica et Biophysica Acta **1273**: 150-158.

Demmig-Adams, B. and Adams, W. W. (2006) “Photoprotection in an ecological context: the remarkable complexity of thermal energy dissipation.” New Phytologist **172:** 11-21.

De Mooij, T., De Vries, G., Latsos, C., Wijffels, R. and Janssen, M. (2016) “Impact of light color on photobioreactor productivity.” Algal Research **15**: 32-42.

Dillschneider, R. (2014) “Die Effizienz der Kultivierung von Mikroalgen zur Biodieselgewinnung – Prozessentwicklung auf der Grundlage von Energiebilanzierung, Simulation und Integration modellprädiktiver Regelungskonzepte.” Dissertation, Institut für Bio-und Lebensmitteltechnik (BLT), Karlsruher Institut für Technologie, KIT.

Dionisio, M. L., Tsuzuki, M. and Miyachi, S. (1989 a) “Blue light induction of carbonic-anhydrase activity in *Chlamydomonas reinhardtii*.” Plant Cell Physiology **30**: 215-219.

Dionisio, M. L., Tsuzuki, K. and Miyachi, S. (1989 b) “Light requirement for carbonic anhydrase induction in *Chlamydomonas reinhardtii*.” Plant Cell Physiology **30**: 207-213.

Dreuw, A., Fleming, G. R. and Head-Gordon, M. (2005) “Role of electron transfer quenching of chlorophyll fluorescence by carotenoids in non-photochemical quenching of green plants. Biochemical Society Transactions **33**: 858-862.

Drexler, I. L. C. and Yeh, D. H. (2014) “Membrane applications for microalgae cultivation and harvesting: a review.” Reviews in Environmental Science and Biotechnology **13**: 487-504.

Drioli, E., Santoro, S., Simone, S., Barbieri, G., Brunetti, A., et al. (2014) “ECTFE membrane

preparation for recovery of humidified gas streams using membrane condenser." Reactive and Functional Polymers **79**: 1-7.

Eberhard, S., Finazzi, G., and Wollman, F. A. (2008) "The dynamics of photosynthesis." Annual Review of Genetics **42**: 463-515.

Eckart, P. (1996) "Spaceflight Life Support and Biospherics." Kluwer Academic Publishers, Dordrecht.

Ehrenberg, G. S. (1883) „Die Infusionstierchen als vollkommene Organismen." In: Engelmann TW (ed), Leipzig, p. 15.

Elwakeel, K. Z. (2010) "Environmental application of chitosan resins for the treatment of water and wastewater: a review." Journal of Dispersion Science Technology **31**: 273-288.

Emerson, R. and Lewis, C. M. (1943) "The Dependence of the Quantum Yield of *Chlorella* photosynthesis on wave length of light." American Journal of Botany **30**(3): 165-178.

Emerson, R. and Rabinowitsch, E. (1960) "Red drop and role of auxiliary pigments in photosynthesis." Plant Physiology **35**(4): 477-485.

Endo, T. and Asada, K. (1996) "Dark induction of the non-photochemical quenching of chlorophyll fluorescence by acetate in *Chlamydomonas reinhardtii*." Plant and cell physiology **37**: 551-555.

Evangelista, V., Frassanito, A., Passarelli, V., Barsanti, L. and Gualtieri, P. (2006) "Microspectroscopy of the photosynthetic compartment of Algae." Photochemistry and Photobiology **82**: 1039-1046.

Falkowski, P. G. and Raven, J. A. (1997) "Aquatic Photosynthesis", Blackwell Science, London.

Fan, L. H., Zhang, Y. T., Cheng, L. H., Zhang, L. and Chen, H. L. (2008) "Evaluation of a membrane-sparged helical tubular photobioreactor for carbon dioxide biofixation by *Chlorella vulgaris*." Journal of Membrance Science **325**: 336-345.

Farges, B., Poughon L., Creuly, C., Cornet, J. F., Dussap, C. G., et al. (2008) "Dynamic aspects and controllability of the MELISSA project: Bioregenerative system to provide life support in space." Applied Biochemistry and Biotechnology **151**: 686-699.

Farges, B., Duchez, D., Dussap, C. G. and Cornet, J. F. (2012) "Preliminary characterization of carbon dioxide transfer in a hollow fiber membrane module as a possible solution for gas-liquid transfer in microgravity conditions." Advances in Space Research **49**: 254-261.

Farmintzin, A. (1878) „Die Wirkung des Lichtes auf Algen und einige andere ihnen verwandte Organismen." Jahrbücher für Wissenschaftliche Botanik VI.

Federspiel, W. J. and Henchir, K. A. (2014) "Lung, Artificial: Basic principles and current applications." Encyclopedia of Biomaterials and Biomedical Engineering second edition, Taylor Francis online.

Fernandez, F. G. A., Camacho, F. G., Perez, J. A. S., Sevilla, J. M. F. and Grima, E. M. (1997) "A model for light distribution and average solar irradiance inside outdoor tubular photobioreactors for the microalgal mass culture." Biotechnology and Bioengineering **55**: 701-714.

Ferreira, B. S., Fernandes, H. L., Reis, A. and Mateus, M. (1998) "Microporous hollow fibers for carbon dioxide absorption: mass transfer model fitting and the supplying of carbon dioxide to microalgal cultures." Journal of Chemical Technology and Biotechnology **71**: 61-70.

Fett, J. P. and Coleman, J. R. (1994) "Regulation of Periplasmic Carbonic-Anhydrase Expression in *Chlamydomonas reinhardtii* by acetate and pH." Plant Physiology **106**: 103-108.

Figoli, A., Sager, W. F. C. and Mulder, M. H. V. (2001) "Facilitated oxygen transport in liquid membranes: review and new concepts" Journal of Membrane Science **181**: 97-110.

Finazzi, G., Rappaport, F., Furia, A., Fleischmann, M., Rochaix, J. D., et al. (2002) "Involvement of state transitions in the switch between linear and cyclic electron flow in *Chlamydomonas reinhardtii*." EMBO Reports **31**(31): 280-285.

Finazzi, G. (2005) "The central role of the green alga *Chlamydomonas reinhardtii* in revealing the mechanism of state transitions." Journal of Experimental Botany **56**: 383-388.

Finazzi, G., Johnson, G. N., Dall'Osto, L., Zito, F., Bonente, G., et al. (2006) "Nonphotochemical quenching of chlorophyll fluorescence in *Chlamydomonas reinhardtii.* " Biochemistry, **45**: 1490-1498.

Fischer, F. and Pfleiderer, G. (1922) "Über die Löslichkeit von Sauerstoff in verschiedenen organischen Lösungsmitteln." Zeitschrift für anorganische und allgemeine Chemie **124**: 61-69.

Folta, K. M. and Maruhnich, S. A. (2007) “Green light: a signal to slow down or stop.” Journal of experimental botany **58**(12): 3099-3111.

Forbes-Stovall, J., Howton, J., Young, M., Davis, G., Chandler, T., et al. (2014) “*Chlamydomonas reinhardtii* strain CC-124 is highly sensitive to blue light in addition to green and red light in resetting its circadian clock, with the blue-light photoreceptor plant cryptochrome likely acting as negative modulator.” Plant Physiology and Biochemistry **75**: 14-23.

Foster, K. W., Saranak, J., Patel, N., Zarilli, G., Okabe, M., et al. (1984) “A rhodopsin is the functional photoreceptor for phototaxis in the unicellular eukaryote *Chlamydomonas*.” Nature **311**: 756-759.

Foster, K. W., Saranak, J. and Zarilli, G. (1988) “Autoregulation of rhodopsin synthesis in *Chlamydomonas reinhardtii*.“ Proceedings of the National Academy of Sciences USA **85**: 6379-6383.

Frahm, B., Kirchner, S., Kauling, J., Brod, H., Langer, U. and Bödeker, B. (2007) “Dynamische Membranbegasung im Bioreaktor zur Intensivierung der Sauerstoffversorgung empfindlicher Zelllinien.“ Chemie Ingenieur Technik **79**(7): 1052-1058.

Frahm, B., Brod, H. and Langer, U. (2009) “Improving bioreactor cultivation conditions for sensitive cell lines by dynamic membrane aeration.” Cytotechnology **59**: 17-30.

Frenkel, A. W. (1952) “Hydrogen Evolution by the Flagellate Green Alga, *Chlamydomonas Moewusii*.” Archives of Biochemistry and Biophysics **38**: 219-230.

Fujiu, K., Nakayama, Y., Iida, H., Sokabe, M. and Yoshimura, K. (2011) “Mechanoreception in motile flagella of *Chlamydomonas*.” Nature cell biology. **13**: 630-632.

Gallucci, F., et al. (2011) "Introduction–A Review of Membrane Reactors." Membranes for Membrane Reactors: Preparation, optimization and selection: 1-61.

Garcia-Ochoa, F., Gomez, E., Santos, V. E. and Merchuk, J. C. (2010) “Oxygen uptake rate in microbial processes: An overview.” Biochemical Engineering Journal **49**: 289-307.

Gardner, R. D., Lohman, E., Gerlach, R., Cooksey, K. E. and Peyton, B. M. (2013) “Comparison of CO_2 and bicarbonate as inorganic carbon sources for triacylglycerol and starch accumulation in *Chlamydomonas reinhardtii*.” Biotechnology and Bioengineering **110**: 87-96.

Gasset, G., Tixador, R., Eche B., Lapchine, L., Moattt, N., et al. (1994) "Growth and division of *Escherichia coli* under microgravity conditions." Research in Microbiology **145**: 111-120.

Geider, R. J. and Osborne, B. A. (1992) „Algal photosynthesis." Chapman and Hall, New York.

Germain, E., Stephenson, T. and Pearce, P. (2005) "Biomass characteristics and membrane aeration: toward a better understanding of membrane fouling in submerged membrane bioreactors (MBRs)." Biotechnology and Bioengineering **90**(3): 316-322.

Giancoli, D. C. and Boyle, J. J. (2005) "Physics: principles with applications" Pearson Education.

Gille, A., Trautmann, A., Posten, C. and Briviba, K. (2016) "Bioaccessibility of carotenoids from *Chlorella vulgaris* and *Chlamydomonas reinhardtii*. " International Journal of Food Sciences and Nutrition **67**(5): 507-513.

Giordano, M., Beardall, J. and Raven, J. A. (2005) "CO_2 concentrating mechanisms in algae: Mechanisms, environmental modulation and evolution." Annual Review of Plant Biology **56**: 99-131.

Gitelson, I. I., Terskov, I. A., Kovrov, B. G., Sidko, F. Y, Lisovsky, G. M., et al. (1976) "Life Support System with autonomous control employing plant photosynthesis." Acta Astronautica **3**: 633-650.

Gitelson, I. I., Degermendzhy, A. G. and Rodicheva, E. K. (2003) "Self-restoration as fundamental property of CES providing their sustainability." Advances in Space Research **31**(7): 1641-1648.

Gódia, F., Albiol, J., Montesinos, J. L., Pérez, J., Creus, N., et al. (2002) "MELISSA: a loop of interconnected bioreactors to develop life support in space." Journal of Biotechnology **99**: 319-330.

Goldschmidt-Clermont, M. (1986) "The two genes for the small subunit of RuBP Carboxylase/oxygenase are closely linked in *Chlamydomonas reinhardtii*." Plant Molecular Biology **6**: 13-21.

Goodenough, U. W. and Heuser, J. E. (1985) "The Chlamydomonas cell wall and its constituent glycoproteins analyzed by the quick-freeze, deep-etch technique." The Journal of cell biology **101**: 1550-1568.

Gordon, J. and Polle, J. (2007) "Ultrahigh bioproductivity from algae." Applied Microbiology and Biotechnology **76**: 969-975.

Grossmann, A. R., Lohr, M. and Im, C. S. (2004) "*Chlamydomonas reinhardtii* in the landscape of pigments." Annual Review of Genetics **38**: 119-173.

Gualtieri, P., Passarelli, V. and Barsanti, L. (1989) "A simple instrument to perform *in vivo* absorption spectra of pigmented cellular organelles." Micron Microscopica Acta **20** (2): 107-110.

Häder, D. P., Colombetti, G., Lenci, F. and Quaglia, M. (1981) "Phototaxis in the flagellates, *Euglena gracilis* and *Ochromonas danica*." Archives of Microbiology **130**: 78-82.

Häder, D. P. (Ed.) (1999) "Photosynthese", Thieme, Stuttgart.

Häder, D. P., Hemmersbach, R. and Lebert, M. (2005) "Gravity and the behaviour of unicellular organisms." Cambridge University Press, Cambridge.

Haldall, P. (1957) "Importance of calcium and magnesium ions in phototaxis of motile green algae." Nature **26**: 215-216.

Harris, E. H. (2001) "*Chlamydomonas* as a model organism." Annual Review of Plant Physiology and Plant Molecular Biology **52**: 363-406.

Harris, E. H., Stern, D. B., and Witman, G. (2009) "The Chlamydomonas sourcebook". 2nd ed; Academic Press: Amsterdam, Boston.

Harvey, H. H. (1975) "Gas disease in fishes – a review." Proc. Chemistry and Physics of Aqueous Gas Solutions., Electrothermics and Metallurgy and Industrial Electrolytic Divisions, Electrochemical Society, Princeton, N.J., 450-485.

Haupt, W. (1959) „Phototaxis der Algen." Handbuch der Pflanzenphysiologie. Bd. 17/1. S. 318-370. E. Bünning. Springer, Berlin-Göttingen-Heidelberg.

Hegemann, P., Hegemann, U. and Foster, K. W. (1988) "Reversible bleaching of *Chlamydomonas reinhardtii* rhodopsin *in vivo*." Photochemistry and Photobiology **48**: 123-128.

Hegemann, P. and Harz, H. (1998) "How microalgae see the light. Microbial responses to light and time." Cambridge University Press, Cambridge.

Heifetz, P. B., Forster, B., Osmond, C. B., Giles, L. J. and Boynton, J. E. (2000) "Effects of acetate on facultative autotrophy in *Chlamydomonas reinhardtii* assessed by photosynthetic measurements and stable isotope analyses." Plant Physiology **122**: 1439-1445.

Heussler, P., Castillo, J., Merino, S. and Vasquez, V. (1978) "Improvement in pond construction and CO_2 supply for the mass production of microalgae." Archiv für Hydrobiologie **11**: 254-260.

Hey, M. J., Hilton, A. M. and Bee, R. D. (1994) "The formation and growth of carbon dioxide gas bubbles from supersaturated aqueous solutions." Food Chemistry **51**: 349-357.

Hikita, H. and Konishi, Y. (1984) "Desorption of carbon dioxide from supersaturated water in an agitated vessel." American Institute of Chemical Engineers Journal **30**(6): 945-950.

Hill, A. E., Shachar-Hill, B., Shachar-Hill, Y. (2004) "What are aquaporins for?" Journal of Membrane Biology **197**: 1-32.

Hoek, C.v.d., Mann, D. G., Jahns, H. M. (2002) "Algae: an introduction to phycology." Cambridge University Press, Cambridge.

Horneck, G. (1999) "Impact of microgravity on radiobiological processes and efficiency of DNA repair." Mutation Research **430**: 221-228.

Huang, K. and Beck, C. F. (2003) "Phototropin is the blue-light receptor that controls multiple steps in the sexual life cycle of the green alga *Chlamydomonas reinhardtii*." PNAS **100**(10): 6269-6274.

Hwang, T., Park, S. J., Oh, Y. K., Rashid, N. and Han, J. I. (2013) "Harvesting of *Chlorella sp*. KR-1 using a cross flow membrane filtration system equipped with an anti-fouling membrane." Bioresource Technology **139**: 379-382.

Jackson, M. L. (1994) "Energy effects in bubble nucleation." Industrial and Engineering Chemistry Research **33**: 929-933.

Jacobi, A., Steinweg, C., Rosello Sastre, R., and Posten, C. (2012 a) "Advanced photobioreactor LED illumination system: Scale-down approach to study microalga growth kinetics." Engineering in Life Sciences **12**(6): 621-630.

Jacobi, A., Bucharsky, E. C., Schell, K. G., Habisreuther, P., et al. (2012 b) "The application of transparent glass sponges for improvement of light distribution in photobioreactors." Journal

of Bioprocessing and Biotechniques **2**: 1-8.

Jacobi, A. (2013) "Optimierung der Lichtverteilung in Photobioreaktoren – Potentiale Antennen-reduzierter Mikroalgen Mutanten als biologischer Ansatz und transparenter Schwammstrukturen als technisches Konzept." Dissertation, Institut für Bio- und Lebensmitteltechnik (BLT), Karlsruher Institut für Technologie, KIT.

Javanmardian, M. and Palsson, B. (1991) "High-density photoautotrophic algal cultures: design, construction, and operation of a novel photo-bioreactor system." Biotechnology and Bioengineering **38** (10): 1182-1189.

Javanmardian, M. and Palsson, B. (1992) "Design and operation of an algal photobioreactor system." Advances in Space Research **12** (5): 5231-5235.

Johkan, M., Shoji, K., Goto, F., Hahida, S. and Yoshihara, T. (2012) "Effect of green light wavelength and intensity on photomorphogenesis and photosynthesis in *Lactuca sativa*." Environmental and Experimental Botany **75**: 128-133.

John, R. P., Anisha, G. S., Nampoothiri, K. M., Pandey, A. (2011) "Micro and macroalgal biomass: a renewable source for bioethanol." Bioresource Technology **102**(1): 186-193.

Juergens, M. T., Deshpande, R. R., Lucker, B. F., Park, J. J., Wang, H., et al. (2015) "The regulation of photosynthetic structure and function during nitrogen deprivation in *Chlamydomonas reinhardtii*." Plant physiology **167**: 558-573.

Jungandreas, A., Schellenberger, C. B., Jakob, T., von Bergen, M., Baumann, S., et al. (2014) "The acclimation of *Phaeodactylum tricornutum* to blue and red light does not influence the photosynthetic light reaction but strongly disturbs the carbon allocation pattern." PLOS-One **9**(8): 1-14.

Kam, V., Moseyko, N., Nemson, J. and Feldman, L. J. (1999) "Gravitaxis in *Chlamydomonas reinhardtii*: Characterization Using Video Microscopy and Computer Analysis." International Journal of Plant Sciences **160**: 1093-1098.

Kessler, J. O. (1985) "Hydrodynamic focusing of motile algal cells." Nature **313**: 218-220.

Khulbe, K. C., Feng, C. Y. and Matsuura, T. (2007) "Synthetic polymeric membranes, characterization by atomic force microscopy" Springer.

Kim, H. H., Goins, G. D., Wheeler, R. M. and Sager, J. C. (2004) "Green-light supplementation for enhanced lettuce growth under red- and blue-light-emitting diodes." HortScience, a publication of the American Society for Horticultural Science **39**(7): 1617-1622.

Kim, D. G., Lee, C., Park, S. M. and Choi, Y. E. (2014) "Manipulation of light wavelength at appropriate growth stage to enhance biomass productivity and fatty acid methyl ester yield using *Chlorella vulgaris*." Bioresource Technology **159**: 240-248.

Kindle, K. L. (1987) "Expression of a Gene for a Light-Harvesting Chlorophyll-a-Binding Chlorophyll-B-Binding Protein in *Chlamydomonas reinhardtii* - Effect of Light and Acetate." Plant Molecular Biology **9**: 547-563.

Klanjscek, T. and Legovic, T. (2001) "Toward a closed life support system for interplanetary missions." Ecological Modeling **138**: 41-54.

Klempnauer, K. H., Fischer, L. and Otto, M. K. (2008) "Einführung in die Biochemie" In: Bioprozesstechnik, Chmiel, H. (Ed), Spektrum Akademischer Verlag, Heidelberg.

Kliphuis, A. M. J., Martens, D. E., Janssen, M. and Wijffels, R. H. (2011) "Effect of O_2:CO_2 ratio on the primary metabolism of *Chlamydomonas reinhardtii*." Biotechnology and Bioengineering **108**: 2390-2402.

Kommareddy, A. and Anderson, G. (2003) "Study of light as parameter in the growth of algae in a photo-bio-reactor (PBR)." ASAE annual international meeting presentation 034057, Las Vegas, USA.

Komsic-Buchmann, K., Wöstehoff, L. and Becker, B. (2014) "The contractile vacuole as a key regulator of cellular water flow in *Chlamydomonas reinhardtii*." Eukaryotic Cell **13**(11): 1421-1430.

Kondo, T., Hirschie Johnson, C. and Woodland Hastings, J. (1991) "Action Spectrum for resetting the circadian phototaxis rhythm in the cw15 strain of *Chlamydomonas*." Plant Physiology **95**: 197-205.

Kong, Q. X., Li, L. Martinez, B., Chen, P and Ruan, R. (2010) "Culture of microalgae *Chlamydomonas reinhardtii* in wastewater for biomass feedstock production." Appl. Biochem. Biotechnol. **160**: 9-18.

Kordyum, E. (1997) "Biology of plant cells in microgravity and under clinostating." International

Review of Cytology **17**: 1-78.

Korogodin, V. I. (1966) "Problems of Post-Radiation Restoration." Atomizdat, Moscow. p. 392.

Kostoglou, M. and Karapantsios, T. D. (2007) "Bubble dynamics during the non-isothermal degassing of liquids. Exploiting microgravity conditions." Advances in colloid and interface science **134**: 125-137.

Kozaki, A. and Takeba, G. (1996) "Photorespiration protects C3 plants from photooxidation." Nature **384**: 557-560.

Kreimer, G. and Melkonian, M. (1990) "Reflection confocal laser scanning microscopy of eyespots in flagellated green algae." European Journal of Cell Biology **53**(1): 101-111.

Kropat, J., Hong-Hermesdorf, A., Casero, D., Ent, P., Castruita, M., et al. (2011) "A revised mineral nutrient supplement increases biomass and growth rate in *Chlamydomonas reinhardtii*." The Plant Journal **66**: 770-780.

Kruse, O., Rupprecht, J., Mussgnug, J. H., Dismukes, G. C. and Hankamer, B. (2005) "Photosynthesis: a blueprint for solar energy capture and biohydrogen production technologies." Photochemical and Photobiological Science **4**: 957-969.

Kuchitsu, K., Tsuzuki, M. and Miyachi, S. (1988) "Changes of Starch Localization within the Chloroplast induced by Changes in CO_2 Concentration during Growth of *Chlamydomonas reinhardtii*: Independent Regulation of Pyrenoid Starch and Stroma Starch." Plant and Cell Physiology **29**: 1269-1278.

Kulkarni, A. A. and Joshi, J. B. (2005) "Bubble formation and bubble rise velocity in gas-liquid systems: A review." Industrial & Engineering Chemistry Research **44**(16): 5873-5931.

Kung, C. (2005) "A possible unifying principle for mechanosensation." Nature **436**: 647-654.

Kuwahara, S. S., Cuello, J. L., Myhre, G. and Pau, S. (2011) "Growth of the green algae *Chlamydomonas reinhardtii* under red and blue lasers." Optics and Lasers in Engineering **49**: 434-438.

Lamers, P. P., van de Laack, C. C. W., Kaasenbrood, P. S., Lorier, J., Janssen, M., et al. (2010) "Carotenoid and fatty acid metabolism in light-stressed *Dunaliella salina*." Biotechnology and Bioengineering **106**(4): 638-648.

Lee, Y. K. and Hing, H. K. (1989) "Supplying CO_2 to photosynthetic algal cultures by diffusion through gas-permeable membranes." Applied Microbiology and Biotechnology **31**: 298-301.

Lee, C. G. and Palsson, B. (1994) "High-density algal photo-bioreactors using light-emitting diodes." Biotechnology and Bioengineering **44**(10): 1161-1167.

Lehmann, J., Piehl, G. W. and Schulz, R. (1987) "Bubble-free cell culture aeration with porous moving membranes." Developments in Biological Standardization **66**: 227-240.

Lehr, F. and Posten, C. (2009) "Closed photo-bioreactors as tools for biofuel production." Current Opinion in Biotechnology **20**: 280-285.

Lehr, F., Morweiser, M., Rosello Sastre, R., Kruse, O. and Posten, C. (2012) "Process development for hydrogen production with *Chlamydomonas reinhardtii* based on growth and product formation kinetics." Journal of Biotechnology **162** (1): 89-96.

Leiseifer, H. et al. (1983) "Biological Life Support Systems Environmental and Thermal Control for Space Vehicles." ESA SP-200, p.289-298.

Li, G. B., Liu, Y. D., Wang, G. H. and Song, L. R. (2004) "Reactive oxygen species and antioxidant enzymes activity of Anabena sp. PCC 7120 (Cyanobacterium) under simulated microgravity." Acta Astronautica **55**: 953-957.

Lichtenthaler, H. K. and Buschmann, C. (2001) "Chlorophylls and Carotenoids: Measurement and Characterization by UV-Vis Spectroscopy" John Wiley & Sons, Inc.

Lindsay, W. L. (1979) "Chemical equilibria in soils." Wiley.

Lubetkin, S. D. (1989) "The nucleation and detachment of bubbles." Journal of the Chemical Society, Faraday Transactions Journal **85**(7): 1753-1764.

Lund, L. W., Hattler, B. G. and Federspiel, W. J. (2002) "Gas permeance measurement of hollow fiber membranes in gas-liquid environment." American Institute of Chemical Engineers. AIChE Journal **48**(3): 635-643.

Luykx, P., Hoppenrath, M. and Robinson, D. G. (1997) "Structure and behavior of contractile vacuoles in *Chlamydomonas reinhardtii*." Protoplasma **198**: 73-84.

Lunze, J. (2008) „Regelungstechnik 1". Number Bd. 1 in Springer-Lehrbuch, Springer.

Maeda, I., Seto, Y., Ueda, S., Yukoh, C. G., Heri, J., et al. (2006) "Simultaneous control of turbidity and dilution rate through adjustment of medium composition in semi-continuous Chlamydomonas cultures." Biotechnology and Bioengineering **94** (4): 722-729.

Mann, H., Schiffelgen, H. and Froriep, R. (2009) "Analoge Übertragungsglieder" In: Einführung in die Regelungstechnik: Analoge und digitale Regelung, Fuzzy-Regler, Regler-Realisierung, Software, Carl Hanser Verlag München.

Marino, B., Mahato, T. R., Druitt, J. W., Leigh, L. and Lin, G. (1999) "The agricultural biome of Biosphere 2: Structure, composition and function." Ecological Engineering **13**: 199-234.

Massa, G. D., Emmerich, J. C., Morrow, R.C., Bourget, C. M. and Mitchell, C. A. (2006) "Plant-Growth lighting for space life support: a review." Gravitational Space Biology **19**(2): 19-30.

Mattoni, R. H. T., Keller, E. C., Ebersold, W. T., Eiserling, F. A. and Romig, W. R. (1971) "Induction of lysogenic bacteria in the space environment." In: The Experiments of Biosatellite II, J. Saunders (ed) NASA, Washington DC, NASA SP-204, pp: 309-324.

Mattos, E. R., Singh, M., Cabrera, M. L. and Das, K. C. (2015) "Enhancement of biomass production in *Scenedesmus bijuga* high-density culture using weakly absorbed green light." Biomass and Bioenergy **81**: 473-478.

Mayer, A. M. (1968) "*Chlamydomonas*: adaptation phenomena in phototaxis." Nature **217**: 875-876.

McCree, K. J. (1972) "The action spectrum, absorptance and quantum yield of photosynthesis in crop plants." Agricultural Meteorology **9**: 191-216.

Melis, A., Murakami, A., Nemson, J. A., Aizawa, K., Ohki, K. et al. (1996) "Chromatic regulation in *Chlamydomonas reinhardtii* alters photosystem stoichiometry and improves the quantum efficiency of photosynthesis." Photosynthesis research **47**: 253-265.

Melis, A., Zhang, L., Forestier, M., Ghirardi, M. L. and Seibert, M. (2000) "Sustained photobiological hydrogen gas production upon reversible inactivation of oxygen evolution in the green alga *Chlamydomonas reinhardtii*." Plant physiology **122**: 127-136.

Melkonian, M. and Robeneck, H. (1984) "The eyespot apparatus of flagellated green algae: a critical review." Progress in Phycological Research **3**: 193-286.

Meng, F., Chae, S. R., Drews, A., Kraume, M., Shin H. S., et al. (2009) "Recent advances in

membrane bioreactors (MBRs): Membrane fouling and membrane material." Water Research **43**: 1489-1512.

Mennigmann, H. D. and Lange, M. (1986) "Growth and differentiation of *Bacillus subtilis* under microgravity." Naturwissenschaften **73**: 415-417.

Merchant, S. S., Prochnik, S. E., Vallon, O., Harris, E. H., Karpowicz, S. J., et al. (2007) "The *Chlamydomonas* genome reveals the evolution of key animal and plant functions." Science **318**: 245-250.

Merkys, A. J. and Laurinavicius, R. S. (1990) "Plant growth in space." In: Fundamentals of Space Biology, M. Ashima and G. M. Laurinavicius (eds) Springer-Verlag, Berlin, pp: 69-83.

Mezhevikin, V. V., Okhonin, V. A., Bartsev, S. I. and Gitelson, J. I. (1994) "Indications and counterindications for applying different versions of closed ecosystems for space and terrestrial problems of life support." Advances in Space Research **14**(11): 11135-11142.

Min, S. K., Yoon G. H., Joo J. H., Sim S. J. and Shin, H. S. (2014) "Mechanosensitive physiology of *Chlamydomonas reinhardtii* under direct membrane distortion." Scientific reports **4**: 4675.

Mirmohseni, A., Seyed Dorraji, M. S., Figoli, A. and Tasselli, F. (2012) "Chitosan hollow fibres as effective biosorbent toward dye: Preparation and modeling." Bioresource Technology **121**: 212-220.

Miroshnichenko, L. I. (2003) "Radiation hazard in Space" Vol. 297, Dordrecht, The Netherlands: Astrophysics and Space Science Library.

Mittag, M., Kiaulehn, S. and Johnson, C. H. (2005) "The circadian clock in *Chlamydomonas reinhardtii*. What is it for? What is it similar to?" Plant Physiology **137**(2): 399-409.

Mohanty, K. and Purkait, M. K. (2011) "Membrane Technologies and Applications", CRC Press.

Mori, K., Ohya, H., Matsumoto, K., Furuune, H., Isozaki, K., et al. (1989) "Design for a bioreactor with sunlight supply and operations systems for use in the space environment." Advances in Space Research **9**(8): 8161-8168.

Moroney, J. V. (2001) "Carbon concentrating mechanisms in aquatic photosynthetic organisms: A report on CCM." Journal of Phycology **37**: 928-931.

Müller, P., Li, X. P. and Niyogi, K. K. (2001) "Non-photochemical quenching. A response to excess light energy." Plant Physiology **125**: 1558-1566.

Münzner, P. and Voigt, J. (1992) "Blue light regulation of cell division in *Chlamydomonas reinhardtii*." Plant Physiology **99**: 1370-1375.

Myers, J. (1963) "Space biology: ecological aspects: introductory remarks." The American Biology Teacher **25**: 409-411.

Nagel, G. D. O., Fuhrmann, M., Kateriya, S., Musti, A. M., Bamberg, E., et al. (2002) "Channelrhodopsin-1: a light-gated proton channel in green algae." Science **296**(5577): 2395-2398.

Nagel, G. T., Szellas, T., Kateriya, S., Adeishvili, N., Hegemann, P., et al. (2005) "Channelrhodopsins: directly light-gated cation channels." Biochemical Society Transactions **33**(4): 863-886.

Nakamura, Y., Kanakagiri, S., Van, K., He, W. and Spalding, M. H. (2005) "Disruption of the glycolate dehydrogenase gene in the high-CO2-requiring mutant HCR89 of *Chlamydomonas reinhardtii*." Canadian Journal of Botany-Revue Canadienne De Botanique **83**: 820-833.

Nakayama, Y., Fujiu, K., Sokabe, M. and Yoshimura, K. (2007) "Molecular and electrophysiological characterization of a mechanosensitive channel expressed in the chloroplasts of Chlamydomonas." Proceedings of the National Academy of Sciences of the United States of America. **104**: 5883-5888.

NASA (2004) "Advanced Life Support Program. Bounding the design space for space-craft internal atmosphere pressure and composition." Office of Biological and Physical Research, NASA Headquarters, Houston, Texas, USA.

Nedbal, L., Trtilek, M., Cerveny, J., Komárek, O. and Pakrasi, H. B. (2008) "A photobioreactor system for precision cultivation of photoautotrophic microorganisms and for high-content analysis of suspension dynamics." Biotechnology and Bioengineering **100**(5): 902-910.

Nedukha, E. M. (1996) "Possible mechanisms of plant cell wall changes at microgravity." Advances in Space Research **17**: 37-45.

Nelson, M., Allen J., Alling A., Dempster W. F. and Silverstone, S. (2003) "Earth applications of closed ecological systems: Relevance to the development of sustainability in our global

biosphere.” Advances in Space Research **31**(7): 1649-1655.

Nickelsen, J. and Kück, U. (2000) “The Unicellular Green Alga *Chlamydomonas reinhardtii* as an Experimental System to study Chloroplast RNA Metabolism.” Naturwissenschaften **87**: 97-107.

Nultsch, W., Thorm, G. and Rimscha, I. V. (1971) „Phototaktische Untersuchungen an *Chlamydomonas reinhardtii* Dangeard in homokontinuierlicher Kultur.“ Archives of Microbiology **80**: 351-369.

Ohad, I., Kyle, D. J. and Arntzen, C. J. (1984) “Membrane-Protein Damage and Repair - Removal and Replacement of Inactivated 32-Kilodalton Polypeptides in Chloroplast Membranes.” Journal of Cell Biology **99**: 481-485.

Oldenhof, H., Bisová, K., van den Ende, H. and Zachleder, V. (2004 a) “Effect of red and blue light on the timing of cyclin-dependent kinase activity and the timing of cell division in *Chlamydomonas reinhardtii*.” Plant Physiology and Biochemistry **42**: 341-348.

Oldenhof, H., Zachleder, V. and van den Ende, H. (2004 b) “Blue light delays commitment to cell division in *Chlamydomonas reinhardtii*.” Plant Biology **6**: 689-695.

Oguchi, M., Otsubo, K., Nitta, K., Shimada, A., Fujii, S., et al. (1989) “Closed and continuous algae cultivation system for food production and gas exchange in CELSS.” Advances in Space Research **9**(8): 8169-8177.

O'Toole, E. T., Giddings, T. H., McIntosh, J. R. and Dutcher, S. K. (2003) “Three-dimensional organization of basal bodies from wild-type and delta-tubulin deletion strains of *Chlamydomonas reinhardtii*.” Molecular biology of the cell **14**: 2999-3012.

Ozdemir, S.S., Buonomenna, M.G. and Drioli, E. (2006) “Catalytic polymeric membranes: next term preparation and application.” Applied Catalysis A: General Journal **307**: 167-183.

Paul, D. P. and Koros, W. J. (1976) “Effect of partially immobilizing sorption on permeability and the diffusion time lag.” Journal of Polymer Science: Polymer Physics **14**: 675-685.

Perez-Garcia, O., Escalante, F. M. E., de Bashan, L. E. and Bashan, Y. (2011) “Heterotrophic cultures of microalgae: Metabolism and potential products.” Water Research **45**: 11-36.

Petropoulos, J. H. (1970) “Quantitative analysis of gaseous diffusion in glassy polymers.” Journal of

Polymer Science: Polymer Physics **8**: 1797-1801.

Pinho, P., Jokinen, K. and Halonen, L. (2012) "Horticultural lighting - present and future challenges." Lighting Research and Technology **44**: 427-437.

Pirt, S. J., Lee, Y.K., Richmond, A. and Watts-Pirt, M. (1980) "The photosynthetic efficiency of *Chlorella* biomass growth with reference to solar energy utilization." Journal of Chemical Technology and Biotechnology **30**: 25-34.

Pittman, J. K., Dean A. P. and Osundenko, O. (2011) "The potential of sustainable algal biofuel production using wastewater resources." Bioresource Technology **102**(1): 17-25.

Planel, H., Tixador, R., Nefedov, Y., Gretchko, G. and Richoilley, G. (1982) "Effect of space flight factors at the cellular level: Results of the CYTOS experiment." Aviation, Space and Environmental Medicine **53**: 370-374.

Planel, H. (2004) "Space and Life. An Introduction to Space Biology and Medicine." CRC Press, Boca Raton.

Podhajsky, S., Slenzka, K., Harting, B., Di Capua, M., Posten, C., et al. (2014) "Physiological research and functional verification of the ModuLES-PBR". In: Presented at the 65th international astronautical congress IAC, Toronto

Polyakov, Y., Musaev, I., and Polyakov, S. (2010) "Closed bioregenerative life support systems: Applicability to hot deserts." Nature Precedings, doi.org/10.1038/npre.2010.3926.2.

Pope, D. H. and Berger, L. R. (1973) "Algal photosynthesis at increased hydrostatic pressure and constant pO_2." Archives of Microbiology **89**: 321-325.

Porra, R. (2002) "The chequered history of the development and use of simultaneous equations for the accurate determination of chlorophylls a and b." Photosynthesis Research **73**: 149-156.

Posten, C. and Walter, C. (2012) "Microalgal biotechnology: potential and production." De Gruyter, Berlin/Boston.

Pröschold, T., Harris E.H. and Coleman, A. W. (2005) "Portrait of a Species: *Chlamydomonas reinhardtii*." Genetics **170**(4): 1601-1610.

Pruvost, J. and Cornet, J. F. (2012) "Knowledge models for engineering and optimization of

photobioreactors.” In: Microalgal Biotechnology, C. Walter, C. Posten a. Ed. De Gruyter GmbH&Co. KG, pp. 181-224.

Qin, L., Yu, Q., Ai, W. and Guo, S. S. (2014) “Response of cyanobacteria to low atmospheric pressure.” Life Sciences in Space Research **3**: 55-62.

Qiu, D., Dhir, V. K., Chao, D., Hasan, M. M., Neumann, E., et al. (2002) “Single-bubble dynamics during pool boiling under low gravity conditions." Journal of thermophysics and heat transfer **16**(3): 336-345.

Radmer, R., Behrens, P. and Arnett, K. (1987) “Analysis of the productivity of a continuous algal culture system.” Biotechnology and Bioengineering **29**: 488-492.

Raven, P.H., Evert, R.F. and Eichhorn, S.E. (2005) “Biology of Plants” W. H. Freeman and Company, New York.

Rea, G., Esposito, D., Damasso, M., Serafini A., Margonelli, A., et al. (2008) “Ionizing radiation impacts photochemical quantum yield and oxygen evolution activity of Photosystem II in photosynthetic microorganisms.” International Journal of Radiation Biology **84** (11): 867-877.

Reitz, G., Facius, R. and Sandler, H. (1995) “Radiation protection in space.“ Acta Astronautica **35**: 313-338.

Richards, J. T., Corey, K. A., Paul, A. L., Ferl, R. J., Wheeler, R. M., et al. (2006) “Exposure of *Arabidopsis thaliana* to hypobaric environments: implications for low-pressure bioregenerative life support systems for human exploration missions and terraforming on Mars.” Astrobiology **6**(6): 851-866.

Ringo, D. L. (1967) “Flagellar motion and fine structure of the flagellar apparatus in Chlamydomonas.” The Journal of cell biology **33**: 543-571.

Robb, W. (1968) "Thin silicone membranes - their permeation properties and some applications." Annals of the New York Academy of Sciences **146**(1): 119-137.

Roberts, A. M. (2006) “Mechanisms of Gravitaxis in Chlamydomonas.” The Biological Bulletin **210**: 78-80.

Robeson, L. M. (2008) “The upper bound revisited.” Journal of Membrane Science **320**: 390-400.

Robinson, D. G. and Schlösser, U. G. (1978) "Cell wall regeneration by protoplasts of Chlamydomonas." Planta **141**: 83-92.

Rochaix, J. D. (1995) "*Chlamydomonas reinhardtii* as the photosynthetic yeast." Annual Review of Genetics **29**: 209-230.

Rodríguez, M. C., Barsanti, L., Passarelli, V., Evangelista, V., Conforti, V., et al. (2007) "Effects of chromium on the photosynthetic and photoreceptive apparatus of the alga *Chlamydomonas reinhardtii*." Environmental Research **105**: 234-239.

Rubio, F. C., Fernandez, F. G., Perez, J. A., Camacho, F.G. and Grima, E. M. (1999) "Prediction of dissolved oxygen and carbon dioxide concentration profiles in tubular photobioreactors for microalgal culture." Biotechnology and Bioengineering **62**(1): 71-86.

Ryan, W. L. and Hemmingsen, E. A. (1998) "Bubble formation at porous hydrophobic surfaces." Journal of Colloid and Interface Science **197**: 101-107.

Rygalov, V. Y. and Holmer, C. (2014) "Correlation between closure degree, trophic network complexity, and stability level for closed ecological systems designed for autonomous functioning in space." In: Presented at the 65th international astronautical congress IAC, Toronto.

Sager, R. (1955) "Inheritance in the green alga *Chlamydomonas reinhardtii*. " Genetics **40**: 476-489.

Sawdon, A. and Peng, C. A. (2015) "Internal deoxygenation of tubular photobioreactor for mass production of microalgae by perfluorocarbon emulsions." Journal of Chemical Technology and Biotechnology **90**: 1426-1432.

Scardina, P. and Edwards, M. (2001) "Prediction and measurement of bubble formation in water treatment." Journal of Environmental Engineering **127**(11): 968-973.

Scardina, P. and Edwards, M. (2002) "Practical Implications of Bubble Formation in Conventional Treatment." Journal American Water Works Association **94**(8): 85.

Scardina, P. (2004) "Effects of dissolved gas supersaturation and bubble formation on water treatment plant performance." Virginia Polytechnic Institute and State University.

Schaller, K. R. D. and Uhl, R. (1997) "How *Chlamydomonas* keeps track of the light once it has reached the right phototactic orientation." Biophysical Journal **73**(3): 1562-1572.

Schaub, G. and Vetter, A. (2007) "Biofuels – a review". Chemie Ingenieur Technik **79**: 569-578.

Schneider, M., Reymond, F., Marison, I. W. and von Stockar, U. (1995) "Bubble-free oxygenation by means of hydrophobic porous membranes." Enzyme and Microbial Technology **17**: 839-847.

Schönfeld, C., Wobbe, L., Borgstädt, R., Kienast A., Nixon, P. J., et al. (2004) "The Nucleus-encoded Protein MOC1 is Essential for Mitochondrial Light Acclimation in *Chlamydomonas reinhardtii*." Journal of Biological Chemistry **279**(48): 50366-50374.

Schreiber, U. and Vidaver, W. (1973) "Hydrostatic pressure: a reversible inhibitor of primary photosynthetic processes." Zeitschrift für Naturforschung. Teil C: Biochemie, Biophysik, Biologie, Virologie. **28**: 704-709.

Schwartzkopf, S. H. (1992) "Design of a controlled ecological life support system." Bioscience **42**(7): 526-535.

Schwister, K. (2005) "Taschenbuch der Verfahrenstechnik" Fachbuchverlag Leipzig im Carl Hanser Verlag.

Schwuchoh, J. M., Kern, V. D., White, N. J. and Sack, F. D. (2002) "Conservation of the plastid sedimentation zone in all moss genera with known gravitropic protonemata." Journal of Plant Growth Regulation **21**: 146-155.

Shanableh, A. (2007) "pH-Dependance and contributions of the carbonic species to CO_2 flux across the gas/liquid interface." Jordan Journal of Civil Engineering **1**(1): 109-122.

Shikanai, T. (2007) "Cyclic electron transport around photosystem I: Genetic approaches." Annual Review of Plant Biology **58**: 199-217.

Siaut, M., Cuiné, S., Cagnon, C., Fessler, B., Nguyen, M., et al. (2011) "Oil accumulation in the model green alga *Chlamydomonas reinhardtii*: characterization, variability between common laboratory strains and relationship with starch reserves." BMC biotechnology **11**, 7, doi: 10.1186/1472-6750-11-7.

Sievers, A., Buchen, B. and Hodick, D. (1996) "Gravity sensing in tip-growing cells." Trends in Plant Science **1**: 273-279.

Simone, S., Figoli, A., Criscuoli, A., Carnevale, M. C., Alfadul, S. M., et al. (2014) "Effect of selected spinning parameters on PVDF hollow fiber morphology for potential application in

desalination by VMD." Desalination **344**: 28-35.

Sineshchekov, O. A., Jung, K. H. and Spudich, J. L. (2002) "Two rhodopsins mediate phototaxis to lowand high-intensity light in *Chlamydomonas reinhardtii*." PNAS **99**(13): 8689-8694.

Slenzka, K. (2002) "Life Support for Aquatic Species – Past; Present; Future" Advances in Space Research **30**(4): 789-795.

Smith, A. H. (1975) "Principles of gravitational biology." In: Foundation of Space Biology and Medicine. Calvin M, Gazenko O (eds) NASA Washington DC, Vol II, Book 1, pp. 139-162.

Soeder, C. J. (1986) "An historical outline of applied algology." In: Richmond A (ed) CRC handbook of microalgal mass culture, pp. 25-41.

Souliès, A., Legrand, J., Marec, H. and Pruvost, J. (2016) "Investigation and modeling of the effects of the light spectrum and incident angle on the growth of *Chlorella vulgaris* in photobioreactors." Biotechnology Progress **32**(2): 247-261.

Spalding, M. H. (2008) "Microalgal carbon-dioxide-concentrating mechanisms: *Chlamydomonas* inorganic carbon transporters." Journal of Experimental Botany **59**: 1463-1473.

Spolaore, P., Joannis-Cassan, C., Duran, E. and Isamber, A. (2006) "Commercial Applications of Microalgae." Journal of Bioscience and Bioengineering **101**(2): 87-96.

Stabenau, H. and Winkler, U. (2005) "Glycolate metabolism in green algae" Physiologia Plantarum **123**: 235-245.

Stavis, R. L. and Hirschberg, R. (1973) "Phototaxis in *Chlamydomonas reinhardtii*." Journal of Cell Biology **59**: 367-377.

Stern, D. B. (2009) "The Chlamydomonas sourcebook: Organellar and metabolic processes" Vol. 2, 2. ed., Academic Press, Amsterdam.

Storhas, W. (1994) "Bioreaktoren und periphere Einrichtungen." Vieweg, Braunschweig, ISBN 3-528-06510-9.

Strauch, S. M., Schuster, M., Lebert, M., Richter, P., Schmittnägel, M., et al. (2008) "A closed ecological system in a space experiment." Journal of gravitational physiology **15**(2).

Stumm, W. and Morgan, J. J. (1981) "Aquatic chemistry: an introduction emphasizing chemical equilibria in natural waters." John Wiley.

Stutte, G. W., Monje, O., Goins, G. D. and Tripathy, B. C. (2005) "Microgravity effects on thylakoid, single leaf, and whole canopy photosynthesis of dwarf wheat." Planta **223**: 46-56.

Sun, J., Nishio, J. N. and Vogelmann, T. C. (1998) "Green Light Drives CO_2 Fixation Deep within Leaves." Plant and Cell Physiology **39**(10): 1020-1026.

Sun, X., Wang, C., Tang, Y., Wang, W. and Wie, J. (2013) "A comparative study of microfiltration and ultrafiltration for algae harvesting." Algal Research **2**: 437-444.

Tabony, J., Glade, N., Papaseit, C. and Demongeot, J. (2002) "Microtubule self-organization and its gravity dependence" In: Cell Biology and Biotechnology in Space, A Cogoli (ed) Advances in Space Biology and Medicine 8, Elsevier, Amsterdam, pp. 19-58.

Takache, H., Pruvost, J. and Cornet, J. F. (2012) "Kinetic modeling of the photosynthetic growth of *Chlamydomonas reinhardtii* in a photobioreactor." Biotechnology Progress **28**(3): 681-692.

Takahashi, T. and Watanabe, M. (1993) "Photosynthesis modulates the sign of phototaxis of wild-type *Chlamydomonas reinhardtii*. Effects of red background illumination and 3-(3',4'-dichlorophenyl)-1,1-dimethylurea." FEBS Letters **336**(3): 516-520.

Takemiya, A., Inoue, S. I., Doi, M., Kinoshita, T. and Shimazaki, K. I. (2005) "Phototropins promote plant growth in response to blue light in low light environments." The Plant cell **17**(4): 1120-1127.

Talbot, P., Gortares, M. P., Lencki, R. W. and de la Noue, J. (1991) "Absorption of CO_2 in algal mass culture systems: a different characterization approach." Biotechnology and Bioengineering **37**(9): 834-842.

Tamburic, B., Szabó, M., Tran, N. A. T., Larkum, A. W. D., Sugget, D. J., et al. (2014) "Action Spectra of oxygen production and chlorophyll a fluorescence in the green microalga *Nannochloropsis oculata*." Bioresource Technology **169**: 320-327.

Tamponnet, C. (1991) "Man in Space – A European Challenge in Biological Life Support." ESA Bulletin **67**: 38-49.

Tang, H., Chen, M., Simon, N. K. Y. and Salley, S. O. (2012) Continuous Microalgae Cultivation in a

Photobioreactor. Biotechnology and Bioengineering **109**(10): 2468-2474.

Teramoto, H., Nakamori, A., Minagawa, J. and Ono, T. (2002) "Light-intensity-dependent expression of Lhc gene family encoding light-harvesting chlorophyll-a/b proteins of photosystem II in *Chlamydomonas reinhardtii*." Plant Physiology **130**: 325-333.

Terashima, I., Fujita, T., Inoue, T., Chow, W. S. and Oguchi, R. (2009) "Green light drives leaf photosynthesis more efficiently than red light in strong white light: Revisiting the enigmatic question of why leaves are green." Plant Cell Physiology **50**(4): 684-697.

Terashima, I., Hanba, Y. T., Tholen, D. and Niinemets, U. (2011) "Leaf functional anatomy in relation to photosynthesis." Plant Physiology **155**: 108-116.

Tredici, M. R. (2010) "Photobiology of microalgae mass cultures: understanding the tools for next green revolution." Biofuels **1**(1): 143-162.

Turner, M. H. (1989) "Building an ecosystem from scratch." BioScience **39**: 147-150.

Vance, P. and Spalding, M. H., (2005) "Growth, photosynthesis, and gene expression in *Chlamydomonas* over a range of CO_2 concentrations and CO_2/O_2 ratios: CO_2 regulates multiple acclimation states." Canadian Journal of Botany-Revue Canadienne De Botanique **83**: 796-809.

Vítová, M., Bišová, K., Umysová, D., Hlavová, M., Kawano, S., et al. (2011) "*Chlamydomonas reinhardtii*: duration of its cell cycle and phases at growth rates affected by light intensity." Planta **233**: 75-86.

Vogelmann, T. C. (1993) "Plant tissue optics." Annual Review of Plant Physiology and Plant Molecular Biology **44**: 231-251.

Vorlop, J. and Lehmann, J. (1988) "Scale-up of bioreactors for fermentation of mammalian cell cultures with special reference to oxygen." Chemical Engineering and Technology **11**: 171-178.

Wagner, I., Braun, M., Slenzka, K. and Posten, C. (2015) "Photobioreactors in Life Support Systems" In: Advances in Biochemical Engineering/Biotechnology, Springer Berlin Heidelberg, pp.1-42.

Wagner, I., Steinweg, C. and Posten, C. (2016) "Mono- and dichromatic LED illumination leads to

enhanced growth and energy conversion for high-efficiency cultivation of microalgae for application in space.“ Biotechnology Journal **11**: 1060-1071.

Wagner, I. and Posten, C. (2017) “Pressure reduction affects growth and morphology of *Chlamydomonas reinhardtii*.” Engineering in Life Sciences **17**(5): 552-560.

Wang, G. H., Li G. B., Li D. H., Liu Y. D., Song, L. R., et al. (2004 a) “Real-time studies on microalgae under microgravity.” Acta Astronautica **55**: 131-137.

Wang, G. H., Li, G. B., Hu, C. X., Liu, Y. D., Song L. R., et al. (2004 b) “Performance of a simple closed aquatic ecosystem (CAES) in space.” Advances in Space Research **34**: 1455-1460.

Wang, G., Liu, Y., Li, G., Hu, C., Zhang, D. et al. (2008) “A simple closed aquatic ecosystem (CAES) for space.” Advances in Space Research **41**: 684-690.

Wayne, R., Staves, M. P. and Leopold, A. C. (1992) “The contribution of the extracellular matrix to gravisensing in characean cells.” Journal of Cell Science **101**: 611-623.

Weers, P. M. M. and Gulati, R. D. (1997) “Growth and reproduction of *Daphnia galeata* in response to changes in fatty acids, phosphorus, and nitrogen in *Chlamydomonas reinhardtii*.” Limnology and Oceanography **42**: 1584-1589.

Weger, H. G., Guy, R. D. and Turpin, D. H. (1990) “Cytochrome and Alternative Pathway Respiration in Green-Algae - Measurements Using Inhibitors and O-18(2) Discrimination.” Plant Physiology **93**: 356-360.

Weissig, H. and Beck, C. F. (1991) “Action spectrum for the light-dependent step in gamete differentiation in *Chlamydomonas reinhardtii*.” Plant Physiology **97**: 118-121.

Weitkamp, D. E. and Katz, M. (1980) "A review of dissolved gas supersaturation literature." Transactions of the American Fisheries Society **109**(6): 659-702.

Wharton, R. A., Smernoff D. T. and Averner, M. M. (1988) “Algae in Space.” Algae and Human Affairs, eds. C. A. Lembi and J. R. Waaland. Cambridge University Press, pp. 486-509.

Wingler, A., Lea, P. J., Quick, W. P. and Leegood, R. C., (2000) “Photorespiration: metabolic pathways and their role in stress protection.” Philosophical Transactions of the Royal Society of London. Series B: Biological Sciences **355**: 1517-1529.

Witman, G. B. (2009) "The Chlamydomonas sourcebook: Cell motility and behavior." Vol. 3, 2. ed., Academic Press, Amsterdam.

Wollman, F. A. (2001) "State transitions reveal the dynamics and flexibility of the photosynthetic apparatus:" The EMBO Journal **20**(14): 3623-3630.

Xia, Y., Lu, Y., Kamata, K., Gates, B., and Yin, Y. (2003) "Macroporous materials containing threedimensionally periodic structures" In: The Chemistry of Nanostructured Materials (Ed.: Yang, P.), World Scientific Publishing, pp. 69-100.

Xiao, Y., Liu, Y., Wang, G., Hao, Z. and An, Y. (2010) "Simulated microgravity alters growth and microcystin production in Microcystis aeruginosa (cyanophyta)." Toxicon **56**: 1-7.

Yoshimura, K. (1996) "A novel type of mechanoreception by the flagella of *Chlamydomonas*." The Journal of Experimental Biology **199**: 295-302.

Yoshimura, K. (1998) "Mechanosensitive Channels in the Cell Body of *Chlamydomonas*." Journal of Membrane Biology **166**: 149-155.

Yoshimura, K. (2003) "Gravitaxis in *Chlamydomonas reinhardtii* Studied with Novel Mutants." Plant and Cell Physiology **44**: 1112-1118.

Yun, Y. S. and Park, J. M. (2001) "Attenuation of monochromatic and polychromatic lights in *Chlorella vulgaris* suspensions." Applied Microbiology and Biotechnology **55**(6): 765-770.

Zhu, X. G., Long, S. P and Ort, D. R. (2008) "What is the maximum efficiency with which photosynthesis can convert solar energy into biomass?" Current Opinion in Biotechnology **19**: 153-159.

Zonia, L. and Munnik, T. (2007) "Life under pressure: hydrostatic pressure in cell growth and function." Trends in Plant Science **12**(3): 90-97.

11 Appendix

11.1 Medium used

11.1.1 TP-NO_3 medium for *C. reinhardtii* CC-1690 for 1 L culture medium

Table 11-1. 1 L culture medium for *C. reinhardtii* CC-1690.

TP-NO_3 medium
7.5 ml KNO_3 (1M stock solution)
10 ml $CaCl_2$ (5 g per L stock)
10 ml $MgSO_4$ (9.86 g per L stock)
8.33 ml Phosphate solution (14.34 g K_2HPO_4 and 7.26 g KH_2PO_4 per L stock)
10 ml Tris (1L stock solution) if no pH control
2 g KCl if pH control
1 ml of each individual stock solution of trace elements
Add to 1000 ml H_2O distilled

Table 11-2. Phosphate solution for 1 L TP-NO_3 medium

Phosphate solution (1000 ml)	Concentration of phosphate component
14.34 g K_2HPO_4 (anhydrous)	0.68 mM
7.26 g KH_2PO_4 (anhydrous)	0.45 mM

Table 11-3. Tris stock solution for 1 L TP-NO_3 medium

Tris stock solution (1000 ml)	Concentration
242 g Tris base	20 mM

Table 11-4. Trace elements: preliminary concentrated stock solutions

Preliminary stock solutions	Concentration	Composition
Pre-1 EDTA-Na_2 concentrate	125 mM	13.959 g in ~ 250 mM, titrate to pH 8.0 with trace element grade KOH (~1.7 g), and bring up to a volume of 300 mL
Pre-2 $(NH_4)_6Mo_7O_{24}$	285 μM	$(NH_4)_6Mo_7O_{24}\cdot 4H_2O$: 0.088 g, bring up to a

concentrate		volume of 250 mL
Pre-2a $Na_2MoO_4 \cdot 2H_2O$	2.43 mM	$Na_2MoO_4 \cdot 2H_2O$: 0.125 g bring up to a volume of 250 mL
Pre-3 Na_2SeO_3 concentrate	1 mM	Na_2SeO_3: 0.043 g, bring up to a volume of 250 mL

Table 11-5. Individual trace elements stock solution (1000x)

Stock solution	Concentration in stock	Composition
1. EDTA-Na_2	25 mM	EDTA-Na_2: 50 mL of 125 mM EDTA-Na_2 concentrate (Pre-1) from step A
2. $(NH_4)_6Mo_7O_{24}$	28.5 µM*	$(NH_4)_6Mo_7O_{24} \cdot 4H_2O$: 25 mL of 285 µm $(NH_4)_6Mo_7O_{24}$ concentrate (Pre-2) from step A
2.a $Na_2MoO_4 \cdot 2H_2O$	0.243 mM	$Na_2MoO_4 \cdot 2H_2O$: 25 mL of 2.43 mM $Na_2MoO_4 \cdot 2H_2O$ (Pre-2a) from step A
3. Na_2SeO_3	0.1 mM	Na_2SeO_3: 25 mL of 1 mM Na_2SeO_3 concentrate (Pre-3) from step A
4. Zn·EDTA	2.5 mM	$ZnSO_4 \cdot 7H_2O$: 0.18 g
	2.75 mM	EDTA-Na_2: 5.5 mL of 125 mM EDTA-Na_2 concentrate (Pre-1) from step A
5. Mn·EDTA	6 mM	$MnCl_2 \cdot 4H_2O$: 0.297 g
	6 mM	EDTA-Na_2: 12 mL of 125 mM EDTA-Na_2 concentrate (Pre-1) from step A
6. Fe·EDTA	20 mM	$FeCl_3 \cdot 6H_2O$: 1.35 g
	22 mM	EDTA-Na_2: 2.05 g
	22 mM	Na_2CO_3 (sodium carbonate): 0.58 g
	Combine EDTA-Na_2 with sodium carbonate in water and mix. Add $FeCl_3 \cdot 6H_2O$ after the first two components dissolve. Do not use Pre-1	
7. Cu·EDTA	2 mM	$CuCl_2 \cdot 2H_2O$: 0.085 g
	2 mM	EDTA-Na_2: 4 mL of 125 mM EDTA-

	Na_2 concentrate (Pre-1) from step A

Notes:

*The final [Mo] in the 1x medium is 0.2 µM; total [EDTA] in 1x medium: (25 + 2.75 + 6 + 22 + 2) = 57.75 µM

11.1.2 TP-medium for *C. reinhardtii* WT13 for 1L culture medium

Table 11-6. TP-medium for *C. reinhardtii* WT13

1 L TP-medium
2.42 g Tris
25 ml TP salt solution
375 µl p-solution
10 ml Hutners' trace (100x)
pH 7, add to 1000 ml H_2O distilled
for plates, 15 g agar agar per 1 L

Note: 10x TP-NO_3 medium was prepared with the same amounts of components, just filled up to 100 ml H_2O distilled without adjustment of pH.

Table 11-7. 1 L salt solution for TP-medium

Salt	Amount
NH_4Cl	15.0 g
$MgSO_4 \cdot 7H_2O$	4.0 g
$CaCl_2 \cdot 2H_2O$	2.0 g
Add to 1000 ml H_2O distilled	

Table 11-8. p-solution for TP-medium

Component	Amount
K_2HPO_4	28.8 g
KH_2PO_4	14.4 g
Add to 100 ml H_2O distilled	

Table 11-9. Hutner's trace elements

Hutner's trace solution	
EDTA disodium salt	5.0 g
H_3BO_3	1.14 g
$ZnSO_4 \cdot 7H_2O$	2.2 g
$MnCl_2 \cdot 4H_2O$	0.51 g
$FeSO_4 \cdot 7H_2O$	0.5 g
$CoCl_2 \cdot 6H_2O$	0.16 g
$CuSO_4 \cdot 5H_2O$	0.16 g
$(NH_4)_6Mo_7O_{24} \cdot 4H_2O$	0.11 g
Add to 1000 ml H_2O distilled	

11.1.3 Media for sterile tests

Table 11-10. Medium for bacterial plates

Component	Concentration [g L^{-1}]
peptone	15
yeast extract	3
glucose	1
NaCl	6
agar	12

Table 11-11. Medium for fungal plates

Component	Concentration [g L^{-1}]
peptone	1
malt extract	20
glucose	20
agar	15

11.2 Experimental setups

11.2.1 Setup for membrane tests

A

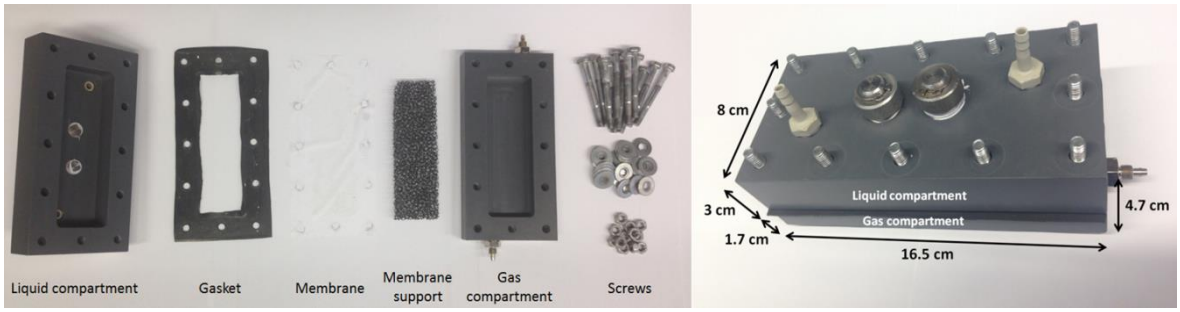

B

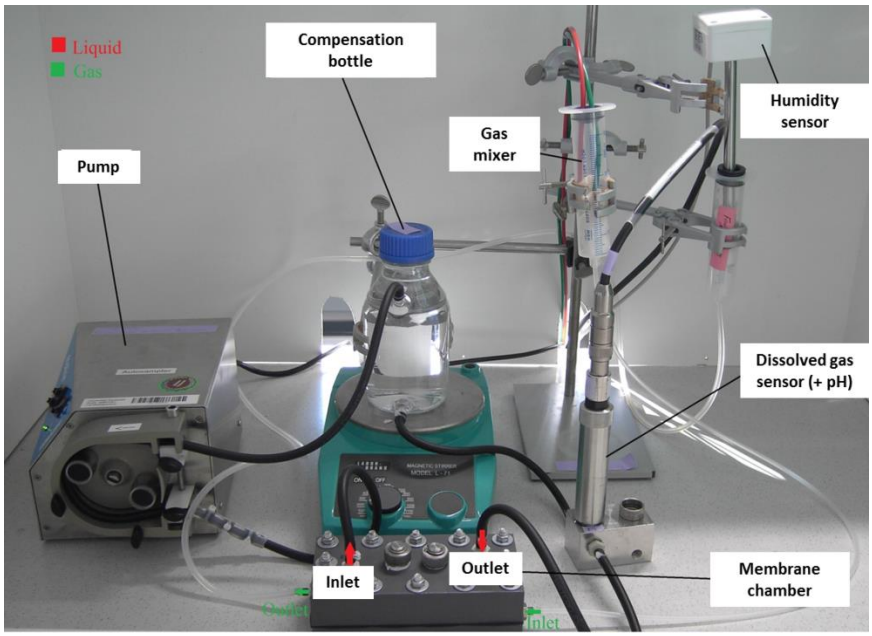

Figure 11-1. Membrane testing unit. A) Single parts of testing chamber with dimensions. B) Overall setup for membrane tests.

11.2.2 Membrane-aerated lab scale modular photobioreactor

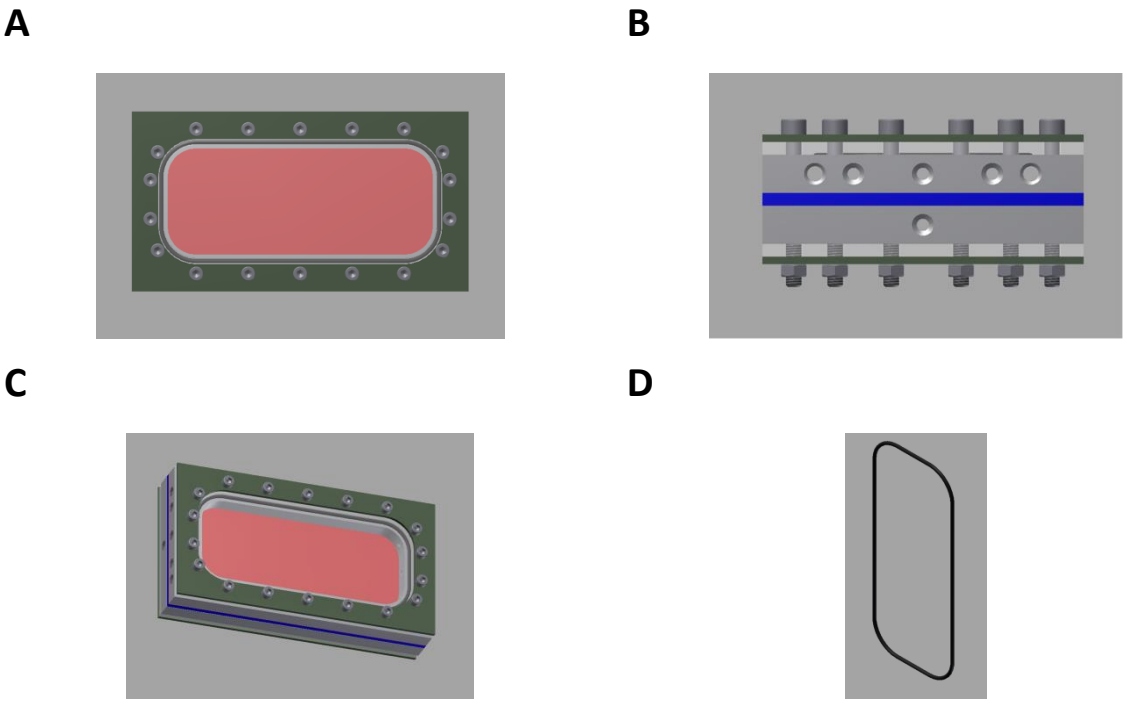

Figure 11-2. Technical drawings of the membrane-aerated photobioreactor. A) Top view B) Side view with liquid and gas inlets. C) Position of ring gasket. D) Ring gasket made from fluoroelastomer.

11.2.3 Stirred tank photobioreactor

Figure 11-3. 1.8L model reactor. KLF 2000 bioreactor (Bioengineering AG).

11.3 Pump calibration curves

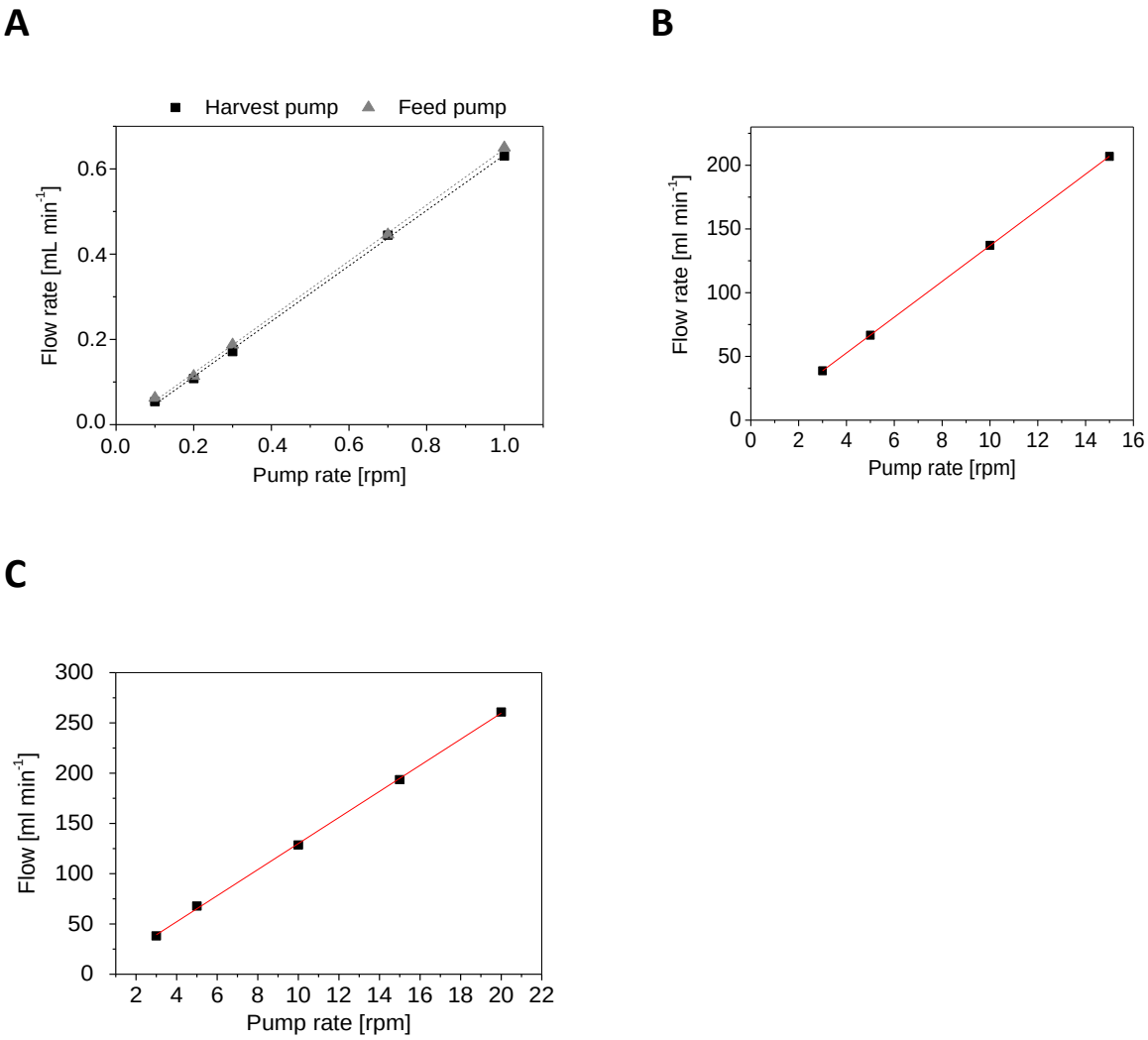

Figure 11-4. Calibration curves of pumps. A) Miniplus pumps for feed and harvest flows during continuous cultivations in stirred tank photobioreactor. Correlation between set up pump stage and flow rate in ml min^{-1} Harvest: y = 0.65·x-0.02; Feed: y = 0.66·x-0.01. B) Calibration curve for the peristaltic pump in the bypass loop of the membrane testing unit, Ecoline ISM1-B, pumphead 280: y = 14.025·x-3.35. C) Calibration curve for the peristaltic pump in the bypass loop of the membrane testing unit, Ecoline ISM1-B, pumphead 380: y = 12.969·x-0.306.

11.4 LED data sheets

11.4.1 ModuLES-PBR

11.4.1.1 First parabolic flight campaign

curve of spectrum power distributing

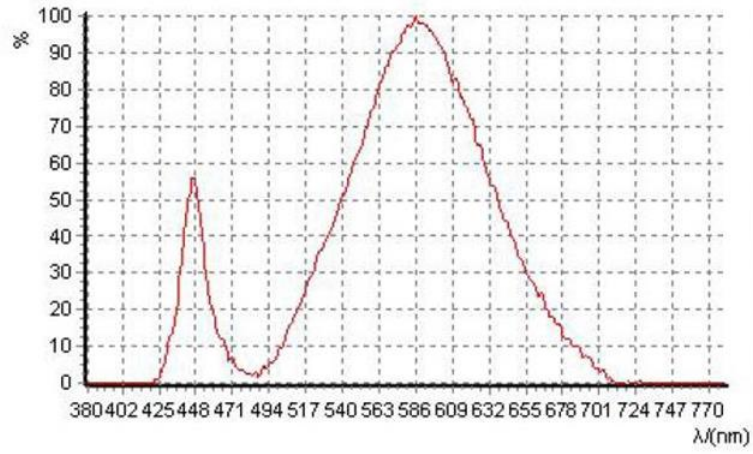

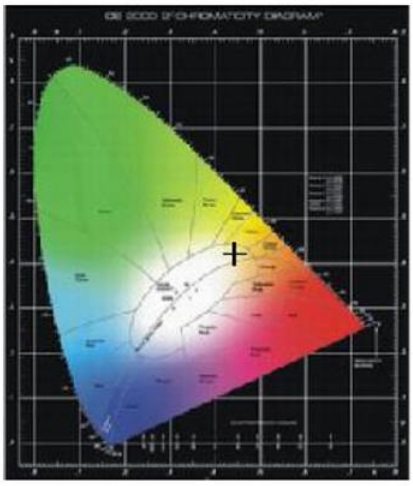

Spectrum		Electrical	
λp:	586.0 nm	I(warm-up):	mA
λd:	582.4 nm	warm-up Time:	ms
λm:	545.2 nm	I(test):	mA
λc:	524.0 nm	V(Forward):	3.18 V
Δλ:	98.0 nm	φv:	6789.3 mlm
Tc:	2906 K	Light Effi:	0.000 lm/w
CIE(x,y):	0.4477, 0.4141	Light Power:	17.2775 mw
CIE(u,v):	0.2531, 0.3512		
Ra:	59.8		
Purity:	0.587	V(reverse):	V
		I(Leakage):	0.0 uA

Figure 11-5. LED emission spectrum, first parabolic flight campaign, PFC 23, warm-white, 3000 K, Ledxon.

11.4.1.2 Second parabolic flight campaign

epitex

Opto-Device & Custom LED SMD TYPE LED SMT450

Lead (Pb) Free Product – RoHS Compliant

SMT450

High Performance Blue color TOP LED

SMT450 consists of an InGaN LED mounted on the lead frame as TOP LED package and is 200mcd typical of Brightness.
It emits a spectral band of radiation at 450nm.

♦Specifications

1) Product Name	TOP LED
2) Type No.	SMT450
3) Chip	
(1) Chip Material	InGaN
(2) Peak Wavelength	450nm typ.
4) Package	
(1) Lead Frame Die	Silver Plated
(2) Package Resin	PPA Resin
(3) Lens	Epoxy Resin

♦Outer dimension (Unit: mm)

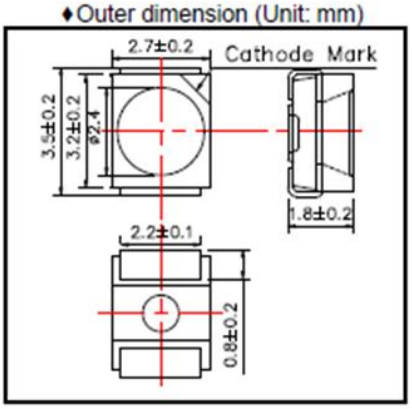

♦Absolute Maximum Ratings

Item	Symbol	Maximum Rated Value	Unit	Ambient Temperature
Power Dissipation	P_D	190	mW	Ta=25°C
Forward Current	I_F	50	mA	Ta=25°C
Pulse Forward Current	I_{FP}	200	mA	Ta=25°C
Reverse Voltage	V_R	5	V	Ta=25°C
Operating Temperature	T_{OPR}	-30 ~ +80	°C	
Storage Temperature	T_{STG}	-40 ~ +80	°C	
Soldering Temperature	T_{SOL}	250	°C	

‡Pulse Forward Current condition: Duty=1% and Pulse Width=10us.
‡Soldering condition: Soldering condition must be completed within 5 seconds at 250°C

♦Electro-Optical Characteristics [Ta=25°C]

Item	Symbol	Condition	Minimum	Typical	Maximum	Unit
Forward Voltage	V_F	I_F=20mA		3.3	4.0	V
Reverse Current	I_R	V_R=5V			10	uA
Radiated Power	P_O	I_F=20mA		16		mW
Radiant Intensity	I_E	I_F=20mA		4		mW/sr
Brightness	I_V	I_F=20mA	100	200		mcd
Peak Wavelength	λ_P	I_F=20mA	440	450	460	nm
Half Width	$\Delta\lambda$	I_F=20mA		20		nm
Viewing Half Angle	$\theta_{1/2}$	I_F=20mA		±55		deg.

‡Radiated Power is measured by S3584-08.
‡Radiant Intensity is measured by Tektronix J-6512.
‡Brightness is measured by Tektronix J-16.

EPITEX INC.: 66-3 Minami-Kawabe Cho, Higashi-Kujyo, Minami-Ku, Kyoto, Japan
Tel: ++81-75-682-2338 Fax: ++81-75-682-2267
e-mail: sales-dep@epitex.com http://www.epitex.com

Figure 11-6: Datasheet blue LEDs for second parabolic flight campaign with ModuLES-PBR.

epitex

Opto-Device & Custom LED TOP IR LED SMT680

Lead (Pb) Free Product – RoHS Compliant

SMT680

High Performance Infrared TOP IR LED

SMT680 consists of an AlGaAs LED mounted on the lead frame as TOP LED package and is sealed with epoxy or silicone resin.
It emits a spectral band of radiation at 690nm.

♦Outer dimension (Unit:mm)

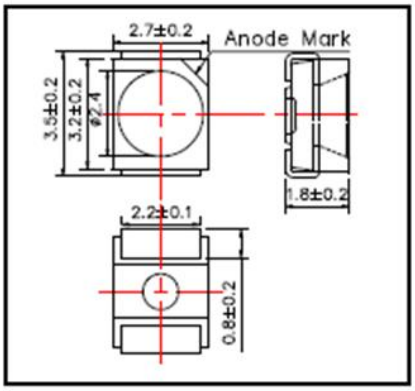

♦Specifications

1) Product Name	TOP IR LED
2) Type No.	SMT680
3) Chip	
(1) Chip Material	AlGaAs
(2) Peak Wavelength	680nm typ.
4) Package	
(1) Lead Frame Die	Silver Plated
(2) Package Resin	PPA Resin
(3) Lens	Epoxy or silicone Resin

♦Absolute Maximum Rating

Item	Symbol	Maximum Rated Value	Unit	Ambient Temperature
Power Dissipation	P_D	100	mW	Ta=25°C
Forward Current	I_F	50	mA	Ta=25°C
Pulse Forward Current	I_{FP}	200	mA	Ta=25°C
Reverse Voltage	V_R	5	V	Ta=25°C
Operating Temperature	T_{OPR}	-40 ~ +80	°C	
Storage Temperature	T_{STG}	-40 ~ +80	°C	
Soldering Temperature	T_{SOL}	250	°C	

‡Pulse Forward Current condition: Duty=1% and Pulse Width=10us.
‡Soldering condition: Soldering condition must be completed within 5 seconds at 250°C

♦Electro-Optical Characteristics [Ta=25°C]

Item	Symbol	Condition	Minimum	Typical	Maximum	Unit
Forward Voltage	V_F	I_F=50mA		1.90	2.30	V
Reverse Current	I_R	V_R=5V			10	uA
Total Radiated Power	P_O	I_F=50mA	5.0	8.0		mW
Radiant Intensity	I_E	I_F=50mA		6.0		mW/sr
Peak Wavelength	λ_P	I_F=50mA	670	680	690	nm
Half Width	$\Delta\lambda$	I_F=50mA		25		nm
Viewing Half Angle	$\theta_{1/2}$	I_F=50mA		±55		deg.
Rise Time	tr	I_F=50mA		80		ns
Fall Time	tf	I_F=50mA		80		ns

‡Total Radiated Power is measured by Photodyne #500
‡Radiant Intensity is measured by Tektronix J-6512.

EPITEX INC.: 66-3 Minami-Kawabe Cho, Higashi-Kujyo, Minami-Ku, Kyoto, Japan
Tel: ++81-75-682-2338 Fax: ++81-75-682-2267
e-mail: sales-dep@epitex.com http://www.epitex.com

Figure 11-7. Datasheet red LEDs for second parabolic flight campaign with ModuLES-PBR.

11.5 Analytical procedures

11.5.1 CDW-OD_{750} correlation factor

In order to obtain a correlation of CDW and OD_{750} values for *C. reinhardtii* CC-1690 and WT13 cells, the alga was cultivated in surface-aerated shaking flasks on a LED rotary shaker with warm-white LED illumination at a PFD of 50 µE m^{-2} s^{-1}. After analyzing samples for OD_{750} and CDW (determined gravimetrically) the results were fitted to a linear equation, where the slope of the curve displays the correlation factor. By this means the correlation curve was established:

For *C. reinhardtii* CC-1690 cells:

$$CDW\ [g\ L^{-1}] = 0.28\ [g\ L^{-1}\ AU^{-1})] \cdot OD_{750}\ [AU]$$

For *C. reinhardtii* WT13 cells:

$$CDW\ [g\ L^{-1}] = 0.45\ [g\ L^{-1}\ AU^{-1})] \cdot OD_{750}\ [AU]$$

In case of aggregate formation (palmelloids or secondary aggregates) for CC-1690 cells, this correlation could not be used and individual samples were withdrawn during linear growth phases of batch and fed-batch processes (or during steady-state phases of continuous cultivations) for gravimetrical analysis of CDW in relation to the photometrically determined OD_{750} value.

11.5.2 Starch analysis

Starch content of *C. reinhardtii* cells was analyzed using a sulfur anthrone method. This method is based on the acidic hydrolysis of polysaccharides to obtain monosaccharides and a later reaction with the anthrone reagent to a color complex which can be photometrically determined at 625 nm. Cell pellets were resuspended and diluted to a CDW of 0.2 to 0.5 g L^{-1} with distilled water to achieve a final volume of 400 µL. 800 µL of anthrone reagent were added, composed of 1 g L^{-1} anthrone in 96% sulphuric acid. The mixture was gently mixed and the sample was placed on ice for five minutes. Following this, the sample was placed in a thermomixer for 16 minutes at 95°C. After the reaction the reaction tubes were cooled down on ice for another 5 minutes followed by centrifugation for 10 min, at 4°C and 10,000 rpm. The supernatant was then used for the absorption measurement at 625 nm against pure water as blank. A calibration curve for different starch concentration and the corresponding A625 was established by using solutions with 0.02, 0.05, 0.1, 0.125, 0.13, 0.15 and 0.2 g L^{-1} starch. A linear correlation between concentration and absorption exists within the range of 0.22 to 0.26 g L^{-1}.

11.6 Further experimental data and supporting information

11.6.1 Efficient illumination of microalgae cultures

11.6.1.1 Spectral response curve of the planar quantum sensor

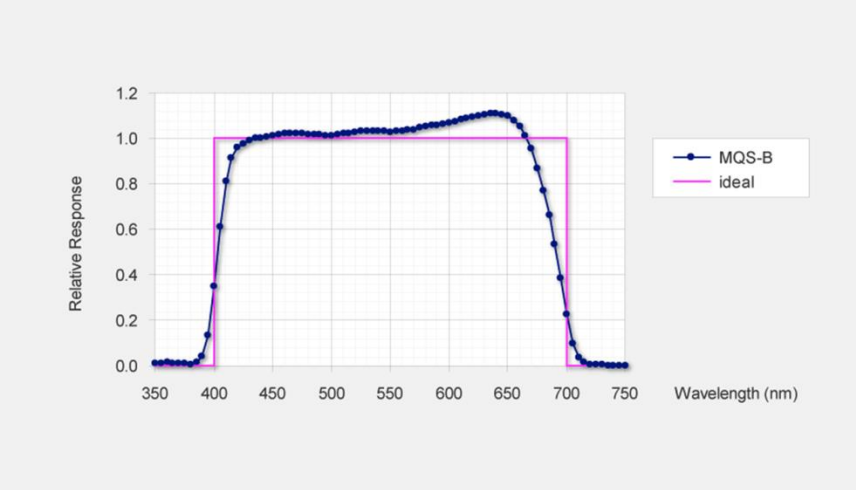

Figure 11-8. Spectral response curve of MQS-B sensor (blue line with dots). Pink line shows the ideal response of a photon flux sensor for photosynthetically active radiation. Source: Datasheet planar quantum sensor MQS-B, Walz Mess- und Regelungstechnik, Effeltrich, Germany.

11.6.1.2 Calibration curves of mini- and midiplate LED panels

In case of warm-white mini- and midiplate illumination, LED calibration curves were derived from a previous work (Jacobi 2013).

A

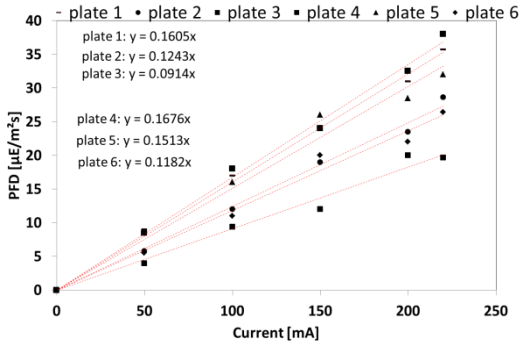

B

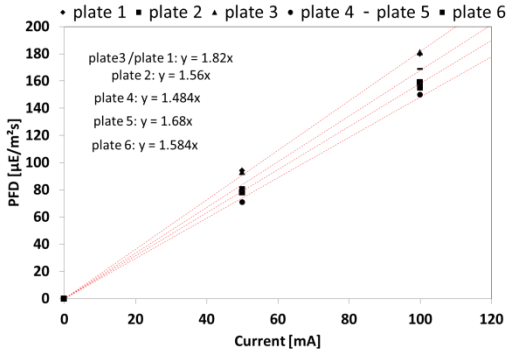

C

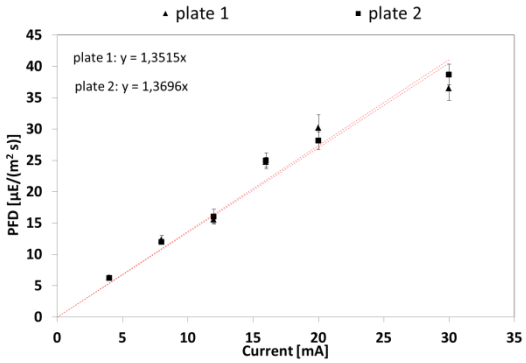

Figure 11-9. LED calibration curves for mini- and midiplate illumination. A) Red LEDs miniplates. B) Blue LEDs miniplates. C) Green LEDs miniplates.

11.6.1.3 Effects of light color and intensity on pigment content

In relation to Chapter 4.4, the following tables show the measured specific pigment concentrations in dependence on the applied light color and intensity.

Table 11-12. Specific pigment concentrations for low PFDs (25 µE m^{-2} s^{-1}) in miniplate reactors at 25°C.

Light color/Mixture	Chl a [mg g^{-1} CDW]	Chl b [mg g^{-1} CDW]	Car [mg g^{-1} CDW]
Warm-white	45.6 ± 6.5	16.9 ± 1.0	14.6 ± 2.1
Red (680 nm)	33.5 ± 0.3	10.2 ± 0.3	12.3 ± 3.8
Blue (447 nm)	50.3 ± 12.6	18.4 ± 3.1	16.2 ± 4.0
Green (520 nm)	55.7 ± 9.9	19.8 ± 3.7	17.9 ± 3.5
Shift (blue to red)	39.6 ± 2.6	14.3 ± 0.9	14.7 ± 1.0
90% red 10% blue	41.6 ± 1.5	12.8 ± 2.1	14.7 ± 1.1
80% red 20% blue	58.0 ± 2.4	20.8 ± 1.0	19.1 ± 0.5
70% red 30% blue	50.9 ± 7.4	19.7 ± 5.7	16.6 ± 5.9
50% red 50% blue	51.2 ± 2.7	17.4 ± 3.8	16.8 ± 0.1
25% red 75% blue	49.3 ± 3.8	17.6 ± 3.4	15.5 ± 2.3
90% red 10% green	32.2 ± 3.7	12.6 ± 4.0	10.1 ± 1.9

Table 11-13. Specific pigment concentrations for warm-white control and 90/10 red/blue illumination in miniplate reactors at 25°C.

PFD [µE m^{-2} s^{-1}]	Light color/ Mixture	Chl a [mg g^{-1} CDW]	Chl b [mg g^{-1} CDW]	Car [mg g^{-1} CDW]
25	ww	45.6 ± 6.5	16.9 ± 1.0	14.6 ± 2.1
	90/10 r/b	41.6 ± 1.5	12.8 ± 2.1	14.7 ± 1.1
50	ww	44.6 ± 4.5	18.9 ± 3.9	17.8 ± 1.8
	90/10 r/b	26.9 ± 0.6	12.5 ± 1.3	10.6 ± 1.4
100	ww	32.1 ± 4.8	12.7 ± 1.7	13.6 ± 1.9
	90/10 r/b	15.6 ± 2.3	12.5 ± 0.8	15.8 ± 1.2
150	ww	14.7 ± 5.7	11.6 ± 3.9	12.0 ± 3.9
	90/10 r/b	15.2 ± 0.1	13.6 ± 1.0	12.1 ± 0.8
200	ww	15.0 ± 2.5	7.6 ± 1.8	8.2 ± 0.6

Table 11-14. Specific pigment concentrations for warm-white control and 90/10 red/blue illumination in midiplate reactors at 25°C.

PFD [µE m^{-2} s^{-1}]	Light color/ Mixture	Chl a [mg g^{-1} CDW]	Chl b [mg g^{-1} CDW]	Car [mg g^{-1} CDW]
25	ww	54.6 ± 0.1	20.6 ± 0.0	17.4 ± 0.0
	90/10 r/b	36.0 ± 0.0	13.9 ± 0.0	12.3 ± 0.0
50	ww	18.8 ± 0.2	7.8 ± 0.2	8.9 ± 0.2
	90/10 r/b	23.2 ± 0.2	10.4 ± 0.2	11.1 ± 0.2
100	ww	25.7 ± 0.9	13.2 ± 0.5	13.5 ± 0.3
	90/10 r/b	18.1 ± 0.5	8.8 ± 0.3	8.9 ± 0.2
150	ww	13.1 ± 4.3	6.3 ± 2.0	7.5 ± 3.9
	90/10 r/b	14.0 ± 3.6	6.0 ± 3.0	7.4 ± 1.7
200	ww	16.0 ± 1.3	12.1 ± 1.5	5.8 ± 0.4
	90/10 r/b	25.9 ± 2.4	17.7 ± 3.2	8.0 ± 1.0

11.6.1.4 Starch content in dependence on applied wavelengths and intensity

Starch content of the cells was analyzed for samples in the linear to stationary growth phase of the cultures. In Figure 11-10 the dependency of starch concentration on illumination regimes with respect to the applied light color and PFD is depicted. Figure 11-10 A shows results for specific starch content for all tested light colors at low PFDs in miniplates except for red/blue 25/75 and red/green 90/10 (see

also Table 11-15). With respect to the displayed error bars no tremendous differences in specific starch content can be noticed between the different lighting approaches.

A

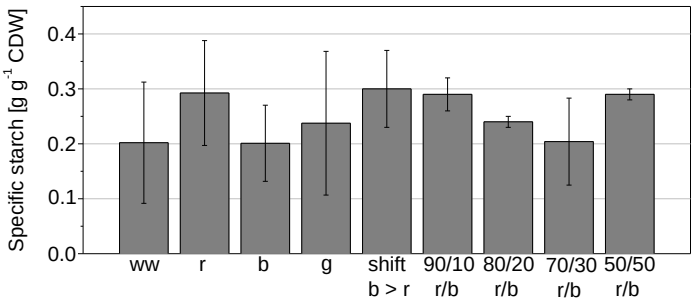

B

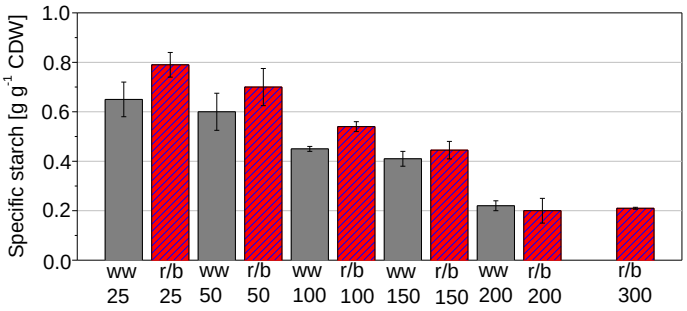

Figure 11-10. Dependency of specific starch content on light color and PFD. A) Specific starch content of cells illuminated with different light colors compared to full spectrum at low light intensities of 25 µE m^{-2} s^{-1} in miniplates at 25°C. B) Specific starch content with higher PFDs for dichromatic 90/10 red/blue in comparison to full spectrum illumination in midiplates at 25°C.

Specific concentrations vary between 0.2 and 0.3 g g^{-1} CDW where no clear tendency can be manifested. Large standard deviations may be the result from an analytical protocol which has not been specifically modified to *C. reinhardtii*. Figure 11-10 B shows results for specific starch concentrations for dichromatic 90/10 red/blue illumination in comparison to full spectrum illumination in midiplates at 25°C.

Table 11-15. Specific starch concentrations for the tested light colors and color mixtures in comparison with full spectrum illumination in miniplates at 25°C.

Light color/Mixture	Starch [g g^{-1} CDW]
Warm-white	0.2 ± 0.1
Red (680 nm)	0.3 ± 0.1
Blue (447 nm)	0.2 ± 0.1

Green (520 nm)	0.2 ± 0.1
Shift (blue to red)	0.3 ± 0.1
90 % red 10 % blue	0.3 ± 0.0
80 % red 20 % blue	0.2 ± 0.0
70 % red 30 % blue	0.2 ± 0.1
50 % red 50 % blue	0.3 ± 0.0

For further starch analysis the protocol was specified in a certain extent for *C. reinhardtii* concerning CDW concentration in samples analyzed which is reflected as smaller standard deviations. Although there are quantitatively large differences between values for low PFDs of 25 µE m^{-2} s^{-1} between small scale and larger scale reactor cultivations, there is a tendency for a decline of specific starch content with increasing PFDs for both approaches where above saturation point there is, at least for dichromatic approach tested, no further decline of value (see also Table 11-16).

Table 11-16. Specific starch concentrations with increasing PFD for dichromatic 90/10 red/blue illumination and warm-white control in midiplate reactors at 25°C.

PFD [µE m^{-2} s^{-1}]	Light color/ Mixture	Starch [g g^{-1} CDW]
25	ww	0.7 ± 0.1
	90/10 r/b	0.8 ± 0.1
50	ww	0.6 ± 0.1
	90/10 r/b	0.7 ± 0.1
100	ww	0.5 ± 0.0
	90/10 r/b	0.5 ± 0.0
150	ww	0.4 ± 0.0
	90/10 r/b	0.5 ± 0.0
200	ww	0.2 ± 0.0
	90/10 r/b	0.2 ± 0.1
300	90/10 r/b	0.2 ± 0.0

Following the thesis, that starch production is enhanced under stress conditions, the decreasing amounts of specific starch with decreasing PFD can be explained in terms of light limitation stress at lower PFDs. However, this thesis cannot explain the result that specific starch contents are higher for the well absorbing red/blue 90/10 dichromatic illumination except for intensities around saturation

point where no clear differences are monitored. In both respects starch content reflects the behavior of PCE in dependency on applied light color and with increasing PFD. In that extent the starch content positively correlates with photosynthesis efficiency in terms of light energy to biomass conversion. According to Ball and coworkers (1990), starch in *C. reinhardtii* is produced especially under nutrient limitation and a decline in specific growth rate. It can be assumed that with increasing PFD the decline in growth rate during cultivation is more rapid for highly absorbing wavelengths then for white control leading to a higher induction of starch production rate explaining higher values for dichromatic approach for intensities below saturation point.

11.6.1.5 Long-term effects of mono-and dichromatic red/blue illumination on starch content

In relation to chapter 4.6.3, specific starch contents of cells continuously cultivated under red/blue illumination at a low PFD of 25 µE m^{-2} s^{-1} are shown in Figure 11-11.

Also for long-term cultivations no clear influence of light color has been monitored on specific starch content in accordance to the results in fed-batch cultures at low light (compare to Figure 11-10 A).

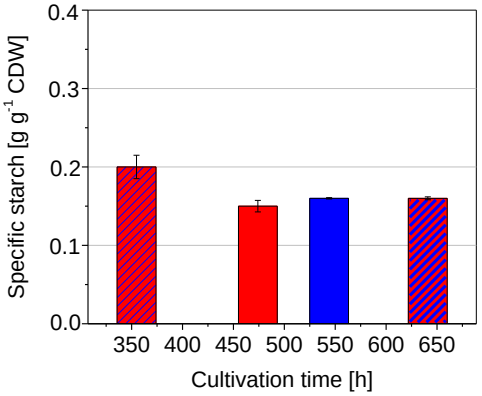

Figure 11-11. Specific starch concentration of cells during continuous cultivation in midiplate reactor under mono- and dichromatic red/blue illumination at a PFD of 25 µE m^{-2} s^{-1}. The first value is derived for 90/10 red/blue, second for pure red, third for pure blue and fourth for 50/50 red/blue illumination. Each sample was taken before a light color change was applied.

11.6.2 Pressure effects on microalgae cultures

11.6.2.1 Calibration procedure for mass flow meters at lowered pressure

Mass flow meters for CO_2 and air were calibrated for each of the applied lowered pressures of 0.9, 0.8 and 0.7 bar. In between the air inlet and the inlet sterile filter a device for measuring the volumetric flow (Gilian Gilibrator 2, NIOSH Primary Standard Air Flow Calibrator, Sensidyne) was installed in case of air; in case of CO_2 a smaller bubble flowmeter (20562, Supelco) was used. In both cases the measurement is based on the rise of a soap bubble within a certain time. For calibration the bioreactor was filled with water and the vacuum pump was connected to the exhaust gas line. An obstacle for

calibration was the discontinuous operation of the vacuum pump which was controlling pressure with a tolerance of 10 mbar. For this reason the pump, once the desired lowered pressure was installed, was stopped for the short time of the bubble rising to avoid interferences.

11.6.2.2 Calibration of cylindrical LED panel

For calibration of the new cylindrical LED panel (cold-white, type NFSW036BT, Nichia) a spherical quantum sensor (Biospherical Instruments Inc. QSL2101) was used. For experiments under lowered pressure the reactor was filled with an algae (CC-1690) suspension at a CDW concentration of 0.4-0.5 g L^{-1} where a homogenous light distribution can be expected according to the light intensity profile, Figure 11-14. The sensor was placed at 15 cm height and 1.3 cm distance from inner radius. Using the corresponding software Loggerlight the photon flux density was measured, while the current was stepwise increased in 0.5 A steps up to a PFD of 400 µE m^{-2} s^{-1}. The calibration curve of the old warm-white LED panel was taken from previous works (Jacobi 2013).

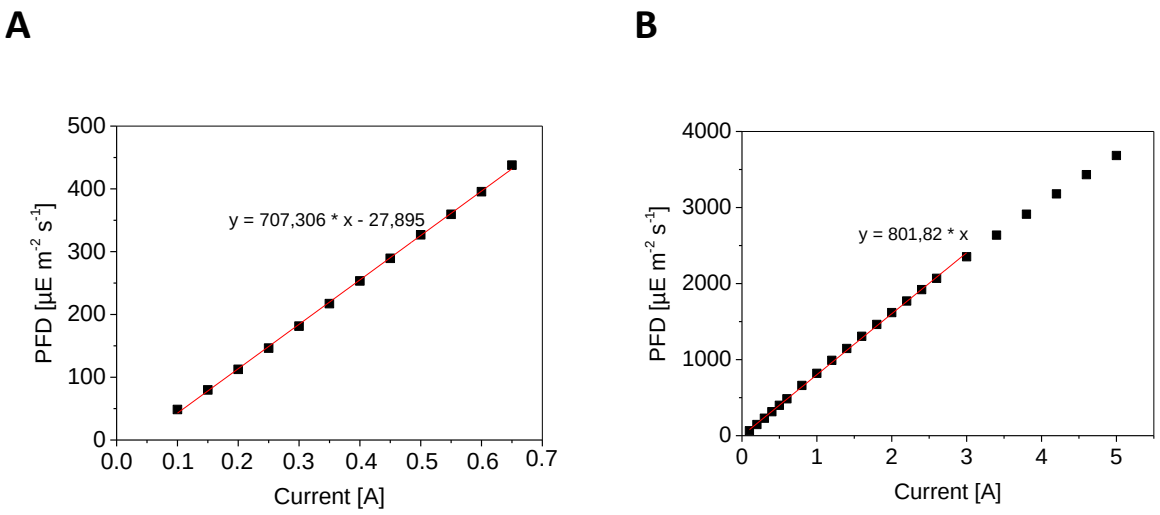

Figure 11-12. Calibration curves of cylindrical LED panels of the bubble-aerated stirred photobioreactor. A) New cold-white LED panel. B) Old warm-white LED panel (NS6L083AT, Nichia) with collimating lenses; Jacobi (2013). Both calibration curves were established with algae suspensions of cell densities where light is homogenously distributed.

11.6.2.3 Influence of pressure reduction on starch formation

Figure 11-13 shows results for specific starch content for cultivations under reduced pressure. As results show, for warm-white light values seem to fluctuate for different pressures, whereas under cold-white light the values are constant at 0.4 g g^{-1}. Hence, no effects of reduced pressure on specific starch concentrations can be shown with these experiments within the range of measurement accuracy (Wagner 2017). Values account for: 0.46 ± 0.01 and 0.45 ± 0.01 g g^{-1} starch per CDW for 1000 mbar, 0.34 ± 0.01 g g^{-1} for 900 mbar (ww), 0.2 ± 0.09 g g^{-1} for ww and 0.46 ± 0.01 g g^{-1} for cw at 800 mbar and for 0.31 ± 0.01 g g^{-1} (ww) and 0.47 ± 0.02 g g^{-1} (cw) at 700 mbar.

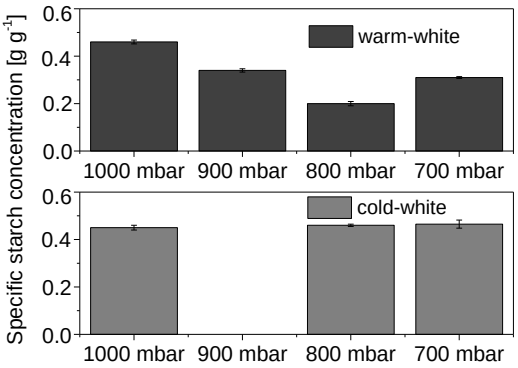

Figure 11-13. Specific starch concentration for batch cultivations with *C. reinhardtii* CC-1690 under different pressures. Specific starch concentrations of CC-1690 cells for cultivations under different pressures for both lighting colors.

11.6.3 Long-term cultivations of continuous microalgae cultures

11.6.3.1 Light intensity profile for cylindrical illumination

For the continuous cultures in the bubble-aerated stirred tank photobioreactor a light intensity profile was measured at different cell densities and for different incident light intensities based on the calibration curve in Figure 11-12 B, with the help of a spherical quantum sensor (Biospherical Instruments Inc. QSL2101). These graphs show that for CDW concentrations of 0.3 g L^{-1} the PFD increases towards the center as a result from overlapping light beams of the cylindrical panel. In contrast to that, for CDW concentrations of 0.6 g L^{-1} the PFD decreases toward the inner reactor volume as a result from increasing mutual shading of cells. At a specific cell density (in this case about 0.4 g L^{-1}) there is a homogenous light distribution throughout the reactor volume.

A **B**

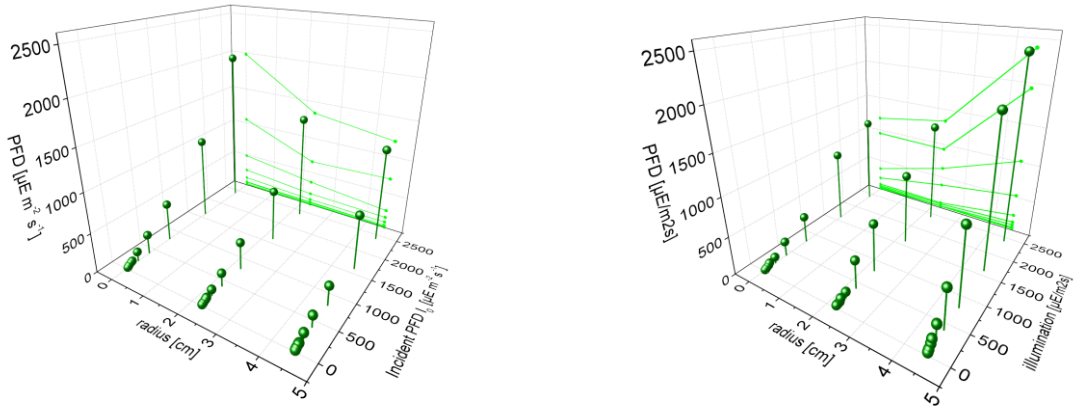

Figure 11-14. 3D light profile for cylindrical illumination of the stirred tank photobioreactor with old warm-white LED panel for different incident PFDs and different cell densities from center (radius = 0 cm) to reactor wall (radius = 4.5 cm). A) for a CDW of 0.3 g L^{-1}. B) for a CDW of 0.6 g L^{-1}.

11.6.3.2 µ-I-curve for *C. reinhardtii* CC-1690 in the stirred tank photobioreactor with cylindrical illumination

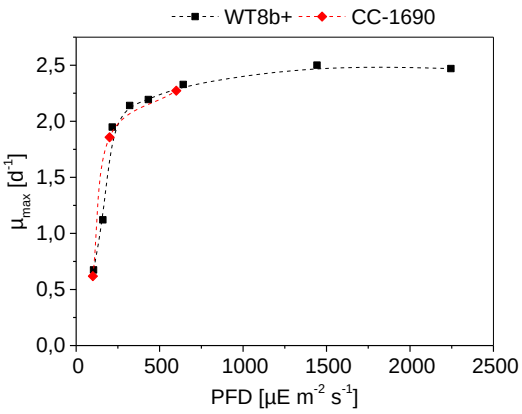

Figure 11-15. μ_{max}-I-curve of *C. reinhardtii* CC-1690 cells compared to *C. reinhardtii* WT8b+ cells in bubble-aerated 1.8 L photobioreactor. Data of WT8b+ (described in Bonente 2011) was originating from Jacobi (2013).

11.6.4 ModuLES-PBR: experimental data from parabolic flight and ground

Table 11-17. Times of light step changes and step increments during batch cultivation of the first flight with dichromatic illumination. The time range from t = 0 min to t = 50 min is included here, presenting the duration where the system was running under limited energy supply with a minimal PFD of 20 µE m^{-2} s^{-1}.

Time [min]	Light intensity PFD step change [µE m^{-2} s^{-1}]
50	20 to 200
110	200 to 100
140	100 to 200
155	200 to 100
178	100 to 70
205	70 to 100
218	100 to 200
235	200 to 60

11.7 Symbols and abbreviations

Greek symbols

α	Selectivity factor	-
γ	Illuminated fraction of reactor volume	-
ε	Extinction coefficient	$m^2\ g^{-1}$
λ	Wavelength of light	nm
μ	Specific growth rate	h^{-1}
ρ	Density	$kg\ m^{-3}$
Φ	Quantum efficiency	$mol\ mol^{-1}$
τ	Residence time	h

Latin symbols

a	Specific mass transfer area membrane	m^{-1}
a	Slope in light-limited range of PI-curve	$m^2\ s\ h^{-1}\ \mu E^{-1}$
A	Surface Area	m^2
c	Concentration	$g\ L^{-1}$
CUR	Carbon dioxide uptake rate	$mmol\ L^{-1}\ h^{-1}$
D	Dilution rate	h^{-1}
D	Diffusion coefficient	$m^2\ s^{-1}$
d	diameter	µm, mm
d, D	thickness, layer thickness	cm, mm, µm
h, H	Height	mm
H_B	Calorific value biomass	$J\ g^{-1}$
I	Light intensity	$\mu E\ m^{-2}\ s^{-1}$
I_0	Irradiated light intensity on surface	$\mu E\ m^{-2}\ s^{-1}$
I_c	Compensation point (photosynthesis	$\mu E\ m^{-2}\ s^{-1}$

	and maintenance)	
I_h	Inhibiting light intensity	µE m^{-2} s^{-1}
I_k	Optimal light intensity	µE m^{-2} s^{-1}
I_s	Saturation intensity	µE m^{-2} s^{-1}
k_L	Mass transfer coefficient	m s^{-1}
n	Refractive index	-
OPR	Oxygen production rate	mmol L^{-1} h^{-1}
p	Pressure	bar
pCO_2	Relative saturation of dissolved carbon dioxide	%
pO_2	Relative saturation of dissolved oxygen	%
q_{CO2}	Specific CO_2 uptake rate	mol g^{-1} h^{-1}
R	Reflected light	µE m^{-2} s^{-1}
r	Radius	mm
T	Temperature	°C, K
T	Transmitted light	µE m^{-2} s^{-1}
t	Time	h
v	Velocity	m s^{-1}
V	Volume	m^3, L
$\dot{V}$	Volumetric flow rate	ml min^{-1}
x	Molar fraction	mol mol^{-1}
Y	Yield	g mol^{-1}, mol^{-1} mol^{-1}

Physical constants

c	Speed of light	$2.998 \cdot 10^{8}$	$m\ s^{-1}$
g	Gravitation constant	9.81	$m\ s^{-2}$
h	Planck's constant	$6.626 \cdot 10^{-34}$	J s
N	Avogadro's number	$6.022 \cdot 10^{23}$	mol^{-1}
R	Ideal gas constant	8.314	$J\ mol^{-1}\ K^{-1}$
V_M	Molar volume of ideal gas	22.4	$L\ mol^{-1}$

Indices

*	Equilibrium condition
0	Initial condition, first, primary, outer
1	Compartment 1, inlet
2	Compartment 2, outlet
abs	Absorbed
aq	Aqueous
av	Average
b	Bubble
B	Biomass
CO_2	Carbon dioxide
g, G	Gas, gas phase
L	Light
l, L	Liquid, liquid phase
M	Membrane
M	Molar
max	Maximum

O_2	Oxygen
OD	Optical density
i, I	Inner, intrinsic
i	Compound i
j	Compound j
o, O	outer
p	Particle
S	Stirrer
V	Volume
wv	Water vapor
X	Biomass

Abbreviations

A_0	primary acceptor in light reaction of photosynthesis
A_λ	Absorption at a specific wavelength λ
ACP	Acrylic copolymer
ADP	Adenosine diphosphate
ATCC	American type culture collection
ATP	Adenosine triphosphate
AU	Absorption units
BLSS	Biological Life Support System
Car	Carotenoids
CCM	Carbon concentrating mechanisms
CDW	Cell dry weight
CELSS	Closed (or Controlled) Environmental (or Energy) Life Support Systems

Chl	Chlorophyll
Chl a	Chlorophyll a
Chl b	Chlorophyll b
ChR1, 2	Channelrhodopsin 1, 2
dH_2O, ddH_2O	Demineralized water, double-distilled water
dCO_2	Dissolved carbon dioxide
DCU	Digital control unit
DO	Dissolved oxygen
dO_2	Dissolved oxygen
EDTA	Ethylenediaminetetraacetic acid
EPS	Extracellular polysaccharides
EtOH	Ethanol
FIC	Flow indication control
k_L	Mass transfer coefficient
LED	Light emitting diode
LHC (I and II)	Light harvesting complex (I and II)
LSS	Life Support System
MBR	Membrane reactor
ModuLES	Modular life support and energy system
ModuLES-PBR	Modular life support and energy system photobioreactor
$NADPH+H^+$	Nicotinamide adenine dinucleotide (phosphate)
NPQ	Non-photochemical quenching
OD	Optical density
PAR	Photosynthetic active radiation

PBR	Photobioreactor
PCE	Photo conversion efficiency
PE	Polyethylene
PE	Photosynthesis efficiency
PFC	Parabolic flight campaign
PFD	Photon flux density
PP	Polypropylene
PS (I and II)	Photosystem (I and II)
PTFE	Polytetrafluoroethylene
PVDF	Polyvinylidene fluoride
qE	Energy-dependent quenching (of NPQ)
qT	State transitions (of NPQ)
rH	Relative humidity
ROS	Reactive oxygen species
RuBisCO	Ribulose-1,5-bisphosphate carboxylase/oxygenase
S_x (x = 0,1,2)	Electron states during excitation in photosynthesis
spec.	Specific
STPBR	Stirred tank photobioreactor
TAG	Triacylglyceride
TAP	TRIS-acetate-phosphate
TIC	Temperature indication control
TP	TRIS-phosphate
TRIS	Tris(hydroxymethyl)aminomethane
Vol.	Volumetric

11.8 Publications and students' thesis

Peer-reviewed publications

Wagner, I., Steinweg, C. and Posten, C. (2016) "Mono- and dichromatic LED illumination leads to enhanced growth and energy conversion for high-efficiency cultivation of microalgae for application in space." Biotechnology Journal **11**: 1060-1071.

Wagner, I. and Posten, C. (2017) "Pressure reduction affects growth and morphology of *Chlamydomonas reinhardtii*." Engineering in Life Sciences **17**(5): 552-560.

Students' thesis

Noemi Gutiérrez Carmona: "Investigation of a membrane-aerated reactor concept for the cultivation of microalgae." Master thesis.

Chloe Vanessa Smith: "Usage of membranes for aeration of photobioreactors." Master thesis.

Hannes Frey: „Verwendung von Membranen zur blasenfreien Begasung von Photobioreaktoren." Bachelor thesis.

Johannes Kühn: „Verwendung von Membranen zur blasenfreien Begasung von Photobioreaktoren unter warmweißer- und dichromatischer Beleuchtung. " Bachelor thesis.

Felix Kasper: "Influence of mono- and dichromatic illumination on microalgae cultures and dependency of oxygen production on light regimes in continuous *Chlamydomonas reinhardtii* cultures." Diploma thesis.

Marius Meier: „Einfluss mono- und dichromatischer Beleuchtung auf Mikroalgenkulturen." Bachelor thesis.

Virag Anna Sari: "Influence of mono- and dichromatic illumination on microalgae cultures and dependency of oxygen production on red and blue light regimes in continuous *Chlamydomonas reinhardtii* cultures." Bachelor thesis.

Gina Kaysan: "Influence of mono- and dichromatic illumination on microalgae cultures during continuous cultivations and at saturating light intensities of *Chlamydomonas reinhardtii*

cultures.” Bachelor thesis.

Manuel Merkel: „Kultivierung der Grünalge *Chlamydomonas reinhardtii* bei Unterdruck.” Bachelor thesis.